

TECHNICAL NOTE

D-1510

COLLECTED PAPERS ON INSTABILITY

OF SHELL STRUCTURES - 1962

Langley Research Center
Langley Station, Hampton, Va.

NATIONAL AERONAUTICS AND SPACE ADMINISTRATION
WASHINGTON

NATIONAL AERONAUTICS AND SPACE ADMINISTRATION

TECHNICAL NOTE D-1510

COLLECTED PAPERS ON INSTABILITY
OF SHELL STRUCTURES - 1962

FOREWORD

Shell structures are important components of airplanes, missiles, and space vehicles, but present capabilities for predicting the local and general instability of many such structures are inadequate. A large effort continues to be devoted to the stability analysis of shell structures, and considerable progress has been made. Results are slowly disseminated, however, and many engaged in research are not fully cognizant of the problems and practices of the vehicle designers who utilize research results. Therefore, an NASA SYMPOSIUM ON INSTABILITY OF SHELL STRUCTURES was organized by the Langley Research Center with sessions scheduled to be held there on October 24 and 25, 1962. Participants were limited to persons contributing papers and to certain officials of the U.S. Government.

This symposium was planned to provide those persons concerned with shell instability at research laboratories, at educational institutions, and in the aerospace industry with a comprehensive view of the present state of the art, including the voids in present knowledge, important current problems, and the most fruitful directions for future theoretical and experimental research on the instability of all types of shell structures.

Individuals actively engaged in research on shell stability or design were invited to contribute written papers for inclusion in a compilation to be distributed to the participants prior to the symposium. A few papers were selected by a steering committee for oral presentation at the symposium. Provision was made, also, for a discussion of all papers.

Individual authors prepared their final manuscripts and figures in a form that could be directly reproduced in this volume. The material provided was neither checked nor edited by NASA. Opinions and data presented are the responsibility of the authors and do not represent official views of the NASA.

The following steering committee guided and assisted the Langley Research Center personnel in the organization of the symposium:

R. R. Heldenfels, Chairman, NASA Langley Research Center
George Gerard, Allied Research Associates
M. G. Rosche, NASA Headquarters
E. E. Sechler, California Institute of Technology
R. S. Shorey, General Dynamics/Astronautics

NATIONAL AERONAUTICS AND SPACE ADMINISTRATION

TECHNICAL NOTE D-1510

COLLECTED PAPERS ON INSTABILITY
OF SHELL STRUCTURES - 1962

ABSTRACT

This collection of papers provides a comprehensive view of the present state of the art, including the voids in present knowledge, important current problems, and the most fruitful directions for future theoretical and experimental research on the instability of all types of shell structures.

CONTENTS

	Page
FOREWORD	i
I. THE DESIGNER'S VIEWPOINT	
SHELL INSTABILITY PROBLEMS AS RELATED TO DESIGN . . . by Lewis H. Abraham and Mortimer J. Lowy (Douglas Aircraft Company Inc.)	1
STABILITY PROBLEMS IN MISSILE STRUCTURES . . . by Richard J. Sylvester (The Catholic University of America)	11
SOME TYPICAL SHELL STABILITY PROBLEMS ENCOUNTERED IN THE DESIGN OF BALLISTIC MISSILES . . . by A. Kaplan, E. J. Morgan, and W. Zophres (Space Technology Laboratories, Inc.)	21
SOME SHELL STABILITY PROBLEMS IN MISSILE AND SPACE VEHICLE ANALYSIS . . . by D. O. Brush (Lockheed Missiles & Space Company, Sunnyvale, California)	35
DEVELOPMENT OF DESIGN STRENGTH LEVELS FOR THE ELASTIC STABILITY OF MONOCOQUE CONES UNDER AXIAL COMPRESSION . . . by A. H. Hausrath and F. A. Dittoe (General Dynamics/Astronautics)	45
SHELL STABILITY PROBLEMS IN THE DESIGN OF LARGE SPACE VEHICLE BOOSTERS . . . by James B. Sterett, Jr. (NASA Marshall Space Flight Center)	57
PROBLEMS ASSOCIATED WITH THE DESIGN OF LARGE SHELL STRUCTURE . . . by W. M. Moseley (General Dynamics/Fort Worth)	67
DESIGN OF STIFFENED CYLINDERS IN AXIAL COMPRESSION . . . by John M. Hedgepeth (Space Systems Division, Martin Marietta Corporation)	77
ELASTIC STABILITY CONSIDERATIONS IN AIRCRAFT STRUCTURAL DESIGN . . . by Richard L. Schleicher (North American Aviation, Inc.)	85
DESIGN AND TEST EXPERIENCES WITH INSTABILITY OF MAJOR AIRFRAME COMPONENTS . . . by Walter E. Binz, Jr. (The Boeing Company, Transport Division)	95

II. CYLINDRICAL SHELLS

ON THE BUCKLING OF THIN ELASTIC SHELLS . . . by Ellis Harold Dill (University of Washington)	105
BUCKLING AND POST-BUCKLING OF ELASTIC SHELLS . . . by H. Langhaar and A. Boresi (University of Illinois)	115
THE EFFECT OF INITIAL IMPERFECTIONS ON THE BUCKLING STRESS OF CYLINDRICAL SHELLS . . . by C. D. Babcock and E. E. Sechler (California Institute of Technology)	135
EFFECTS OF MODES OF INITIAL IMPERFECTIONS ON THE STABILITY OF CYLINDRICAL SHELLS UNDER AXIAL COMPRESSION . . . by L. H. N. Lee (University of Notre Dame)	143
A REPORT ON THREE SERIES OF EXPERIMENTS AND THE DESCRIPTION OF A SIMPLIFIED MODEL OF THE THIN WALL CYLINDER AND CONE BUCKLING MECHANISM . . . by Octavio G. S. Ricardo (Instituto Tecnologico de Aeronautica, Brasil)	163
SOME RESULTS ON BUCKLING AND POSTBUCKLING OF CYLINDRICAL SHELLS . . . by Joseph Kempner (Polytechnic Institute of Brooklyn) . . .	173
BUCKLING OF INITIALLY IMPERFECT AXIALLY COMPRESSED CYLINDRICAL SHELLS . . . by S. Y. Lu and William A. Nash (University of Florida)	187
ON THE POSTBUCKLING BEHAVIOR OF THIN CYLINDRICAL SHELLS . . . by W. F. Thielemann (Deutsche Forschungsanstalt für Luft- und Raumfahrt e.V. (DFL), Braunschweig (Germany))	203
THE EFFECT ON THE BUCKLING OF PERFECT CYLINDERS OF PREBUCKLING DEFORMATIONS AND STRESSES INDUCED BY EDGE SUPPORT . . . by Manuel Stein (NASA Langley Research Center)	217
THE MEMBRANE APPROACH TO BENDING INSTABILITY OF PRESSURIZED CYLINDRICAL SHELLS . . . by Harvey G. McComb, Jr., George W. Zender, and Martin M. Mikulas, Jr. (NASA Langley Research Center)	229
INSTABILITY ANALYSIS OF CYLINDRICAL SHELLS UNDER HYDROSTATIC PRESSURE . . . by George Herrmann (Northwestern University) . . .	239

	Page
INVESTIGATION OF YIELD COLLAPSE OF STIFFENED CIRCULAR CYLINDRICAL SHELLS WITH A GIVEN OUT-OF-ROUNDNESS . . . by Robert C. DeHart and Nicholas L. Basdekas (Southwest Research Institute, San Antonio, Texas)	245
THERMAL BUCKLING OF CYLINDERS . . . by Melvin S. Anderson (NASA Langley Research Center)	255
LOCAL CIRCUMFERENTIAL BUCKLING OF THIN CIRCULAR CYLINDRICAL SHELLS . . . by David J. Johns (College of Aeronautics, Cranfield, U.K.)	267
ELASTIC AND PLASTIC STABILITY OF ORTHOTROPIC CYLINDERS . . . by George Gerard (Allied Research Associates)	277
ON THE INSTABILITY OF ORTHOTROPIC CYLINDERS . . . by Michael F. Card and James P. Peterson (NASA Langley Research Center) . . .	297
GENERAL INSTABILITY OF ORTHOGONALLY STIFFENED CYLINDRICAL SHELLS . . . by Arie van der Neut (Technological University, Delft (Netherlands), Aeronautical Department)	309
BUCKLING OF LAYERED ORTHOTROPIC AND SANDWICH CYLINDRICAL SHELLS IN AXIAL COMPRESSION . . . by Edward W. Kuenzi (U.S. Forest Products Laboratory)	323
ELASTIC STABILITY OF SIMPLY SUPPORTED CORRUGATED CORE SANDWICH CYLINDERS . . . by Leonard A. Harris and Edward H. Baker (North American Aviation, Inc., Space and Information Systems Division)	331
DESIGN AND TESTING OF HONEYCOMB SANDWICH CYLINDERS UNDER AXIAL COMPRESSION . . . by John H. Cunningham and Marcus J. Jacobson (Douglas Aircraft Company, Inc., Missile Structural Systems Section, Missile and Space Division, Santa Monica, California)	341
THE BUCKLING OF CIRCULAR CYLINDRICAL SHELLS SUBJECT TO AXIAL IMPACT . . . by Anthony P. Coppa (Space Sciences Laboratory, Missile and Space Division, General Electric Company)	361

III. CONICAL SHELLS

A SURVEY OF BUCKLING THEORY AND EXPERIMENT FOR CIRCULAR CONICAL SHELLS OF CONSTANT THICKNESS . . . by Paul Seide (Aerospace Corporation)	401
ELASTIC INSTABILITY OF CONICAL SHELLS UNDER COMBINED LOADING . . . by P. P. Radkowski (Avco Research and Advanced Development Division)	427
BUCKLING OF CONICAL SHELLS UNDER EXTERNAL PRESSURE . . . by P. P. Bijlaard (Cornell University and Bell Aerosystems Company)	441
AXISYMMETRIC SNAP BUCKLING OF CONICAL SHELLS . . . by Malcolm Newman and Edward L. Reiss (Republic Aviation Corporation and New York University)	451
BUCKLING OF ORTHOTROPIC AND STIFFENED CONICAL SHELLS . . . by Josef Singer (Technion, Israel Institute of Technology)	463

IV. SPHERICAL SHELLS

ASYMMETRIC BUCKLING OF CLAMPED SHALLOW SPHERICAL SHELLS . . . by Hubertus J. Weinitschke (Hughes Aircraft Company, Ground Systems Group)	481
ON THE INFLUENCE OF NON-SYMMETRICAL MODES ON THE BUCKLING OF SHALLOW SPHERICAL SHELLS UNDER UNIFORM PRESSURE . . . by R. R. Parmerter and Y. C. Fung (California Institute of Technology)	491
SOME RECENT RESULTS ON THE BUCKLING MECHANISM OF SPHERICAL CAPS . . . by Herbert B. Keller and Edward L. Reiss (New York University)	503
COMPARISON OF EXPERIMENTAL AND THEORETICAL BUCKLING PRESSURES FOR SPHERICAL CAPS . . . by Gaylen A. Thurston (General Electric Company)	515
LOWER BOUNDS FOR THE BUCKLING PRESSURE OF SPHERICAL SHELLS . . . by Nicholas J. Hoff and Tsai-Chen Soong (Stanford University)	523

	Page
A SURVEY OF RESEARCH ON THE STABILITY OF HYDROSTATICALLY-LOADED SHELL STRUCTURES CONDUCTED AT THE DAVID TAYLOR MODEL BASIN . . . by Thomas E. Reynolds (David Taylor Model Basin)	545
BUCKLING OF A SPHERE OF EXTREMELY HIGH RADIUS-THICKNESS RATIO . . . by Harvey G. McComb, Jr., and Wilbur B. Fichter (NASA Langley Research Center)	555
DEFORMATIONS AND STABILITY OF SPHERICAL SHELLS SUBJECTED TO THE ACTION OF ASYMMETRICAL LOADINGS - EXPERIMENTAL STUDY . . . by R. M. Evan-Iwanowski (Syracuse University Research Institute)	565
EXPERIMENTAL OBSERVATIONS ON CREEP BUCKLING OF SPHERICAL SHELLS . . . by K. N. Tong (Syracuse University) and B. L. Greenstreet (Oak Ridge National Laboratory)	581
AXISYMMETRIC DYNAMIC BUCKLING OF CLAMPED SHALLOW SPHERICAL SHELLS . . . by Bernard Budiansky and Robert S. Roth (Harvard University and AVCO Corporation)	591
DYNAMIC DEFORMATION AND BUCKLING OF SPHERICAL SHELLS UNDER BLAST AND IMPACT LOADING . . . by Emmett A. Witmer, Theodore H. H. Pian, and Hans A. Balmer (Massachusetts Institute of Technology)	601
NONLINEAR TRANSVERSE AXISYMMETRIC VIBRATIONS OF SHALLOW SPHERICAL SHELLS . . . by J. Connor, Jr. (Watertown Arsenal Laboratories)	617

V. OTHER SHELL PROBLEMS

STRUCTURAL INSTABILITY OF SOLID PROPELLANT ROCKET MOTORS . . . by Adam R. Zak and Max L. Williams (California Institute of Technology)	637
SIMILITUDE REQUIREMENTS FOR SCALE MODEL DETERMINATION OF SHELL BUCKLING UNDER IMPULSIVE PRESSURES . . . by Arthur A. Ezra (Martin Company, Denver, Colorado)	655
STABILITY OF THIN TORISPHERICAL SHELLS UNDER UNIFORM INTERNAL PRESSURE . . . by John Mescall (Watertown Arsenal Laboratories, Watertown, Massachusetts)	665

	Page
ON SEVERAL RESEARCH PROBLEMS OF THE INSTABILITY OF SHELL STRUCTURES . . . by Masatsugu Kuranishi (Nihon University, Japan)	687
RECENT SOVIET CONTRIBUTIONS TO INSTABILITY OF SHELL STRUCTURES . . . by George Herrmann (Northwestern University)	715
A REVIEW OF SOME AVAILABLE TECHNIQUES FOR PREDICTING GENERAL INSTABILITY OF SHELL STRUCTURES . . . by Walter J. Crichlow (Lockheed-California Company)	725
A DIGITAL METHOD FOR THE ANALYSIS OF LARGE DEFLECTIONS AND STABILITY OF COMPLEX STRUCTURES . . . by Dale S. Warren (Douglas Aircraft Company, Inc.)	737
NON-LINEAR SHALLOW SHELL ANALYSIS BY THE MATRIX FORCE METHOD . . . by Warner Lansing, Irving W. Jones, and Paul Ratner (Grumman Aircraft Engineering Corporation)	747

I THE DESIGNER'S VIEWPOINT

SHELL INSTABILITY PROBLEMS AS RELATED TO DESIGN

By Lewis H. Abraham
and
Mortimer J. Lowy

Douglas Aircraft Company Inc.

SUMMARY

A presentation is made which highlights several current shell stability problems. A searching reappraisal of shell stability research is advocated in the light of the current rapidly mounting intensity of shell research which in many cases is disproportionately academic and non-design orientated.

INTRODUCTION

In scanning the list of participants in this symposium one can only marvel to see that so many serious investigators in the field of elastic stability can be gathered at any one time. Likewise, the papers presented cover a cross section of the important recent works being accomplished in the field of shell stability. At such a distinguished gathering, however, the responsibility of pointing out areas which are not receiving sufficient emphasis, is of equal importance to the task of reporting accomplishments. It is the hope of the authors that in pointing out specific problem areas and, where possible, indicating their relative importance in the design process, that interest will be aroused and solutions be expedited. Contrary to what has quite often become the expected plea, this paper will not ask for more effort in the discipline of shell instability, rather a diversion of the serious worker to the problem areas offering a maximum return potential. Even a casual glance at Figure 1 would indicate the widespread interest in shell stability as evidenced by the increase in the quantity of literature being published on shell analysis. Unfortunately much of it is concerned with peripheral problems and much deals with trivia. Perhaps it was this inundation of mediocre and inconsequential papers that prompted the editorial board of the Journal of Applied Mechanics to adopt a policy which excludes from consideration, without review, papers in the field of shell stability which employ small deflection theory or otherwise apply established techniques to the solutions, "no matter how interesting," (reference 3). While not a deterrent to all, at least such a policy will discourage waste effort involving trivial refinements and mathematical gymnastics. In the face of a limited and in-

expandable supply of competent talent we must turn our attention from the inconsequential problems to those where increased knowledge and analytical techniques hold promise of increased structural reliability and efficiency.

DESIGNING FOR STABILITY

A missile or spacecraft is primarily a pressure sustaining structure. Perhaps in excess of 90% of the structure may be sustaining pressure loads. In the early missile designs most shells were pressure critical and stabilization was not necessary except for certain handling conditions. However, as material applications and properties have advanced, wall thicknesses have diminished until today many shells which have been previously designed by pressure vessel criteria are now at or beyond the threshold of the instability problem. Figure 2 represents a design problem involving a solid propellant motor case which illustrates this situation. The case, a second stage sustainer, is subjected to axial compression and bending loads during the initial boost stage. After first stage booster cut-off the sustainer is fired and the case is subjected to an internal pressure condition. Figure 2 shows the required wall thickness of this 18-inch radius, steel cylindrical shell versus the tensile stress of the material considered. For the condition of internal pressure the typical hyperbolic relationship is obtained. However, consideration of the condition which induces compression in the shell establishes a lower limit of wall thickness which can be drawn as a horizontal cut-off line. This cut-off line, when derived for an unsupported shell by the method of reference 4 intersects the hyperbola at an ultimate tensile stress of 251,000 psi. This approaches very closely the ultimate strength of the material selected for the motor case. Thus it can be seen that additional improvements in the strength of case materials would be pointless without something being done about the shell stabilization problem.

Where previously it was conservative to neglect core stabilizing effects they now are a first order consideration. Figure 2 shows two additional cut-off lines. The intermediate one is based upon the work of Seide on cylinders stabilized by elastic cores (reference 5) and the lower one is based upon a value obtained in a full-scale compression test of a motor case filled with inert propellant. If the case were designed to the lowest cut-off value a weight saving of approximately 40% would result. These particular values of the limitations due to compressive instability are cited merely to illustrate the problems rather than define actual allowables. Methods of predicting stabilizing-effects of viscoelastic cores are rather difficult to apply in practice. For example, in applying Seide's theory it was necessary to assume a value for the modulus of elasticity of the core. This is difficult to obtain,

as it is well known that core materials behave in a viscoelastic manner and any test program must realistically account for the actual temperature and strain rate if it is to be an acceptable analog of the operational problem. Here then is a fertile field of investigation.

STIFFENED SHELLS

The designer, faced with the problem of shell instability must ask, "why monocoque?" It is well known that, except for the limiting cases of minimum-gage handling problems and thick-walled shells the monocoque is structurally the least efficient mode of material disposition for non-stabilized shells in compression.

In general, then, it behooves the designer to either avoid monocoque or stabilize it wherever possible. Some methods of avoiding monocoque include the following construction:

- (a) Conventional frame and/or stringer combinations
- (b) Integral stiffening
- (c) Sandwich construction
 - (1) Isotropic core (e.g. foam)
 - (2) Orthotropic core (e.g. honeycomb)
 - (3) Unidirectional core (e.g. corrugations)

The integrally stiffened shell is illustrated in Figure 3 which shows a machined waffle pattern that has been successfully used for design of several cryogenic fuel tanks. This simple configuration at first represented a fabrication challenge. Now that it has been successfully produced for several designs, attention has been given to optimizing the stiffener configuration. Interestingly enough, the most difficult problems here are not those concerned with optimizing the shell for strength only, but rather optimization consistent with the conditions imposed by manufacturing limitations and other design considerations.

Figure 4 shows a weight comparison of several systems of construction for cylinders as a function of loading intensity for an actual design case involving combined axial compression and bending. Similar consideration is given to spherical caps under external pressure in Figure 5. Here the treatment is more general in that weight, or gage, has been normalized as has the loading. There are several items worthy of note in this figure. First, we find a substantial difference between classical theory for monocoque and the empirical curve based on test data. The empirical curve shown is based upon a constant coefficient of 0.2 in the classical formula. This agrees within 10% with the available experimental data. Further examination of Figures 4 and 5 shows that there is a much larger potential pay-off in attempting to apply

sandwich construction to the design problem than there is in operating on the monocoque theory. One problem which looms large in designing for sandwich construction --- especially in cryogenic tankage, is that of thermal stress and the technique of combining thermal stresses with load-induced stresses. A rigorous address to this problem should provide useful information to the designer. An even more pertinent observation is that the weight advantages shown for sandwich construction are often lost in the reduction to design practice, especially in the design of joints and attachments. Thus the question must be raised whether a portion of funds spent on shell research and development could not, in many cases show greater returns, even for the long term, if spent on development of design and fabrication techniques rather than analytical methods. The problems of the stability of stiffened shells afford a propitious interface for the interests of the researcher and the designer and the contributions of both are essential.

SCATTER AND RELIABILITY

One problem of the designer which is even difficult to state, let alone operate upon, concerns the relationship among shell instability solutions, product testing and design factor-of-safety philosophy. In the design and construction of large boosters and space vehicles time and economic considerations dictate that full scale test specimens be few in number; yet the reliability of the vehicle must be close to 100%. Under the circumstances the large scatter in test and performance data experienced under present test techniques and the large deviations from predictions cannot be accepted without unwarranted design weight penalties or reduction in vehicle reliability.

It might be argued that many reliable aircraft were designed with limited full scale testing. It can also be argued however that there were many compensating factors in aircraft design that are not found in missiles. Among these were the sometimes meaningless corrections such as material and coupon correction factors, none of which had much direct bearing on shell instability. Nevertheless these corrections inadvertently provided reliability due to a high induced safety factor. Figure 6 reflects the design of a typical thin shell structure. If only specimen No. 1 had been tested and the design based on this value (e.g. the normal 1.5 safety factor applied to this value) the structure produced would have apparently operated satisfactorily and would still not have failed under limit stress even if an actual strength value as low as specimen No. 6 had been realized. Missile and spacecraft designers however, under pressure to produce more and more efficient structures have been forced to reduce this so called ultimate factor of safety from the standard value of 1.5 to 1.25 and even less. Using this criteria the allowable working stress for the illustrative example would have been raised and the reliability of the production structure, based on this

limited test data, would have been reduced to an unacceptable level.

Certainly, there must be a reason for this scatter. Does the observed scatter of test data reflect a variation from specimen to specimen or does the prime variational influence lie in the testing? If the former, perhaps we can control variations by design techniques. If the latter, can we expect similar variations in actual operations? These problems must be answered if the designer is to apply rational reliability criteria to his products. If some of the parameters affecting scatter were known, these data could be reduced to a much narrower scatter band --- even to a reasonably accurate standard value. If this were possible, data from a few tests could be used with greater assurance. Work to reconcile and explain the observed scatter would be most welcome by those of us in the design effort. In any event more rigor must be observed in the reporting of new test data.

OTHER PROBLEMS

Dynamic loading of shells, although not necessarily, or even predominately, a structural stability problem, is another area of great concern to the designer. For the large boosters now in study phases the effects of ground winds, wind shears and gusts, transient thrust and release loads, fuel sloshing and structural cross-coupling and blast exposure loom as first order problems. We feel that these problems are not receiving their proportionate share of attention.

CONCLUDING REMARKS

At the risk of making a presentation - and a short one at that - of perhaps considerably different context than most of those here, we have attempted to expound a philosophy based upon the immediate needs of the design engineer. Certainly we have not covered all important areas. The tremendous increase in the tempo of shell instability research in recent years would indicate such appraisals are periodically necessary if our precious research resources are to be used intelligently. The temptation to work on a problem because it yields a more tractable mathematical model or is academically interesting must be seriously weighed against the gains to be expected. Quite often a less elegant attack on a more abstruse problem will show a greater return in terms of advancement of the state-of-the-art of structural design. Most agencies charged with expenditure of the structural research dollars are forced into continuing reappraisal of the emphases and aims of contract-supported shell instability investigations in the light of the near and far term mission requirements. The point of philosophy we wish to reiterate in that things now appear out of balance. Perhaps some of the research dollars now spent on shell instability might be given up and spent in more lucrative endeavors.

REFERENCES

1. Nash, William A.: Bibliography on Shells and Shell-Like Structures. Report 863, David Taylor Model Basin, November, 1954.
2. Nash, William A.: Bibliography on Shells and Shell-Like Structures (1954-1956). University of Florida, June 1957.
3. Technical Editors: Editorial Policy Announcement. Journal of Applied Mechanics, Volume 29, Series E, No. 1, March 1962, back cover.
4. Gerard, George and Becker, Herbert: Handbook of Structural Stability, Part III - Buckling of Curved Plates and Shells. NACA TN3783, August 1957.
5. Seide, Paul: The Stability Under Axial Compression and Lateral Pressure of a Circular Cylindrical Shell with an Elastic Core. STL/TR-60-000-09032, Space Tech. Labs., Inc.
6. Weingarten, V. I., Morgan, E. J., and Seide, P.: Final Report on Development of Design Criteria for Elastic Stability of Thin Shell Structures. STL/TR-60-0000-19425 (AFBMD/TR-61-7), Space Tech. Labs., Inc., December 31, 1960, P. 134.
7. Lu, S. Y. and Nash, W. A.: Elastic Instability of Pressurized Cylindrical Shells under Compression or Bending. Presented at the 4th U. S. National Congress and Applied Mechanics held at University of California, Berkeley, June 18-21, 1962.

ARTICLES ON SHELLS & SHELL-LIKE STRUCTURE

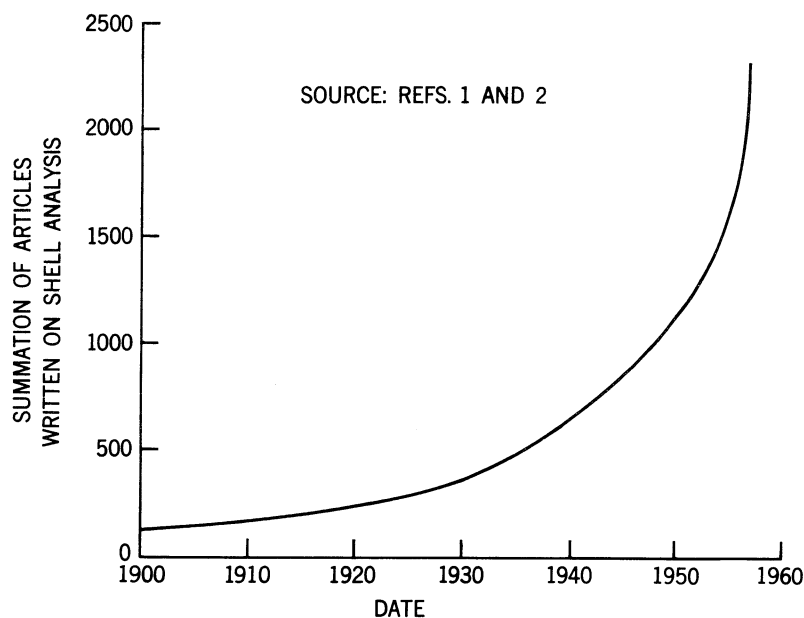


Figure 1

STRENGTH AS A FUNCTION OF CASE THICKNESS FOR AN ACTUAL MOTOR CASE

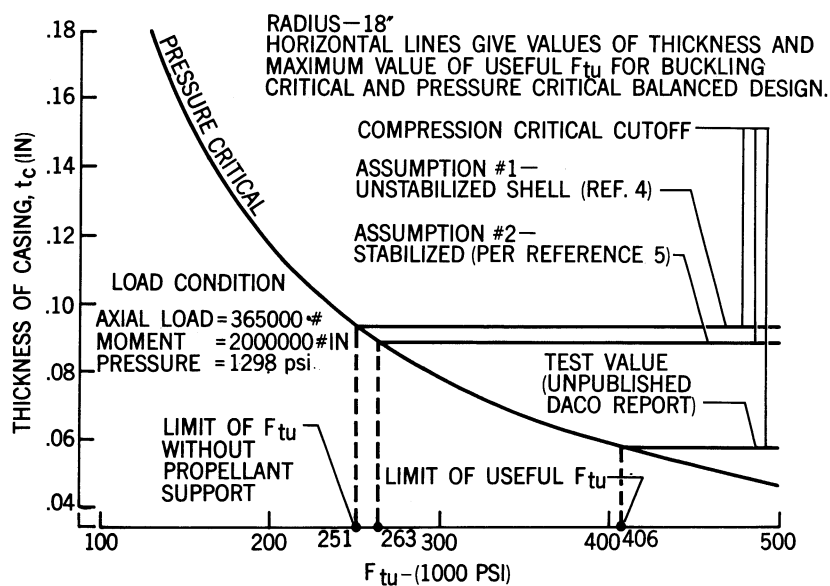


Figure 2

SEGMENT OF AN INTEGRALLY STIFFENED SHELL

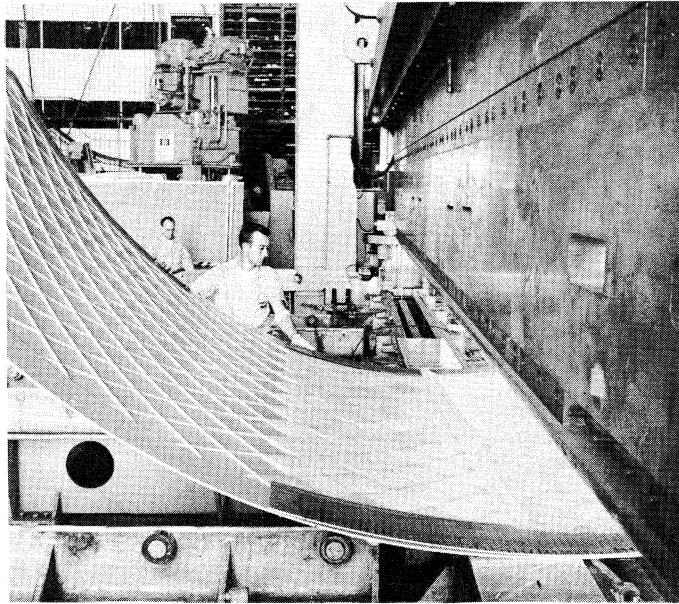


Figure 3

COMPARISON OF MINIMUM WEIGHT DESIGNS FOR VARIOUS STRUCTURAL SYSTEMS AND MATERIALS IN AN AXIALLY LOADED CYLINDER

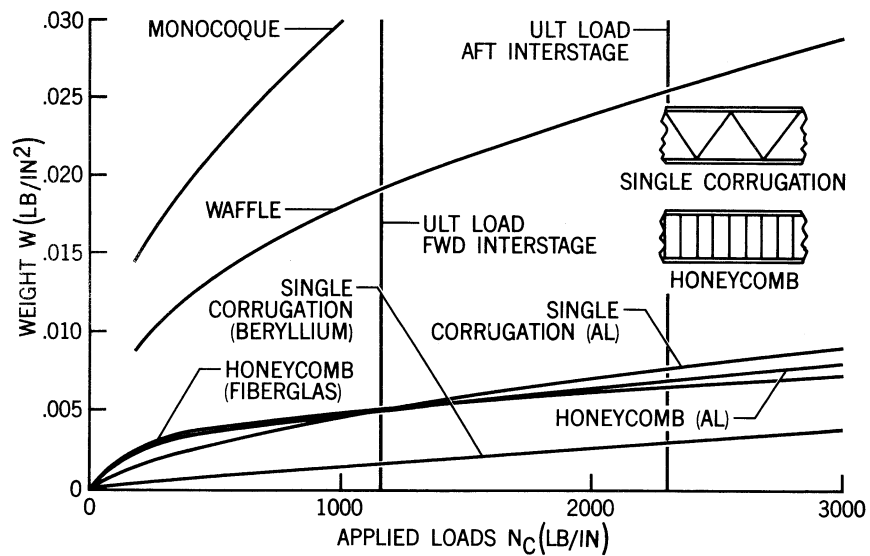


Figure 4

STRENGTH TO WEIGHT COMPARISON OF DEEP SPHERICAL CAPS UNDER EXTERNAL BUCKLING PRESSURE

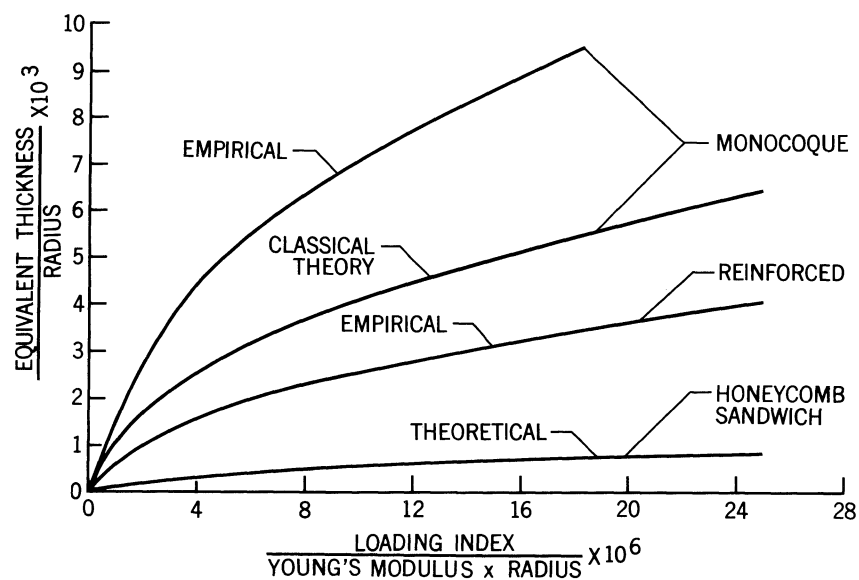


Figure 5

INFLUENCE OF SAFETY FACTOR AND SCATTER ON STRUCTURAL RELIABILITY

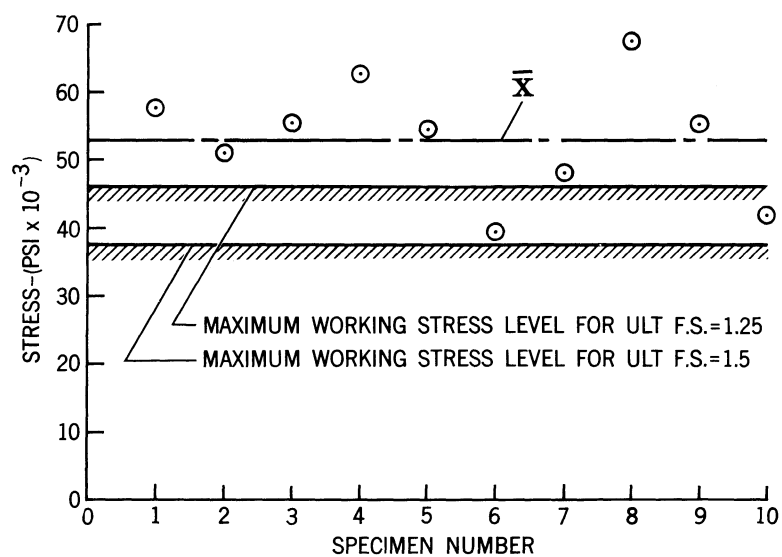


Figure 6

STABILITY PROBLEMS IN MISSILE STRUCTURES

By Richard J. Sylvester

The Catholic University of America

SUMMARY

A number of specific buckling problems relating to missile propellant tanks and transition sections are enumerated. In some cases approximate techniques used by missile designers to determine stability are mentioned. The inadequacies of these approximate methods and the unavailability of appropriate usable information is stressed.

Furthermore, the mathematical complexities of nonlinear buckling problems are considered. Some possibly fruitful areas of mathematics to simplify these complexities are discussed with the hope that research in these areas will provide a better means through which the analyst may supply the designer with more realistic and accurate theoretical data.

INTRODUCTION

The desire to reduce structural weight in missiles and space vehicles in order to increase payload has resulted in thin-walled shell construction subject to elastic and inelastic buckling as one primary mode of failure. In many instances an adequate buckling analysis, or method of analysis, or experimental information is not available. Consequently, very crude but hopefully conservative approximations or idealizations are employed for analysis of the design. Often designers even avoid entirely particular lightweight configurations because of the complete lack of experimental or theoretical information on potential instability problems. The results of the above situations may be either the choice of a design which may not be near optimum or, perhaps even worse, a very expensive static test or flight test failure resulting in costly delays and vehicle modifications.

This paper discusses a number of missile shell stability problems which can be categorized among those which cause difficulty for designers. The specific problems are considered under the classifications of tank dome problems, tank barrel problems, or transition section problems. Many of these stability problems may be formulated as boundary value problems in nonlinear partial or ordinary differential equations; however, the solutions of these equations are extremely difficult to obtain or to approximate.

Three distinct sets of ideas are entertained in regard to simplifying the methods of solution for these problems. The first ideas are in regard to high-speed digital computer means of determining parameters resulting from Ritz-type methods used with stationary energy principles. The second set of notions concerns the behavior of approximation to integral equation formulations of shell buckling problems rather than to differential equation formulations. The last group of ideas explore in a very preliminary fashion the possibility of converting the boundary value problems of shell stability into initial value problems by methods similar to those of Ambarzumian or those of "invariant imbedding" used in transport theory. Perhaps then as initial value problems simpler methods may be found to determine stability or multiplicity of solutions.

STABILITY OF TANK DOMES

Elliptical Domes Under Internal Pressure

The thin-walled elliptical shell (hemi-ellipsoidal shell of revolution) whose ratio of length of major to length of minor axis is $\sqrt{2}$ is often chosen as a missile tank dome primarily on the premise that such domes give the shallowest rise and hence minimize transition section length and weight without introducing the possibility of dome circumferential buckling. Rattinger has clearly shown by experiment that flatter elliptical domes will buckle under internal pressure.

Without entertaining the idea that such buckling might not be an adverse phenomenon, two important assumptions underlie the choice of a "root-two" elliptical dome. The first is that linear membrane analysis tells all that the designer needs to know. This implies that the displacements of the dome under load and the effect of edge restraints have little bearing on the dome stresses or stability. The second assumption is that the loading is a constant internal pressure.

Within the framework of linear membrane theory Baltrukonis has shown that for "root-two" elliptical domes under axisymmetric internal hydrostatic pressure compressive circumferential stresses do arise. These stresses appear in the neighborhood of the attachment points of the dome; the extent to which they continue into the dome depends upon the pressure gradient in relation to the total pressure. The fact that a great number of missiles with "root-two" domes which have been flight tested and have not experienced detectable buckling due to this effect may imply any of the following:

1. the domes have sufficient stiffness to withstand the compressive stress without buckling, or

2. the pressure gradient in relation to the maximum pressure is sufficiently small so that the compressive region is confined to the shell boundaries where attachments provide restraint against buckling, or
3. the displacements of the shell are large enough to change substantially shell curvatures and thus invalidate linear theory.

The nonlinear behavior of very thin elliptical domes under internal pressure is still a quantitative unknown. Tests indicate bursting pressures of 20% to 40% over that which linear membrane theory predicts. This phenomenon seems to be due to large curvature changes in domes under high pressure. These observations are offered as part justification for the third reason given above.

The successes of past designs of given geometry, thickness, and "pressure gradient-maximum pressure" relations unhappily do not insure the success of future designs which may incorporate variable thickness "root-two" domes of larger than conventional diameters and with different relationships between pressure gradient and maximum pressure. Consequently, the problem of buckling of elliptical domes under axisymmetric internal hydrostatic pressure still remains an open question.

When a propellant tank is in the horizontal position and containing a propellant, Baltrukonis has again shown membrane hoop compression under the nonaxisymmetric hydrostatic pressure. Here again is the source of a significant stability problem.

Shallow Spherical Domes Under Internal Pressure

In order to decrease the total length of a missile, decrease its structural weight, and raise its fundamental frequency of lateral vibration one tries to shorten as much as practical transition sections between propellant tanks. To accomplish this shortening some designers have considered using shallow spherical shells for tank domes. Reasoning from linear membrane theory they conclude that the lateral component of the longitudinal membrane stress at the dome-tank juncture must be resisted by a sufficiently stiff ring frame so that buckling of the tank walls and dome is avoided. The ring frame is customarily designed with a stiffness sufficient to prevent first mode "out-of-roundness" buckling were the ring free and under a uniformly distributed line load in the plane of the ring. The intensity of this line load is determined from the lateral component of the membrane stress in the dome. Consequently, the increased weight due to the heavy ring required under the above assumptions does not give the shallow spherical dome design a decided advantage over the elliptical dome design.

The author is not at all certain that for a shallow dome without a ring frame buckling will occur as first mode out-of-roundness. Most certainly large nonlinear local bending effects will occur as internal pressure is increased. The dome and tank wall curvatures will change measurably before buckling occurs. The deformed shape may tend to approach that of a shallow ellipse for which the mode of buckling is not in general first mode out of roundness. The presence of a ring frame may tend to reduce the amount of displacement at the edge of the dome, but the mode of buckling would seem to be dependent upon the stiffness of the ring frame. Hence, the nature of the stability of a shallow spherical shell under internal pressure and attached to a cylindrical tank wall with or without a ring frame of given stiffness is still an unresolved problem.

It seems heuristically reasonable that for sufficiently stiff rings "out-of-roundness" first mode buckling is most likely to govern the ring design. A pertinent suggestion has been to stabilize the ring against such buckling by a series of lightweight tension rods much like the spokes on a bicycle. It is believed that these rods would inhibit first mode buckling by providing restraint against outward motion of the ring. If such stabilization is possible, then a lighter ring may be used designed against buckling at some higher mode. Perhaps a weight-saving may be realized. Thus, the problem of the stability of a shallow spherical dome attached to a cylindrical shell edged by a ring frame which itself is stabilized by tension rods (perhaps prestressed) provides a challenging and useful area of investigation for the shell analyst. Further, weight optimization including the ring and tension rod weights with stability as the failure criterion would be most useful.

Domes for Segmented Tanks

In order to reduce the circumferential stress in propellant tank barrels the segmented tank, whose cross-section resembles the shape of a scalloped round doily, was devised. Domes for such tanks pose a stability problem for the analyst. For relatively flat domes a small radius of curvature is required at the transition from the dome to the segments of the barrel, hence one may legitimately anticipate circumferential compression in these areas when the tank is subjected to internal pressure. These transition segments are not shells of revolution but more closely resemble sections of a football. A computational complexity is thus encountered in determining the linear membrane stresses as well as the buckling behavior of these football segments. Certainly, the solution of this problem would be useful to designers.

Domes Under Static External Pressure

Several environmental and test conditions introduce the occurrence of static or quasistatic external pressures on domes. Such mishaps as rapid emptying of propellant tanks during simple hydrostatic testing without proper vent valve opening, air transport of tanks from higher to lower altitudes with unopened vent valves, and geysering of cryogenics during tank filling have all inadvertently caused situations of external pressures on domes. The frequency of buckling failures due to such mishaps have prompted designers to consider using various "failsafe" valves, which would permit rapid pressure equalization under such conditions. The design of such valves requires the knowledge of the buckling pressure of the domes. The problem of static external pressure on domes arises also in regard to recoverable boosters and in missile tanks in which a common dome separates two varieties of propellant.

Under some of the conditions mentioned above buckling occurs without rupture of the dome but with plastic deformations. Internal pressure may be used to "pop" the domes back into shape. Whether or not such a procedure is harmful to the integrity of the dome has not yet been determined.

Thus, dome buckling under external pressure is a significant large deflection problem complicated by the fact that in practice domes are not always shallow. Judging from the discussions in the literature on the nonlinear solution of the shallow spherical shell problem one may say with assurance that the buckling of deeper domes provides an extreme challenge. Perhaps different mathematical and new numerical schemes are necessary to seek out the solutions to such problems.

Domes Under Dynamic External Pressure

In a number of applications tank domes are subjected to rapidly applied external pressures. For example, in-flight ignition of a higher stage engine in the neighborhood of a lower stage tank dome causes a sudden dynamic blast to impinge on the dome below. In order to prevent damage to the lower stage which may be intended to be recovered or which might, if damaged, explode and cause a disruption of the higher stage the dome must be able to withstand the dynamic load. As the outstanding work of Ezra and Foral of the Martin Company in Denver has shown, for blast loads of short duration a peak external pressure considerably greater than the static buckling pressure can be withstood before permanent buckling is experienced. However, high speed motion pictures by Foral show considerable motion and large displacements due to high pressure impulses. An understanding of the dynamic response under such loads and the relation of this dynamic response to the permanent buckling or tearing

of the shell is not at all apparent. Just what stability means under such dynamic conditions is not at all clear. Here again is a complicated nonlinear problem to test the acuity of the analyst.

Concentrated Loads on Domes

The weight of many missile components is often supported by relatively heavy trusses in the transition section areas. These trusses are usually fastened to ring frames in the walls of the transition sections. Should these components be mounted directly on domes in the transition areas, truss weights could be saved. This practical consideration leads one to be concerned with the effects of concentrated loads on domes.

In testing of some shallow domes under single concentrated loads one of two different types of behavior is usually observed. For thicker domes plastic yielding in a significant neighborhood around the concentrated load is observed. For thinner domes no noticeable plastic yielding takes place; however, the concentrated load causes snapthrough or oil canning. Aside from desiring to know the load which causes snapthrough either local or general on shallow or deep domes, one should also like to know the values of those physical parameters which mark the separation point between the two different phenomena; i.e., elastic snapthrough or local yielding.

Explosively Formed Domes

Explosively forming from flat sheets large diameter domes for missile application has been suggested as a useful and economical manufacturing scheme. Tests on small scale models show that for sufficiently thin sheets of material used in explosively forming domes, wrinkles or buckles can form in the neighborhood of the apex of the dome and also around the supporting edge of the dome. Although methods for preventing these wrinkles are being devised, better understanding of the forming of these wrinkles would certainly be useful.

STABILITY PROBLEMS RELATING TO TANK BARRELS

Problems of Barrel Design

The choice of the type of barrel design to be used in missile propellant tanks is determined by several important considerations. Primarily the function of the tank barrel is to contain the propellant; thus, it must be able to withstand the internal pressures caused by the propellant and the tank pressurization system. Another function relegated to the tank barrel is transmitting the axial thrust of the engines to the

payload; thus, the barrel must be able to withstand the compressions developed. It is the resistance of this compressive loading that often leads to varieties of barrel designs.

A popular choice is the cylindrical tank with integral longitudinal stringers and hoop frames flexibly fastened to the stringer flanges. The stringers are usually designed to some sort of column buckling and crippling criterion which in the hands of a good analyst appears adequate. Whether or not the interior hoop frames provide an aid to stability is an unanswered question. On the basis of a variety of tests with internal pressure the presence of the frames and whether they are attached to the shell or the stringers does not seem to affect the buckling load significantly. A more adequate resolution of this problem is desirable.

For larger diameter rockets requiring relatively less internal pressure honeycomb construction for tank barrels will reduce tank weights. Honeycomb, however, in its customary design is adversely affected by thermal stresses. When the outer skin is heated and the inner skin cooled, the core material is placed under tension stresses which bring about separation between the core and the face sheets. A design which permits periodically spaced creases or ripples in the inner face sheet of a sandwich construction will tend to permit contraction of the inner face and expansion of the outer face without extremely high core tensions. The ripples will merely be pulled flat. The problem of the stability of honeycomb cylinders with such ripple inner face sheets has not at all been examined. Here, too, is a fruitful area of research for the structural analyst in the area of nonlinear buckling of sandwich cylinders.

Concentrated Load on Tank Barrels

Among the causes of concentrated loads on tank barrels one can include

1. struts and straps used in fastening booster rockets in cluster configurations,
2. handling loads in transport of missiles.

Significant problems in shell stability arise from these concentrated loads. Internally pressurized thin shells with identical longitudinal struts of varying cross section equally spaced about the circumference and supporting concentrated loads pose a problem of stability. Not only the behavior of these struts under longitudinal loads, but also under concentrated normal loads is significant. Study of the stability and deformation of such design with two, four, or six longerons would be most useful.

Straps or linkages which may be used to hold clusters of booster rockets together impose concentrated loads. Usually the strength of the barrel shell is ignored in the direct carrying of these loads and interior rings or support structures are assumed to carry the loads. If the degree to which the shell can resist concentrated tangential loads is better assessed, the internal support structure can be lightened or perhaps even eliminated.

The interior hoop frames mentioned in the section entitled, Problems of Barrel Design, are useful in preventing tank collapse due to handling loads. Precisely to what degree they are useful is not known. They are customarily designed by no really rational method. Knowing how these rings interact with the shell structure and maintain stability would be useful.

Dynamic Loads on Tank Barrels

Rapidly applied dynamic loads on tank barrels may arise from three important sources; the launch of a rocket vehicle from an underground silo, a nearby detonation, or a nearby upper-stage ignition. As in the case of dynamic loads on domes just what structural stability means and whether it should be considered in analysis under such loads is still an open question.

STABILITY PROBLEMS IN TRANSITION SECTIONS

Longerons in Transition Sections

The tremendous thrusts of rocket engines in liquid propellant missiles are usually resisted by heavy longerons which distribute these thrusts to cylindrical panels by means of shearing action. The required length of longeron is dictated by the buckling strength of the attached panels. This buckling strength is usually assessed as that of a flat plate of approximately the same dimensions as the curved panel. An adequate stability analysis of curved panels with variable section longerons does not seem to be available.

In order to save weight and shorten transition sections, some designers run the longerons into the tank barrel area. The stability behavior of a longeroned "transition section" and "tank barrel" ensemble is indeed complex and even good approximations to this behavior have not been forthcoming although certain designs employing this principle have been successful.

Should the longeron be made in two sections spliced in some way at the "tank-transition section" junction a noticeable decrease in bending stiffness of the longeron may be realized at this splice. This reduction in bending stiffness will tend to make the configuration more susceptible to buckling. The effect on stability of such a splice should be studied.

Other Transition Section Problems

Transition sections between tanks and between missile and payload must transmit high compressive forces and are designed entirely on stability considerations. To complicate the analysis of such sections is the presence of access doors. The stability of the section often depends strongly on the fastening and load-carrying capability of these doors, complicated by other loading environments such as transonic buffeting.

Still another interesting problem relating to transition sections is that of local elastic buckling on the compressive side of a laterally vibrating missile. The amount of bending stiffness reduction in the missile cross section due to local buckling is not well known. Determining this would enable the analyst to determine the decrease in the fundamental structural frequency of the missile due to such local elastic buckling during large lateral vibrations.

SOME AREAS OF MATHEMATICAL RESEARCH

With Donnell's idea that the buckling of a cylindrical shell under axial load is essentially a nonlinear phenomenon and with the clear confirmation of this notion by Von Karman and Tsien the shell analyst is forced into a mathematical discipline which is both very complicated and still in its infancy. Many shell stability problems can be considered as boundary value problems in the theory of nonlinear partial differential equations. This author would like to mention three different mathematical areas in which he feels research would be of benefit to the shell analyst.

Extremizing Nonlinear Functions

In the work of Von Karman and Tsien and more recently of Kempner concerning the postbuckling behavior of thin cylindrical shells the method of approximate solution of the nonlinear problem stems from the Principle of Stationary Potential Energy. Ignoring the important question of existence of a solution, analysts often employ a Ritz-type procedure. An approximate displacement function containing a number of arbitrary parameters is generated; compatibility in terms of this function is satisfied. The remaining task is to determine the values of the parameters

which minimize or at least make stationary the potential energy function.

Research to determine adequately convergent numerical schemes applicable to high-speed digital computers to minimize or extremize nonlinear functions of many parameters would certainly be fruitful to the shell analyst. Methods of steepest descent seem most promising and should be investigated further.

Integral Equation Formulations

Budiansky appears to be the only author to have employed the discipline of integral equations to shell buckling. His formulation of the shallow shell problem under uniform pressure led to nonlinear Hammerstein-like integral equations defined over a finite domain with a rather complicated kernel of Kelvin functions with singularities at its boundaries. An equivalent formulation with linear kernels but an infinite domain is also possible.

Since generally speaking the boundary conditions of the problem are already incorporated into the integral equation formulations, such questions as existence and uniqueness of solutions or numbers of non-unique solutions should be simpler for integral equation formulations than for differential equation formulations. Also, the rapidly developing field of functional analysis should provide many powerful theorems useful in the study of integral equations. Since nonsingular linear problems in integral equations lend themselves to numerically better behaved approximate solutions than do the equivalent differential equation formulations, one might hope for the same advantage in singular, nonlinear problems. For all these reasons the author would like to encourage the mathematically inclined shell analyst to become interested in and do some research in nonlinear integral equations.

Invariant Imbedding

Recent work by Bellman, Kalaba, and Wing in the mathematics of transport theory, has led to a method of solving boundary value problems called "invariant imbedding" which is an extension of the work of Ambarzumian. A primary objective of the method is the conversion of boundary value problems to initial value problems which seem to be well suited to high-speed digital computation. Although this method has not been applied to shell theory, preliminary investigations indicate that it has good potential. The invariant imbedding technique may be very useful in determining shell stability and should be examined more carefully.

SOME TYPICAL SHELL STABILITY PROBLEMS ENCOUNTERED IN THE DESIGN
OF BALLISTIC MISSILES

by

A. Kaplan, E. J. Morgan and W. Zophres
Space Technology Laboratories, Inc.

INTRODUCTION AND SUMMARY

Investigations carried out at STL on three current problems involving instability of thin shells in applications to aerospace vehicles are discussed. The first concerns the experimental determination of the buckling behavior of longitudinally stiffened pressurized cylinders; the second, the analytic prediction and experimental confirmation of the buckling behavior of multi-layer cylinders and the third involves the behavior of cylinders under combined axial load and lateral pressure. In each case the background of the application is reviewed, followed by a short description of the work. It is indicated that the longitudinally stiffened cylinder shows considerable promise in taking maximum advantage of the strengthening effect of internal pressure, that the use of an external low modulus layer as an insulator can have a significant effect on the buckling capability of a shell, and that the assumption of a linear interaction for pressure and axial load is unnecessarily conservative.

STIFFENED PRESSURIZED CYLINDRICAL SHELLS

The two original ballistic missiles, Atlas and Titan, were engineered with quite different design philosophies. In the Atlas, the primary axial load carrying ability is due to a high internal pressure and the thin walls serve primarily to contain the pressure, although they do make a small but significant contribution to the strength of the structure. This type of design can be quite efficient if high pressures are required for other systems such as the pump, and if high strength materials are employed. Its major disadvantage is the requirement of continual pressurization or axial tension in the structure to prevent collapse.

The Titan criteria specified that the fully-loaded missile be capable of standing erect in a wind with zero internal pressure. To meet this condition, the initial design called for a conventional aluminum aircraft type structure with longitudinal stringers supported by circumferential rings. However, due to the high pressurization stresses and severe aerodynamic heating this design is subjected to very large

secondary stresses at the frame attachments. These were eliminated by supporting the frames with radially slotted fittings. The frames supported the longerons in the unpressurized condition by preventing inward motion, but exerted no restraint to the outward motion resulting from internal pressure and heating. In the pressurized condition the only support for the longerons was obtained from the elastic foundation provided by the stressed skin. The procedure used for design was to size the stringers for the unpressurized ground condition assuming the tank behaved as a conventional stiffened structure, and then to check for the pressurized flight condition assuming that the skins buckled and that the elastically supported stringers failed by crippling. This structural concept was proved out by full scale room temperature tests and programmed heating tests conducted by the Martin Company at their own plant and at Wright field. It has been successfully used on both the Titan I and Titan II missiles. However, for the Titan tanks the unpressurized ground condition is critical, therefore there was no need to determine the effect of the various parameters of the pressurized stiffened structure and thus optimize its design.

To determine the full potentialities of this type of structure, a small scale testing program was started at STL a year and a half ago. It was felt that in addition to the reasons for its use in the Titan design, pressurized stiffened cylinders had the potential of making better use of the stiffening effect of the internal pressure than did the monocoque type of structure. This expectation was based on the observed buckling behavior of pressurized monocoque cylinders. With increasing internal pressure, the monocoque buckling waves become shorter longitudinally and larger circumferentially. When they approach an axially symmetric shape, the buckling stress which has been increasing with the pressure reaches a limit equal to the classical buckling stress for a monocoque cylinder. The addition of longitudinal stiffening would be expected to inhibit the formation of these axially symmetric buckles and thus increase the buckling stress of the skin. Furthermore, after buckling, the skin would be expected to act as a stretched membrane in the circumferential direction and thus continue to provide an elastic foundation for the longerons. These expectations were reinforced by the theoretical results of Thieleman (Reference 1) which indicated that internal pressure has a much stronger effect on the buckling stress of an orthotropic cylinder with the major stiffness in the longitudinal direction than on an isotropic cylinder.

a. Specimen Description

The aim of the test program was to determine the buckling behavior of longitudinally stiffened cylinders as a function of the internal pressure and the geometrical parameters of the cylinder. The latter included the R/t and L/R of the cylinder skin, and the number, size and

shape of the stiffeners. Because of the large number of combinations, it was necessary that a simple, easily made specimen be used. The test specimen and testing technique used were similar to that developed in a previous program and described in detail in Reference 2. The cylinders were formed from thin (2 mil to 10 mil) Mylar plastic and were bonded to plexiglas stringers. The specimens were joined to the end caps by casting them in a ring of Cerrelow, a low melting temperature metal alloy, thus providing a uniform loading of both stringers and skin.

The principal advantage in the use of Mylar is that due to its large range of linear elongation, buckling tests can be repeated without any degradation in performance. This had been demonstrated in the previous program and, in addition, it had been shown that there was no significant difference between the results for Mylar and those for metal, provided the buckling stresses were within the elastic limit.

The basic test cylinder was 8 inches in diameter and 8 inches long, but the effects of length and diameter were checked by spot testing of other sizes covering a range of R/t from 400 to 4,000 and of L/R from 1 to 4. Most of the stringers were of rectangular section, but a few tests using I and H sections were also made. The number of stringers was varied from 4 to 72.

b. Test Procedure

Tests on each specimen were made at a sequence of increasing pressures. The specimen was loaded at a constant displacement rate until the peak load was achieved. The total axial load and the relative axial displacement of the cylinder ends were continuously measured and recorded on an XY plotter. The results of a test sequence for a typical specimen with intermediate size stiffening are shown in Figure 1. The interruption in the curve indicates visual observance of panel buckling, while the horizontal intercept indicates the load carried by the pressure, $\pi R^2 p$.

c. Description of Results

The buckling of the specimens fell into several regions depending primarily upon the internal pressure and the relative size and number of the stringers.

For relatively light stringers at low pressures the specimens behaved as orthotropic cylinders with buckling of the skin and stringers occurring simultaneously. As the pressure was increased, the stringers continued to carry load after buckling of the skin and finally failed as columns. Finally, at high pressure, general failure occurred in an axisymmetric mode (Figure 2) similar to the failure of a monocoque cylinder.

der at high pressure. The onset of the axisymmetric mode was accelerated by an increase in the number of stringers.

For the heavier stringers, skin buckling occurs appreciably earlier than general failure. The skin buckles in the familiar diamond pattern with the longitudinal wave length decreasing with increasing pressure. At low pressure, the stringers buckle in their first or second longitudinal mode. With increasing pressure, the stringer buckling wave length decreases, but at a slower rate than that of the skin. Typical failure mode of a heavily stiffened cylinder at intermediate pressure is shown in Figure 3.

d. Analysis of Results

In line with the experimental evidence, two approaches were used in the theoretical analysis of the problem. In the first, the cylinder was treated as an orthotropic shell and a one term solution obtained for the corresponding Donnell type equation. In the second, the stringers were treated as individual columns supported by the skin acting as an elastic foundation. Neither of these approaches has been very satisfactory as yet but they have indicated the qualitative trends of the data.

In lieu of an analytic theory, an empirical equation indicating the influence of the various parameters was developed. The initial step in this direction was to separate the load carrying capability of the skin from that of the stringers. This was done by subtracting the sum of the load carried by pressure and the calculated buckling load of the monocoque skin from the total failure load, and dividing the result by the number of stringers. This gave P_N , the increase in load above that of pure monocoque cylinder due to each stringer.

Plotting P_N for various numbers of stringers as a function of pressure indicated that over most of the range of configurations tested P_N was independent of the number of stringers and was proportional to the square root of the pressure, except at very low pressures. Continued plotting and analysis led eventually to the following formula

$$P_N = \frac{4\pi^2 E_o I_o}{L^2} + \frac{1}{2} \sqrt{\left(\frac{E_o I_o}{\rho_o} \right) \left(\frac{E_s t^2}{12(1-\mu^2)R} \right)} \left\{ 1 + \sqrt{1 + 12(1-\mu^2) \frac{p}{E_s} \left(\frac{R}{t} \right)^2} \right\}$$

The formula agrees within an accuracy of about 10% with all the experimental results except those for a large number of stringers and high

pressures. For those cases, the formula overestimates the increase in P_N with pressure. The overestimation occurs earlier with relatively light stringers and is evidently associated with the onset of the axially symmetric buckling mode. Methods of including this effect in the formula are still being studied. In Figure 4 the results for similar cylinders with a wide variation in size and number of stringers are compared with the predictions of the formula. The good agreement over most of the range of parameters together with the drop off for the large number of stringers is evident.

The difficulties in obtaining an accurate analysis using the concept of an elastically supported column are evident by comparing the empirical buckling formula with the equation for the buckling of a clamped column on an elastic foundation

$$P_{cr} = 4 \pi \frac{E_o I_o}{L^2} + 2 \sqrt{k E_o I_o}$$

This indicates that the effective elastic foundation is a function of ρ_o and thus evidently cannot be the simple Winkler type foundation which is usually assumed. The comparison also indicates that for large pressures the stiffness is independent of the skin thickness and thus the effective width of the skin is independent of pressure. This conclusion is confirmed by the load deflection curves.

Additional analyses are being performed in an attempt to determine the mechanism of this effect and additional tests are planned to further delineate the region of axially symmetric buckling. To determine if the axial compression results are applicable to bending, a small bending program has been started. Initial results from this program are encouraging and indicate that the bending behavior can be inferred from the axial test results.

LOW R/t MONOCOQUE CYLINDERS SUBJECTED TO COMBINED EXTERNAL PRESSURE AND AXIAL LOAD

The interstage structure of the Minuteman consists of ring stiffened monocoque cone frustums of small included angle and with an R/t of about 200. For the loads encountered by the Minuteman, this monocoque design provides a good combination of high bending stiffness, high heat sink capability to minimize aerodynamic heating, and relatively low weight. The critical loading conditions for the interstages occur at stage burn-out due to a combination of axial compressive load and high temperature,

at maximum dynamic pressure due to a combination of axial compression, bending and a slight external pressure, and at silo launch, due to a combination of axial compression and high external pressure. To optimize the design for the launch condition, a small scale testing program was instituted at STL.

An earlier test program (Reference 2) covering a wide range of cones and cylinders had indicated that the interaction curve for buckling of cylinders under axial compression and external pressure was concave upwards, particularly for low values of R/t . However, there was not enough data to be conclusive and there was no data for R/t less than 400. Additional testing was therefore indicated. Because of the small included angles of the interstages, and because the previous results had indicated good correlation between low angle cones and cylinders, it was decided to simplify the testing by using cylinders. The specimens were similar to those described in the previous section, being made of Mylar plastic sheet joined to the end plates by casting in a Cerrelow ring.

Tests were run on a series of specimens with $R/t = 156$ and approximately 200, and with values of Z ranging from 26 to 739. The results are presented in Figure 5 as the ratios of the experimentally determined buckling pressures and loads to design values for lateral pressure alone and axial load alone, respectively. The reference buckling coefficients for lateral pressure are taken as 90% of the values suggested by Batdorf (Reference 3) while the reference axial buckling coefficients are those recommended in Reference 2, that is

$$C = 0.606 - 0.546 \left(1 - \exp - \frac{1}{16} \sqrt{\frac{R}{t}} \right)$$

It is seen that the interaction curve is strongly non-linear and also asymmetrical. A line drawn through the mean of the data would be definitely non-circular. However, due to the increased scatter for the high axial load conditions, a circular interaction curve is recommended for design. A report describing the details of the experimental work is in preparation.

It is clear that in this low range of R/t the assumption of a linear interaction curve between axial load and lateral pressure is unnecessarily conservative.

COMPOSITE CYLINDERS SUBJECTED TO AXIAL COMPRESSION AND EXTERNAL PRESSURE

The Guidance and Control Compartment of the Minuteman is subjected to similar loading conditions as are the interstages. However, due to its forward position, the load intensities are lower and the aerodynamic heating is higher. As the result of several design studies, it was decided to use an aluminum monocoque shell with one intermediate lateral pressure ring to which was bonded a layer of low conductivity fiberglass insulation. An important factor in the choice of this configuration was the major contribution of the fiberglass insulation to the buckling strength of the shell for silo launch and max q conditions. At these times, particularly the silo launch condition, only the surface layers of the fiberglass were heated and therefore it maintained most of its room temperature properties. At the final burnout condition, the fiberglass was heated throughout and its structural contribution was therefore neglected.

The analytic approach (Reference 4) to the buckling of the two layered cylinder was based on neglecting the difference in Poisson's ratio between the two materials. This approximation allows a simple calculation of the bending and stretching stiffnesses of the composite shell. On substituting these stiffnesses into Donnell's equations, revised expressions were obtained for the curvature parameter Z and the buckling coefficient K. These revised expressions then allow direct utilization of the solutions obtained by Batdorf (Reference 3) and others for the buckling of thin cylindrical shells for various loading conditions.

Thus for a shell consisting of two thicknesses, t_1 and t_2 with elastic moduli E_1 and E_2 , respectively, the composite extensional stiffness B is given by

$$B = \frac{E_1 t_1}{1-\mu^2} \alpha, \quad \alpha = 1 + \frac{E_2 t_2}{E_1 t_1}$$

while the composite bending stiffness D is given by

$$D = \frac{E_1 t_1^3}{12(1-\mu^2)} \beta, \quad \beta = 4 + 4 \frac{E_2}{E_1} \left(\frac{t_2}{t_1} \right)^3 - \frac{3 \left[1 - \frac{E_2}{E_1} \left(\frac{t_2}{t_1} \right)^2 \right]^2}{1 + \frac{E_2 t_2}{E_1 t_1}}$$

Then

$$Z = \frac{L}{R} \sqrt{\frac{1-\mu^2}{12}} \sqrt{\frac{B}{D}} = \sqrt{1-\mu^2} \frac{L^2}{R t_1 \sqrt{\frac{\beta}{\alpha}}}$$

and

$$N_{cr} = K \frac{\pi^2 D}{L^2} = K \frac{\pi^2 E_1 t_1^3}{12(1-\mu^2)L^2} \beta$$

For large Z, the equation for buckling under an axial load is simply

$$K_x = \frac{4\sqrt{3}}{\pi} Z$$

which, on making the proper substitutions becomes

$$N_{cr} = \frac{1}{\sqrt{3(1-\mu^2)}} \frac{E_1 t_1^2}{R} \sqrt{\alpha\beta} = 0.6 \frac{E t_1^2}{R} \sqrt{\alpha\beta}$$

Thus, the theoretical influence of the second layer is proportional to $\sqrt{\alpha\beta}$. Presumably there is a similar reduction in the theoretical coefficient, 0.6, for the multilayer cylinder as there is for the homogeneous cylinder. The actual functional variation can only be determined experimentally, but a likely candidate is to assume the same function of R/t as for a single cylinder based on the effective thickness term in the expression for Z, $t_{eff} = t_1 \sqrt{\beta/\alpha}$.

In Figure 6(a) are shown the results of axial buckling tests of full-scale cylinders representing the Minuteman G&C Compartment. The results are expressed as the ratio of the actual buckling loads to the average buckling load obtained for three single layer aluminum cylinders. The R/t of the aluminum cylinder is 244 and the L/R is 1.8. These tests were conducted by the Space and Information Division of North American Aviation. Also shown are the theoretical predictions for the two assumptions that the buckling coefficient is considered a function of $\sqrt{\alpha/\beta}$ and that it is considered independent of $\sqrt{\alpha/\beta}$. The data is insufficient to confirm the theoretical predictions over a range of thickness ratios, but it does confirm the major increase in load at the tested thickness ratio.

For the buckling of cylinders under lateral pressure, the Batdorf expression for the buckling coefficient for large Z is

$$K_y = 1.04 \sqrt{Z}$$

On substitution, the expression for the lateral buckling pressure, p_{cr} , is obtained

$$p_{cr} = 0.926 E_1 \left(\frac{t_1}{R} \right)^{5/2} \frac{R}{L} 4 \sqrt{\beta^3 \alpha}$$

Thus, for lateral pressure, the influence of the second layer is proportional to

$$\sqrt{\beta^3 \alpha} = \sqrt{\alpha \beta} \sqrt{\beta/\alpha}$$

and is considerably greater than for the axial load case.

In figure 6(b) are shown the results of similar tests performed by North American for the lateral pressure case. The results are presented in the same way as for the axial load case except that the reference value for a single layer is computed. Two of the specimens were cylinders ($R/t_1 = 240$, $L/R = 1.8$) and the other two were conical frustums with a semi angle of 5° ($R/t_1 \approx 240$, $L/R \approx 0.9$). In this case the tests were conducted at a variety of thickness ratios and indicate excellent agreement with the theoretical predictions.

It thus appears that the simple theory presented here gives good correlation with experiment and further that the addition of a relatively thick but low modulus layer has a significant effect on the buckling load of a cylinder, particularly under lateral pressure. It should be noted that for Minuteman interstages, the proportionate amount of insulation required is much smaller and therefore the use of fiberglass would have a much less significant effect on the buckling strength.

One severe problem should be mentioned before closing. The buckling capability of a two layer structure is a critical function of the bond between the layers. This is particularly the case when plastics are bonded to metals because the wide difference in thermal coefficients of expansion can induce significant internal stresses. It is only when these factors are considered in detail in laying out the fabrication and quality control procedures, as was done by North American, that a successful structure can be built.

REFERENCES

1. W. F. Thieleman, "New Developments in the Non-Linear Theories of the Buckling of Thin Cylindrical Shells," Aeronautics and Astronautics Proceedings of the Durant Centennial Conference, N. J. Hoff and W. G. Vincenti, Editors. Pergammon Press, New York, 1960
2. V. I. Weingarten, E. J. Morgan and P. Seide, "Final Report on Development of Design Criteria for Elastic Stability of Thin Shell Structures," Space Technology Laboratories, Inc. Report, TR-60-0000-19425, December 1960.
3. S. B. Batdorf, "A Simplified Method of Elastic-Stability Analysis for Thin Cylindrical Shells," NACA TR 874, 1947.
4. W. Zophres, "Elastic Buckling of Two-Layer Cylinders and Curved Plates," Space Technology Laboratories, Inc. Report, GM-TR-0165-00539, December 1958.

$R=4$ $L=8$ $t=.005$
 $36 \sim 1/8W \times .030D$ STIFFENERS

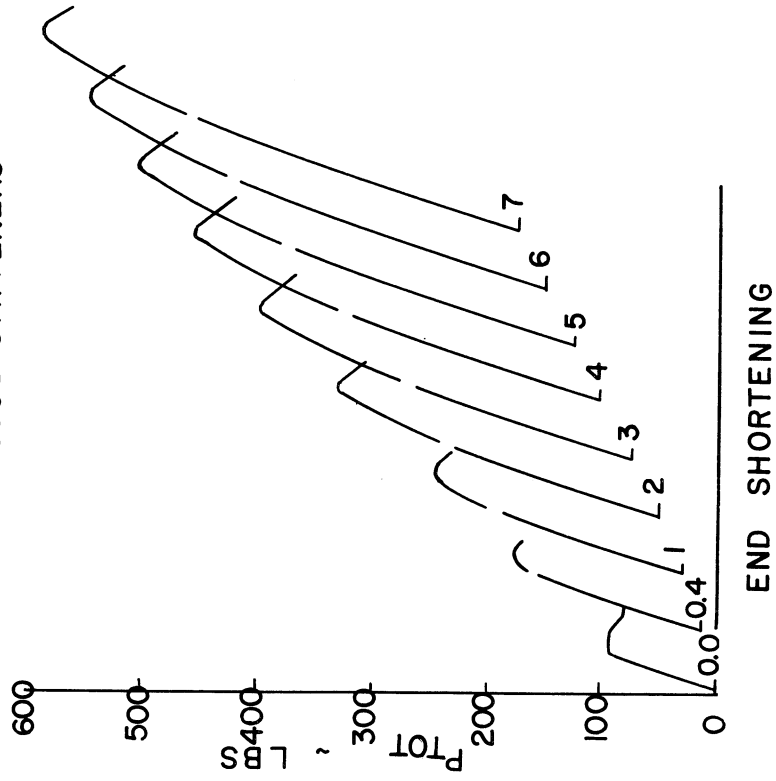


Figure 1.- Typical sequence of load-deflection curves.

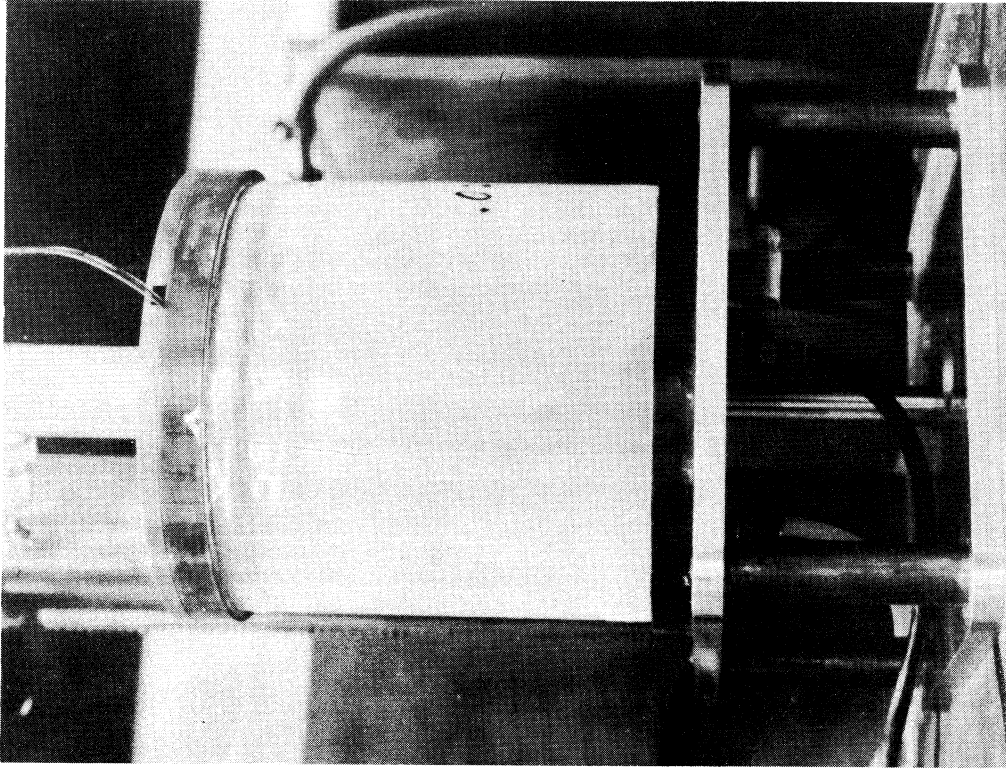


Figure 2.- Axisymmetric buckling mode of a lightly stiffened cylinder (same specimen as fig. 1).

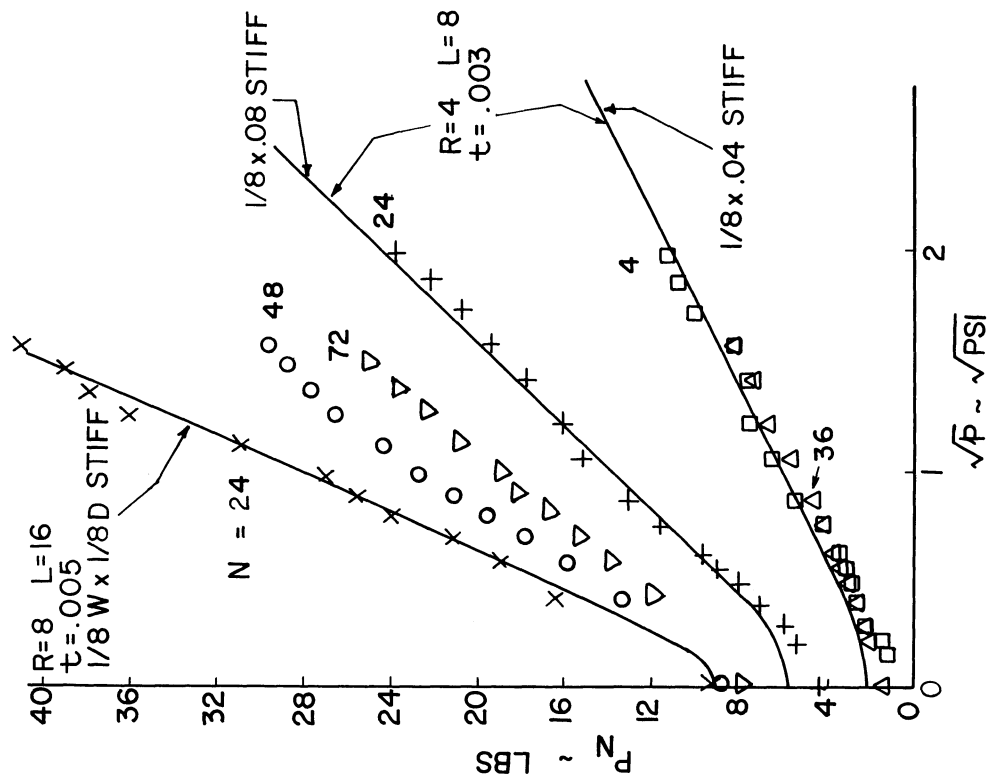


Figure 4.- Comparison of experimental results with empirical prediction.

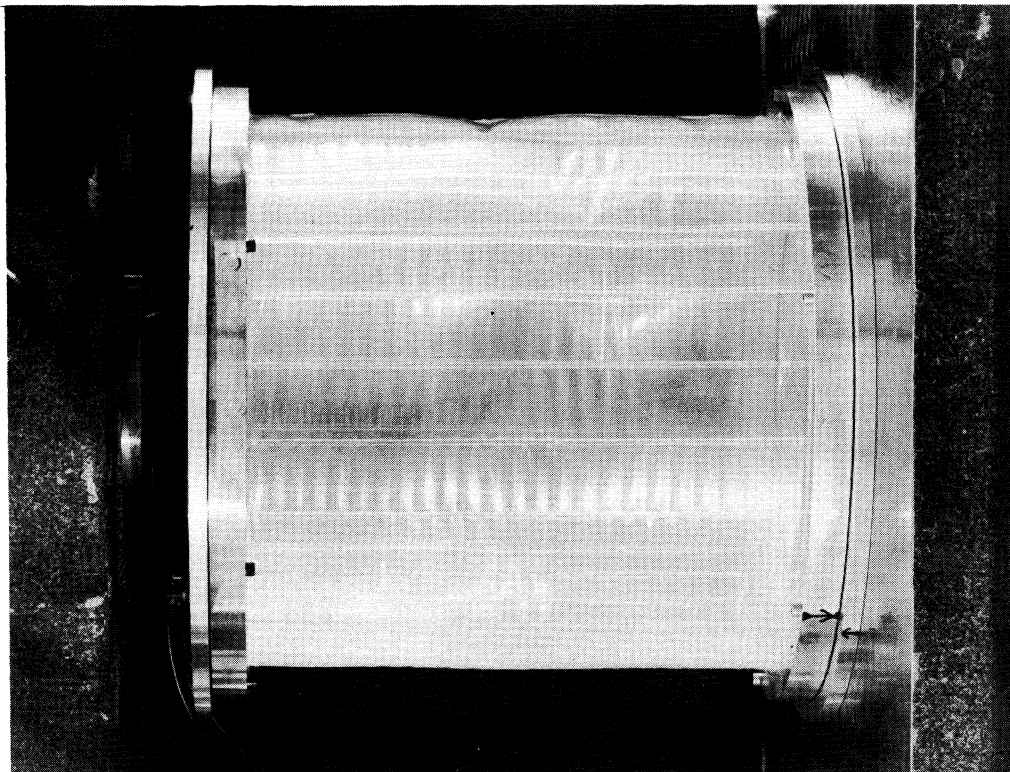


Figure 3.- Typical buckling mode of a heavily stiffened cylinder at intermediate pressure (specimen X of fig. 4).

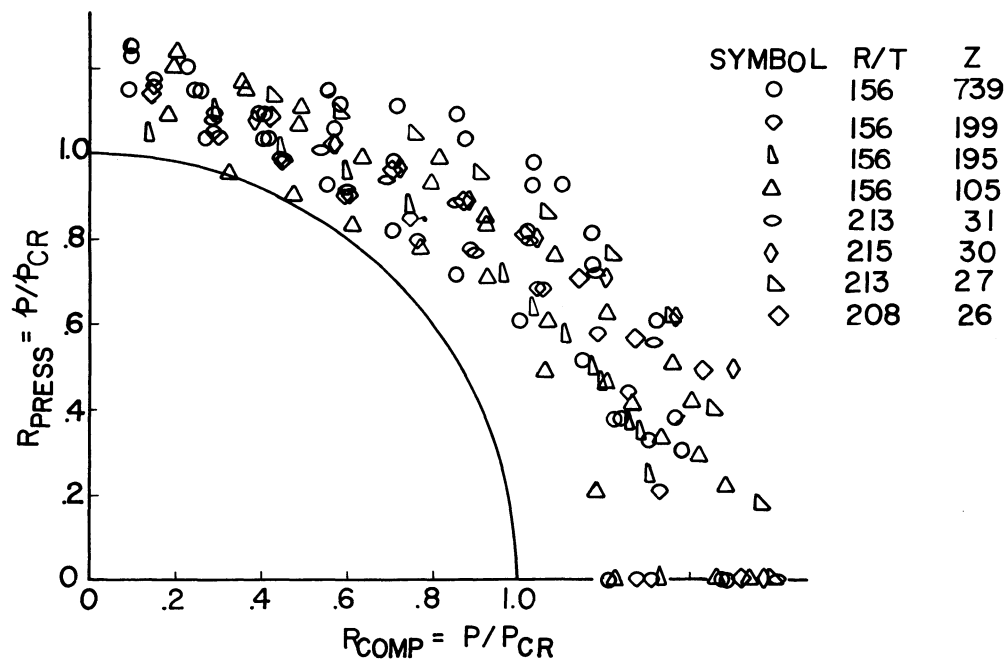


Figure 5.- Experimental results for Mylar cylinders under combined axial compression and external pressure.

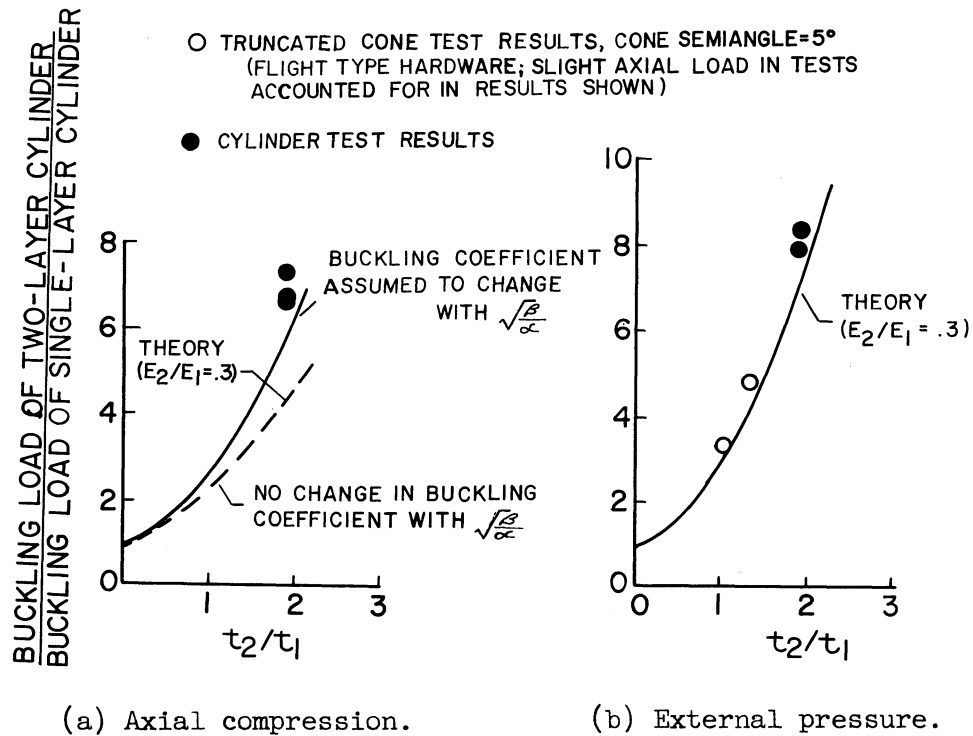


Figure 6.- Buckling of two-layer cylinders (cylinders of aluminum-reinforced plastic combination).

SOME SHELL STABILITY PROBLEMS
IN MISSILE AND SPACE VEHICLE ANALYSIS

By D. O. Brush

Lockheed Missiles & Space Company
Sunnyvale, California

SUMMARY

A brief discussion is presented of three structural shell stability studies in progress at Lockheed Missiles & Space Company: the stabilizing influence of solid propellants, the effect of cushion stiffness on buckling under cushion loading, and the snap-through buckling of axially loaded cylinders. Recent analytical results are compared with test data. Also included is a brief description of a few shell stability problems of present interest to LMSC for which satisfactory methods of analysis are not available.

INTRODUCTION

One of the consequences of the critical importance of weight saving in missile and space vehicle design is that most major structural components consist of thin-walled structural shells. In terms of the usual classifications of shell theory, most of the shells in such applications are not only thin but are extremely thin. This thinness, of course, promotes buckling and large deflections. Consequently, a substantial portion of the structural research effort in any missiles and space company must be devoted to shell stability investigations.

Research and methods-of-analysis studies are presently in progress at Lockheed Missiles & Space Company on a broad range of shell stability problems. This report briefly discusses three of these problems: the stabilizing influence of solid propellants, the effect of cushion stiffness on buckling under cushion loading, and the snap-through buckling of axially loaded cylinders. The first of these concerns analyses in which the propellant is assumed, as a first approximation, to act as a soft elastic foundation. The accuracy of small-deflection buckling theory in such analyses and the suitability of the Winkler-foundation assumption are considered. The second study pertains to the design of large-diameter cylindrical shell structures to resist handling and storage loads. A support load occasionally must be introduced into a

cylindrical shell in an unstiffened region of the shell surface. The possibility of buckling under loads applied by cushioned supports and the effect of cushion stiffness on the buckling strength of the structure are discussed. The third problem, snap-through buckling of axially loaded cylinders, is very well-known. New theoretical results are presented which, for the first time, agree with experimental data for the minimum postbuckling equilibrium load.

Finally, in spite of the research effort devoted to shell stability studies, what may be called the "methods gap" continues to grow. A brief description also is presented of a few shell stability problems of present active interest to LMSC for which satisfactory methods of analysis are not available.

THREE SHELL STABILITY STUDIES

Influence of Soft Elastic Cores

The use of solid-propellant fuels in rocket motor cases has led to widespread interest in the stabilizing influence of soft elastic cores on the buckling strength of circular cylindrical shells. As a consequence, a number of papers on core-stabilized cylinders have appeared in the literature in recent months. A notable example is the recent paper by Seide on buckling under uniform lateral pressure and axial compression (ref. 1).

Axially-symmetrical loading. - An extensive study of core influence has been in progress at LMSC for several months. As a part of this study, an analysis has recently been completed for the buckling of core-filled cylinders subjected to axially-symmetrical loading (ref. 2). A stability equation is derived for a simply-supported cylinder subjected to axially-symmetrical lateral pressure of arbitrary axial distribution, combined with a central axial force. The analysis is an extension of a corresponding empty-cylinder analysis in reference 3, and the treatment of the core effect is based on Seide's general elastic-core analysis in reference 1.

Numerical results are presented in reference 2 for certain lateral pressure distributions of interest in motor-case analysis. For a cylinder subjected to an axially-symmetrical band of pressure, it is found that the magnitude of the buckling pressure is independent of both band location and cylinder length, unless the band is located near one end of the cylinder or the cylinder is extremely short. Furthermore, for sufficiently wide pressure bands, the magnitude of the buckling pressure is also independent of the bandwidth.

As would be expected, the buckling pressures for wide pressure bands are found to be the same as those given in reference 1 for relatively long core-filled cylinders pressurized over their entire length. These buckling pressures also may be shown to be the same as those given by the following relatively simple equation derived in reference 4 for a wide ring of rectangular cross section, filled with a soft elastic core, and subjected to uniform external pressure:

$$\frac{p}{1 + E_c r / \left[(1 - \mu_c) Et \right]} = n^2 \frac{D}{r^3} + \frac{1}{n} \frac{E_c}{2(1 - \mu_c^2)} \quad (1)$$

where:

$$D = Et^3 / \left[12(1 - \mu^2) \right]$$

E, E_c = Young's modulus, ring and core

μ, μ_c = Poisson's ratio, ring and core

r = ring radius

t = thickness

n = number of circumferential waves in buckle pattern

The physical significance of individual factors in the analysis is much more evident in equation (1) than in the more complex, cylinder equations. The second term in the denominator on the left side of the equation represents the prebuckling influence of the core, and usually is negligibly small. The first term on the right side represents the ring bending stiffness, and the second term the core effect during buckling. For $E_c = 0$, equation (1) reduces to the well-known Donnell solution for an empty ring.

The Winkler-foundation assumption. - Equation (1) was derived in terms of the assumption that the core in the ring is an elastic medium in a state of plane stress. It is important to note that the alternative assumption that the core acts as a Winkler foundation, i.e., as a set of uncoupled springs, may be shown to lead to a factor $(1/n^2)$ instead of $(1/n)$ in the last term in the above equation. In the range of practical stiffnesses for solid propellants, n is much greater than unity. Therefore omission of shear coupling in the foundation (as was

done, for example, in refs. 5 and 6) greatly underestimates the stabilizing influence of the core, and may lead to results which are grossly conservative.

Accuracy of small-deflection theory. - Both Seide's analysis and the analysis in reference 2 are based on small-deflection buckling theory. As is well-known, this theory does not always yield results in agreement with test data. However, it is generally recognized that, for empty cylindrical shells, the agreement is reasonably close for loadings in which the prebuckling membrane stresses are predominantly circumferential. Seide has shown in reference 1 that reasonably close agreement also may be obtained for core-filled cylinders, for the case of uniform lateral pressure loading. An additional comparison for core-filled cylinders is shown in figure 1 for a case of nonuniform lateral pressure, namely, for a circumferential band of pressure. The theoretical results are based on reference 2, and the test data are from reference 7. In view of the fact that it is quite difficult to determine an appropriate experimental value for Young's modulus of the core material, the agreement between theoretical and experimental values again may be said to be reasonably close.

Elastic Cushion Loading

Cushioned support-saddles pressing against the unsupported lateral surface of a large-diameter cylindrical shell structure induce compressive hoop stresses in the shell wall which can cause the shell to buckle. However, the cushions also act as an elastic foundation which tends to stabilize the shell wall. The stabilizing restraint is similar to that derived from a soft elastic core. Consequently, the stiffness of the support-saddle cushioning material is a strong factor in determining the magnitude of the applied pressure at which buckling failure may occur under cushion loading. The allowable pressure is lower for relatively soft cushions, with fluid-pressure loading constituting a limiting case corresponding to cushions of zero stiffness.

Unsymmetrical loading. - Both axially symmetrical and unsymmetrical (i.e., transverse) cushion loading are of practical interest at LMSC. Of course, if the circumferential distribution of the pressure applied to a cylindrical shell is such that a significant amount of circumferential bending is induced in the shell wall from the outset, the shell may fail by local bending or local beam-column action rather than by buckling. However, axial symmetry of the applied pressure is not a necessary condition for bifurcation instability. A band of pressure circumferentially distributed according to the relation:

$$p = p_{\max} (1 + \cos \varphi)/2 \quad (2)$$

where φ is the circumferential coordinate, causes the cylinder cross sections to translate and decrease in diameter, but does not induce significant circumferential bending prior to buckling. An analysis of bifurcation instability under the pressure distribution of equation (2) was carried out as part of the present study, and is reported in reference 8. Results of the analysis indicate that the maximum allowable fluid pressure for the unsymmetrical loading treated in reference 8 is somewhat greater than that for the corresponding axially-symmetrical case, but the difference is not great. Therefore, subsequent studies of bifurcation instability under cushion pressure have been limited to axially-symmetrical loading in the present investigation.

Axially-symmetrical loading. - The most recent result of the axially symmetrical loading investigation is a pilot study of a core-filled circular ring subjected to external pressure applied by soft elastic cushions (ref. 4). The equation determined for the buckling pressure in that analysis is:

$$\frac{p}{1 + E_c r / [(1 - \mu_c) E t]} = n^2 \frac{D}{r^3} + \frac{1}{n} \left[\frac{E_c}{2(1 - \mu_c^2)} + \frac{R(n) E_s}{2(1 - \mu_s^2)} \right]$$

$$R(n) = \frac{\left(1 + \frac{t_s}{r}\right)^n + 1}{\left(1 + \frac{t_s}{r}\right)^n - 1} \quad (3)$$

where the subscript s denotes cushion, and the remaining symbols are defined above. For $E_s = 0$, this equation reduces to the relation given in equation (1) for fluid pressure loading. Equation (3) indicates that the stability of the structure may be increased by increasing the stiffness of the cushion material or by decreasing the cushion's thickness.

The Axially Loaded Cylinder

A study of the snap-through buckling of axially loaded circular cylindrical shells has been in progress at IMSC for quite some time. This is a well-known problem which has challenged investigators in the field of structural shell stability analysis for many years. The continuing interest in the problem is indicated by the relatively large

number of references to it in the collected abstracts of papers for the present symposium.

Large-deflection analysis. - The first phase of the LMSC study of this problem has recently been completed, and is reported in reference 9. This phase treats the theoretical postbuckling behavior of isotropic cylinders which are free from initial geometric imperfections. General interest in this aspect of the problem was first stimulated by the findings of von Karman and Tsien in 1941 (ref. 10). Results of their analysis indicate that if large displacements are considered, the load can be shown to drop sharply from the bifurcation point given by small-deflection theory to a relatively low minimum in the postbuckling range. Their analysis was later improved by other investigators, among whom, Kempner (ref. 11) gave the most accurate solution. However, the ratio given in reference 11 between the minimum postbuckling equilibrium load and the classical, small-deflection buckling load is $P/P_{CL} = 0.30$. The corresponding experimental values reported by Thielemann in reference 12 are only 0.10 to 0.12

In the LMSC analysis, as in the previous analyses, the Rayleigh-Ritz procedure is used to represent the elastic system in terms of a countable number of degrees of freedom. The Newton-Raphson iteration method was employed to obtain solutions to the nonlinear equation system, and an IBM 7090 computer was used in the numerical work. The number of degrees of freedom in the Rayleigh-Ritz analysis was successively increased until no significant change occurred in the magnitude of the minimum postbuckling equilibrium load.

Results of the analysis of reference 9 are shown in figure 2. The expression assumed for the radial displacement component is of the form:

$$w = \sum \sum a_{ij} \cos (i m \pi x) \cos (j n \pi y) \quad (4)$$

where m, n are wavelength parameters, x, y are the axial and circumferential coordinates, and i, j are integers. Curve A in figure 2 represents the case in which all coefficients a_{ij} except a_{20}, a_{11}, a_{02} are set to zero, and coincides with the Kempner solution. By successively including additional degrees of freedom in the displacement function, equation (4), the results represented by curves B, C, and D are obtained. It may be seen that:

- the magnitude of the minimum postbuckling equilibrium load decreases as the number of degrees of freedom is increased,

- the rate of decrease diminishes as the number of degrees of freedom is increased,
- the minimum value found for the greatest number of degrees of freedom, Case D, is approximately $P/P_{CL} = 0.11$ and,
- this value is in close agreement with the corresponding experimental values (0.10 to 0.12) reported by Thielemann.

Reference 9 also presents information on the energy levels associated with various postbuckling equilibrium configurations.

Experimental investigation. - Of course, the objective of investigations of postbuckling behavior such as those in references 9 through 11 is to furnish information which may contribute to the ultimate establishment of an adequate buckling criterion. It is believed that extensive additional testing will be necessary before such a criterion can be formulated. Unfortunately many of the early tests of axially loaded cylinders were designed to determine simply the load level at which snap-through occurs. It is now widely recognized that experimental evidence is needed on a much broader range of questions, such as the influence of initial geometric imperfections of known form, the response to dead-weight loading, changes in buckle pattern during loading and unloading in the postbuckling region, etc. A test program designed to furnish certain information of this kind has been initiated at LMSC. It is believed that the results of such tests, together with continued theoretical effort, can ultimately serve as a rational basis for design of the axially loaded cylinder.

Pressurized and core-filled cylinders. - The analysis reported in reference 9 of theoretical postbuckling behavior under axial compression may be extended with relatively little difficulty to internally pressurized cylinders and to cylinders filled with a soft elastic core. This work also is in progress. Results in reference 12 and elsewhere indicate that the load range within which buckling is possible for internally pressurized cylinders (i.e., the range between the classical buckling load and the minimum postbuckling equilibrium load) diminishes with increasing internal pressure. The same tendency also may be expected with soft elastic cores. Hence, the choice of a buckling criterion in these cases may well be less critical.

FUTURE RESEARCH

Although the number of papers in the literature on structural shell stability has increased to a substantial volume, the present growth of aerospace technology is creating new problems at an even

greater rate. A few shell stability problems which are of present interest to LMSC and for which satisfactory methods of analysis are not available are briefly listed below.

Methods of analysis for the influence of solid propellants on the buckling strength of motor cases are needed in which the propellant is treated as a viscoelastic rather than an elastic medium. Results are required for an entire class of load distributions and load-time profiles. Another broad class of problems of particular interest is that of structural instability under dynamic loading. Included in this category are impulsive loading of only a few microseconds duration. Within the field of ordinary static buckling analysis, insufficient information is available on the buckling of shells whose principal radii of curvature are functions of one or both of the shell coordinates, e.g., a deep ellipsoidal dome subjected to, say, uniform external pressure.

A particularly troublesome task for the structures analyst is the assessment of the effect of a large cutout on the buckling strength of a cylindrical or conical shell. Information seems to be lacking for both reinforced and unreinforced openings and for monocoque and stiffened shells.

The increasing use of filament-wound motor cases has given renewed emphasis to the need for information on the buckling of both orthotropic and bi-layered cylinders. Similarly, the immense size of booster fuel tanks for recently proposed vehicles has increased the interest in methods of analyzing cylinders of both orthotropic and sandwich construction.

Finally, in shell stability investigations, relatively greater emphasis must be given to experimental research. Although it is often more difficult to obtain funding for testing than for analysis, the uncertain reliability of small-deflection buckling theory makes the role of experimental data especially critical in shell applications.

REFERENCES

1. Seide, P.: The Stability under Axial Compression and Lateral Pressure of Circular Cylindrical Shells with a Soft Elastic Core. Jour. Aerospace Sci., vol. 29, no. 7, Jul. 1962, pp. 851-862.
2. Brush, D.O., and Almroth, B.O.: Buckling of Core-Stabilized Cylinders under Axially-Symmetrical External Loads. Jour. Aerospace Sci. (in press).

3. Brush, D.O., and Almroth, B.O.: Thin Shell Buckling Analysis - A General Expression for the Second Variation of the Strain Energy. Presented at 4th U. S. National Congress of Applied Mechanics, Berkeley, Calif. Jun 1962.
4. Brush, D.O., and Pittner, E.V.: Buckling of Core-Filled, Two-Layered Rings Subjected to Elastic Shoe Loading. LMSC 6-90-62-29. Lockheed Missiles & Space Co. Feb. 1962.
5. Brush, D.O., and Field, F.A.: Buckling of a Cylindrical Shell Pressurized Over a Circumferential Band and Stabilized by a Soft Elastic Core. General Research in Flight Sciences - Vol. 5, LMSD 48381, Lockheed Missiles & Space Co. Jan. 1959, pp. 257-281.
6. Zak, A.R., and Bollard, R.J.H.: Elastic Buckling of Cylindrical Thin Shells Filled with an Elastic Core. ARS Jour., vol. 32, no. 4, May 1962, pp. 588-593.
7. Goree, W.S., and Nash, W.A.: Elastic Stability of Circular Cylindrical Shells Stabilized by a Soft Elastic Core. Experimental Mechanics, vol. 2, no. 5, May 1962, pp. 142-149.
8. Almroth, B.O.: Buckling of a Cylindrical Shell Subjected to Nonuniform External Pressure. Jour. Appl. Mech., (in press).
9. Almroth, B.O.: On the Buckling of Circular Cylinders Subjected To Axial Compression. LMSC 6-90-61-115, Lockheed Missiles & Space Co., Jun. 1962.
10. von Kármán, T., and Tsien, H.S.: The Buckling of Thin Cylindrical Shells Under Axial Compression. Jour. Aeronautical Sci., vol. 8, no. 8, Jun. 1941, pp. 303-312.
11. Kempner, J.: Post-Buckling Behavior of Axially Compressed Cylindrical Shells. Jour. Aeronautical Sci., vol. 21, no. 5, May 1954, pp. 329-342.
12. Thielemann, W: New Developments in the Nonlinear Theories of Buckling of Thin Cylindrical Shells. Proc. Durand Cent. Conf. Stanford University, Stanford, Calif., 1959.

COMPARISON OF THEORY AND TESTS FOR BUCKLING UNDER CIRCUMFERENTIAL BAND OF PRESSURE

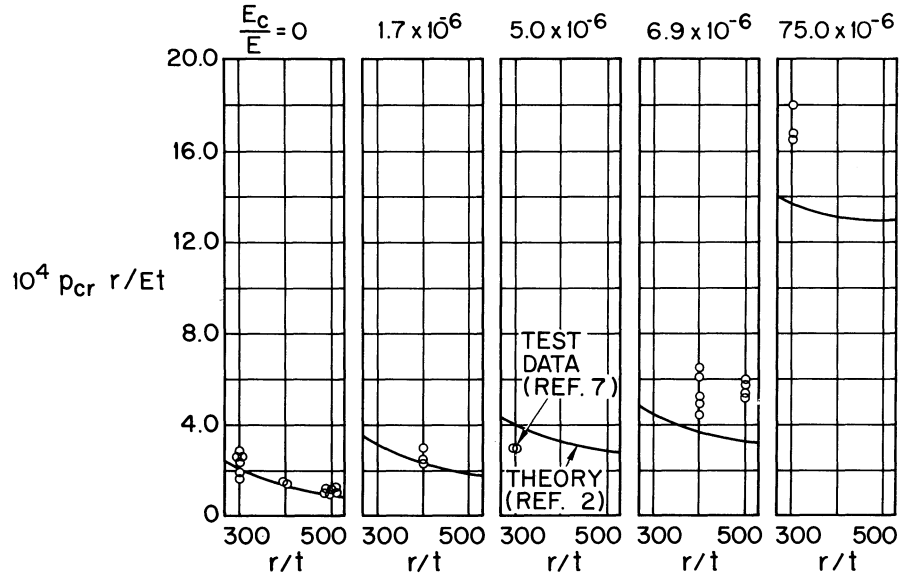


Figure 1

THEORETICAL LOAD-DISPLACEMENT CURVES FOR THE AXIALLY LOADED CYLINDER (FROM REF. 9)

$$w = \sum \sum a_{ij} \cos(im\pi x) \cos(jn\pi y)$$

COEFFICIENTS INCLUDED:

A - a_{20}, a_{11}, a_{02} (ALSO KEMPNER)

B - $a_{20}, a_{11}, a_{40}, a_{22}$

C - $a_{20}, a_{11}, a_{40}, a_{22}, a_{60}, a_{33}$

D - $a_{20}, a_{11}, a_{02}, a_{40}, a_{31}, a_{22}, a_{13},$
 $a_{60}, a_{33},$

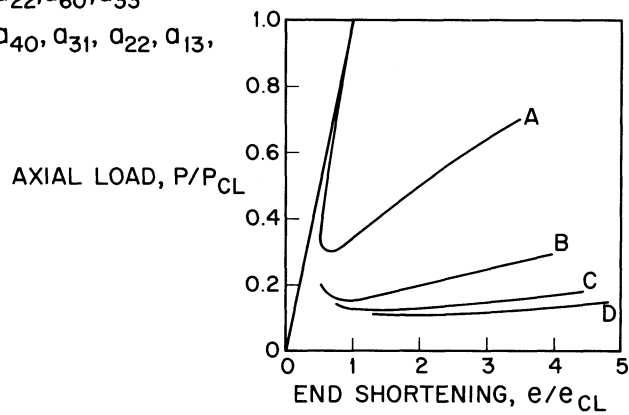


Figure 2

DEVELOPMENT OF DESIGN STRENGTH LEVELS
FOR THE ELASTIC STABILITY OF
MONOCOQUE CONES UNDER AXIAL COMPRESSION

By A. H. Hausrath and F. A. Dittoe

General Dynamics/Astronautics

SUMMARY

Design relationships have been derived for the determination of elastic buckling strength levels for unpressurized monocoque truncated cones under axial compression. Theoretical implications have been considered in the establishment of a semi-empirical analysis leading to the development of probability based design expressions. Data from 170 tests by various investigators were statistically evaluated for the expected mean, 90%, and 99% probability strength levels. Dispersion of data was found to be slightly less than that of monocoque cylinders. Non-linear effects of radius to thickness ratio or strength deterioration with length to radius ratio were not discernible.

INTRODUCTION

The elastic buckling of unpressurized monocoque right truncated circular cones under axial compression is analyzed statistically to establish design strength levels. The resulting prediction equations were derived from data in the ranges of semi-vertex angle from 2.87° to 75° , mid-height radius of curvature to thickness ratios of 98 to 4160, and slant height to mid-height radius of curvature ratios of 0.133 to 4.45. The resulting equations are intended for the design of cones where applicable in aerospace vehicles and other structures requiring high levels of structural reliability.

SYMBOLS

- A subscript indicating the "A" level.
- "A" level that level which would be exceeded by at least 99% of the entire population with 95% confidence; i.e., the confidence is 95% that at least 99% of the stability strengths of all

	cones in axial compression can be expected to exceed the "A" level.
B	subscript indicating the "B" level.
"B" level	that level which would be exceeded by at least 90% of the entire population with 95% confidence; i.e., the confidence is 95% that at least 90% of the stability strengths of all cones in axial compression can be expected to exceed the "B" level.
C	buckling coefficient; see eq. (2).
\bar{C}	mean value of C; see eq. (7).
E	material modulus of elasticity in compression.
e_i	theoretical frequencies for intervals in grouped data.
i	subscript indicating i th value.
k	one-sided tolerance factor for the normal distribution; a function of sample size, probability level, and confidence level.
l	slant height of conical frustum.
m	number of intervals in grouped data.
N	number of data values in sample.
n_i	observed frequencies for intervals in grouped data.
P_{cr}	axial compressive load, lbs., just prior to buckling.
\bar{P}_{cr}	expected mean value of P_{cr} .
$P_{cyl \infty}$	axisymmetric axial-buckling load of infinite cylinder with constant-thickness walls.
r	radius of cylindrical shell.
r_1	radius at small end of conical shell, measured in plane normal to axis of cone.
r_2	radius at large end of conical shell, measured in plane normal to axis of cone.
s	sample standard deviation; see eq. (8).

t	shell thickness.
α	semi-vertex angle of cone.
μ	mean value for a total population.
ν	Poisson's ratio.
ρ	radius of curvature.
$\bar{\rho}$	radius of curvature of conical shell at mid-height.
σ	standard deviation for a total population.
χ^2	statistical parameter indicating goodness-of-fit of data to a distribution function.

DISCUSSIONS

Justification for the Statistical Approach

Large variations in the actual buckling strengths of unpressurized truncated cones can be expected due to the unstable nature of pre-buckling load-deflection relationships for monocoque shells in compression. Cylinders, for example, tend to follow the familiar peaked load-deflection curve toward the bifurcation point and then into the post-buckling regime; however, to attain classical values of the buckling coefficient, all conditions (imperfections, eccentricities, end conditions, etc.) must be ideal. Since actual shells are subject to less than ideal conditions, the resulting buckling strengths will be not only significantly lower than theoretically indicated, but also widely dispersed. Existing data from cylinders are slightly more dispersed than from cones for axial compression and the response of spherical shells under external pressure shows similar scatter, probably for related reasons.

An examination of the test data presented in fig. 1 shows approximately equal scatter for all values of the semi-vertex angle. The cause of such variations in test results is not currently quantitatively defined. The high sensitivity to unmeasured or unmeasurable parameters makes an accurate analytical prediction of general instability strength improbable for the types of applied structure used in aerospace vehicles. Thus, in order to guarantee a reliable structure, statistical methods are used to establish practical design strength levels. These levels should not be considered as final. Analysis will eventually reveal the quantitative relationships between the buckling load and the above discussed conditions. This will permit a better evaluation of the test scatter and new statistical analyses resulting in more accurate prediction equations.

Designing at mean or typical strength levels acknowledges that 50% of structures so designed would fail before reaching design ultimate loads. A previous statistical analysis (ref. 1) indicates that 10% of cylinders designed to mean strength levels would fail at 75% or less of design ultimate strength in axial compression. A similar situation exists for cones.

Although the dispersion of test data for monocoque shells is generally recognized, mean expected strength levels are often erroneously advocated for design. "Eyeball" estimates of a lower bound to test data are also sometimes used, particularly when only a limited amount of test data are available. Unfortunately, the lower bound approach does not result in a quantitative evaluation of the reliability of the solution. Statistical analyses result in strength level estimates at desired levels of probability and confidence and thus make it possible to design to the required level of structural reliability.

This study endeavors to establish practical design relationships for the elastic stability of unpressurized monocoque cones under axial compression. The statistical levels adopted correspond to "A" and "B" levels as defined in SYMBOLS.

Test Data

The total number of pertinent tests known to the authors is 174. Refs. 2-6 contain data from 18 steel, 133 mylar, 15 nickel, and 8 aluminum cone tests. Although the preponderance of data are from the mylar specimens of ref. 2, the remaining data with four exceptions, fit into the mylar distribution satisfactorily, as may be seen in fig. 1. The value of mylar as a material for model stability test specimens was treated in ref. 2 where it was concluded that mylar was quite attractive for testing of this kind. A close scrutiny of the data reveals that the mylar results tend to be slightly higher than those of the metal specimens. Reasons for this may include experience gained in fabricating and testing a large number of mylar specimens and the low probability for local yielding of these specimens prior to buckling. The metal specimens were worked closer to their proportional limits and thus were more susceptible to failures precipitated by local yielding. In the cases of one aluminum and three nickel specimens, early failures may be directly attributed to local yielding. In the aluminum specimen, the failure load produced gross stresses in the cone wall above the material proportional limit while in the nickel tests there were questionable end conditions. These four tests were omitted from the statistical analysis but are shown in figs. 1 and 3 for reference purposes.

The remaining sample size of 170 consists of cones having $2.87^\circ \leq \alpha \leq 75^\circ$, $98 \leq \bar{p}/t \leq 4160$ and $0.133 \leq l/\bar{p} \leq 4.45$.

METHODS OF ANALYSIS

It is certainly to be recognized that from a statistician's point of view the sample population is far from ideal. The experiments were not statistically designed, there was no particular effort to randomize the combinations of geometrical parameters, and there are several obvious sources of bias in the sample population; however, distribution charts of $l/\bar{\rho}$ and α vs. $\bar{\rho}/t$ (tables 1 and 2) reveal some sampling in many of the usual ranges of interest.

The plot of the buckling coefficient C vs. $\bar{\rho}/t$ shown in fig. 1 discloses the most interesting implication that C is independent of $\bar{\rho}/t$. This finding is contrary to the conclusions of refs. 2, 3, 4, and 7 where functional relationships between C and some ρ/t were assumed similar to that for cylinders.

The theoretical result for cones presented in ref. 7 and affirmed in ref. 6 is

$$P_{cr} = P_{cyl} \cos^2 \alpha \quad (1)$$

which may be written

$$P_{cr} = C 2\pi E t^2 \cos^2 \alpha \quad (2)$$

The well-known classical value for C is

$$C = \frac{1}{\sqrt{3(1-\nu^2)}} \quad (3)$$

which, for $\nu = 0.3$, is 0.605. However, experimental results for cylinders are such that $0.07 \approx C \approx 0.5$ and that C is strongly dependent upon radius/thickness ratios. The experimental evidence for cones is presently such that $0.194 \approx C \approx 0.478$ and that C is independent of radius/thickness ratios, at least for the range of data available. Additional influences of α or length effects are not discernible from plots of cone data.

An examination of the frequency distribution of C by means of a histogram (fig. 2) indicates near normalcy. If the variations in C could be attributed to eccentricities in loading and specimen geometry, local irregularities, etc., and if each of these could be assumed to occur in a random manner, then it can be shown that the values of C would be expected to be normally distributed.

The normal or Gaussian distribution function is given by

$$f(x) = \frac{1}{\sigma\sqrt{2\pi}} \exp\left[-\frac{(x-\mu)^2}{2\sigma^2}\right] \quad (4)$$

so that

$$\int_a^{\infty} f(x)dx = \text{probability that } x > a \quad (5)$$

In eq. (4), μ and σ are respectively the mean value and standard deviation for a total (infinite) population. As is the usual case, only estimates of μ and σ are available. These are the sample mean, \bar{x} , and the sample standard deviation, s , which were used to obtain the fitted normal curve shown in fig. 2 for comparison with the histogram.

An analytical evaluation of the conformity of the grouped data to the normal distribution was conducted using the χ^2 test. This test, discussed in most texts on basic statistics, consists of evaluating the parameter χ^2 from eq. (6) and comparing the result to tabulated percentage points for the χ^2 distribution. If the calculated value of χ^2 is less than the value tabulated for the applicable significance level and number of degrees of freedom, then there is no reason to reject the hypothesis that the data are from a normal population.

$$\chi^2 = \sum_{i=1}^m \frac{(n_i - e_i)^2}{e_i} \quad (6)$$

In eq. (6), m is the number of intervals over which the summation takes place, n_i are the observed frequencies in the intervals, and e_i are the theoretical frequencies for the intervals from the fitted normal distribution.

The χ^2 goodness-of-fit test was conducted for the test data and resulted in the conclusion that at the 5% level of significance, the sample distribution is consistent with the hypothesis that the parent distribution is normal. The 5% level of significance, generally used for χ^2 tests for normality, was generously exceeded by the data. For the purposes of this paper, the values of C were thus assumed to be normally distributed.

The mean value of C and standard deviation were obtained from the 170 data values using eqs. (7) and (8).

$$\bar{C} = \frac{1}{N} \sum_{i=1}^N C_i \quad (7)$$

$$s = \sqrt{\frac{1}{N-1} \sum_{i=1}^N (\bar{C} - C_i)^2} \quad (8)$$

The "B" and "A" level estimates of C were then calculated from

$$C_B = \bar{C} - k_B s \quad (9)$$

$$C_A = \bar{C} - k_A s \quad (10)$$

where k_B and k_A are the proper probability tolerance factors. Values of k have been calculated using procedures outlined in chapter 1 of ref. 8 and tabulated in ref. 9. The values of k were calculated for the normal distribution such that the confidence is 95% that at least the desired proportions will exceed the "B" and "A" levels. For 169 degrees of freedom, $k_B = 1.465$ and $k_A = 2.592$.

The results of calculations using eqs. (7) through (10) are:

$$\bar{C} = 0.316 \quad (11)$$

$$s = 0.06077 \quad (12)$$

$$C_B = 0.227 \quad (13)$$

$$C_A = 0.158 \quad (14)$$

Plots of the expected mean, "B", and "A" levels are shown in figs. 1, 2, and 3 for comparison with available data.

RECOMMENDATIONS

The "A" and "B" levels are recommended for the practical design of unpressurized monocoque cones critical in buckling due to axial compression. The "A" level, eq. (14), is recommended for use for those structures the single failure of which could result in catastrophic loss or injury to personnel. The "B" level, eq. (13), may be used for structures not requiring the "A" level.

Application of eqs. (13) and (14) as coefficients for eq. (2) should be limited to cones having the following approximate geometries: $100 < \bar{\rho}/t < 4000$, $10^\circ < \alpha < 75^\circ$, and $0.25 < l/\bar{\rho} < 5$. Table 1 and 2 may be consulted to determine the number of known tests for a desired cone geometry. The stress level at the small end of the cone should be checked to preclude the possibility of an early failure precipitated by inelastic stresses.

Structural substantiation tests should be conducted on cones designed by the use of eqs. (2), (13), and (14) because of the influences of fabrication techniques, size, and end conditions in each particular design.

FUTURE RESEARCH

Additional testing of cones should be conducted in the sparsely populated ranges of tables 1 and 2. Of particular interest would be additional elastic tests in the high and low $\bar{\rho}/t$ and small α groups. These could permit a better understanding of the present experimentally indicated independence of buckling coefficient with radius/thickness ratio. The influence of end conditions on buckling of cones would seem to be greater than for cylinders and, if adequately evaluated, might be used to reduce the scatter of test data. Tests of larger and longer specimens should indicate the effects of size and length which are not discernible from existing data.

Accurate determinations of the compressive modulus of elasticity of specimen materials should be reported in all future stability test reports. Although difficult to obtain for thin gages, this information is helpful in statistically evaluating test data and may, in fact, be responsible for a significant amount of scatter in the existing data.

CONCLUDING REMARKS

For practical design purposes, reliable design buckling load levels may be established if sufficient data exist. Recent shell stability testing has greatly enhanced the fact that for unpressurized monocoque shells, existing theoretical solutions are unrealistic for design. The use of mean expected buckling strengths is also unconservative while lower bound estimates are of unknown reliability. Statistically determined allowable strength levels acknowledge the inevitable scatter of test data and permit the estimation of strengths at desired levels of probability and confidence. The application of statistics to other loading conditions and shell configurations would be desirable when enough data are available.

REFERENCES

1. Schumacher, J. G.: Development of Design Curves for the Stability of Thin Pressurized and Unpressurized Circular Cylinders. General Dynamics/Astronautics report no. AZS-27-275B, May 8, 1959, revised July 22, 1960.
2. Seide, P., Weingarten, V. I., and Morgan, E. J.: Final Report on Development of Design Criteria for Elastic Stability of Thin Shell Structures. Space Technology Laboratories, Inc. report no. STL/TR-60-0000-19425, Dec. 31, 1960.
3. Lackman, L., and Penzien, J.: Buckling of Circular Cones Under Axial Compression. Journal of Applied Mechanics, vol. 27, no. 3, Sept. 1960.
4. Homewood, R. H., Brine, A. C., and Johnson, A. E. Jr.: Buckling Instability of Monocoque Shells. AVCO Corporation report no. RAD-TR-9-59-20, August 18, 1959.
5. Lofblad, R. P. Jr.: Elastic Stability of Thin-Walled Cylinders and Cones with Internal Pressure Under Axial Compression. Mass. Inst. of Tech. ASRL TR 25-29, May 1959.
6. Lundquist, E. E., and Schuette, E. H.: Strength Tests of Thin-Wall Truncated Cones of Circular Section. N.A.C.A. report WRL-442, Dec. 1942.
7. Seide, P.: Axisymmetrical Buckling of Circular Cones Under Axial Compression. Journal of Applied Mechanics, vol. 23, no. 4, Dec. 1956.
8. Eisenhart, C., Hastay, M. W., and Wallis, W. A.: Selected Techniques of Statistical Analysis for Scientific and Industrial Research and Production and Management Engineering. McGraw-Hill Book Co., 1947.
9. Schumacher, J. G.: Statistical Determination of Strength Properties. General Dynamics/Astronautics report no. AZS-27-274A, Nov. 11, 1958, revised Dec. 29, 1959.

TABLE 1

DISTRIBUTION CHART $\bar{\rho}/t$ VS $\ell/\bar{\rho}$

$\bar{\rho}/t$	$\ell/\bar{\rho}$									
	0.12	0.25	0.5	0.75	1.0	1.5	2	3	5	≥ 8
200			1			5				
300			2			2	1	3		
450			4		6	17	7	4		
650			2	3	3	1	5	5		
900			1	2	3	11	5	5	1	
1,400	2	5	14	8	6	12	2	4		
2,000		3	6	4		3	2	2		
3,000					2					
4,000		1								
Σ	2	9	30	17	20	50	18	23	1	
										170

TABLE 2

DISTRIBUTION CHART $\bar{\rho}/t$ VS α

$\bar{\rho}/t$	α (DEG.)							
	3	10	15	20	30	45	60	75
200			3	2		1		
300				5	1	2		
450		6		7	14	11		
650		5		3	1		5	
900	1	5		5	8	7	2	
1,400		6		4	7	13	22	1
2,000				4	9	2	2	3
3,000						2		
4,000								1
Σ	1	22	3	30	40	38	31	5

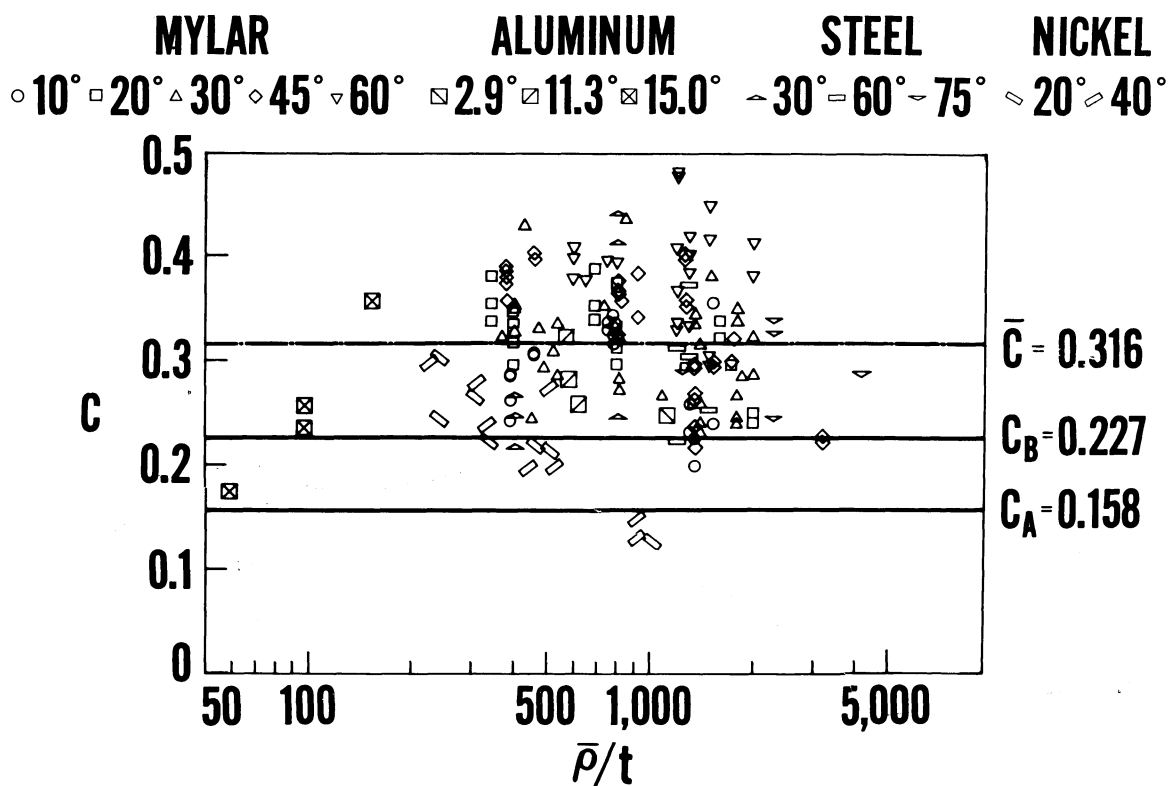


Figure 1.- Experimental evidence of the independence of buckling coefficient with respect to mean radius of curvature/thickness ratio in tested region.

CONE DATA

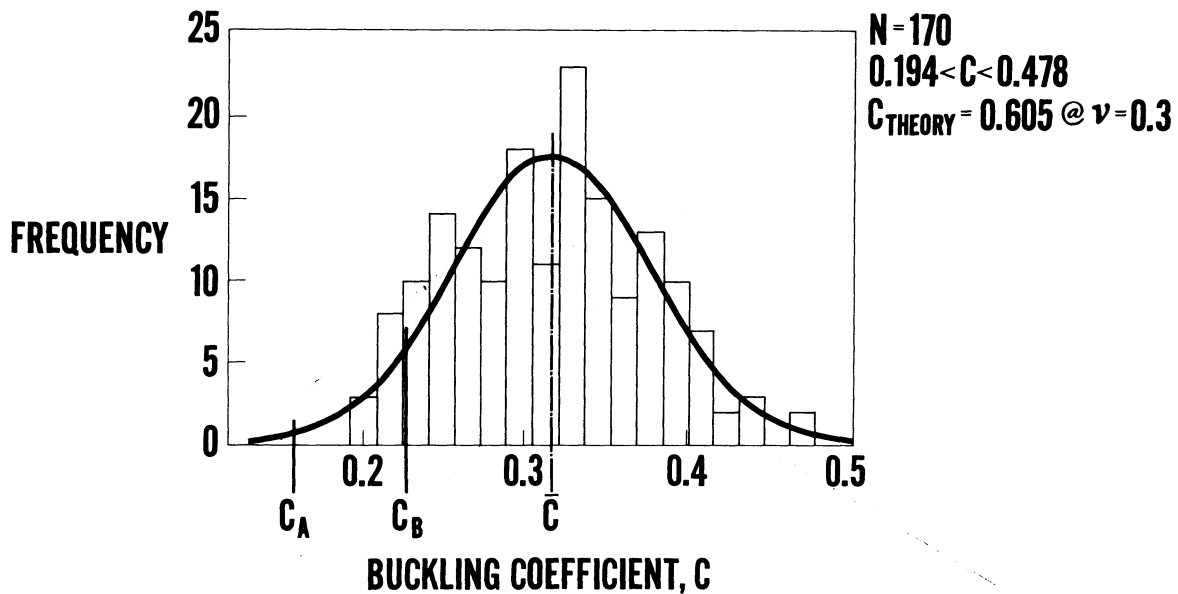


Figure 2.- Histogram of cone data and fitted normal curve.

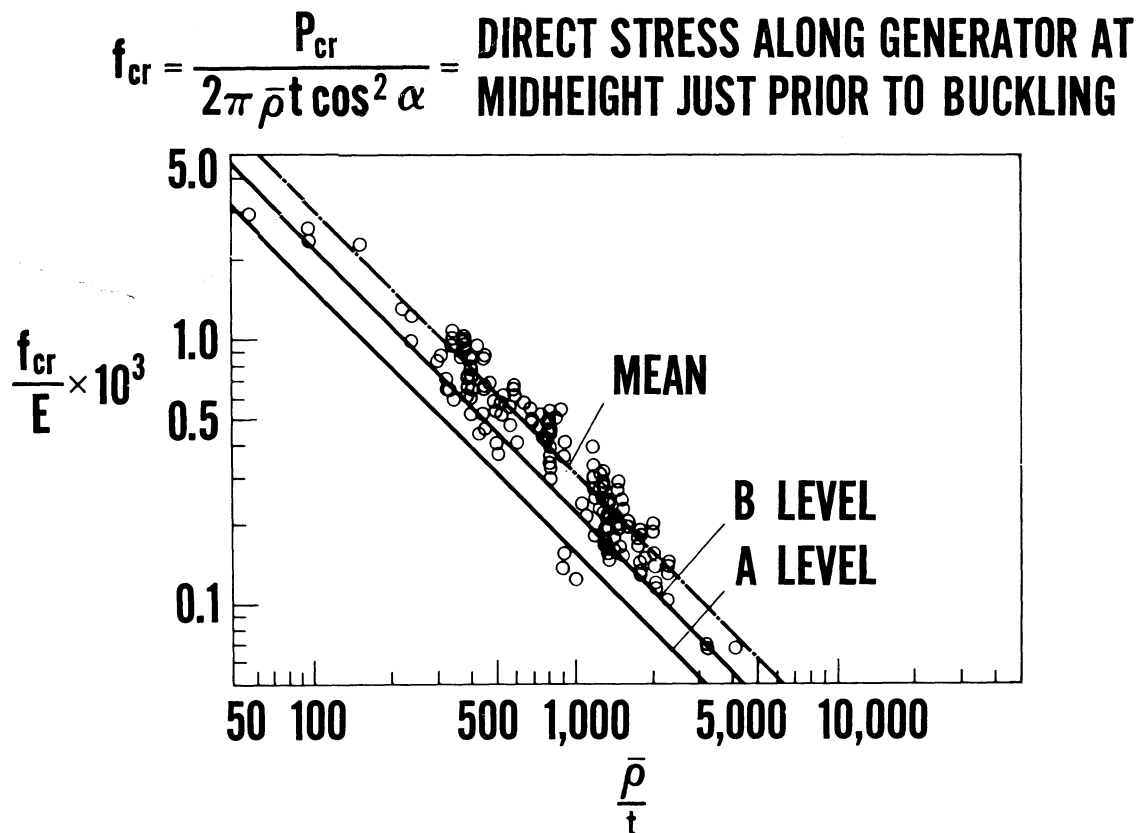


Figure 3.- Non-dimensional comparison of cone data with statistical levels.

SHELL STABILITY PROBLEMS IN THE DESIGN OF
LARGE SPACE VEHICLE BOOSTERS

By James B. Sterett, Jr.

NASA Marshall Space Flight Center

SUMMARY

A discussion of the current methods used to design the Saturn type booster shell structures is presented covering bending and axial compression, with and without internal pressure. Problem areas encountered in the application of available shell stability data to these designs are delineated; as well as, suggested areas of future research for shell configurations anticipated in advanced designs.

INTRODUCTION

The pressurized and unpressurized cylindrical shell portions of the Saturn Boosters have changed considerably in configuration as payload requirements became more stringent. Various cylindrical cross-sections were investigated to optimize structural designs, with corrugated skins in the unpressurized areas and "tee" stiffened tank walls indicating minimum weight structures. Additional weight savings might be realized with the use of multicell tanks for large diameter Boosters.

SYMBOLS

C_f	frame stiffness coefficient
D	shell diameter
E	Young's modulus of elasticity
F_c	ultimate compressive stress
I	area moment of inertia
K	shell buckling constant

L	shell length (between transverse frames)
q	axial load per unit of circumference
R	shell radius
t	monocoque shell thickness
\bar{t}	equivalent weight monocoque shell thickness
t*	equivalent strength monocoque shell thickness

DEVELOPMENT OF SHELL CONFIGURATIONS

FOR THE SATURN C-1 BOOSTERS

Pressurized Areas

Pressurized shell designs for the Saturn C-1 Boosters were based on water hydrostatic test pressure requirements. The particular aluminum selected, 5456-H343, is a work hardening alloy and develops excellent mechanical properties after pressure cycling. Weld areas in the tanks have final tensile yield strengths as high as 90% of the parent material. Since the payload requirements were not critical for these Boosters, the test pressures shown in table 1 were acceptable, especially considering the resulting high structural integrity. Buckling instability of the monocoque shells, under combined bending and axial compression, is not critical compared to the hoop tension stresses.

Unpressurized Areas

The unpressurized cylindrical portions of the Saturn C-1 Boosters were designed more efficiently than the tanks although subsequent load reductions have increased their safety margins. The forward and aft skirts of the 70 and 105 inch diameter tanks are semi-monocoque shells except for short intermediate modified monocoque sections (as defined in reference 1) attaching these skirts to the tank walls. The most critical areas of these skirts, in each case, are the modified monocoque portions. The classical buckling equation, $F_c = KEt/R$, with a K value = 0.30, has been used to establish these shell thicknesses and compares favorably with the structural test results. The R/t range of from 140 to 390 as shown in table 1, falls within the limits of the application of the 0.30 constant suggested in reference 2.

ADVANCED SATURN C-5 BOOSTER SHELLS

Pressurized Areas

Development of the pressurized portions of the advanced Saturn C-5 Booster followed a completely different design philosophy from the early Saturn vehicles. Stringent requirements for maximum payload capacity, for both lunar and earth orbital rendezvous, dictated a refined approach to shell design. Initially, preliminary design concepts depicted an integrally milled 45° waffle pattern for the skins with a full length cruciform anti-slosh baffle dividing the tanks into four quarters. Further shell optimization studies, coupled with the possibility of a redesign of the baffles to annular rings, indicated a substantial structural weight reduction by incorporating integrally milled longitudinal "tee" stringers in place of the 45° waffle. A comparison of these shell designs are shown in tables 2 and 3. The values presented are for the actual C-5 design pressures, bending moments and longitudinal forces, within the plate thickness limitations for the 2219-T87 aluminum sheet sizes required. Since the skin thickness for the "tee" stiffened design is significantly influenced by pressure stresses, additional shell weights were investigated for both waffle and "tee" stiffened segments considering pressure increases. The "tee" stiffened cross sections were sized, based on optimization of skin to stiffener area ratios, with the skin fully effective in compression (no local buckling). The waffle sections were developed through application of the work accomplished by Seide (ref. 4).

An interesting phenomena, concerning the annular rings, developed in the optimization studies. To suppress sloshing within acceptable limits, the ring baffles required a depth of approximately 30 inches, several times that necessary to provide column stability for the stiffened shell. In addition, longitudinal structural ties between rings on the inner flanges were required to support the normal forces on the ring webs due to sloshing pressures. This configuration of deep rings, with the inner flanges supported against lateral instability, permitted reduction of the \bar{t} contribution by the rings. A standard ring section, required to stabilize the shell, was generated using the following equation from reference 3:

$$EI = \frac{C_f q \pi D^4}{4L} \cdot$$

This ring would add .078 inches to the skin-stringer \bar{t} , compared to .048 inches for the deep anti-slosh rings. Sketches of the typical C-5 tank structures are shown in figures 1 and 2.

Unpressurized Areas

Cylindrical skirt areas of the Advanced Saturn without internal pressure have been designed based on minimum weight criteria from reference 3 and are of fabricated (riveted) 7075-T6 aluminum sheet and stringer combinations, with the exception of the inter-tank shell. This section attaches the fuel tank to the oxidizer tank and is composed of 7075-T6 corrugated sheet with transverse stabilizing ring frames. In contrast with the C-1 Boosters, the monocoque skirt areas are restricted to negligibly short segments which exist only at bulkhead to shell junctures. Weights of the skirts are as follows:

SEGMENT	WEIGHT PER INCH
Forward Skirt	40
Intertank Skirt	35
Aft Skirt	48

Manufacturing and access requirements preclude the use of corrugated skins for all of the skirts, although this cross section is structurally the more efficient.

FUTURE RESEARCH

Monocoque Buckling Allowables

Tables 2 and 3 present weights for waffle pattern designs based on three sources for buckling allowables (references 5 and 6). The basic waffle dimensions are established from reference 4, but when the t^* value is selected from each buckling reference, different shell weights are developed. For Boosters in the size range of the Advanced Saturn and Nova, these differences amount to thousands of pounds of structural weight. Extensive research should be conducted to establish uniform, generally accepted cylinder buckling curves.

Multicell Designs

An area which shows extreme promise in future space vehicle designs is the multicell configuration. Extensive studies accomplished at Marshall Space Flight Center on cylindrical versus multicell tanks and total Booster structures indicate weight savings for the multicell, which

increase in percentage with larger vehicles. Figure 3 presents the results of these studies ranging from a 360 inch diameter Booster to 600 inches. The typical cross section, shown in figure 4, does not present unusual structural problems except in the transition areas between the shell walls and bulkheads. These areas are geometrically difficult to define and defy presently available methods of analysis for local shell stability.

CONCLUDING REMARKS

Minimum weight designs for large space vehicle Booster cylindrical shells require comprehensive studies to establish each individual configuration. Shell skins with integral milled stiffeners appear especially attractive for propellant tanks. The selection of mill patterns such as 45° waffle or longitudinal "tees" depends on loads and other design criteria peculiar to that tank. Uniformly accepted and proven cylinder buckling curves would permit further refinement of shell designs. For future Boosters, research is needed on multicell designs and their stability problems.

REFERENCES

1. Bruhn, E. F.: Analysis and Design of Airplane Structures. Tri-State Offset Co., Cincinnati, Ohio, 1952.
2. Peery, D. J.: Aircraft Structures. McGraw-Hill Book Company, Inc., 1950.
3. Shanley, F. R.: Weight-Strength Analysis of Aircraft Structures. Dover Publications, Inc., New York, 1960.
4. Seide, P.: The Effectiveness of Integral Waffle-Like Stiffening for Long, Thin, Circular Cylinders Under Axial Compression, Part II, Mechanically Milled Sheet. Ramo-Wooldridge Corp. Report AM-6-10, STL Report GM-TR-38, June 15, 1956.
5. Marshall Space Flight Center: Astronautics Structures Manual.
6. Schumacher, J. G.: Development of Design Curves for the Stability of Thin Pressurized and Unpressurized Circular Cylinders. Convair Astronautics Report AZS-27-275 (Contract Number AF04(645)-4), May 8, 1959.

TABLE 1.- PRESSURE, SHELL THICKNESS, AND R/t VALUES FOR SATURN C-1 TANKS

BOOSTER	TANK	FLIGHT DESIGN PRESSURE (psig)	HYDROSTATIC TEST PRESSURE (psig)	PRESSURIZED SHELL THICKNESS (inches)	UNPRESSURIZED SHELLS			
					THICKNESS		R/t	
					FORWARD	AFT	FORWARD	AFT
					(inches)			
SATURN C-1, BLOCK I	70" FUEL	41	53	.090	.090	.100	389	350
	70" LOX	78	92	.119	.190	.190	184	184
	105" LOX	78	92	.250	.305	.375	172	140
SATURN C-1, BLOCK II	70" FUEL	40	51	.081	.090	.100	389	350
	70" LOX	79	109	.131	.249	.249	141	141
	105" LOX	79	109	.173	.305	.305	172	172

TABLE 2.- COMPARISON OF WAFFLE AND "TEE" STIFFENED DESIGNS FOR C-5 BOOSTER OXIDIZER TANKS

% DESIGN PRESSURE	NO. OF RING FRAMES	45° WAFFLE PATTERN												PRESENT C-5 "TEE" STIFFENED SHELL	
		BUCKLING ALLOWABLE PER REFERENCE 5 (1)				BUCKLING ALLOWABLE PER REFERENCE 6 (99% Probability)				BUCKLING ALLOWABLE PER REFERENCE 6 (90% Probability)					
		t*	- t	TOTAL SHELL WEIGHT	inches	t*	- t	TOTAL SHELL WEIGHT	lbs.	t*	- t	TOTAL SHELL WEIGHT	lbs.	- t	TOTAL SHELL WEIGHT
		inches	inches	lbs.	inches	inches	inches	lbs.	inches	inches	inches	lbs.	inches	inches	lbs.
100	2	.750	.467	28,850	.862	.535	.728	33,090	.728	.453	.728	28,040			
	3	.740	.444	27,740	.793	.479	.692	29,880	.692	.421	.692	26,230			
	4	.740	.446	29,380	.774	.465	.674	29,280	.674	.409	.674	25,860			
	12	.690	.536	35,540	.656	.386	.584	26,840	.584	.359	.584	24,800	.383	26,740	
150	2	.740	.623	38,400	.723	.608	.604	37,530	.604	.536	.604	33,120			
	3	.740	.591	36,860	.627	.514	.558	32,050	.558	.501	.558	31,260			
	4	.720	.600	37,470	.605	.504	.551	31,630	.551	.491	.551	30,870			
	12	.697	.539	35,740	.460	.421	.460	28,540	.460	.414	.460	28,140	.416	28,800	

(1) Total Shell Weights Include Required Ring Frames.
t Values Do Not Include Frames.

TABLE 3.- COMPARISON OF WAFFLE AND "TEE" STIFFENED DESIGNS FOR C-5 BOOSTER FUEL TANKS

% DESIGN PRESSURE	NO. OF RING FRAMES	45% WAFFLE PATTERN												PRESENT C-5 "TEE" STIFFENED SHELL		
		BUCKLING ALLOWABLE PER REFERENCE 5 (1)				BUCKLING ALLOWABLE PER REFERENCE 6 (99% Probability)				BUCKLING ALLOWABLE PER REFERENCE 6 (90% Probability)						
		TOTAL SHELL WEIGHT		t		t*		t		t*		t		TOTAL SHELL WEIGHT		
		inches	lbs.	inches	lbs.	inches	lbs.	inches	lbs.	inches	lbs.	inches	lbs.	inches	lbs.	
100	2	.920	16,500	.543	16,170	.901	.533	.787	.430	.787	.430	.787	.430	13,180		
	3	.860	15,800	.512	15,000	.828	.485	.742	.393	.742	.393	.742	.393	12,300		
	4	.820	14,770	.469	14,430	.795	.457	.706	.371	.706	.371	.706	.371	11,910		
	12	.750	14,160	.414	13,240	.717	.382	.648	.326	.648	.326	.648	.326	11,160	.274	9,500
150	2	.920	16,490	.543	16,160	.901	.532	.787	.475	.787	.475	.787	.475	14,530		
	3	.865	15,530	.501	14,890	.828	.480	.742	.436	.742	.436	.742	.436	13,590		
	4	.820	15,060	.476	14,580	.795	.461	.706	.412	.706	.412	.706	.412	13,130		
	12	.755	14,960	.441	15,160	.719	.448	.658	.363	.658	.363	.658	.363	12,620	.356	11,900

(1) Total Shell Weights Include Required Ring Frames.
t Values Do Not Include Frames.

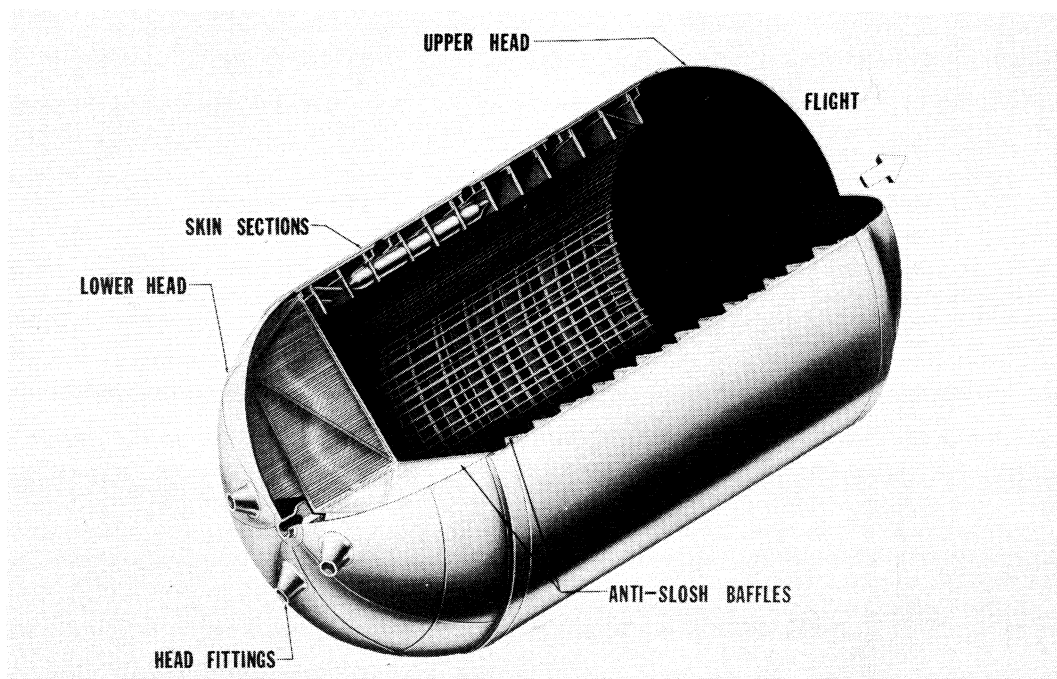


Figure 1.- Typical tank assembly for Advanced Saturn C-5 Booster.

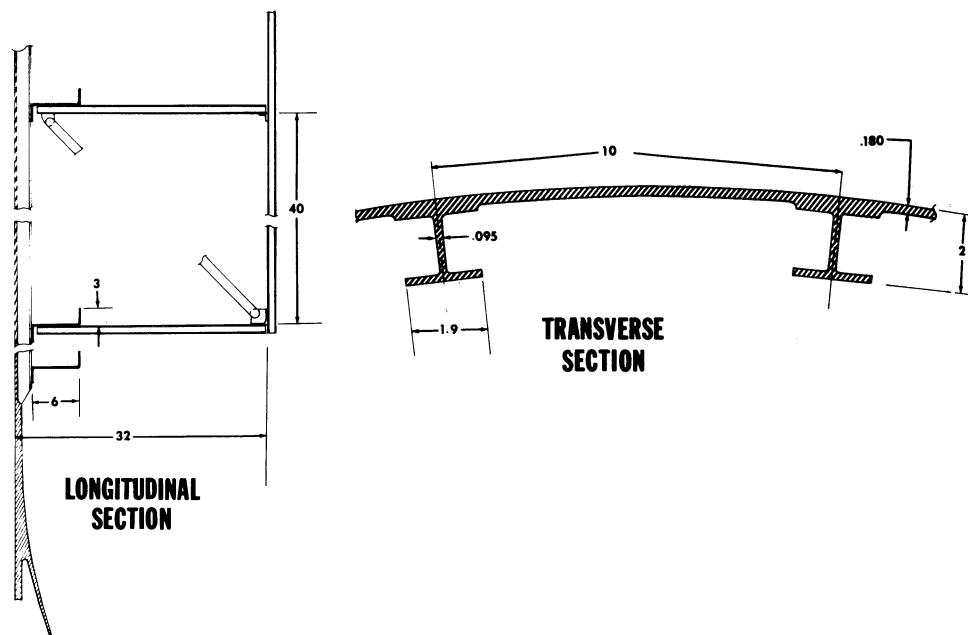


Figure 2.- Cross-sections of the C-5 Booster tank assembly.

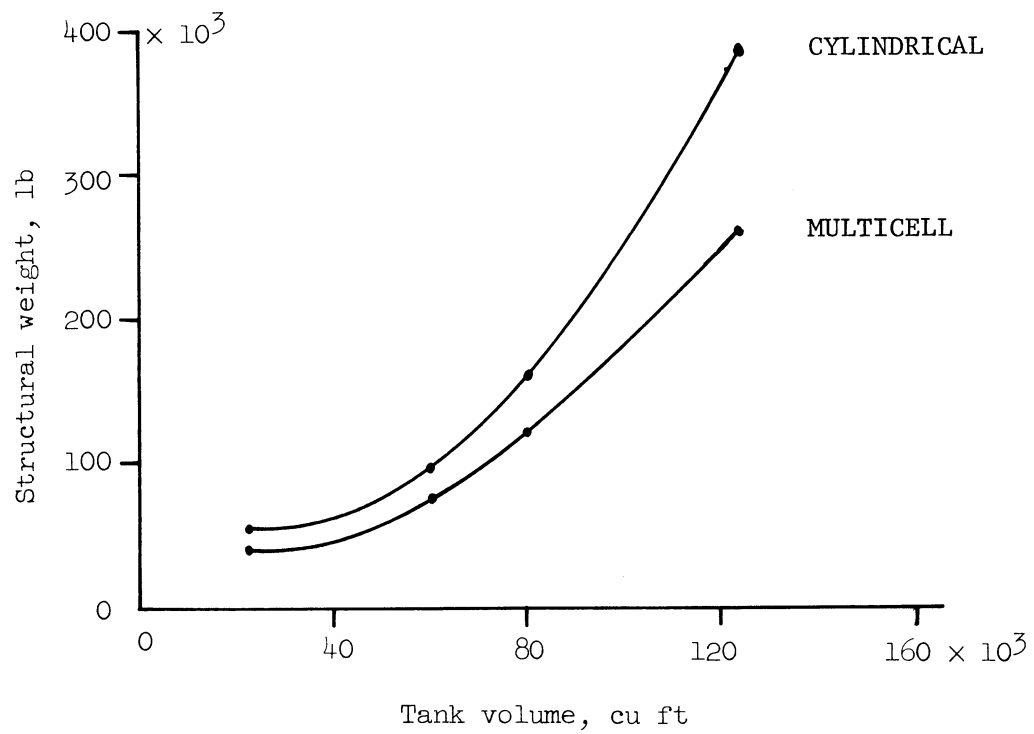


Figure 3.- Multicell versus cylindrical tank weights.

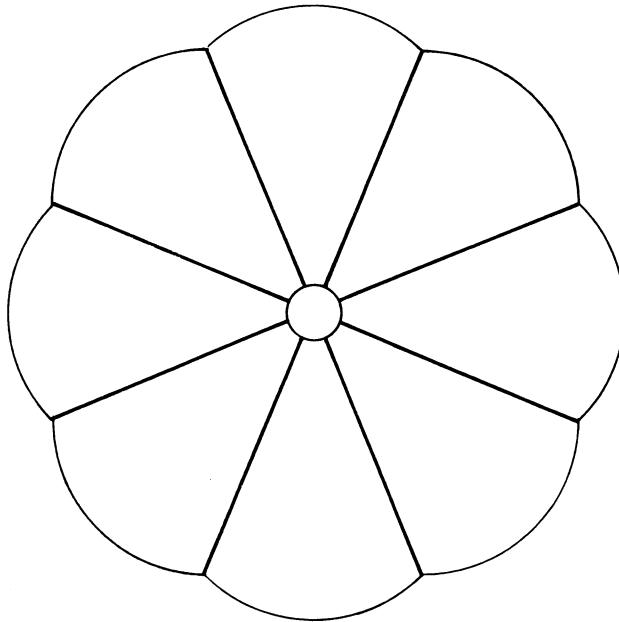


Figure 4.- Typical division of tank into cells.

PROBLEMS ASSOCIATED WITH THE DESIGN
OF LARGE SHELL STRUCTURE

By W. M. Moseley

General Dynamics/Fort Worth

SUMMARY

An account of the approach used in design of a large sandwich construction nose cone is given. The areas in which analytical methods are needed are discussed and a theoretical procedure is proposed.

INTRODUCTION

Many of the space exploration probes and satellites are housed on the nose of large missiles. These payloads require protection during the launch phase and the missile requires fairing to reduce aerodynamic drag. Thus, large jettisonable nose panels are needed in many applications. The panels must possess integral stiffness since there is little or no room for supporting structure. These requirements have resulted in the design of large "split-cone" sections of sandwich construction. Satisfactory methods of analysis do not exist for this type of structure.

SYMBOLS*

x, r, z, p	Linear coordinates
θ, ϕ	Angular coordinates
a, b, c, d, L, L', B	Dimensions
μ, v, w, q, v', S	Displacements
$I, J, F, G, N, M, K, K', H$	Displacement parameters

A (with proper subscript)	Coefficients of displacement parameters
f, g, i, j, k, l, m, n, h	Integers or subscripts

*See also figures 1 and 2.

DESIGN APPROACH

The task under consideration is to design a nose fairing for a 10 foot diameter missile. The purpose of the fairing is to reduce vehicle drag, and to protect the payload from heat and airloads during the boost phase of the flight. A cone-on-cylinder configuration is chosen for the proposed design. The 10 foot diameter cylinder portion is 10 feet long. The conical portion is 16 feet long with a taper of 14.5° per side. There are no internal frames or bulkheads forward of the base. To facilitate jettisoning in flight, the fairing is fabricated in halves. The half shells are then held mated by a few explosive fasteners along the vertical split lines.

The air pressure or loads act in a crushing direction and produce axial and hoop compressive stresses in the shell wall. Since the airload is not uniform, shear and bending are also present. In addition the shell must be able to withstand thermal stresses resulting from rather severe aerodynamic heating.

Environmental conditions indicate the use of fiber-glass sandwich for shell wall construction. The designer must then attempt to establish the required core and laminate thickness to provide the required strength and stability. He can satisfy these by the use of conventional stress equations but he soon finds that these apply to complete cylinders of solid sheet material. The cylinders treated are considered very long or assumed held round at intervals. Only a small amount of information exists on sandwich cylinder allowables, and in each case the author points out the need of further investigation and testing to establish valid design allowables.

In this particular design the engineer does not have a complete cylinder. He has two half cone-cylinders, since moment continuity is lost at the split lines. The

knee area, or juncture between the cone and cylinder, acts as a stiffening ring to some degree. It divides the shell into two distinct bays which might buckle independently if the juncture is stiff enough. The designer finds very little information on the required stiffness of reinforcing rings for cases of this nature.

To determine the elastic buckling pressure of the conical portion of the half shell, the designer will again be forced to use complete cylinder formulas and use assumed values for effective length and radius. The loss in strength due to the split line and the absence of a rigid ring cannot be adequately predicted.

The airloads on a ring (a unit length of shell) can be divided into a uniform crushing component and an asymmetrical component. The uniform component is reacted by hoop compression in the ring and no bending is present. The asymmetrical component induces a shear reaction in the shell, and a ring flattening effect is expected. A quick analysis shows that a shear reaction of the classical VQ/I type produces no ring bending with the asymmetrical airload. However, further checking shows that only slight variations in the distribution of the applied pressure or the reacting shear will produce very high computed ring flattening deflections and bending moments. Thus the stiffness required to prevent flattening becomes a major unknown.

In most such design projects, the designer is aware of the vehicle performance penalty for unnecessary structural weight. Yet he is faced with a schedule and budget that does not permit developmental testing. A nose cone failure could waste a missile and launch effort costing millions of dollars. If a designer is to have a measure of confidence in his product, under these circumstances, the finished hardware is sure to be unnecessarily heavy.

For example, previous analyses of this type panel have treated the problem on an "equivalent-thickness" basis. The sandwich panel is reduced to an equivalent thickness of solid metal and compared with cylinder data of the same effective length, radius, and mean radial pressure distribution. Margins of safety of 50% have been allowed to account for the effects of the split line. Such procedures are believed to result in excessive sandwich core weight.

The cone-on-cylinder shell discussed here is believed to be useful enough to be worthy of further research. The author knows of four existing satellite programs which utilize this shape, and several more that are under consideration.

ADDITIONAL THEORETICAL INVESTIGATION

A limited investigation was initiated to determine if the critical buckling load of the nose cone could be found by theoretical means. For this purpose a structural idealization of the nose cone was made considering its physical features. The configuration was a sandwich shell composed of a spherical nose cap, a conical section, and a cylindrical section. The shell is split into two halves to facilitate jettisoning; the edges of the half shells are reinforced along the parting line by fairly stiff beams. The shell is supported at its base by the missile body and just below its spherical cap by stout bulkheads.

Only the cone-cylinder sections need be considered in a stability analysis. At the juncture of the cone and cylinder the discontinuity angle of the shell plus a local thickening of the sandwich acts as a stiffening ring. Since it would not be decided initially if this stiffening was sufficient to cause the cone and cylinder to buckle as individual elements, provision for buckling of the combination was included in the analysis. It was also decided to include the discontinuity of bending moment along the shell parting line although the effect of this now appears of somewhat minor consequence. It was felt that an essential feature in this analysis should be the low transverse shear stiffness of sandwich construction.

Before attempting an analysis, the load-temperature-time history for the nose cone was considered. It was found that the design loads occurred at near room temperature and were followed at some later time by the peak thermal gradient during which the applied loads were nearly zero. The distribution of pressure and temperature is practically uniform over the conical and cylindrical segments under consideration. Although the design pressures can occur at a slight angle of incidence, it is felt that this affects the bending only since the instability is primarily a function of the mean radial pressure distribution.

Having made the above idealizations, some time was spent in a brief review of applicable literature. Papers on thin cones and cylinders, and on sandwich cylinders were reviewed. From the survey it became apparent that the only feasible analytical approach would be an approximate one based upon an energy method. The inherent hazard of such an approach is that it leads to unconservative values of critical loads if the expression for deformation does not admit the true buckled shape (reference 1, page 90). Several authors state that satisfactory solutions for cylinders subjected to hydrostatic pressure can be obtained with small deflection theory and others suggest that for sandwich construction snap-through type buckling is unlikely (sec. 1.1, ref. 1, p. 498; ref. 2, p. 49; ref. 3, p. 2). Although no such statements were found for cones, there appears no reason for their behaving differently from cylinders as long as the cone angle is not large. With these assumptions it is possible to follow the procedure of reference 4, which also makes use of reference 5, in computing the critical buckling load for the nose cone. The detailed steps taken and the equations are much too lengthy for presentation here so only a brief outline of principles will be shown. The geometry of the cone is shown in figure 1.

Strain components for the cylindrical portion of the shell can be expressed in terms of displacements as equations 12.56 of reference 6. However, in addition to u , v , and w , terms involving transverse shearing strains $\gamma_{\theta x}$ and $\gamma_{\theta z}$ omitted in equations 12.47 (ref. 6) must be included in the last three equations of 12.57 (ref. 6) to account for the low shear modulus of the sandwich core. Similar strain expressions for the cone may be derived in terms of displacements s , v' , and q and shear strains γ_{rp} and $\gamma_{\theta p}$.

The normal deflection (q , w) assumed for each half shell was the sum of the three shapes shown in longitudinal section in figure 2.

The expressions used are:

$$w = (F) (M) + (G) (L) + (N) (K)$$

$$q = (F) (I) + (H) (J) + (N) (K')$$

Where:

$$F = \sum_f \left[-\overbrace{\frac{6}{3\pi-16} \frac{A_f}{f}}^* + \overbrace{\frac{8\sqrt{2}}{3\pi-16} \frac{A_f}{f} \sin \left(\frac{\theta}{2} + \frac{\pi}{4} \right)}^* + A_f \sin f\theta \right]$$

$$G = \sum_g \left[-\overbrace{\frac{6}{3\pi-16} \frac{A_g}{g}}^* + \overbrace{\frac{8\sqrt{2}}{3\pi-16} \frac{A_g}{g} \sin \left(\frac{\theta}{2} + \frac{\pi}{4} \right)}^* + A_g \sin g\theta \right]$$

$$N = \sum_n \left[-\overbrace{\frac{6}{3\pi-16} \frac{A_n}{n}}^* + \overbrace{\frac{8\sqrt{2}}{3\pi-16} \frac{A_n}{n} \sin \left(\frac{\theta}{2} + \frac{\pi}{4} \right)}^* + A_n \sin n\theta \right]$$

$$M = \sum_m A_m \sin \frac{m\pi(x-c)}{(d-c)}$$

$$L = \sum_l A_l \sin \frac{l\pi(x-c)}{(d-c)} \sin \frac{\pi(x-c)}{2(d-c)}$$

$$K = \sum_k A_k \sin \frac{k\pi(x-b)}{(d-b)}$$

$$H = \sum_h \left[-\overbrace{\frac{6}{3\pi-16} \frac{A_h}{h}}^* + \overbrace{\frac{8\sqrt{2}}{3\pi-16} \frac{A_h}{h} \sin \left(\frac{\theta}{2} + \frac{\pi}{4} \right)}^* + A_h \sin h\theta \right]$$

*These terms are zero for $f, g, h, n = \text{even}$, i.e., a continuous shell.

$$I = \sum_i A_i \sin \frac{i\pi(r-B)}{(L-B)} = \sum_i A_i \sin \frac{i\pi(x-b)}{(c-b)}$$

$$J = \sum_j A_j \sin \frac{j\pi(r-B)}{(L-B)} \cos \frac{\pi(r-B)}{2(L-B)}$$

$$= \sum_j A_j \sin \frac{j\pi(x-b)}{(c-b)} \cos \frac{\pi(x-b)}{2(c-b)}$$

$$K' = \sum_k A'_k \sin \frac{k\pi(r-B)}{(L'-B)} = \sum_k \frac{1}{\cos\phi} A_k \sin \frac{k\pi(x-b)}{(d-b)}$$

The above expressions for q and w were found to satisfy all boundary conditions provided shear strains $\gamma_{\theta x}$, $\gamma_{\theta z}$, γ_{rp} , $\gamma_{\theta p}$, and Poissons ratio effects in the strain component expressions previously derived are neglected.

The strain energy of the sandwich cylinder and core, due to deflections q , w , are determined similarly to the method of reference 4. It was found more convenient to take the reference surface at the core mid-height. An expression of similar form to that of equation 47 (ref. 4) is found for the strain energy of the shell, and the flexural energy of the edge beams of the nose cone is added to the term corresponding to B_{15} , of reference 6.

In applying the method of minimizing the total potential, only the change of load potential during buckling need be found. Part of this change comes from the induced radial compression in the nose cone and part from the axial force on the shell. The former can be found using the trick of reference 1, page 288. The equivalent load is

the quantity on the right side of equation (a). The quantity in parenthesis is replaced with the radial curvatures from the expressions for strain components in the nose cone. Radial displacement terms can be eliminated by consideration of inextensible buckling. Longitudinal displacements can be expressed in terms of the "tilting" factors and neutral surface ordinates used for strain energy expressions. For the second part of the change in external energy, the average shortening of an elemental length of genatrix can be taken as

$$1/2 \left[\left(\frac{\partial w}{\partial x} \right)^2 + \left(\frac{\partial v}{\partial x} \right)^2 \right] \text{ or } 1/2 \left[\left(\frac{\partial q}{\partial r} \right)^2 + \left(\frac{\partial v'}{\partial r} \right)^2 \right]$$

where terms in v , v' must be again expressed in terms of "tilting" factors and neutral surface ordinates.

The change in total potential is taken as the sum of load potential and strain energy. Arranging terms involving "tilting" factors and neutral surface ordinates on the right-hand side, these parameters can be eliminated by minimization and result in a right side expression similar to that of equation 59 (ref. 4).

Further minimization of the change in total potential with respect to $A_c A_m$, $A_g A_e$, $A_f A_i$, $A_h A_j$, and $A_n A_k$ results in five simultaneous equations containing q_{cr} (pressure) and the integers f , g , h , i , j , k , l , m , and n . These equations are much too lengthy to show here. They also are much too complex to solve manually and should be programmed onto a large computer.

Due to the time schedule of the particular nose cone being designed, there was insufficient time to attempt solution on the IBM 7090 computer available at this facility. However, this would be an ideal tool to use in this analysis. It is completely feasible and practical to obtain an IBM solution to the equations. The problem is common enough throughout the industry to warrant this research and the majority of the aerospace companies who would use such data have facilities for processing a computer program.

CONCLUDING REMARKS

Tying such a theoretical analysis development program to an experimental investigation of sandwich nose cone models would make an excellent research program. For instance, it is strongly suspected from the tests of thin metal models that the k-mode displacements are unnecessary in the analysis and would affect large simplifications in the analysis by being omitted. At the same time, there also exists the possibility that tests of sandwich shells might reveal that some other displacement mode is required although this does not appear likely from tests to date. In either event, completion of the analysis and test corroboration would give us a very useful design tool.

REFERENCES

1. Timoshenko, S. and Gere, J. M.: Theory of Elastic Stability, 2nd Ed., McGraw-Hill, New York, 1961.
2. Gerard, G., and Becker, H.: Handbook of Structural Stability, Part III - Buckling of Curved Plates and Shells, NACA TN 3783, August 1957.
3. Norris, C. B., and Zahn, J. J.: Design Curves for the Buckling of Sandwich Cylinders of Finite Length Under Uniform External Lateral Pressure, U. S. Forest Products Laboratory Reports No. 1869, May 1959.
4. March, H. W., and Kuezi, E. W.: Buckling of Sandwich Cylinders in Axial Compression, U. S. Forest Products Laboratory Reports No. 1830, December 1957.
5. Ericksen, W. S., and March, H. W.: Effects of Shear Deformation in the Core of a Flat Sandwich Panel, Compressive Buckling of Sandwich Panels Having Facings of Unequal Thickness, U. S. Forest Products Laboratory Reports No. 1583B, November 1950.
6. Wang, Chi-Ten: Applied Elasticity, McGraw-Hill, New York, 1953.

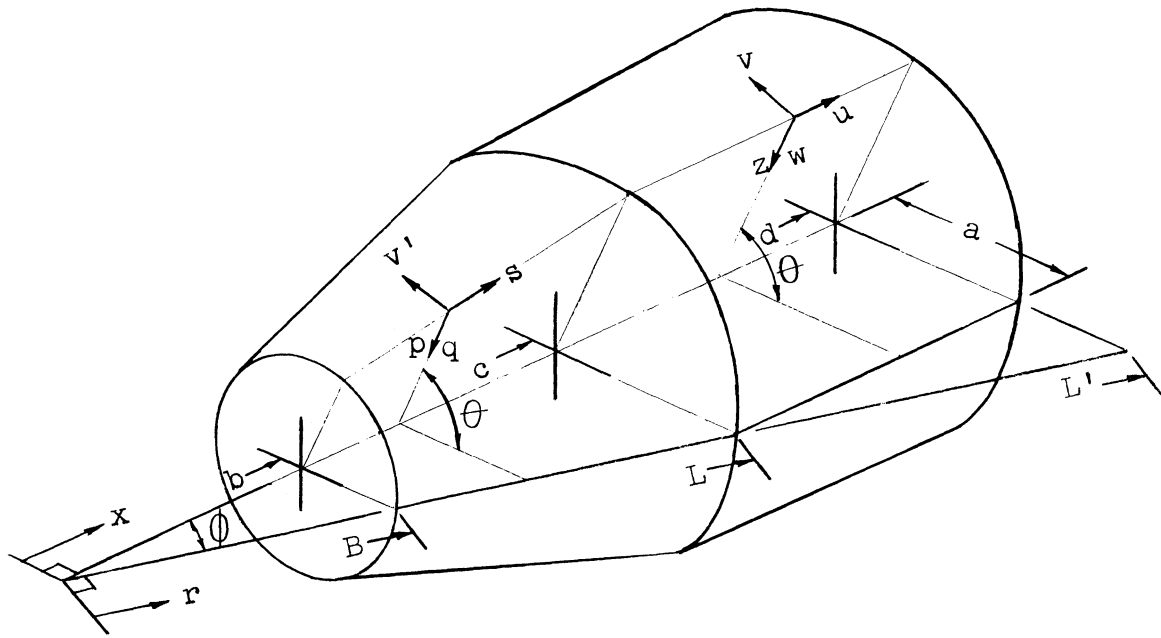


Figure 1.

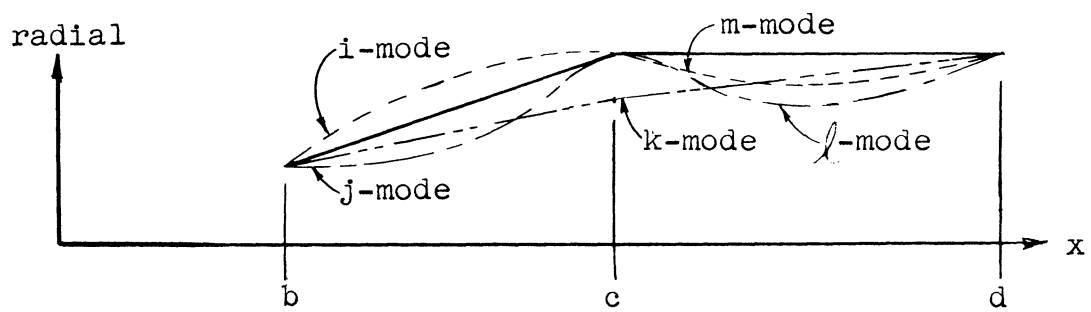


Figure 2.

DESIGN OF STIFFENED CYLINDERS IN AXIAL COMPRESSION

By John M. Hedgepeth

Space Systems Division, Martin Marietta Corporation

SUMMARY

The problem of optimum design of axially compressed cylinders stiffened by rings and stringers is discussed. Particular attention is devoted to configurations suitable for large launch vehicles. Consideration is given to the analytical techniques for determining strength as well as the procedures for optimization.

INTRODUCTION

One of the primary design criteria for circular cylindrical shells in flight vehicles is the necessity of carrying axial compressive loading. In most situations, the loading is light enough so that efficient design precludes the use of an unstabilized, single-thickness shell. Of the various means of stabilization, the one used most often is that of stringer and ring reinforcement.

The purpose of this paper is to discuss methods of analysis and of optimum design of stiffened cylinders. Attention is devoted primarily to types of configurations and loadings which are suitable for large-scale launch vehicles. Only the case in which integral stringers are firmly fixed to the rings and in which premature local buckling of the skin between stiffeners is prohibited is considered, in the belief that these are inherent properties of the most efficient structure. For simplicity, the stiffening elements are assumed to have negligible torsional or sidewise bending stiffness.

Most of the information contained herein is not particularly new or surprising. It is felt, however, that the discussion taken as a whole is a contribution to the field of optimum design.

DISCUSSION

Before looking at the complex stiffened cylinder, there are some lessons to be learned from published analyses of the much simpler stiffened flat plate. For example, a study of the results of reference 1 shows that a longitudinally compressed, longitudinally stiffened rectangular plate with many bays in the transverse direction, buckles as if the bending stiffness of the stiffeners was "smeared out", provided that the stiffeners are not so stiff that local buckling of the plate between stiffeners occurs. For the present case wherein premature skin buckling is prohibited, this means that the stringer stiffening can be very adequately accounted for by means of orthotropic analyses. Since the larger the stringer, the larger the ratio of stiffness to weight, it also means that a necessary condition for optimum design is that local skin buckling, stringer crippling, and overall cylinder buckling should occur at the same load level. In short, for a given required distributed stringer stiffness determined by orthotropic theory, optimum design implies that the stringer spacing be as wide as possible without encountering local skin buckling, and as deep as possible without creating crippling.

The situation with regard to rings is unfortunately not so straightforward. Qualitative help is afforded by the results in reference 2 for the longitudinal loading of transversely stiffened long plates. These results have been replotted in figure 1 in a form suitable for the present discussion. In this form, the buckling curves that occur if the stiffener were stiff enough to force local panel buckling and the curves predicted by an orthotropic analysis are the same for all proportions; these are shown by the dashed straight lines. The exact results for the discrete stiffeners are indicated by the solid curves. These curves are very nearly coincident for practical panel aspect ratios. There are three ranges of the stiffness parameter: For light stiffeners, the curves follow the orthotropic theory; for heavy stiffeners, the panel is forced to buckle between stiffeners. In the intermediate range, the stiffeners participate in the buckling and their discreteness is important.

Several lessons pertaining to the buckling of stiffened cylinders are learned in this figure. For example, there is no need of making the rings stiffer than a certain value. Furthermore, since the larger a ring is the more efficient from a weight standpoint it is, the range in which the orthotropic ring theory is valid should be avoided. The optimum design will have a ring stiffness that would be associated with the intermediate range. This is unfortunate since in this range analysis techniques are

the most difficult. In addition, the optimization procedure would have to include the complicated coupling between the stringer stiffened cylinder and the rings. Without very much cost in weight one can eliminate part of this coupling by adopting the criterion that the rings should be made just stiff enough to force nodes at the rings.

On the basis of this criterion one can design the optimum stringer panels for buckling between rings; this would depend only on the loading and the ring spacing. Then the rings can be sized so that the selected buckling mode would be obtained. A subsequent optimization with respect to ring spacing would yield the final efficient design.

The carrying out of the foregoing optimization procedure is feasible within the present state of the art of analysis techniques. A discussion of some of the interesting aspects of this state of the art follows:

Analysis of Stringer Stiffened Cylinders

If one can ignore the effect of "one sidedness" of the stringers, there are a number of orthotropic cylinder analyses that are applicable to solving this problem. Such an analysis should include the effects of plasticity since optimum design should entail sizable stresses. This is particularly true if the cylinder is pressurized. The inclusion of these plasticity effects for the pressurized case can be a source of trouble because of the difference in effective stress levels between shell and stringers. Analysis shows that the shell becomes plastic at a considerably lower load than do the stringers.

Theoretical results obtained from such orthotropic analysis should be in good agreement with the strength that would be realized experimentally even though small deflection theory is utilized. This conclusion follows from an examination of the kinds of configurations that are optimum for large launch vehicle structures. Here the optimum ring spacing turns out to be relatively small and most of the load carrying ability of the stringer stiffened cylinder is contributed by its wide column capability. The contribution of the curvature, which is most subject to reduction due to large deflection effects, is relatively small. Furthermore, a stringer stiffened cylinder turns out to have a relatively low effective radius-thickness ratio so that the knock-down in cylinder strength is small. These conclusions are based in part on the results obtained in reference 3 by means of an approximation of the orthotropic analysis of reference 4.

An investigation of the influence of the one sidedness of the stringer stiffeners in practical cylinder design is being performed by the author. Preliminary results of the investigation indicate that for the axisymmetric mode of buckling, locating the stringers on the inside yields a significantly higher strength than locating them on the outside. For most asymmetric modes of buckling, the converse is true. Since the critical mode of failure is usually the latter, attention should be given to the possibility of utilizing external stiffeners in design.

Determination of Required Ring Stiffness

As was mentioned before, efficient stiffened cylinder proportions require the rings to be handled as discrete entities rather than by means of orthotropic techniques. An oft used practice is to size the rings in accordance with Shanley's criterion, reference 5, which is a conservative quasiempirical specification based on the envelope of a large number of test data. For large launch vehicles, Shanley's criterion yields rings that contribute significantly to the overall weight of the cylinder. A more refined technique, based on the detailed geometry of the cylinder and its stiffeners and treating the rings as discrete elements, is therefore an important adjunct to efficient design.

Examination of various proposed designs for launch vehicles in the Nova class shows that the tank domes and the manufacturing splices divide the structure into relatively short cylinders. For such configurations only a few additional rings are necessary in each segment. Therefore, analyses of "infinitely long" geometries are of limited usefulness. One must deal with the actual structure, incorporating the restraint effects of domes and other attachments in order to get accurate strength estimates. Mathematically there are two ways of dealing with each of the cylindrical segments. One is by writing the 8th order partial differential equation for the stringer stiffened cylinder with the proper boundary and discontinuity conditions at the ends and across rings. The other would be to use a potential energy approach. In either case, various values of circumferential wave length would have to be examined and the rings sized in order to yield at least as much strength as that already determined for the stringer stiffened cylinder. Of the two approaches, the energy approach would seem to be more suitable for programming on a computer.

Effects of Alternative Design Conditions

As is usual in structural design, launch vehicles are subjected to a variety of loading conditions. The tank barrels, for

instance, must be capable of withstanding not only the very large flight compression loads coming from the combined longitudinal acceleration and wind shears but also less large, but still appreciable, compression loads on the launch pad. The high reliability requirement for man rating dictates capability of any tank's being empty and unpressurized while all upper stages are completely fueled. The necessity of meeting both of these design loadings well may yield a tank structure which is optimum for neither of the loadings since the pressurization existing during flight reduces the requirements for rings but increases the plasticity problems. The first rough cut would be gotten by designing the tank barrels without rings for the flight condition and then adding a sufficient number of rings to handle the launch pad condition. Further refinement is necessary, however, for weight saving.

CONCLUDING REMARKS

All actual designs are affected by the practical aspects of fabricability; off-optimum design therefore usually results. Nevertheless, the optimum configuration should be determined, if for no other reasons than to determine what the cost of such practical considerations is, and to indicate the direction in which improvements in manufacturing technology would be most helpful. In addition, for very large launch vehicles, optimum configurations might well be feasible because of the absence of minimum-gage problems.

REFERENCES

1. Budiansky, Bernard, Seide, Paul, and Weinberger, Robert A.: The Buckling of a Column on Equally Spaced Deflectional and Rotational Springs. NACA TN 1519, 1948.
2. Budiansky, Bernard, and Seide, Paul: Compressive Buckling of Simply Supported Plates with Transverse Stiffeners. NACA TN 1557, 1948.
3. Peterson, James P., and Dow, Marvin B.: Compression Tests on Circular Cylinders Stiffened Longitudinally by Closely Spaced Z-Section Stringers. NASA Memo 2-12-59L, 1959.
4. Stein, Manuel, and Mayers, J.: Compressive Buckling of Simply Supported Curved Plates and Cylinders of Sandwich Construction. NACA TN 2601, 1952.
5. Shanley, F. R.: Simplified Analysis of General Instability of Stiffened Shells in Pure Bending. Jour. Aero. Sci., vol. 16, no. 10, Oct. 1949, pp. 590-592.

LONGITUDINAL BUCKLING OF TRANSVERSELY STIFFENED PLATES

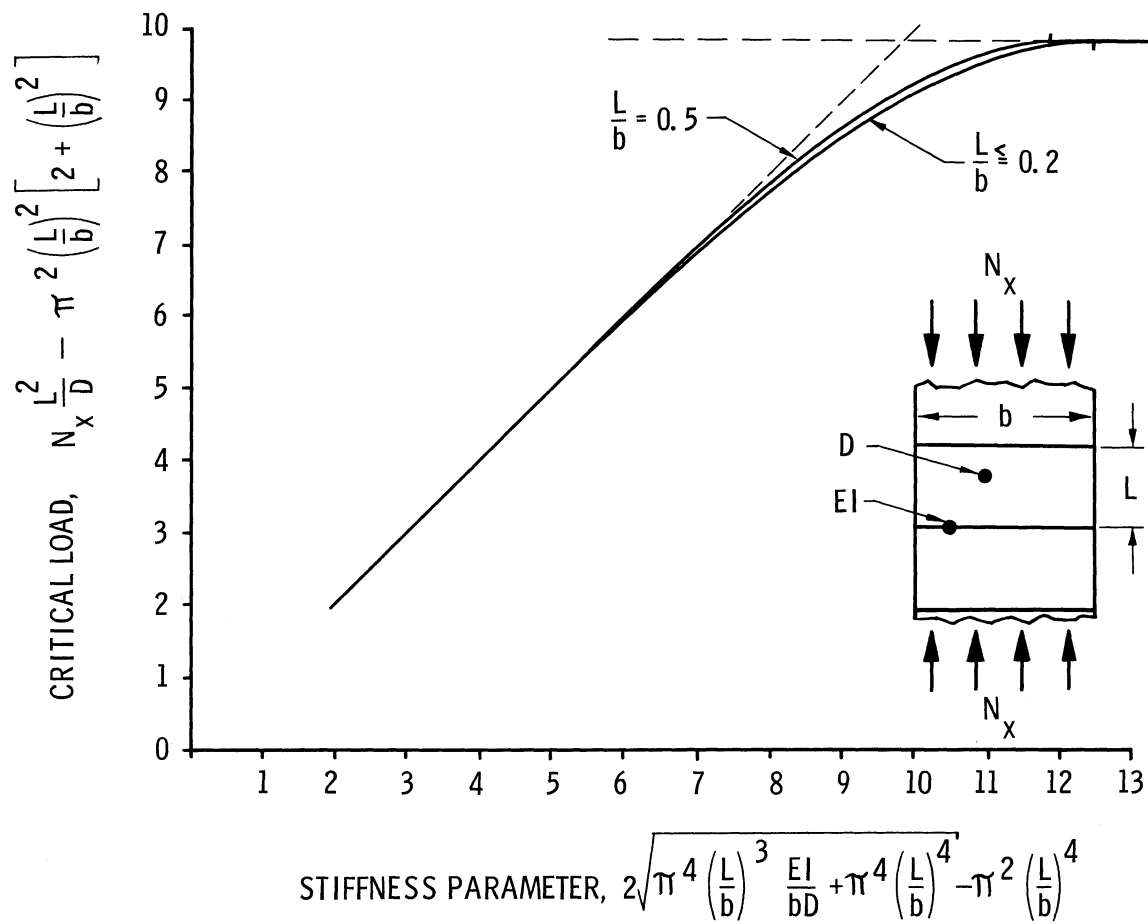


Figure 1

ELASTIC STABILITY CONSIDERATIONS IN AIRCRAFT STRUCTURAL DESIGN

By Richard L. Schleicher

North American Aviation, Inc.

General instability in shell type structures is a relatively infrequent phenomenon. By general instability is meant that a complete section of a structure becomes elastically unstable, as compared with local crippling or buckling. The first step in design is to rough size the structure and determine its compatibility with air vehicle configuration and systems installations. After this step has been completed, it is possible to survey the layouts to determine whether general instability is likely to occur. The general parameters of length, diameter, frame spacing, element stiffness, etc., are then investigated to determine if a general failing stress exists which is less than any local column, beam column, or panel failing stress. In this way, a well-balanced design is determined and general stability failing modes eliminated.

The structural designer has a fairly wide selection of basic parameters during the early phases of design. These diminish, however, as the design progresses and consideration for systems installations becomes more important. In many cases the ideal arrangement of structural elements soon gives way to marked discontinuities. The classical example of a circular cylinder with symmetrically spaced elements is seldom realized. Uniform frame sections and spacing give way to deeper utility frames at random spacing. The effective stiffness of the deeper frames may be 20 - 50 times greater than the minimum required to prevent instability, considering the general proportions of the shell. In like manner, the uniform distribution of longitudinal stiffeners is replaced by a system of longerons supplying the axial compressive elements. Major frames serve as base points in support of beam-column longerons. The intermediate frames give elastic column support to the longerons and form boundary members for the shear panels in the shell covering. It has been found that longitudinal stringers become superfluous and are more difficult to accommodate than longerons, even though these too may be interrupted. Without longitudinal stringers, frame stiffness may actually be increased through simplified design.

A situation frequently arises in which frame depths must be arbitrarily increased to accommodate aircraft systems installations; namely, pipe lines, conduits, etc. This results in deep frames having unstable inner flanges. When the auxiliary systems fail to supply the necessary stability, other means must be employed. Straps of sheet metal are sometimes fastened to the inside flanges of frames, lacing them together

and terminating at convenient major frames. These latter ties serve as node points to the frame flanges.

When major frames or bulkheads are spaced too far apart to stabilize the longerons laterally, other means must be provided. Each design must be inspected to ascertain whether the longeron is supporting intermediate frames or vice versa. Normally, the side skin will give continuous vertical stability to the longerons with the intermediate frames serving to stabilize the inside flanges. Cross plane flooring or shelving generally serves this purpose. In some instances, the lower longerons on both sides of the weapons bay in bombers have been stabilized by the doors attached to them. Continuous piano hinges are excellent for this purpose. During the transition from closed to open, the longeron has reduced lateral stability. However, since bombing runs are made during unaccelerated flight conditions, high loads are not encountered during the quick opening and closing cycles. In general, careful attention to frame design offsets instability failures in fuselage structures.

Wing structures are seldom affected by general instability if proper attention has been paid to rib and spar design. In thin wing box structures, bending deflections may be appreciable. Rib designs must be checked for the compressive loads brought about by the surface deflection. This consideration usually provides enough stiffness to support the wing surface against general instability. When closely spaced ribs are not feasible in thin wings, the skin thickness is increased and surface stiffness is achieved through the use of multi-spars. The problem then reverts to one of simple panel instability. There are a number of wing box structures in service today whose compression surface allowable stress is equal to the compressive yield strength of the material used. This has been achieved through the use of thick milled skins and multi-spar support.

The structural designer is not without constant regard for the general instability problem. He is frequently guided by his sense of proportion based on long experience. This sense has often resulted in stiffening certain areas and thus forestalling the progression of incipient failures.

TESTS OF CURVED PANELS

The structures engineer must frequently obtain verification of the effects of several variables in order to proceed with a particular design. Typical of the above is a series of tests to determine the effect of intermediate frame spacing on the strength of curved sheets in axial compression. The following concerns the test of a group of 4130 steel

curved panels with varying frame spacing. The material was heat-treated to 125 - 140 ksi. The main frames were 2 inch "Z" sections spaced 18-7/16 inches on center and made of the same material. Light intermediate "J" section frames were made from 301 CRES steel. The 28 inch radius of curvature and main frame spacing were held constant - only the intermediate frame spacing was varied. The width of all panels was approximately 67 inches and all frames were riveted to the skin panels. The free edges were lightly clamped between two 3 x 3 x 3/8 steel angles. All specimens were tested in axial compression between two parallel steel loading plates 10 inches thick. The panels were made of two pieces of steel sheet welded longitudinally to form a single panel and heat-treated after welding. The warping caused by heat-treating did not result in flat spots greater than 1/16 inches in depth.

Each specimen failed by inward buckling of large sections of the panel. In each case, the post buckling load was also obtained and this, it was found, could be repeatedly attained after initial failure. The post buckling stress was equal to or greater than 68 per cent of the initial buckling stress for the main frame spacing of 28 inches. The smaller intermediate frame spacings resulted in a value of 79 per cent or greater. The buckling characteristic of the closely spaced frames was a gradual type of failure rather than sudden buckling. The light "J" section frames were quite effective in attaining high buckling stresses. Two of the specimens were reworked after initial failure by adding the intermediate frames and retested. The reworked specimen sustained from 19 to 60 per cent greater load.

One steel panel was subjected to heavy hammer blows to ascertain the additional effects of surface dents. The initial buckling load was reduced approximately 25 per cent whereas the post buckling load was only reduced approximately 4 per cent over the more perfect specimen. There was no reduction in post buckling load over the initial load. The results of these tests showed:

- (a) The initial strength of a curved panel depends on the initial surface conditions.
- (b) The post buckling strength, except for the damaged panels, is less than the initial buckling strength.
- (c) Light intermediate frames add greatly to the buckling strength of curved panels.
- (d) The strength of the panels after initial buckling was consistent and reproducible.

The pertinent stress coefficients derived from the test data are

plotted in Figure 1. Also shown is the characteristic curve taken from Figure 3 of NACA Report 874. It will be noted that the test points fall considerably below the NACA curve. This is no doubt due to the initial condition of the specimens which closely approximated actual construction. The upper symbols indicate initial buckling and the lower symbols post buckling. The familiar stress coefficients are the same as found in Reference 1.

TEST OF A FUSELAGE SPECIMEN

It is sometimes necessary following detail element tests such as the curved panel tests just described, to proceed with a representative component test specimen. This was done in the case of the X-15 fuselage which is essentially a monocoque cylinder subjected to a multitude of loadings and environment.

The test component was a generalized section of the X-15 fuselage in the region of the integral propellant tanks. It was basically a 56 inch diameter cylindrical shell 80 inches long with a $14\frac{1}{2}$ inch diameter inner cylinder, two toroidal bulkhead frames, and two side fairings. The details are shown in Figure 2.

The outer shell was .093 inch Inconel X sheet formed to a 56 inch diameter cylinder. Welding was used except for a mechanical joint at Station 60. Beads were formed in the side areas to provide increased stiffness in the circumferential direction and thermal relief in the longitudinal direction. One typical wing carry-through frame was welded to the shell at Station 16 with four attaching fittings for external loads. Four longitudinal angles were welded to the outside of the shell, acting both as longerons and fairing attachments. The main shell is used to contain LOX. The $14\frac{1}{2}$ inch inner cylinder, which is used to store helium, was fabricated from .043 inch Inconel X material. Zee section circumferential stiffeners were spotwelded to the outside of the inner cylinder. One of the toroidal bulkheads consisted of two circular segments made from Inconel sheet welded to the large shell wall and the inner cylinder respectively. To these was riveted a .050 inch thick 7075-T6 clad aluminum alloy section to complete the torus. The other torus was formed in two segments welded to the outer and inner cylinders and along a circumferential seam joining the two segments. The side fairings used to house control elements and plumbing details in the X-15 completed the assembly. However, only one fairing duplicated the X-15 design which consisted of a flat outer sheet reinforced by a corrugated inner sheet - both made from Inconel X.

Tests were conducted in five parts. These included pressurization,

external loads, and elevated temperature tests. A general view of the specimen is shown in Figure 3.

The first test was an internal pressure test to determine the collapsing strength of the aluminum alloy torus. Pressure was applied above the aluminum torus and failure occurred at 10.7 psi which was 71.3 per cent of the required pressure. Radial stiffeners spaced 15 degrees apart were required to achieve the 15 psi pressure required.

The object of the second test was to test the welded joints of the Inconel torus, the welded joints of the outer shell, and the strength of the inner shell under a collapsing pressure. Positive pressure was applied internally between Station 0 and the Inconel torus. Failure occurred by compression buckling of the inner shell at 80 psi. Failure was in a multi-node fashion as indicated by theory. As a result of this test the inner cylinder stiffener spacing was reduced in order to carry the required ultimate pressure of 111 psi. Both the Inconel torus and main outer shell withstood the pressure without failure. In addition, 100 cycles of limit pressure (78 psi) were also applied without damage. Likewise, a design negative pressure test of the Inconel torus to 20 psi resulted in no indication of failure.

Following the above tests, a negative pressure test of the outer shell was conducted. For this test, a sealed bulkhead was attached at Station 80. To prevent premature failure, the specimen was filled almost full with deionized water. The space at the top was evacuated to -6 psi with no failure resulting. Due to the head of water within the specimen, the net pressure at the bottom was -3.1 psi. This test was sufficient to demonstrate the collapsing strength of the outer shell.

The next order of tests included both room and elevated temperature load tests of the wing carry-through frame. The specimen was loaded through a set of loading beams attached to the wing fittings. For the room temperature tests, the frame was loaded to failure at 93 per cent of the design ultimate load. Since failure occurred only on one side, a repair was made and retested to a gradient across the frame of 555° F. The gradient was obtained by first cooling the inner flange of the frame with a fine spray of liquid nitrogen. Quartz glass radiant heaters were used on the outside. The temperature gradient was programmed to achieve a maximum value in 300 seconds. Limit load was first applied at room temperature and, while holding the load constant, the temperature gradient was achieved. Next the load was increased and failure took place at 90 per cent design ultimate load. The failure was at the same corresponding location on the side of the frame opposite to the previous failure. A reinforced frame was used in the final design. It is interesting to note that there was only a 3 per cent difference between the identical failures occurring at both room temperature

and with the gradient noted above.

The specimen was then loaded in vertical bending (side fairings at the neutral axis) both at room and elevated temperatures. Moment was applied through a steel bulkhead and loading beams attached to Station 80. It was necessary to precool all four longerons prior to heating to achieve the proper temperature gradient. The room temperature load tests were carried to the required ultimate moment of 6,300,000 inch pounds without failure. The elevated temperature tests, to a gradient of 550° F., were run at increasing load levels (10 per cent increments) with a cool-down after each load level. In every case the cool-down was followed by load application and then the heat reapplied. Failure of the outer shell occurred at 160 per cent design ultimate load as the heating cycle was applied.

The remaining bending test was a side bending case in which the side fairing was placed in compression. This test, like the preceding one, was conducted both at room and elevated temperatures. The test setup was also the same as for the case of vertical bending. In addition to the side bending moment of 2,940,000 inch pounds, an axial compression of 9,900 pounds was applied to the side fairing. At room temperature, the main shell withstood 100 per cent side bending moment. The side fairing however failed at 43 per cent maximum load through the spotwelds connecting the outer skin to the corrugated inner skin. The spotwelds were replaced with monel rivets and the fairing failed at 85 per cent design ultimate load by crippling of the outer skin in an area which was beyond the support of the inner corrugated skin. The spotwelding used in the specimen was changed to a stitch weld of greater strength in the vehicle side fairing to achieve 100 per cent strength. During the elevated temperature part of the test, the outer shell withstood 150 per cent design ultimate bending moment without failure. However, during a subsequent loading the outer shell failed at 140 per cent design ultimate load.

The final major test was a transverse shear test in which an ultimate load of 46,700 pounds was applied at Station 80 and reacted at the floor mounting. This test was conducted at room temperature and was completed without failure.

This series of tests is typical of the procedure followed in the design of an airframe of unusual structural characteristics.

TESTS OF A LARGE CYLINDRICAL SPECIMEN

The purpose of this test was to evaluate the longerons, frames, and frame stabilizing straps of a large fuselage specimen shown in

Figure 4. This specimen was circular with a diameter of 100 inches and length of 64 inches. The shell wall was 6V - 4AL titanium riveted to 4AL - 3Mo - 1V titanium frames and ten H-11 steel longerons. The specimen was subjected to bending about mutually perpendicular axes, both singly and in combination as listed below:

$$\text{I} \quad - M_y = 45,000,000 \text{ inch pounds} \quad S_z = 210,000 \text{ pounds}$$

$$\text{II} \quad - M_z = 32,500,000 \text{ inch pounds} \quad S_y = 60,000 \text{ pounds}$$

$$\text{III} \quad - M_y = 42,000,000 \text{ inch pounds} \quad S_z = 91,000 \text{ pounds} \quad \left. \begin{array}{l} \\ M_z = 23,000,000 \text{ inch pounds} \quad S_y = 50,000 \text{ pounds} \end{array} \right\}$$

The basic internal stresses were obtained by elementary bending theory plus the effects of diagonal tension as these might affect the longerons. A multi-support beam-column analysis was developed for the longeron. Frame loads were derived considering the skin diagonal tension and the frame solution was based on the theory of minimum strain energy. The calculated strength of the frame inner flanges indicated low compressive strength and these were to be investigated as part of this test.

In calculating the beam column strength of the longerons, the interaction effects of the other longerons were not considered. The frame stiffnesses at each longeron were calculated and used as flexible supports. Considering the frame and longeron geometries, the deflection pattern of the longeron could be determined. Using an iteration process, the critical load of any longeron could then be determined. The predicted buckling stress of the side longeron was 195,000 psi. At 90 per cent of the side bending test (.90 x 32,500,000 inch pounds), visual observations gave signs of impending failure. The strain gages indicated stresses of 220,000 and 120,000 psi measured on opposite sides of a longeron element. The calculated stress level, however, was 180,000 psi. It was concluded that the calculated and predicted failing stresses were in good agreement. The strain gage readings also indicated a decrease in stress at the 90 per cent load increment. The test was stopped at this load level.

At the same time that the side longeron was at the point of failure, the upper and lower shoulder longerons were also indicating failure because of increased deflections. The critical predicted buckling stresses were 120,000 and 182,000 psi, respectively, for these longerons. The calculated stresses at this point in the test were 104,000 psi and 171,000 psi. Strain gages monitored during the test indicated 100,000 and 160,000 psi. The test in side bending was not carried beyond this point since design requirements were met and other tests were still

planned. The test did indicate that the calculated and predicted critical longeron loads were close, considering that failure was imminent and not actual.

An energy solution of typical frames, considering the skin diagonal tension stresses and longeron effects, indicated that the optimum strap spacing for the inner flanges was 11.5 inches. After sustaining the maximum vertical loading condition of 45,000,000 inch pounds moment and 210,000 pounds shear, one half of the straps were removed and the frames continued to carry this test loading. Strain gage readings indicated impending failure of the flanges. The original strap spacing was resumed and failure occurred at 110 per cent of the above loading condition in the outer flanges of the frames. This failure was considered a general instability failure of the shell. Once the lateral strap spacing was determined, the calculated and predicted frame flange loadings of 1659 pounds and 1980 pounds, respectively, could be determined. Considering the many variables involved, this engineering approach to a typical shell instability problem proved adequate.

RECOMMENDATIONS FOR RESEARCH

- (1) Expand present theory and techniques to include non-circular and unsymmetrical sections, especially with areas of re-entrant curvature.
- (2) Expand present theory and techniques to include sandwich shells where the shear rigidity of surface elements is significant.
- (3) Develop structural concepts embodying a high degree of post-buckling strength to minimize the hazard of immediate total collapse.
- (4) Develop and verify methods of analysis to include interaction effects of multiple loading.

REFERENCES

- (1) NACA Technical Report No. 874, "A Simplified Method of Elastic Stability Analysis for Thin Cylindrical Shells", by S. B. Batdorf.
- (2) NASA Technical Note 3735, "Bending Tests of Ring-Stiffened Circular Cylinders", by James P. Peterson.

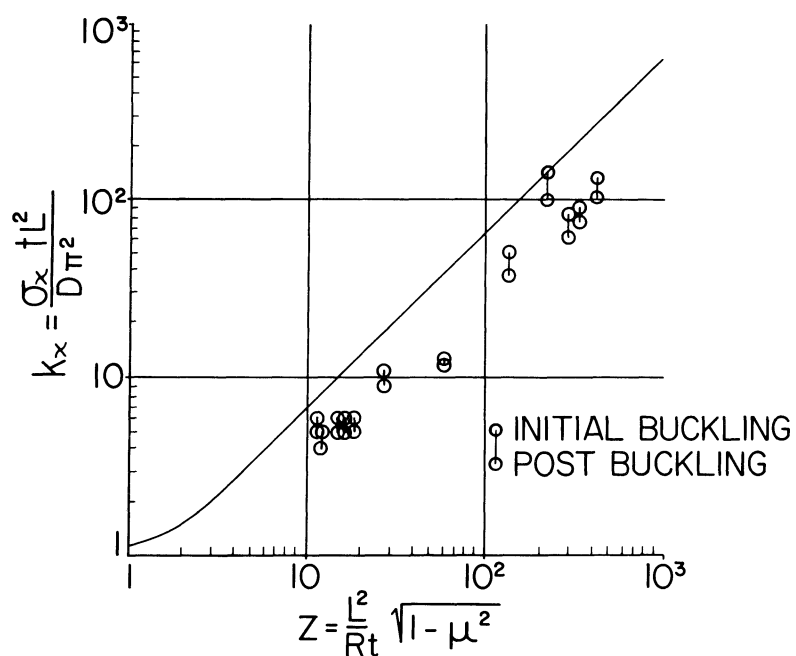


Figure 1 - AXIAL STRESS COEFFICIENTS FOR CURVED PANELS

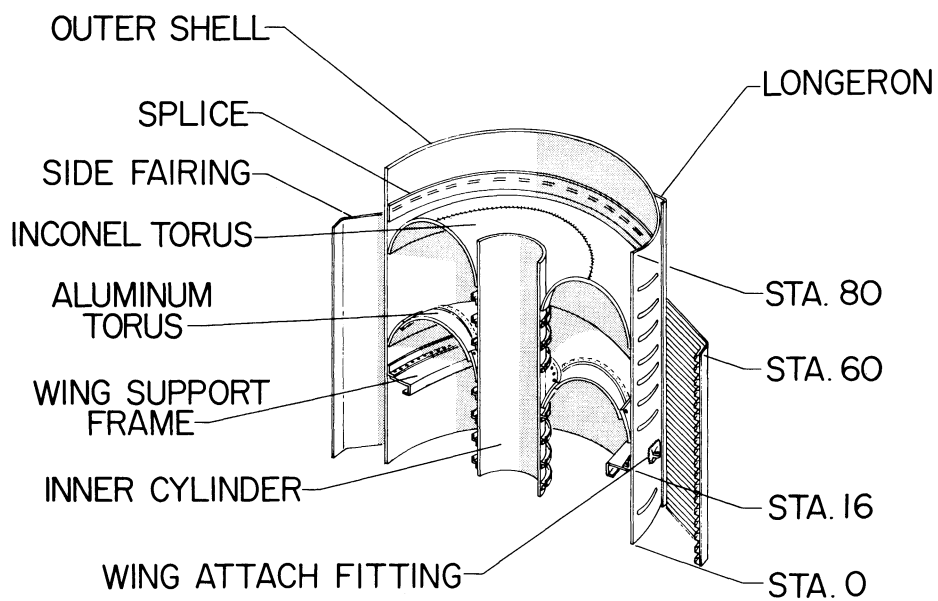


Figure 2 - X-15 FUSELAGE SPECIMEN

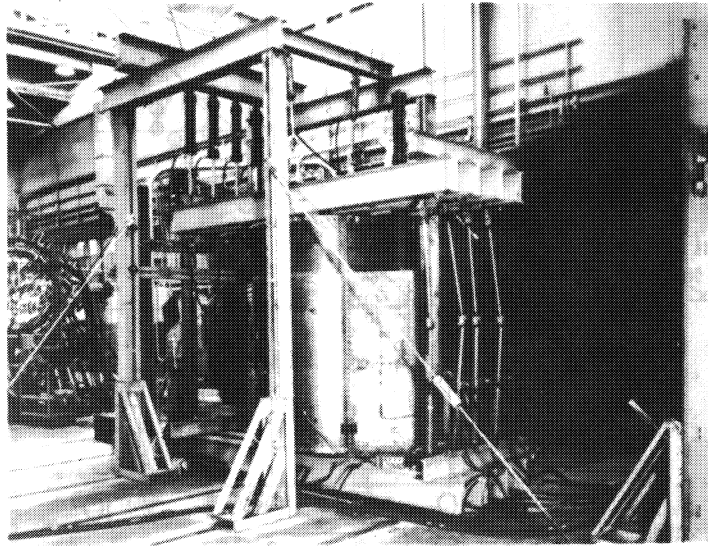


Figure 3 - X-15 FUSELAGE SPECIMEN

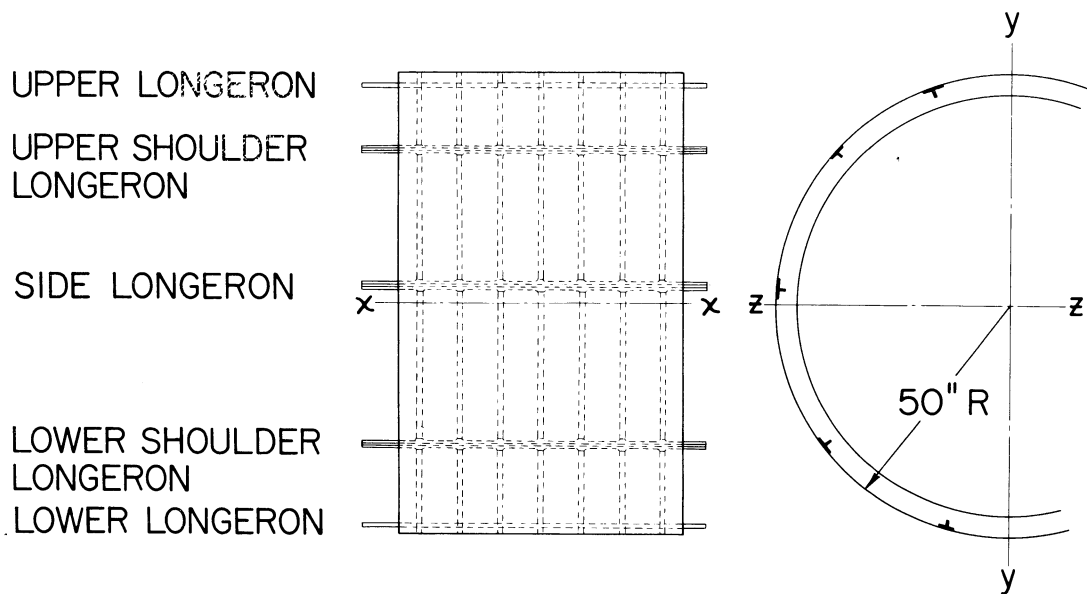


Figure 4 - FUSELAGE SHELL SPECIMEN

DESIGN AND TEST EXPERIENCES WITH INSTABILITY
OF MAJOR AIRFRAME COMPONENTS

By Walter E. Binz, Jr.

The Boeing Company
Transport Division

SUMMARY

Two test incidents involving instability of large scale commercially built structures are described. Two classes of structure are discussed; the first, a fuselage with skin designed to buckle at low stress, and the second, a wing whose surface remains unbuckled to failure. The structure in the region of failure is defined and the failures described and illustrated. Insofar as possible, the stresses in the critical area at the time of failure are reported and compared to strength determined by analysis. Both fuselage and wing surfaces were observed to fail in the mode of a medium range column when adequate support was provided by ribs and frames. Initial failure in the wing example was premature due to a design deficiency in rib strength. A clear illustration is given of the effect of rib stiffness on wing surface stability. Adding stiffness to wing ribs increases the limit of surface stability to the theoretical flat panel value.

INTRODUCTION

Tests of large, full scale, stiffened shell structures, built by production quality mechanics with production tools, rarely get attention in the technical literature. Individuals in the technical community have limited access to data from these types of tests. Investigators of structural stability have recognized that imperfections exist in all structures and have attempted to evaluate their effects on the limits of stability. The tested structures described in this report are imperfect to the degree which may be expected for commercially built airframes. These imperfections are not specifically defined but one might expect that their effect could be qualitatively evaluated by observing any marked deviation in the behavior of these structures from the theoretical or experimental behavior of near perfect specimens.

SYMBOLS

b	stiffener spacing, in.
b _e	effective width of skin between stringers, in.
c	coefficient of fixity in Euler column formula
D ₁	plate flexural stiffness in longitudinal direction, in.-kips
D ₂	plate flexural stiffness in circumferential direction, in.-kips
E	Young's modulus, ksi
E ₁	plate extensional stiffness in longitudinal direction, kips/in.
h _e	average depth of wing box, in.
h _x	width of wing box, in.
I	moment of inertia of effective wing bending section, in. ⁴
K	buckling coefficient of flat plate, $\frac{\sigma_{cr} b^2}{\eta E t^2}$
l	length of surface between frames or ribs, in.
M	spanwise wing bending moment, in.-lbs.
N _p	compressive load per inch at panel buckling, kips/in.
P	rib crushing load, lbs./in.
r	initial radius of curvature of wing, in.
R	radius of cylinder, in.
t	thickness of skin, in.
γ	empirical correction for initial imperfections
ε̄	unit shortening
η	plasticity reduction factor
ρ	radius of gyration, in.
σ _{edge}	edge stress corresponding to strain ε̄, ksi

σ_{cc} local crushing stress of effective section, ksi

σ_{cr} compressive stress at local buckling of skin, ksi

A FUSELAGE INSTABILITY PROBLEM

During the static test program of the KC-135 jet tanker, one instability type failure occurred in the fuselage monocoque structure. This failure, in the lower aft body under the stabilizer, is shown in Figure 1 at the instant of failure. The critical section was loaded by a combination of bending, vertical shear and a small amount of torsion.

The structure in the vicinity of the failure may be described as a single cell tapered shell, any section of which is made up of an upper radius and a lower radius separated by a flat segment at the sides. Longitudinal stiffening was provided by hat section stringers which were spaced at about seven inches. Stringers had an area of .23 square inches and a $\rho = .475$ in. The monocoque skin was .040 - 7075-T6 clad curved to a radius of 35 inches. Frames were connected to the upstanding legs of the hat section stringers and did not interrupt the stringer continuity. The frame forward of the failure area was a partial bulkhead. The frame aft was a formed .051 gage 7075-T6 Z section 2.44 inches deep. The frame spacing was 24 inches.

Loads were applied in small increments up to failure and instrumentation read at each increment. Compression wrinkles in the lower surface skin were noticed at about 50% of the failure load. At 95% of the failure load, these buckles were very sharp. All load systems had stabilized after the application of the final load, however, the fuselage collapsed before data could be recorded.

Failure was initiated in the skin-stringer panel midway between the frames described. An inside view of the fuselage after failure is shown in Figure 2. The frames appeared to be in good condition after failure with no indication of lateral permanent set.

A group of strain gages were located on the critical stiffener within inches of the point of failure initiation. An analysis of these gage readings indicates that at the time of failure, the average stress in the effective bending structure was -43,000 psi. The stress computed using the elementary flexure formula applied to the effective body bending section is also -43,000 psi.

Allowable Stress Computation

At the time of this design, allowable compressive stresses were computed by the Johnson Parabolic formula

$$\sigma_{edge} = \sigma_{cc} - \frac{\sigma_{cc}^2 \left(\frac{l}{\rho \sqrt{c}} \right)^2}{4 \pi^2 E}$$

A limited amount of test data was used to substantiate this analysis. A fixity coefficient $c = 1.0$ was assumed and l was taken as the frame spacing. The strengthening effect of the body curvature was neglected. The effective section was calculated using a width of skin

$$b_e = 1.7 t \sqrt{\frac{E}{\sigma_{edge}}}$$

The proportions of the stiffener were such that local crippling could not occur below the compressive yield stress of the material. Therefore,

$$\sigma_{cc} = F_{cy} = 62,000 \text{ psi} .$$

Computation of the allowable compressive stress at the point of test failure using this method yielded $\sigma_{edge} = -41,200$ psi. When compared to the test conditions at failure, this analysis underestimated the surface strength by less than 5%.

An analysis of the critical section using the techniques described by Peterson, Whitley and Deaton in reference 1 was recently completed. Manipulating the flat panel portion of equation 3, reference 1

$$N_p = \frac{c \pi^2 D_1}{l^2} + \gamma \frac{2}{R} \sqrt{E_1 D_2}$$

and again assuming the fixity coefficient $c = 1$, the edge stress at panel buckling was calculated as $\sigma_{edge} = -43,000$ psi. Consideration of curvature in this analysis would raise the edge stress to $-44,700$ psi at panel buckling.

On the strength of these analyses the consideration that the structure behaves as a flat simply supported column appears to be reasonable for structures of these proportions loaded in compression only. The skin, being buckled at a low stress, loses its ability to stabilize the stiffeners by shell action and permits a column failure mode to be predominate. Where the skin between stiffeners is buckled by high shear loads combined with compression, a more sophisticated analysis must be undertaken to account for the interaction of the shear in the skin on the compressive strength of the surface.

A WING INSTABILITY PROBLEM

A wing instability failure was encountered during the static destruction test program of the B-52A airplane. Failure was initiated by instability of the inspar wing structure and resulted in complete collapse of the upper surface of the left hand wing. Failure occurred approximately 25 feet outboard from the side of the body (one-third span) as shown in Figure 3. The critical section of the wing was loaded by a combination of bending, shear and torsion.

The primary structure is a single-cell, two-spar, box beam of constant width and tapered depth. Upper and lower surfaces are cambered in the chord direction. In the failure area, the wing box is approximately ten feet wide with an average depth of 33 inches. Upper surface spanwise stiffening is provided by extruded "J" section stiffeners spaced at approximately 8.5 inches and supported by chordwise ribs spaced at 30 inches. Ribs are of a stiffened web construction and constitute a beam member between front and rear spars. Spanwise stringers are continuous with their outstanding flanges attached to the chords of the supporting ribs. All primary structure is fabricated from 7075-T6 aluminum material with the exception of rib webs which are 2024-T3 aluminum material. In the region of failure, the upper surface skin-stringer combination has an area of .5 square inches per inch of width and a radius of gyration of 1.0 inches.

Loads were applied in small increments and instrumentation data obtained at each load level. At 88% of failure load, the deflection indicators used to measure rib crushing began to show a nonlinear load-deflection relationship. Incremental loading was continued until a sudden and complete failure occurred. At the final load application, the structure collapsed before instrumentation data could be obtained.

Failure was initiated by crushing of the ribs with the simultaneous collapse of the upper compression material in the aft portion of the box. Internal damage in the area of primary failure is shown in Figure 4. From an analysis of the recorded data taken from strain gages located in the failure area, the average stress in the upper surface material was -45,000 psi at failure. The stresses calculated in the failure area by the elementary flexure formula average approximately -50,000 psi. It seems likely that the softness of the supporting ribs in the test structure caused some of the upper surface load to shift to the more lightly loaded structure in the forward part of the box, thereby explaining the discrepancy between the measured test stresses and the calculated stresses in the aft portion of the box. Unfortunately, no strain gages were located on the forward part of the wing to substantiate this argument.

Ribs are generally used as stiffening members in flexible wings to prevent the collapse of the surface material. Rib crushing loads are proportional to the curvature of the wing. Rib loads for the critical wing rib were computed according to the formula:

$$P = \frac{Ml}{h_e h_x r} + \frac{M^2 l}{h_e h_x EI_x}$$

which includes the effect of initial surface curvature and primary wing bending curvature. The computed rib loads were 380 lbs per inch of surface width under the failure conditions. A subsequent test of the rib under crushing loads indicated an ultimate strength of 600 lbs per inch of surface width. Its spring rate was found to be 4,800 lbs per inch deflection per inch of surface width. Since the rib was the primary cause of failure, the foregoing formula obviously did not account for the total rib crushing load experienced in the test.

In attempting to discover the reason for this discrepancy, it was observed that the rib adjacent to the critical rib had a considerably higher extensional stiffness since it formed a fuel tank bulkhead. As a consequence, the upper surface curvature was higher than expected at the critical rib and lower at the adjacent stiffer rib. The opposite effect occurred at the lower surface. A subsequent analysis, accounting for the differences in rib stiffness and the shearing deformations in the ribs caused by the unbalanced crushing loads, showed that the upper surface crushing load at the critical rib was actually 610 lbs per inch of surface width for the failure condition. This is in close agreement with the tested ultimate strength of this rib and emphasizes the importance of including all secondary effects in rib stress analysis.

Allowable Stress Computation

Curves of allowable wing surface stress versus $\frac{l}{\rho \sqrt{c}}$ were established on the basis of a large amount of experimental data accumulated for this airplane as well as previous Boeing airplanes. Since the surface skins were required to remain unbuckled at ultimate load, these design curves were modified in the short column range according to the formula

$$\sigma_{cr} = K \eta E \left(\frac{t}{b} \right)^2$$

A buckling coefficient of 5.0 was used to account for the skin being continuous over the stringers, curvature of the surface, and torsional restraint provided the stringers by the ribs.

The allowable surface stress in the failure area was computed as -56,000 psi using these procedures and assuming a fixity coefficient $c = 1.0$. An analysis using the formula

$$N_P = \frac{c\pi^2 D_1}{l^2}$$

with a fixity coefficient $c = 1.0$ gives an allowable edge stress equal to -56,000 psi. Premature rib failure restricted the surface stress level to -45,000 psi. As a result of this failure, the rib was reinforced to an ultimate strength of 890 lbs per inch of surface width. In a subsequent test of the wing incorporating these rib changes, the upper surface material reached a stress level of -53,000 psi. A failure in another part of the wing prevented further load application and testing was discontinued.

In an attempt to further substantiate the strength of the upper surface, a separate test program was initiated. Several tests were made on portions of the upper surface, curved to the shape of the deflected wing and laterally supported on springs simulating rib flexibility. Destruction tests of these panels established that the surface allowable of the wing as originally tested was -54,000 psi, and that, after improving the rib stiffness, the surface allowable increased to -55,500 psi. Further increases in rib stiffness produced no major improvement in strength. Similar tests on initially straight specimens (without wing bending curvature) indicated no improvement in strength over specimens that were initially curved.

CONCLUDING REMARKS

In the example of fuselage instability, the structure did not fail in a mode typical of cylindrical shells but tended to behave in much the same manner as a column. This might be expected in the case where the skin is designed to buckle in compression at low applied loads. The curvature of the section seemed to have only a minor effect on its strength.

In both the wing and fuselage examples the fact that the ribs and frames were uniformly spaced and offered little resistance to rotation of the surface structure seemed to permit the surfaces to deform to the characteristic single half wave shape between supports in the manner of a simply supported column. This is evidenced by the fact that the fixity coefficient for simple supports yields an analysis which closely approximates the actual tested strength.

The wing program gives definite indication that there is an optimum amount of rib stiffness required to develop the full surface strength. The radius of curvature of the wing (~ 2000 inches) had no appreciable effect on the surface strength.

REFERENCES

1. Peterson, James P., Whitley, Ralph O., and Deaton, Jerry W.: Structural Behavior and Compressive Strength of Circular Cylinders with Longitudinal Stiffening. NASA TN D-1251, 1962.

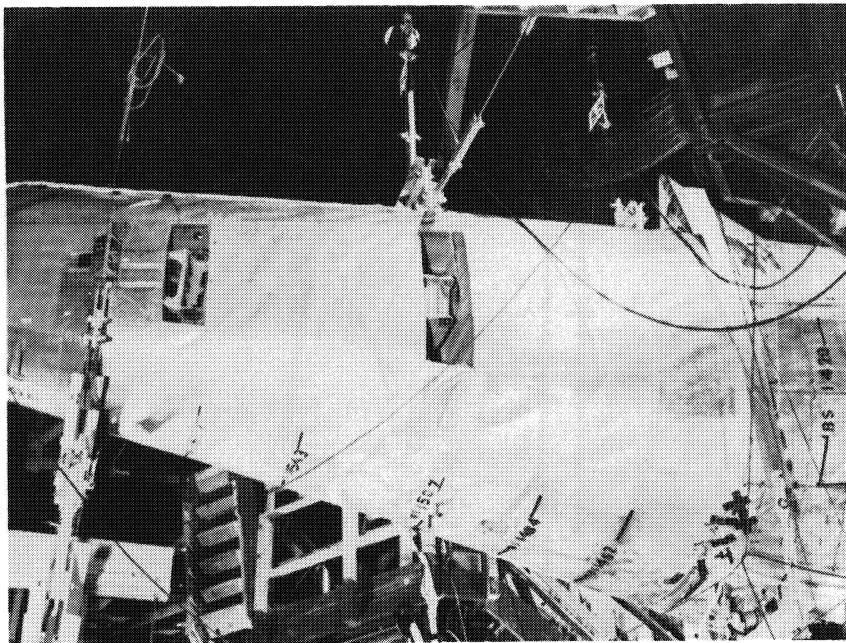


Figure 1.- Fuselage instability failure.

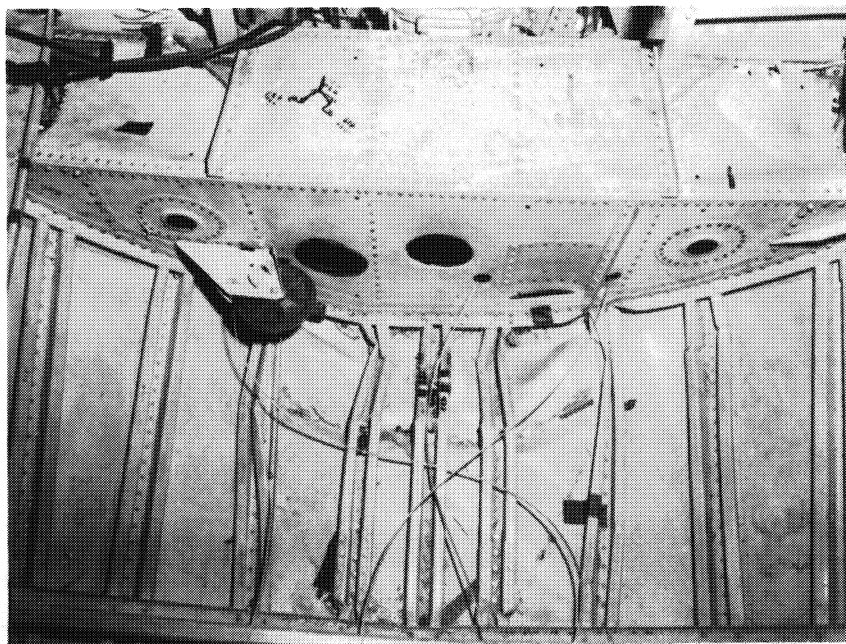


Figure 2.- Inside view - fuselage instability failure.

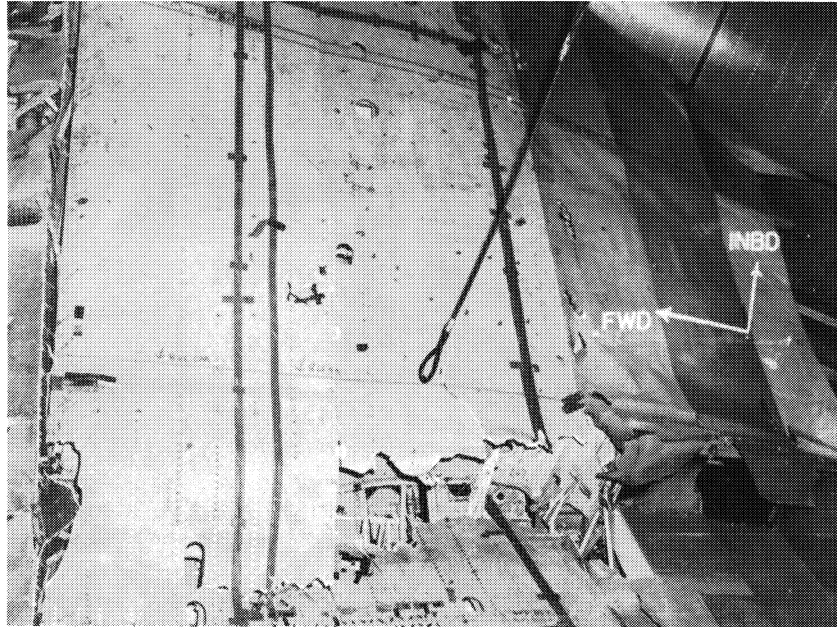


Figure 3.- Wing upper surface instability failure.

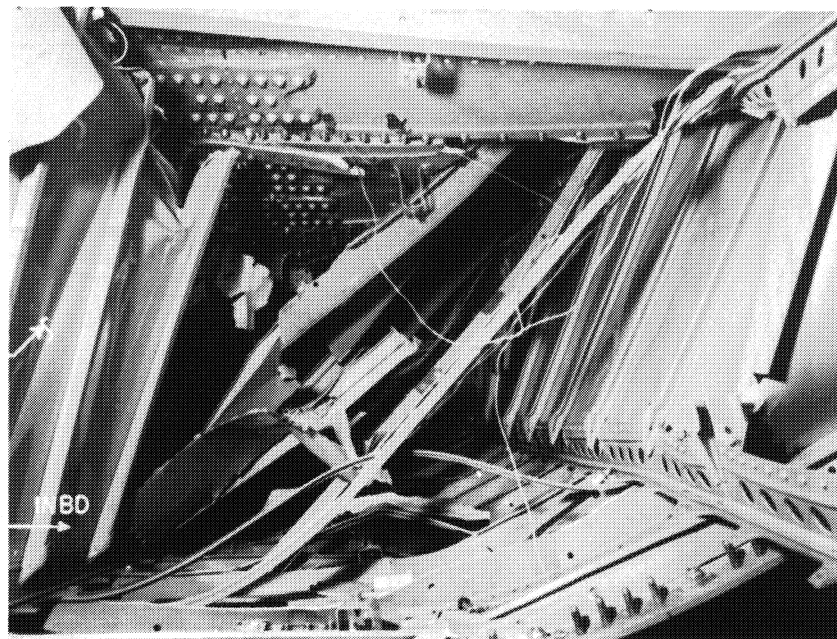


Figure 4.- Rear inside view - wing instability failure.

II CYLINDRICAL SHELLS

ON THE BUCKLING OF THIN ELASTIC SHELLS

By Ellis Harold Dill

University of Washington

SUMMARY

The differential equations which must be solved to predict the buckling load are reviewed. The different possible physical interpretations of these equations are discussed.

INTRODUCTION

This article is concerned with the prediction of the response to arbitrary disturbances of a structure initially at rest in a deformed state under known static loads. The response to loads varying in time is not considered. This problem will be called the elastic buckling problem. In the elastic buckling problem, certain general conclusions can be drawn about linear systems (ref. 2). But shells are characterized by the importance of non-linearities (ref. 1). So far, no similar comprehensive study of the possible instabilities of non-linear elastic systems has been made.

There are several possible versions of the elastic buckling problem for non-linear systems¹. Any of the following questions might be asked. (1) Are there loads for which two infinitesimally different equilibrium states exist? (2) Are there loads for which the second variation of strain energy ceases to be positive definite? (3) Are there loads for which infinitesimal oscillations diverge? (4) Will the stiffness decrease greatly at some load so that intolerable deflections occur? (5) Will a dynamic jump from one equilibrium configuration to another occur at some load due to a given magnitude of disturbance? (6) Will a limit cycle develop as a result of finite disturbances? The fundamental question here is the equivalence of these problems.

¹ref. 1, pg. 123

²ref. 3, pg. 54

STATIC EQUILIBRIUM

The exact equations governing the deformations of linearly elastic solids are geometrically non-linear. The restriction to linear elasticity implies, for most materials, a restriction to small stretches and small shears. For such deformations, the displacement gradients will be small and therefore the non-linearities negligible unless one or two dimensions of the body are small compared to the others². Thin elastic shells are three dimensional linearly elastic solids for which one dimension, the thickness, is much smaller than the other two. For shell problems, the geometric non-linearities may therefore be important. However, because of the two-dimensional nature of the shell, not all of the non-linear terms can be of equal importance³. Some simplifications result because of the thinness and because of the flatness. Equations which systematically introduce simplifications appropriate to the relative magnitude of these two parameters for various possible modes of deformation have been accomplished (ref. 4). However, much further work remains to be done. In particular, the strain-displacement and curvature-displacement relations corresponding to each family of basic equations must be determined before application to special problems and comparison with existing special theories is possible.

Since the general theory of linearly elastic solids can be formulated as the stationary condition of the potential energy, each set of shell equations will also provide the Euler equations for the stationary value of a functional, the potential energy, W . The static equilibrium states are thus determined by

$$\delta W = 0 \quad . \quad (1)$$

Unlike the linear theory, non-uniqueness of equilibrium states is to be expected for a wide variety of loads (refs. 5,6,7).

The usual problem is concerned with the stability of static equilibrium positions which differ only slightly from the undeformed configuration. The non-linear terms might, therefore, be of negligible importance. No exact solutions are available which clearly resolve this question, and test results on spherical caps (ref. 9) indicate that

²ref. 3, pg. 54
³ref. 3, pg. 182

the non-linear terms can not be neglected in determining the equilibrium state even before buckling.

STABILITY

Suppose the shell is subject to loads derivable from a potential, then the rest position is determined by a set of non-linear differential equations and boundary conditions corresponding to the stationary condition for the potential energy. If a disturbance in the form of finite displacements and velocities is introduced, the equations which describe the motion will be non-linear.

The motion may subside, diverge, or reach a limit cycle. For a given rest state, the motion will depend upon the magnitude of the initial disturbances. Should there exist other static equilibrium positions (at the same loads), disturbances of sufficient magnitude could cause the structure to jump from its initial static equilibrium position and come to rest in a second static equilibrium position. An important question, not yet solved, is the relation between such motions and the von Karman-Tsien energy criterion (ref. 10). With disturbances of sufficient magnitude it would appear possible to have a jump from one static equilibrium position to another at loads less than those predicted by this criterion. No general results are known about the motion of non-linear structures subjected to finite disturbances.

If only infinitesimal vibrations are superposed on the deformed system, then, as for linear systems, the motion will be harmonic if $\delta^2 W > 0$ and diverging if $\delta^2 W < 0$. The first case will be called stable. All other cases (including "neutral equilibrium") will be called unstable and the corresponding loads will be called the buckling loads.

It is generally not possible to directly investigate a static equilibrium state to determine the sign of the second variation for all possible variations from it. Instead the function which minimizes the second variation is determined. The differential equations governing such a function are the Euler equations of

$$\delta(\delta^2 W) = 0 \quad . \quad (2)$$

The minimum is then investigated to see whether it is positive or negative. Generally $\delta^2 W > 0$ for small loads. As

the load is increased, the least value of the second variation becomes smaller and finally becomes zero and then negative. The lowest value of the load for which the second variation is non-negative is thus the buckling load. The differential equations determined by Eq. 2 are linear equations with variable coefficients. When the loads are derivable from a potential, they will be the same equations as those found by considering the differential equations satisfied by the difference between two infinitesimally different static equilibrium states⁴ (corresponding to the same load). Thus problems (4), (5), (6) as stated above are equivalent when the loads are derivable from a potential.

A DONNELL TYPE THEORY

The notation followed is that of ref. 11 wherever possible: Greek letters will have the range (1,2). Curvilinear (material) coordinates in the middle surface will be denoted by x^α and are chosen so that x^1, x^2, \bar{n} form a right-handed system when \bar{n} is the unit, inward normal. The components of the metric tensor of the surface are $a_{\alpha\beta}$. The coefficients of the second quadratic form are $e_{\alpha\beta}$. The $e_{\alpha\beta}$ system is skew-symmetric and $e_{12} = \sqrt{a}$ where a is the determinant of the metric tensor. A bar denotes covariant differentiation based on the $a_{\alpha\beta}$. The components of tangential displacement are u^α . The normal displacement, positive inward is denoted by w .

The Donnell type theory for large deflections (ref. 12) leads to the set of equations:

$$n^{\alpha\beta} |_\beta + p^\alpha = 0 \quad , \quad (3)$$

$$m^{\alpha\beta} |_{\alpha\beta} + b_{\alpha\beta} n^{\alpha\beta} + n^{\alpha\beta} w |_{\alpha\beta} - p^\alpha w |_\alpha + p = 0 \quad , \quad (4)$$

$$n^{\alpha\beta} = B H^{\alpha\beta\nu\lambda} a_{\nu\lambda} \quad , \quad (5)$$

⁴ref. 3, Chap. 5

$$m^{\alpha\beta} = -D H^{\alpha\beta\nu\lambda} w|_{\nu\lambda} , \quad (6)$$

$$B = \frac{E t}{1-\nu^2} , \quad D = \frac{E t^3}{12(1-\nu^2)} ,$$

$$a_{\nu\lambda} = \frac{1}{2} (u_\nu|_\lambda + u_\lambda|_\nu - 2 b_{\nu\lambda} w + w|_\nu w|_\lambda) , \quad (7)$$

$$H^{\alpha\beta\nu\lambda} = \frac{1}{2} (a^{\alpha\nu} a^{\beta\lambda} + a^{\alpha\lambda} a^{\beta\nu} + \nu [e^{\alpha\nu} e^{\beta\lambda} + e^{\alpha\lambda} e^{\beta\nu}]) .$$

The $n^{\alpha\beta}$ is a symmetric tensor that may be interpreted as the membrane stress, $m^{\alpha\beta}$ is a symmetric tensor that may be interpreted as the bending moment, and $a_{\nu\lambda}$ is the membrane strain tensor. The tangential surface loads are p^α and the normal pressure is p , positive inward. The boundary conditions to be satisfied on the edge with unit, outward normal in the middle surface m^α consist of specifying the quantities

$$u_\nu \quad \text{or} \quad n^{\nu\lambda} m_\lambda , \quad (8)$$

$$w \quad \text{or} \quad m^{\alpha\beta}|_\alpha m_\beta + n^{\alpha\beta} w|_\alpha m_\beta + \frac{\partial}{\partial s} (e_{\nu\alpha} m_\beta m^\nu m^{\alpha\beta}) , \quad (9)$$

$$\frac{\partial w}{\partial n} \quad \text{or} \quad m^{\alpha\beta} m_\alpha m_\beta , \quad (10)$$

where n and s are distances normal and tangential to the boundary.

These equations are derived from the necessary conditions for the stationary of the potential energy

$$W = \frac{1}{2} \iint H^{\alpha\beta\nu\lambda} (B a_{\alpha\beta} a_{\nu\lambda} + D w|_{\alpha\beta} w|_{\nu\lambda}) dS - \iint (p^\alpha u_\alpha + p w) dS \quad (11)$$

when the surface loads are fixed in magnitude and direction and either displacements are given on the edges or the given edge forces are specified to be zero.

The equations governing an equilibrium state corresponding to the same loads and differing only by an infinitesimal amount can be derived⁵ in the manner of ref. 3. Denoting the difference between the quantities, defining the

⁵Report 62-1, Feb. 1962, Dept. of Aeronautical Engineering, University of Washington, by E. H. Dill: Stability of Thin Elastic Shells.

two states, by superposed bars, these equations are

$$\bar{n}^{\alpha\beta}|_{\beta} = 0 \quad , \quad (12)$$

$$\bar{m}^{\alpha\beta}|_{\alpha\beta} + b_{\alpha\beta} \bar{n}^{\alpha\beta} + n^{\alpha\beta} \bar{w}|_{\alpha\beta} + \bar{n}^{\alpha\beta} w|_{\alpha\beta} - p^{\alpha} \bar{w}|_{\alpha} = 0 \quad , \quad (13)$$

$$\bar{n}^{\alpha\beta} = B H^{\alpha\beta\nu\lambda} \bar{a}_{\nu\lambda} \quad , \quad (14)$$

$$\bar{m}^{\alpha\beta} = -D H^{\alpha\beta\nu\lambda} \bar{w}|_{\nu\lambda} \quad , \quad (15)$$

$$\bar{a}_{\nu\lambda} = \frac{1}{2} (\bar{u}_{\nu}|_{\lambda} + \bar{u}_{\lambda}|_{\nu} - 2 b_{\nu\lambda} \bar{w} + \bar{w}|_{\nu} w|_{\lambda} + w|_{\nu} \bar{w}|_{\lambda}) \quad . \quad (16)$$

The quantities

$$\bar{u}_{\nu} \quad \text{or} \quad \bar{n}^{\nu\beta} m_{\beta} \quad , \quad (17)$$

$$\bar{w} \quad \text{or} \quad \bar{m}^{\alpha\beta}|_{\alpha} m_{\beta} + \bar{n}^{\alpha\beta} m_{\beta} w|_{\alpha} + n^{\alpha\beta} m_{\beta} w|_{\alpha} + \frac{\partial}{\partial s} (e_{\nu\lambda} m_{\beta} m^{\lambda} \bar{m}^{\nu\beta}) \quad , \quad (18)$$

$$\frac{\partial w}{\partial n} \quad \text{or} \quad \bar{m}^{\alpha\beta} m_{\alpha} m_{\beta} \quad . \quad (19)$$

must be given on the edge.

It can be shown that equations (12) to (19) result from Eq. (2) when the direction and magnitude of the surface loads are fixed.

SYMMETRICAL DEFORMATIONS OF CYLINDRICAL SHELLS

For a cylindrical shell of radius R , let $x^1 = x$ be the distance along the generator, and $x^2 = R\theta$ be the circumferential distance from a given generator. The coordinates x^1, x^2 and the inward normal form a right-hand system. Consider an axially compressed cylinder undergoing only axially symmetric deformations. Then

$$u_2 = 0 \quad , \quad n^{12} = 0 \quad , \quad m^{12} = 0 \quad , \quad p^{\alpha} = 0 \quad , \quad p = 0 \quad , \quad (20)$$

and all derivatives with respect to x^2 are zero.

For free ends, the boundary conditions are

$$n^{11} = -P, \quad w|_{11} = 0, \quad -Dw|_{111} + n^{11}w|_1 = 0. \quad (21)$$

A solution of Eqs. (3) to (7) is easily seen to be

$$w = -\frac{\nu P R}{Et}, \quad n^{11} = -P, \quad n^{22} = 0, \quad \text{etc.} \quad (22)$$

However, if the ends are restrained the result is different. For simply supported ends, the boundary conditions are

$$n^{11} = -P, \quad w = 0, \quad w|_{11} = 0. \quad (23)$$

The solution for

$$P < P_c, \quad P_c = Et \left(\frac{d}{R} \right)^2, \quad d^2 = \frac{Rt}{[3(1-\nu^2)]} \quad (24)$$

is

$$n^{11} = -P, \quad n^{22} = -w \frac{Et}{R} - \nu P, \quad (25)$$

$$w = -\nu \frac{PR}{Et} + e^{\beta x} (C_1 \cos \alpha x + C_2 \sin \alpha x) + e^{-\beta x} (C_3 \cos \alpha x + C_4 \sin \alpha x)$$

$$\beta^2 = \frac{1-\lambda}{d^2}, \quad \alpha^2 = \frac{1+\lambda}{d^2}, \quad \lambda = \frac{P}{P_c} \quad (26)$$

The constants can be adjusted to satisfy the boundary conditions. The axially symmetric solution for $P \geq P_c$ can be written in terms of similar terms.

With restrained ends there will be lateral deflections, moments, and circumferential stress whose magnitude and distribution depend upon the load but is always confined to a narrow edge zone. Usually the membrane solution, which is the same as Eq. (22), is assumed to be a sufficiently accurate estimate of the state before buckling even for restrained ends.

STABILITY OF CYLINDERS

For the axially compressed cylinder, the stability of the axially symmetric initial state is determined by seeking a solution of equations (12) to (19). For the free

ends, the solution⁶ shows that an axially symmetric buckling mode exists, localized near the ends, for which the buckling load is $p = \frac{1}{2} P_c$.

It may be shown that no axially-symmetric buckling mode exists for the simply supported ends for $P < P_c$. Therefore no axially-symmetric buckling mode is possible. This does not imply that the axially-symmetric deformations are stable; that question remains to be answered by solving equations (12) to (19). This solution has not been accomplished exactly.

REFERENCES

1. Fung, Y. C., and Sechler, E. E.: Instability of Thin Shells. Proc. First Symposium on Naval Structural Mechanics (Aug. 11-14, 1958, Stanford Univ.), Pergamon Press (New York), 1960, p. 115.
2. Ziegler, H.: On the Concept of Elastic Stability. Advances in Applied Mathematics, vol. 4, 1956, p. 351, Academic Press.
3. Novozhilov, V. V.: Foundations of the Non-linear Theory of Elasticity. Graylock Press. 1953.
4. Chien, W. Z.: The Intrinsic Theory of Thin Shells and Plates. Quart. Appl. Math. vol. 1, 1943, pp. 297-327, vol. 2, 1944, pp. 43-59, 120-135.
5. von Karman, T. and Tsien, H. S.: The Buckling of Thin Cylindrical Shells under Axial Compression. Jour. Aero. Sci., vol. 7, no. 2, 1939, p. 43.
6. von Karman, T. and Tsien, H. S.: The Buckling of Thin Cylindrical Shells under Axial Compression. Jour. Aero. Sci., vol. 8, no. 8, 1941, p. 302.

⁶N. J. Hoff, Buckling of Thin Shells, Dept. of Aeronautical Engr., Stanford University, SUDAER No. 114, Aug. 1961, p. 7.

7. Grigoluk, E. I.: On the Instability under Large Deformation of a Multi-layered Conical Shell under a Uniform Pressure. (In Russia) Inzhenernyi Sbornik, vol. 22, 1955, p. 111.
8. Donnell, L. H. and Wan, C. C.: Effect of Imperfections on Buckling of Thin Cylinders and Columns under Axial Compression. Jour. Appl. Mech. vol. 17, no. 1, 1950, p. 73.
9. Kaplan, A. and Fung, Y. C.: A Non-linear Theory of Bending and Buckling of Thin Elastic Shallow Shells. NACA TN 3212, 1954.
10. Tsien, H. S.: A Theory for the Buckling of Thin Shells. Jour. Aero. Sci., vol. 9, 1942, p. 373.
11. Green, A. E. and Zerna, W.: Theoretical Elasticity. Oxford Univ. Press, 1954.
12. Dill, E. H.: General Theory of Large Deflections of Thin Shells. NASA TN D-826, 1961.

BUCKLING AND POST-BUCKLING OF ELASTIC SHELLS

by

H. Langhaar and A. Boresi
University of Illinois

SUMMARY

Some theoretical investigations of buckling of elastic shells are surveyed in this report. Only geometrically perfect shells are considered; initial dents and out-of-roundness are not taken into account. Several questions raised by the studies are: (a) Under what conditions is the infinitesimal theory of buckling of shells adequate? (b) How does the energy theory of buckling of shells correlate with the method based on equilibrium equations for bending moments, tensions, and shears in a buckled configuration? (c) How important are nonlinear terms in the tangential displacements u , v in the strain-displacement relations for buckling and post-buckling studies? (d) How important are the boundary conditions for u , v in affecting stability? (e) If a condition of snap-through is approached, how much external work is required to push the shell "over the hump" into the buckled configuration? (f) How reliable are mathematical approximations used previously in the infinitesimal theory of buckling of shells? Tentative and incomplete answers to some of these questions are suggested.

INFINITESIMAL THEORY OF BUCKLING

One of the objectives of nonlinear theories of shells is to show how good (or bad) the linear eigenvalue theory of buckling is. It is to be expected that a shell that is heavily reinforced by stringers approximates roughly the behavior of a set of parallel columns. The linear eigenvalue theory of buckling is known to be satisfactory for columns; consequently, it may be expected to determine the buckling load of a shell that derives its strength mainly from stringers. This conjecture is supported by an analysis of buckling of cylindrical stringer-reinforced sheet panels subjected to nonuniform axial compression (1). Cylinders of arbitrary cross-sectional form were considered. A panel was considered to be supported by bulkheads at its ends and by spars along its longitudinal edges. The bulkheads prevented normal and circumferential displacements of the sheet at the ends, whereas only normal displacements were prevented by the spars. Elastic rotational restraints of the bulkhead chord members were taken into account. A panel was considered to be so short that the wave form of a buckled stringer was a single loop. However, several loops were admitted in the wave form of a buckled cross section transverse to the stringers. The analysis was based on the principle that the work of the external forces equals the increment of strain energy when an infinitesimal buckling deformation occurs. The equation $w = w_0 \sin m\xi \sin \eta$ was adopted for the normal displacement due to buckling, where ξ and η are respectively dimensionless circumferential and axial coordinates. Euler's equation of the calculus of variations was used to determine the circumferential displacement u to minimize the buckling load. Results of the theory were compared with experimental data from five box beams having cambered

stringer-reinforced compression surfaces. The beams were subjected to pure bending. Although ideal buckling did not occur, the deflection curves of the test panels relative to the spars showed well-defined knees. In all cases, the computed buckling loads fell nicely on the knees. When the buckling loads were represented by the Euler column formula, the plate-stringer column-fixity factors ranged from 1 to 3. Consequently, the specification of a single constant fixity factor (or reduced column length) for computing allowable compression stresses in cambered plate-stringer panels may be either dangerous or exceedingly conservative.

Another investigation treated the infinitesimal theory of buckling of a circular cylindrical shell reinforced by rings and subjected to uniform external hydrostatic pressure and uniform axial compression (2). The axial compression was considered to be so small that the typical fluted buckling pattern was not impaired. The end plates were considered to be so flexible that no restraints were imposed on the axial displacement u at the ends. The Kirchhoff assumption that radial line elements remain straight and normal to the middle surface was used. Also, the stresses σ_r , $\tau_{r\theta}$, τ_{rx} were neglected. Without loss of generality, the length of the shell was set equal to π . The axial, circumferential, and radial displacements were assumed to be represented respectively by $u = u_0 + x_1 \sin x \cos n\theta$, $v = y_1 \cos x \sin n\theta$, $w = (z_0 + z_1 \cos n\theta) \cos x$. Here the axial coordinate x is measured from the center cross section; u_0 is a function of x , and x_1 , y_1 , z_0 , z_1 are constants. The term $z_0 \cos x$ is an approximation for the deflection before buckling and the other terms represent the infinitesimal deformation that results from buckling. By the calculus of variations, u_0 was chosen to minimize the total potential energy V . The previous equations differ from those adopted by von Mises only by the introduction of u_0 . After elimination of u_0 , V was approximated as a cubic polynomial in the generalized coordinates x_1 , y_1 , z_0 , z_1 ; this degree of approximation is adequate for the infinitesimal theory of buckling, since higher degree terms would introduce nonlinear forms in x_1 , y_1 , z_0 , z_1 into the second variation of V . The second variation of V is a quadratic form in the virtual increments of the generalized coordinates x_1 , y_1 , z_0 , z_1 ; the buckling criterion is that the determinant of the coefficients in this quadratic form be zero.

Results of the analysis agree very well with von Mises' theory if the ratio of length to radius L/a is greater than 1. However, if $L/a < 1$, the computed buckling pressures for unreinforced shells are considerably less than those given by von Mises' theory; in some cases the difference is as great as 25%. In the range $L/a < 1$ the infinitesimal theory has been reported to give buckling pressures larger than the experimental values; consequently, from a practical standpoint, the new theory introduces an improvement. A comparison with test data for a machined ring-reinforced cylindrical shell also shows better agreement with the new theory than with other infinitesimal theories of buckling of perfect shells. The results suggest that discrepancies between theory and experiment for buckling of hydrostatically loaded cylindrical shells may derive partly from inadmissible mathematical approximations in the infinitesimal theories, rather than from weak stability preceding

snap-through. The reason for the lowered buckling pressure given by the new theory is not easy to trace, since other investigators have not approached the problem by way of the second variation of potential energy. It is hoped that further investigations will disclose the cause of the difference.

SNAP-THROUGH OF HYDROSTATICALLY LOADED CYLINDRICAL SHELLS.

Despite the fact that the infinitesimal theory of buckling yields results in fair agreement with tests of cylindrical shells subjected to external hydrostatic pressure, snap-through is a definite possibility. This fact is disclosed by some theoretical studies of post-buckling behavior of unreinforced elastic cylindrical shells loaded by external normal pressure (3). The analysis was based on the principle of minimum potential energy. When the Ritz method is used in this type of analysis, it is imperative that the assumed deflection pattern shall not impose excessive membrane strains, for then the membrane strain energy is far too large. Approximations concerning the strain energy of bending may be rather rough, but the membrane strain energy is a delicate matter. As Lord Rayleigh remarked, "We can bend a piece of sheet metal easily with our fingers, but we can not stretch it noticeably."

The displacement pattern due to buckling was assumed to be represented by $u = u_0 + u_1 \cos n\theta + u_2 \cos 2n\theta + u_3 \cos 3n\theta$, $v = v_1 \sin n\theta + v_2 \sin 2n\theta + v_3 \sin 3n\theta$, $w = w_0 + w_1 \cos n\theta + w_2 \cos 2n\theta + w_3 \cos 3n\theta$, where u , v , w are axial, circumferential, and radial displacement components of the middle surface. The coefficients u_i , v_i , w_i are functions of x . Excessive membrane strains were avoided by the assumption that there is no increment of the membrane hoop strain ϵ_θ caused by buckling. This assumption undoubtedly causes ϵ_x to be too large in some regions, and it consequently leads to Euler buckling pressures that are too large in the case of short thick shells. However, it yields a comparatively simple theory that readily provides numerical results. The assumption $\Delta\epsilon_\theta = 0$ leads to explicit formulas for v_1 , v_2 , v_3 , w_0 , w_2 , w_3 , in terms of w_1 . After the strain energy was linearized in u , the functions u_0 , u_1 , u_2 , u_3 were obtained with the aid of Euler's equation of the calculus of variations so that the potential energy V was minimized. Observations of buckled shells usually enable us to estimate approximate functions for w quite accurately, but much greater difficulties are encountered with u and v . Consequently, it is desirable to determine u and v by means of the exact formulas of the calculus of variations, rather than by the Rayleigh-Ritz procedure, whenever possible.

The remaining unknown function w_1 was assumed to be given by $w_1 = (W_0 \cos \pi x/L) / (n - \frac{1}{n})$ where W_0 is a constant and n is the number of waves in the cross section of the buckled cylinder. Thus, the shell was effectively reduced to a system with one degree of freedom, the generalized coordinate being W_0 . The results exhibit the typical snap-through behavior. Figure 1 illustrates qualitatively the nature of the load-deflection curves that were derived. The falling part of the curve (dotted in Fig. 1) represents unstable equilibrium configurations. Also, the continuation of line OE (dotted) represents unstable unbuckled configurations. Actually, the shell snaps from some configuration A to another configuration B, as indicated

by the dashed line. Theoretically, point A coincides with the Euler critical pressure E , but initial imperfections, residual stresses, or accidental shocks may prevent the shell from reaching point E. In any case, point A is higher than the minimum point C. The pressure at point C is the smallest pressure at which a buckled form can persist; when the pressure drops below this value, the shell snaps back to the unbuckled form.

An analysis of the post-buckling behavior of a structure determines the buckling load automatically. For example, an analysis of the form of a buckled column reveals that there is no real nonzero solution unless the load exceeds a certain value, the Euler critical load. Accordingly, in principle, the nonlinear theory of equilibrium eliminates the need for a special theory of buckling. However, in practice, it is usually easier to determine the Euler buckling load of a structure by solving a linear eigenvalue problem than by determining a bifurcated curve in configuration space that represents all equilibrium configurations.

Since the shell was reduced to a system with a single degree of freedom the theory provides an equation which expresses the increment of potential energy ΔV due to buckling as a function of the deflection parameter W_0 . Thus, for any given value of the external pressure p , a curve of ΔV versus W_0 may be plotted. The forms of the graphs corresponding to several values of p are illustrated by Fig. 2. The pressures indicated on the curves are such that $p_1 < p_2 < p_3 < p_4$. The minima on the curves represent configurations of stable equilibrium, and the maxima represent configurations of unstable equilibrium. If $p < p_4$, the unbuckled state is stable, since the configuration $W_0 = 0$ then provides a relative minimum to the potential energy. However, if $p \geq p_4$, the unbuckled state becomes a configuration of maximum potential energy; hence, it is unstable. Accordingly, p_4 is the Euler critical pressure. The curve corresponding to p_1 has an inflection point at which the tangent is horizontal; hence, p_1 corresponds to point C on Fig. 1; it is the smallest pressure at which a buckled form can persist. For any pressure greater than p_1 there is a state of minimum potential energy with $W_0 > 0$; hence snap-through is possible. Let us take, for example, the curve corresponding to p_2 , for which the value of ΔV at the minimum is zero. In other words, for $p = p_2$, the potential energies of the buckled and unbuckled configurations are equal. Tsien suggested that this condition be taken as a criterion for buckling; accordingly, p_2 may be called the Tsien critical pressure. The maximum on the curve for p_2 represents a potential energy barrier that the shell must cross to reach the buckled form. If this maximum is high, there is little danger of snap-through, since a large amount of external work must be provided to carry the shell "over the hump." However, if the potential-energy hill is low, snap-through is imminent. Of course, this argument is not linked to the Tsien hypothesis; it applies for any of the curves in the range $p_1 < p < p_4$. It appears that the snap-through theory of ideal shells would be enhanced by further studies of the potential-energy barriers separating the buckled and unbuckled forms. Such studies might enable us to evade the extremely complicated problems of initially dented shells, since accidental shocks may be used as a criterion for design instead of initial dents or out-of-roundness. If

anticipated shocks will not provide enough energy to carry a shell over the hill to the buckled form, the design may be considered to be safe.

One numerical calculation was performed for a shell with $L/a = 0.60$, $a/h = 1000$, $E = 30,000,000 \text{ lb/in.}^2$, $a = 20 \text{ in.}$, where L is the length of the shell, a is the radius, and h is the thickness. It was found that, with the pressure equal to the Tsien critical value, 0.23 ft lb of work would carry the shell over the hill to the buckled form. Since this small amount of work might easily come from accidental disturbances, we see why the Euler critical pressure is practically unattainable in some cases.

Another interesting conclusion arose from a study of end constraints. In all cases, the end plates were considered to provide simple support to the cylindrical wall, so that the bending moment M_x vanished at the ends. Also, the end plates imposed the boundary conditions $\bar{v} = w = 0$. However, with regard to the axial displacement u , two different conditions were considered. In one case, the end plates were free to warp, so that no restraints were imposed on u at the ends. In the second case, the end plates were rigid, so that u had a constant value at either end. Surprisingly, the constraint imposed upon u by a rigid end plate raised the buckling pressure significantly. In general, the number n of waves in the periphery of a buckled cylinder is greater for rigid end plates than for flexible end plates. The results are illustrated by Fig. 3, which shows computed load-deflection curves for $a/h = 100$ with both flexible and rigid end plates. Besides the pressure p on the lateral surface, the cylinder was subjected to an axial compression force $F = \pi a^2 p$, which would result from uniform hydrostatic pressure on the end plates. Instead of the pressure p , the ordinate in Fig. 3 is a dimensionless coefficient K , defined by $p = K E h/a$. The Euler critical pressures represented by the intercepts of the curves with the K -axis in Fig. 3 are too high, since the present theory employed the assumption $\Delta\epsilon_\theta = 0$. The improved infinitesimal theory of buckling (2), discussed earlier, yields Euler critical pressures that are considerably lower for short shells, and therefore the effect of snap-through would not be so pronounced as one might infer from the steep curves in Fig. 3.

A generalization of the nonlinear theory of Ref. 3 has been given by the authors. (4). In this generalization, the shell was reduced to a system of 21 degrees of freedom. However, it was found unfeasible to handle the nonlinear equilibrium problem for a system with 21 degrees of freedom. Consequently, for the numerical work, some higher harmonics were discarded so that the system was reduced to 7 degrees of freedom. Calculations were confined principally to the determination of the minimum point C on the post-buckling curve (Fig. 1), that is, to the determination of the pressure at which a buckled form can exist. It was found that the ordinate of point C , as determined in (3), was somewhat too high. The numerical studies indicated that the theory of (4) may be used effectively with an electronic digital computer. However, for cursory studies of post-buckling behavior, the theory and the tables of (3) are recommended.

BUCKLING OF UNREINFORCED PRESSURIZED CYLINDRICAL SHELLS SUBJECTED TO AXIAL COMPRESSION

The strain-energy formulas developed in (3) apply without modification for a cylindrical shell that is subjected to internal pressure and uniform axial compression. Again, a snap-through condition is anticipated.

In an analysis of post-buckling behavior of an axially compressed cylindrical shell (5), the strain formulas are linearized in the axial displacement u . For the time being, consideration of end effects is avoided by the supposition that the shell is infinitely long. Then, as is well known, the buckling pattern consists of diamond-shaped lobes (Fig. 4). This pattern signifies that the radial deflection w is doubly periodic, with its fundamental region in the form of a rhombus. In any rhombus (e.g., the cross-hatched rhombus in Fig. 4), the function w assumes all its values; the function is merely duplicated in any other rhombus. A rhombus subtends the angle 2β from the axis of the cylinder; hence, $\beta = \pi/n$, where n is an integer representing the number of rhombuses in the circumference of the cylinder. The function w is symmetrical about the diagonals of a rhombus. Consequently, if the origin of the (x, θ) plane is taken at the center of a rhombus, the function w is even in x and θ (Fig. 4).

The rhomboidal pattern and the associated symmetry properties of u , v , w require that these functions be represented by series of the following forms* if the origin for x and θ is taken at the center of a rhombus:

$$u = c_0 + c_1 x + \sum_{i=0}^{\infty} \sum_{j=1}^{\infty} a_{ij} \cos i\theta \sin \frac{j\pi x}{\lambda}, \quad a_{ij} = 0 \text{ if } i+j \text{ is odd}$$

$$v = \sum_{i=1}^{\infty} \sum_{j=0}^{\infty} b_{ij} \sin i\theta \cos \frac{j\pi x}{\lambda}, \quad b_{ij} = 0 \text{ if } i+j \text{ is odd}$$

$$w = \sum_{i=0}^{\infty} \sum_{j=0}^{\infty} c_{ij} \cos i\theta \cos \frac{j\pi x}{\lambda}, \quad c_{ij} = 0 \text{ if } i+j \text{ is odd}$$

Here c_0 , c_1 , a_{ij} , b_{ij} , c_{ij} are constants, and λ is half the length of a diagonal of a rhombus in the x -direction (Fig. 4). Writing these equations in expanded form as far as second harmonics, we obtain

$$u = c + u_0 x + u_1 \cos n\theta \sin \frac{\pi x}{\lambda} + u_2 \sin \frac{2\pi x}{\lambda} + u_3 \cos 2n\theta \sin \frac{2\pi x}{\lambda}$$

$$v = v_0 \sin n\theta \cos \frac{\pi x}{\lambda} + v_1 \sin 2n\theta + v_2 \sin 2n\theta \cos \frac{2\pi x}{\lambda}$$

* By error, some additional terms were included in the formula for u in Ref. 5.

$$w = w_0 + w_1 \cos n\theta \cos \frac{\pi x}{\lambda} + w_2 \cos \frac{2\pi x}{\lambda} + w_3 \cos 2n\theta + w_4 \cos 2n\theta \cos \frac{2\pi x}{\lambda}$$

The coefficients u_i , v_i , w_i are constants. The additive constant c is irrelevant, since it represents a translation.

The preceding equations were developed for a shell of infinite length. Experiments indicate that the number of half waves in the length of a finite shell is an integer. Therefore, the length L of the shell is assumed to be a multiple of λ ; that is, $\lambda = L/m$, where m is an integer. To satisfy the boundary conditions $v = w = 0$ at the ends $x = 0$ and $x = L$, the factor $\sin \pi x/L$ was introduced in the formulas for v and w in the last equations. The formula for u is unchanged if the end plates are flexible.

The preceding equations are somewhat more general than the buckling patterns that have been used to study this problem. For correlation with the buckling patterns assumed by some other investigators, a translation of the origin from the center of a rhombus to the midpoint of an edge of a rhombus may be required. In studying the infinitesimal theory of buckling, Timoshenko discarded all terms except u_1 , v_0 , w_1 . Von Karman and Tsien adopted a function w that is equivalent to the preceding if $w_4 = 0$ and $w_2 = w_3$. Donnell and Wan concluded that the relation $w_2 = w_3$ is not plausible on the basis of observed buckling patterns.

If all coefficients are retained in the expansion to second harmonics, there are 12 degrees of freedom. It is highly desirable to retain all 12 of these generalized coordinates, but the problem of minimization of the potential energy then becomes exceedingly complicated. A part of the trouble lies in the quadratic terms in v in the strain-displacement relations. Kempner and other investigators have neglected this quadratic term, and workable results have been obtained.

SLENDER CIRCULAR CYLINDERS (RINGS)

Since Levy (6) first published his classical theory on the buckling of rings, several theories on the buckling of rings and cylinders have appeared. Levy obtained the result

$$P_{cr} = K_{cr} EI/r_0^3, \quad K_{cr} = 3$$

as the critical pressure for a uniformly loaded ring, where r_0 is the radius of the centroidal axis, I is the moment of inertia of the cross section and E is the modulus of elasticity of the material. Levy did not consider the effects of ring thickness h and of Poisson's ratio ν . The load was considered to remain normal to the ring surface throughout the deformation process. In 1914, R. v. Mises (7) starting with the general differential equations of equilibrium and considering only linear terms in the strain tensor, developed a theory which yielded a buckling pressure of $3 Eh^3 / (1 - \nu^2) r_0^3$ for the uniformly loaded infinitely long circular cylinder. In 1933, Donnell (8), by making several simplifications of the general shell equations, arrived at a theory for the buckling of thin cylindrical shells. For the infinitely long circular cylinder (for which Donnell's theory is not strictly valid), Donnell's

theory predicts a critical pressure of $4Eh^3 / (1 - \nu^2) r_0^3$. The theoretical result that is generally accepted for a long circular cylinder is $3Eh^3 / (1 - \nu^2) r_0^3$ (provided the load remains directed perpendicular to the cylinder's surface).

Several authors have noted that the critical pressure depends strongly upon the post-buckling direction of the load (9, 10, 11). For example, for a ring subjected to a uniform pressure that remains directed toward the center of the ring $K_{cr} = 4.5$, (9), and if the load remains constant in direction $K_{cr} = 4$ (11). The effects of ring thickness h and of Poisson's ratio upon p_{cr} for uniformly loaded rings have been studied in (9), the general result being a decrease in K_{cr} with an increase in h . The sway buckling of a semi-circular arch loaded by vertical point load P at the midsection of the arch has been studied in (12), where the result $P_{cr} = 6.54 EI / r_0^2$ was obtained. The sway buckling of a semi-circular arch loaded by vertical inertia forces (or by dead weight of the arch) has been discussed in (13), where it was shown that $w_{cr} = 2.68 EI / r_0^3$, where $w_{cr} = \rho a$, ρ = mass density per unit length of arc and a = vertical acceleration of the supports of the arch. The problem of stability and large deflection of rings, including the effects of ring thickness and of Poisson's ratio, subjected to nonuniform loads is relatively unexplored.

EQUILIBRIUM APPROACH TO THE NONLINEAR THEORY OF SHELLS

The middle surface of any shell is defined by $\bar{r} = \bar{r}(x, y)$, where \bar{r} is a position vector and (x, y) are parameters called "surface coordinates." Attention will here be restricted to orthogonal surface coordinates. Then, since the derivative vectors \bar{r}_x and \bar{r}_y are tangent respectively to the x and y coordinate lines, $\bar{r}_x \cdot \bar{r}_y = 0$. In this case, the distance ds between neighboring points on the middle surface S is given by

$$ds^2 = A^2 dx^2 + B^2 dy^2 \quad (1)$$

where $A^2 = \bar{r}_x \cdot \bar{r}_x$ and $B^2 = \bar{r}_y \cdot \bar{r}_y$. Accordingly, the unit tangent vectors to the x and y coordinate lines are \bar{r}_x/A and \bar{r}_y/B , respectively. The unit normal \hat{n} to the middle surface S is accordingly,

$$\hat{n} = \frac{\bar{r}_x \times \bar{r}_y}{AB} \quad (2)$$

The coefficients of the second differential quadratic form of S are

$$e = \hat{n} \cdot \bar{r}_{xx}, \quad f = \hat{n} \cdot \bar{r}_{xy}, \quad g = \hat{n} \cdot \bar{r}_{yy} \quad (3)$$

If the coordinate lines on S are the lines of principal curvature, $f = 0$, and the principal curvatures of S are $1/r_1 = e/A^2$, $1/r_2 = g/B^2$. However, we shall not make the restriction $f = 0$.

The tensions N_x , N_y , the shears N_{xy} , N_{yx} , Q_x , Q_y , the bending moments M_x , M_y , and the twisting moments M_{xy} , M_{yx} , referred to an element of the middle surface of the shell, are shown with their positive senses in Fig. 5. The normals to the element dS of the middle surface

generate a volume element of the shell. The external force on this element is denoted by $\bar{P} dS = \bar{P} A B dx dy$. This force ordinarily results from the weight of the volume element and from loads applied to the external faces of the shell. The force $\bar{P} dS$ is specified to act at a point in dS . Then there may be an external couple $\bar{L} dS$ that acts on the volume element; usually it results from tangential external distributed loads applied to the faces of the shell. The components of the vectors \bar{P} and \bar{L} in the directions of the orthogonal vectors \bar{r}_x , \bar{r}_y , \hat{n} are denoted by P_x , P_y , P_z and L_x , L_y . The vector \bar{L} has no component in the direction \hat{n} .

The equilibrium equations for the quantities N_x , N_y , etc. may be derived in an elementary manner by Gibbs' vector theory; they were derived more than twenty years ago in tensor form by Synge and Chien. In the present notations, their equilibrium equations are

$$\frac{\partial}{\partial x} (B N_x) + \frac{\partial}{\partial y} (A N_{yx}) + A_y N_{xy} - B_x N_y - \frac{B e}{A} Q_x - f Q_y + A B P_x = 0 \quad (4)$$

$$\frac{\partial}{\partial x} (B N_{xy}) + \frac{\partial}{\partial y} (A N_y) - A_y N_x + B_x N_{yx} - f Q_x - \frac{A g}{B} Q_y + A B P_y = 0 \quad (5)$$

$$\frac{\partial}{\partial x} (B Q_x) + \frac{\partial}{\partial y} (A Q_y) + \frac{B e}{A} N_x + \frac{A g}{B} N_y + (N_{xy} + N_{yx}) f + A B P_z = 0 \quad (6)$$

$$\frac{\partial}{\partial x} (B M_x) + \frac{\partial}{\partial y} (A M_{yx}) + A_y M_{xy} - B_x M_y + A B L_y = A B Q_x \quad (7)$$

$$\frac{\partial}{\partial x} (B M_{xy}) + \frac{\partial}{\partial y} (A M_y) - A_y M_x + B_x M_{yx} - A B L_x = A B Q_y \quad (8)$$

$$N_{xy} - N_{yx} - \frac{e}{A^2} M_{xy} + \frac{f}{A B} (M_x - M_y) + \frac{g}{B^2} M_{yx} = 0 \quad (9)$$

Equations (7) and (8) may be used to eliminate Q_x and Q_y from Eq. (6); thus, the moment equilibrium equation is obtained. The shears Q_x and Q_y are usually discarded from Eqs. (4) and (5), since they are small compared to N_x , N_y , N_{xy} . Furthermore, the terms Q_x and Q_y that occur in Eqs. (4) and (5) represent only components of the transverse shears tangent to surface S which arise because the volume element is slightly tapered. For a flat plate, these terms drop from Eqs. (4) and (5) automatically, since then $e = f = g = 0$. Also, the approximations $N_{xy} = N_{yx}$ and $M_{xy} = M_{yx}$ are nearly always legitimate; they are exactly true for a flat plate. When the approximation $N_{xy} = N_{yx}$ is used, Eq. (9) is disregarded.

The weight of the material often contributes to the tangential loads (P_x , P_y), but frequently the effect of the weight on the stresses is negligible. Then, if no tangential distributed loads are applied to the exterior faces of the shell, the terms (P_x , P_y) are practically zero. In this case, if the terms Q_x and Q_y are discarded from Eqs. (4) and (5), and if the approximation $N_{xy} = N_{yx}$ is introduced, the general solution of Eqs. (4) and (5) may be expressed as follows in terms of a generalized Airy stress function $H(x, y)$ for the case in

which the Gaussian curvature K of surface S is constant (14):

$$\begin{aligned} N_x &= B^{-2} H_{yy} + A^{-2} B^{-1} B_x H_x - B^{-3} B_y H_y + K H \\ N_y &= A^{-2} H_{xx} - A^{-3} A_x H_x + A^{-1} B^{-2} A_y H_y + K H \\ N_{xy} &= N_{yx} = -A^{-1} B^{-1} H_{xy} + A^{-2} B^{-1} A_y H_x + A^{-1} B^{-2} B_x H_y \end{aligned} \quad (10)$$

The case $K = \text{constant}$, to which Eq. (10) is restricted, includes flat plates, spheres, cylinders, and cones, as well as many less common surfaces. For example, any surface that can be obtained by bending a thin flat piece of sheet metal or a piece of a thin spherical shell without stretching it has constant K , since the Gaussian curvature is a bending invariant. There are also surfaces of constant negative Gaussian curvature, called pseudospheres. For flat plates, $K = 0$, and H is a generalized Airy stress function that is applicable to any orthogonal coordinates in the middle plane of the plate.

The equilibrium equations naturally refer to the stressed state. Sometimes the deformation caused by stressing alters the geometry of the shell appreciably. For example, a plate that is initially flat becomes a curved shell when it is loaded, and the curvature may have important effects on the equilibrium conditions. Likewise, a shell that is initially rotationally symmetric may lose its symmetry because of elastic or plastic deformations. Accordingly, if (e, f, g) are the components of the curvature tensor of the undeformed reference surface S , some modifications of these coefficients may be required to account for the effects of the deformation on the equilibrium conditions. This is always true in problems of post-buckling behavior.

When the shell is deformed, the reference surface S passes into another surface S^* . The asterisk or star will be used generally to denote the stressed state. The displacement vector of S is denoted by $\bar{q}(x, y)$; that is, the point \bar{R} on S^* corresponding to point \bar{r} on S is $\bar{R} = \bar{r} + \bar{q}$. Evidently, if the vector function $\bar{q}(x, y)$ is known, the position vector \bar{R} is a known function of (x, y) . Thus, the same coordinates (x, y) serve for surfaces S and S^* . The metric coefficients of S^* are $E^* = \bar{R}_x \cdot \bar{R}_x$, $F^* = \bar{R}_x \cdot \bar{R}_y$, $G^* = \bar{R}_y \cdot \bar{R}_y$. The distance between two neighboring points on S^* is determined by $(ds^*)^2 = E^* dx^2 + 2 F^* dx dy + G^* dy^2$. If surface S is bent without straining, $E^* = A^2$, $F^* = 0$, $G^* = B^2$, since $ds = ds^*$. If the strains of surface S are small, as usually happens, ds is very nearly equal to ds^* . Consequently, even in the large-deflection theories of shells, changes of A and B caused by straining of surface S need not be taken into account in the equilibrium equations. Seemingly, this approximation is not generally appreciated, for some of the modern investigations of buckling of shells introduce undue complications into the equilibrium equations as a consequence of incremental changes in the metric coefficients due to straining. In particular, if the coordinates (x, y) on S are orthogonal, as is here assumed they are orthogonal on S^* too, for the equation $F = 0$ signifies that F^* is nearly zero. Since the Gaussian curvature K and the Christoffel symbols Γ_{jk}^i

are determined by the metric tensor alone, they may also be considered to be unaffected by the deformation, insofar as the equilibrium are concerned. However, in nonlinear theories of shells, the quantities (e, f, g) must be replaced by the corresponding quantities (e^*, f^*, g^*) in Eq. (6). It is not important to make this change in Eqs. (4) and (5), since the terms Q_x and Q_y are ordinarily dropped from these equations anyway.

The components of the displacement vector \mathbf{u} in the directions of the vectors $\mathbf{e}_x, \mathbf{e}_y, \mathbf{n}$ are denoted by (u, v, w) , respectively. The effects of the tangential displacements (u, v) on the changes of curvature are usually small. Consequently, for computation of e^*, f^*, g^* , the equation $\mathbf{R} = \mathbf{r} + \mathbf{u}$ is approximated by $\mathbf{R} = \mathbf{r} + \mathbf{n} w$. The curvature tensor for S^* is $e^* = \mathbf{n}^* \cdot \mathbf{R}_{xx}$, $f^* = \mathbf{n}^* \cdot \mathbf{R}_{xy}$, $g^* = \mathbf{n}^* \cdot \mathbf{R}_{yy}$. The following notations are introduced:

$$K_x = e^* - e, \quad K_y = g^* - g, \quad K_{xy} = f^* - f \quad (11)$$

It is a routine problem of differential geometry to derive K_x, K_y, K_{xy} . The results have been obtained by Koiter, with (u, v) terms included (15). Dropping the (u, v) terms, we get

$$K_x = -\frac{A_x}{A} w_x + \frac{A_y}{B^2} w_y + w_{xx}, \quad K_y = \frac{B_x}{A^2} w_x - \frac{B_y}{B} w_y + w_{yy}$$

$$K_{xy} = -\frac{A_y}{A} w_x - \frac{B_x}{B} w_y + w_{xy} \quad (12)$$

These equations are merely first-degree approximations; nonlinear terms in derivatives of w have been neglected. Also, a linear undifferentiated w -term has been dropped. This term may be interpreted by considering the case, $w = \text{constant}$. For example, if w is constant for a circular cylindrical shell, there is a small change of curvature because the radius is changed. However, since A, B have been retained instead of E^*, F^*, G^* , it would be inconsistent to retain the undifferentiated w -term, since the effect of this term is about the same as effects of changes of the metric tensor due to straining of surface S .

Equations (11) and (12) determine the quantities (e^*, f^*, g^*) that are to be introduced into Eq. (6) instead of (e, f, g) when large deflections or buckling problems are considered. To obtain this generalization, the term f must be retained in Eq. (6), for, even though coordinates are chosen so that $f = 0$, f^* is not generally zero. In other words, in nonlinear theories, the lines of principal curvature on S are altered significantly by the deformation. For example, for a flat plate referred to rectangular coordinates, $A = B = 1$ and $e = f = g = 0$. Equations (11) and (12) give $e^* = w_{xx}$, $f^* = w_{xy}$, $g^* = w_{yy}$. Introducing these quantities into Eq. (6) instead of (e, f, g) , supposing that $L_x = L_y = 0$, and eliminating Q_x and Q_y by means of Eqs. (7) and (8), we obtain a well-known equation in the theory of buckling of flat plates:

$$\frac{\partial^2 M_x}{\partial x^2} + 2 \frac{\partial^2 M_{xy}}{\partial x \partial y} + \frac{\partial^2 M_y}{\partial y^2} + N_x w_{xx} + N_y w_{yy} + 2 N_{xy} w_{xy} + P_z = 0$$

STRAINS OF A SURFACE

The strains of surface S due to the displacement vector (u, v, w) have been derived by Love and many others. If only quadratic terms in w_x, w_y are retained, these equations are

$$\begin{aligned} \epsilon_x &= \frac{u_x}{A} + \frac{A_y v}{A B} - \frac{e w}{A^2} + \frac{w_x^2}{2 A^2}, & \epsilon_y &= \frac{v_y}{B} + \frac{B_x u}{A B} - \frac{g w}{B^2} + \frac{w_y^2}{2 B^2} \\ \gamma_{xy} &= \frac{u_y}{B} + \frac{v_x}{A} - \frac{A_y u}{A B} - \frac{B_x v}{A B} - \frac{2 f w}{A B} + \frac{w_x w_y}{A B} \end{aligned} \quad (13)$$

The metric tensor of the deformed surface S^* is given by $E^* = A^2 (1 + 2\epsilon_x)$, $G^* = B^2 (1 + 2\epsilon_y)$, $F^* = A B \gamma_{xy}$. Since, by differential geometry, the Gaussian curvature K^* of surface S^* can be expressed in terms of E^* , F^* , G^* alone, the increment of K due to the deformation can accordingly be expressed in terms of $\epsilon_x, \epsilon_y, \gamma_{xy}$. The result of this calculation is

$$\begin{aligned} A B (K^* - K) &= \frac{\partial^2 \gamma_{xy}}{\partial x \partial y} - \frac{A}{B} \frac{\partial^2 \epsilon_x}{\partial y^2} - \frac{B}{A} \frac{\partial^2 \epsilon_y}{\partial x^2} + \frac{B_x}{A} \frac{\partial \epsilon_x}{\partial x} + \frac{A_y}{B} \frac{\partial \epsilon_y}{\partial y} \\ &+ \left(\frac{A B_y}{B^2} - \frac{2 A_y}{B} \right) \frac{\partial \epsilon_x}{\partial y} + \left(\frac{B A_x}{A^2} - \frac{2 B_x}{A} \right) \frac{\partial \epsilon_y}{\partial x} + \frac{A_y}{A} \frac{\partial \gamma_{xy}}{\partial x} + \frac{B_x}{B} \frac{\partial \gamma_{xy}}{\partial y} \\ &+ 2 \left(\frac{B_{xx}}{A} - \frac{A_x B_x}{A^2} \right) \epsilon_x + 2 \left(\frac{A_{yy}}{B} - \frac{A_y B_y}{B^2} \right) \epsilon_y \\ &+ \left(\frac{A_{xy}}{A} + \frac{B_{xy}}{B} - \frac{A_x A_y}{A^2} - \frac{B_x B_y}{B^2} \right) \gamma_{xy} \end{aligned} \quad (14)$$

Substituting Eq. (13) into Eq. (14), and simplifying the result with the Gauss and Codazzi equations, we obtain

$$\begin{aligned} A B (K^* - K) &= B K_x u + A K_y v + 2 A B K M w + \frac{1}{A^2 B} \left(-\frac{B B_x e}{A} + 2 A_y f - A_x g \right) w_x \\ &+ \frac{1}{A B^2} \left(-\frac{A A_y g}{B} + 2 B_x f - B_y e \right) w_y + \frac{g}{A B} w_{xx} - \frac{2 f}{A B} w_{xy} + \frac{e}{A B} w_{yy} \end{aligned}$$

$$\begin{aligned}
& -\frac{1}{A^3} \left(\frac{A_x B_x}{A} + \frac{A_y^2}{B} + K A^2 B \right) w_x^2 - \frac{1}{B^3} \left(\frac{A_y B_y}{B} + \frac{B_x^2}{A} + K A B^2 \right) w_y^2 + \frac{B_x}{A^3} w_x w_{xx} \\
& + \frac{2 A_y}{A^2 B} w_x w_{xy} - \frac{A_x}{A^2 B} w_x w_{yy} - \frac{B_y}{A B^2} w_y w_{xx} + \frac{2 B_x}{A B^2} w_y w_{xy} + \frac{A_y}{B^3} w_y w_{yy} \\
& + \frac{w_{xx} w_{yy} - w_{xy}^2}{A B}
\end{aligned} \quad (15)$$

In the linear theory of shells, all nonlinear terms are dropped from Eq. (15). The term M represents the mean curvature of S ; i.e., $2M = 1/r_1 + 1/r_2$.

For brevity, Eqs. (14) and (15) are written as follows: $A B (K^* - K) = L(\epsilon_x, \epsilon_y, \gamma_{xy})$, $A B (K^* - K) = B K_x u + A K_y v + \psi(w)$. These equations yield

$$L(\epsilon_x, \epsilon_y, \gamma_{xy}) = B K_x u + A K_y v + \psi(w) \quad (16)$$

If K is constant, u and v disappear from Eq. (16). Then Eq. (16) is a compatibility equation for the strain components of surface S . If K is not constant, u and v can not be eliminated without the use of differential operators of order greater than 2. For example, if a flat plate is referred to rectangular coordinates, $A = B = 1$ and $e = f = g = K = M = 0$. Then Eq. (16) yields

$$\frac{\partial^2 \gamma_{xy}}{\partial x \partial y} - \frac{\partial^2 \epsilon_x}{\partial y^2} - \frac{\partial^2 \epsilon_y}{\partial x^2} = w_{xx} w_{yy} - w_{xy}^2$$

This is an important equation in the large-deflection theory of plates.

Shell problems may be formulated in terms of the displacement components (u, v, w) or in terms of the stress function and the normal displacement (H, w) . If (u, v, w) are regarded as the unknowns, only the equilibrium equations and the boundary conditions are needed; there is no need to consider compatibility equations. Certainly, this is the more general approach, since the stress function H is limited to shells of constant Gaussian curvature, although a generalization to cover all rotationally symmetric shells is possible (14). Furthermore, the boundary conditions can always be formulated in terms of (u, v, w) , but they can not always be expressed in terms of stresses. The compatibility equation represented by Eq. (16) is useful only for shells of constant Gaussian curvature, since only then do the terms u and v drop out. However, it is only for shells of constant Gaussian curvature that a compatibility equation is needed, since the (u, v, w) formulation will be used for other shells.

Equations (1) to (16) do not involve stress-strain relations and they remain valid if shear deformation is significant. For a complete formulation of the shell problem, we must express (N_x, N_y, N_{xy}) in terms of $(\epsilon_x, \epsilon_y, \gamma_{xy})$ and also (M_x, M_y, M_{xy}) in terms of (K_x, K_y, K_{xy}) . Here, the simplest approximations to adopt are exactly the same as in flat-plate theory. Ques-

tions of nonlinear geometric relations do not enter here, since they arise only in the strain-displacement relations [Eq. (13)]. It is a moot point whether nonlinear terms in (u, v) should be retained in Eq. (13). A rigorous analysis of stress-strain relations and moment-curvature relations, with thermal effects included, was developed on the basis of the Kirchhoff assumption by the authors (16). Some investigators have concluded, on the basis of order-of-magnitude considerations, that, when the Kirchhoff assumption is used, consistency requires that the strains be linearized in the normal coordinate z . However, if this argument is applied to beams, it signifies that the Winkler theory of curved beams is no better than straight-beam theory. A striking example of an error that can be incurred by linearization with respect to z is provided by a curved cantilever beam of rectangular cross section with depth h and width b (Fig. 6). The load P is applied at the centroid of the end section. By Winkler's theory, the stress σ_θ at ordinate z is

$$\sigma_\theta = \frac{P}{bh} + \frac{Pz(1 - \sin \theta)}{b(aC - h)(a + z)}, \quad C = \log \frac{2a + h}{2a - h} \quad (a)$$

The net tension and the bending moment are

$$F = b \int_{-h/2}^{h/2} \sigma_\theta dz, \quad M = b \int_{-h/2}^{h/2} z \sigma_\theta dz \quad (b)$$

Substituting Eq. (a) into Eq. (b), we get $F = P \sin \theta$, $M = Pa(1 - \sin \theta)$. These relations agree with elementary statics. Suppose now that C is replaced by the first two terms in its power series; that is,

$$C = \frac{h}{a} + \frac{h^3}{12a^3}$$

Also, let us drop z from the denominator of Eq. (a), so that the equation is linearized in z . Thus, we get the equation of straight-beam theory:

$$\sigma_\theta = \frac{P}{A} + \frac{Mz}{I}$$

With this value of σ_θ , the net tension calculated by $F = \int_{-h/2}^{h/2} \sigma_\theta dA$ is $F = P$. This relation disagrees grossly with statics.

The sensitivity in this example comes from the fact that the stress σ_θ has a large negative value on the inside of the beam, and a large positive value on the outside. Therefore, σ_θ must be given quite accurately if $\int \sigma_\theta dA$ is to be evaluated correctly. We may conclude that linearization of the stresses or strains with respect to z is usually admissible if the objective is to predict yielding or other types of failure of the material. However, it is a questionable approximation if the stresses are to be integrated through the thickness for the purpose of determining N_x , M_x , etc.

If linearization with respect to z is admissible, we obtain from (7), when temperature terms and nonlinear terms in h are discarded,

$$N_x = \frac{E h}{1 - \nu^2} (\epsilon_x + \nu \epsilon_y), \quad N_y = \frac{E h}{1 - \nu^2} (\epsilon_y + \nu \epsilon_x) \quad (17)$$

$$N_{xy} = N_{yx} = G h \gamma_{xy}$$

where E is Young's modulus, ν is Poisson's ratio, G is the shear modulus, and h is the thickness of the shell. Naturally, these relations are restricted to isotropic elastic shells. Also, if effects of u and v on the bending moments are neglected, we obtain

$$M_x = -D \left[\frac{K_x}{A^2} + \frac{\nu K_y}{B^2} + w k_1 (k_1 - k_2) \right]$$

$$M_y = -D \left[\frac{K_y}{B^2} + \frac{\nu K_x}{A^2} + w k_2 (k_2 - k_1) \right] \quad (18)$$

$$M_{xy} = M_{yx} = -\frac{D(1 - \nu)}{A B} K_{xy}, \quad D = \frac{E h^3}{12(1 - \nu^2)}$$

Here, k_1 and k_2 are the principal curvatures of the middle surface. The quantities K_x , K_y , K_{xy} are defined by Eq. (12). Most writers have dropped w from Eq. (18). However, in some cases, this term has a significant effect on computed buckling loads. For example, if a very long cylindrical shell of radius a is subjected to uniform external pressure, the buckling pressure is $p_{cr} = 3 D/a^3$. This result is obtained if w is retained in Eq. (18), but we get $p_{cr} = 4 D/a^3$ if w is dropped.

Some special applications of the preceding equations have been studied. For example, if w is dropped from Eq. (18), Donnell's equation for cylindrical shells is obtained readily. Also, the equations of Reiss, Greenberg, and Keller for snap-through of a shallow spherical cap are obtained immediately, although in a different form. For flat plates, von Kármán's equations are obtained. By further studies, the authors hope to get a better correlation between the equilibrium approach and the energy approach to problems of buckling and post-buckling.

REFERENCES

1. H. Langhaar, Stability of Semimonocoque Wing Structures, Jour. Aero. Sci., 13, 3, 119-125, Mar., 1946.
2. H. Langhaar and A. Boresi, Buckling of a Cylindrical Shell Subjected to External Pressure, Osterreichisches Ingenieur-Archiv, XIV, 3, 189-203, 1960.
3. H. Langhaar and A. Boresi, Snap-Through and Post-Buckling Behavior of Cylindrical Shells Under the Action of External Pressure, Univ. of Illinois Engineering Exper. Station Bulletin No. 443, vol. 54, no. 59. April, 1957.
4. H. Langhaar and A. Boresi, Buckling and Post-Buckling Behavior of a Cylindrical Shell Subjected to External Pressure, Univ. of Illinois, T. & A. M. Report No. 93, April, 1956.
5. H. Langhaar and A. Boresi, Buckling of Axially Compressed Cylindrical Shells Subjected to Internal Pressure, Univ. of Illinois, T. & A.M. Report No. 121, July, 1957.
6. M. Levy, J. Math pure et appl. (Liouville) series 3, Vol. 10, 1884, p. 5.
7. R. von Mises, Der kritische Aussendruck Zylindrischer Rohre, V.D.I. Zeitschr., Vol. 58, 1914, p. 750.
8. L. H. Donnell, Stability of Thin-Walled Tubes Under Torsion, NACA Rep. 479, 1933.
9. A. Boresi, A Refinement of the Theory of Buckling of Rings Under Uniform Pressure, J. of Appl. Mechs., Vol. 22, No. 1, March, 1955, p. 95.
10. G. W. H. Stevens, The Stability of a Compressed Elastic Ring...., Quart. J. of Mechs and Appl. Math., Vol. 5, pt. 2, June, 1952, p. 221.
11. S. R. Bodner, On the Conservativeness of Various Distributed Force Systems, J. of the Aero. Sciences, Vol. 25, No. 2, Feb., 1958, p. 132.
12. H. Langhaar, A. Boresi, D. Carver, Energy Theory of Buckling of Circular Elastic Rings and Arches, Proc. of Second U. S. Nat. Cong. of Appl. Mechs., 1955, p. 437.
13. G. E. Sliter, Some Nonlinear Problems in Structural Mechanics, M.S. Thesis, Univ. of Illinois, Urbana, Feb., 1962.
14. H. Langhaar, An Invariant Membrane Stress Function for Shells, Jour. App. Mech., 20, 2, June, 1953.
15. Koiter, W. T., A Consistent First Approximation in the General Theory of Thin Elastic Shells, Proc. of Symposium on Theory of Thin Elastic Shells, Delft, Netherlands, Aug., 1959.
16. H. Langhaar and A. Boresi, Strain Energy and Equilibrium of a Shell Subjected to Arbitrary Temperature Distribution, Proc. 3rd U.S. Nat. Congress Appl. Mech., ASME, New York, 1958.

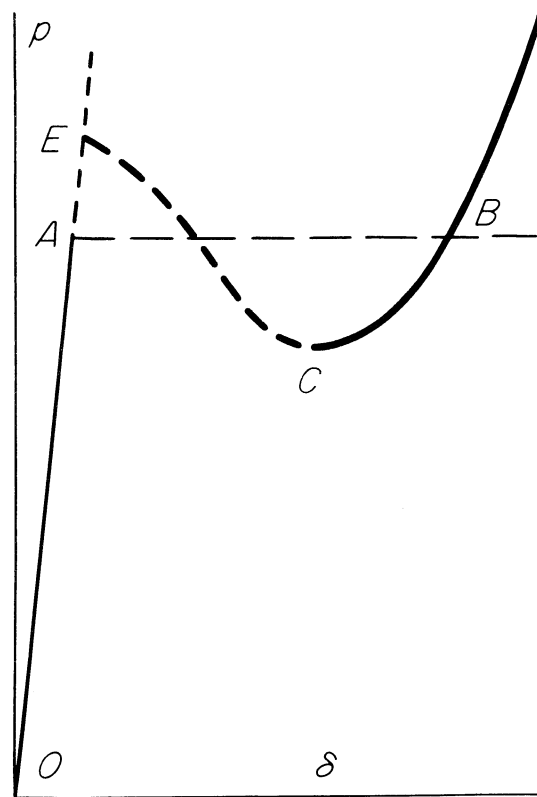


Figure 1.- Pressure-deflection curve.

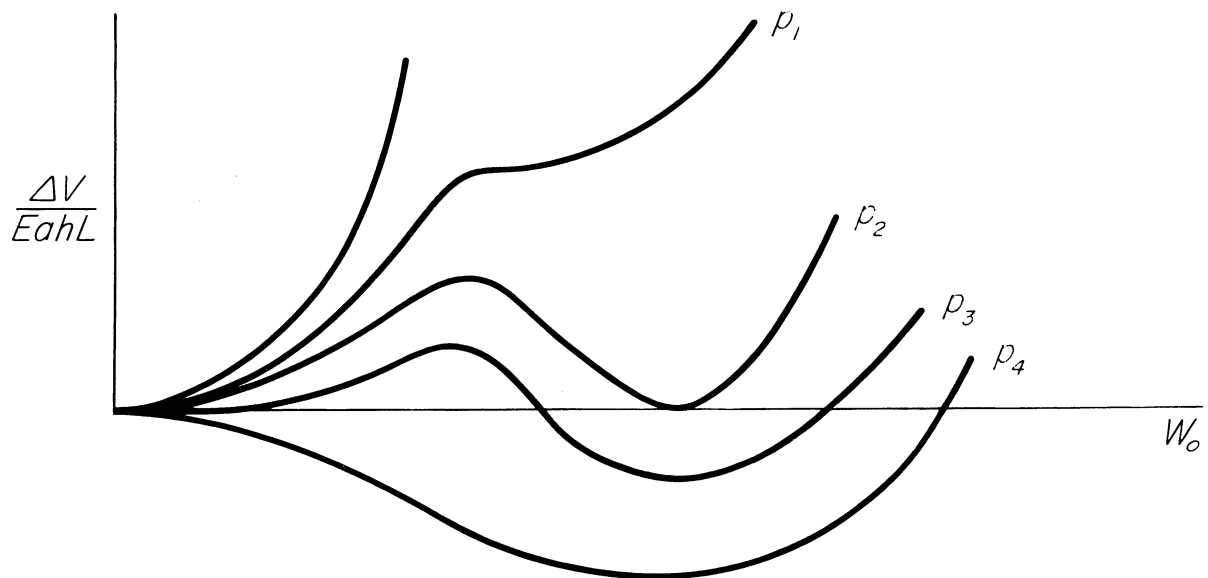


Figure 2.- Increment of potential energy versus deflection parameter.

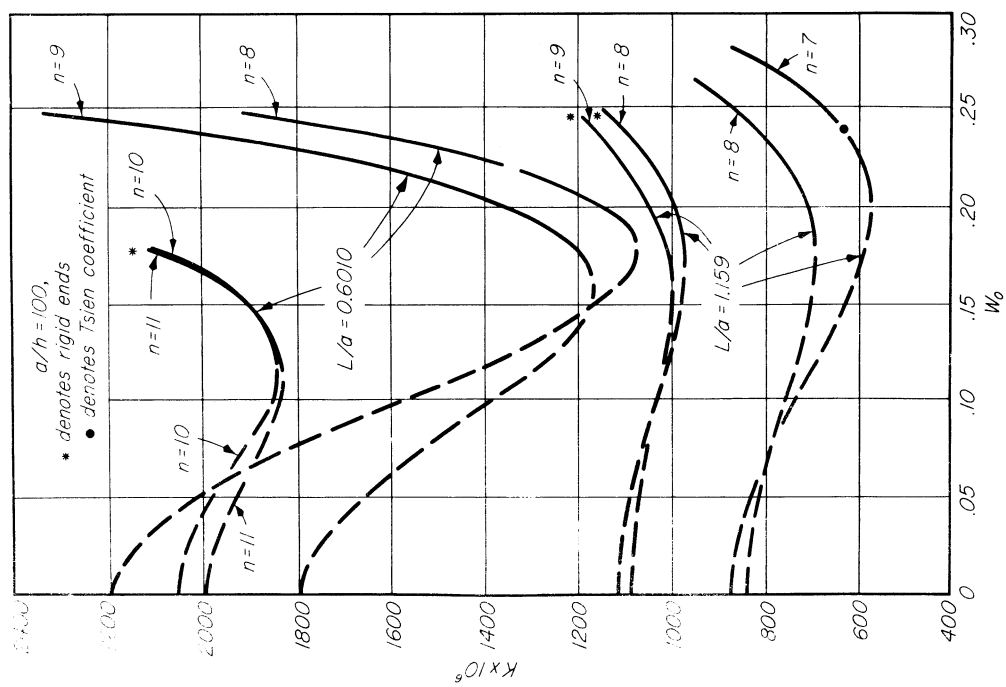


Figure 3.- Buckling coefficient K versus deflection parameter W_0 .

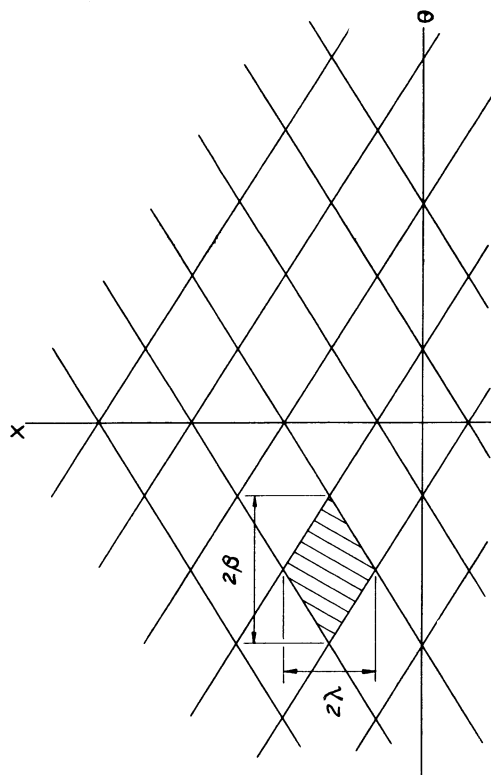


Figure 4.- Deflection pattern.

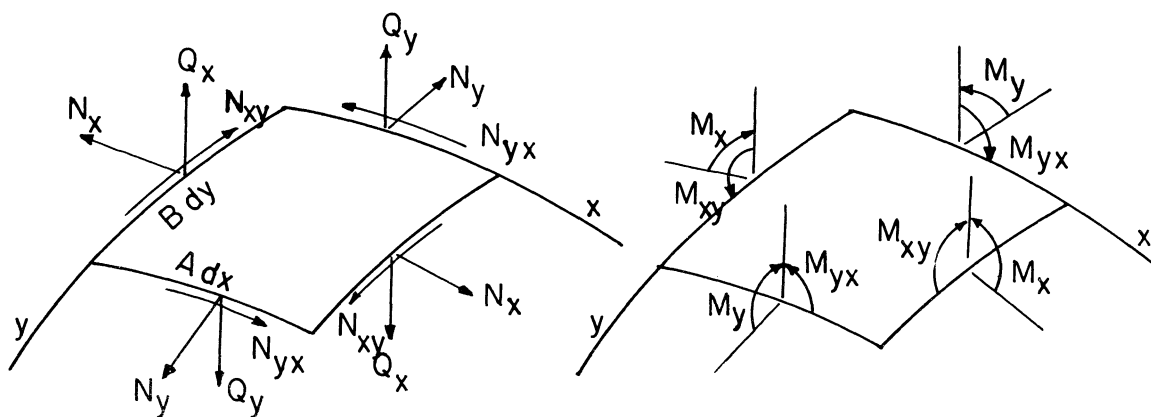


Figure 5.- Notation and sign convention for tractions, bending moments and twisting moments.

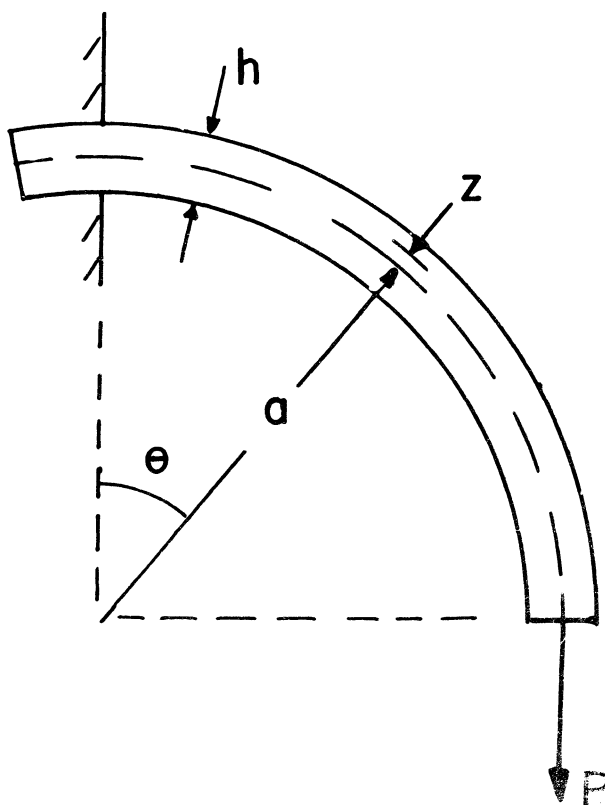


Figure 6.

THE EFFECT OF INITIAL IMPERFECTIONS ON THE BUCKLING STRESS OF CYLINDRICAL SHELLS

By C. D. Babcock and E. E. Sechler

California Institute of Technology

SUMMARY

Techniques have been developed for making essentially "perfect" thin cylindrical shells and for making shells with definite types of initial deformations. The "perfect" shells give buckling stresses much higher than have previously been obtained. Initial deformations of the form $\Delta R = a_0 \sin \frac{\pi x}{L}$ have been tested and ranges of positive a_0 were found in which there was no lowering of the buckling stress. Negative values of a_0 caused a decrease in the failure load. A theoretical solution which indicated the same trends as were found experimentally has been carried out.

INTRODUCTION

Ever since the great disagreement between theory and experiment on the buckling stress of axially compressed cylinders was discovered efforts have been made to determine the cause of this disagreement. One approach was to refine the theoretical analysis to determine 1) whether or not the lowest eigenvalue has been established and 2) whether initial deformations might have an effect on the buckling stress. These studies showed that, if the cylinder was assumed perfect and, if end effects were neglected, the buckling stress was given by $\sigma_{cr} = Et/R \sqrt{3(1 - \mu^2)}$ which, for $\mu = 0.3$ becomes $\sigma_{cr} = 0.605 Et/R$. Secondly, the work of Donnell and others indicated that there was probably a considerable effect from initial deformations. In these studies it was assumed that the initial deformations had essentially the wave form of the post buckling mode and no attempt was made to determine the effect of other types of initial deformations.

The experimental investigations that were carried out were never as good as the theoretical studies. The specimens contained eccentricities and discontinuities from seams and other fabrication techniques, had unknown internal stresses, and the testing methods

in most cases were relatively crude. For example, the actual stress distribution in the specimen was seldom measured during test. For the above reasons it was felt desirable to carry out carefully controlled tests on specimens whose imperfections were accurately known and to correlate the data obtained with new theoretical studies. The work was carried out under NASA research grant no. NsG-18-59.

SYMBOLS

a_o	maximum amplitude of initial deformation, inches
D	plate stiffness = $Et^3/12(1 - \mu^2)$ lb inch
E	Young's modulus, psi
F	stress function defined as $F_{xx} = N_y$, $F_{yy} = N_x$, $F_{xy} = -N_{xy}$
K	buckling stress coefficient in the equation $\sigma_{cr} = KEt/R$
L	length of shell, inches
N_x, N_y, N_{xy}	membrane forces, lb/inch
R	shell radius, inches
ΔR	radial value of initial deformation, inches
t	shell thickness, inches
w	radial displacement of shell, inches
x	axial distance along the shell, inches
y	circumferential distance around shell, inches
μ	Poisson's ratio
σ_{cr}	buckling stress of the shell, psi
Subscripts:	
xx, xy, yy	denote $\partial/\partial x^2, \partial/\partial xy, \partial/\partial y^2$

THE EXPERIMENTAL PROGRAM

The objectives of this program were:

- 1) to develop a method of making cylindrical shells which were as nearly perfect as possible;
- 2) to establish testing techniques in which the stress distribution was controllable and measurable;
- 3) to determine the axial buckling stress of these nearly perfect shells
- 4) to add known imperfections to the shells and determine the effect of these imperfections on the buckling stress; and
- 5) to attempt to isolate the most damaging forms of initial deformations so they could be avoided in manufacture whenever possible.

To date, items 1) through 3) have been completed and some work has been carried out in 4).

The method of manufacturing of the cylindrical shells is not new with GALCIT (see reference 1) but a number of refinements were required in order to obtain the uniformity and accuracy desired. Basically it consisted of plating a copper shell on an accurately machined wax mandrel and then melting the mandrel out of the shell. For a shell 8 inches in diameter and 10 inches long, a steel cylinder 7 inches in diameter and 13 inches long was used as a core (this provided a means of water cooling the wax to harden it). On this core was cast a layer of wax consisting of a two to one mixture of refined paraffin and Mobile Cerese Wax 2305. This was cooled, machined to the proper shape, and sprayed with silver paint thinned with toluene. The plating was done in a Cupric Fluoborate, $\text{Cu}(\text{BF}_4)_2$, bath with a 15 inch diameter copper anode which was bagged in fine mesh Dynel fabric. During plating the mandrel was rotated and the bath was given additional agitation by forcing air through it. Using voltages less than 10 volts and current densities up to 55 amperes per square foot, the plating time was approximately 20 minutes per 0.001 inches of plate.

After plating, the ends of the cylinder were removed (some thickness increase occurred just at the ends), the wax was carefully melted out, and the residual wax and silver paint was removed with benzene. The shell thickness used in this series of tests was approximately 0.0045 inches. The thickness variation in any shell could be held to less than 3 per cent. In the radial direction, the desired radius could be held to $\pm t/2$ or approximately ± 0.0025 inches.

The specimen was mounted (using Cerrobend) to a load measuring ring instrumented with 24 strain gages which gave the stress distribution in the shell. The assembly of specimen and loading ring were then placed in a very stiff, controlled displacement testing machine in which the displacement was controlled by three fine pitch screws (one turn of the screw gave 0.025 inches displacement). These could either be operated together or could be adjusted individually to correct for nonuniformity in stress distribution. See figure 1.

Two types of axially symmetric initial deformations were tested, a sine wave in which $\Delta R = a_o \sin \pi x/L$ and a constant curvature form given by $\Delta R = a_o [2(2x/L) - (2x/L)^2]$. Values of a_o/t ranging from -20 to +45 were tested.

EXPERIMENTAL RESULTS

Figure 2 shows the results of this first test series in which σ_{cr}/σ_c is plotted against a_o/t . These are compared with the Kanemitsu and Nojima value which for the L/R and the R/t corresponding to these specimens gives $K = 0.17$. The following important features can be seen:

1. That with proper care in manufacturing and testing, values of the buckling stresses can be obtained which are much higher than those usually found.
2. That, for the displacement forms tested, small departures from initial straightness lower the buckling stress and that the effect for inward displacements is greater than that for outward displacements.
3. That if the outward displacements are increased the value of the buckling stress again rises until it reaches essentially the same value as that for the initially straight cylinder.
4. That the constant curvature and sine wave shapes give essentially the same values of σ_{cr} for the larger values of a_o/t .

The drop in the value of σ_{cr} for $0 < a_o/t < 10$ and the return to the "perfect" value for $a_o/t > 20$ cannot be explained at this time. Although considerable effort was made to keep the stress uniform around the circumference of the cylinder, variations of ± 10 per cent were common and this probably accounts for some of the scatter

in the experimental results. Since the classical theoretical solutions have assumed edges which were free to expand radially and, since the edges of the present cylinder were rigidly clamped, it may be that the lowering of the value of σ_{cr} below the classical value may be due in part to this fact.

THEORETICAL SOLUTION

The theoretical approach was as follows:

- 1) Determination of the stresses and deflections in the shell that occur during the loading and before buckling.
- 2) Consideration of the stresses and deflections occurring during buckling as small perturbations about step 1) and linearizing the resulting equations.
- 3) Solving the eigenvalue problem obtained in 2) for the minimum eigenvalue.

To simplify the problem, the shallow shell equations of Marguerre (reference 2) were used. These give

$$\nabla^4 F = Et \left[w_{xy}^2 - w_{xx} w_{yy} + 2w_{o_{xy}} w_{xy} - w_{o_{xx}} w_{yy} - w_{xx} w_{o_{yy}} \right] \quad (1)$$

$$D \nabla^4 w = F_{yy} (w_{xx} + w_{o_{xx}}) - 2F_{xy} (w_{xy} + w_{o_{xy}}) + F_{xx} (w_{yy} + w_{o_{yy}}) \quad (2)$$

where w_o is the initial deviation from the flat plate and F is the stress function. For the circular cylindrical shell, w_o is given by $w_o = (y^2 - y^2)/2R$. Using this equation for w_o one arrives at the set of equations originally derived by Donnell and used in his studies of initial imperfections (reference 3). For the initial deformations of the present tests the equation for w_o becomes

$$w_o = \frac{1}{2R} (y^2 - y_o^2) - a_o \sin \frac{\pi x}{L} \quad (3)$$

which when substituted into equations 1 and 2 gives

$$\nabla^4 F = Et \left[w_{xy}^2 - w_{xx} w_{yy} - a_o \left(\frac{\pi}{L} \right)^2 \sin \frac{\pi x}{L} w_{yy} - \frac{1}{R} w_{xx} \right] \quad (4)$$

$$D \nabla^4 w = F_{yy} (w_{xx} + a_o \left(\frac{\pi}{L} \right)^2 \sin \frac{\pi x}{L}) - 2F_{xy} w_{xy} + F_{xx} w_{yy} + \frac{1}{R} F_{xx} \quad (5)$$

Letting F^* and w^* be the solutions of the axially symmetric problem and \bar{F} and \bar{w} be the perturbation values occurring during buckling, we have $F = F^* + \bar{F}$ and $w = w^* + \bar{w}$. Substituting into 4 and 5 and linearizing by neglecting higher order terms one obtains a set of equations in \bar{F} and \bar{w} which can be solved for the eigenvalues. The boundary conditions used were: 1) The ends of the shell are free to expand radially and, while so doing, they are simply supported; 2) for the axially symmetric problem u^* and w^* (deflection in axial and radial directions) must be independent of y and v^* (circumferential displacement) must be zero; 3) Axial motion of the ends of the shell (usually a periodic function in y) is permitted.

Carrying out the remainder of the mathematics leads to the dotted curve shown in figure 2 showing that, for $a_o > 0$ no decrease in buckling stress should occur and that for $a_o < 0$ an appreciable drop in load carrying ability should be observed. Comparing this with the experimental data we find that the trends are correct but that the reduction in σ_{cr} for $a_o < 0$ is actually less than that predicted theoretically. Also, it was found that the number of circumferential waves was higher than the theory predicts and, if the experimental value for this wave number were to be used in the theoretical solution the agreement was better.

FUTURE PROGRAM

The continuation of this program calls for

- 1) An attempt to reduce the scatter in the experimental data by striving for a more uniform axial stress distribution in the shell.
- 2) A detailed study of the effect of the clamped end of the shell on the buckling stress - possibly trying to make a shell with a negative Poisson displacement so that it would be straight at the buckling stress.
- 3) Extension of the experimental program to other forms of initial deformation.
- 4) Consideration of other R/t ratios.
- 5) A more sophisticated theoretical treatment of the problem.

REFERENCES

1. Thompson, J.M.T.: Making of Thin Metal Shells for Model Stress Analysis. Jour. Mech. Eng. Sciences, vol. 2, no. 2, 1960.
2. Marguerre, K.: Zur Theorie der gekrummten Platte grosser Formanderung. Proc. 5th Int. Cong. App. Mech., p. 93, 1938.
3. Donnell, L. H.: A New Theory for the Buckling of Thin Cylinders under Axial Compression and Bending. Trans. of A.S.M.E., vol. 56, p. 795, Nov. 1934.

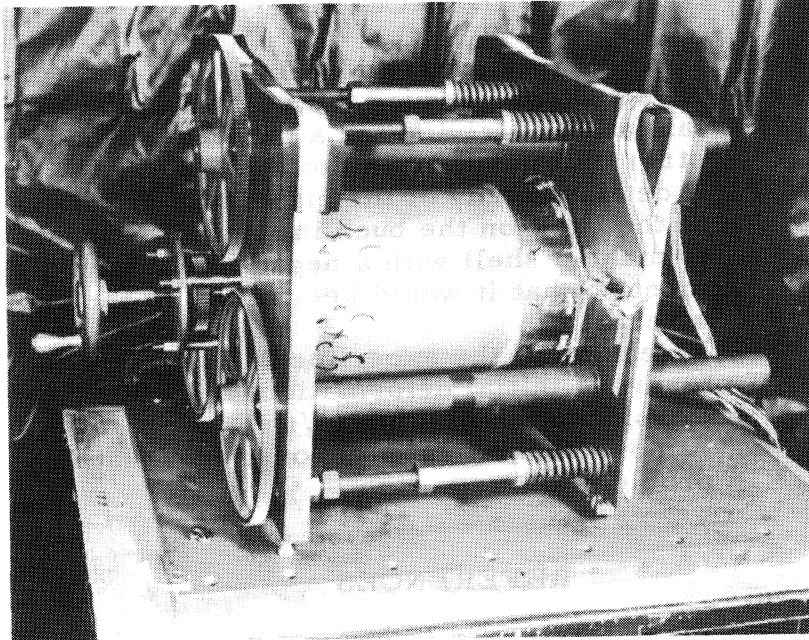


Figure 1.- Testing machine, specimen, and load ring.

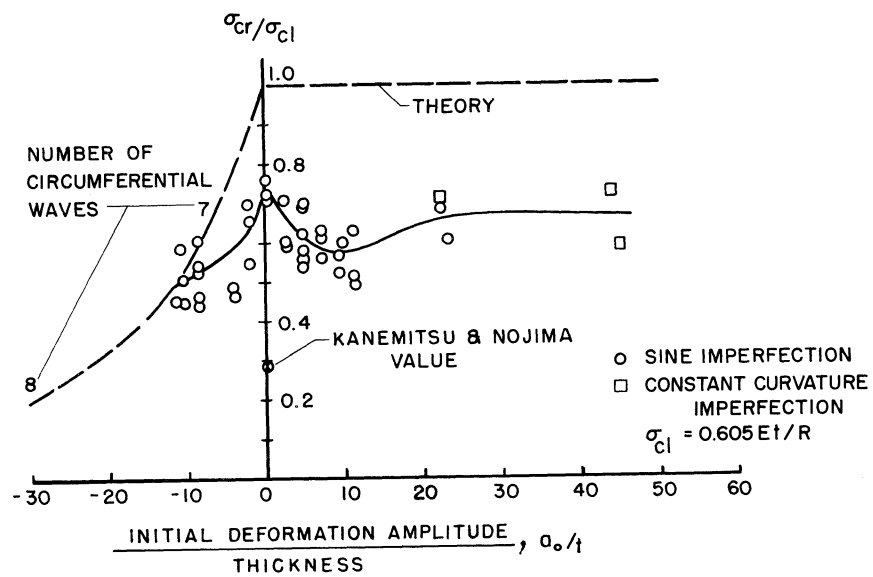


Figure 2.- Buckling stress variation with initial imperfection amplitude.

EFFECTS OF MODES OF INITIAL IMPERFECTIONS
ON THE STABILITY OF CYLINDRICAL
SHELLS UNDER AXIAL COMPRESSION

By L. H. N. Lee

University of Notre Dame

SUMMARY

The effects of definite and "indefinite" initial imperfections on the buckling and postbuckling behavior of an axially compressed cylindrical shell are analyzed by a non-linear theory. The definite initial imperfections considered do not contribute to the reduction of the peak buckling load; while the "indefinite" imperfections, expressed in terms of a single factor introduced by Donnell¹, cause a reduction in the buckling strength. The physical meaning of the imperfection factor, however, needs further clarification. Two theoretical buckling processes are found to be possible. In the early stage of buckling, the cylinder may deform with a comparatively large number of waves of small amplitudes or the cylinder may deform with a comparatively small number of waves of large amplitudes. Further theoretical and experimental studies of the effects of initial imperfections and the process of buckling are suggested.

INTRODUCTION

The problem of elastic buckling of axially compressed cylindrical shells has not yet been completely solved in spite of being the subject of intensive research in recent years. To explain the fact that buckling loads obtained by experiments are much lower than that predicted by the classical linear theory^{2,3}, Donnell (1934) introduced a non-linear theory and the concept of initial imperfections. The non-linear theory was further developed by von Kármán and Tsien (1941)⁴. Their analysis, in turn, was refined by Leggett and Jones (1942)⁵, Michielsen (1948)⁶, and Kempner (1954)⁷.

The non-linear theory does indicate a large drop of resistance as soon as buckling takes place. This is con-

sistent with the observed phenomena. For a conceptually perfect cylinder, however, the buckling load predicted by the non-linear theory is still the same as that given by the classical theory. By considering the effects of initial imperfections, Donnell and Wan⁸ were able to explain in a reasonable way the discrepancies between experimental and theoretical buckling loads. For the convenience of analysis, Donnell assumes that the geometrical and material imperfections of a cylinder may be replaced by an equivalent geometrical deviation. He assumes further that the equivalent geometrical deviation is proportional to the deformation of the cylinder and may be expressed by a single imperfection factor indicating essentially its magnitude. It is the purpose of this paper to evaluate the implication of this assumption.

Timoshenko⁹ has shown, by a linear theory, that the initial curvature of an axially compressed, elastic column has substantial effects on the load-deflection relationship but relatively little effect on the maximum load. The initial shape of the column can be expressed by a series of functions giving the normal buckling mode shapes of the column. According to the linear theory, the term in the series describing the principal buckling mode has the predominant effect on the behavior of the column. In general, an axially compressed column having arbitrary small initial deviation most likely buckles in its principal mode. The assumption made by Donnell and Wan is apparently in accord with this fact. However, it has been shown¹⁰ that the mode as well as the amplitude of the initial imperfections of a geometrically or physically non-linear structure may influence the buckling load and the corresponding mode of buckling. Therefore, the effects of definite initial imperfections as well as "indefinite" initial imperfections, in terms of the imperfection factor introduced by Donnell, on the buckling behavior of axially compressed cylinders are analyzed in this paper.

The present analysis is based on the Love-Kirchoff assumption for thin shells and the principle of stationary potential energy for load-deformation relationships.

ANALYSIS

Strain-Displacement Relationships

Consider an initially imperfect but nearly circular cylindrical shell of mean radius r , length L , and thickness t . Let the radial difference between the radial distance of a point at the initial median surface and the mean radius be denoted by w_0 . Let x , s and z (positive inward) be the axial, circumferential and radial coordinate, respectively. The corresponding components of the displacement of the point, denoted by u , v and w (positive inward) respectively, are measured from the position at the initial median surface. Based on Donnell's assumptions⁸, it may be shown that the bending strains depend only on the axial and circumferential curvature changes, $(\partial^2 w / \partial x^2)$ and $(\partial^2 w / \partial s^2)$, and the twist of the median surface $(\partial^2 w / \partial x \partial s)$. Including the effects of the initial radial deviations and the second order terms, the axial and circumferential membrane strains, ϵ_x and ϵ_s , and the membrane shear strain γ_{xs} , are¹¹

$$\begin{aligned}\epsilon_x &= \frac{\partial u}{\partial x} + \frac{1}{2} \left(\frac{\partial w}{\partial x} \right)^2 + \frac{\partial w}{\partial x} \frac{\partial w_0}{\partial x} \\ \epsilon_s &= \frac{\partial v}{\partial s} + \frac{1}{2} \left(\frac{\partial w}{\partial s} \right)^2 + \frac{\partial w}{\partial s} \frac{\partial w_0}{\partial s} - \frac{w}{r} \\ \gamma_{xs} &= \frac{\partial u}{\partial s} + \frac{\partial v}{\partial x} + \frac{\partial w}{\partial x} \frac{\partial w}{\partial s} + \frac{\partial w}{\partial x} \frac{\partial w_0}{\partial s} + \frac{\partial w_0}{\partial x} \frac{\partial w}{\partial s}\end{aligned}\tag{1}$$

The axial, circumferential and shear membrane stress, σ_x , σ_s and τ_{xs} , may now be expressed in terms of the membrane strains, the modulus of elasticity E and the Poisson's ratio ν by the Hooke's law for the isotropic material.

Equilibrium and Compatibility Equations

By omitting higher-order terms, it may be shown that the membrane stresses satisfy the equilibrium equations

$$\begin{aligned}\frac{\partial \sigma_x}{\partial x} + \frac{\partial \tau_{xs}}{\partial s} &= 0 \\ \frac{\partial \tau_{xs}}{\partial x} + \frac{\partial \sigma_s}{\partial s} &= 0\end{aligned}\tag{2}$$

Equations (2) are identically satisfied by the introduction of the Airy stress function $\phi(x,y)$ defined by the relations

$$\sigma_x = \frac{\partial^2 \phi}{\partial s^2}, \quad \sigma_s = \frac{\partial^2 \phi}{\partial x^2}, \quad \tau_{xs} = - \frac{\partial^2 \phi}{\partial x \partial s}\tag{3}$$

By Hooke's law, the membrane strains may be expressed as

$$\begin{aligned}\epsilon_x &= \frac{1}{E} \left(\frac{\partial^2 \phi}{\partial s^2} - \nu \frac{\partial^2 \phi}{\partial x^2} \right) \\ \epsilon_s &= \frac{1}{E} \left(\frac{\partial^2 \phi}{\partial x^2} - \nu \frac{\partial^2 \phi}{\partial s^2} \right) \\ \gamma_{xs} &= - \frac{2(1+\nu)}{E} \frac{\partial^2 \phi}{\partial x \partial s}\end{aligned}\tag{4}$$

Elimination of axial and circumferential displacement components between Eqs. (1) and combination of Eqs. (1) and (4) yield the compatibility equation

$$\begin{aligned}\nabla^4 \phi &= E \left[\left(\frac{\partial^2 w}{\partial x \partial s} \right)^2 - \frac{\partial^2 w}{\partial x^2} \frac{\partial^2 w}{\partial s^2} - \frac{1}{r} \frac{\partial^2 w}{\partial x^2} \right. \\ &\quad \left. + 2 \frac{\partial^2 w}{\partial x \partial s} \frac{\partial^2 w_0}{\partial x \partial s} - \frac{\partial^2 w}{\partial x^2} \frac{\partial^2 w_0}{\partial s^2} - \frac{\partial^2 w_0}{\partial x^2} \frac{\partial^2 w}{\partial s^2} \right]\end{aligned}\tag{5}$$

in which $\nabla^4 = \left(\frac{\partial^4}{\partial x^4} + 2 \frac{\partial^4}{\partial x^2 \partial s^2} + \frac{\partial^4}{\partial s^4} \right)$

The stress function and the membrane stresses may now be determined by Eq. (5) if the initial imperfection and the the radial displacement are obtained or assumed.

Initial Imperfections and Deformations

The initial geometrical imperfections or the deformation of the cylinder can be completely described by an infinite double Fourier series. The degree of approximation which can be attained in the description largely depends on the choice of a proper number of terms of the series. However, the mathematical difficulties of solving the problem multiply rapidly with increasing number of terms considered. To simplify the analysis, it is assumed that the initial radial deviation may be described by

$$w_0 = At \cos \frac{\pi x}{L_x} \cos \frac{\pi s}{L_s} + \frac{a_0}{a} w \quad (6)$$

where A and a_0 are the given or known dimensionless amplitude parameters, L_x and L_s are the given or known half wave lengths in the axial and circumferential directions respectively. The first term at the right-hand side of Eq. (6) describes a definite shape. The second term, introduced by Donnell⁸, is definite in amplitude but indefinite in shape, because the radial displacement w varies with the applied load. It may be interpreted that the second term is used to replace all terms in the infinite series which may have effects on the deformation. It also implies that only one of these implicit terms influences the deformation at one time.

The deformation of the cylinder is assumed to be given by

$$w = at \left[\cos \frac{\pi x}{\ell_x} \cos \frac{\pi s}{\ell_s} + b \cos \frac{2\pi x}{\ell_x} + d \right] \quad (7)$$

where a and b are arbitrary parameters, ℓ_x and ℓ_s are the unknown half-wave lengths of the deformation waves in the axial and circumferential directions. d is not an independent parameter. d may be determined by the condition that v is a periodic function of s . The deformation function by Eq. (7) is essentially the one adopted by Donnell⁸ and Kempner⁷ except that a term of $\cos \frac{2\pi s}{\ell_s}$ is not included.

Stress Function

By introducing w_0 from Eq. (6) and w from Eq. (7) into Eq. (5), the stress function is found to be

$$\begin{aligned}
 \phi = & -\frac{Et^2}{\mu^2\eta} \left\{ \frac{a(aK\eta - 8b)}{32} \cos \frac{2\pi x}{\ell_x} + \frac{a^2K\eta\mu^4}{32} \cos \frac{2\pi s}{\ell_s} + \right. \\
 & a(2abK\eta - 1)P_{11}^2 \cos \frac{\pi x}{\ell_x} \cos \frac{\pi s}{\ell_s} + 2a^2bK\eta P_{31}^2 \cos \frac{3\pi x}{\ell_x} \cos \frac{\pi s}{\ell_s} \\
 & + \frac{Aa\eta_0}{4} \left[\frac{\mu^2}{(\mu - \mu_0)^2} \left[Q_{11}^2 \cos \frac{(\mu n - \mu_0 n_0)x}{r} \cos \frac{(n - n_0)s}{r} \right. \right. \\
 & + Q_{22}^2 \cos \frac{(\mu n + \mu_0 n_0)x}{r} \cos \frac{(n + n_0)s}{r} \Big] + \frac{\mu^2}{(\mu + \mu_0)^2} \cdot \left[\right. \\
 & Q_{12}^2 \cos \frac{(\mu n - \mu_0 n_0)x}{r} \cos \frac{(n + n_0)s}{r} + Q_{21}^2 \cos \frac{(\mu n + \mu_0 n_0)x}{r} \\
 & \cos \frac{(n - n_0)s}{r} \Big] + 8b \left[Q_{33}^2 \cos \frac{(2\mu n - \mu_0 n_0)x}{r} \cos \frac{n_0 s}{r} \right. \\
 & \left. \left. + Q_{44}^2 \cos \frac{(2\mu n + \mu_0 n_0)x}{r} \cos \frac{n_0 s}{r} \right] \right] \Big\} - \frac{\sigma s^2}{2} \quad (8)
 \end{aligned}$$

in which

$$K = 1 + \frac{2a_0}{a} = 1 + \frac{V}{a}, \quad \mu = \frac{\ell_s}{\ell_x}, \quad \mu_0 = \frac{L_s}{L_x}$$

$$n = \frac{\pi r}{\ell_s}, \quad n_0 = \frac{\pi r}{L_s}, \quad \eta = \frac{n^2 t}{r}, \quad \eta_0 = \frac{n_0^2 t}{r}$$

$$\begin{aligned}
P_{11} &= \frac{\mu^2}{1 + \mu^2}, \quad P_{31} = \frac{\mu^2}{1 + 9\mu^2}, \quad \alpha = \sqrt{\frac{\eta_0}{\eta}} \\
Q_{11} &= \frac{(\mu - \mu_0)^2}{(\mu - \alpha\mu_0)^2 + (1 - \alpha)^2}, \quad Q_{22} = \frac{(\mu - \mu_0)^2}{(\mu + \alpha\mu_0)^2 + (1 + \alpha)^2} \\
Q_{12} &= \frac{(\mu + \mu_0)^2}{(\mu - \alpha\mu_0)^2 + (1 + \alpha)^2}, \quad Q_{21} = \frac{(\mu + \mu_0)^2}{(\mu + \alpha\mu_0)^2 + (1 - \alpha)^2} \\
Q_{33} &= \frac{\mu^2}{(2\mu - \alpha\mu_0)^2 + \alpha^2}, \quad Q_{44} = \frac{\mu^2}{(2\mu + \alpha\mu_0)^2 + \alpha^2}
\end{aligned}$$

In Eq. (8) σ is the applied average axial compressive stress.

Potential Energy

The total potential energy of the system consists of the potential energy of the applied load and the internal strain energy in the cylinder. There are two parts in the strain energy, the membrane strain energy U_m and the bending strain energy U_b . They can be expressed as

$$U_m = \frac{t}{2E} \int_0^L \int_0^{2\pi r} \left[(\sigma_x + \sigma_s)^2 - 2(1+\nu)(\sigma_x \sigma_s - \tau_{xs}^2) \right] dx ds \quad (9)$$

and

$$U_b = \frac{D}{2} \int_0^L \int_0^{2\pi r} \left\{ (\nabla^2 w)^2 + 2(1-\nu) \left[\left(\frac{\partial^2 w}{\partial x \partial s} \right)^2 - \frac{\partial^2 w}{\partial x^2} \frac{\partial^2 w}{\partial s^2} \right] \right\} dx ds \quad (10)$$

in which $D = (1/12) Et^3/(1-\nu^2)$.

From Eqs. (3), (4), (7), (8), (9) and (10), the total internal strain energy, U_i , is found to be

$$\begin{aligned}
 U_i = (\pi E t^3 L / r) \bigg\{ & a^2 (a K \eta - 8b)^2 / 128 + a^4 K^2 \eta^2 \mu^4 / 128 \\
 & + a^2 (2abK\eta - 1)^2 P_{11}^2 / 4 + a^4 b^2 K^2 \eta^2 P_{31}^2 \\
 & + (A^2 a^2 \eta^2 / 64) [Q_{11}^2 + Q_{22}^2 + Q_{12}^2 + Q_{21}^2 \\
 & + 64b^2 (Q_{33}^2 + Q_{44}^2)] + (\sigma r / Et)^2 \\
 & + [a^2 \eta^2 / 48 \cdot (1 - \nu^2)] [(1 + \mu^2)^2 + 32b^2 \mu^4] \bigg\} \quad (11)
 \end{aligned}$$

The potential energy of the axial load applied to the ends of the cylinder, U_a , can be expressed as

$$U_a = 2\pi r t \sigma \int_0^L \left(\frac{\partial u}{\partial x} \right) dx \quad (12)$$

The integral in Eq. (12) gives the total end shortening in the axial direction. From the first of Eqs. (1) and the first of Eq. (4), the integrand is found to be

$$\frac{\partial u}{\partial x} = \frac{1}{E} \left(\frac{\partial^2 \phi}{\partial s^2} - \nu \frac{\partial^2 \phi}{\partial x^2} \right) - \frac{1}{2} \left(\frac{\partial w}{\partial x} \right)^2 - \left(\frac{\partial w}{\partial x} \right) \left(\frac{\partial w_0}{\partial x} \right) \quad (13)$$

If ϵ is defined as the average unit end shortening in the axial direction or the ratio of the total end shortening and the cylinder length, it is found that

$$(\epsilon r / t) = (\sigma r / Et) + a^2 K \eta \mu^2 (1 + 8b^2) / 8 \quad (14)$$

In carrying out the integral in Eq. (12), it is assumed that $\ell_x \neq L_x$ and that the initial and deformed axial wave lengths are small compared to the entire length of

the cylinder.

Determination of Parameters

The deflection parameters, expressed in terms of a , b , η and μ , may be determined by the principle of stationary potential energy. When the total potential energy of the system, $U_i + U_a$, is made stationary for a small variation of each of the four parameters, the following four simultaneous algebraic equations are obtained:

$$\begin{aligned}
 & (aK\eta - 8b) [a\eta(1+K) - 8b] + a^2K\eta^2\mu^4(1+K) + 32 \cdot \\
 & (2abK\eta - 1) [2ab\eta(1+K) - 1] P_{11}^2 + 128 a^2b^2\eta^2K \cdot \\
 & (1+K)P_{31}^2 + 2A^2\eta_0^2 [Q_{11}^2 + Q_{22}^2 + Q_{12}^2 + Q_{21}^2 + \\
 & 64b^2(Q_{33}^2 + Q_{44}^2)] + 8\eta^2 [(1+\mu^2)^2 + 32b^2\mu^4]/3(1-\nu^2) \\
 & - 16(\sigma r/Et)\eta\mu^2(1+K)(1+8b^2) = 0
 \end{aligned} \tag{15}$$

$$\begin{aligned}
 b = aK\eta \left[(1/8) + P_{11}^2 \right] & \div \left[1 + 2a^2K^2\eta^2(P_{11}^2 + P_{31}^2) \right. \\
 & + 2A^2\eta_0^2 (Q_{33}^2 + Q_{44}^2) + 4\eta^2\mu^4/3(1-\nu^2) \\
 & \left. - 4(\sigma r/Et)\eta K\mu^2 \right]
 \end{aligned} \tag{16}$$

$$\begin{aligned}
 & a^2K^2\eta (1 + \mu^4) - 8abK + 64abK(2abK\eta - 1)P_{11}^2 \\
 & + 128 a^2b^2K^2\eta P_{31}^2 + 2A^2\eta_0^2 \left\{ Q_{22}^2 [\mu_0(\mu + \nu\mu_0)] \right.
 \end{aligned}$$

$$\begin{aligned}
& + 1 + \alpha] / (\mu - \mu_0)^2 - Q_{11}^3 [\mu_0(\mu - \alpha\mu_0) + 1 - \alpha] / (\mu - \mu_0)^2 \\
& + Q_{21}^3 [\mu_0(\mu + \alpha\mu_0) - 1 + \alpha] / (\mu + \mu_0)^2 \\
& - Q_{12}^3 [\mu_0(\mu - \alpha\mu_0) - 1 - \alpha] / (\mu + \mu_0)^2 \\
& + (128 A^2 b^2 \eta_0 \alpha^3 / \mu^2) \left\{ [\mu_0(2\mu + \alpha\mu_0) + \alpha] Q_{44}^3 \right. \\
& \left. - [\mu_0(2\mu - \alpha\mu_0) - \alpha] Q_{33}^3 \right\} \\
& + 8\eta [(1 + \mu^2)^2 + 32 b^2 \mu^4] / 3(1 - \nu^2) \\
& - 16 (\sigma r / Et) K \mu^2 (1 + 8b^2) = 0
\end{aligned} \tag{17}$$

$$\begin{aligned}
& a^2 K^2 \eta^2 \mu^3 / 32 + (2abK\eta - 1)^2 P_{11}^3 / \mu^3 \\
& + 4a^2 b^2 K^2 \eta^2 P_{31}^3 / \mu^3 + (A^2 \eta_0^2 / 16) \left\{ \right. \\
& (1 - \alpha) [\mu_0(\mu - \alpha\mu_0) + 1 - \alpha] Q_{11}^3 / (\mu - \mu_0)^3 \\
& + (1 + \alpha) [\mu_0(\mu + \alpha\mu_0) + 1 + \alpha] Q_{22}^3 / (\mu - \mu_0)^3 \\
& + (1 + \alpha) [1 + \alpha - \mu_0(\mu - \alpha\mu_0)] Q_{12}^3 / (\mu + \mu_0)^3 \\
& \left. + (1 - \alpha) [1 - \alpha - \mu_0(\mu + \alpha\mu_0)] Q_{21}^3 / (\mu + \mu_0)^3 \right\} \\
& + (4\alpha A^2 b^2 \eta_0^2 / \mu^3) \left\{ [\alpha - \mu_0(2\mu - \alpha\mu_0)] Q_{33}^3 \right. \\
& \left. + [\alpha + \mu_0(2\mu + \alpha\mu_0)] Q_{44}^3 \right\}
\end{aligned}$$

$$\begin{aligned}
& + \eta^2 \mu [1 + \mu^2 + 32b^2 \mu^2] / 12(1 - \nu^2) \\
& - (\sigma r / Et) K \eta \mu (1 + 8b^2) / 2 = 0
\end{aligned} \tag{18}$$

In the variational procedure, it is considered that $\sigma =$ constant, the case of dead-weight loading. The deflection parameters for a given load may now be determined by solving Eqs. (15) to (18) simultaneously. The following procedure of obtaining numerical solutions is considered.

Eq. (16) is first used to eliminate b from the other three equations. The values of the parameters, A , a_0 , η_0 and μ_0 defining the initial imperfections are preassigned.

For assumed values of a , η , and μ , a value of σ may be computed from each of the three equations. The correct set of a , μ , and η yields the same σ value from each of the three equations. For a fixed value of a , a pair of η and μ may be found by systematic coarse scanning such that the three corresponding values of σ are reasonably close to each other. Then by keeping one of the two parameters constant and adding a small increment to the other one, the effects of the increment on the σ -values are determined. Knowing these effects, a new pair of η and μ may be extrapolated. This process may be repeated until a pair of η and μ values are found such that the three σ -values agree with each other to within a desired accuracy.

For a fixed value of a , there may be more than one set of η , μ and σ values satisfying the three equations. Knowing a set of a , η , μ and σ values, the corresponding values of b and $(\epsilon r / t)$ may be calculated by Eqs. (16) and (14). The entire procedure may be repeated for a suitable number of a -values. The computation involved in this method of solution was programmed by the Fortran language on an IBM 1620 digital computer.

NUMERICAL RESULTS AND DISCUSSIONS

The numerical results of the solution of Eqs. (15) to (18) for a number of cases are shown in Figs. 1 to 6 as

functions of the unit end shortening parameter $(\epsilon r/t)$. For comparison, the $(\sigma r/Et)$ vs $(\epsilon r/t)$ relationship of a perfect cylinder, Case I: $A = 0$, $V = 0$, is also shown in Fig. 1. For this case, the minimum value of the applied stress in the postbuckling region is $\sigma = 0.193 (Et/r)$ at $\mu = 0.397$ and $(\epsilon r/t) = 0.462$. These results compare favorably with the corresponding results of $\sigma = 0.195 (Et/r)$ at $\mu \cong 0.40$ by Leggett and Jones⁵ and Michielsen⁶. The minimum stress obtained by Kempner⁷, by using five parameters in the variational procedure, is $0.182 (Et/r)$ at $\mu = 0.362$. Fig. 1 shows the departure of the results by the present analysis and that of Michielsen⁶ in the region $(\epsilon r/t) > 0.5$. The difference is due to the deformation functions employed in the two analyses being slightly different. The results of the present analysis in the region $(\epsilon r/t) > 0.5$ practically coincide with that by Kempner⁷. The variations of the deflection parameters with unit shortening for this case are shown in Fig. 2.

Fig. 1 also shows the $(\sigma r/Et)$ vs $(\epsilon r/t)$ curves of three other cases having essentially definite initial imperfections. These curves deviate only slightly from that of the perfect cylinder. It is also to be noted that the values of the parameters defining the initial imperfections are in the critical ranges of the deflection parameters giving the shapes of the deformation waves of the perfect cylinder. The maximum applied stress for Case II is $0.621 (Et/r)$. For cases III and IV it is $0.617 (Et/r)$. These maximum stresses are slightly higher than the critical value of $0.605 (Et/r)$ for the perfect cylinder. It indicates that definite initial imperfections, at least, of the type considered do not cause lower buckling stresses. However, the characteristics of the curves in Fig. 1 indicate that the imperfect cylinders, when subject to external disturbances, may become unstable at critical stresses less than the maximum applied stresses and snap through into other states of equilibrium which are connected with considerably smaller axial loads. But, it is to be noted that the imperfect cylinders II, III and IV are comparatively more stable than the perfect cylinder. The curves indicate that a comparatively larger amount of external disturbance may be needed to cause the snapthrough bucklings of the imperfect cylinders than that of the perfect cylinder.

Although the $(\sigma r/Et)$ vs $(\epsilon r/t)$ curves of the imperfect and perfect cylinders appear to be similar, their deflection parameters do not vary in a similar manner. Fig. 3 shows the variations of the deflection parameters with unit end shortening for Case II, which are similar to that of Case I. However, the variations of the deflection parameters with unit end shortening for Case IV, shown in Fig. 4, (similar results for Case III) are quite different from the other two cases. It indicates that the initial imperfections may affect the buckling process of a cylinder. It also indicates that the following two buckling processes are possible. In the early stage of buckling, a cylinder may deform with a comparatively small number of waves of comparatively large amplitudes (Case II) or a cylinder may deform with a comparatively large number of waves of comparatively small amplitudes (Case IV).

Fig. 5 represents the influences of the imperfection factor, V , ($V = 2a_0$), on the behavior of an axially compressed cylinder. The segment of Curve 1 in solid line was obtained by the process previously described. The minimum applied stress indicated by Curve 1 is $0.187 (Et/r)$ at $(\epsilon r/t) = 0.451$ and $\mu = 0.349$. In the region of the dotted line of Curve 1, an exhaustive search did not produce a set of parameters that satisfies the three simultaneous equations. However, other sets of parameters that yield points in the $(\sigma r/Et)$ vs $(\epsilon r/t)$ plane above Curve 1 were found. This difficulty may be due to the insufficient number of terms included in the deflection function.

Curve 2 in Fig. 5 was obtained by using the following deflection function previously employed by Lool².

$$w = a't \left[\sin \frac{ns}{r} \sin \frac{\pi x}{\ell_x} + b' \left(\cos \frac{2\pi x}{\ell_x} - 1 \right) + d' \right] \quad (19)$$

It may be shown that the total potential energy of a cylinder having the initial imperfection given by Eq. (6) and the deflection given by Eq. (19) may still be expressed by Eqs. (11), (12), and (14) provided that a is replaced by a' and b is replaced by $(-b')$ in these equations. By using a numerical procedure identical to the previous one, Curve 2 in Fig. 5 as well as the variations of the parameters with unit end shortening shown in Fig. 6 were

obtained. For comparison, Fig. 5 also shows the results by Loo¹² for cases of $V = 0$ and $V = .2$. These results, which compared reasonably well with that of the present analysis, were obtained by assuming the constant values of η and μ given by the classical small deflection theory. It is to be noted that the values of a' in Fig. 6 are much less than the values of a of the Cases I to IV. It is also to be noted that the values of η and μ in Fig. 6 are close to the corresponding values predicted by the small-deflection theory. The results also indicate that the number of waves, given by η , decreases in the later stage of the buckling process. This has also been indicated by Von Karman and Tsien⁴.

CONCLUDING REMARKS

The foregoing analysis and numerical results indicate that the theoretical axial buckling stresses of cylinders having definite initial imperfections, at least of the periodic type considered, are not necessarily lower than that of a perfect cylinder. In other words, it is possible that certain types of definite initial deviations may increase the buckling resistance of a cylindrical shell. The imperfection factor introduced by Donnell¹ leads to lower theoretical buckling stresses. However, the physical meaning of the factor needs further clarification.

The usage of the imperfection factor implies the following assumption. The initial imperfections may be described by an infinite double Fourier series having all terms, each of which is a function of the space coordinates only, of equal amplitude; the terms interact with the deflection function, a function of the space coordinates and the applied load one at a time. However, the present analysis indicates that all the terms may interact with the deflection function. The interactions may not necessarily reduce the theoretical buckling stress.

It has also been found that two theoretical buckling processes are possible. In the early stage of buckling, a cylinder may deform with a comparatively large number of waves of comparatively small amplitudes or it may deform with a comparatively small number of waves of comparatively large amplitudes.

It is obvious that further research on the effects of initial imperfections and the process of buckling is needed. The theoretical analysis may be improved by considering (a) higher order terms in the strain-displacement relationships and the equilibrium equations, and (b) more accurate descriptions of the initial imperfections and the deflection. From the present analysis, it appears that aperiodic as well as periodic functions should be used to describe the initial imperfections and the deflection.

A great deal of mathematical difficulty is expected in any theoretical refinement. They may be alleviated, however, if the theoretical development is guided by refined experiments. Most of the experimental results available in the literature are usually presented in terms of only the critical buckling load and the final mode of buckling. New experimental results on the complete development of the buckling stress pattern, prebuckling and postbuckling, may provide a physical basis for a better theoretical insight into this difficult problem.

REFERENCES

1. Donnell, L. H.: A New Theory for the Buckling of Thin Cylinders under Axial Compression. Trans. ASME, Vol. 56, 1934, p. 795.
2. Timoshenko, S.: Einige Stabilitätsprobleme der Elastizitätstheorie. Z. Math. Phys., Vol. 58, No. 4, 1910, p. 337.
3. Southwell, R. V.: On the General Theory of Elastic Stability. Phil. Mag., Series A, Vol. 213, 1914, p. 187.
4. Von Kármán, Th., and Tsien, H. S.: The Buckling of Thin Cylindrical Shells under Axial Compression. J. Aeronaut. Sci., Vol. 8, No. 8, 1941, p. 303.
5. Leggett, D. M. A., and Jones, R. P. N.: The Behavior of a Cylindrical Shell under Axial Compression when the Buckling Load has been Exceeded. A.R.C.R. and M., No. 2190, Aug. 1942.

6. Michielsen, H. F.: The Behavior of Thin Cylindrical Shells After Buckling under Axial Compression. J. Aeronaut. Sci., Vol. 15, No. 12, 1948, p. 739.
7. Kempner, J.: Postbuckling Behavior of Axially Compressed Circular Cylindrical Shells. J. Aeronaut. Sci., Vol. 21, No. 5, 1954, p. 329.
8. Donnell, L. H. and Wan, C. C.: Effects of Imperfections on Buckling of Thin Cylinders and Columns Under Axial Compression. Trans. ASME, Vol. 72, No. 1, 1950, p. 73.
9. Timoshenko, S. and Gere, J. M.: Theory of Elastic Stability. McGraw-Hill Book Co., New York, 1961, p. 31.
10. Lee, L. H. N.: Stability of Non-Linear Systems. J. Engr. Mech., ASCE Proceedings, Vol. 88, No. EM2, Part 1, April, 1962, p. 81.
11. Thielemann, W. F.: New Developments in the Non-linear Theories of the Buckling of Thin Cylindrical Shells. Aeronautics and Astronautics, Pergamon Press, New York, 1960, p. 76.
12. Loo, T. T.: Effects of Large Deflections and Imperfections on the Elastic Buckling of Cylinders under Torsion and Axial Compression. Proc. 2nd U. S. Congr. Appl. Mechanics, 1954, p. 345.

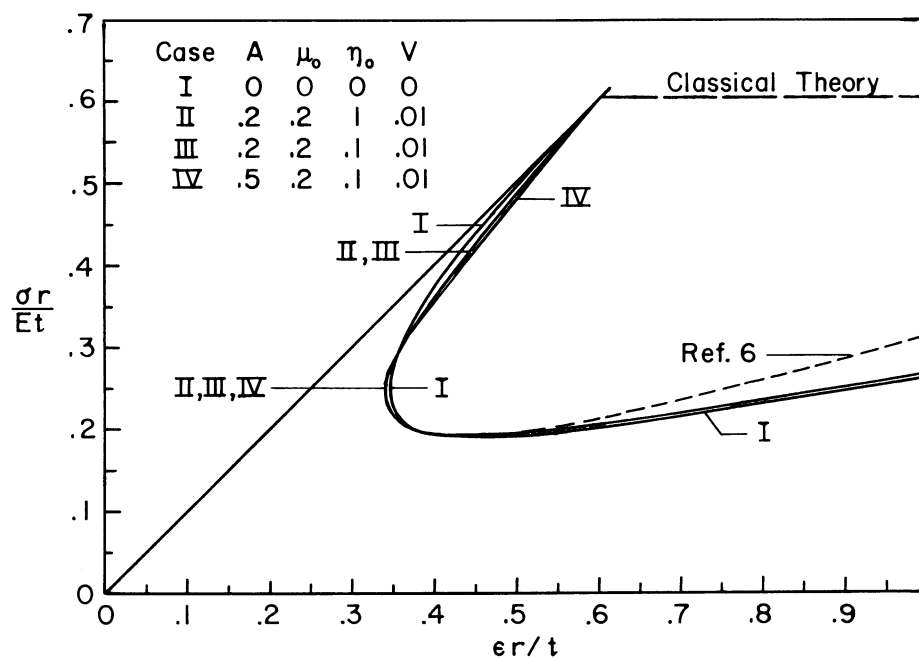


Figure 1.- Variation of applied stress with unit end shortening.

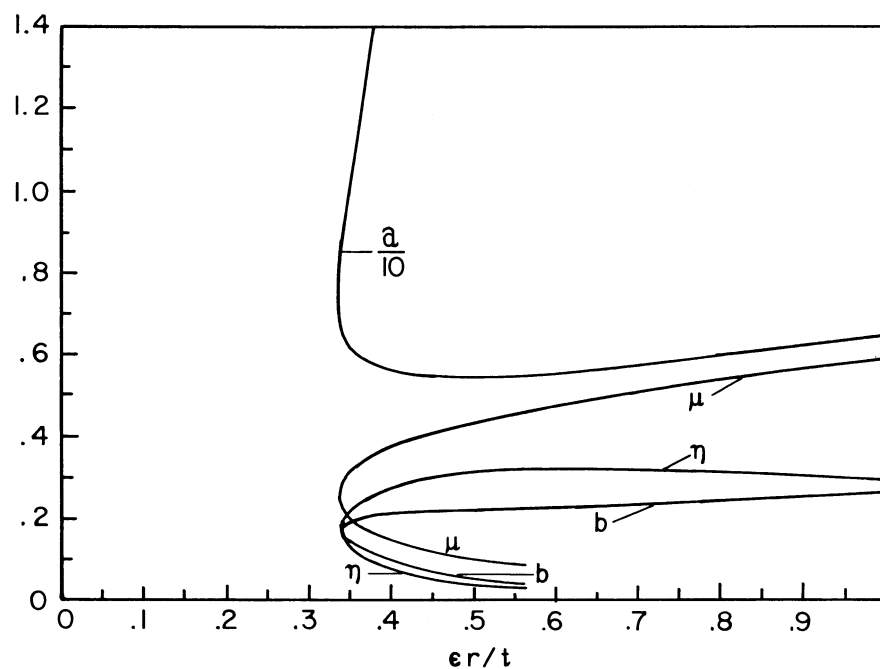


Figure 2.- Variation of deflection parameters with unit end shortening.
Case I: A = 0; V = 0.

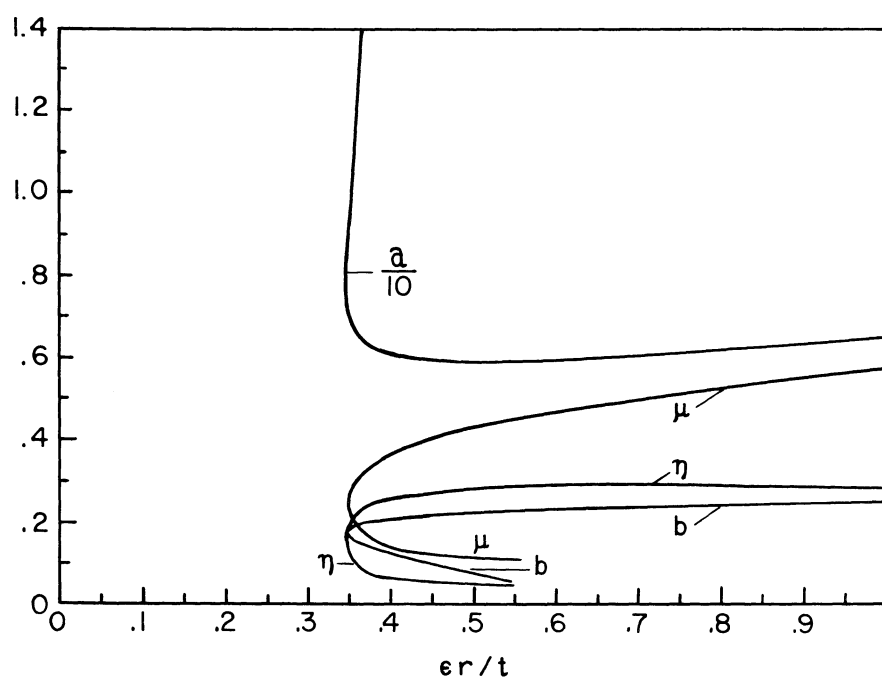


Figure 3.- Variation of deflection parameters with unit end shortening.
Case II: $A = .2$; $\eta_0 = 1.0$; $\mu_0 = .2$; $V = .01$.

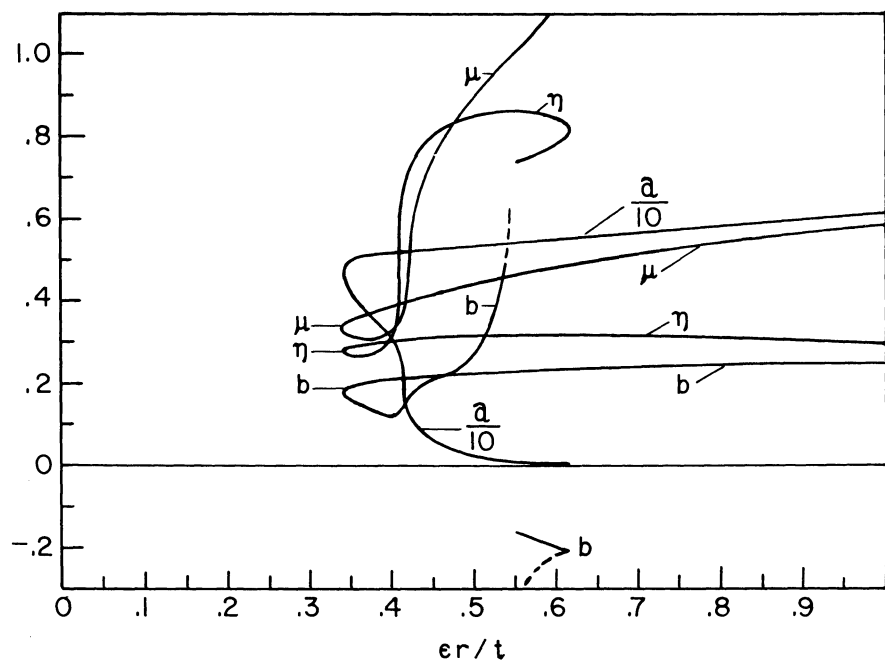


Figure 4.- Variation of deflection parameters with unit end shortening.
Case IV: $A = .5$; $\eta_0 = .1$; $\mu_0 = .2$; $V = .01$.

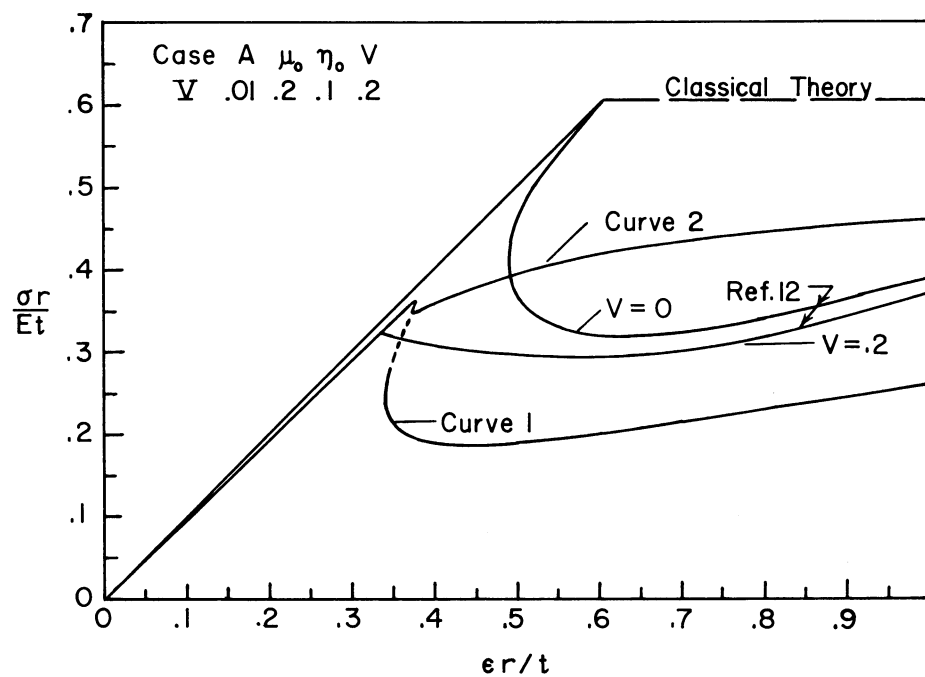


Figure 5.- Variation of applied stress with unit end shortening.

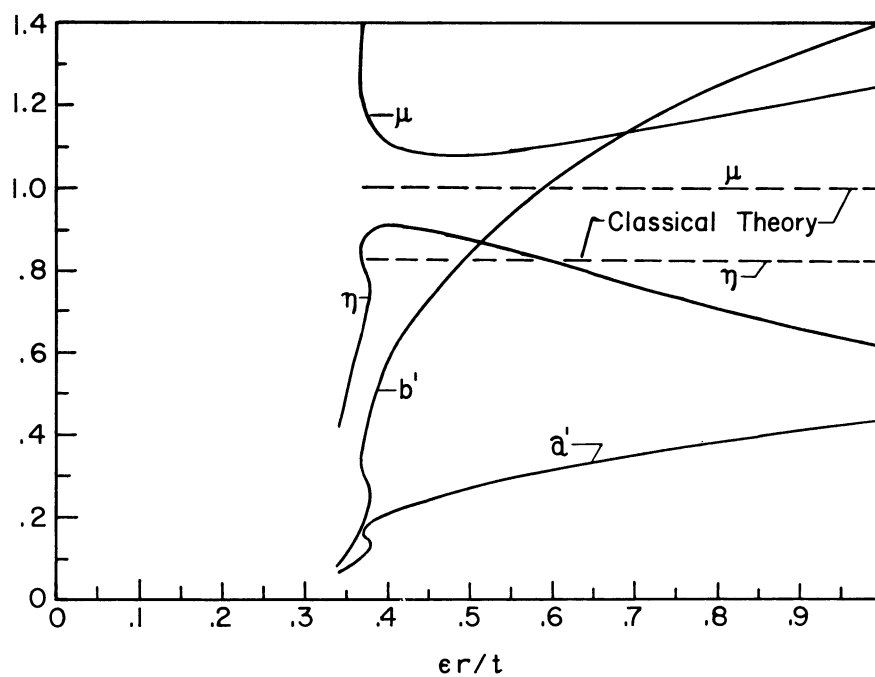


Figure 6.- Variation of deflection parameters with unit end shortening.
 Case V: $A = .01$; $\eta_0 = .1$; $\mu_0 = .2$; $V = .2$.

A REPORT ON THREE SERIES OF EXPERIMENTS AND
THE DESCRIPTION OF A SIMPLIFIED MODEL OF THE THIN
WALL CYLINDER AND CONE BUCKLING MECHANISM

By Octavio G. S. Ricardo

Instituto Tecnológico de Aeronautica, Brasil

SUMMARY

Three series of experiments were performed to investigate the nature of the buckling phenomenon. They were: a) influence of an increasing dimple on the buckling load of a cylinder; b) investigation of the strain distribution on one cylinder, after one or more waves were imposed on it; c) measurements of lateral deflections at buckling. The results of such experiments give some support to the idea of a buckling model, which can be of eventual interest to the thin wall cylinder and cone buckling problem, where a non-linear system (the buckled band) is considered in series with a linear system (the unbuckled portion of the cylinder, plus the testing-machine).

INTRODUCTION

The classical literature that deals with the mechanism of buckling of thin wall cylinders presents, in the post-buckling region, a non-linear relation between axial load and axial deflection, in such a way that large lateral deflections of the cylinder wall correspond to a large decrease of the load with which the cylinder reacts to an increasing imposed shortening. (Buckling is considered here in its engineering sense, i.e., collapse). These lateral deflections increase from zero to large finite values following a continuous curve, corresponding to (unstable or stable) equilibrium conditions. Therefore, this curve always starts at the classical value $K \approx 0.6$.

These infinitesimal lateral deflections are always associated with membrane and bending stresses.

However, it is possible to imagine that the axial shortening imposed on the cylinder could be absorbed by its walls taking an almost developable polyhedral configuration (developable, except at its vertices), in which the membrane strain energy could be relatively small in comparison to the bending energy stored at the diamond borders. In this way

the total strain energy (and the load) could possibly be smaller, and the resulting load vs. strain curve would become independent of the classical buckling load at $K \cong 0.6$. Buckling would be, in this way, a discontinuous process, with the cylinder jumping from a first mode (simple compression) of absorbing the axial shortening, to a second mode (a polyhedral buckled band, plus an unbuckled region of the cylinder). Thus, this second mode could be entirely independent of the first one.

In order to investigate this possibility, the experiments described below were performed, and some support to this approach was obtained. A very much simplified model of the cylinder and cone buckling phenomenon was studied, yielding simple and interesting results, which may eventually be useful. This model enables one to explain the buckling problem without the necessity of supposing a jump over the "energy hump".

SYMBOLS

A	semi-vertex angle of the cone
d	distance between recording points
E	Young's modulus
H	height of the cylinder
j	see figure 6
K	coefficient for the collapse of a cylinder
k	H/R
n	number of sides of the basic polygon of the buckled cross-section
n_0	value of n that minimizes the bending energy
P	axial force on the cylinder
Q	lateral force acting on the cylinder wall
R	radius
t	wall thickness
U	strain-energy
δ	axial shortening of the cylinder or cone
ϵ	ratio of the shortening to the height of the cylinder
ϵ_R	ratio of the shortening to the average radius of the buckled band (cone case)
η	lateral deflection of the cylinder wall

σ compressive stress

Subscripts:

b for bending

c for simple compression

l for linear system (unbuckled portion of the cylinder, plus the testing-machine)

EXPERIMENTAL RESULTS

Influence of a small increasing dimple on the collapse load of cylinders.- A constant lateral force Q was imposed on the wall of mylar cylinders, and the lateral deflections η at the loading point were measured when the axial load P on the cylinder increased. The collapse load was also measured. In this way, fig. 1 was obtained. It can be seen that dimples of depth to about one wall thickness do not affect the collapse load. Larger dimples cause one-wave initial buckling, which brings the collapse load to a lower level, where it remains practically unaffected by further very large imposed lateral deflections. When two or three initial waves appeared, they gave similar results. Cross-plots of these P, Q, η graphs were also obtained, and they show the distinct regions of one, two, and three initial waves, and collapse.

These graphs seem to show very strongly that for $R/t \cong 300$, collapse has a discontinuous nature. Also it appears that if an initial local imperfection is to affect collapse, the width of the initial imperfection has to be larger than a critical value.

Similar experiments were performed at various points around the cylinder, and they called attention to the influence of a non-uniform compression stress distribution on the one-wave initial buckling.

Strain measurements.- A mylar cylinder with $t = 0.010$ in., $R/t = 250$, and $H = 12$ in. was loaded with $\sim 70\%$ of the collapse load. Twenty-four half-diamond waves were imposed simultaneously on one section, simulating a buckled band (i.e., two dodecagons, out of phase). Properly placed strain-gages picked up the induced longitudinal and transverse, direct and bending strains. Because the strain-gage length and stiffness made it impossible to measure the crests of the bending-strain curves at the diamond borders, only qualitative conclusions were possible. However, it can be said that close to the polyhedral band, the bending energy is much larger than the change that occurs in the compression energy, when the waves are imposed on the wall.

When only one wave was imposed, and in spite of the experimental difficulty mentioned above, the bending energy was ~ 10 times the change of the compression energy, in a region close to the wave; and they were about equal at a section 4 in. away from the center of the wave.

It was also clear that most of this bending energy had to be provided by the elasticity of the loading device.

Recording of the lateral deflections at collapse.- The aim of these experiments was to try to record the cylinder wall movements at collapse, and to interpret them from the point of view of the continuity of the buckling process. In particular it was desired to detect any evidence of the existence during the "jump" of the unstable equilibrium stage, which corresponds to Tsien's "hump" problem. Eight mylar cylinders were studied, with $R \approx 2.2$ to 4.8 in., $t = 0.007 \sim 0.010$ in., $H = 4.3$ in. Their ends were embedded in "cerrolow" metal. Ten small eye-pins were cemented to the wall, at the same height, and each one connected to a special wire potentiometer. The signals were recorded by a ten-channel recording oscillograph. Obviously, this arrangement provided an appreciable lateral support to the wall (the friction was ~ 8 gr for each channel). Therefore, the height of the cylinder had to be kept small, and the load had to be applied a little off the center, in order that the buckled band would occur at the studied section.

About 50 recordings were performed, with very consistent results. Fig. 2 shows the recording paper of Exp. no. 190, with $R = 4.75$ ", $t = 0.007$ ", $d = 1.18$ ". No initial waves were present, and the buckling occurred simultaneously along the studied section. It can also be seen from fig. 2 that 0.01 sec. after collapse, the cross-section was already a 10- or 11-sided polygon, and its shape changed to an 8- or 10-sided polygon after further shortening was imposed on the cylinder (the testing-machine was not immediately stopped). No evidence was found of an intermediate polygon between the circle and the 11-sided one.

Fig. 3 shows the recording paper of Exp. no. 152, with $R = 4.75$ ", $t = 0.010$ ", $d = 1.18$ ". Initial waves can be seen at channels 2, 4, 5, 6, but apparently they had not much influence on the mode of collapse. It is interesting to note that all these channels reversed their senses at collapse. This is a strong indication that the mode of deflection at collapse is independent of initial small irregularities.

Fig. 3 also shows the cross-sections drawn according to the observed final configuration of the cylinder. The studied section stayed at half-height of the buckled band, showing a polygon with twice the number of sides of the basic one.

The results of the other experiments generally confirmed these conclusions.

A SIMPLIFIED MODEL FOR THE BUCKLING MECHANISM

Bending energy of the buckled band.- Following the lines presented above, the bending energy of the buckled band, corresponding to large lateral deflections, can be easily estimated if simplifying assumptions are made.

The simplest mode of buckling, which can be observed experimentally if a "stiff" machine is used, is obtained if the buckled portion of the cylinder or cone is considered to be a band of $2n$ triangles (fig.4). These triangles are half-diamonds, but the other halves are not considered, because they involve only relatively large radii of curvature. The bending energy is assumed to be stored at the borders of such triangles, and at the vertices, where the radii are small and assumed constant. Two non-dimensional parameters have to be empirically estimated, and they are N and γ as shown in fig. 4. The angles are estimated from the geometry.

The bending energy is minimized for n . Then, for a family of cylinders with $k = 4$, one obtains,

$$U_b = 21.8Et_b^3 \epsilon_b^{1/3} \quad (1)$$

$$P_b = 7.3 \frac{Et_b^3}{H} \epsilon_b^{-2/3} \quad (2)$$

For simple compression:

$$U_c = k\pi R_0^2 t E \epsilon_c^2 \quad (3)$$

$$P_c = 2\pi E R_0 t \epsilon_c \quad (4)$$

Two modes of absorbing axial shortenings.- The axial shortening imposed on the cylinder can be absorbed: a) by simple compression or b) by two systems in series: a non-linear system consisting of the buckled band, and a linear system consisting of the unbuckled portion of the cylinder (or cone), plus the testing-machine. The mechanism of the collapse would be, for this simplified model, the mechanism of "jumping" from the first to the second mode of absorbing the axial shortening.

The second mode is controlled by the equilibrium or minimum energy condition (after collapse):

$$P_c = P_b \quad (5)$$

This condition allows a graphical solution for $(U_c + U_b)$ after collapse, and the "jump" can occur when the $(U_c + U_b)$ curve crosses the U_c curve for the first mode alone.

Fig. 5 shows two solutions for the same cylinder. In a rigid-machine $K \approx 0.34$. In a "soft" machine (assumed in this example 20 times more flexible than the cylinder alone, as in the case where a dynamometer is inserted) $K \approx 0.11$.

The same process can be applied to cones, using the equations shown in fig. 4. A graph was made for the "soft" machine case, with results of the same order of magnitude as in ref. 1. The results of ref. 2 are about twice as large as the estimated ones. However, their trends coincide for A and R_m/t , while the graph over-emphasizes the influence of R_2/R_1 . (Note that the experiments of ref. 2 apparently were not performed with a "soft" loading device).

For the internal pressure case, the same reasoning was applied, with waves disposed along one helix around the cylinder. The main parameter was found to be $\frac{p}{E} \left(\frac{R}{t} \right)^2$, and the results were of the same order of magnitude as the experimental ones, for small values of p , while the assumption of a developable surface remains acceptable. In this sense, the role of high internal pressures would be only indirect, changing the wave pattern from the almost-developable "diamonds" involving change of volume to the undevelopable sinusoidal surface, involving no change of volume, with large membrane strains. K increases accordingly, until attaining the limit, that is the classical value $K = 0.6$.

A possible collapse mechanism.— The minimum strain energy theorem requires that if a cylinder and a shortening are given, there is only one possible value n_0 for the number of sides of the basic polygon. n_0 decreases as the shortening increases. A graph can be made, relating the energy levels before and after collapse, the lateral wall deflections (bounded internally by j_1 and externally by j_e), and n_0 (fig. 6). The graph is self-explanatory, showing the regions where the second mode is impossible, possible but requiring external energy $((U_c + U_b) > U_c)$, or effective $((U_c + U_b) < U_c)$.

In terms of the "energy hump" idea, the cylinder would pass through an unstable equilibrium stage before reaching the stable stage. This unstable stage corresponds to a basic polygon with a larger number of sides (n_u) than the stable one (n_s). But, when changing from n_u to n_s , some points have necessarily to reverse their sense of motion, while others, which stayed motionless during the first stage, have to move now. It is more likely that these points, which start at or cross the $j = 0$ line during the second stage, do so without regard to the first stage.

Therefore, the strips or regions corresponding to these points would buckle directly into the stable lower energy level configuration, dragging the adjacent regions or strips directly to the n_s polygon. The process is possible, because the total amount of energy is available. In this way, the waves would initiate at certain points, and propagate laterally until completing the buckled band around the cylinder. But the intermediate steps (the growing waves) would only be dynamically possible. The process would be intrinsically discontinuous, as far as equilibrium positions are concerned. The waves would grow towards a well defined size and shape.

This explanation agrees with the experimental results mentioned before, where no evidence of intermediate polygons was found.

SUGGESTIONS FOR FUTURE RESEARCH

At the ITA Structures Laboratory, two series of experiments are being prepared: a) an investigation on the influence of the cylinder height and of the testing-machine stiffness on the collapse load; b) a correlation between lateral deflection, cylinder load and vertical displacement.

ACKNOWLEDGEMENTS

The author wants to express his deep appreciation to Dr. E. E. Sechler of the California Institute of Technology, to Prof. P. C. Dunne, of the Instituto Tecnológico de Aeronautica, Brasil, and to the ITA and NASA authorities, who made his work and this report possible.

REFERENCES

1. Semi-annual report on the development of design criteria for elastic instability of thin shell structures, Jan. 1, 1959 to July 1, 1959. Space Technology Laboratories, Inc.
2. Seide, P., Weingarten, V. I., and Morgan, E. J.: Final Report on the Development of Design Criteria for Elastic Stability of Thin Shell Structures. STL/TR-60-0000-19425 (AFBMD/TR-61-7), Space Tech. Labs., Inc., Dec. 31, 1960.

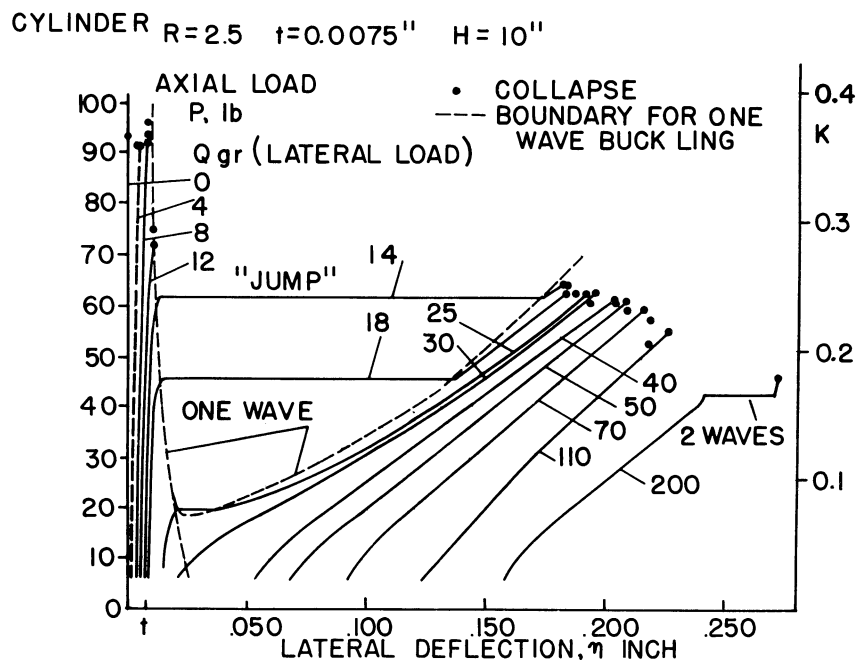


Figure 1.- Influence of an imposed dimple on the collapse load of a cylinder.

EXP. No. 190 DIA. 9.5 IN $t=0.007$ IN.

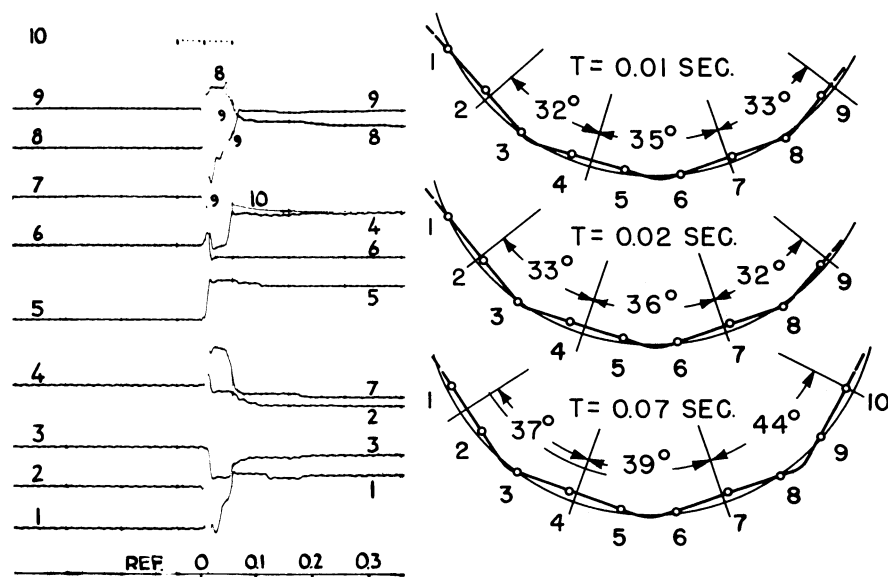


Figure 2.- Recording of lateral deflections at collapse.
Left: Recording paper. Right: Results.

EXP. No. 152 DIA. 9.5 IN. $t = 0.010$ IN.

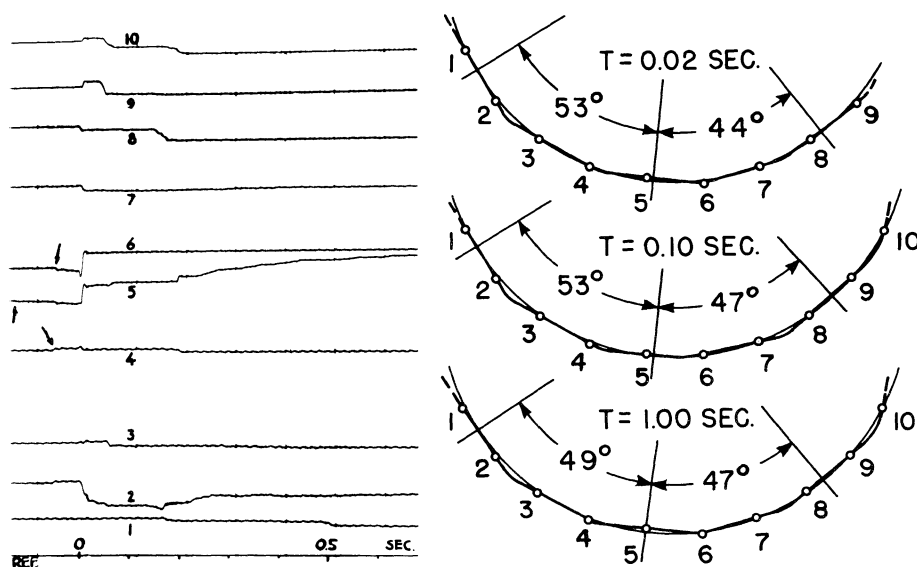


Figure 3.- Recording of lateral deflections at collapse.
Left: Recording paper. Right: Results.

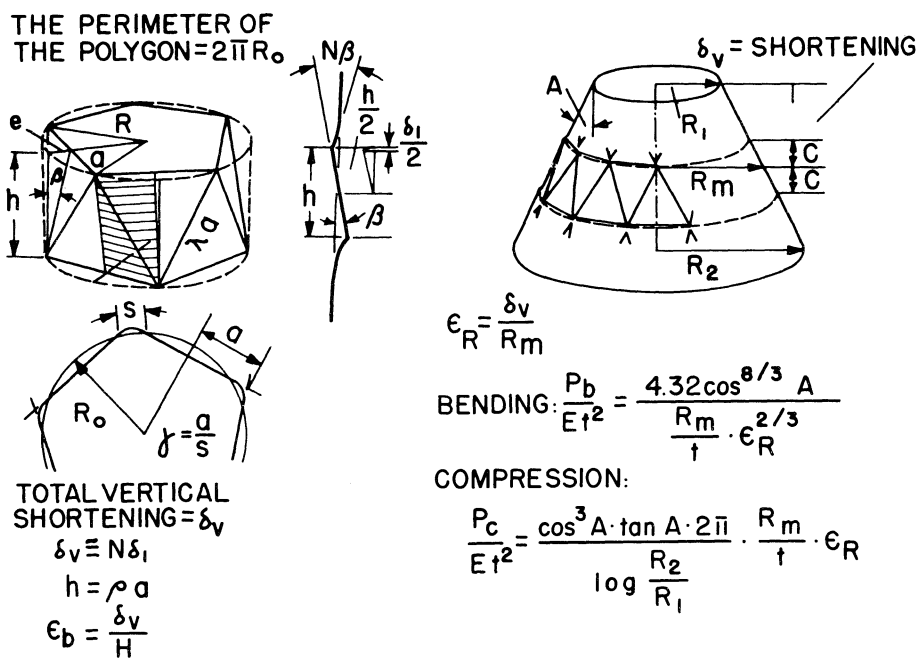


Figure 4.- A simplified model for the buckling problem.

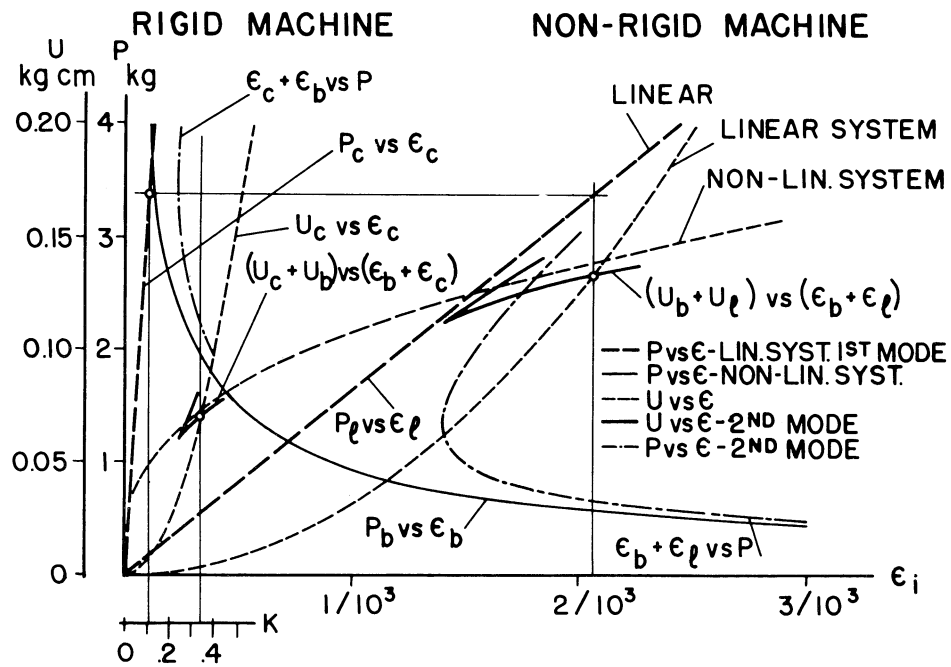


Figure 5.- Graphical calculation of the collapse load.

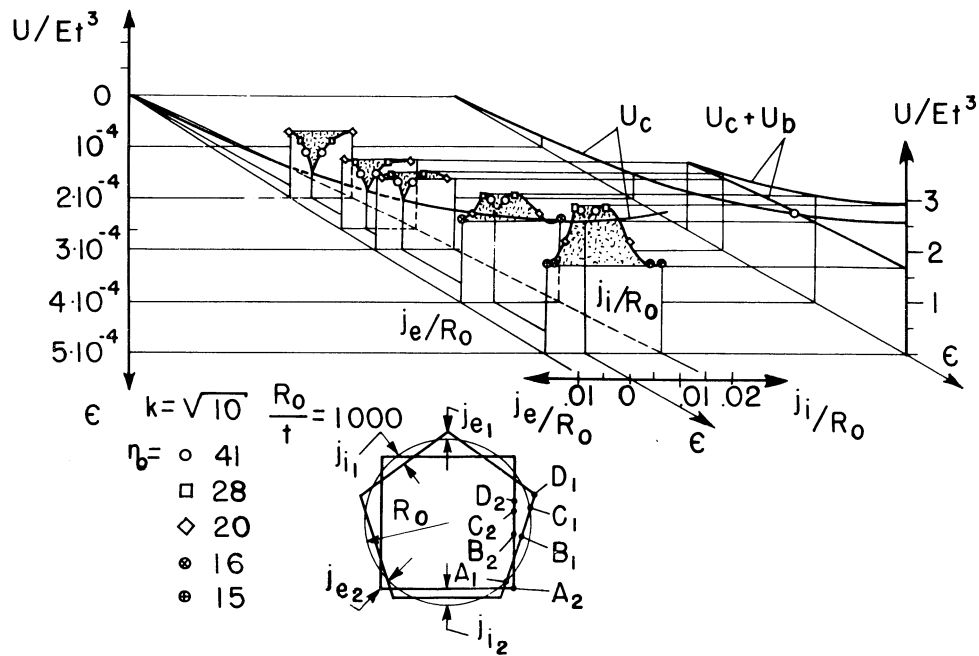


Figure 6.- Graph showing the changes of the energy level, lateral deflection, number of sides of the basic polygon, when a shortening is imposed on the cylinder.

SOME RESULTS ON BUCKLING AND POSTBUCKLING
OF CYLINDRICAL SHELLS

By Joseph Kempner

Polytechnic Institute of Brooklyn

SUMMARY

In this summary paper, the effects of initial deformations on the buckling and postbuckling characteristics of circular cylindrical shells under hydrostatic pressure is determined in an approximate manner. The influence of initial axisymmetric deformations is stressed. Also, the classical buckling of an axially compressed, noncircular (oval) cylindrical shell is studied. The results show that the major-minor axis ratio of the cross section has a marked effect on the critical load, and that use of the maximum radius of curvature in the formula for the classical buckling stress of a circular cylindrical shell leads to good results for moderate eccentricities.

INTRODUCTION

In view of the success of large-deflection theory in revealing equilibrium states of deformation at loads considerably less than the classical buckling load for axially compressed circular cylinders, a large-deflection analysis of cylinders under external hydrostatic pressure was initiated in the belief that similar results would be obtained in this case. Such results would help to explain the discrepancy between theory and experiment which appeared to exist for relatively short cylinders (ref. 1).

Hence, the postbuckling behavior of initially perfect circular cylinders under external hydrostatic pressure was investigated in a manner analogous to that applied in previous studies of axially compressed cylinders; i.e., with the aid of the Rayleigh-Ritz procedure (ref. 2). The results of this approximate analysis indicated that stable postbuckling equilibrium states exist for pressures greater than as well as less than the critical pressure determined from classical (small-deflection) theory. Postbuckling pressures less than the critical pressure were found to exist only within a finite range of a parameter indicative of shell geometry. This range is approximately that found in reference 1 to be one in which considerable discrepancy between experiment and theory was exhibited. However, the calculated

minimum value of the postbuckling load was found to be only 3% less than the corresponding classical von Mises buckling load, while experimental collapse pressures are as little as 60% of this load. These results suggested that the analysis of reference 2 should be extended to include the effects of axisymmetric and asymmetric initial radial deformations on the large-deflection characteristics of circular cylindrical shells under external hydrostatic pressure. Initial work on this problem was presented in reference 3. The first part of the present summary paper describes this and subsequent work on the problem, with particular emphasis being placed upon the effects of initial axisymmetric deformations on the buckling and postbuckling characteristics. For all outward initial axisymmetric deformations and for large inward initial axisymmetric deformations, the buckling load was found to be greater than the von Mises buckling load and less than or equal to the axisymmetric small-deflection buckling load. For smaller inward initial deformation amplitudes of the order of the shell thickness, the buckling load was found to be of the order of 90% of the von Mises load.

In the second part of the present summary a brief description of an investigation of the classical buckling of noncircular (oval) cylindrical shells under axial compression is presented. In particular, the effect of varying the eccentricity of the oval cross section of cylinders having different ratios of the mean radius to thickness is studied. The results show that within the framework of classical theory the use of the maximum radius of curvature in the formula for the classical buckling stress of a circular cylindrical shell yields good results for moderate eccentricities, particularly for very thin shells.

LARGE DEFLECTIONS OF HYDROSTATICALLY LOADED

INITIALLY IMPERFECT CIRCULAR CYLINDERS

Analysis

The basic relations (i.e., strain-displacement relations, stress-strain laws, energy expressions) applied to the study of initially imperfect circular cylindrical shells under external hydrostatic pressure are the same as those discussed in references 4 and 5. The assumed deflected shape is prescribed in the simplified form found to be adequate for initially perfect shells in reference 2, i.e., it consists of the sum of an asymmetric term corresponding to small-deflection theory, of a purely axisymmetric term, and of a term independent of the shell coordinates. Thus, the inward radial displacement w (due to loads) is expressed in the form

$$w/t = \left[\varphi - \xi \cos (\pi y / \lambda_c) \right] \cos (\pi x / L) + \delta \quad (1)$$

in which t and L , respectively, are the wall thickness and length of the cylinder, x is the axial and y the circumferential coordinate of a point on the median surface with origin at the midpoint of a generator, and φ , ξ , and δ are undetermined deflection parameters. The quantity λ_c is the half-wave length of circumferential buckles obtained from the limiting case of vanishingly small asymmetric wave amplitudes, and can be determined from the results of small-deflection theory (see refs. 1 and 2). Justification for fixing the value of λ_c (and, hence, the number of circumferential waves) in this manner was given in reference 2.

The edge conditions implied by equation (1) are that the axial moment resultant vanishes and that the deflection equals the uniform radial displacement $t\delta$ at $x = \pm(L/2)$. This displacement component is included in equation (1) to account for the uniform radial contraction prior to buckling assumed in classical solutions (ref. 1).

It is further assumed that the cylinder has an initial radial deformation w_0 of the form

$$w_0/t = \left[\varphi_0 - \xi_0 \cos (\pi y / \lambda_c) \right] \cos (\pi x / L) \quad (2)$$

in which ξ_0 and φ_0 are independent constants.

Equations (1) and (2), together with an approximate expression for the stress function which satisfies the nonlinear compatibility equation, are employed in the determination of the total potential energy of the hydrostatically loaded shell (ref. 3). Minimization of the total potential with respect to the three deflection parameters leads to a set of three nonlinear algebraic equations which are used to determine the nonlinear load-deflection characteristics of a given family of cylinders for prescribed values of the amplitudes of the initial deformation components. These equations simplify considerably when only axisymmetric initial deformations are present, i.e., when $\xi_0 = 0$. They can then be expressed as

$$\xi f_1(\xi, \varphi, \varphi_0, p, B) = 0 \quad (3)$$

$$\varphi = f_2(\xi, \varphi_0, p, B) \quad (4)$$

$$\delta = f_3(\xi, \varphi, p, B) \quad (5)$$

in which the functions f_1 , f_2 , f_3 are in general nonlinearly dependent

upon ξ , φ , φ_0 , as well as on the hydrostatic pressure p and the cylinder parameter B . The latter quantity is defined by the relation $B = (\pi^4/48)(Rt/L^2)^2/(1-\nu^2)$, where R is the cylinder radius and ν is Poisson's ratio.

Equation (3) shows that either the asymmetric deflection amplitude ξ is identically zero or $f_1 = 0$. Consideration of the first of these possible solutions together with equation (4) leads to a relation for φ which corresponds to the axisymmetric small-deflection solution $w = w^*$, where ($\xi_0 = 0$)

$$w^*/t = \varphi_0 \left[k_p / (k_{p_{c.1}} - k_p) \right] \left[\cos(\pi x/L) - (2/\pi) \right] + \bar{w} \quad (6)$$

in which the load parameter $k_p = \pi^2(R^3/tL^2)(p/E)$ (E is Young's modulus), and $k_{p_{c.1}} = 2 \left[1 - (8/\pi^2) + 4B \right]$ is the critical-load parameter corresponding to axisymmetric small-deflection buckling ($\xi = 0$, $\varphi \neq 0$, $\delta \neq 0$ in eq. (1), and $\varphi_0 = \xi_0 = 0$ in eq. (2)). The uniform radial displacement of the prebuckled state when φ_0 (and ξ_0) = 0 is given by the relation

$$\bar{w}/t = k_p \left[1 - (\nu/2) \right] / \left[48(1 - \nu^2)B \right]^{1/2}.$$

The second solution of equation (3), i.e., $f_1 = 0$, together with equation (4), represent two simultaneous nonlinear algebraic equations for the determination of the finite asymmetric and axisymmetric deflection amplitudes ξ and φ . Elimination of φ between these equations yields a relation which is of third degree in both ξ^2 and k_p ; elimination of ξ yields a relation which is of third degree in φ and linear in k_p .

Results and Discussion

Studies of the two solutions described above show that during the early stages of loading of a given cylinder with prescribed initial axisymmetric deformation the load-deflection characteristics are those predicted by small-deflection theory (eq. (6)). However, at a later stage a bifurcation point exists, after which both the axisymmetric small-deflection solution and the large-deflection solution (the latter exhibiting both axisymmetric and asymmetric components) represent possible equilibrium states. The load corresponding to the bifurcation point can be interpreted as a buckling load consistent with

finite-deformation theory. Its value depends upon the stresses in and the deformations of the cylinder, which in turn depend upon the amplitude of axisymmetric initial deformations.

Upon examination of the solutions, a cubic equation for the buckling loads (the bifurcation points) as a function of the initial deformation amplitude φ_0 and cylinder geometry parameter B can be readily determined (ref. 3). For the technically interesting range of cylinder geometry in which the von Mises (asymmetric) buckling load is less than the axisymmetric small-deflection buckling load, the cubic equation has either three real roots, or one real root and a pair of complex conjugate roots. In the former case two of the roots lie below and the other root lies above the small-deflection axisymmetric buckling load. Such results are shown in figure 1, for which the load parameter k_p has been evaluated at the bifurcation points and designated as $k_{p_{c.o}}$. It may be seen that for an initially perfect cylinder ($\varphi_0 = (w_0/t)_{x=0} = 0$) the cubic equation for the buckling-load parameter $k_{p_{c.o}}$ yields a double root whose value is equal to $k_{p_{c.1}}$ and a single root corresponding to the von Mises buckling load (designated as k_{p_c} in fig. 1).

Stability analyses based upon the second variation of the total potential show that only the lowest root in the region of three real roots, and no root in the remaining regions, correspond to stable branches of the large-deflection solution. Furthermore, it is found that the lowest root can take on values not only significantly less than those corresponding to the axisymmetric small-deflection buckling load but also to values less than the von Mises load for small inward initial deformations. For large inward initial deformations and for all outward initial deformations, the buckling load is found to be greater than the von Mises load and less than or equal to the small-deflection axisymmetric buckling load (i.e., $k_{p_c} < k_{p_{c.o}} \leq k_{p_{c.1}}$). The manner in which $k_{p_{c.o}}$ varies with φ_0 and B is shown in figure 2, in which the extremities of the region in which $k_{p_{c.o}}$ takes on three real roots are indicated. For inward initial deformation amplitudes limited to the order of the shell thickness, the lowest buckling load varies between 90% and 100% of the von Mises load.

The postbuckling characteristics are determined from solutions to equations (3) to (5) for ξ not identically zero. Corresponding results

are indicated in figure 3, where the two hyperbolic branches associated with the axisymmetric small-deflection solution (see eq. (6)) and the three branches of the large-deflection solution are plotted for one value of B and several values of φ_0 . Only the lower ($k_p < k_{p_{c.1}}$) of

the two branches of the small-deflection solution and the lowest of the three branches of the large-deflection solution include stable and, hence, physically admissible solutions. The other branches have been included in order to display the nature of the complete solution of equations (3) to (5), and to indicate the role played by the roots $k_{p_{c.o}}$.

The large-deflection branch of the solution that emanates from the lowest of the three real bifurcation points for given values of B and φ_0 is of two types. In one of these, the load first decreases in an unstable manner with increasing deflection, reaches a minimum value, and thereafter exhibits a stable increase; in the other, the load monotonically increases in a stable fashion. The lowest curves corresponding to $\varphi_0 = -0.05$ and $\varphi_0 = 0.2$, respectively, (see figure 3) are examples of the two forms of load-deflection curves. Thus, while both types of load-deflection relations afford the possibility of a snap-through form of buckling at pressures in the regime bounded by the buckling load $k_{p_{c.o}}$ and by the axisymmetric small-deflection buckling load $k_{p_{c.1}}$, the former type also presents the possibility of snap-through buckling in the additional region bounded by the minimum postbuckling load and $k_{p_{c.o}}$.

Reference 3 and the results of additional calculations which will appear in an enlarged report based on reference 3 indicate that with inward initial deformations of the order of the wall thickness of the cylinder the lowest value of the minimum postbuckling load is of the order of 90% of the von Mises buckling load for the range of B values considered in figure 2. When minimum postbuckling loads less than the von Mises load exist, they correspond to loads only slightly less than the related buckling loads $k_{p_{c.o}}$. This occurs for small positive values of φ_0 , i.e.,

when the cylinder is initially slightly spool shaped. When $\varphi_0 < 0$ (i.e., when the shell is barrel shaped) and when φ_0 is considerably greater than $(\varphi_0)_m$ (see fig. 2), values of $k_{p_{c.o}}$ can be found which consider-

ably exceed the classical von Mises buckling load (see, for example, ref. 3 and fig. 2). However, in such cases the minimum value of the postbuckling load is significantly less than the buckling load $k_{p_{c.o}}$

and, hence, the possibility of a snap-through form of buckling places

strong restrictions on the use of $k_{p_{c.o}}$ for purposes of design.

For values of φ_o exterior to the region bounded by $(\varphi_o)_1$ and $(\varphi_o)_r$ in figure 2 physically admissible bifurcation points do not exist. However, stable postbuckling load-deflection curves can be found for these regions. Such curves were discussed in reference 3 and will be discussed in the subsequent report mentioned previously.

Current studies include the application of equations (1) and (2) modified by the addition of axisymmetric terms proportional to $\cos(3\pi x/L)$; see "Large Deflection Buckling of Initially Deformed Circular Cylindrical Shells Under Hydrostatic Pressure" by A. Misovec, Thesis for B.S. (Aerospace Engineering), Polytechnic Institute of Brooklyn, June 1962. Such terms are required for accurate calculations of axisymmetric small-deflection buckling loads when B is very small, e.g., for long cylinders, (see ref. 2). Corresponding values of $k_{p_{c.o}}$ are now determined from solutions of a fifth degree polynomial. Results to date indicate that, when a $\cos(3\pi x/L)$ -term is included only in equation (1), the loop curves in figure 2 are replaced by curves having two connected loops (figure-eight like) the lower of which yields values of $k_{p_{c.o}}$ in good agreement with the physically admissible values discussed previously.

When the initial deformations consist either of an asymmetric component or of a combination of asymmetric and axisymmetric components (see eq.(2)), the load-deflection curves differ from those described in the foregoing (see ref. 3). Two sets of such curves are displayed in figures 4 and 5 where they are compared with the results of small-deflection theory. The curves corresponding to $\xi_o = 0$ are taken from figure 3.

The load-deflection curves in figures 4 and 5 are seen to be analogous to those obtained from the large-deflection theory of rectangular plates. In view of this, no clear cut buckling criterion can be applied. Rather, a lower limit on the collapse load can be prescribed, for example, in terms of the von Mises yield criterion.

BUCKLING OF AN AXIALLY COMPRESSED NONCIRCULAR CYLINDRICAL SHELL

Analysis

The basic relations used in the buckling analysis of an axially compressed, noncircular (oval) cylindrical shell are equivalent in accuracy to those of Donnell. In the present work the median curve of the doubly symmetric cross section of the cylinder is defined in terms of its curvature $1/r$ which is expressed as a function of the running perimetrical length s in the following form:

$$1/r = (1/r_o) \left[1 + q \cos (4\pi s/L_o) \right] \quad (7)$$

where q and r_o are constants, the former being a measure of the eccentricity of the oval and obeying the inequality $|q| \leq 1$, and the latter representing the radius of a circle whose circumference $L_o = 2\pi r_o$ is equal to that of the oval. Equation (7) represents a simplified version of a relation used by Marguerre in reference 6. The limitation on the eccentricity parameter q is imposed in order to restrict the curvature to positive values. The corresponding major-minor axis ratio b/a (see fig. 6) therefore varies between 1 and 2.06.

The analysis is performed in a manner similar to that described earlier in this paper. However, the assumed deflection function is taken in the form (see "Buckling of an Axially Compressed Noncircular Cylindrical Shell" by J. Kempner and Y.-N. Chen, PIBAL Rep. in preparation)

$$w/r_o = \cos (\pi x/\lambda) \sum_{n=0}^{\infty} A_n \cos (ns/r_o) \quad (8)$$

in which A_n is a constant, and λ represents the half-wave length of buckles in the axial (x) direction. The origin of the coordinate s is the same as that implied by equation (7), i.e., either at an end of the semi-major axis (when $q > 0$) or at an end of the semi-minor axis (when $q < 0$).

Equation (8) represents a solution to the problem of a long cylinder, i.e., one for which edge effects are negligible. This expression for w and an expression for the stress function which satisfies the linear compatibility equation are used to calculate the total potential energy of the axially compressed cylinder. Since small-deflection buckling loads are sought, only quadratic terms are retained.

Minimization of the total potential with respect to A_n leads to an infinite set of simultaneous homogeneous linear algebraic equations for each value of λ . This set is separable into two sets corresponding to n being either odd or even. The eigenvalues of this system correspond to possible buckling loads. Practical calculations are performed with truncated sets of equations containing successively larger numbers of terms until the lowest eigenvalue is determined with sufficient accuracy for a selected value of λ . This procedure is repeated for different selections of λ until the minimum applied stress corresponding to buckling is computed with satisfactory accuracy.

Results and Discussion

Some of the results of the analysis are indicated in figure 6 in which σ_{cr} and σ_{cr}^0 , respectively, represent the applied uniform axially compressive buckling stress of the oval cylinder and of a circular cylinder having the same wall thickness t and circumferential length L_0 . The parameter K which enters the calculations is defined as $K =$

$\left[12(1-\nu^2)\right]^{1/2} (r_0/t)$. The results show that for a given value of this parameter the buckling stress decreases rapidly with increasing eccentricity of the cross section. The oval cylinder can be significantly weaker than a circular cylinder having the same wall thickness and circumferential length. In fact the dashed line in figure 6 is ob-

tained by letting $\sigma_{cr} = \sigma_{cr}^*$, where $\sigma_{cr}^* r_{max}/Et = \left[3(1-\nu^2)\right]^{-1/2} \approx 0.6$

and from equation 7, $r_{max} = r_0/(1 - |q|)$. Thus, substituting the expression for the maximum radius of curvature into the well-known relation for the classical buckling stress of a circular cylinder yields a simple expression for a lower bound on the buckling stress of the noncircular cylinder (see fig. 6). The corresponding relation

$\sigma_{cr}^*/\sigma_{cr}^0 = 1 - |q|$ is also determined from the analysis in the limit when $K \rightarrow \infty$.

Determination of the eigenvectors corresponding to the buckling stresses in figure 6 reveals that the distortion of the cylinder is localized about the ends of the minor axis, i.e., in the neighborhood of r_{max} . A typical buckled shape is indicated in the sketch in figure 6. As the value of either $|q|$ or K increases, the deformation becomes more localized.

FUTURE RESEARCH

In the problem of the buckling of a hydrostatically loaded circular cylinder undergoing large deformations the need exists for the introduction of assumed deflected shapes more extensive than those considered herein. Such work should include the consideration of boundary conditions likely to be met in practice, e.g., edge supports provided by elastic frames. In addition, the problem of the initially imperfect axially compressed circular cylinder should be examined in the light of the present analysis. It is anticipated that if such calculations were performed, buckling loads corresponding to bifurcation points on the prebuckled axially symmetric load-deflection curves would be revealed.

With regard to noncircular cylindrical shells, efforts should be directed towards the attainment of as complete an understanding of their behavior as now exists for circular cylinders. The use of different functional representations of the cross section should be examined. Stress and buckling analyses and experiments should be performed for classical load and boundary conditions. Some such work is currently being performed at the Polytechnic, including the problem of the postbuckling behavior of axially compressed oval cylinders. Such work should serve to indicate the usefulness of results such as those presented in figure 6.

CONCLUDING REMARKS

A brief summary of work performed on the problem of the large deflections of initially imperfect circular cylindrical shells under hydrostatic pressure as well as on the problem of the small-deflection buckling of a noncircular (oval) cylindrical shell under axial compression has been presented. The results of the first problem indicate that initial deformations have a significant effect on the buckling and postbuckling characteristics of hydrostatically loaded cylinders. The results of the second problem show that the buckling stress of an oval cylinder depends strongly on the amount of eccentricity of the cross section, and that a reasonable estimate of this stress can be obtained by the use of the formula for the buckling stress of an axially compressed circular cylinder having a radius equal to the maximum radius of curvature of the oval.

ACKNOWLEDGEMENT

The results described in the foregoing were obtained on Contract Nonr 839(14), Project No. NR 064-167 sponsored by the Office of Naval Research and the Bureau of Ships, and on Grant AF-AFOSR 62-200 sponsored by the Office of Aerospace Research.

REFERENCES

1. Batdorf, S.B.: A Simplified Method of Elastic-Stability Analysis for Thin Cylindrical Shells. I - Donnell's Equation. NACA TN 1341, June 1947.
2. Kempner, Joseph; Pandalai, K.A.V.; Patel, Sharad A., and Crouzet-Pascal, Jacques: Postbuckling Behavior of Circular Cylindrical Shells Under Hydrostatic Pressure. Jour. Aero. Sci., vol. 24, no. 4, Apr. 1957, pp. 253-264.
3. Kempner, Joseph, and Crouzet-Pascal, Jacques: Finite Deflection of Initially Imperfect Cylindrical Shells Under Hydrostatic Pressure. Presented at Xth Int. Cong. Appl. Mech., Aug. 31 to Sept. 7, 1960, Stresa; also, PIBAL Rep. No. 572, presented at A Symposium on the Mechanics of Plates and Shells for Industry Research Associates, Polytechnic Institute of Brooklyn, Mar. 9-11, 1960.
4. Donnell, L.H.: A New Theory for the Buckling of Thin Cylinders Under Axial Compression and Bending. Trans. ASME, vol. 56, 1934, pp. 795-806.
5. von Kármán, Th., and Tsien, Hsue-Shen: The Buckling of Thin Cylindrical Shells Under Axial Compression. Jour. Aero. Sci., vol. 8, no. 8, June 1941, pp. 303-312.
6. Marguerre, K.: Stability of the Cylindrical Shell of Variable Curvature. NACA TM 1302, July 1951.

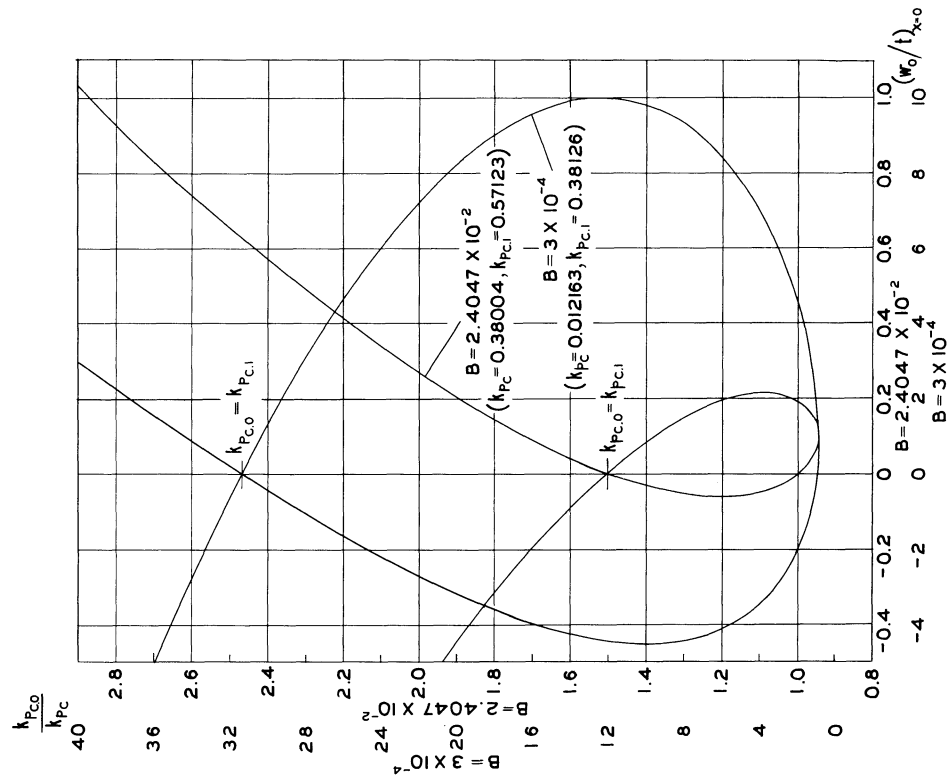


FIG. 1 VARIATION OF $k_{pc,0}$ WITH AMPLITUDE OF INITIAL DEFORMATION
($\xi_0 = 0$, $B = 3 \times 10^{-4}$ AND 2.4047×10^{-2})

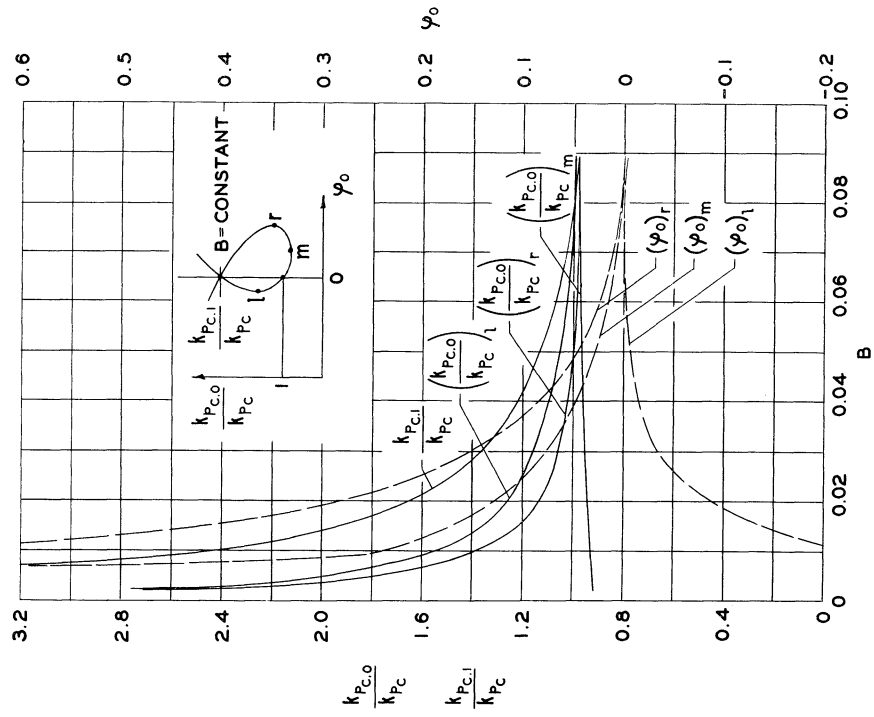


FIG. 2 LOAD AND INITIAL DEFORMATION PARAMETERS CHARACTERIZING THE DEPENDENCE OF $k_{pc,0}$ ON B

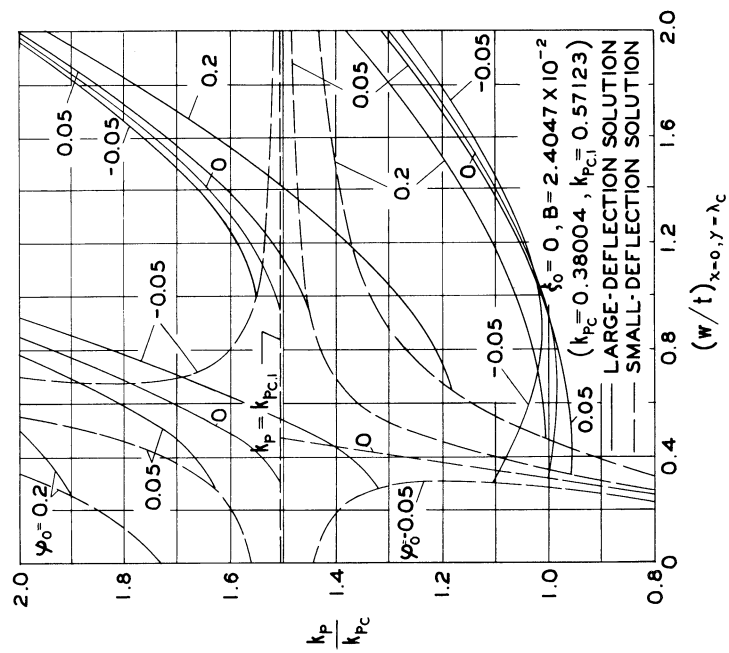


FIG. 3 LOAD-DEFLECTION DIAGRAMS FOR CYLINDERS WITH AXISYMMETRIC INITIAL DEFORMATION ONLY
($\xi_0 = 0, B = 2.4047 \times 10^{-2}$)

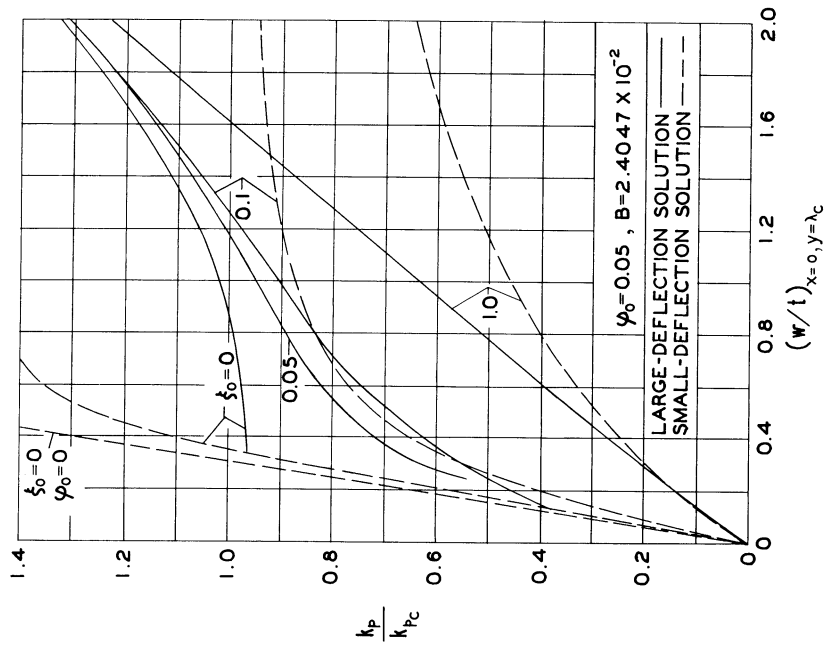


FIG. 4 LOAD-DEFLECTION DIAGRAMS FOR CYLINDERS WITH COMBINED ASYMMETRIC AND AXISYMMETRIC INITIAL DEFORMATION
($\xi_0 = 0.05, B = 2.4047 \times 10^{-2}$)

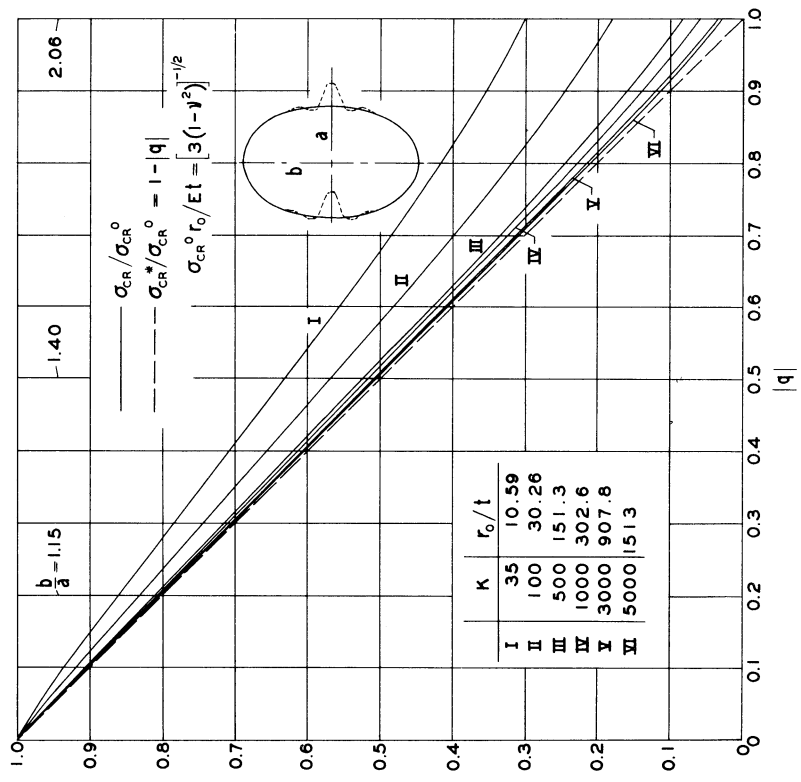


FIG. 6 VARIATION OF CRITICAL STRESS WITH ECCENTRICITY PARAMETER

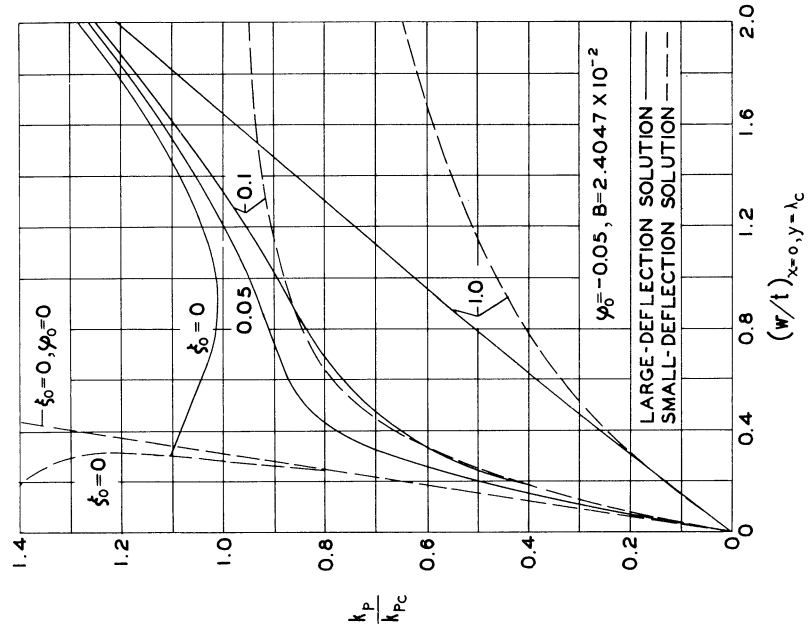


FIG. 5 LOAD-DEFLECTION DIAGRAMS FOR CYLINDERS WITH COMBINED ASYMMETRIC AND AXISYMMETRIC INITIAL DEFORMATION ($\varphi_0 = -0.05, B = 2.4047 \times 10^{-2}$)

BUCKLING OF INITIALLY IMPERFECT AXIALLY
COMPRESSED CYLINDRICAL SHELLS

By S. Y. Lu and William A. Nash

University of Florida

SUMMARY

The effects of imperfections on the buckling strength of pressurized cylinders under axial compression are studied. The imperfection factor is considered in the finite-deflection compatibility equation, as well as in the equilibrium equation. A new relation to express the imperfection as an explicit exponential function of pressure and radius-thickness ratio is proposed. A method for finding the exponential function is described, and the solution for the critical stress is found in a fairly simple form. The relation of decrease of stability with respect to magnitude of imperfections is found.

INTRODUCTION

The elastic postbuckling behavior of initially perfect cylindrical shells subject to internal pressure together with axial compression or bending has been discussed in references 1, 2, 3, and 4. It was observed that the available test results (refs. 2, 3, and 4) were lower than the critical stress found by the analysis in reference 1. On the other hand, the ratio of the increment of critical stress, due to the internal pressure, to the critical stress in an unpressurized cylinder, found in the analysis in reference 1, was fairly close to the test data in references 2, 3, and 4. This indicates that practically no shell can be considered perfect and that the solution to the "perfect" shell can only serve as an upper bound. Therefore, an investigation of the effect of imperfections is necessary.

The influence of initial imperfections was first studied by Donnell in 1934 (ref. 5). The solution for cylindrical shells under axial compression was later carried out by Donnell and Wan (ref. 6). For shells under external pressure, the effects of imperfections and finite deflections were studied by Nash (ref. 7), while the case of fixed edges was discussed by Donnell in 1958 (ref. 8).

SYMBOLS

C	index in the exponential function defined in equation 11
D	flexural rigidity, $D = Et^3 / 12(1 - \nu^2)$
E	Young's modulus
F	Airy stress function
R	radius of middle surface of shell
m, n	number of waves in axial and circumferential directions, respectively
p	internal pressure
t	wall thickness of shell
w	total normal deflection
w_i	initial deflection
x, s	co-ordinates of point in middle surface of shell
Γ	w_i/w , imperfection ratio
α	R/m^2t
η	$b_3/t\alpha$

μ	n^2/m^2
γ	imperfection coefficient defined in equation 24
ν	Poisson's ratio, $\nu = 0.3$
∇^4	$= \frac{\partial^4}{\partial x^4} + 2 \frac{\partial^4}{\partial x^2 \partial s^2} + \frac{\partial^4}{\partial s^4}$
φ	stress parameter defined in equation 18
σ	axial stress
o	superscript indicating perfect shell
cr	subscript indicating critical condition

BASIC EQUATIONS

Let w equal the total radial deflection; w_i , the initial imperfection in the radial direction; and F , the Airy stress function. The strain-displacement relations are:

$$\left. \begin{aligned} \epsilon_x &= \frac{\partial u}{\partial x} + \frac{1}{2} \left(\frac{\partial w}{\partial x} \right)^2 - \frac{1}{2} \left(\frac{\partial w_i}{\partial x} \right)^2 \\ \epsilon_s &= \frac{\partial v}{\partial s} - \frac{(w - w_i)}{R} + \frac{1}{2} \left(\frac{\partial w}{\partial s} \right)^2 - \frac{1}{2} \left(\frac{\partial w_i}{\partial s} \right)^2 \\ \epsilon_{xs} &= \frac{\partial u}{\partial s} + \frac{\partial v}{\partial x} + \frac{\partial w}{\partial x} \frac{\partial w}{\partial s} - \frac{\partial w_i}{\partial x} \frac{\partial w_i}{\partial s} \end{aligned} \right\} \quad (1)$$

The strain-stress relations in the x-s plane are:

$$\left. \begin{aligned} \epsilon_x &= \frac{1}{E} \left(\frac{\partial^2 F}{\partial s^2} - \nu \frac{\partial^2 F}{\partial x^2} \right) \\ \epsilon_s &= \frac{1}{E} \left(\frac{\partial^2 F}{\partial x^2} - \nu \frac{\partial^2 F}{\partial s^2} \right) \\ \epsilon_{xs} &= - \frac{2(1+\nu)}{E} \frac{\partial^2 F}{\partial x \partial s} \end{aligned} \right\} \quad (2)$$

The compatibility equation derived from equation 2 is:

$$\nabla^4 F = E \left(\frac{\partial^2 \epsilon_x}{\partial s^2} + \frac{\partial^2 \epsilon_s}{\partial x^2} - \frac{\partial^2 \epsilon_{xs}}{\partial x \partial s} \right) \quad (3)$$

After equation 1 is substituted in equation 3, the finite-deflection compatibility equation has the following form:

$$\begin{aligned} \nabla^4 F = E \left[\left(\frac{\partial^2 W}{\partial x \partial s} \right)^2 - \frac{\partial^2 W}{\partial x^2} \frac{\partial^2 W}{\partial s^2} - \frac{1}{R} \frac{\partial^2 W}{\partial x^2} - \left(\frac{\partial^2 W_i}{\partial x \partial s} \right)^2 \right. \\ \left. + \frac{\partial^2 W_i}{\partial x^2} \frac{\partial^2 W_i}{\partial s^2} + \frac{1}{R} \frac{\partial^2 W_i}{\partial x^2} \right] \quad (4) \end{aligned}$$

The equilibrium equation in the radial direction is:

$$D \nabla^4 (w - w_i) = \frac{t}{R} \frac{\partial^2 F}{\partial x^2} + t \left[\frac{\partial^2 F}{\partial s^2} \frac{\partial^2 w}{\partial x^2} - 2 \frac{\partial^2 F}{\partial x \partial s} \frac{\partial^2 w}{\partial x \partial s} + \frac{\partial^2 F}{\partial x^2} \frac{\partial^2 w}{\partial s^2} \right] - p \quad (5)$$

When w_i is a known function, the solution may be found by solving for w and F in equations 4 and 5 simultaneously. However, w_i is, in general, unknown. For simplicity, w is assumed to be proportional to w_i as in references 5 through 8, that is,

$$w_i/w = \Gamma = \text{imperfection ratio} \quad (6)$$

where Γ is independent of x and s . The expression for Γ will be discussed in the next section. The critical stress to be found is then a function of Γ .

With the relation from equation 6, the compatibility and equilibrium equations are expressed, respectively, as:

$$\left(\frac{1}{1-\Gamma} \right) \nabla^4 F = E(1+\Gamma) \left[\left(\frac{\partial^2 w}{\partial x \partial s} \right)^2 - \frac{\partial^2 w}{\partial x^2} \frac{\partial^2 w}{\partial s^2} \right] - \frac{E}{R} \frac{\partial^2 w}{\partial x^2} \quad (7)$$

and

$$D(1-\Gamma) \nabla^4 w = \frac{t}{R} \frac{\partial^2 F}{\partial x^2} + t \left[\frac{\partial^2 F}{\partial s^2} \frac{\partial^2 w}{\partial x^2} - 2 \frac{\partial^2 F}{\partial x \partial s} \frac{\partial^2 w}{\partial x \partial s} + \frac{\partial^2 F}{\partial x^2} \frac{\partial^2 w}{\partial s^2} \right] - p \quad (8)$$

DEFLECTION FUNCTION w AND IMPERFECTION RATIO Γ

In the present study, the deflection function for a cylindrical shell under internal pressure and axial compression is assumed to be:

$$w = b_1 + b_2 \cos \frac{mX}{R} \cos \frac{nS}{R} + b_3 \cos \frac{2mX}{R} + b_3 \cos \frac{2nS}{R} \quad (9)$$

The parameter b_1 is not independent but is used to satisfy the condition of periodicity of circumferential displacement.

The Airy stress function, accordingly, is assumed to be:

$$F = -\frac{\sigma}{2} S^2 + \frac{p}{2} \frac{R}{t} X^2 + a_{11} \cos \frac{mX}{R} \cos \frac{nS}{R} + a_{20} \cos \frac{2mX}{R} \\ + a_{22} \cos \frac{2mX}{R} \cos \frac{2nS}{R} + a_{02} \cos \frac{2nS}{R} \quad (10)$$

Before the solution is discussed, the expression for the imperfection ratio, Γ , should be studied. Evidence from previous tests (refs. 2, 3, and 4) reveals that imperfections have the greatest effect on shells having the largest ratio of R/t . The simplest way to express this relation is to assume that Γ increases linearly with R/t and then to determine the proportionality constant by means of available test data. However, this method may fit only a certain range of values of R/t . The limiting physical conditions require that: (1) $\Gamma = 0$ when $R/t = 0$, and (2) $\Gamma = 1$ only when $R/t \rightarrow \infty$. A relation to express Γ as a function of both R/t and the internal pressure p is now proposed, such that:

$$\Gamma = 1 - \exp\left(-C \frac{R}{t}\right) \quad (11)$$

The index C in the above equation is always positive and is assumed to be a function of internal pressure only. The method for determining C will be discussed later.

SOLUTIONS

The Galerkin method was employed to solve equations 7 and 8 when the assumed forms of F and w in equations 10 and 9, respectively, were used. The coefficients of the stress function F are found first as follows:

$$\left. \begin{aligned} \frac{1}{1-\Gamma} \frac{\partial_{11}}{Et^2} &= \frac{1}{(1+\mu)^2} \left[1 - 4\mu(1+\Gamma)\eta \right] \alpha \left(\frac{b_2}{t} \right) \\ \frac{1}{1-\Gamma} \frac{\partial_{22}}{Et^2} &= - \frac{1+\Gamma}{(1+\mu)^2} \mu \eta^2 \alpha^2 \\ \frac{1}{1-\Gamma} \frac{\partial_{02}}{Et^2} &= - \frac{1+\Gamma}{32\mu} \left(\frac{b_2}{t} \right)^2 \\ \frac{1}{1-\Gamma} \frac{\partial_{20}}{Et^2} &= \frac{1}{16} \left[4\eta \alpha^2 - \frac{\mu}{2} (1+\Gamma) \left(\frac{b_2}{t} \right)^2 \right] \end{aligned} \right\} \quad (12)$$

where

$$\mu = \frac{n^2}{m^2} \quad (13)$$

$$\alpha = \frac{R}{m^2 t} \quad (14)$$

$$\eta = \frac{b_3/t}{\alpha} \quad (15)$$

From the integration of equation 8 and the relation in equation 12, the following two equations are established after simplification:

$$\begin{aligned} \frac{1}{1-\Gamma} \varphi = & \frac{(1+\mu)^2}{12(1-\nu^2)} \frac{1}{\alpha} + \alpha \left\{ \frac{1}{(1+\mu)^2} - \left[\frac{4(2+\Gamma)}{(1+\mu)^2} + \frac{1}{2} \right] \mu \eta \right. \\ & \left. + (1+\Gamma) \frac{16\mu^2 \eta^2}{(1+\mu)^2} \right\} + \frac{(1+\Gamma)(1+\mu^2)}{16\alpha} \left(\frac{b_2}{t} \right)^2 \quad (16) \end{aligned}$$

and

$$\begin{aligned} \frac{1}{1-\Gamma} \varphi = & \frac{1+\mu^2}{3(1-\nu^2)} \frac{1}{\alpha} + \left[\frac{1}{4} + \frac{4(1+\Gamma)}{(1+\mu)^2} \mu^2 \eta^2 \right] \alpha \\ & + \frac{1}{\alpha} \left\{ \frac{2(1+\Gamma)}{(1+\mu)^2} \mu^2 - \frac{1}{\eta} \left[\frac{\mu}{2(1+\mu)^2} + \frac{1+\Gamma}{32} \mu \right] \right\} \left(\frac{b_2}{t} \right)^2 \quad (17) \end{aligned}$$

In the above equations, φ is a dimensionless stress parameter and

$$\varphi = \frac{\sigma R}{Et} - \mu \frac{p R^2}{E t^2} \quad (18)$$

Equations 16 and 17 can be rewritten as:

$$\frac{1}{1-\Gamma} \varphi = \frac{A_1}{\alpha} + \alpha (A_2 + A_3 \eta + A_4 \eta^2) + \frac{A_5}{\alpha} \left(\frac{b_2}{t} \right)^2 \quad (16a)$$

$$\frac{1}{1-\Gamma} \varphi = \frac{B_1}{\alpha} + \alpha (B_2 + B_4 \eta^2) + \left(\frac{B_5 + B_6/\eta}{\alpha} \right) \left(\frac{b_2}{t} \right)^2 \quad (17a)$$

In the above equations, the following notations are used:

$$\left. \begin{aligned} A_1 &= \frac{(1+\mu)^2}{12(1-\nu^2)} & B_1 &= \frac{1+\mu^2}{3(1-\nu^2)} \\ A_2 &= \frac{1}{(1+\mu)^2} & B_2 &= \frac{1}{4} \\ A_3 &= - \left[\frac{4(2+\Gamma)}{(1+\mu)^2} + \frac{1}{2} \right] \mu & B_4 &= \frac{4(1+\Gamma)\mu^2}{(1+\mu)^2} \\ A_4 &= \frac{16(1+\Gamma)\mu^2}{(1+\mu)^2} & B_5 &= \frac{2(1+\Gamma)\mu^2}{(1+\mu)^2} \\ A_5 &= \frac{(1+\Gamma)(1+\mu^2)}{16} & B_6 &= -\mu \left[\frac{1}{2(1+\mu)^2} + \frac{1+\Gamma}{32} \right] \end{aligned} \right\} \quad (19)$$

To eliminate b_2/t from equations 16a and 17a it has been found that:

$$\frac{1}{1-\Gamma} \varphi = \frac{C_1 A_1}{\alpha} + C_2 A_2 \alpha \quad (20)$$

where

$$C_1 = \frac{\frac{A_5}{A_1} B_1 - B_5 - \frac{B_6}{\eta}}{A_5 - B_5 - \frac{B_6}{\eta}} \quad (21a)$$

$$C_2 = \frac{(A_5 B_2 - A_3 B_6 - A_2 B_5) - \frac{A_2 B_6}{\eta} - (A_3 B_5 + A_4 B_6) \eta + (A_5 B_4 - A_4 B_5) \eta^2}{A_2 \left(A_5 - B_5 - \frac{B_6}{\eta} \right)} \quad (21b)$$

When φ is assumed to be a continuous function of α , the minimization of φ with respect to α leads to:

$$\frac{\partial \varphi}{\partial \alpha} = 0$$

Thus, from equation 20,

$$\alpha = \sqrt{\frac{C_1 A_1}{C_2 A_2}} \quad (22)$$

and we have

$$\varphi_\alpha = 2(1-\Gamma) \sqrt{C_1 C_2} \sqrt{A_1 A_2} = (1-\Gamma) \sqrt{C_1 C_2} \sqrt{\frac{1}{3(1-\nu^2)}} \quad (23)$$

The notation φ_α represents the value of φ that has been minimized with respect to α . It is to be noted that $\sqrt{\frac{1}{3(1-\nu^2)}}$ is the classical value from the small-deflection solution for perfect shells. However, the expressions C_1 and C_2 are dependent on Γ and, therefore, are different from those used for the case of the perfect shell, which can be considered as a limiting case by taking $\Gamma = 0$ in the present solution. The solution reduces to the small-deflection solution by letting b_3 or η approach zero and letting $C_1 = C_2 = 1$ for either perfect or imperfect shells.

The next step is to find the minimum of φ_α versus η when μ and Γ are given. This minimized value is denoted as $\varphi_{\alpha,\eta}$, which is, therefore, a function of μ and Γ . The superscript o is hereafter used to indicate the parameters of perfect shells, for which $\Gamma = 0$ identically. The magnitudes of $\varphi_{\alpha,\eta}^o$ versus μ were found in reference 1.

Let us introduce the notation

$$\gamma = \frac{\varphi_{\alpha,\eta}}{\varphi_{\alpha,\eta}^o} \quad (24)$$

The ratio γ is here called an "imperfection coefficient." The variation of γ with Γ for different values of μ is shown in figure 1. Note that curve IV ($\mu = 1.5$) is for unpressurized shells, while curve I ($\mu = 0$) is for shells subject to rather high pressures, for example, $pR^2/Et^2 \geq 1$. Let us rewrite equation 18 as

$$\frac{\sigma R}{Et} = \gamma \varphi_{\alpha,\eta}^o + \mu \frac{pR^2}{Et^2} \quad (25)$$

At the critical condition,

$$\left(\frac{\sigma R}{Et}\right)_{cr} = \gamma \varphi_{\alpha, \eta}^0 + \mu_{cr} \frac{p R^2}{E t^2} \quad (25a)$$

The notation μ_{cr} represents the value of μ at which the magnitude of σ is minimum.

The problem, now, is to determine the index C in equation 11. Since C is assumed to change only with p , it can, of course, be found by a series of tests on shells of the same R/t under different pressures. However, C is essentially an experimental constant, and the simple approach discussed in the next paragraph will reduce the necessary number of tests to one.

Previous experiences (refs. 1 and 2) indicate that μ decreases with increasing p . When $p R^2 / E t^2$ increases to approximately unity, or even greater, μ_{cr} approaches zero. It is also physically true that Γ becomes smaller at greater values of p . The exact relations among these variables are, of course, unknown. In figure 1 it can be seen that γ is a decreasing function of Γ but an increasing function of μ . Therefore, the change of pressure should not significantly change the magnitude of γ due to the somewhat counter effect of Γ and μ . At the time C is determined, γ is here assumed to be independent of p . Hence, from equation 25, it can be assumed that at certain values of R/t :

$$\left(\frac{\sigma}{\sigma^0}\right)_{p=0} = \left(\frac{\varphi_{\alpha, \eta}}{\varphi_{\alpha, \eta}^0}\right)_{p=0} \approx \left(\frac{\varphi_{\alpha, \eta}}{\varphi_{\alpha, \eta}^0}\right) \frac{p R^2}{E t^2} \geq 1 = \left(\frac{\sigma}{\sigma^0}\right) \frac{p R^2}{E t^2} \geq 1 \approx \bar{\gamma} \quad (26)$$

In the above equation, $\bar{\gamma}$ is taken as an average value of γ for all pressures. Equation 26 is used only for the

purpose of estimating C . When pR^2/Et^2 varies, the ratio $\frac{\sigma}{\sigma_0}$ is not expected to be much different from $\bar{\gamma}$. Tests can be made at any one value of pressure to find σ . The σ_0 is the corresponding critical stress in the perfect shell under the same pressure and can be found in reference 1. Then $\bar{\gamma}$ ($= \frac{\sigma}{\sigma_0}$) is determined.

After $\bar{\gamma}$ is chosen, the relation between Γ and μ is found from figure 1. With the value of R/t known in equation 11, C can be found in terms of Γ and, hence, in terms of μ . Also, μ can be found in terms of pR^2/Et^2 from equation 25a. The index C is thus determined as a function of p .

NUMERICAL EVALUATION

For the purpose of illustrating the method of finding the index C , assume $\bar{\gamma} = 0.6$ at $R/t = 1,500$. From figure 1, the change of Γ with μ can be found, and, from equation 11, C can be determined in terms of Γ . For the perfect shell, the relation between $\varphi_{\alpha,\eta}^0$ and μ has been found previously. From equation 25a the μ_{cr} at which the shell buckles can be evaluated at various values of p . Some of the numerical relations are listed in the following table.

μ, μ_{cr}	1.5	1.0	0.5	$\rightarrow 0$
Γ	0.63	0.565	0.49	0.4
$C \times 10^3$	0.662	0.555	0.448	0.34
$\varphi_{\alpha,\eta}^0$	0.161	0.183	0.29	0.605
$\frac{pR^2}{Et^2}$	0	0.06	0.19	≥ 1.0

From the above table, C versus p is plotted in figure 2.

REFERENCES

1. Lu, S. Y., and Nash, W. A.: Elastic Instability of Pressurized Cylindrical Shells Under Compression or Bending. Scheduled for publication in Proc. 4th U.S. Nat. Cong. Appl. Mech., 1962.
2. Fung, Y. C., and Sechler, E. E.: Buckling of Thin-Walled Circular Cylinders Under Axial Compression and Internal Pressure. Jour. Aeronautical Sci., vol. 24, no. 5, May 1957, pp. 351-356.
3. Lofblad, R. P., Jr.: Elastic Stability of Thin-Walled Cylinders and Cones with Internal Pressure Under Axial Compression. MIT TR 25-29, May 1959.
4. Thielemann, W. F.: New Developments in the Nonlinear Theories of the Buckling of Thin Cylindrical Shells. Deutsche Versuchsanstalt fur Luftfahrt E.V.
5. Donnell, L. H.: A New Theory for the Buckling of Thin Cylinders Under Axial Compression and Bending. ASME Trans., vol. 56, Nov. 1934, pp. 795-806.
6. Donnell, L. H., and Wan, C. C.: Effect of Imperfections on Buckling of Thin Cylinders and Columns Under Axial Compression. Jour. Appl. Mech., vol. 17, no. 1, Mar. 1950, pp. 73-83.
7. Nash, W. A.: Effect of Large Deflections and Initial Imperfections on the Buckling of Cylindrical Shells Subject to Hydrostatic Pressure. Jour. Aeronautical Sci., vol. 22, no. 4, Apr. 1955, pp. 264-269.
8. Donnell, L. H.: Effect of Imperfections on Buckling of Thin Cylinders with Fixed Edges Under External Pressure. Proc. 3rd U.S. Nat. Cong. Appl. Mech., 1958, pp. 305-311.

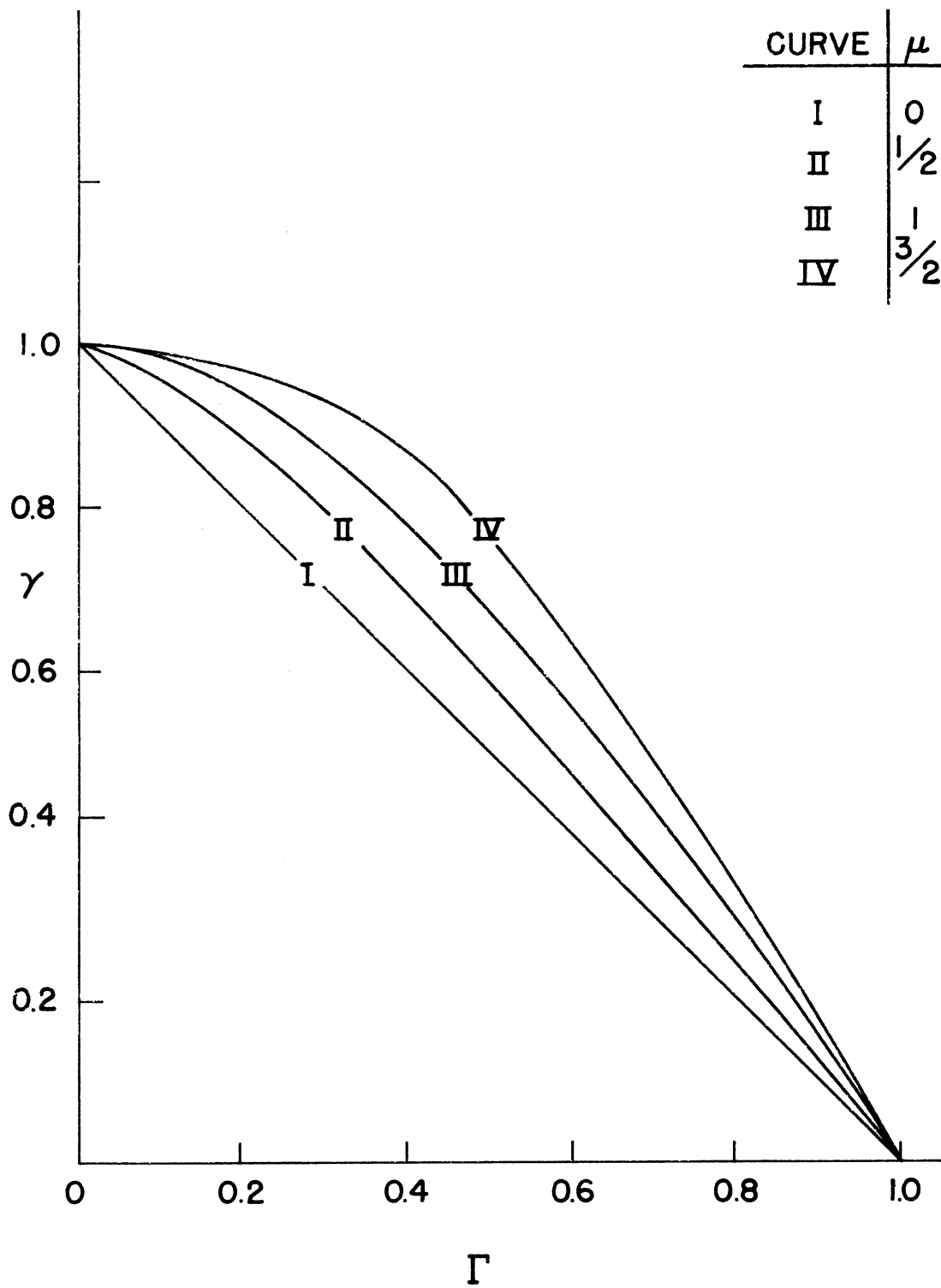


Figure 1.- Variation of imperfection coefficient with imperfection ratio.

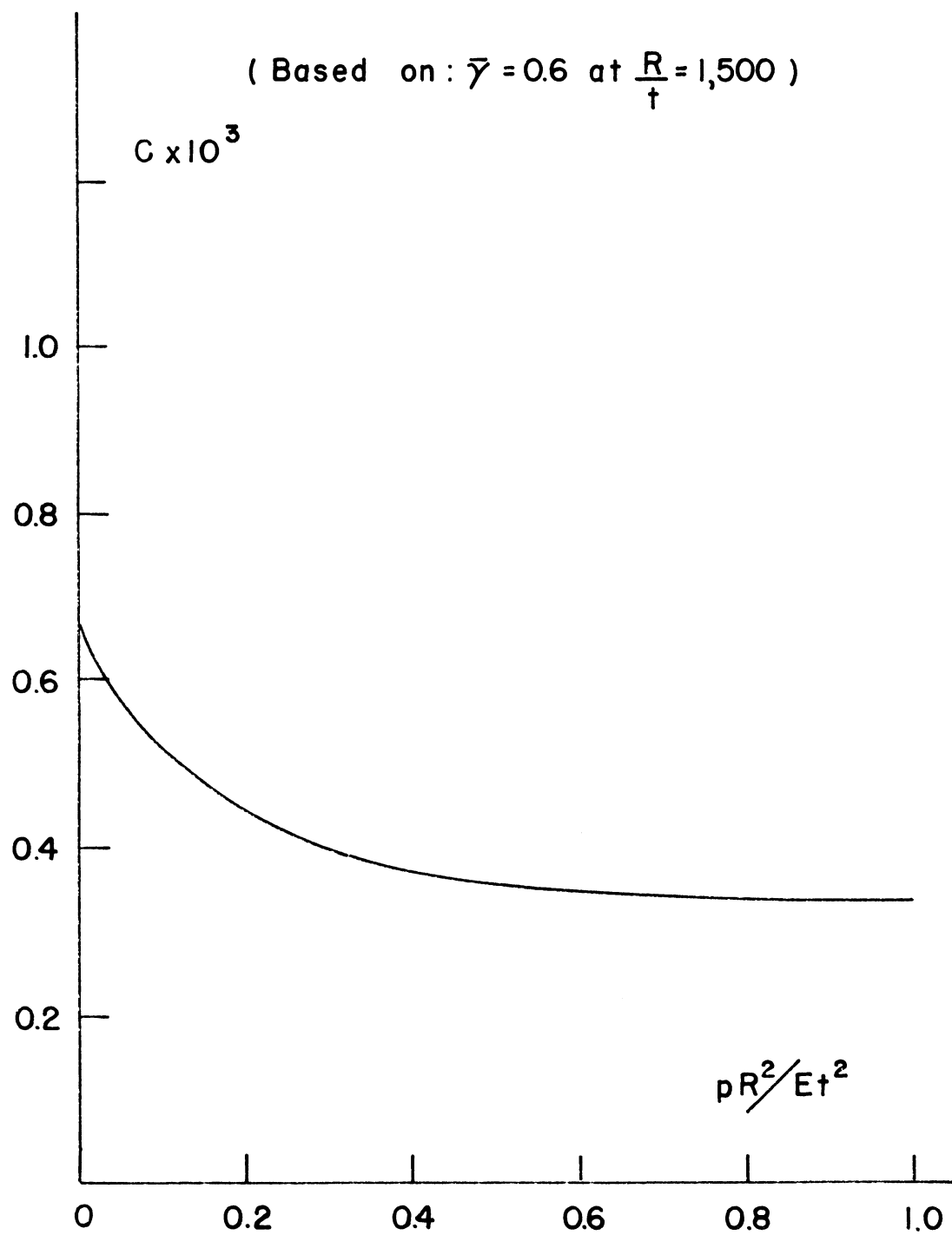


Figure 2.- Variation of index C with pressure.

ON THE POSTBUCKLING BEHAVIOR OF THIN CYLINDRICAL SHELLS

By W.F. Thielemann

Deutsche Forschungsanstalt für Luft- und Raumfahrt e.V. (DFL)
Braunschweig (Germany)

SUMMARY

Results of tests on postbuckling equilibrium positions of isotropic thin-walled circular cylindrical shells under axial compression, external pressure and combined loading are reported and compared with available theoretical results.

INTRODUCTION

Since, in 1941, von Kármán and Tsien in their basic work on the postbuckling behavior of axially compressed thin-walled circular cylinders [1] gave an explanation for the discrepancy between experimental collapse loads and the buckling loads predicted by classical small-deflection theory, many investigators improved the results of von Kármán and Tsien and extended the methods used by these authors to other loading cases (references see [2]).

The non-linear problem of the postbuckling behavior of thin shells can be represented by two partial differential equations [2]. Their approximate solution by energy methods generally involves a large amount of numerical work. Therefore, in most of the investigations known the approximations to the "exact" solution are not yet fully satisfying.

The degree of approximation of the theoretical results should be measured by tests on cylindrical shells made in the postbuckling region. Unfortunately, tests in this region are difficult to perform since the large deflections of the walls of the shells may result in plastic deformations, the effect of which is generally not included in the theoretical investigations on the postbuckling behavior. However, cylinders made of Mylar, which have been used by several experimenters in the recent time, show elastic properties even at large deflections of the walls, so that by using this material a possibility is given to investigate experimentally the postbuckling behavior of thin shells, and to compare the test results with the known results of theoretical investigations on this problem.

In the following, some results of experimental investigations on the postbuckling behavior of thin isotropic cylindrical shells under axial compression, external pressure, and combinations of these loadings, made at the DFL at Braunschweig (Germany) will be reported and the agreement with available theoretical results will be discussed.

REMARKS ON THE THEORY OF POSTBUCKLING BEHAVIOR

In the investigations known on the postbuckling behavior of thin-walled shells, in most cases, the Ritz energy method has been used. In this method, the total potential energy of the system will be varied with respect to the free amplitudes of a trigonometric series approximating the buckling pattern of the shell.

At axisymmetrically loaded circular cylinders buckling patterns with periodic buckles (number of buckles n) in the circumferential direction can be observed in tests, whereas in longitudinal direction no periodicity of the buckles occurs (fig. 1). These buckling patterns may be generally described by the series:

$$w = \sum_{j=0}^{\infty} f_j(x) \cos j \frac{ny}{r} . \quad (1)$$

$f_j(x)$ can be expanded to the Fourier series

$$f_j(x) = \sum_{i=0}^{\infty} \left(a_{ij} \cos i \frac{\pi x}{l} + b_{ij} \sin i \frac{\pi x}{l} \right) , \quad (2)$$

where l is the length of the cylinder.

In spite of the fact that in tests on axially compressed cylinders local buckles are observed (see fig. 1a), which should be described by (1), in the work of von Kármán and Tsien and in the later works on this problem it was assumed that the buckles are periodically distributed over the entire length of the cylinder. The influence of the length of the cylinder and the boundary conditions on the buckling pattern was neglected. In this case, the buckling pattern can be described in the simplified form:

$$w = \sum_{j=0}^{\infty} \sum_{i=0}^{\infty} a_{ij} \cos i \frac{\pi x}{l_x} \cos j \frac{ny}{r} ; \quad (i+j) \text{ even} , \quad (3)$$

where l_x is the half-wave length of a buckle in axial direction.

Von Kármán and Tsien, in their investigation on the axially compressed cylinder [1], approximated the buckling pattern using three terms out of the series (3), and varied the potential energy with respect to the amplitudes of these terms. They kept the number n of the buckles in circumferential direction constant and also fixed the half-wave length l_x of the buckles. For constant values of the ratio $\mu = l_y/l_x$ ($l_y = \pi r/n$, half-wave length of buckles in circumferential direction), the states of equilibrium of the buckled shell were represented in a series of load-shortening curves with integral numbers n as parameter. For small values of μ , states of equilibrium of the buckled shell connected with axial tensile forces were found, a result which was regarded to be unlikely. In the later investigations [3], [4], the potential energy of the system was not only varied with respect to the amplitudes of the terms of the Fourier series but also with respect to the wave lengths l_x and l_y . This procedure resulted in one single curve for the states of equilibrium in the post-buckling region, all these states of equilibrium being connected with compression forces.

However, the variation of the total potential energy with respect to l_y , i.e. to the number n of the buckles in circumferential direction, is not admissible since by applying the Ritz method according to Lagrange's principle only such displacements can be admitted which do not violate the condition of geometric compatibility of the system. It is obvious that a continuous variation of n would violate the condition of periodicity in the circumferential direction. Therefore, n should be kept constant in the investigation of the postbuckling behavior of shells.

The variation of the total potential energy with respect to the half-wave length l_x is only admissible, if the influence of the length of the cylinder on the buckling pattern is neglected, as assumed in the investigations mentioned above. For the description of actual buckling patterns of cylinders with finite length the series (1) and (2) should be used rather than the series (3). In this case the variation with respect to a half-wave length in axial direction will become meaningless.

The proposed procedure which is based on a more rigorous application of the principles of mechanics will result in a series of load-deflection curves with integral values of n as parameters. Consequently, at given values of load or deformation several equilibrium positions may exist with different numbers n of buckles in the circumferential direction, which is in agreement with the behavior of cylinders observed in tests (see fig. 2, 3 and 4).

These equilibrium positions are, of course, connected with different values of potential energy. The cylinder not necessarily adopts the equilibrium position with the lowest level of potential energy in the postbuckling region. The transition, at a given load or deformation, from a stable equilibrium position of higher energy level to another stable finitely adjacent equilibrium position with lower energy level generally requires the surmounting of an "energy hump", i.e. the input of additional external energy of finite magnitude into the system. At certain critical values of given load or deformation the transition from a position of higher energy level to another one with lower energy level occurs without input of additional external energy: the equilibrium at these critical values becomes indifferent. These critical loads shall be called "secondary buckling loads".

Unfortunately little can be said about the stability of the states of equilibrium by the results of the Ritz method. The theoretical determination of the secondary buckling loads involves more difficulties than the determination of the classical primary buckling load, since, in the latter case, a pure membrane state of stress is assumed in the prebuckling region, whereas in the former case the stability of a complicated combined membrane and bending state of stress has to be investigated.

CYLINDERS UNDER AXIAL COMPRESSION

Tests in the Postbuckling Region

The tests were made on circular cylinders manufactured of Mylar. Dimensions of the specimen: length $l = 400$ mm, radius $r = 200$ mm, and wall thickness $t = 0,254$ mm. Young's modulus of Mylar is approximately $E = 500$ kp/mm² and Poisson's ratio $\nu = 0,3$. The modulus of elasticity of each specimen has been measured. The edges of the cylinders were clamped by plastic cement to end plates. The cylinders were tested in a rigid test equipment allowing a control of the shortening. The loads and the deformations of the specimen in axial direction were measured and registered by an x-y-plotter. The loading of the specimen was performed continuously.

Fig. 2 shows the load-shortening curves of the cylinder in the postbuckling region obtained in the test. At the critical value of shortening of the specimen, according to an axial stress ratio of $\sigma / \sigma_{cl} = 0,63$ ($\sigma_{cl} = Et/r \sqrt{3(1 - \nu^2)}$), the initial form of the cylinder becomes unstable, and the cylinder jumps into a

new stable equilibrium position, which is connected with a local buckling pattern of two staggered rows of buckles ($n = 14$) near the middle region of the cylinder (see fig. 1a).

With increasing shortening the equilibrium of the buckled cylinder also becomes unstable at a critical load, which has been called secondary buckling load in the preceding section. The specimen jumps into a new similar buckling pattern the number of buckles of which is reduced by one ($n = 13$). This process will be repeated with increasing shortening of the specimen. By loading and unloading the specimen a series of curves representing stable equilibrium positions in the postbuckling region can be obtained. It can be seen from fig. 2, that indeed several stable equilibrium positions exist for the same value of shortening of the specimen. The fact that the transition from one buckling pattern (n) to the other ($n - 1$) is connected with a jump indicates that the stable equilibrium position (n) near the critical secondary buckling load is connected with a higher energy level than the adjacent equilibrium position ($n - 1$),

A characteristic feature of the postbuckling behavior of cylinders under axial compression is the low load carrying capacity in the postbuckling region which is in the order of 10 - 25 per cent of the classical buckling load. No considerable increase of the axial load can be obtained with increasing shortening due to the low values of the secondary buckling loads.

Comparison with Theory

No theoretical results are known which could be directly compared with the test results, since no attempt has been made yet to describe the local buckling pattern (fig. 1a) by a Fourier series in the form of (1) and to use integral numbers of n as parameters in the investigation. But there are results from the theoretical work of Kempner [4] and of Almroth^{*}). In both investigations it was assumed that the buckles are distributed over the entire length of the cylinder, and terms of Fourier series (3) were used to describe the buckling pattern. The potential energy was varied with respect to n , so that the postbuckling equilibrium positions are represented by a single load-deflection curve. Kempner used three terms of (3) with the amplitudes a_{20} , a_{11} and a_{02} while Almroth took into consideration nine terms of (3) with the amplitudes a_{20} , a_{40} , a_{60} , a_{11} , a_{31} , a_{02} , a_{22} , a_{13} , a_{33} . The results of the two investigations are compared

^{*}) Private communication to the author of May 11, 1962

with the test results in fig. 2 . It is interesting to note that Almroth's more complete description of the buckling pattern results in a considerable improvement of Kempner's solution. The agreement of Almroth's solution with the test results is remarkable with regard to the fact, that the buckling pattern used in the theoretical investigation is considerably different from the local buckling pattern observed in tests.

CYLINDERS UNDER EXTERNAL PRESSURE

Tests in the Postbuckling Region

Tests were performed on two Mylar cylinders. One specimen had the same dimension as the specimen for axial loading, and the second one had a length of 200 mm, while the other dimensions remained unchanged. The edges of the cylinders were again clamped by plastic cement to end plates. The external pressure produced by decreasing the pressure in the cylinder was controlled. The pressure and the axial shortening of the cylinder were registered on an x-y-plotter.

Fig. 3 shows the stable equilibrium positions of the cylinders in the postbuckling region. At critical values of external pressure the initial form of the cylinder becomes unstable. The buckling pattern develops in a progressive fashion rather than with a sudden appearance of the buckles around the entire cylinder. But after a small increase of the external pressure the complete buckling pattern can be observed ($n_{cr} = 10$ and $n_{cr} = 14$, resp.) (see fig. 1c). This postbuckling configuration of the cylinder shows a remarkable degree of stability under increasing external pressure loading. Contrary to the case of axial loading no secondary buckling pressure could be observed. To avoid a final uncontrolled collapse of the specimen the increase of the loading was stopped at values of about 150 per cent of the critical value of external pressure. However, by applying additional local external loads to the surface of the cylinder transition to an adjacent buckling pattern with a number of buckles $n - 1$ can be achieved at loads below the secondary buckling pressure.

This process can be repeated, and a series of curves representing stable equilibrium positions in the postbuckling region for different values of n can be registered by loading and unloading the cylinder. It can again be noticed from fig. 3 that for a given external pressure several stable equilibrium positions of the cylinder exist in the postbuckling region related to different values of n .

During unloading the cylinder in a buckling configuration $n < n_{cr}$, at a critical value of external pressure, the cylinder jumps back into a buckling configuration with the number of buckles $n + 1$. Equilibrium positions with number of buckles n below this critical value of external pressure are unstable. By further decrease of the loading this process will be repeated, until the cylinder jumps into its initial unbuckled configuration. (Since during the snap-through process the pressure in the cylinder cannot be kept constant, the curves representing the jumps, are not horizontal straight lines as it should be expected for jumps at controlled external pressure.)

The test results indicate that due to the very high degree of stability of the buckling configuration, only the buckling pattern $n = n_{cr}$ can be expected to be observed in tests after buckling. Transitions to other configurations ($n < n_{cr}$) require a considerable increase of the external pressure loading beyond the critical pressure. This behavior is in contrast to the behavior of axially compressed cylinders. Since in the latter case the stability of the postbuckling configurations is lost at values far below the critical buckling load the cylinder may jump into buckling patterns with different numbers of n , depending on the stiffness of the test equipment.

Comparison with Theory

Direct comparison of the test results with results of theoretical investigations of the postbuckling behavior of cylinders under external pressure is difficult, since available results either do not take into account the actual boundary conditions of the test cylinders (clamped edges) or do not use a sufficient number of terms of a Fourier-series to describe the buckling pattern in a satisfying manner.

The influence of the boundary conditions on the buckling load and the postbuckling behavior of a cylinder under external pressure is considerably stronger than in the case of axial compression. In the latter case for cylinders with ratios $l/r \geq 1,5$ the influence of length and boundary conditions on the buckling load can be neglected [5], while in the former case the classical buckling load found for cylinders with simply supported edges (v. Mises' theory) will be increased for cylinders with clamped edges by a factor of approximately 1.3. This factor is not well established, since for clamped edges only approximate solutions [6] for the buckling load of the cylinder are known, the accuracy of the results depending on the degree of approximation of the buckling pattern by the Fourier series.

Under the assumption that the theoretical critical pressure p_{cr} of cylinders with clamped edges is 1.3 of the classical v. Mises buckling pressure for hinged edges the actual buckling pressures of the two test cylinders were 70 % and 92 % of the theoretical buckling load p_{cr} .

The buckling pattern in the postbuckling region of the cylinder with clamped edges can be described by the equations (1) and (2), which for hinged edges will be simplified to

$$w = \sum_{i=1}^{\infty} \sum_{j=0}^{\infty} a_{ij} \sin i \frac{\pi x}{l} \cos j \frac{\pi y}{r}; \quad i \text{ odd}, \quad (4)$$

the origin of the coordinate-system being on the one edge of the cylinder.

Fig. 4 shows theoretical load deformation curves of simply supported cylinders under external pressure. For different length parameters $\lambda = \sqrt{3(1-\nu^2)}l/\sqrt{r t}$ these curves have been calculated at the DFL using the Ritz method. Four terms with the amplitudes a_{10} , a_{11} , a_{30} and a_{31} out of the series (4) have been used to describe the buckling pattern approximately. A similar investigation has been performed by Kempner [7], who introduced two terms with the amplitudes a_{10} and a_{11} in his calculations. He restricted his investigation to a single load-deformation curve of the equilibrium states related to the buckling pattern with the number of buckles $n = n_{cl}$, where n_{cl} is the number of buckles received from linear buckling theory.

The theoretical load-deflection curves of fig. 4 show the same principal trend as the experimental curves of fig. 3. For cylinders with higher values of λ the approximate theoretical investigation indicates equilibrium positions related to negative values of external pressure (internal pressure). This result of the theory is not confirmed by the tests. The reason for this unsatisfactory theoretical result is without doubt - beside the assumption of hinged edges - the incomplete description of the buckling pattern by only four terms of the series (4), which, apparently, is not sufficient for long cylinders and large values of deformation. Under these conditions the buckling pattern of fig. 1c will be changed to a pattern, showing some kind of corrugation with approximately constant amplitude of the buckles in axial direction on a considerable part of the cylinder length. The transition from the corrugated form to the circular form at the ends of the cylinder is limited to a relatively narrow edge region (see fig. 1d). This buckling pattern, of course, cannot be described by the four terms used in the theoretical investigation with satisfying accuracy.

However, the buckling patterns with $n < n_{cr}$ are of more academic interest, as, due to the high degree of stability of the buckling pattern $n = n_{cr}$, only this pattern will be observed in tests without input of additional external energy.

In fig. 4 the minimum loads in the postbuckling region for the buckling pattern $n = n_{cr}$ are given as function of the length parameter λ . This value can be approximately regarded as a lower limit for the actual buckling load of the cylinder. Due to initial imperfections the actual buckling load may vary between the theoretical buckling load p_{cr} and the minimum load in the postbuckling region p_{min} .

In fig. 4 theoretical results for p_{min}/p_{cr} for cylinders with hinged edges from the investigations of Kempner and the DFL are compared with results obtained in tests for cylinders with clamped edges. Donnell [6] investigated theoretically the postbuckling behavior of circular cylinders under external pressure with clamped edges, using a two-terms expression for the buckling pattern, but did not succeed in finding a minimum load in the postbuckling region.

CYLINDER UNDER COMBINED LOADING

Experimental curves of postbuckling states of equilibrium for different numbers of buckles n are given for a cylinder tested under combined axial compression and external pressure as a further example for the postbuckling behavior of isotropic cylinders. The external pressure $p/p_{cr} = 0.7$ has been kept constant during the test while the shortening of the cylinder has been varied. As in the cases of pure axial loading and pure external pressure loading, it can be seen from fig. 5 that the postbuckling behavior of the cylinder is represented by a series of load-deflection curves rather than by a single curve. Fig. 1b shows the buckling pattern of this loading case.

Again the transition from one buckling pattern to the adjacent one occurs at secondary buckling loads. No theoretical investigation of the combined loading case is known, the results of which could be compared with the test results.

CONCLUSIONS

The test results discussed in this report indicate that cylindrical shells under axisymmetrical loading show in the postbuckling region for given values of end shortening or loading several stable equilibrium positions related to different integral circumferential wave numbers n . With increasing shortening or loading the equilibrium positions may become unstable and transition to an adjacent stable equilibrium position may occur. In theoretical investigations on the postbuckling behavior the variation of the potential energy with respect to n is not in agreement with a rigorous application of the principles of mechanics, and should be abandoned, as the results of such theoretical investigations may deviate considerably from the actual postbuckling behavior of the shell.

The theoretical determination of the secondary buckling loads involves more difficulties than the determination of the classical primary buckling load. For external pressure loading, such a theoretical investigation on secondary buckling loads has approximately been performed by Ivanov [8].

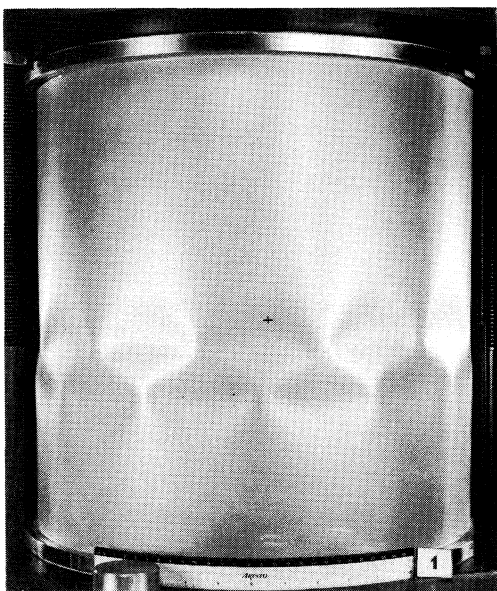
The results of the available theoretical investigations of the postbuckling behavior of shells under axisymmetric loading are not yet satisfactory. For axially loaded cylinders remarkable progress has been made by Almroth. In a future extension of the investigations equation (1) should be used for the description of the local buckling pattern of fig. 1a, taking into account the boundary conditions and the length of the cylinder.

For cylinders under external pressure loading the investigation on the postbuckling behavior of the, practically, important case of clamped edges should be extended to more complete descriptions of the buckling pattern by equation (1), in order to get better agreement of experimental and test results. Even the primary theoretical buckling load of cylinders with clamped edges should be better determined.

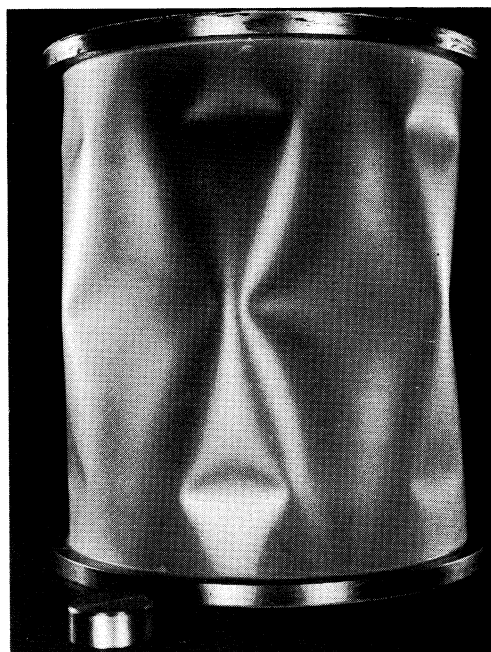
The experimental investigation of the DFL on the postbuckling behavior of isotropic circular cylindrical shells under axisymmetrical loading will be continued.

REFERENCES

1. Kármán, Th. von, and Tsien, H.S.: The Buckling of Thin Cylindrical Shells under Axial Compression. Jour.Aero.Sci. Vol. 8, No. 8, 1941 pp. 303-312
2. Thielemann, W.F.: New Developments in the Nonlinear Theories of the Buckling of Thin Cylindrical Shells. Aeronautics and Astronautics, Proc. Durand Centennial Conf., Pergamon Press (London), 1960, pp. 76-119
3. Michielsen, Hermann F.: The Behavior of Thin Cylindrical Shells after Buckling under Axial Compression. Jour.Aero. Sci. Vol. 15, No. 12, 1948, pp. 738-744
4. Kempner, J.: Postbuckling Behavior of Axially Compressed Circular Cylindrical Shells. Jour.Aero.Sci., Vol. 21, No. 5, 1954, pp. 329-335,342
5. Kanemitsu, S. and Nojima, N.M.: Axial Compression Tests of Thin Circular Cylinders. M.S. thesis, Calif. Inst. Technol. 1939
6. Donnell, L.H.: Effect of Imperfections on Buckling of Thin Cylinders with Fixed Edges under External Pressure. Proc. 3rd U.S. Nat. Congr. Appl. Mech. (June 1958, Providence, R.I.) ASME 1958, pp. 305-311
7. Kempner, J., Pandalai, K.A.V., Patel, S.A., and Crouzet-Pascal, J.: Postbuckling Behavior of Circular Cylindrical Shells under Hydrostatic Pressure. Jour. Aero. Sci., Vol. 24, No. 4, 1957, pp. 253-264
8. Ivanov, V.S.: On the Problem of a Static Elastic Circular Cylindrical Shell with Initial Deflection. PMM, Vol. 22, No. 5, 1958, pp. 687-690, Jour. Appl. Math. Mech., Vol. 22, No. 5, 1958, pp.965-971



(a) Axial compression.



(b) Combined axial compression and external pressure.

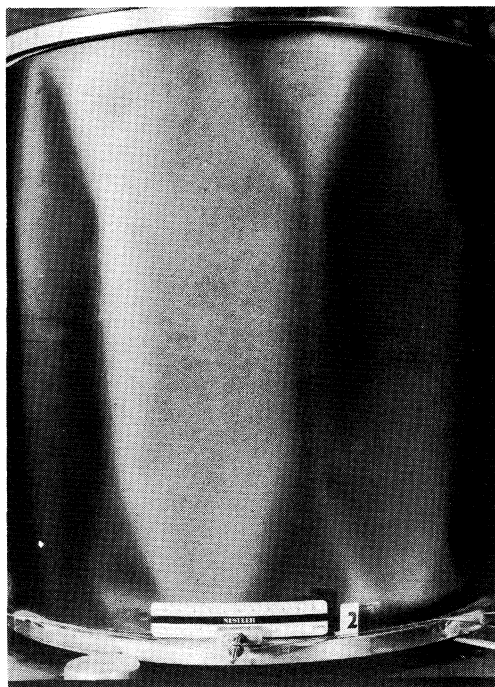
(c) External pressure.
 $n = n_{cr} = 10.$ (d) External pressure. $n = 9.$

Figure 1.- Buckling patterns of axisymmetrically loaded cylinders.

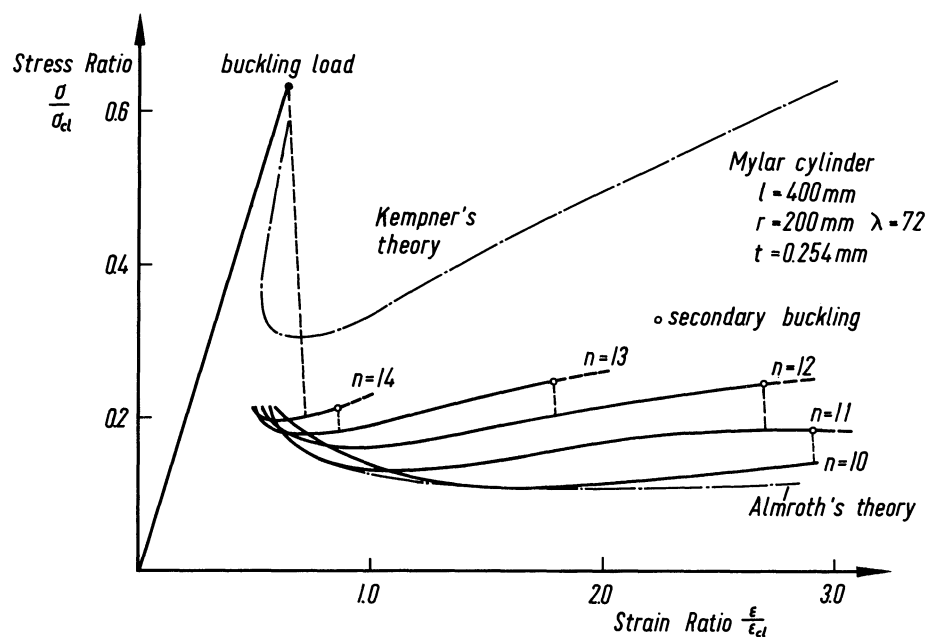


Figure 2.- Cylinder under axial compression. Postbuckling states of equilibrium - test results.

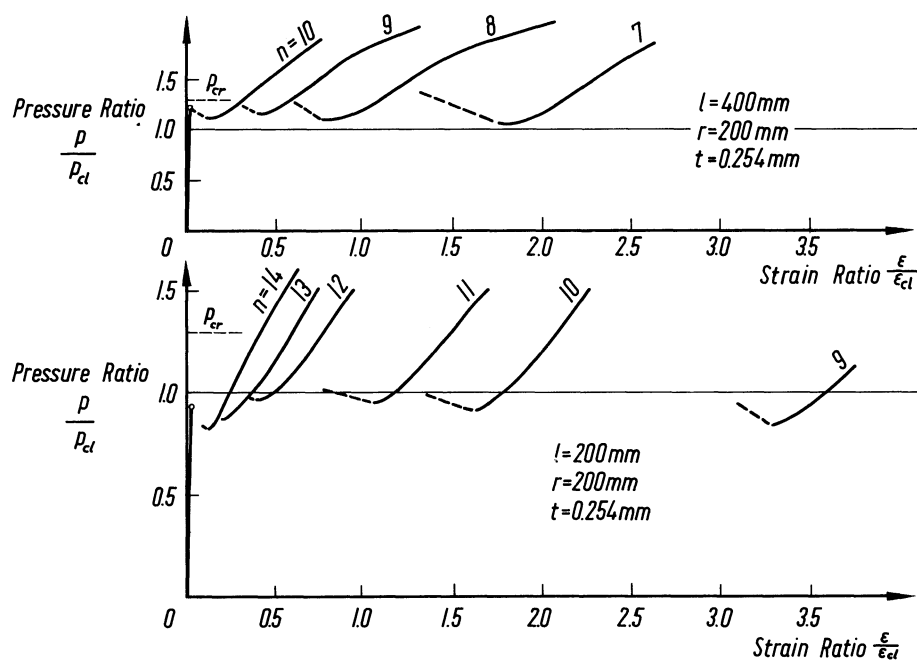


Figure 3.- Cylinders under external pressure. Test results.

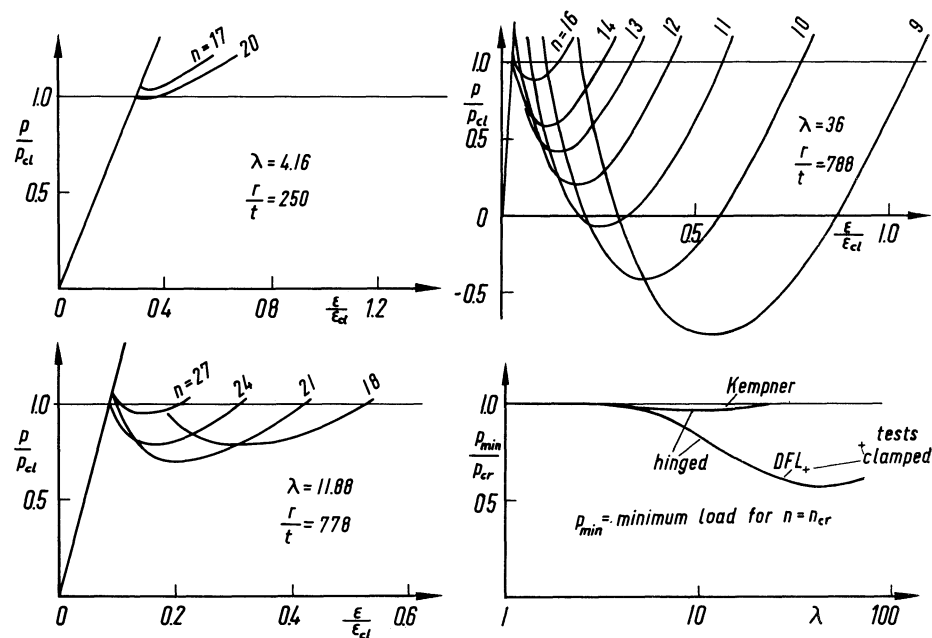


Figure 4.- Cylinders under external pressure. Theoretical results.

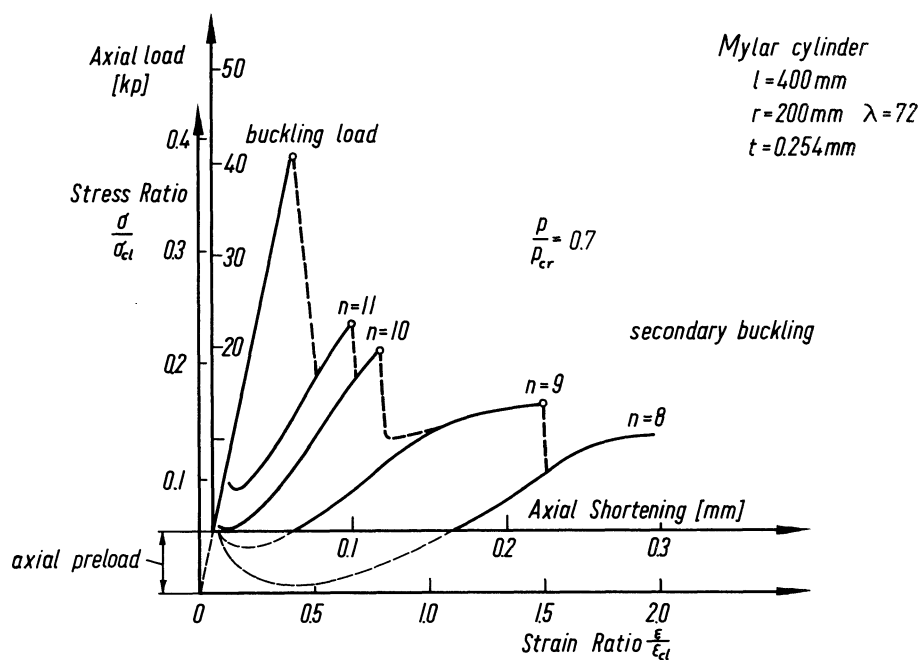


Figure 5.- Cylinder under axial compression and external pressure. Postbuckling states of equilibrium - test results.

THE EFFECT ON THE BUCKLING OF PERFECT CYLINDERS
OF PREBUCKLING DEFORMATIONS AND STRESSES
INDUCED BY EDGE SUPPORT

By Manuel Stein

NASA Langley Research Center

SUMMARY

Large deflection theory is used to compute buckling loads of simply supported initially perfect cylinders under axial compression, external hydrostatic pressure, and combinations of axial compression and internal or external pressure. Important results are obtained by taking into account prebuckling deformations and stresses induced by edge support. For example, the presence of these deformations and stresses can decrease the axial-compression buckling load of an unpressurized perfect cylinder by 50 percent or more.

INTRODUCTION

Classical theory and experiment are in good agreement for buckling of circular cylindrical shells under uniform external lateral pressure. (See ref. 1.) For external hydrostatic pressure there is similar agreement between experiment and theory except for the lower range of curvature parameter ($Ir^2/rt < 100$). For axial compression, however, severe disagreement exists; experiments have shown that the actual buckling stress is from 15 to 50 percent of that predicted by classical theory. (See ref. 2.) The disagreement found in hydrostatic pressure tests at low values of the curvature parameter is probably also due to the inability of classical theory to account for axial compression. (See ref. 1.)

Convincing arguments have been made that the occurrence of lower-than-expected buckling stresses for axial compression is due in part to initial imperfections. For example, the results of large deflection analysis (see ref. 3) have indicated that small initial imperfections can lead to large reductions in the buckling load. However, another potential reason for this disagreement of classical theory and experiment has, until recently, been unexplored. This potential reason for the disagreement is the inconsistent assumption of classical theory with regard to prebuckling and buckling-edge conditions. It is assumed

that the prebuckling deflection and stress components are either constant or zero and imply that the edges of the shell are free until buckling occurs; however, during the buckling process the edges are assumed to be radially restrained (simply supported or clamped).

The effect of one deviation from the classical-edge conditions has already been investigated (see refs. 4 and 5) for buckling in axial compression by use of linear equations. The edges of the shell were allowed to remain free during the buckling process. The resulting buckling load was less than half the classical load; the result demonstrates effectively the importance of the edge conditions. In practice, however, the occurrence of free edges is rare; the edges of the shell are usually attached to a ring or pressed against the platens of a testing machine. Thus, it seems more realistic to take a consistent but opposite approach, wherein from the inception of loading through buckling the edges of the cylinder are radially restrained. Moreover, it is apparent that such restraint must lead to nonuniform prebuckling deflections and stresses throughout the cylinder, the importance of which should be determined. This approach to cylinder buckling analysis has been adopted in the present investigation.

A cylinder without initial imperfections is considered, and large deflection theory is used to determine the deformations and stresses prior to buckling and to determine the buckling equation. Results are obtained for buckling of simply supported cylinders under axial compression, external hydrostatic pressure, and combinations of axial compression and internal or external pressure.

SYMBOLS

n	number of waves in circumferential direction
p	pressure
r	radius of cylinder
t	thickness of cylinder wall
u,v,w	displacements in the x-, y-, and radial directions, respectively
x,y	axial and circumferential directions
D	plate stiffness, $Et^3/12(1 - \mu^2)$
E	Young's modulus for material

L	length of cylinder
M	number of stations in half length
P	applied axial midplane compressive force per unit length
U,V,W	functions of x which appear in the buckling displacements u_B , v_B , and w_B , respectively
Z	curvature parameter $\left(\frac{L^2}{rt} \sqrt{1 - \mu^2} \right)$
μ	Poisson's ratio for material
u_A, w_A	prebuckling displacements (functions of x)
u_B, v_B, w_B	buckling displacements (functions of x and y)
N_x, N_y, N_{xy}	midplane forces per unit length
$\epsilon_x, \epsilon_y, \gamma_{xy}$	midplane strains

$$\nabla^4 = \frac{\partial^4}{\partial x^4} + 2 \frac{\partial^4}{\partial x^2 \partial y^2} + \frac{\partial^4}{\partial y^4}$$

When the subscripts x and y follow a comma, they indicate partial differentiation of the principal symbol with respect to x and y .

ANALYSIS

In the large-deflection Donnell theory, the basic differential equations of equilibrium of a cylinder:

$$\left. \begin{aligned} N_{x,x} + N_{xy,y} &= 0 \\ N_{y,y} + N_{xy,x} &= 0 \\ D \nabla^4 w + \frac{N_y}{r} - (N_x w_{,xx} + N_y w_{,yy} + 2N_{xy} w_{,xy}) &= p \end{aligned} \right\} \quad (1)$$

together with Hooke's law:

$$\left. \begin{aligned} N_x &= \frac{Et}{1 - \mu^2} (\epsilon_x + \mu \epsilon_y) \\ N_y &= \frac{Et}{1 - \mu^2} (\epsilon_y + \mu \epsilon_x) \\ N_{xy} &= \frac{Et}{2(1 + \mu)} \gamma_{xy} \end{aligned} \right\} \quad (2)$$

and the nonlinear strain-deformation relations:

$$\left. \begin{aligned} \epsilon_x &= u_{,x} + \frac{1}{2} w_{,x}^2 \\ \epsilon_y &= v_{,y} + \frac{w}{r} + \frac{1}{2} w_{,y}^2 \\ \gamma_{xy} &= u_{,y} + v_{,x} + w_{,x} w_{,y} \end{aligned} \right\} \quad (3)$$

provide a complete set of 9 equations in the 9 unknown forces, strains, and deformations which, together with boundary conditions, specify the problem.

It is to be expected that prebuckling deformations are axisymmetric; that is, they are functions of x only and may be obtained directly from equations (1) to (3) and boundary conditions which include zero radial displacement at the edges from the onset of loading. A solution to the axisymmetric problem was first obtained in reference 6 and is reported in reference 7.

Let the solution to the prebuckling axisymmetric problem just described be identified as u_A , w_A (and $v_A = 0$). To the prebuckling deformations are added infinitesimal nonaxisymmetric changes u_B , v_B , and w_B that occur at buckling:

$$\left. \begin{aligned} u &= u_A(x) + u_B(x, y) \\ v &= v_B(x, y) \\ w &= w_A(x) + w_B(x, y) \end{aligned} \right\} \quad (4)$$

The displacements u_B , v_B , and w_B also satisfy simple support boundary conditions consistent with the axisymmetric solution. The following buckling equations may now be obtained by substituting equations (4) into equations (1) to (3) and then neglecting nonlinear subscript B deformations (and subtracting out identities relating subscript A deformations):

$$\left. \begin{aligned} u_{B,xx} + \frac{1-\mu}{2} u_{B,yy} + \frac{1+\mu}{2} v_{B,xy} + \frac{\mu}{r} w_{B,x} + (w_{A,x} w_{B,x})_{,x} \\ + \frac{1-\mu}{2} w_{A,x} w_{B,yy} = 0 \\ \frac{1+\mu}{2} u_{B,xy} + v_{B,yy} + \frac{1-\mu}{2} v_{B,xx} + \frac{1}{r} w_{B,y} + \frac{1-\mu}{2} w_{A,xx} w_{B,y} \\ + \frac{1+\mu}{2} w_{A,x} w_{B,xy} = 0 \\ DV^4 w_B + \frac{1}{r} N_{yB} + P w_{B,xx} + \left(\mu P - \frac{Et}{r} w_A \right) w_{B,yy} - w_{A,xx} N_{xB} = 0 \end{aligned} \right\} \quad (5)$$

where

$$\begin{aligned} N_{xB} &= \frac{Et}{1-\mu^2} \left[u_{B,x} + w_{A,x} w_{B,x} + \mu \left(v_{B,y} + \frac{w_B}{r} \right) \right] \\ N_{yB} &= \frac{Et}{1-\mu^2} \left[v_{B,y} + \frac{w_B}{r} + \mu \left(u_{B,x} + w_{A,x} w_{B,x} \right) \right] \end{aligned}$$

The physical conditions of continuity around the cylinder are satisfied if

$$\left. \begin{aligned} u_B &= U(x) \sin \frac{ny}{r} \\ v_B &= V(x) \cos \frac{ny}{r} \\ w_B &= W(x) \sin \frac{ny}{r} \end{aligned} \right\} \quad (6)$$

where n , the number of waves around the cylinder, is an integer. Equations (5) may now be converted to ordinary differential equations relating U , V , W , and the eigenvalues. Of course, the subscript A displacements introduce variable coefficients, and these equations are difficult to solve. Instead of solving the ordinary differential equations directly, equivalent numerical expressions for U , V , and W at M stations in a half length (W as an even function of x being assumed) were developed by using the energy method and solved for the necessary eigenvalue.

LIMITATIONS OF THE CALCULATIONS

In order to obtain accurate results, M was arbitrarily taken large enough so that there were at least five stations for each prebuckling (inward or outward) wrinkle. For $Z > 1,000$, this criterion led to equations involving determinants that were too large for economical application of the computing machine used. Hence, calculations have been limited to $Z \leq 1,000$.

The proper value of n is the integral value which yields the lowest buckling load with the physical restriction that n cannot be less than 2 (since $n = 1$ is simple translation and $n = 0$ is an axisymmetric form). Little accuracy is lost, however, if n is considered to be continuously variable for $n > 2$. It was found that $n = 2$ gave the condition for instability for almost every case except for the range of higher external pressures. The differential equations of equilibrium (eqs. (1)) are accurate for the $n = 2$ case only if there are present at least three wrinkles in every part of a length equal to the radius so that the deformations are extensional. (See ref. 8.) For this reason small values of the curvature parameter ($Z < 50$) could not be treated for axial compression and for combinations of axial compression and internal pressure.

RESULTS

In figures 1 and 2 interaction curves are presented for a low value (50) and a high value (500), respectively, of the curvature parameter Z . Each point on the curve presents a combination of axial compression and lateral pressure that causes buckling. Where the curves depend on r/t they correspond to $n = 2$; at the higher external pressures, the results were given by $n > 2$ with n assumed continuously variable. At the end points to the left the curves give the buckling pressures for cylinders under external lateral pressure alone. The hydrostatic pressure for buckling is given by the point on the curve marked by a cross. When

the pressure is zero, note that the axial buckling stress is 50 percent or less of the classical value. With internal pressure present, the axial stress required for buckling increases until it approaches the classical value. Stress coefficients for external hydrostatic pressure alone and axial compression alone are presented in figures 3 and 4, respectively, for a wide range of curvature parameter Z (within the limitations specified in the previous section).

DISCUSSION

Experimental results are available in reference 9 for cylinders with combinations of internal pressure and axial compression and with curvature parameters about equal to those presented in figures 1 and 2. The experimentally obtained buckling stress coefficients are plotted along with the theoretical curves in figures 1 and 2. A comparison of the results shows that, although the experimental cylinders were ring supported and the theory was for simply supported cylinders, there is much better quantitative agreement of experiment with present theory than with classical theory. The evident disagreement in the shapes of the theoretical and experimental interaction curves has not been explained.

In figure 3 results of the present investigation for external hydrostatic pressure are plotted against the curvature parameter Z together with the corresponding classical curve and with experiment. Comparison of the theoretical results shows that prebuckling stresses and deformations serve to stiffen the cylinder by about 25 percent for higher values of Z . In the range of lower Z this stiffening effect disappears and prebuckling stresses and deformations serve to weaken the cylinder to about 80 percent of the classical value. Thus, whereas the classical theory agrees with experiment in the range of higher values of Z and disagrees for lower values of Z , the present results follow the trend of experiment and yield buckling pressures roughly 25 percent high in both regions.

For axial compression of unpressurized cylinders the present results are more than 50 percent below the classical values. (See fig. 4.) Thus, the axial buckling load is sensitive to the prebuckling deformations and stresses resulting from restraint of the edges. The value of the buckling load from the present theory is dependent on radius-thickness ratio whereas in the classical theory it is not. The dependence on radius-thickness ratio occurs because the critical wave form is determined to have two waves in the circumferential direction. It can be seen from figure 4 that the empirical curves of reference 2 - and therefore experimental results - are also dependent on radius-thickness ratio, and that agreement between theory and experiment is much better with present theory than with classical theory especially for low radius-thickness ratios.

Neither the results of the present theory nor the results of classical theory for buckling in axial compression indicate that the buckle wave form is of the diamond pattern as indicated by buckled experimental cylinders. The results of present theory which specify two waves in the circumferential direction at buckling deviate even further from the experimental buckled wave form than the results of classical theory. However, previous work has shown (see ref. 10) that the equilibrium configuration which is the mode at buckling need not be stable under usual conditions of loading. If the buckling mode is not stable, it might not necessarily resemble the final shape of a buckled experimental cylinder.

CONCLUDING REMARKS

The present paper has focused attention on a serious shortcoming of classical buckling theory. To avoid complicated prebuckling deformations and stresses, the classical approach is to relax completely the supports in the prebuckling range and thus assume that the prebuckling stresses are zero or constant and the prebuckling deformations are zero, constant, or linear. Prebuckling deformations and stresses due to edge support have been ignored even in studies of effects of initial imperfections. Yet, in every practical cylindrical shell structure, some measure of radial support is present from the beginning of loading so that, prior to buckling, complicated axisymmetric deformations and stresses are present to modify the load-shortening behavior of the cylinder and to influence its buckling load. This influence is especially notable for cylinders in axial compression and for short cylinders under external hydrostatic pressure, where it accounts for a large part of the disagreement between classical theory and experiment.

Further work needed in this field includes studies of cylinders with clamped edges and flexible rings at the edges. In order to study the behavior of longer cylinders (cylinders of larger Z) in axial compression, it would also be desirable to analyze the semi-infinite cylinder. Further, in future cylinder studies, it would be useful to extend this work by using a more exact theory that is valid for buckling into two circumferential waves for less than three wrinkles in the axial direction. It is also clear that the adoption of the present approach - seeking an infinitesimal nonaxisymmetric change at buckling from a symmetric prebuckling state which satisfies the boundary conditions - would probably clarify greatly the problem of buckling of a spherical cap under external pressure.

REFERENCES

1. Batdorf, S. B.: A Simplified Method of Elastic-Stability Analysis for Thin Cylindrical Shells. NACA Rep. 874, 1947. (Formerly included in NACA TN's 1341 and 1342.)
2. Batdorf, S. B., Schildcrout, Murry, and Stein, Manuel: Critical Stress of Thin-Walled Cylinders in Axial Compression. NACA Rep. 887, 1947. (Formerly NACA TN 1343.)
3. Donnell, L. H., and Wan, C. C.: Effect of Imperfections on Buckling of Thin Cylinders and Columns under Axial Compression. Jour. Appl. Mech., vol. 17, no. 1, Mar. 1950, pp. 73-83.
4. Hoff, Nicholas J.: Buckling of Thin Shells. SUDAER No. 114 (AFOSR-TN-61-1422), Dept. Aero. Eng., Stanford Univ., Aug. 1961.
5. Nachbar, W., and Hoff, N. J.: On Edge Buckling of Axially-Compressed, Circular Cylindrical Shells. SUDAER No. 115 (NsG.93-60), Dept. Aero. Eng., Stanford University, Nov. 1961.
6. Föppl, L.: Achsensymmetrisches Ausknicken Zylindrischer Schalen, S.-B. Bayr. Akad. Wiss. 1926, pp. 27-40.
7. Flügge, Wilhelm: Stresses in Shells. Springer-Verlag (Berlin), 1960.
8. Kempner, Joseph: Unified Thin-Shell Theory. Symposium on the Mechanics of Plates and Shells for Industry Research Associates, Polytechnic Inst. of Brooklyn, Mar. 1960.
9. Dow, Marvin B., and Peterson, James P.: Bending and Compression Tests of Pressurized Ring-Stiffened Cylinders. NASA TN D-360, 1960.
10. Stein, Manuel: The Phenomenon of Change in Buckle Pattern in Elastic Structures. NASA TR R-39, 1959.

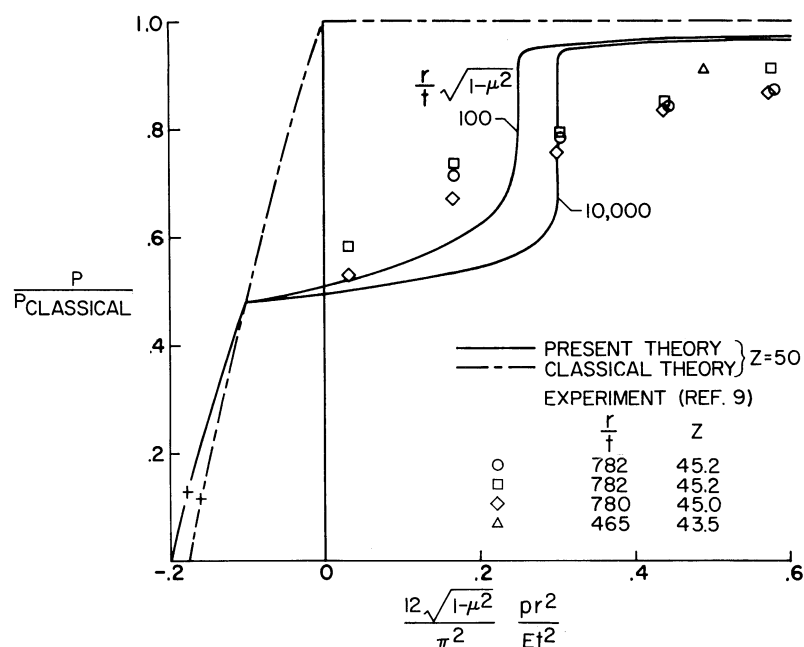


Figure 1.- Theoretical and experimental results for buckling of a cylinder of low Z under combinations of axial compression and internal pressure. Crosses indicate hydrostatic external pressure for buckling.

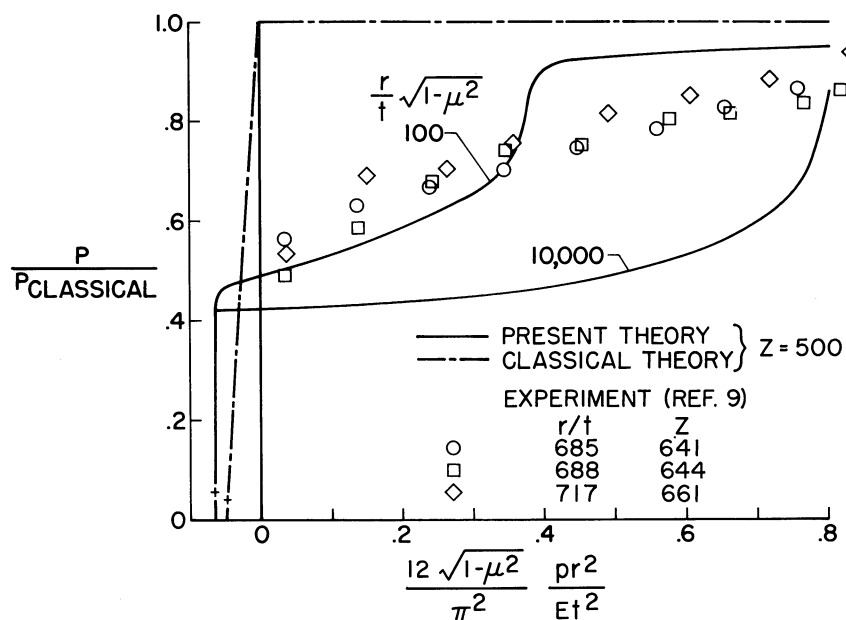


Figure 2.- Theoretical and experimental results for buckling of a cylinder of high Z under combinations of axial compression and internal pressure. Crosses indicate hydrostatic external pressure for buckling.

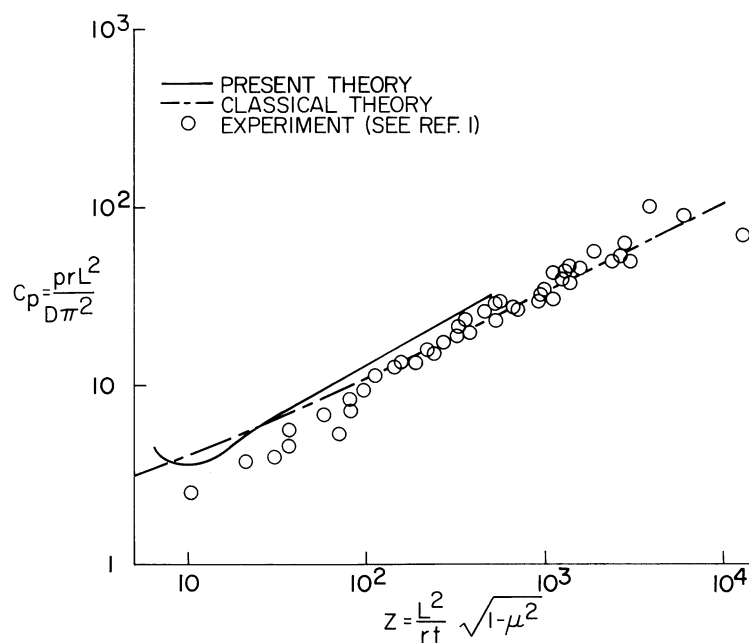


Figure 3.- Theoretical and experimental results for buckling of cylinders under hydrostatic pressure.

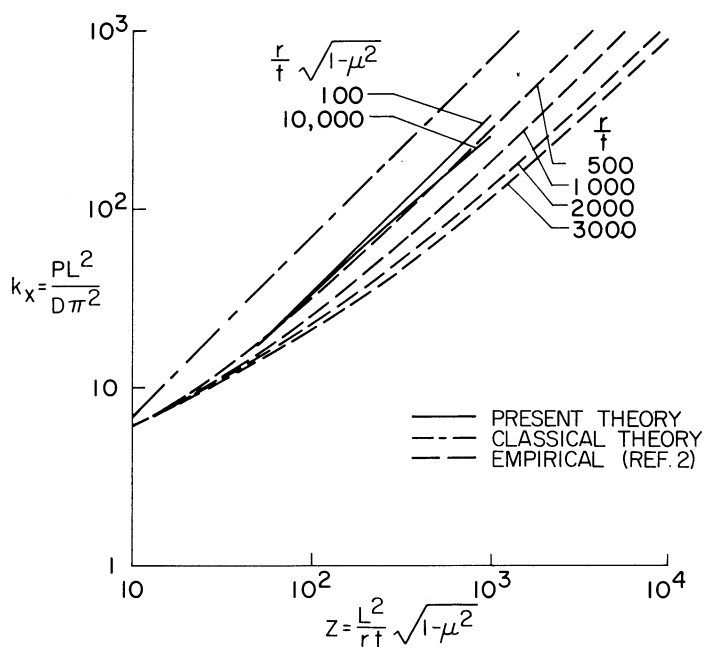


Figure 4.- Theoretical and empirical results for buckling of cylinders in axial compression.

THE MEMBRANE APPROACH TO BENDING INSTABILITY OF
PRESSURIZED CYLINDRICAL SHELLS

By Harvey G. McComb, Jr., George W. Zender,
and Martin M. Mikulas, Jr.

NASA Langley Research Center

SUMMARY

Recent theoretical and experimental research is briefly described to trace the development of deformation and the occurrence of collapse in pressurized circular cylindrical membranes under applied moment loading. The collapse of pure membrane cylinders is then compared with instability of pressurized cylindrical shells. This approach leads to a better understanding of the behavior of pressurized cylinders under bending loads. The results suggest possibilities for further research utilizing the membrane approach.

INTRODUCTION

The fuel and oxidizer tanks of large launch vehicles are often highly pressurized circular cylindrical shells and, during the launch phase of flight, may be subjected to large bending moments from aerodynamic and inertia loads. The strength of pressurized cylinders in bending is thus an important consideration in launch vehicle design, and considerable work has been done on this problem from the usual standpoint of buckling of shells with finite wall bending stiffness. (See, for example, refs. 1, 2, and 3.) In the present paper, it is shown that the study of pure membrane cylinders having no wall bending stiffness but maintaining their shape only by virtue of internal pressure leads to an explanation of pressurized cylinder behavior. With wall bending stiffness accounted for in an approximate way, a simple formula for the strength of pressurized cylinders in bending is obtained.

SYMBOLS

E	Young's modulus
F	applied axial compressive load

K	curvature of axis of circular cylinder due to bending moment
M	applied bending moment
P	total axial force (due to internal pressure and externally applied load)
p	internal pressure
p*	pressure parameter, $\sqrt{12(1 - \mu^2)} \frac{p(r)}{E(t)}^2$
r	radius of circular cylinder
t	thickness of cylinder wall
μ	Poisson's ratio
Subscript:	
c	collapse

BENDING OF CYLINDRICAL MEMBRANES

Experiments on Membrane Cylinders

As one phase of a study of the behavior of membrane structures, tests have been made at the NASA Langley Research Center on 6-inch diameter cylinders made of 1/2 mil Mylar $\left(\frac{r}{t} = 6,000\right)$. A photograph of one such specimen is shown in figure 1. This specimen is loaded by internal pressure, bending, and axial tension. Note that wrinkles of very short wavelength have appeared on the right side where compressive stress due to bending moment has canceled the tensile stress due to pressure and axial load.

The behavior of these specimens in bending is illustrated in figure 2. In this figure the ordinate is the applied bending moment divided by the moment required to reduce the stress to zero at one point on the cross section. The abscissa is a dimensionless parameter representing the curvature of the axis of the cylinder. The circles and squares are test points obtained on a specimen similar to that shown in figure 1.

Theoretical Behavior

The solid-line curve in figure 2 is a result of the theory presented in reference 4. This theory describes the behavior of membranes in a partly wrinkled condition with the assumption that, when one of the principal stresses in a membrane becomes zero, many small wrinkles will occur in a direction normal to the direction of zero principal stress. Correspondingly, the membrane is assumed to carry no stress whatsoever normal to the wrinkles. According to reference 4, the theoretical behavior of a membrane cylinder is as follows: For moments such that $\frac{2M}{Pr} < 1$, the cylinder bends like an elastic beam and the response is linear (fig. 2). At $\frac{2M}{Pr} = 1$ wrinkling begins along one generator of the cylinder and, as the moment is increased further, the extent of the wrinkled region increases circumferentially. The moment-curvature curve becomes nonlinear after wrinkling begins, and its slope (representing the bending stiffness of the cylinder) decreases as moment increases. Only when the wrinkled region has progressed all the way around the cylinder does the slope become zero so that instability (collapse) of the cylinder theoretically occurs. The collapse moment $\left(\frac{2M}{Pr}\right) = 2$ is approached asymptotically. Notice that the theoretical collapse moment of a membrane cylinder is precisely twice the initial wrinkling moment.

Correlation of Tests and Theory

In the membrane-cylinder theory presented in reference 4, moments due to externally applied axial load are neglected. Thus, in order for this theory to be compared with experiment, the test specimens had to be shortened until such moments were negligible. The test points shown in figure 2 (obtained from a specimen having a length-radius ratio of about unity) were found to be essentially independent of the proportions of axial load contributed by internal pressure and by externally applied load. Therefore, the previously mentioned requirement of negligible moment due to axial load was satisfied. Nevertheless, the test points in figure 2 are somewhat above the curve from reference 4 and show a dependence on the magnitude of the total axial load.

In an attempt to account for the disparity between membrane theory and the tests, a modification was made in the theory by assuming that over the wrinkled portion of the cylinder the skin could carry a small uniform compressive stress normal to the wrinkles. When this compressive stress was taken to be $\frac{0.6Et}{r}$ (the buckling stress for a highly pressurized cylinder in axial compression) the dash-dot curves shown in figure 2 were obtained. These curves are seen to agree well with the test results.

The need for the modified theory to predict these results for pressurized Mylar cylinders with $\frac{r}{t} = 6,000$ testifies to the importance in pre-collapse behavior of even very small wall bending stiffness in pressurized cylinders.

If the modified theory is projected to collapse as in figure 2, it predicts a collapse moment greater than the theoretical collapse moment for a true membrane cylinder - specifically, the predicted moment is twice the moment at which one point on the cylinder first reaches a compressive stress of $\frac{0.6Et}{r}$. This ideal condition is not reached in practice, however, and collapse actually occurs before the wrinkles can envelop the whole circumference of the cylinder. For example, in the Mylar test specimens of figure 2, collapse was observed at moments slightly above the upper test points when the uniform pattern of small wrinkles (fig. 1) abruptly shifted to a few deep wrinkles concentrated in one or two zones. (In some instances, these deep wrinkles assumed a pattern resembling elongated diamond buckles.) It is of some interest, then, to determine just when bending collapse of practical pressurized cylinders does occur in relation to the collapse moments predicted by the unmodified and modified membrane theories. This comparison has been made in reference 5 and is reviewed briefly in the following section.

COLLAPSE OF THIN-WALLED PRESSURIZED CYLINDERS IN BENDING

Presentation of Shell Data in Membrane Terms

Experimental data on instability of pressurized cylindrical shells in bending are compared in figure 3 with the theoretical collapse moment for pressurized cylindrical membranes. In this figure the ordinate is the ratio of the shell collapse moment to the theoretical initial wrinkling moment of a cylindrical membrane and the abscissa is a dimensionless pressure parameter which is proportional to the internal pressure and the square of the shell radius-thickness ratio.

The theoretical collapse moment for a cylindrical membrane (twice the initial wrinkling moment) is shown as the horizontal dashed line in figure 3. The solid-line curve shows the collapse moment according to the modified membrane theory, in which, instead of zero stress, the cylinder walls are assumed capable of carrying a uniform compressive stress of $\frac{0.6Et}{r}$ normal to the wrinkles over the entire circumference. It is expected that this curve would represent an upper limit for the collapse

moment of cylindrical shells; its equation is simply

$$M_c = p\pi r^3 \left(1 + \frac{4}{p^*}\right) \quad (1)$$

The test points represent failure of pressurized Mylar and 7075-T6 aluminum-alloy cylinders in bending $\left(291 < \frac{r}{t} < 1,333\right)$ obtained by several investigators (refs. 1 and 2). These cylinders failed at moments greater than the membrane collapse moment by virtue of the bending stiffness of the cylinder walls; but their collapse moments lie below the solid curve representing the limiting moment. On the average, somewhat less than half of the difference between the limiting moment and the membrane collapse moment is realized in the tests. In many cases failure was accompanied by a change from wrinkles to diamond shape buckles.

Contribution of the Membrane Approach

In the study of the bending of cylindrical membranes, a clear distinction is made between wrinkling and collapse (fig. 2). A membrane cylinder can carry moments twice the wrinkling moment and does not lose stiffness suddenly when first wrinkling occurs. Similarly, for a pressurized shell, the limiting moment (the solid-line curve of fig. 3) is twice the moment which initially induces a compressive stress of $\frac{0.6Et}{r}$ in an extreme fiber. According to classical linear theory (refs. 6 and 7), buckling of practical pressurized cylinders in bending occurs when a compressive stress only slightly higher than $\frac{0.6Et}{r}$ is reached in an extreme fiber. It appears from figure 3, then, that for p^* greater than about 2, considerable moment-carrying ability remains in a shell beyond this classical buckling moment. Thus, the classical buckling phenomenon is revealed as a comparatively mild local instability analogous to initial wrinkling in a membrane cylinder, and the test points of figure 3 apparently represent a second instability analogous to membrane collapse. For p^* less than about 2, these two instabilities are not distinguishable. This distinctive behavior of cylindrical shells in bending has also been pointed out in references 2 and 7.

An extremely complex analysis would be required for a detailed description of the shell behavior subsequent to classical buckling. On the other hand, a good lower boundary to the test data in figure 3 over

a wide range of p^* is given by the simple empirical expression

$$M_c = p\pi r^3 \left(1 + \frac{1}{p^*}\right) \quad (2)$$

which retains the form of the upper limit expression, equation (1).

FUTURE RESEARCH

Additional research is needed to explore further the membrane approach to the study of pressurized shell behavior. The test data available at present are largely based on very small cylinders of foil-like materials. Unfortunately, the data which are presented in figure 3 for cylinders of sheet gages are limited to very low values of the pressure parameter p^* ($p^* < 3$). Test data are needed for shells made of sheet gages at large values of the pressure parameter. Plasticity, a consideration which has been ignored in this report, may play in important role in such an investigation.

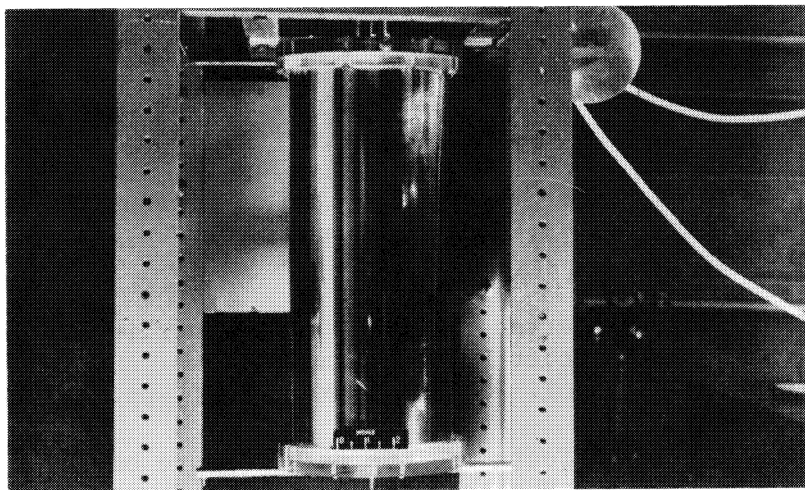
The importance of the combined bending-axial-compression load condition in launch vehicles suggests that pressurized cylinders under these loads should also be investigated from the membrane point of view. Theoretically, for short cylinders the extension of figure 3 to the case of combined axial load F and bending moment M is simple; the only requirement is that the quantity M_c be replaced by $M_c + F_c r$, where M_c and F_c are the applied moment and axial compressive load which jointly cause collapse. However, for cylinders of practical length the added moments due to the axial compression load may have to be taken into account. In addition, test data are needed for the combined load condition for both foil and sheet gages.

CONCLUDING REMARKS

Recent research results on bending of pressurized membrane cylinders, when viewed together with experimental collapse data on pressurized thin-walled cylindrical shells, have clarified the bending behavior and failure of such shells. Additional research would be beneficial in exploiting the membrane approach to the study of the instability of pressurized shells. Experimental data are needed on large pressurized cylindrical shells of sheet gage at large values of the pressure parameter. Such tests should include combined axial and bending moment loading as well as pure moment loading.

REFERENCES

1. Dow, Marvin B., and Peterson, James P.: Bending and Compression Tests of Pressurized Ring-Stiffened Cylinders. NASA TN D-360, 1960.
2. Seide, P., Weingarten, V. I., and Morgan, E. J.: Final Report on the Development of Design Criteria for Elastic Stability of Thin Shell Structures. STL/TR-60-0000-19425 (AFBMD/TR-61-7), Space Tech. Labs., Inc., Dec. 31, 1960.
3. Suer, Herbert S., Harris, Leonard A., Skene, William T., and Benjamin, Roland J.: The Bending Stability of Thin-Walled Unstiffened Circular Cylinders Including Effects of Internal Pressure. Jour. Aero. Sci., vol. 25, no. 5, May 1958, pp. 281-287.
4. Stein, Manuel, and Hedgepeth, John M.: Analysis of Partly Wrinkled Membranes. NASA TN D-813, 1961.
5. Zender, George W.: The Bending Strength of Pressurized Cylinders. Jour. Aerospace Sci. (Readers' Forum), vol. 29, no. 3, Mar. 1962, pp. 362-363.
6. Seide, Paul, and Weingarten, V. I.: On the Buckling of Circular Cylindrical Shells Under Pure Bending. Trans. ASME, Ser. E - Jour. Appl. Mech., vol. 28, no. 1, Mar. 1961, pp. 112-116.
7. Weingarten, V. I.: Effects of Internal Pressure on the Buckling of Circular-Cylindrical Shells Under Bending. Jour. Aerospace Sci., vol. 29, no. 7, July 1962, pp. 804-807.



L-61-5949

Figure 1.- Thin pressurized Mylar cylinder in combined bending and tension.

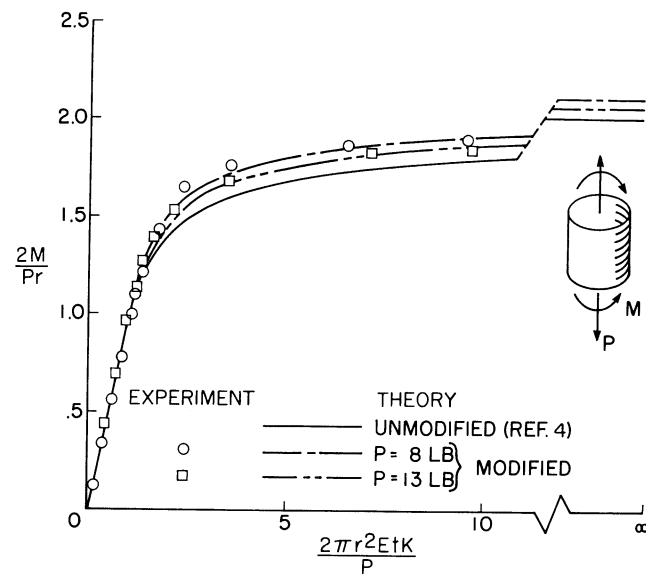


Figure 2.- Moment-curvature relationship for Mylar cylinders in bending. $r/t = 6,000$.

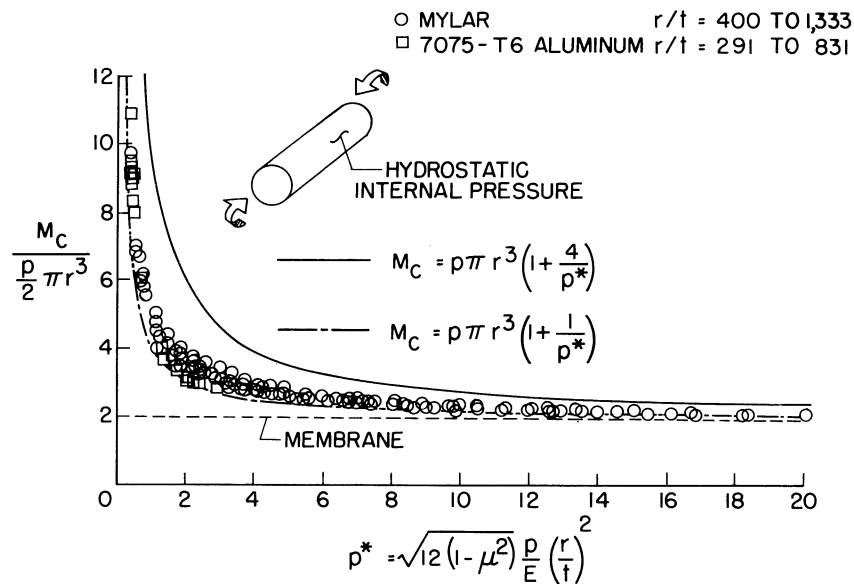


Figure 3.- Bending strength of pressurized cylinders.

INSTABILITY ANALYSIS OF CYLINDRICAL SHELLS
UNDER HYDROSTATIC PRESSURE

By George Herrmann

Northwestern University

SUMMARY

To determine the elastic buckling pressure of simply supported cylindrical shells subjected to lateral and axial hydrostatic forces, various versions of linear bending theories have been employed in the past. For certain shell dimensions, however, the expressions commonly used may yield substantially differing results. In what follows, recent work on this problem by A. E. Armenakas and the writer is briefly reviewed. This work consisted primarily in employing a general bending theory of circular cylindrical shells under the influence of initial stress, developed earlier by the same authors, to re-examine the problem mentioned, and compare the results with those of previous investigations. The outcome was the establishment of a simple but accurate expression for the buckling pressure applicable to a wide range of shell dimensions.

INTRODUCTION

In the past, various versions of linear bending theories have been employed in establishing the buckling value of the external pressure acting on circular cylindrical shells. One of the earliest investigations by von Mises (ref. 1) resulted in a simple expression for the critical uniform lateral pressure (no axial stress) that has been utilized extensively. Timoshenko (ref. 2) indicated that this formula is in close agreement with a more intricate formula obtained by Flügge (ref. 3). Much later, von Mises also considered the case of a shell under all around pressure (axial stress equals one half of the circumferential stress) and presented a formula for the critical pressure (see ref. 2, page 498).

More recently, Batdorf (ref. 4) reinvestigated this problem and using the Donnell equations (ref. 5) obtained the same expression as von Mises for the case of all around pressure, and a somewhat different expression for the case of only lateral pressure. As is well known, however, for shells whose dimensions conduce to buckling in modes with

a small number of circumferential waves, the assumptions made in deriving the Donnell equations are not valid and, concomitantly, for such shells the Batdorf results are inaccurate. Mushtari and Galimov (ref. 6) present an analysis of the same problem also using the Donnell equations and their results are thus subject to the same limitations. Loo (ref. 7) attempted to use, in establishing the buckling pressure, an extended Donnell equation which included the effect of transverse shear forces on the equilibrium in the circumferential direction. Calculations based on this modification appear, for long shells, to be in reasonable agreement with the results obtained by von Mises.

Some of the aforementioned formulas have been referred to frequently in the literature. For certain ranges of shell dimensions, however, they yield substantially differing results. Thus, it is evident that a systematic re-examination of the buckling of circular cylindrical shells under hydrostatic pressure was desirable. For this purpose, the bending theory of cylindrical shells, under the influence of a general state of initial stress, presented recently by Herrmann and Armenakas (ref. 8), was used to establish the value of the critical pressure acting on a cylindrical shell. The results were compared with those of previous investigations and a simplified but accurate expression for the buckling pressure, applicable to a wide range of shell dimensions, was evolved, valid for simple supports. A detailed account of this work, including considerations concerning the character of the external pressure, is given in ref. 9.

SYMBOLS

L	shell length
R	shell radius
h	shell thickness
E	Young's modulus
ν	Poisson's ratio
D	flexural stiffness, $\frac{Eh^3}{12(1 - \nu^2)}$
n	number of circumferential waves (lobes)
m	number of axial half-waves

s	thickness parameter, $\frac{h}{2R}$
β	length parameter, $\frac{Ln}{\pi R}$
Z	curvature parameter, $\frac{L^2 \sqrt{1 - \nu^2}}{Rh}$
p	external pressure
N	circumferential shell stress
T	axial shell stress
K	buckling coefficient
Subscript:	
cr	critical

CYLINDRICAL SHELLS UNDER HYDROSTATIC PRESSURE

Exact Expression for Buckling Pressure

Hydrostatic pressure (as distinct, for example, from constant-directional pressure) is defined as a pressure acting always perpendicular to the area element and having during the process of deformation a constant magnitude per unit actual area. It can act on the lateral surface of the shell, inducing a stress N, or at the end of the shell, inducing a stress T.

$\frac{T}{N} = \frac{1}{2}$ corresponds to all around pressure,

$\frac{T}{N} = 0$ to lateral pressure only.

If the shell is assumed to be simply supported, i. e. the circumferential displacement, the radial displacement, the axial force and the axial bending moment are all zero, then the following expression for the critical hydrostatic pressure p_{cr} is obtained, on the basis of the equations presented in ref. 8.

$$p_{cr} = K \frac{\pi^2 D}{L^2 R}$$

$$K = \frac{G}{H}$$

$$\begin{aligned} G = & n^4(\beta^2 + m^2)^4 + 12Z^2 n^4 m^2 \pi^{-4} + \beta^8(1 - 2n^2) \\ & + 2m^2 \beta^6 \left[2(1 - 2n^2) + v(n^2 - 1) \right] - 6m^4 n^2 \beta^4 - 2m^6 n^2 \beta^2 v \\ H = & \beta^2 n^4(\beta^2 + m^2) + \frac{T}{N} (1 + s) m^2 n^4(\beta^2 + m^2)^2 + \frac{T}{N} (1 + s) m^2 n^2 \beta^2 \left[\beta^2 \right. \\ & \left. + m^2(3 + 2v) \right] - \beta^4 n^2(\beta^2 + 3m^2) + m^2 n^2 s \left[\beta^4 + n^2(\beta^2 + m^2) \right] \end{aligned}$$

Terms involving s result from taking into account the fact that the pressure is not acting on the middle surface of the shell. The above expression for p_{cr} is similar, but not identical to the one obtained by Flügge (ref. 3). For thin shells this expression is unnecessarily complicated and may be simplified considerably.

Approximate expression for Buckling Pressure

It is well known that shells having a small curvature parameter Z buckle into a large number of circumferential waves, and therefore $\frac{1}{n^2}$ may be disregarded as compared to unity. The buckling coefficient K may then be simplified to, with $m = 1$,

$$K = \frac{(1 + \beta^2)^2}{\frac{T}{N} + \beta^2} + \frac{12Z^2}{\pi^4(1 + \beta^2)^2 \left(\frac{T}{N} + \beta^2 \right)}$$

For $\frac{T}{N} = \frac{1}{2}$, this expression is identical to that obtained by von Mises (ref. 2, p. 498) and Batdorf (ref. 4). For the range of shell dimensions for which the above equation is not valid, that is for shells buckling into a small number of circumferential waves n , β^2 is large as compared to unity. Therefore, the exact expression for K may be simplified by disregarding in it terms not included in the approximate expression above, whose order of magnitude is $\frac{1}{\beta^2}$ times that of terms retained. The following expression for the buckling coefficient is then obtained, valid for a wide range of shell dimensions

$$K = \frac{(1 + \beta^2)^2 (n^2 - 1)}{(\frac{T}{N} + \beta^2)n^2} + \frac{12Z^2 n^2}{\pi^4 (1 + \beta^2)^2 (\frac{T}{N} + \beta^2) (n^2 - 1)}$$

In order to evaluate this buckling coefficient for a shell of specified dimensions, it is necessary to establish first the buckling mode (number of circumferential waves n) which yields the smallest value of K for given $\frac{T}{N}$, β and Z . This can be done by repeated calculations, or by using the chart given in ref. 9, which is an extension of curves presented in ref. 10.

Concluding Remarks

An evaluation of earlier work is presented in ref. 9 and the conclusion was reached that neither von Mises' nor Loo's expressions are based on consistent, admissible shell theories, and that they yield, for certain shell dimensions, incorrect results. Donnell-type equations, such as used by Batdorf (ref. 4) cannot be expected to yield good results for long shells.

Further, it is of interest to point out that the new expression for the buckling pressure cannot be derived directly from a consistent simplified shell theory. It appears that this expression can be obtained only on the basis of the complete bending theory, followed by a simplification of the expression for the buckling coefficient. In future work it might be worthwhile to attempt constructing a similar expression for the buckling coefficient valid for more realistic boundary conditions.

REFERENCES

1. von Mises, R.: Der kritische Aussendruck zylindrischer Rohre. Ver. deut. Ingr., vol. 58, 1914, p. 750.
2. Timoshenko, S. P., and Gere, J. M.: Theory of Elastic Stability. Mc Graw-Hill Book Co., (New York), 1961.
3. Flügge, W.: Statik und Dynamik der Schalen. Springer Verlag, (Berlin), 1934, and Stresses in Shells, Springer Verlag, (Berlin), 1960.
4. Batdorf, S. B.: A Simplified Method of Elastic Stability Analysis for Thin Cylindrical Shells. NACA Report, no. 874, 1947.

5. Donnell, L. H.: Stability of Thin-Walled Tubes under Torsion. NACA Report, no. 479, 1933.
6. Mushtari, Kh, M., and Galimov, K. Z.: Nonlinear Theory of Thin Elastic Shells. 1957. Translation from the Russian published for NSF and NASA by Israel Program for Scientific Translations, 1961.
7. Loo, T. T.: An Extension of Donnell's Equation for a Circular Cylindrical Shell. Journal Aero. Sci., May 1957, pp. 390-391.
8. Herrmann, G., and Armenakas, A. E.: Dynamic Behavior of Cylindrical Shells under Initial Stress. Air Force Office of Scientific Research, Technical Note, no. 60-425, April 1960. To be published in the Proceedings of the Fourth U.S. National Congress of Applied Mechanics.
9. Herrmann, G., and Armenakas, A. E.: On the Buckling of Circular Cylindrical Shells under External Pressure. Air Force Office of Scientific Research, Project No. 9782, Technical Note, no. 7, Columbia University, 1962.
10. Windenburg, D. F., and Trilling, C.: Collapse by Instability of Thin Cylindrical Shells under External Pressure. Trans. American Soc. Mech. Engineers, vol. 56, no. 11, Nov. 1934, pp. 819-825.

INVESTIGATION OF YIELD COLLAPSE OF STIFFENED CIRCULAR
CYLINDRICAL SHELLS WITH A GIVEN OUT-OF-ROUNDNESS

By Robert C. DeHart, and
Nicholas L. Basdekas

Southwest Research Institute
San Antonio, Texas

SUMMARY

The effect of out-of-roundness on the yield collapse strength of ring stiffened circular cylindrical shells under hydrostatic pressure has been determined experimentally. On the basis of the experimental data and theoretical stress distributions, empirical relations have been developed which, in conjunction with the theoretically predictable yield collapse strength of round ring-stiffened circular cylindrical shells, permits the prediction of the yield collapse strength of shells with out-of-roundness.

INTRODUCTION

Procedures for predicting the yield collapse strength of ring-stiffened circular cylindrical shells composed of materials having a non-linear stress-strain curve have been developed by the authors in Reference 1.

Out-of-roundness in the shell and stiffening rings may result from manufacturing procedures, relief of residual stresses with time and severe transient or static loading of stiffened shell structures. The need to determine the yield collapse strength of ring-stiffened shells having out-of-roundness and the absence of an available technique for evaluating the strength of out-of-round stiffened shells lead to the present investigation the results of which are presented herein.

Theoretical Treatment

A survey of existing theoretical treatments of out-of-round stiffened circular cylindrical shells was made and excellent contributions were found in References 2 to 5 and particularly in Reference 6. Of all those treatments none are strictly applicable to the case at hand.

There are several theoretical complexities involved in the problem. A stiffened shell with out-of-roundness under hydrostatic pressure undergoes displacements which introduce nonuniform load distribution on the stiffener. As a result of this, the direct stresses in the stiffener are not constant, and the extent of this variation is not known. The determination of bending stresses in the stiffener is a complex matter because the moment and the effective stiffener change with θ (see Figure 1), shell dimensions and pressure level. The variation in loading and effective stiffener introduce large difficulties in the determination of the stiffener's elastic stability. It is needless to say that the difficulties are multiplied when non-linear and/or elasto-plastic strains exist in the stiffened shell.

Adopted Approach

In spite of all the above-mentioned complications, a meaningful approximation of the strains in the stiffener can be obtained by a procedure based on the following reasoning. The presence of the stiffener in a circular cylindrical stiffened shell under pressure develops in the shell disturbances which die out in a short distance from the stiffener. This distance is a function of the thickness of the shell and its radius. The differential equation for axisymmetric deformations of circular cylindrical shells, as given in Reference 7, is

$$w = e^{-\beta x} [C_3 \cos \beta x + C_4 \sin \beta x] \quad (1)$$

where

$$\beta^4 = \frac{3(1 - \nu^2)}{a^2 h^2}$$

a = Radius of Shell

h = Thickness of Shell

ν = Poisson's Ratio

Using equation (1), the shear in a ring-stiffened shell is obtained and the distance from the ring at which it reaches its first zero, for the shell shown in Figure 1, is shown in Figure 2. If the stiffened shell is cut where the shear first becomes zero, then the ring and the shell, as shown in Figure 3, will act as a ring of T cross section. Using this simple approach, bending stresses have been computed by employing the well known bending moment expression

$$M = q r_0 \frac{w_0}{1 - (q/q_{cr})} \quad (2)$$

where

q = The loading on the T cross-section ring

r_o = Radius of the ring

w_o = Maximum out-of-roundness

q_{cr} = Buckling load of the T cross-section ring

To determine the direct stresses in the stiffener, the shear forces existing at the stiffener-shell junction for a perfectly round stiffened cylindrical shell were obtained and applied to the stiffener. The stiffener was considered to be a thick ring, and the Lamé solution was used to compute the direct stresses in the ring.

Models Tested and Results Obtained

Model data are given in Table 1. All models were made out of 7075-T6 aluminum alloy. A typical compression stress-strain curve is shown in Figure 4. They were machined out of solid stock to a tolerance of ± 0.002 inch in the $\cos 2\theta$ out-of-round mode. Strains were read, by means of SR-4 strain gages, at $\theta = 0^\circ, 90^\circ, 180^\circ$, and 270° , in the circumferential direction. Typical strain reading curves are given in Figures 5 and 6, and they are compared with the theoretically predicted strains and those obtained from perfectly round stiffened shells.

In Table 1 the collapse pressures are given for the out-of-round models as well as the perfectly round ones for the sake of comparison. The ratio

$$\frac{q_f}{\sigma_y} = \frac{\text{Collapse Pressure}}{\text{Yield strength of material used based on 1-2\% offset}}$$

was used to denote the non-dimensional collapse pressure.

Discussion of Experimental Data and Their Utilization

From the typical strain records shown in Figures 5 and 6, it is clear that the deviation of the ring strains is greater than the deviation of the mid-bay strains in the case of out-of-round shells. Thus, it is not surprising to find that the mode of failure was that of stiffener collapse rather than that of free plastic flow at mid-bay for which the perfectly round models were designed. The agreement of experimental and theoretical strains in the stiffener and particularly of the maximum strain in it can be of use in determining the pressure which will collapse the stiffener.

The presence of the stiffener, in out-of-round stiffened shells under pressure, results in shell displacements which are non-axisymmetric. It appears that the non-axisymmetric displacements which propagate almost without decay along the shell are directed such that the mid-bay out-of-roundness is reduced and the spread in circumferential mid-bay strains is narrowed.

When the collapse of out-of-round stiffened shells results from failure of the stiffener in the elasto-plastic range, the maximum stress produced in the stiffener is responsible for the creation and spread of plasticity. The establishment of the extent of the plastic region necessary to produce an elasto-plastic stability failure of the stiffener is not easy. Using the experimental data and/or the theoretical predictions which agree very well, the following scheme has been devised in which the pressure producing maximum elastic strains in the stiffener of perfectly round and out-of-round models can be manipulated to predict the collapse strength of aluminum stiffened shells. If P_p is the pressure producing a strain in the stiffener of a perfectly round, efficiently designed stiffened shell equal to the proportional limit, and P_o is the pressure producing a maximum strain in the stiffener of an out-of-round stiffened shell equal to the proportional limit, then it is apparent that the reduction in strength can be correlated with the difference between these two pressures.

An examination of the experimental data disclosed that the reduction in strength can be approximated by the use of a reduction factor, R_f . On this basis, the reduced strength for a given out-of-roundness is given by:

$$\left. \frac{q_f}{\sigma_y} \right|_o = \left. \frac{q_f}{\sigma_y} \right|_p (1 - R_f)$$

where

$$R_f = \frac{1}{2} \left[\frac{P_p - P_o}{P_p} \right]$$

For the out-of-round models tested, only Models 1-0, 3-0, and 3-H-1-0 collapsed, and experimental reduction factors are obtained. Results based on the above procedure, using theoretical and experimental pressure-maximum stiffener strains relations are given in Table 2.

The empirical scheme proposed predicts ultimate strengths, which for the shells tested, differ from the experimentally predicted strengths by no more than 3 per cent.

REFERENCES

1. DeHart, R. C., and Basdekas, N. L., "Yield Collapse of Stiffened Circular Cylindrical Shells," Southwest Research Institute report under Nonr Contract Nr 2650(00), Project Nr 064-435, September 1960.
2. Galletly, G. D., and Bart, R., "Effects of Boundary Conditions and Initial Out-of-Roundness on the Strength of Thin-Walled Cylinders Subjected to External Hydrostatic Pressures," David Taylor Model Basin Report 1066, November 1957.
3. Bodner, S. R., and Berks, W., "The Effect of Imperfections on the Stresses in a Circular Cylindrical Shell under Hydrostatic Pressure," Polytechnic Institute of Brooklyn, Report 210, December 1952.
4. Pulos, J. G., and Hom, K., DTMB Report C-948, June 1958, Confidential.
5. Wenk, E., DTMB Report C-934, June 1958, Confidential.
6. Kendrick, S., Naval Construction Research Establishment Report R.259, October 1953, Confidential.
7. Timoshenko, S., "Theory of Plates and Shells," McGraw-Hill, 1940.

TABLE 1. MODEL DATA

Models	Outside Diameter Inches	Shell Thickness Inches	Stiffener Spacing Inches	Depth of Stiffener Inches	Width of Stiffener Inches	Number of Bays	Relative Stiffness Factor**	$A = \frac{w_0}{h}$	σ_y : 1-2% Offset, psi	Maximum Recorded Strain in the Stiffener, Micros	q_f Collapse Pressure psi	q_f/σ_y
3-D	10	0.550	7.5	1.375	0.550	3	0.382	0	72,500	5,500	9,750	0.1345
1-0	10	0.550	7.5	1.375	0.550	3	0.382	0.0455	78,000	8,150	9,350	0.120
3-0	10	0.550	7.5	1.375	0.550	3	0.382	0.0910	78,000	10,200	9,100	0.1165
3-H	10	0.550	3.75	0.973	0.389	3	0.225	0	72,500	10,700	10,300	0.112*
2-0	10	0.550	3.75	0.973	0.389	3	0.225	0.0910	78,000	17,200	10,050	0.129*
4-0	10	0.550	3.75	0.973	0.389	3	0.225	0.0455	78,000	19,500	10,000	0.1285
3-H-1	6	0.330	2.25	0.584	0.233	7	0.225	0	72,500	9,150	10,200	0.111
3-H-1-0	6	0.330	2.25	0.584	0.233	7	0.225	0.0910	72,500	16,250	9,000	0.124

* Model believed to be at imminent failure. Pressure was greatest that could be obtained during test.

** Quantity first introduced by the authors in Reference 1.

TABLE 2. REDUCTION IN COLLAPSE STRENGTH

Model	1-0	3-0	3-H-1-0
R_f Based on experimental strains	0.12	0.13	0.18
R_f Based on theoretical strains	0.8	0.13	0.16
R_f Based on actual collapse pressures	0.11	0.14	0.12

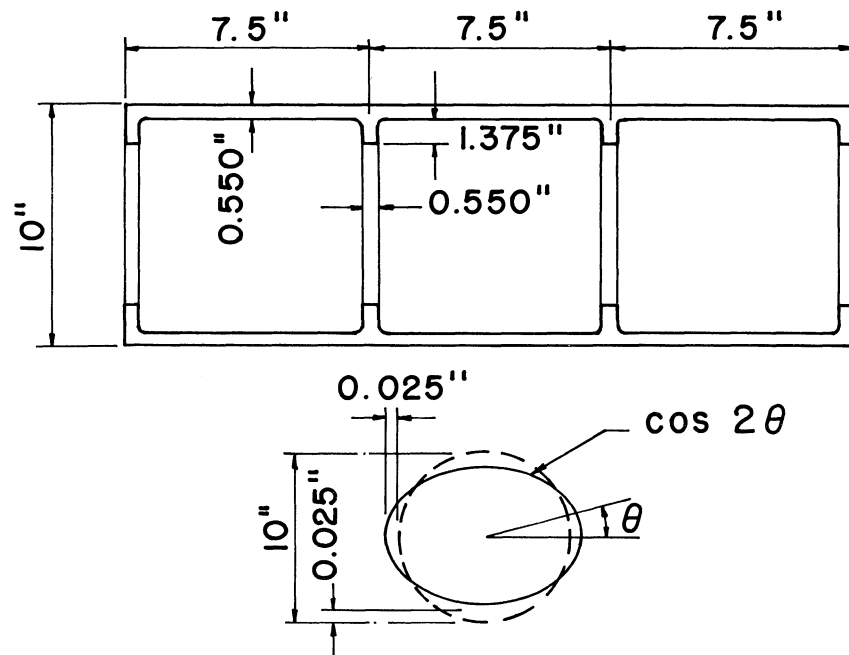


Figure 1.- Dimensions and initial out-of-roundness for model 1-0.

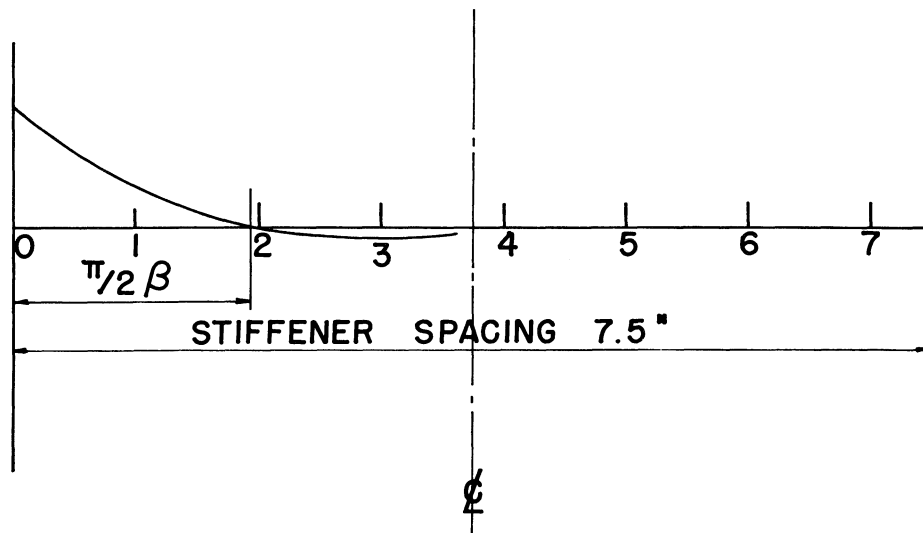


Figure 2.- Shear variation in shell of figure 1.

DISTANCE AT WHICH THE SHEAR REACHES ITS FIRST ZERO VALUE

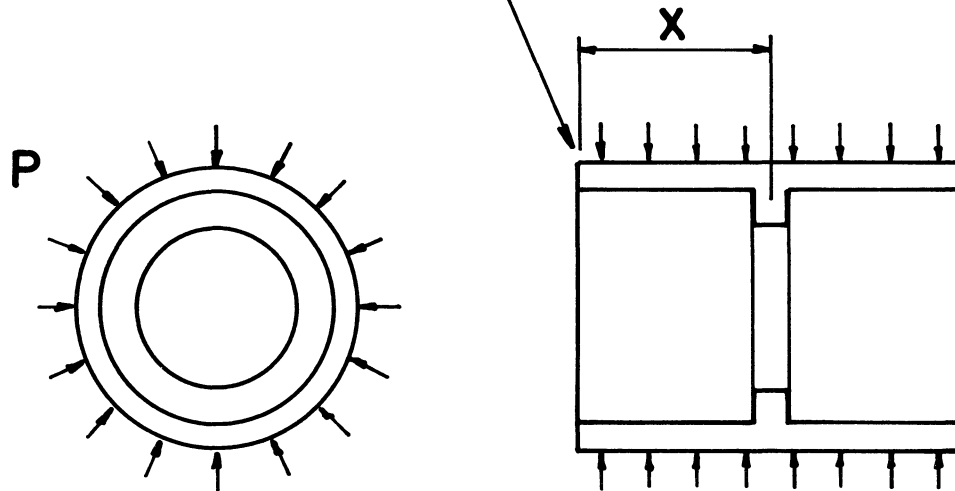


Figure 3.- Sketch of the T cross-section ring.

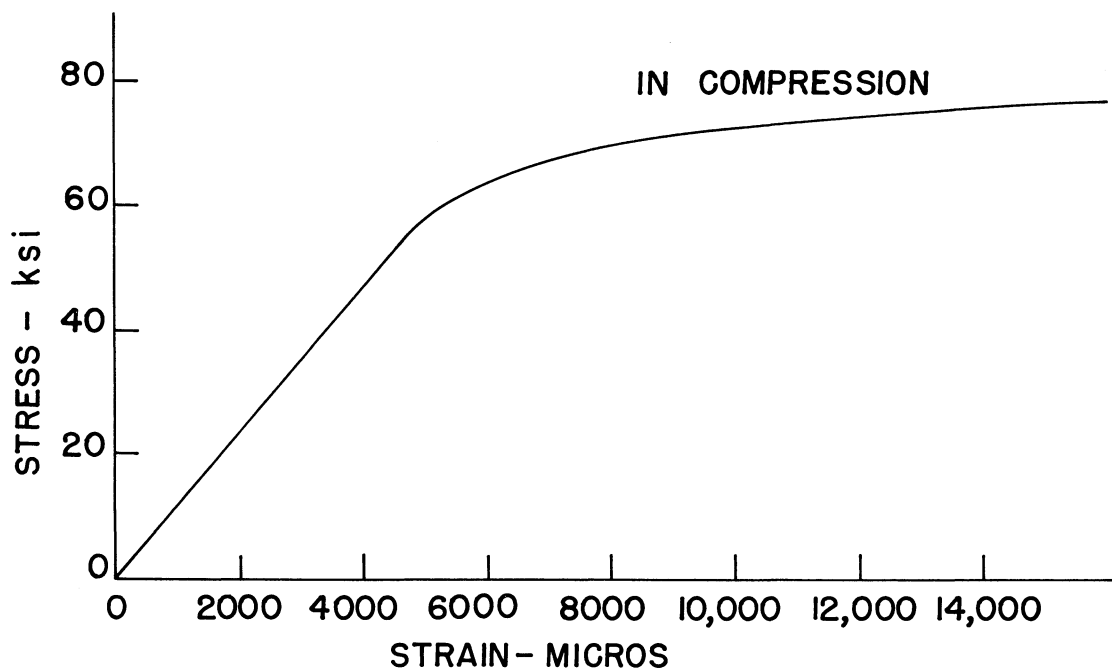


Figure 4.- Typical compression stress-strain curve of 7075-T6 aluminum alloy.

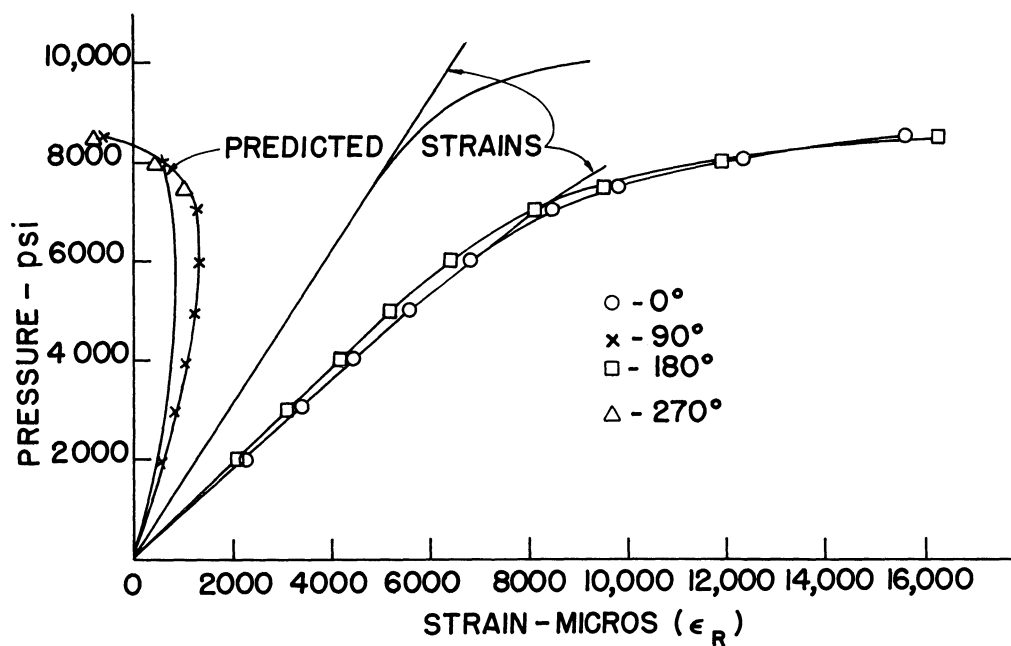


Figure 5.- A typical variation of experimental ring strains in perfectly round and out-of-round stiffened shells and their comparison with the theoretically predicted strains.

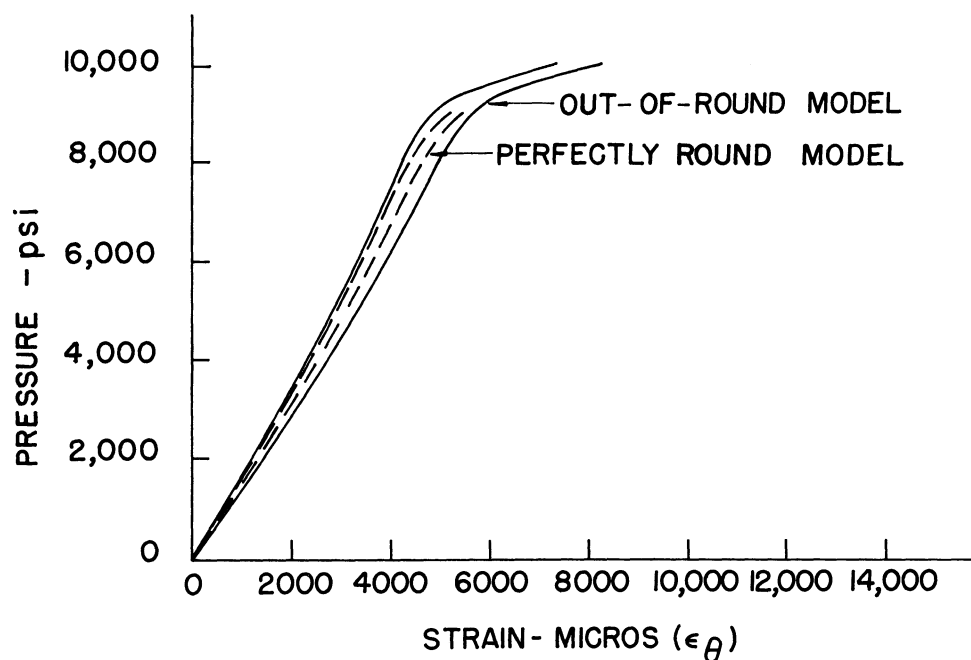


Figure 6.- A typical range of variation of mid-bay circumferential strains in perfectly round and out-of-round ring-stiffened circular cylindrical shells.

THERMAL BUCKLING OF CYLINDERS

By Melvin S. Anderson

NASA Langley Research Center

SUMMARY

Several theoretical and experimental investigations on the buckling of cylinders due to both axial and circumferential thermal stresses are reviewed. Differences that exist among the various results are discussed and areas of future work are indicated.

INTRODUCTION

In recent years numerous investigators have obtained theoretical solutions to various problems on the buckling of cylinders due to thermal stress and in some cases have obtained the interaction of thermal stresses with stresses due to externally applied loads. In the solution of these problems thermal stresses caused by arbitrary temperature distributions are generally represented by a Fourier series and then a Fourier series solution of the buckling problem is obtained. For a specific temperature distribution, the Fourier coefficients for the thermal stress are evaluated and the buckling conditions are determined. It can be seen that any varying stress distribution problem could be treated in the same manner; thus, the work that has been done is not necessarily limited to thermal stress problems.

Two general cases have been considered in the literature. The first case, which was investigated in references 1 to 3, is buckling of a cylinder due to circumferential stresses that vary in the axial direction. Circumferential thermal stresses are caused mainly by restraint of thermal expansion in the vicinity of the cooler rings. The interaction of circumferential thermal stress with uniform axial compression is treated in reference 3. Buckling of a cylinder due to axial stresses that vary in the circumferential direction was considered in references 4 and 5. Such a stress distribution results when a cylinder is heated nonuniformly around the circumference. For combinations of these cases, in which both circumferential and axial stresses are varying, no theoretical solution is available, but certain conclusions based on the results of the separate analyses can be inferred.

In the theory applied throughout references 1 to 5, either the Donnell equation or the modified Donnell equation (see ref. 6) was used.

Some of the more significant aspects of the various solutions are discussed in this paper.

SYMBOLS

E	Young's modulus
L	cylinder length between rings
r	cylinder radius
t	cylinder wall thickness
T_{\max}	maximum cylinder temperature
ΔT	temperature difference between rings and skin
x	axial coordinate
α	coefficient of linear thermal expansion
γ	ratio of axial stress to the classical cylinder buckling stress, $\frac{\sigma \sqrt{3(1 - \mu^2)}r}{Et}$
μ	Poisson's ratio
σ	axial stress
σ_x	maximum bending stress
σ_{Tx}, σ_{Ty}	thermal stress in axial and circumferential directions, positive in tension
τ	temperature buckling coefficient, $\alpha \Delta T \frac{r}{t}$
φ	circumferential coordinate

BUCKLING OF CYLINDERS DUE TO CIRCUMFERENTIAL STRESSES THAT VARY IN THE AXIAL DIRECTION

When a ring-stiffened cylinder is heated rapidly, cooler rings cause circumferential thermal stresses which are a maximum in compression over the rings and generally decay to zero away from the rings. The interaction of these thermal stresses with uniform axial compression to cause buckling is shown in figure 1. It is assumed that the rings and skin are both at constant temperatures, the difference in these temperatures being ΔT which is plotted as the ordinate in the form of the temperature buckling coefficient τ . The abscissa γ is the ratio of the axial compressive stress to the classical buckling stress for a cylinder under uniform compression.

The solid curve from reference 3 applies to a cylinder of many bays with each bay simply supported. A similar problem was considered in reference 1 for the case of heating alone, except that the cylinder was considered to be one-bay long. The value of τ from reference 1 indicated by the circle symbol at γ equal to zero is about $2\frac{1}{2}$ times the value obtained for a cylinder with many bays. This difference does not at first appear reasonable since the equations used in references 1 and 3 lead to the same stability determinant. However, as shown in figure 2 the thermal stress distribution is not the same for the two problems. In figure 2 the theoretical circumferential thermal stress σ_{Ty} is plotted in nondimensional form against $\frac{x}{L}$. The stress distribution for a cylinder of many bays is given by the solid curve while the dashed curve applies to a one-bay simply supported cylinder. The extent of the region of compressive stresses is greater for the cylinder of many bays than for the one-bay cylinder. The reason for the difference between the two curves is that, in a cylinder of many bays, the radial expansion of the cylinder wall is symmetric about a ring which effectively clamps the ends of each bay as far as circumferential thermal stress is concerned. For a given temperature, the average thermal stress in a cylinder of many bays is over twice the average thermal stress for a cylinder of one bay. If the results of references 1 and 3 are compared on the basis of average stress at buckling, the cylinder of one bay is found to have an average stress only 20 percent greater than a cylinder of many bays, even though, as shown in figure 1, the buckling temperature for a cylinder of one bay is over $2\frac{1}{2}$ times that for a cylinder of many bays. On the basis of this explanation, the result is reasonable and is similar to that found for buckling of flat plates where the average stress at buckling increases somewhat as the stress is concentrated more toward the edges.

The curves in figure 1 indicate that a significant portion of the classical buckling stress can be applied without lowering the buckling temperature. This behavior can be explained by examining again the average circumferential stress in the cylinder. For a given temperature, it can be shown (see fig. 8 of ref. 3) that the addition of axial compression reduces the average circumferential thermal stress. For a simply supported cylinder (solid curve in fig. 1) the reduction in average thermal stress compensates for the destabilizing effect of the axial compression and results in essentially no change of the buckling temperature. For a clamped cylinder (long-dash—short-dash curve in fig. 1), this compensation is even greater so there is a net temperature increase for buckling. At high values of γ , the axial stress becomes the dominant factor in buckling and the temperature rise at buckling quickly drops to zero at γ equal to 0.95. This 5-percent reduction in buckling stress from the classical value is caused by circumferential stresses produced by the restraint of Poisson's expansion in the vicinity of the rings.

An analysis of the buckling temperature of a clamped end cylinder is also given in reference 2. The result of this analysis is indicated by the square symbol in figure 1 and is seen to be almost twice the value obtained in reference 3 (long-dash—short-dash curve at γ equal to zero). The stress distribution and the boundary conditions were the same in the two references; however, the eighth-order Donnell equation was used in reference 2 whereas the fourth-order modified Donnell equation was used in reference 3. A preliminary check of the results of reference 2 indicates there may be some numerical errors in the calculations; however, the correct numerical results obtained from the Donnell equation would still be significantly higher than those obtained in reference 3. Batdorf (ref. 6) indicated that the use of the Donnell equation in combination with a Galerkin solution, as was done in reference 2, could lead to incorrect results for clamped cylinders. The discrepancy is possibly due to divergent series resulting from differentiating the deflection function 8 times. Additional information on the accuracy of the Donnell equation for clamped cylinders is obtained from calculations made for a clamped cylinder loaded to produce a uniform circumferential stress, which is a limiting case of the more general thermal stress problem. For this case the result obtained from the Donnell equation is as much as 50 percent higher than either the result obtained by Sturm (ref. 7) or the result obtained from the modified Donnell equation. The reason for the differences between the two equations has not been completely explained, but it does appear that the Donnell equation gives incorrect results for clamped cylinders and that the modified equation should be used.

It is well known that experimental buckling results are lower than values calculated by using small-deflection theory for cylinders in axial

compression. However, for circumferential compression, theoretical results are in agreement with tests. Thus, one could expect good agreement between theory and experiment at lower values of γ where circumferential compression is dominant but at higher values of γ the theory will be unconservative. The test points in figure 1 at τ equal to zero are for room-temperature bending tests, reported in reference 8, of 7075-T6 aluminum-alloy cylinders and indicate the magnitude of the reduction in buckling stress from the classical value for $\frac{r}{t}$ equal to 300. In reference 3 it is proposed that γ be reduced at any value of τ by the same percentage as the reduction at room temperature. This procedure results in the dashed curve in figure 1. The two test points for the heating tests are from the results of reference 9 for 2024-T3 aluminum-alloy cylinders loaded in pure bending and then heated. Reasonable agreement is shown between the tests and the dashed curve.

BUCKLING OF CYLINDERS DUE TO AXIAL STRESSES THAT VARY IN THE CIRCUMFERENTIAL DIRECTION

If a cylinder is heated such that the temperature varies around the circumference, nonuniform axial thermal stresses will arise. The effect of these thermal stresses on the load-carrying ability of the cylinder can be inferred from the analyses given in references 4 and 5. It was shown in reference 4 that, based on small deflection theory for pure bending of a cylinder, the maximum compressive stress for practical cylinder proportions is essentially the classical buckling stress for a cylinder in uniform compression. For most cases of nonuniform heating, the axial thermal stress distribution in a cylinder is similar to a bending-moment stress distribution in the vicinity of maximum compressive stress. Thus, the theoretical maximum axial compressive thermal stress at buckling can also be taken as the classical buckling stress for uniform compression. An exception occurs if the region of compressive stress is very small in the circumferential direction. For example, in reference 10 a theoretical buckling stress slightly higher than the classical value is indicated for a cylinder heated along a very narrow longitudinal strip.

In reference 5, buckling of a cylinder under a varying axial stress is also investigated. The stress distribution is represented by a Fourier cosine series and the resulting stability determinant is evaluated with the aid of certain simplifying assumptions. It is shown that the maximum stress for a bending distribution ($\cos \phi$) or the distribution given by the next higher term ($\cos 2\phi$) approaches the classical value as the size of the determinant is increased. It is of interest to note that with the use of the same simplifying assumptions the stability

determinant for these two cases can be put in closed form, and the maximum stress at buckling can be shown to be precisely the classical buckling stress for uniform compression when the size of the determinant approaches infinity.

It has been mentioned previously that theoretical buckling stresses for cylinders must be reduced to correspond to values observed in tests. Thermal stress distributions are more likely to be similar to bending stress distributions than uniform compression so that the experimental results obtained in bending tests of cylinders should be a good estimate of the maximum thermal stress at cylinder buckling. Experimental buckling stresses for uniform compression, which are slightly lower than the results obtained in bending tests, would provide a conservative estimate of the thermal buckling stress.

Even though the maximum stress at cylinder buckling has been specified, it is still somewhat of a problem to determine the temperature at which this stress occurs. The usual elementary analysis of thermal stress will not be sufficient in many cases as is illustrated in figure 3 where the longitudinal and circumferential variation of axial thermal stress is shown for a typical heating condition. Figure 3 was obtained from the results of reference 11 where an analysis is given of the axial thermal stress present in a cylinder with a nonuniform temperature distribution. The dashed curves represent the elementary thermal stress in each bay, and they differ considerably from either the experimental points or the solid curves, which were calculated by the theory of reference 11. The thermal stresses shown in figure 3 were the result of heating a cylinder on one side only over the central portion of the cylinder. Strains were not measured in the areas directly under the heating lamps but, in the other regions of the cylinder, stresses determined from measured strains agree reasonably well with theoretical values.

As previously mentioned, the results of references 4 and 5 indicate that, if the classical buckling stress for uniform compression is acting over only a portion of the circumference of a cylinder, buckling still occurs. Hence, it is reasonable to assume that the interaction curve obtained in reference 5 for uniform heating and uniform compression would also apply to stresses acting over a portion of the cylinder circumference. Using this assumption and the results of the various buckling analyses that have been previously discussed, the experimental results of reference 11 can be correlated with theory as shown in figure 4. In figure 4, the maximum cylinder bending stress σ_x is plotted against maximum cylinder temperature T_{max} . The upper curve is the result that would be obtained if there were no thermal stress and the bending strength was reduced in proportion to the reduction of Young's modulus with temperature. The middle curve was calculated from reference 3 for

a cylinder that is uniformly heated. The curve represents the interaction of a uniform compressive stress with the circumferential thermal stresses present due to the cooler rings. The cylinders represented by the test points on figure 4 were not heated uniformly but were heated as indicated in figure 3; this heating caused axial thermal stresses in addition to the load-induced stress. The maximum compressive bending stress was at the bottom of the cylinders which was also the point of maximum heating and high compressive thermal stresses; therefore, this region was critical for buckling. The load-carrying ability of the cylinder is indicated by the lower curve which represents the allowable load-induced stress and was obtained by subtracting the calculated axial thermal stress at the bottom of the cylinder from the value given by the middle curve. The data exhibit scatter which is about the same as observed in the results of room-temperature tests and is in reasonable agreement with predicted values.

AREAS OF FUTURE RESEARCH

For the problem of buckling due to circumferential thermal stress, experimental results have been obtained for the case in which significant amounts of axial compression have also been present. Further research is needed in this area to determine experimental buckling results for cylinders that buckle due to temperature alone. In addition the load-carrying ability of the temperature-buckled cylinder would be of interest.

Axial thermal stresses could be a significant factor in buckling of longitudinally stiffened cylinders which might be used as an interstage structure of launch vehicles. Therefore, it would appear that extension of the method of reference 11 for calculating thermal stresses to include stiffened cylinders with the possibility of local buckling between stiffeners should be an area for future research. Also the effect of a varying axial stress on the buckling behavior of a longitudinally stiffened cylinder should be investigated in order to determine whether there is any significant difference from the case of uniform compression.

CONCLUDING REMARKS

The work of several investigators on the buckling of cylinders under varying axial and circumferential thermal stresses has been reviewed. It has been shown that the severity of the circumferential thermal stress is strongly dependent on the boundary conditions. The interaction of circumferential thermal stresses with axial compression is also discussed. A method of incorporating these results with the observed reduction in

axial buckling stress from the theoretical value is indicated and is shown to agree with experimental results.

For cylinders that are heated nonuniformly, the axial thermal stress cannot in general be predicted by elementary theory. A method is available to predict these stresses which can be added to the load-induced stresses to obtain the complete axial stress distribution. Buckling can then be determined by assuming that the maximum axial stress is equal to the buckling stress that would be obtained in a cylinder heated uniformly and loaded by bending or compression.

REFERENCES

1. Hoff, N. J.: Buckling of Thin Cylindrical Shell Under Hoop Stresses Varying in Axial Direction. Jour. Appl. Mech., vol. 24, no. 3, Sept. 1957, pp. 405-412.
2. Johns, D. J., Houghton, D. S., and Webber, J. P. H.: Buckling Due To Thermal Stress of Cylindrical Shells Subjected to Axial Temperature Distributions. Rep. No. 147, The College of Aeronautics, Cranfield (British), May 1961.
3. Anderson, Melvin S.: Combinations of Temperature and Axial Compression Required for Buckling of a Ring-Stiffened Cylinder. NASA TN D-1224, 1962.
4. Seide, Paul, and Weingarten, V. I.: On the Buckling of Circular Cylindrical Shells Under Pure Bending. Trans. ASME, Ser. E - Jour. Appl. Mech., vol. 28, no. 1, Mar. 1961, pp. 112-116.
5. Abir, David, Hoff, N. J., Nardo, S. V., Pohle, Frederick V., Vafakos, William, and Wan, Koon-Sang: Thermal Buckling of Circular Cylindrical and Conical Thin-Walled Shells. WADC Tech. Rep. 58-104 ASTIA Doc. No. AD 151068, U.S. Air Force, Apr. 1958.
6. Batdorf, S. B.: A Simplified Method of Elastic-Stability Analysis for Thin Cylindrical Shells. NACA Rep. 874, 1947. (Formerly included in NACA TN's 1341 and 1342.)
7. Sturm, Rolland G.: A Study of the Collapsing Pressure of Thin-Walled Cylinders. Eng. Exp. Sta. Bull. No. 329, Univ. Ill., 1941.
8. Peterson, James P.: Bending Tests of Ring-Stiffened Circular Cylinders. NACA TN 3735, 1956.
9. Pride, Richard A., Hall, John B., Jr., and Anderson, Melvin S.: Effects of Rapid Heating on Strength of Airframe Components. NACA TN 4051, 1957.
10. Hill, D. W.: Buckling of a Thin Circular Cylindrical Shell Heated Along an Axial Strip. SUDAER No. 88 (AFOSR-TN-59-1250), Dept. Aero. Eng., Stanford Univ., Dec. 1959.
11. Anderson, Melvin S., and Card, Michael F.: Buckling of Ring-Stiffened Cylinders Under a Pure Bending Moment and a Nonuniform Temperature Distribution. NASA TN D-1513, 1962.

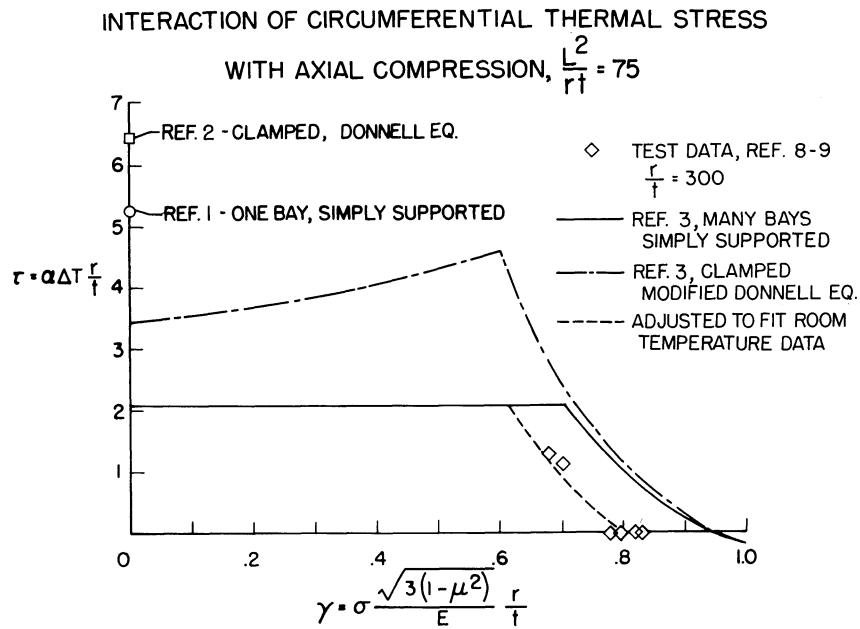


Figure 1

VARIATION OF CIRCUMFERENTIAL THERMAL STRESS ALONG BAY LENGTH

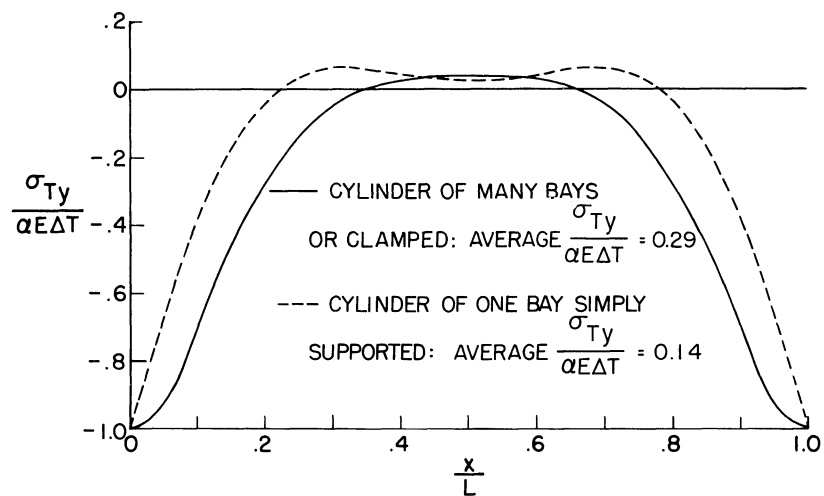


Figure 2

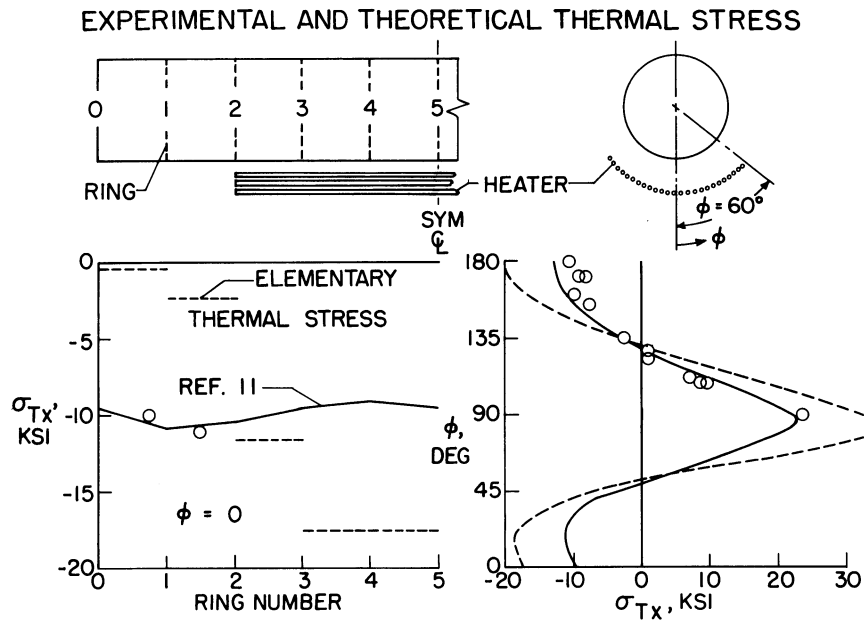


Figure 3

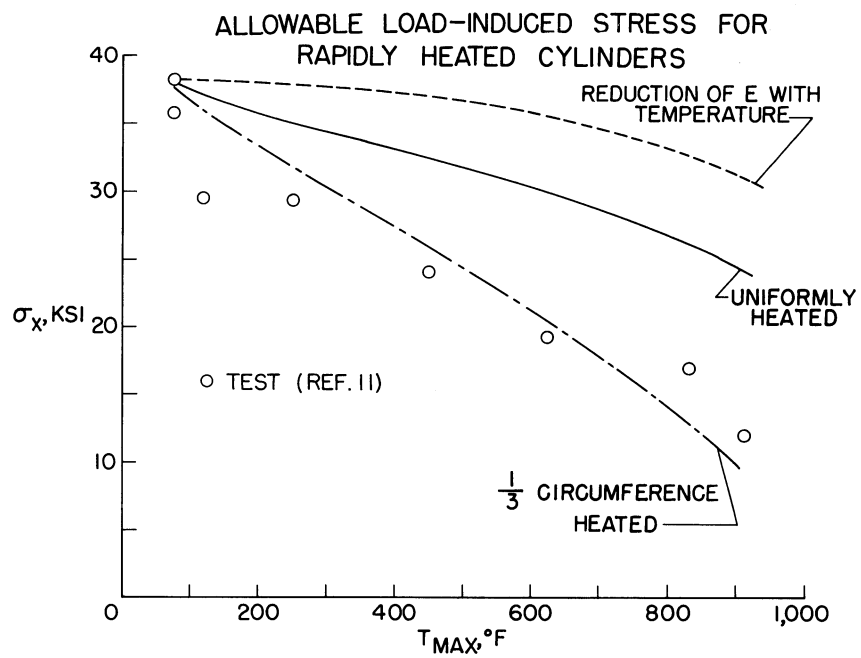


Figure 4

LOCAL CIRCUMFERENTIAL BUCKLING OF THIN CIRCULAR

CYLINDRICAL SHELLS

By David J. Johns

College of Aeronautics, Cranfield, U.K.

SUMMARY

The problem of circumferential buckling of a thin circular cylindrical shell due to compressive hoop stresses which vary in the axial direction is examined. For extremely localised compressive hoop stress distributions resulting from thermal discontinuity effects, or from a uniform, radial line loading, the buckle pattern should also be localised. Simplified analyses into these two types of problem are considered which show that only a limited number of buckle deflection modes needs to be assumed.

INTRODUCTION

The compressive hoop stresses set up near the junction of a cylindrical shell heated axisymmetrically, and a cooler, stiffening ring or bulkhead, may be high enough to cause buckling of the shell. Similar stress distributions are caused by an axisymmetric radial line loading in an unstiffened shell. For both types of problem the localised nature of the high compressive hoop stresses suggests that the buckling mode may also be local.

This paper reviews the problems and discusses some simplified theoretical analyses which only consider the conditions in the shell close to the region in which the compressive hoop stresses are acting. No attempt is made, as in other published solutions, to represent the conditions over the entire length of the shell. By this means it is hoped to show that a realistic solution is obtained when using only a limited number of modes for the buckle deflection pattern.

SYMBOLS

a radius of shell

a_p, a_N, b_N deflection coefficients in radial displacement functions

C	a number
D	flexural rigidity
E	Young's modulus
h	shell thickness
L	shell length
L_β	"compressed" length of shell
P	radial line load
R	thermal buckling factor $(\alpha T)_c$
T	uniform shell temperature rise
w	shell radial displacement
x	axial shell co-ordinate measured from position of maximum hoop stress
y	circumferential shell co-ordinate
α	coefficient of thermal expansion
β	shell parameter $\left[\frac{3(1-\nu^2)}{E} \frac{1}{h^3} \right]^{\frac{1}{4}}$
λ	half wave length of buckling in circumferential direction
σ_y	circumferential membrane stress
Subscript:	
c	critical

CIRCUMFERENTIAL THERMAL BUCKLING

Review

Hoff (ref.1) first investigated the stability of a simply supported cylindrical shell subjected to a uniform temperature rise. Infinite trigonometric series are used to represent the radial deformation of the shell and the axial stress distribution, and Donnell's simplified small deflection theory (ref.2) is used to obtain a solution in the form of an infinite determinant which can be truncated to give a solution to any desired degree of accuracy.

For clamped edged shells such a direct analysis is not possible and a solution of Donnell's equation requires the application of Galerkin's method (refs.3 and 4). In a more recent paper by Anderson (ref.5) a similar approach is made, for both clamped and simply supported edges, using the modified equation of equilibrium proposed by Batdorf (ref.6).

The result is shown in both references 1 and 5 that for long shells many terms are required in the radial deformation function to describe the buckle pattern accurately when it is expressed in the form

$$w = \sin \frac{\pi y}{\lambda} \sum_{p=1}^{\infty} a_p \sin \frac{\pi x}{L} \sin \frac{p\pi x}{L}, \quad (1)$$

for clamped edges, or,

$$w = \sin \frac{\pi y}{\lambda} \sum_{p=1}^{\infty} a_p \sin \frac{p\pi x}{L} \quad (2)$$

for simply supported edges.

For a uniformly heated shell attached to a rigid, non-expanding ring or bulkhead, the exact hoop stress distributions are shown in figure 1 and may be written as

$$\sigma_y / E\alpha T = \phi = e^{-\beta x} (\cos \beta x + \sin \beta x) \quad (3)$$

for clamped edges, and

$$\sigma_y / E\alpha T = \theta = e^{-\beta x} \cos \beta x \quad (4)$$

for simply supported edges.

It is evident that these stresses decrease rapidly away from the shell-bulkhead joint and, if the hoop stress distribution is represented by

$$\sigma_y = RE \sum_{m=0}^{\infty} S_m \cos \frac{m\pi x}{L}, \quad (5)$$

many terms S_m would be required for adequate representation of σ_y over the entire length of the shell. Because of this it was suggested by the author (ref.7) that a more important parameter in this problem than the shell length would be that length of the shell near to each joint for which the hoop stresses are compressive (see figure 1), i.e. L should be replaced by L_β where for clamped edges

$$L_\beta = 3\pi/2\beta \quad (6)$$

and for simply supported edges,

$$L_\beta = \pi/\beta . \quad (7)$$

This concept was used in reference 4 where both the assumed buckle pattern and the hoop stress distribution were only represented over a region close to the shell-bulkhead joint. The small number of terms required to get convergence of the solution and the agreement which was obtained with an experimental investigation suggested that the line of approach was indeed valid.

Hemp (ref.8) has also recently considered this thermal buckling problem and the energy method of solution he presents requires only a consideration of the buckle deformations close to the shell bulkhead joint. In the method of reference 8 allowance is made for the presence of initial longitudinal curvature in the shell in the region of maximum compressive hoop stress. Preliminary calculations by the present author have shown that the effect of the initial curvature is stabilising. A more detailed investigation into this aspect is now in progress.

Analysis

Donnell's simplified equation (ref.2) may be written as

$$D\nabla^4 w + \frac{Eh}{a^2} \left(\frac{\partial^4 w}{\partial x^4} \right) + h\nabla^4 \left\{ \sigma_y \frac{\partial^2 w}{\partial y^2} \right\} = 0 \quad (8)$$

The clamped edged boundary conditions $w = \frac{dw}{dx} = 0$ at $x = 0$ and $x = \frac{NL_\beta}{2}$ are satisfied if we assume an expression for w of the form

$$w = \sin \frac{\pi y}{\lambda} \sum_{p=1}^{\infty} a_p \sin \frac{2\pi x}{NL_{\beta}} \sin \frac{2p\pi x}{NL_{\beta}} \quad (9)$$

In this expression the parameter N defines the buckle pattern length in terms of the parameter, L_{β} . In equation (5) L is replaced by L_{β} and in a given problem the coefficients S_m characterising the particular stress distribution are inserted. The substitution of the modified equation (5) and equation (9) into equation (8) yields an equation which is not satisfied identically by any choice of the coefficients a_p . Recourse is therefore had to Galerkin's method of solution. The resultant stability determinant containing terms in R and λ is then analysed to find the value of λ which makes R a minimum. Various approximations are made by truncating the determinant and increasingly more terms are retained until convergence on the minimum value of R is found.

In reference 4 it was assumed that $N = 2$ and equation (5) could be replaced by

$$\sigma_y = \frac{RE}{2} \left[1 + \cos \frac{2\pi x}{L_{\beta}} \right] \quad 0 < x < \frac{L_{\beta}}{2} \quad (10)$$

Adequate convergence was obtained from only a 3×3 determinant the results of which are plotted in figure 2. The corresponding results for a simply supported shell are also shown and it is seen to have a critical buckling temperature 20% lower than for the clamped edged shell. This relatively close agreement is not surprising because although in the region of the shell-bulkhead joint clamping gives a more rigid support to the shell, the compressive hoop stresses are larger and act over a 50% greater length of shell than for the simply-supported shell. These two effects tend to cancel each other.

It is now thought that a more realistic approach would have been to vary N in the range $N \geq 1$ and so determine R_{\min} as a function of N . However, a first order solution using the above method with $N = p = 1$ produces the following simple result for clamped edges which is in excellent agreement with figure 2, viz

$$(\alpha T)_c = 6.45 \frac{h}{a} \quad (11)$$

The corresponding coefficient from reference 5 for a long, clamped edged shell is 3.6. However, for long shells the size of the determinant needed in reference 5 for convergence was greater than the computer programme allowed (greater than 13×13). This fact coupled with the relative simplicity of the present method and the correlation obtained with experiment leads the author to think that the present approach is probably more valid.

For a non-uniform, axial shell temperature distribution and for a flexible, expanding bulkhead the method above applies directly provided the shell stress distribution is correctly represented in the analysis.

This approach has been used in reference 4 in correlating the theory with the results of an experimental investigation. The steel shell concerned had a radius-thickness ratio of 2540 which for clamped edges gives a theoretical uniform shell buckling temperature of 230°C . For the measured temperature distribution at buckling the theoretical maximum shell temperature was derived as 324°C whereas the experimental value was 300°C . This is considered to be fair agreement. A photograph of the buckled pattern is shown in figure 3.

CIRCUMFERENTIAL BUCKLING DUE TO A RADIAL LINE LOADING

Analysis

For an axisymmetric, radial line loading the compressive hoop stress distribution is similar to that in the thermal buckling problem of the clamped edged shell (equation (3)) and may be approximated by

$$\sigma_y = \frac{P\beta a}{4h} \left(1 + \cos \frac{2\pi x}{L_\beta} \right), \quad 0 < x < \frac{L_\beta}{2} \quad (12)$$

The buckle deflection function is assumed to be

$$w = \sin \frac{\pi y}{\lambda} \left[a_N \left(1 + \cos \frac{2\pi x}{NL_\beta} \right) + b_N \left(1 - \cos \frac{4\pi x}{NL_\beta} \right) \right], \quad (13)$$

$$0 < x < \frac{NL_\beta}{2},$$

where the second term in b_N is a correction term.

The results obtained from the various analyses, using Donnell's simplified equation as described earlier, can be expressed in the form

$$P_c = CEh\left(\frac{h}{a}\right)^{3/2}, \quad (14)$$

and are summarised below.

N	a_N	b_N	C
1	YES	YES	1.41
1	YES	NO	1.44
2	YES	NO	0.80
3	YES	NO	1.11
4	YES	NO	2.19

Comparison of the two results for $N = 1$ suggests that the effect of the correction term b_N is small. Also it is seen that the minimum value of C corresponds to a value of $N = 2$ when the buckle deflection pattern extends over a length twice that for which the hoop stresses are compressive. It should be pointed out that for $N > 1$ no allowance was made for the presence of the small tensile hoop stresses in the region $\frac{3\pi}{4\beta} < x < \frac{7\pi}{4\beta}$ and there is some error in the assumed distribution for σ_y in equation (12).

There are very few other analyses into this problem in the literature but in reference 9 a solution is quoted for a long shell having the value $\frac{a}{h} = 100$. The result quoted for P_c is

$$P_c = 4.2 \times 10^{-4} Eh, \quad (15)$$

whilst from this present paper a coefficient of 8 is found. For $100 < \frac{a}{h} < 1000$ there is an approximate 2:1 relationship between equation (14) with $C = 0.8$ and the result of reference 9.

It is worth noting that the analysis in reference 9 attempted to represent the conditions over the entire length of shell and required twelve terms in the buckle deflection function. Thus the point can again be made that for local loading problems considerable simplification occurs and reasonable accuracy is retained by only considering the local buckling problem.

CONCLUSIONS

Analyses have been discussed which consider the problem of circumferential buckling of thin cylindrical shells. It has been shown that when the compressive hoop stresses are localised considerable simplicity results by also assuming the buckling mode to be local. Reasonable correlation with an experimental result has been obtained for a thermal buckling problem.

REFERENCES

1. Hoff, N.J., Buckling of Thin Cylindrical Shell Under Hoop Stresses Varying in Axial Direction. Jour. App. Mech. Vol.24, No.3, Sept. 1957, pp.405-412.
2. Donnell, L.H., Stability of Thin Walled Tubes Under Torsion. NACA Tech. Rep. No.479, 1933.
3. Zuk, W., Thermal Buckling of Clamped Cylindrical Shells. Jour. Aero. Sci. (Readers Forum) Vol.24, No.5, May 1957, p.359.
4. Johns, D.J., Houghton, D.S., Webber, J., Buckling Due to Thermal Stress of Cylindrical Shells Subjected to Axial Temperature Distributions. College of Aeronautics Rep. No.147, May 1961.
5. Anderson, Melvin S., Combinations of Temperature and Axial Compression Required for Buckling of a Ring-Stiffened Cylinder. NASA TN D-1224, April, 1962.
6. Batdorf, S.B., A Simplified Method of Elastic Stability Analysis for Thin Cylindrical Shells. NACA Rep.874, 1947.
7. Johns, D.J., Comments on Thermal Buckling of Clamped Cylindrical Shells. Jour. Aerospace Sci. (Readers Forum) Vol.26, No.1, Jan. 1959, p.59.
8. Hemp, W.S., Deformation of Heated Shells. SUDAER, No.103, (AFSOF-TN-61-770) Stanford University, April, 1961.
9. Almroth, B.O., and Brush, D.O., Buckling of a Finite Length Cylindrical Shell Under a Circumferential Band of Pressure. Jour. Aerospace Sci. Vol.28, No.7, July 1961, pp.573-578, 592.

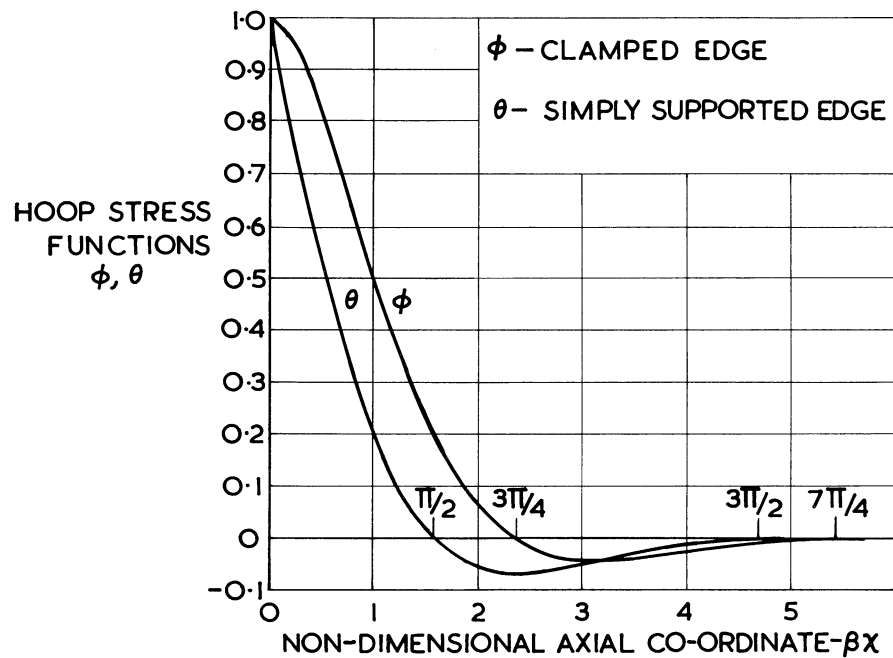


Figure 1.- Hoop stress functions for a cylindrical shell. Uniform shell temperature rise.

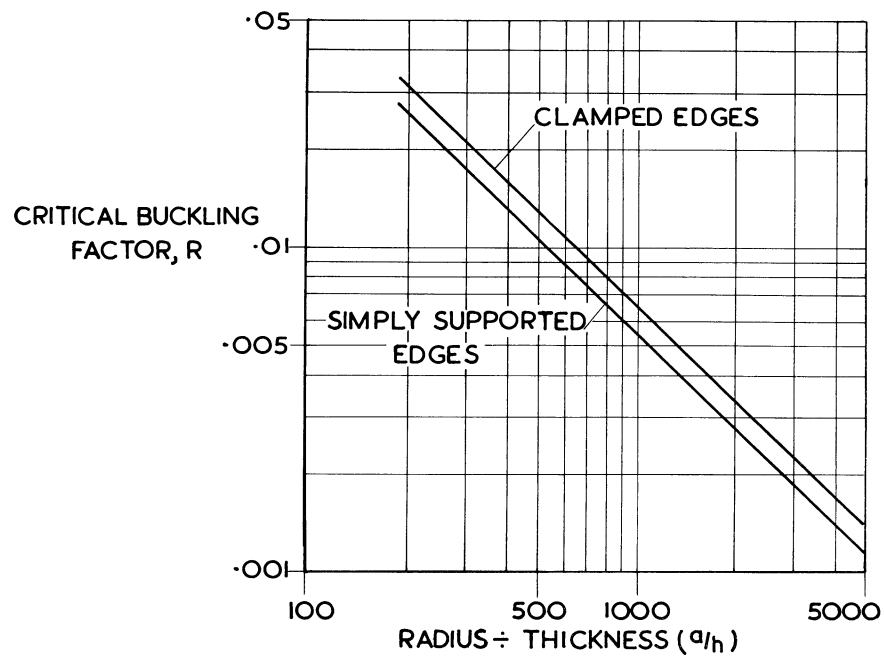


Figure 2.- Critical buckling factor for cylinders subjected to uniform shell temperature rise.

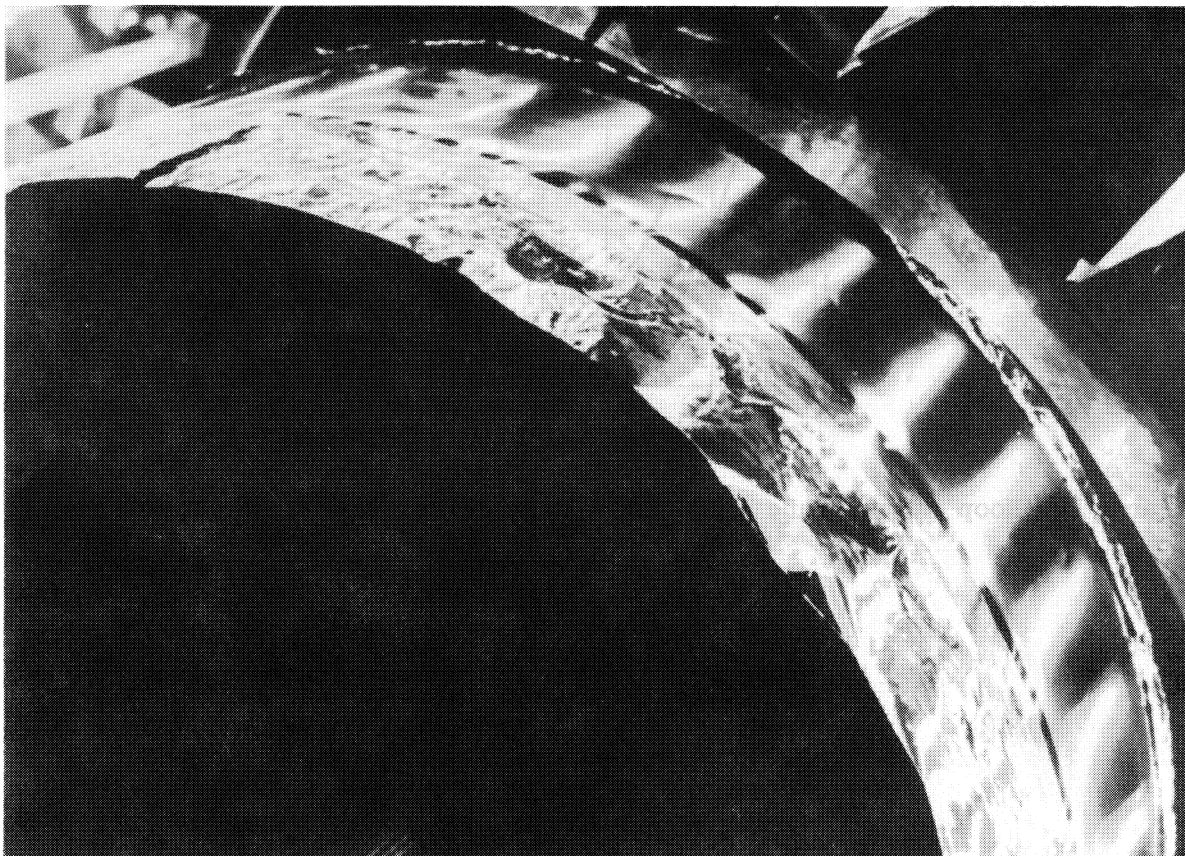


Figure 3.- Thermal buckles due to discontinuity stresses in a thin cylindrical shell.

ELASTIC AND PLASTIC STABILITY OF ORTHOTROPIC CYLINDERS

By George Gerard

Allied Research Associates

SUMMARY

By utilizing linear stability theory, solutions for elastic buckling of short and moderate length orthotropic cylinders under axial compression are presented and correlated with experimental results on circumferentially stiffened cylinders. The plastic buckling of short and moderate length isotropic and orthotropic cylinders is also investigated and the theoretical results correlated with available experimental data. A discussion of the effects of finite deflections and initial imperfections is presented in order to explain the correlation obtained between the theory and the experimental data.

INTRODUCTION

It is the objective here to summarize the significant results obtained on an NASA sponsored investigation* into the general instability characteristics of stiffened circular cylinders¹⁻⁴. One of the major results of this program was the development of a linear general stability theory for elastic and plastic buckling of orthotropic cylindrical shells under axial compression, external pressure and torsion over the complete length range and the correlation obtained with experimental data.

Since linear theory was employed, it is particularly important for shells to correlate the theory with experimental results. Consequently, all available data on stiffened and unstiffened shells were correlated with the theory on a unified basis. For the lateral pressure case, the experimental results were in good agreement with the predictions of the linear theory¹. Under torsional loading, the stiffened cylinder data exhibited somewhat more scatter but were in reasonably good agreement with the linear theory to the same extent

*NASA Research Grant NSG-17-59 with New York University

that the unstiffened cylinder data correlated¹. Thus, it was concluded that for lateral pressure and torsion, linear theory provides a satisfactory approach.

For orthotropically stiffened cylinders under axial compression, which is the area of greatest interest in launch and space vehicle applications, there was almost a complete lack of published test data. As a consequence, an experimental program was conducted on machined orthotropic cylinders of 2014-T6 aluminum alloy under axial compression. In all cases the stiffening system consisted of circumferential rings.

The test data obtained in this program⁴ when compared to the predictions of the linear stability theory revealed a most significant trend. Most of the test data fell within 90 to 100 percent of the linear theory which is in remarkable contrast with the corresponding isotropic cylinder case where the test data generally fall at a small fraction of the linear theory. Furthermore, the test data on the circumferentially stiffened cylinders which were obtained primarily on 8 in. diameter cylinders exhibited relatively little scatter. Corresponding tests on several larger diameter cylinders indicated no significant scale effect.

The theoretical reasons advanced for the behavior of the circumferentially stiffened cylinders are related to the fact that such cylinders first buckle in the axisymmetric mode³. Since this mode is stable in the post-buckling region, the deleterious effects of initial imperfections are minimized and circumferentially stiffened shells fail close to the predictions of linear theory.

SYMBOLS

A_1	plasticity coefficient, $A_1 = (1/4)(1 + 3 E_t/E_s)$
B_i	extensional rigidity, $B_i = E_s t_i / (1 - \nu^2)$
\bar{B}/B_3	$4(A_1 - \nu^2)(B_2/B_3) - \nu(B_1 + B_2)/B_1$
D_i	flexural rigidity, $D_i = E_s I_i / (1 - \nu^2)$
\bar{D}/D_1	$[\nu(D_1 + D_2) + D_3]/D_1$
E	modulus of elasticity

E_s	secant modulus
E_t	tangent modulus
I_i	moment of inertia per unit width
k_x	compressive buckling coefficient
k_{asy}	buckling coefficient, asymmetric mode
k_{axi}	buckling coefficient, axisymmetric mode
L	length
m	number of longitudinal half wave lengths
n	number of circumferential wave lengths
N	loading per unit width
R	radius
t_i	extensional thickness
U	buckling coefficient ratio, $U = k_{asy}/k_{axi}$
w	radial displacement
x, y	coordinates
Z	cylinder curvature parameter, $Z^2 = B_2 L^4 / 12 R^2 D_1$
Z_o	lower limit of short cylinder region
Z^*	upper limit of short cylinder region
α	$\alpha = B_1 D_2 / B_2 D_1$
β	wavelength parameter, $\beta = nL / m\pi R$
$\bar{\beta}$	see Eq.(1)
β^*	wavelength parameter for moderate length region
γ	$\gamma = B_3 \bar{D} / \bar{B} D_1$

δ	$\delta = 4 A_1 B_2 B_3^2 / B_1 \bar{B}^2$
η	plasticity reduction factor
$\bar{\eta}$	see Eq.(9)
ν	Poisson's ratio
ν_e	elastic value of Poisson's ratio
σ	axial stress

ELASTIC STABILITY OF ORTHOTROPIC CYLINDERS

The basic solutions for the compressive stability of orthotropic cylinders for the axisymmetric and asymmetric modes, and the behavior of these solutions over the length ranges associated with flat plates, short cylinders and moderate length cylinders was presented in Ref. 3. We shall be concerned here with a review of the essential results.

Moderate Length Range

In the moderate length range, the wavelength parameters for the asymmetric mode m and β can be treated as continuous variables. As a consequence, the following result is obtained for the wavelength ratio,

$$\bar{\beta}^2 = \beta^2 \left(2 \frac{B_2}{B_1} \frac{B_3}{\bar{B}} \right) = \frac{\delta}{2} \left\{ \frac{1-\alpha}{\alpha-\gamma} \pm \left[\left(\frac{1-\alpha}{\alpha-\gamma} \right)^2 + \frac{4}{\delta} \frac{1-\gamma}{\alpha-\gamma} \right]^{1/2} \right\} \quad (1)$$

where:

$$\alpha = B_1 D_2 / B_2 D_1$$

$$\gamma = B_3 \bar{D} / \bar{B} D_1$$

$$\delta = 4 A_1 B_2 B_3^2 / B_1 \bar{B}^2$$

By use of Eq.(1), the following solution for asymmetric buckling of moderate length orthotropic cylinders can be obtained

$$k_x = 0.702(A_1 - \nu^2)^{1/2} ZU \quad (2)$$

where:

$$U = \left[\frac{\alpha \bar{\beta}^2 + \gamma}{\bar{\beta}^2 + 1} \right]^{1/2} \quad (3)$$

Aside from the factor U , Eq.(2) is identical with that for the axisymmetric mode.

From the definitions of k_x and Z and the solutions for k_x given by Eq.(2) the buckling load for a moderate length cylinder is

$$N_{cr} = \frac{0.702\pi^2}{(12)^{1/2}} \frac{(B_2 D_1)^{1/2}}{R} (A_1 - \nu^2)^{1/2} U \quad (4)$$

It is apparent that in cases where $U < 1$ the asymmetric mode will govern while for $U > 1$ the axisymmetric mode will govern.

Since for the asymmetric mode U depends upon $\bar{\beta}$ which, in turn, depends upon the three orthotropic parameters, α , β and δ , it is of interest to examine Eq.(1) in some detail. It is immediately apparent that real or imaginary values of $\bar{\beta}$ can be obtained for various combinations of α and γ . In fact, the critical combinations are $\alpha = \gamma$ and $\gamma = 1$ as illustrated in Fig. 1.

Here, the shaded areas enclosed by the lines $\gamma = \alpha$ and $\gamma = 1$ represent the regions where β is imaginary for asymmetric buckling. Since the axisymmetric mode is real in the entire domain, it is reasonable to assume that buckling in the axisymmetric mode is the only one possible in the shaded regions.

A further study of Eqs.(1) and (3) for the regions where β is real reveals that $U < 1$ for $\gamma < 1$ and that $U > 1$ for $\gamma > 1$. Consequently, the asymmetric mode is theoretically possible in the region $\gamma \leq 1$ for $\alpha \geq \gamma$ only. On the other hand, the axisymmetric mode governs in the remainder of this domain by virtue of either $U > 1$ or imaginary β for the asymmetric mode.

Of further interest is the location of the solution for the isotropic cylinder which lies at the point 1,1. In terms of β this is rather a confused region since theoretically $-\infty < \beta < \infty$. In fact, direct solution of the isotropic elastic cylinder case from the eighth-order Donnell equation results in an indeterminacy for β . However, by proceeding to the limit of the isotropic cylinder from the orthotropic cylinder solution, it is found that for $\alpha = 1$, Eq.(1) reduces directly

to

$$\beta = (A_1 B_1 / B_2)^{1/4} \quad (5)$$

Since Eq.(5) is valid along $\alpha = 1$ as shown in Fig. 1, and this includes the isotropic cylinder point, the indeterminacy in β is removed. In fact, for the isotropic elastic cylinder, Eq.(5) reduces to $\beta = 1$.

A study of the orthotropic parameters indicates that longitudinally stiffened moderate length cylinders are defined by $\alpha < 1$. Similarly, circumferentially stiffened cylinders are defined by $\alpha > 1$. Furthermore, for many practical types of stiffened construction, it appears that γ is not greatly different from unity. Thus, it appears that the region $\gamma, \alpha < 1$ contains all practical longitudinally stiffened cylinders. The region $\alpha > \gamma > 1$ appears to contain all practical circumferentially stiffened cylinders that buckle in the axisymmetric mode. For the former, both α and γ are important in determining U and hence the buckling load, whereas for the circumferentially stiffened case $U = 1$ theoretically for $\alpha, \gamma > 1$.

Short Cylinder Range

Now that the moderate length range has been considered in some detail, we turn to the short cylinder range where the wavelength parameter $m = 1$, the lowest integer value. For the axisymmetric case, the results shown in Fig. 2 for the $\beta = 0$ case are obtained for all orthotropic elastic cylinders ($A_1 = 1$). At

$$Z = \pi^2 / [12(1-\nu^2)]^{1/2} \quad (6)$$

the short cylinder solution merges with the 45° dashed line which represents the moderate length solution given by Eq.(2). However, to be strictly correct, it is necessary to take into account the integer values of m in this region. Consequently, the cusps shown for $m = 2, 3, 4 \dots$ are obtained.

For the asymmetric case, β is constant in the moderate length range and is given by Eq.(1). We now denote this value of the wavelength parameter by β^* . It can be observed from Fig. 2 that the lowest value of Z corresponding to this value of β^* is denoted by Z^* which marks the upper limit of the short cylinder region for the particular orthotropic cylinder depicted.

For the asymmetric mode, $0 < \beta \leq \beta^*$ in the short cylinder range and $m = 1$. The lowest value of Z for the asymmetric mode denoted by Z_0 is given by

$$Z_0 = \frac{\pi^2 A_1 \gamma^{1/2}}{[12(A_1 - \nu^2)]^{1/2}} \quad (7)$$

The corresponding value of k_x for Z_0 is

$$k_x = A_1(1 + \gamma) \quad ; \quad \text{for } Z = Z_0 \quad (8)$$

This value of k_x is the lowest value at which the asymmetric mode can occur. Thus, the short cylinder region for this mode is bounded by $Z_0 < Z \leq Z^*$.

In the short cylinder region of Fig. 2, the axisymmetric mode governs below $Z_0 = 1.4$ as obtained from Eq.(7) for $\gamma = 1/4$. In the region between Z_0 and $Z^* = 27.4$, a numerical procedure given in Ref. 3 was used to obtain the asymmetric curve shown in Fig. 2. At Z^* , the short cylinder curve merges with the dashed line representing the moderate length solution given by Eq.(2) where $\beta^* = 1.074$ in this case and $U = 0.619$. As in the axisymmetric case, the cusps in the moderate length region result from using the integer values $m = 1, 2, 3 \dots$ and $\beta^* = 1.074$.

PLASTIC STABILITY OF CYLINDERS

In the previous section the solution for elastic buckling of a moderate length isotropic cylinder was obtained as the limiting case of an orthotropic cylinder. Because of the additional complexities that are introduced when plastic buckling is considered, it appears desirable to treat the plastic stability of an isotropic cylinder in some detail before considering the orthotropic cylinder.

In Ref. 2, explicit solutions for plastic buckling of an isotropic cylinder in the axisymmetric and asymmetric modes were obtained for the flat plate and moderate length regions. It is the objective here to present plastic buckling solutions for the short cylinder region and also to define the ranges of validity of the two explicit

solutions for the isotropic cylinder.

For the moderate length region of the plastic isotropic cylinder in terms of the parameters of Fig. 1, $\alpha = 1$ and $\gamma = (2A_1 - 1)^{-1}$. Thus, the effect of plasticity is to move vertically upward from the isotropic elastic point (1,1) as shown in Fig. 1 as E_t/E_s decreases. As a consequence, the axisymmetric solution should always govern for moderate length cylinders subject to plastic buckling.

Short Cylinder Range

By utilizing the procedures given in Ref. 3, k_x -Z curves have been computed for values of $E_t/E_s = 0.75, 0.50, 0.25^x$ and 0. The data for the axisymmetric mode are shown in Fig. 3. It can be observed that the axisymmetric plastic solutions closely resemble the elastic case and that for the limiting case $E_t/E_s = 0$, the solution is independent of Z and corresponds to the flat plate solution.

It is convenient to separate out the plasticity effects through the use of a plasticity reduction factor defined as

$$\bar{\eta} = \eta \frac{(1-\nu^2)_e E}{(1-\nu_e^2) E_s} = \frac{(k_x)_{\text{plastic}}}{(k_x)_{\text{elastic}}} \quad (9)$$

By use of the plasticity reduction factor, the elastic and plastic buckling load can be jointly written as

$$N_x = \frac{\pi^2 \eta k_x E I_1}{(1-\nu_e^2) L^2} \quad (10)$$

Following Eq.(9), values of $\bar{\eta}$ have been determined for the axisymmetric and asymmetric modes. These data are presented in Fig. 4 and cover the Z-range from flat plates through the short cylinder region into the moderate length region.

In the flat plate region $\bar{\eta}$ corresponds to the explicit solution

$$\bar{\eta} = (1/4)(1 + 3 E_t/E_s) \quad (11)$$

In the moderate length region, the following explicit solutions of Ref. 2 apply. For the axisymmetric case,

$$\bar{\eta} = (E_t/E_s)^{1/2} \quad (12)$$

For the asymmetric case,

$$\bar{\eta} = \left(\frac{E_t}{E_s}\right)^{1/2} \left[\frac{2 + (1+3 E_t/E_s)^{1/2}}{3(E_t/E_s) - 1 + (1 + 3 E_t/E_s)^{1/2}} \right]^{1/2} \quad (13)$$

Orthotropic Cylinders

Although the asymmetric load may be lower than the axisymmetric load for certain cases of elastic buckling of orthotropic cylinders as shown in Fig. 2, it is to be expected from the plastic isotropic cylinder investigation that this situation will reverse itself as E_t/E_s is reduced sufficiently. Since the asymmetric buckling load as well as this crossover point are functions of the orthotropic parameters as well as E_t/E_s , it is evident that it is hardly feasible to construct $k_x - Z$ charts covering a significant range of parameters.

The axisymmetric solution is independent of the orthotropic parameters and therefore the form of the plastic buckling solution for orthotropic cylinders is identical with that for isotropic cylinders as shown in Ref. 2. As a consequence, the data presented in Figs. 3 and 4 for the axisymmetric mode may be used directly for short and moderate length orthotropic cylinders.

For the asymmetric plastic case, the procedure used to construct Fig. 2 for the elastic orthotropic cylinder may be used directly by inserting the proper value of A_1 in the pertinent equations. To illustrate the influence of plasticity upon a moderate length orthotropic cylinder, consider the point $\alpha = 1/2$, $\gamma = 1/4$ which corresponds to the orthotropic cylinder example used in Fig. 2. Although α does not depend upon A_1 , γ does, and therefore as A_1 decreases in the plastic range, the effect upon Fig. 1 is to move vertically upward from the point $1/2, 1/4$. Beyond the $1/2, 1/2$ point, it is apparent that the axisymmetric solution will govern.

CORRELATION WITH EXPERIMENTAL DATA

For moderate length cylinders under axial compression, it is of

particular importance to correlate theoretical results with experimental data because of the well known discrepancy that exists for isotropic elastic cylinders. Consequently, the test data obtained in Ref. 4 for elastic buckling of circumferentially stiffened orthotropic cylinders are presented. In addition, available test data on isotropic plastic cylinders are also presented in order to check another phase of the general theory.

Orthotropic Elastic Cylinders

In Ref. 4, experiments were conducted primarily on a series of 8 in. diameter circumferentially stiffened elastic cylinders of moderate length under axial compressive loading. In terms of the parameters of Fig. 1, the range of stiffening parameters covered $3 < \alpha < 20$ (closely spaced to widely spaced rings) and in all cases $\gamma > 1$. The cylinders were designed such that local instability did not occur before failure in the general instability mode. Because of the fact that $\gamma > 1$ for all cylinders, theoretically they should all buckle initially in the axisymmetric mode.

The test data on the failing strength of each cylinder is shown in Fig. 5 as compared to the results of the linear axisymmetric orthotropic theory. It can be observed that excellent agreement exists in remarkable contrast with the results obtained for isotropic elastic cylinders. The small experimental scatter evident in Fig. 5 together with the good correlation with linear theory are important indications of the potential reliability of this type of construction.

Isotropic Plastic Cylinders

Available test data on the failure strength of moderate length aluminum alloy cylinders that buckled plastically have been assembled in Fig. 6. The test data include low⁵, medium⁶ and high⁷ strength aluminum alloys and thus cover a broad range of interest. The cylinders that could be identified as failing in the axisymmetric and asymmetric modes are so indicated in Fig. 6. Also included for comparison is the axisymmetric plasticity reduction factor for moderate length cylinders as given by Eq.(12). In each case, the theoretical curves were computed by using the compressive stress strain data associated with the test specimens.

It can be observed from Fig. 6, in distinct contrast with well known results for the elastic case, that the axisymmetric buckling theory is in relatively good agreement with the test data for the aluminum alloy cylinders that failed in the axisymmetric mode. On the other hand, the 7075-T6 cylinders that failed in the asymmetric mode in the region between the proportional limit and compressive yield

strength exhibit the discrepancy with linear theory characteristic of the elastic case.

POST-BUCKLING BEHAVIOR OF CYLINDERS

From the correlation between theory and test data obtained in the previous section, it is apparent that the orthotropic and plastic aspects of the problem can have a profound influence on the post-buckling behavior. Consequently, we shall be concerned now with a qualitative evaluation of this region. Because of the obvious complexities of the finite deflection, non-linear features of this region, much of this discussion is somewhat conjectural. It is indeed fortunate, however, that the non-linear features of elastic orthotropic cylinders have been investigated by Thielemann⁸ and that Lee⁵ has similarly treated the plastic isotropic cylinder.

Elastic Cylinders

A schematic representation of the behavior of perfect, elastic, moderate length cylinders is illustrated in Fig. 7 in terms of the axisymmetric buckling parameters. It can be observed for the isotropic cylinder that the axisymmetric and asymmetric buckling loads are equal and that the post-buckling behavior for the asymmetric mode is unstable whereas that for the axisymmetric mode is stable.

For a typical longitudinally stiffened cylinder, the asymmetric buckling load may be considerably below that of the axisymmetric case. The post-buckling behavior in this case appears to be similar to that of the isotropic cylinder⁷.

For a typical circumferentially stiffened cylinder, only the axisymmetric load is possible since the asymmetric case generally leads to imaginary values of β . Thus, as the end shortening is increased beyond buckling, it follows the stable, horizontal axisymmetric path. However, at some point in this finite deflection region it is entirely possible that the β values associated with the asymmetric mode may become real resulting in the second bifurcation shown in Fig. 7. Beyond this point, the asymmetric path may be unstable.

The preceding discussion considered perfect cylinders and it is now instructive to consider the behavior of cylinders containing small initial imperfections. A possible loading path for such cylinders is shown by the dashed line in Fig. 7. As the load is increased, the

dashed line intersects the unstable asymmetric post-buckling curves for the longitudinally stiffened and isotropic cylinders considerably below the linear buckling load. It appears to be reasonable to assume that after the intersection point the asymmetric finite deflection paths would be followed. Thus, failure can occur considerably below the linear buckling load in the presence of small initial imperfections.

In the case of the circumferentially stiffened cylinder, the small stable axisymmetric post-buckling region plays a most essential role in significantly reducing the deleterious effects of initial imperfections. As illustrated in Fig. 7, the initial imperfection load path intersects the asymmetric finite deflection path well beyond the end shortening associated with buckling. Thus, failure occurs at a load not significantly below the axisymmetric buckling load depending upon the extent of the stable axisymmetric post-buckling region.

It is important to note that in all three cases failure generally occurs at the intersection of the initial imperfection path with the asymmetric finite deflections path. Thus, it is to be expected that the well known diamond buckle pattern should be observed at the conclusion of many cylinder experiments as shown in Fig. 8a. Under proper conditions, however, it should be possible to observe the formation of an axisymmetric buckle pattern for a circumferentially stiffened cylinder prior to failure in the diamond mode. In other cases such as an orthotropic elastic cylinder circumferentially stiffened (high α), the axisymmetric mode was actually observed⁴ at the conclusion of the test as shown in Fig. 8b.

Plastic Cylinders

A schematic representation, based in part on Lee's analysis^{5,9} of the post-buckling behavior of plastic isotropic moderate length cylinders, is illustrated in Fig. 9 in terms of the axisymmetric buckling parameters. The two cases shown are for the proportional limit region where the two buckling modes are slightly different and the yield region where the two buckling modes are significantly different.

Considering the yield region first, it can be observed that the stable axisymmetric post-buckling region is relatively large in extent by virtue of the significant separation of the asymmetric and axisymmetric buckling loads. As a consequence, cylinders containing small initial imperfections and following the dashed line in Fig. 9b tend to fail upon reaching the axisymmetric load. Here, failure occurs without intersection of the initial imperfection and unstable post-buckling asymmetric paths.

Thus, it can be anticipated that the axisymmetric buckle mode

should be observed at the conclusion of the test and that the failure load should be in good agreement with the axisymmetric buckling load. This is indeed the case for the test data shown in Fig. 6. Initial⁹ imperfections can be expected to play a negligible role in this case⁹.

The probable conditions in the proportional limit region are depicted in Fig. 9a. Here, the stable axisymmetric post-buckling region is sharply reduced as compared to Fig. 9b by virtue of the small separation of the two buckling loads. As a result, the initial imperfection load path can intersect the unstable asymmetric post-buckling path and thus fail well below the axisymmetric and asymmetric buckling loads. Such cylinders would fail in the diamond buckle pattern and initial imperfections are significant here⁹. It is believed that such behavior is associated with the 7075-T6 test points in Fig. 6 that exhibited asymmetric buckles at failure.

CONCLUDING REMARKS

The experimental and theoretical results reported herein present some very significant practical implications for the shell structures of launch and space vehicles. Use of orthotropic circumferential stiffening of shells through either ring stiffeners or possibly through circumferentially oriented filaments appears to be an attractive way to achieve an important improvement in structural reliability over that associated with isotropic cylinders. Improved structural reliability can be realized through the ability to predict the failing load with far greater accuracy than for the isotropic case and through the statistical aspects associated with the much smaller scatter of the circumferentially stiffened cylinder experiments.

REFERENCES

1. Becker, H. and Gerard, G., "Elastic Stability of Orthotropic Shells," Journal of the Aerospace Sciences, Vol. 29, No. 5, pp. 505-512, 520, May 1962.
2. Gerard, G., "Plastic Stability Theory of Geometrically Orthotropic Plates and Cylindrical Shells," New York University Tech. Rep. SM 61-11, July 1961. (Journal of the Aerospace Sciences, accepted for publication).
3. Gerard, G., "Compressive Stability of Orthotropic Cylinders," New York University Tech. Rep. SM 62-4, May 1962.
4. Becker, H., Gerard, G. and Winter, R. W., "Experiments on Axially Compressive General Instability of Monolithic Circumferentially Stiffened Circular Cylindrical Shells," New York University Tech. Rep. SM 62-5, May 1962.
5. Lee, L. H. N., "Inelastic Buckling of Initially Imperfect Cylindrical Shells Subject to Axial Compression," Journal of the Aerospace Sciences, Vol. 29, No. 1, pp. 87-95, Jan. 1962.
6. Osgood, W. R., "The Crinkling Strength and the Bending Strength of Round Aircraft Tubing," NACA Rep. 632, 1938.
7. Moore, R. L. and Clark, J. W., "Torsion, Compression and Bending Tests of Tubular Sections Machined from 75S-T6 Rolled Round Rod," NACA RM 52125, Nov. 1952.
8. Thielemann, W. F., "New Developments in the Nonlinear Theories of the Buckling of Thin Cylindrical Shells," Aeronautics and Astronautics, Pergamon Press, 1960, pp. 76-119.
9. Gerard, G., "On the Role of Initial Imperfections in Plastic Buckling of Cylinders Under Axial Compression," Journal of the Aerospace Sciences, Vol. 29, No. 6, pp. 744-745, June 1962.

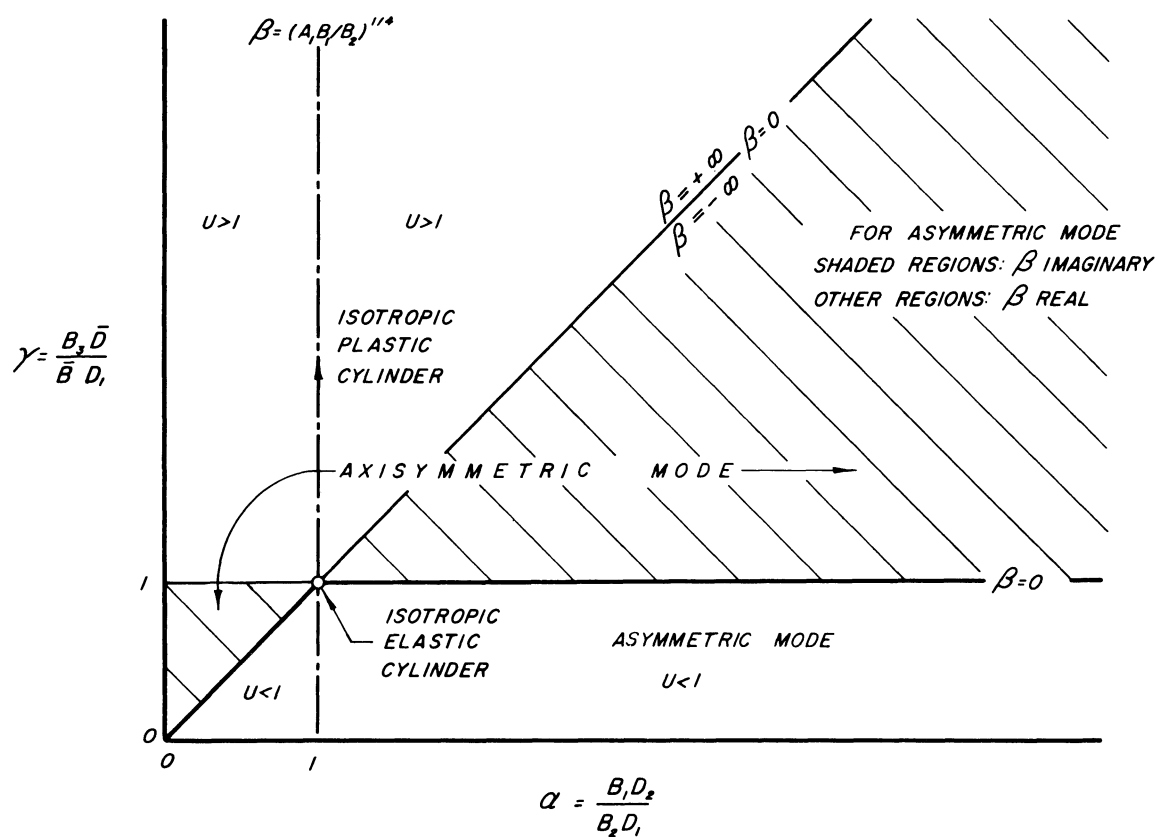


Figure 1.- Domains of β for the asymmetric mode.

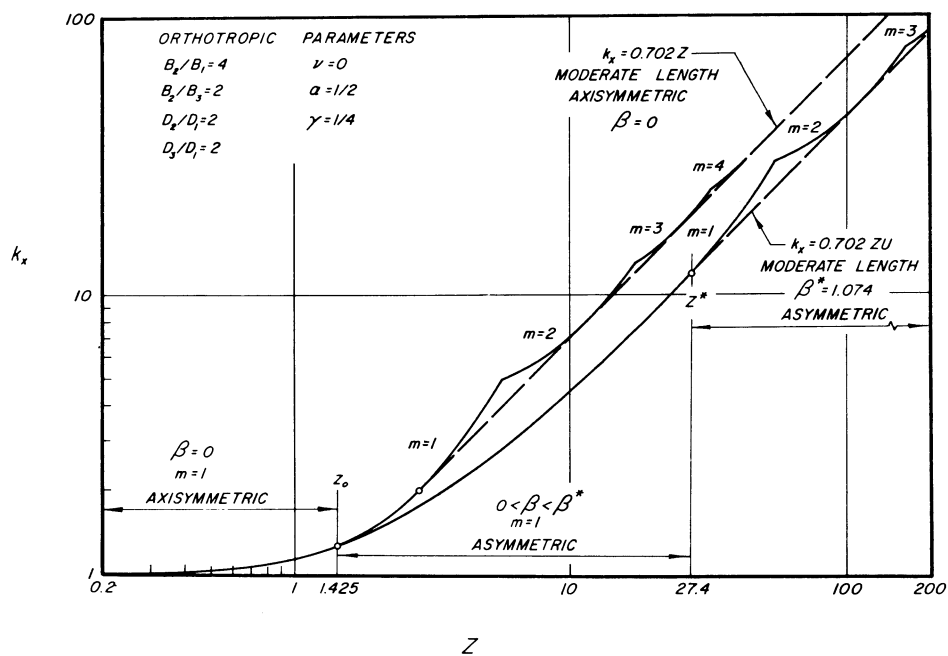


Figure 2.- Buckling coefficients for an elastic orthotropic cylinder.
 $B_2/B_1 = 4$, $B_2/B_3 = D_2/D_1 = D_3/D_1 = 2$ and $\nu = 0$.

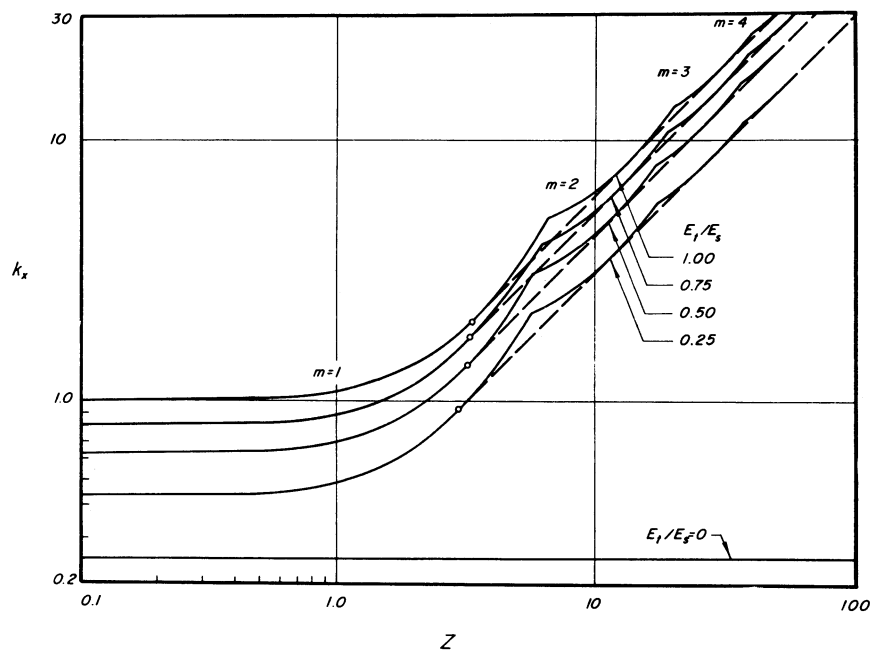


Figure 3.- Axisymmetric plastic buckling coefficients for isotropic cylinders.

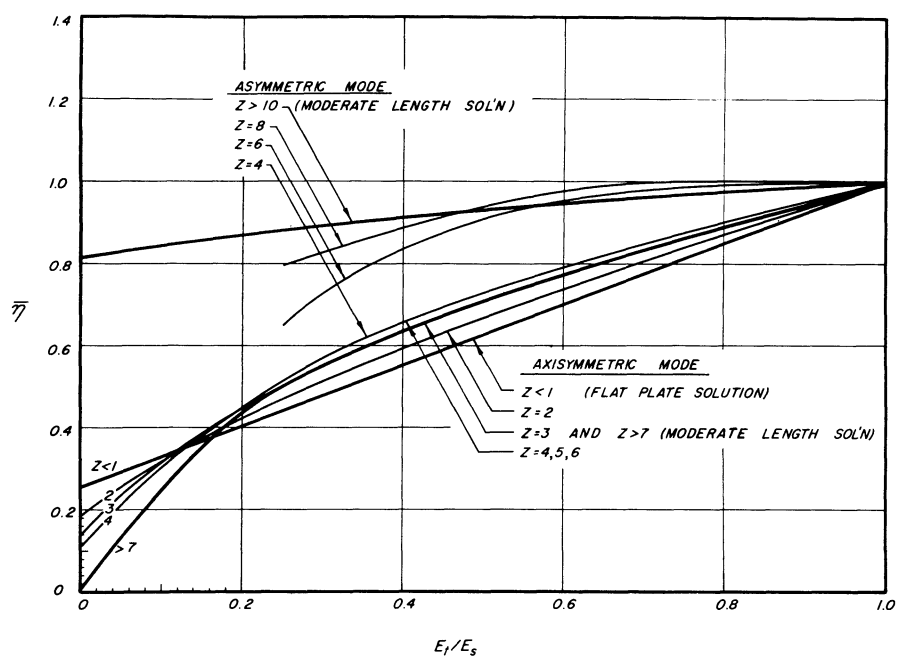


Figure 4.- Plasticity reduction factors as a function of E_t/E_s .

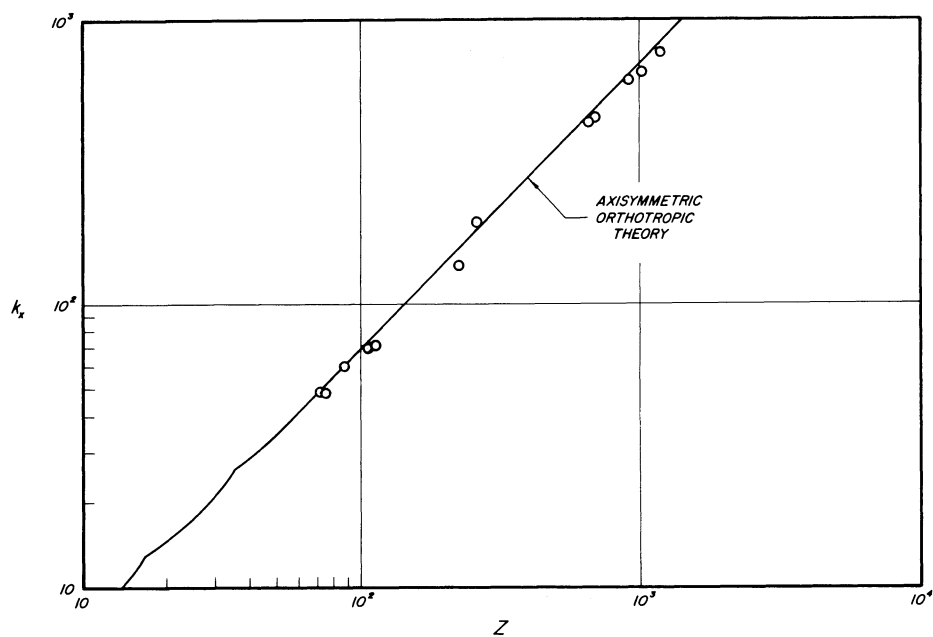


Figure 5.- Test data on elastic general instability of circumferentially stiffened cylinders in axial compression.

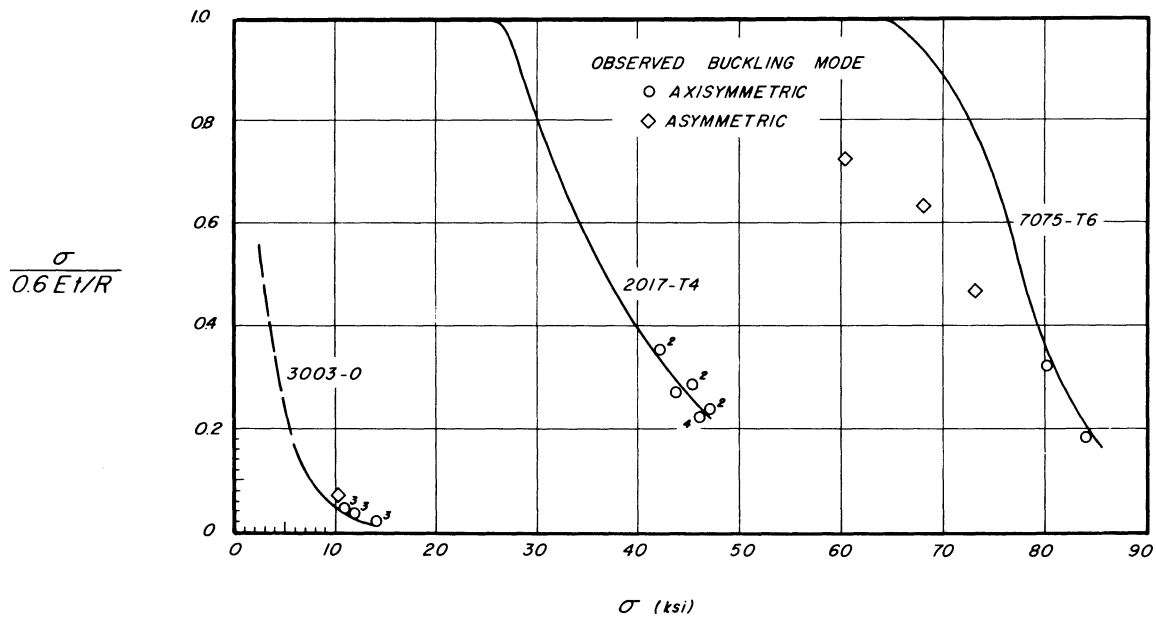


Figure 6.- Test data on plastic buckling of aluminum alloy isotropic cylinders under axial compression compared with axisymmetric theory.

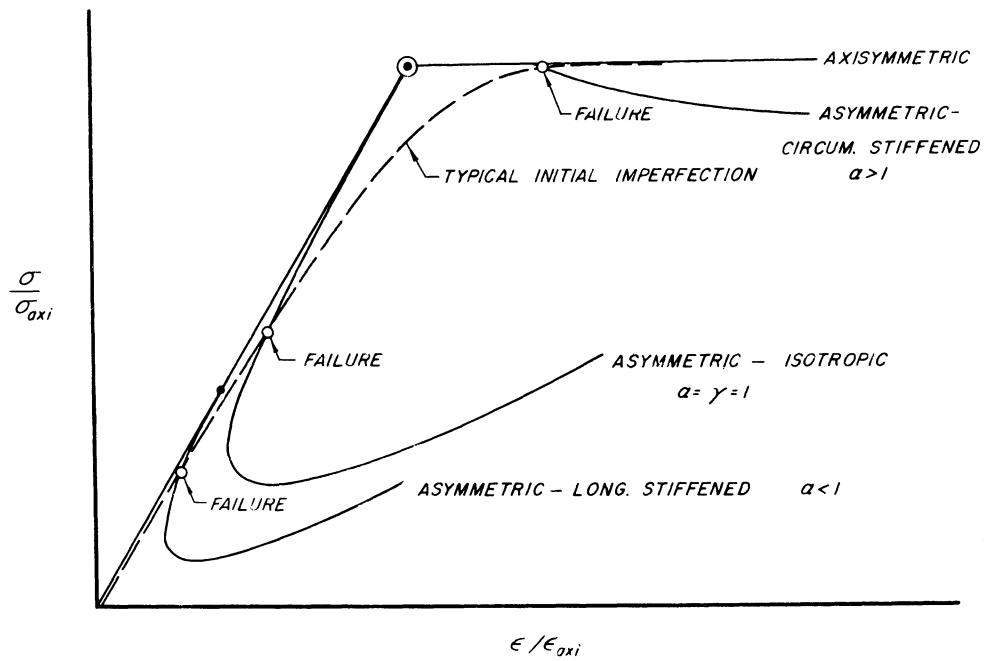


Figure 7.- Post-buckling behavior of moderate length, elastic, orthotropic cylinders (schematic).

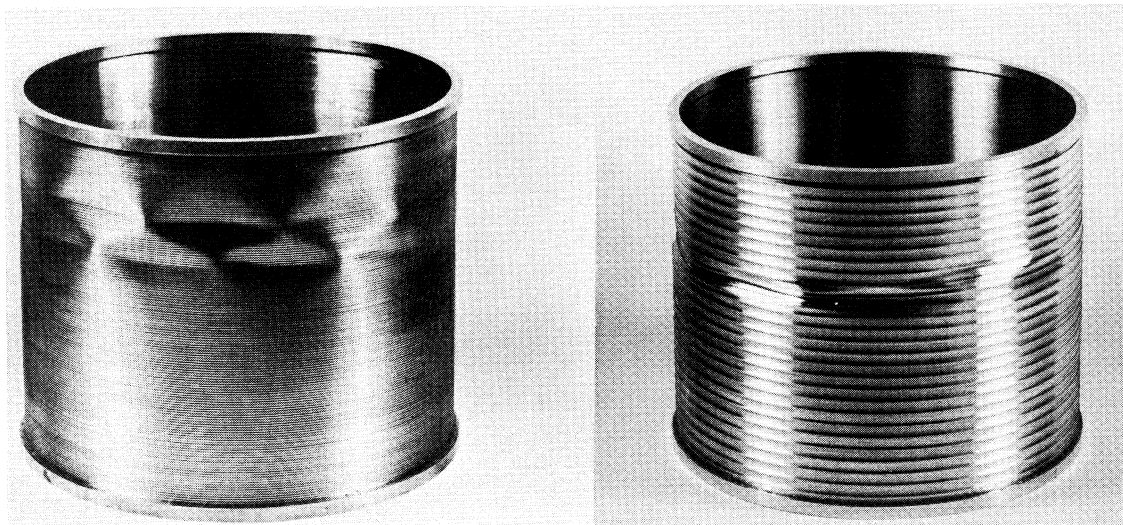
(a) $\alpha = 3$.(b) $\alpha = 20$.

Figure 8.- Circumferentially stiffened buckle patterns at the conclusion of the test.

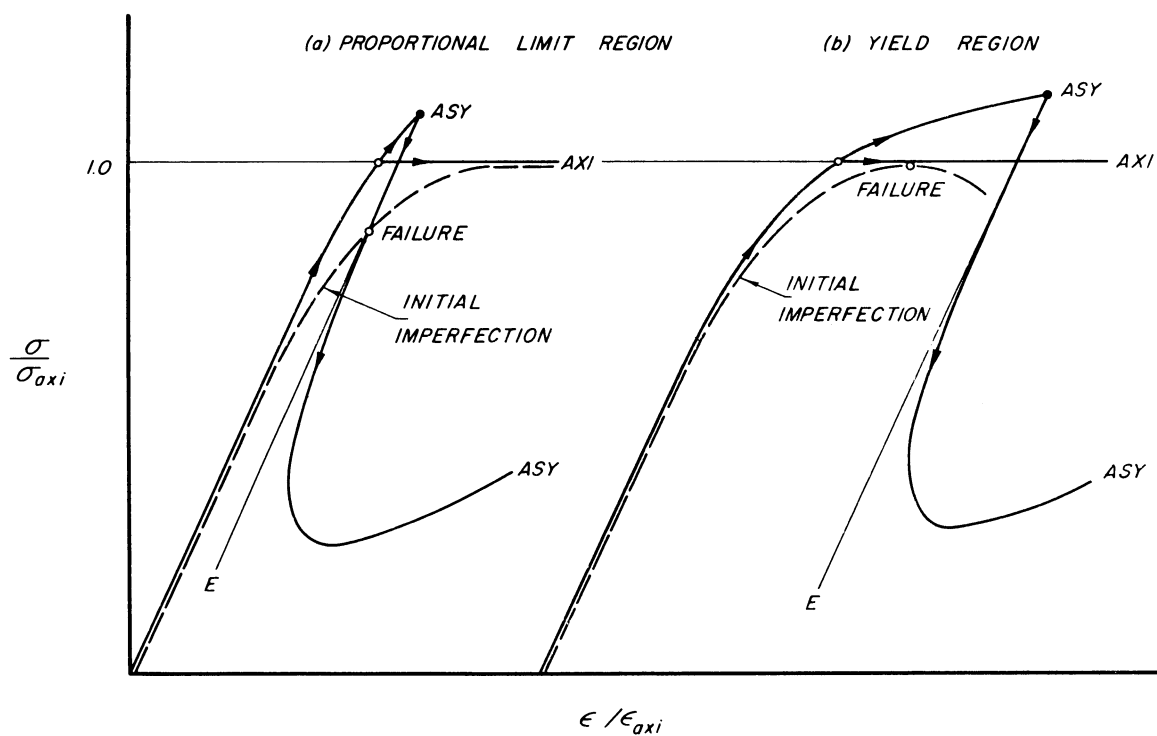


Figure 9.- Post-buckling behavior of moderate length, plastic, isotropic cylinders (schematic).

ON THE INSTABILITY OF ORTHOTROPIC CYLINDERS

By Michael F. Card and James P. Peterson

NASA Langley Research Center

SUMMARY

Preliminary results from experimental investigations on the buckling strength of ring-and-stringer stiffened aluminum cylinders and filament-wound glass-epoxy cylinders are compared with instability calculations based on small-deflection orthotropic cylinder theory. Correlation between experiment and calculation was reasonably good for the glass-epoxy cylinders; however, correlation for the ring-and-stringer stiffened cylinders can be achieved only when some of the basic wall stiffnesses for stiffened cylinders with buckled skin can be better defined. In particular, the wall shear stiffness and the wall bending stiffness in the circumferential direction need better definition.

INTRODUCTION

The test results reported herein were obtained from two separate test programs entailing instability failures of orthotropic cylinders subjected to compressive stresses. In the first program, bending tests were made on 77-inch-diameter cylinders stiffened with Z-section stringers and hat-section rings. The rings were purposely made small to induce "general instability" failures involving collapse of a section of wall large enough to include several stringers and one or more rings. The width-thickness ratio of the skin between stringers was large so that skin buckling occurred early in the tests. In the second program, 15-inch-diameter filament-wound glass-epoxy cylinders were tested in axial compression. Windings of the cylinders consisted of alternate layers of circumferential windings and helical windings such that orthotropic properties were achieved with orthogonal planes of elastic symmetry in the axial and circumferential directions.

Buckling data from these investigations are compared with instability calculations based on small-deflection orthotropic cylinder theory. Wall stiffnesses are needed for the calculations and a considerable portion of the presentation is allotted to the discussion of, and determination of, wall stiffnesses.

SYMBOLS

b	distance between stringers in ring-and-stringer stiffened cylinders
D	wall bending or twisting stiffness as indicated by subscript
E	Young's modulus or extensional stiffness of wall or basic wall element as denoted by subscript; also used to denote equivalent value for Young's modulus of wall composite
G	shear modulus or shear stiffness of wall or basic wall element as indicated by subscript; also used to denote equivalent value for shear modulus of wall composite
k	volumetric ratio of glass in cylinder wall
M	moment at buckling
R	radius of cylinder
t	skin thickness of ring-and-stringer stiffened cylinders
α	helix angle measured from cylinder axis
$\bar{\epsilon}$	edge strain or unit shortening
ϵ_{cr}	buckling strain
σ_{cr}	buckling stress
μ	Poisson's ratio for material or that associated with bending of orthotropic material, used with subscript to denote material or element and direction
μ'	Poisson's ratio associated with extensional strains, used with subscript to denote element and direction

Subscripts:

e	epoxy
g	glass
x	denotes axial direction of cylinder wall
y	denotes circumferential direction of cylinder wall

xy	denotes twisting or shear stiffness of cylinder wall with respect to x- and y-directions
w	denotes with-grain direction of basic wall element
c	denotes cross-grain direction of basic wall element
wc	denotes shear stiffness of basic wall element with respect to w- and c-directions

RING-AND-STRINGER STIFFENED CYLINDERS

Discussion of Pertinent Wall Stiffnesses

Values of some of the stiffnesses needed for the calculation of instability loads for ring-and-stringer stiffened cylinders are known with reasonable accuracy; others are known with very little accuracy. The structural behavior of longitudinally stiffened curved cylinders in compression was investigated in reference 1. Good correlation was achieved between calculation and experiment in predicting load-shortening curves for these cylinders which had a range of structural parameters encompassing the range of the present tests. This result implies that the extensional stiffness of the cylinder wall in the longitudinal direction can be predicted with reasonable accuracy; it also implies that the wall bending stiffness D_x can be estimated with reasonable accuracy. Reference 1 presents the necessary equations for evaluating E_x and D_x .

It can be shown from the study of reference 2 that Poisson's ratio μ'_x is small for sheet buckled in compression. Figure 1, which was constructed from numerical calculations made in reference 2, indicates this effect. Although these calculations were made for flat plates, the result is expected to have approximate application in the present tests because the study of reference 1 indicates that certain curved-plate results approach flat-plate results after skin buckling has been exceeded somewhat. The result indicated in figure 1 implies that μ'_x , and hence μ'_y and μ_x and μ_y , can probably be taken equal to zero without introducing large errors into instability calculations.

Four stiffnesses, E_y , D_y , D_{xy} , and G_{xy} , remained, about which little is known. Some effects of variations of these stiffnesses on the calculated buckling loads are discussed in subsequent sections.

Test Specimens and Test Procedure

The test specimens consisted of seven 77-inch-diameter cylinders stiffened with extruded Z-section stringers on the outer surface and with small, formed, hat-section rings on the inner surface. The stringers were 0.54 inch deep and the rings either 0.54 inch or 0.30 inch deep. The cylinders with 0.54-inch rings had a stringer-spacing—skin-thickness ratio b/t of 125, and those with 0.30-inch rings, $b/t = 200$. Further references to the cylinders will be made by specifying b/t of the cylinder wall. The skin, stringer, and rings were made of 7075-T6 aluminum alloy.

The cylinders were loaded in bending through a loading frame with the use of a hydraulic testing machine. The test setup was similar to that described in reference 3 for bending tests on ring-stiffened cylinders.

Test Results and Discussion

Test results are given in figure 2 along with calculated results made with the use of the stability equation of reference 4 and selected wall stiffness values. The circular test points represent cylinders with $b/t = 125$ and the square test points represent cylinders with $b/t = 200$. The calculation denoted by the solid curves was made with the use of the values discussed earlier for E_x , D_x , and Poisson's ratios, and with the use of rather arbitrary estimates of the stiffnesses E_y , G_{xy} , D_y , and D_{xy} . For this case G_{xy} was taken as the value given in reference 5 for flat plates, E_y was obtained by considering the effective width of buckled skin to be equal in the longitudinal and circumferential directions, D_y was taken as the value computed for the ring and that portion of skin equal to the width of the ring, and D_{xy} was computed on the assumption that local buckling of the skin could be neglected. This calculation is about 8 percent conservative for cylinders with $b/t = 125$ and about 25 percent conservative for cylinders with $b/t = 200$. (See fig. 2.)

Additional calculations were made to determine the influence of changes in some of the stiffnesses on calculated buckling load. In the several calculations made, only one stiffness at a time was varied from the set of stiffnesses used to construct figure 2. Results of the calculations are essentially as follows: (1) The calculated buckling moment was decreased 5 to 10 percent from that shown when the stiffness D_{xy} was taken to be zero. (2) The buckling moment was practically unchanged for a calculation made with the stiffness E_y calculated on the assumption that the buckled skin contributed nothing. (3) The buckling load was increased 5 to 10 percent over that shown for a calculation made

with D_y calculated on the assumption that the skin was 100 percent effective in contributing toward the moment of inertia of ring and skin. Use of this assumption should not suggest that the skin is very effective insofar as it increases the stiffness D_y in this manner; rather the calculation was made to determine the sensitiveness of buckling to changes in D_y . The suggestion has been made (see ref. 6, p. 165) that the corrugation effect of buckles may increase the stiffness D_y . (4) An increase of 100 percent in the stiffness G_{xy} increased the buckling moment about 15 percent for the cylinders with $b/t = 200$; it increased the buckling moment for the cylinders with $b/t = 125$ about 15 percent for cylinders with large ring spacing and about 25 percent for cylinders with small ring spacings. The 100-percent change in shear stiffness may seem to constitute a rather large change; however, it is well within the limits of uncertainty for the shear stiffness of buckled sheet.

From these calculations it can be concluded that the main source of the discrepancy between calculation and experiment as indicated in figure 2 is probably not associated with the use of uncertain values for the stiffnesses E_y and D_{xy} ; these stiffnesses were varied over their probable range of uncertainty with little influence on the calculated buckling moment. Hence, uncertainties in the values of D_y and G_{xy} remain as a probable cause of the discrepancy. If they are indeed the cause, the values of these stiffnesses would have to be increased more for highly buckled sheet than for moderately buckled sheet (corrugation effect) in order to bring calculation and experiment into agreement; the cylinders with $b/t = 125$ experienced instability at ratios of edge strain to local buckling strain of about half of those for the cylinders with $b/t = 200$. Corrugation effects such as these have been suggested in the literature. (See refs. 6 and 2.) Another cause for the discrepancy may be associated with the use of a stability equation based on small-deflection buckling theory. Theory is known to give erroneous results in the case of unstiffened cylinders, for instance. In an attempt to compensate for discrepancies from this source, a "correlation factor" was used in the calculations made. The factor was taken from reference 7 and has had only limited substantiation. Its value was approximately 90 percent for the cylinders with $b/t = 200$ and nearly 100 percent for the cylinders with $b/t = 125$. The discrepancy probably is not associated with the use of incorrect values of E_x and D_x because moment-shortening curves for the cylinders as determined by calculation and test were in reasonably good agreement.

One further calculation was made to determine the likelihood of some of the cylinders having failed by buckling between rings (panel instability) instead of in a general instability mode. The cylinders most susceptible to panel instability are those denoted by the square symbols at large ring spacings. Hence the calculation was made for those cylinders. It is indicated in figure 2 by the dashed curve and was made with

the use of reference 1 and a column-fixity coefficient of 2.0. The use of other values of the coefficient would simply move the curve to the right or left. From this calculation it can be concluded that one of the test cylinders (the last square test point in fig. 2) may have failed by panel instability; the others probably did not. This result indicates that even very small rings evidently provide considerable restraint to the cylinder wall insofar as influence on the panel-instability mode of failure is concerned; the column-fixity coefficient of 2.0 is a considerable increase over the value of unity usually assumed in calculations for panel instability.

FILAMENT-WOUND GLASS-EPOXY CYLINDERS

Discussion of Pertinent Wall Stiffnesses

In contrast to the previous example of ring-and-stringer stiffened cylinders where some of the wall stiffnesses are known with reasonable accuracy, none of the wall stiffnesses are known very accurately for filament-wound cylinders. A basic element of the wall of glass-epoxy cylinders is one of unidirectional fibers embedded in epoxy. If the extensional stiffnesses of this orthotropic element were known, the extensional and bending stiffnesses of the wall could be calculated with the use of theory of elasticity. Two of the five elemental extensional stiffnesses are rather insensitive to distribution of fibers and epoxy and depend almost solely on the volumetric ratio of glass to glass plus epoxy; hence, they are known with reasonable accuracy. These stiffnesses are E_w (the extensional stiffness of the element in the direction of the fibers) and μ'_w (Poisson's ratio associated with contraction normal to the fibers caused by a load in the direction of the fibers). These stiffnesses can be written with good approximation as

$$E_w = kE_g + (1 - k)E_e$$

and

$$\mu'_w = k\mu_g + (1 - k)\mu_e$$

The remaining stiffnesses E_c and G_{wc} depend heavily upon the distribution of fibers and epoxy and were calculated with the use of a mathematical model similar to the one employed in reference 8 for monofilament laminates. The distribution of fibers and epoxy was taken into account in the calculations by a parameter which was chosen such that certain calculated wall stiffnesses agreed with stiffnesses measured in

the course of the cylinder tests. Poisson's ratio μ'_c was found from the relationship $E_w \mu'_c = E_c \mu'_w$. Young's modulus and Poisson's ratio for glass and epoxy were required for the calculations. The values for glass were taken from the literature as $E_g = 10,500$ ksi and $\mu_g = 0.20$. Those for the epoxy were determined from compression tests on 1-inch by 1-inch by 4-inch blocks of the epoxy.

With the stiffnesses of the basic wall element known, the stiffnesses of helical and circumferential windings in any desired direction can be obtained with the use of equations of elasticity for orthotropic materials (see ref. 9), and then combined to give the extensional and bending stiffnesses of the cylinder walls. Typical calculated values of the extensional stiffnesses of a cylinder wall are given in figure 3 for the case of an equal number of helical and circumferential windings.

It is evident from figure 3 that the shear stiffness G_{xy} is rather insensitive to helix angle; it is small relative to the extensional stiffnesses E_x and E_y when compared with similar relationships for metals. Other observations that can be made are: (1) a large difference exists between the stiffnesses E_x and E_y for all but very small helix angles and (2) Poisson's ratios associated with extension of the cylinder wall are somewhat smaller than those associated with metals.

Test Cylinders and Test Procedure .

The test cylinders were 15 inches in diameter and 15 inches long. The walls of the cylinders consisted of alternate layers of circumferential and helical windings. Each helical winding consisted of two half-windings, one at $+\alpha$ and the other at $-\alpha$ to the longitudinal center line of the cylinders. The walls of the cylinders were built up near each end with additional circumferential windings to prevent end failures. The radius-thickness ratio of the cylinders was about 145. Two epoxies were used in construction of the cylinders, Shell Epon 828 with curing agent D and Shell Epon 826 with curing agent CL. Young's modulus and Poisson's ratio for the two epoxies were nearly equal. The block tests indicated that they could be taken as $E_e = 450$ ksi and $\mu_e = 0.40$.

The cylinders were tested in axial compression between the platens of a hydraulic testing machine until buckling or failure occurred. Two tests were made on nominally identical specimens to determine the consistency of buckling loads. In some cases supplementary tests were conducted to obtain the volumetric ratio of glass in the walls, and photomicrographs were made to obtain an idea of the uniformity of construction. The volumetric ratio of glass appeared to be reasonably consistent from

sample to sample within a cylinder and from cylinder to cylinder; it was taken as 0.65. The photomicrographs indicated some nonuniformity in wall construction although the overall thickness of the walls as determined by micrometer measurements was reasonably uniform.

Test Results and Discussion

The test results are given in figure 4 along with the results of an instability calculation made with the use of reference 4 and the calculated stiffnesses of figure 3. Because of the relatively low shear strength of epoxies, an additional calculation which represents shear failure of the cylinder wall from axial compressive stresses is shown. The shear failure calculation was made with the use of results from a compressive test on a 2.60-inch-diameter tube consisting of all circumferential windings. The dashed curve indicates the stress at which tubes that have an equal number of circumferential and helical windings are expected to fail in shear from an applied compressive stress. Cylinders which have an elastic buckling load not much greater than this stress are expected to fail at a somewhat lower stress because of the interaction between the two failures. That is, as a cylinder is loaded to loads somewhat less than the shear-failure load, epoxy shear stresses become large and the epoxy deforms plastically. This deformation causes a reduction in wall stiffnesses which, in turn, lowers the buckling load. The test cylinders with 45° and $67\frac{1}{2}^\circ$ helical windings showed evidence of this interaction at failure. Buckling was evident in that a buckle pattern covering the complete circumference of the cylinders and about half of the length of the cylinders was observed; and shear failure of the wall in the area of buckling was also observed. The shear-failure evidence was lacking in the tests on the cylinders with helical angles of 25° ; these cylinders appeared undamaged when load was removed and the diamond-shape buckles, which had appeared suddenly at maximum test load, had disappeared. The appearance of the cylinders was somewhat deceptive, however, because the cylinders took less load on reloading than on the first loading. The test loads for these cylinders as well as those for other nominally identical cylinders were nearly equal. (See fig. 4.)

The relatively good agreement between the failing load for the cylinders having a helix angle of 25° with that computed on the basis of small-deflection buckling theory is attributed to the small radius-thickness ratio of the cylinders which was about 145. Previous studies on isotropic metal cylinders have indicated that good-quality cylinders with radius-thickness ratios of this magnitude will experience little deviation from theory. (See, for instance, ref. 3.)

One further observation can be made concerning the magnitude of compressive stress at failure of the tube with circumferential windings.

The applied stress of 10.9 ksi corresponds to a shear stress in the epoxy of about half that value or about 5.45 ksi. Tensile tests made on epoxy specimens by other investigators indicate that the epoxy has an ultimate tensile strength of about 9.5 ksi and failure occurs after considerable elongation (about 4 percent). The corresponding ultimate shear strength of the epoxy is expected to be about $\frac{9.5}{\sqrt{3}}$ or about 5.5 ksi, which is very

close to the shear stress at failure of the tube in compression. Hence, on the basis of this single test, it appears that a tensile test of an epoxy specimen may be used to determine the compressive-failure strength of unidirectional glass-epoxy plates when loaded perpendicular to the direction of the fibers.

CONCLUDING REMARKS

Preliminary results from experimental investigations on the buckling strength of ring-and-stringer stiffened aluminum cylinders and filament-wound glass-epoxy cylinders are presented and discussed. Attempts at predicting test results are also given. Correlation between calculation and experiment for the glass-epoxy cylinders was reasonably good. However, the scope of the test results is extremely limited and additional testing is necessary to prove or disprove the theories set forth. Glass-epoxy cylinders have considerably different wall properties than those associated with metals; as a result, new failure modes may be important. In particular, shear stresses induced by the compressive load on the cylinder wall may cause wall failure. Additional testing is required to establish modes of failure and to establish the stiffness properties of the glass-epoxy walls.

The correlation obtained between calculation and experiment for the ring-and-stringer stiffened cylinders leaves considerable room for improvement. Wall stiffnesses - especially shear and circumferential bending - are known with insufficient accuracy, and "correlation factors" which delineate the discrepancy between theory and experiment for buckling of orthotropic cylinders are not adequately defined. Until these areas of weakness are strengthened, correlation between calculation and experiment cannot be adequately achieved. The tests indicate that even small rings offer considerable restraint to the cylinder wall in the panel-instability mode; but additional work is required to determine the quantitative effect of ring proportions on cylinder strength.

REFERENCES

1. Peterson, James P., Whitley, Ralph O., and Deaton, Jerry W.: Structural Behavior and Compressive Strength of Circular Cylinders With Longitudinal Stiffening. NASA TN D-1251, 1962.
2. Stein, Manuel: Behavior of Buckled Rectangular Plates. Jour. Eng. Mec. Div., Proc. American Soc. Civil Eng., vol. 86, no. EM2, Apr. 1960, pp. 59-76.
3. Peterson, James P.: Bending Tests of Ring-Stiffened Circular Cylinders. NACA TN 3735, 1956.
4. Stein, Manuel, and Mayers, J.: Compressive Buckling of Simply Supported Curved Plates and Cylinders of Sandwich Construction. NACA TN 2601, 1952.
5. Kromm, A., and Marguerre, K.: Behavior of a Plate Strip Under Shear and Compressive Stresses Beyond the Buckling Limit. NACA TM 870, 1938.
6. Argyris, J. H., and Dunne, P. C.: Part 2. Structural Analysis. Structural Principles and Data, Handbook of Aeronautics, No. 1, Pitman Pub. Corp. (New York), 1952.
7. Peterson, James P.: Weight-Strength Studies of Structures Representative of Fuselage Construction. NACA TN 4114, 1957.
8. Ekvall, J. C.: Elastic Properties of Orthotropic Monofilament Laminates. Paper No. 61-AV-56, ASME, 1961.
9. Lekhnitski, S. G. (Elbridge Z. Stowell, trans.): Anisotropic Plates. Contributions to the Metallurgy of Steel, No. 50, American Iron and Steel Inst., June 1956, pp. 41-45.

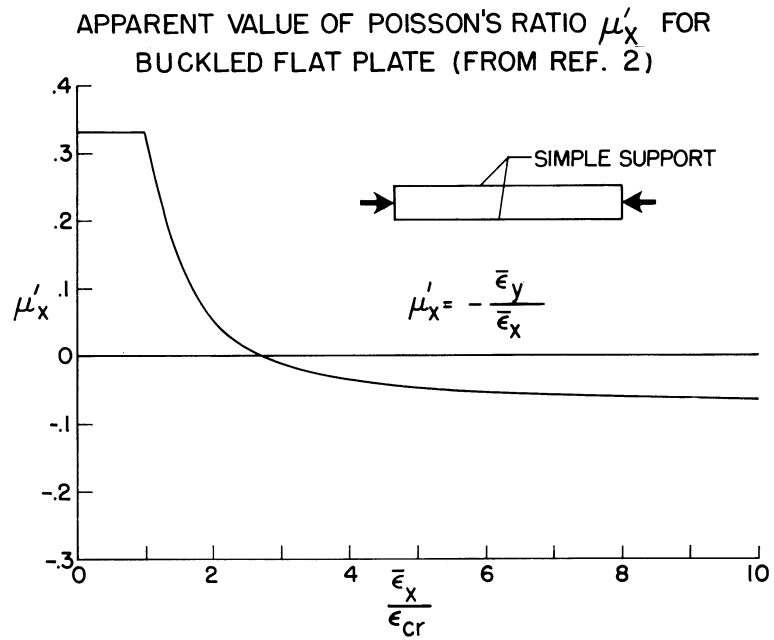


Figure 1

CALCULATED AND EXPERIMENTAL BUCKLING MOMENT
FOR RING-AND-STRINGER STIFFENED CYLINDERS

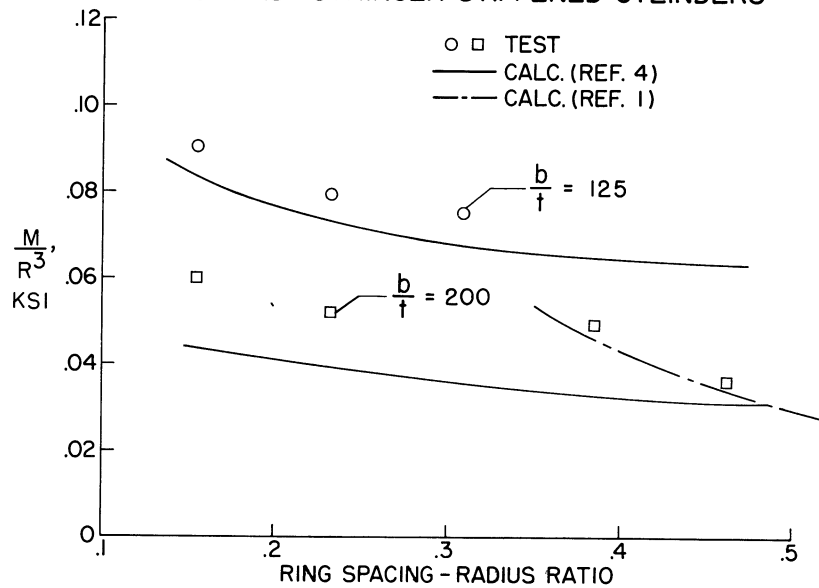


Figure 2

WALL STIFFNESSES OF GLASS-EPOXY CYLINDERS

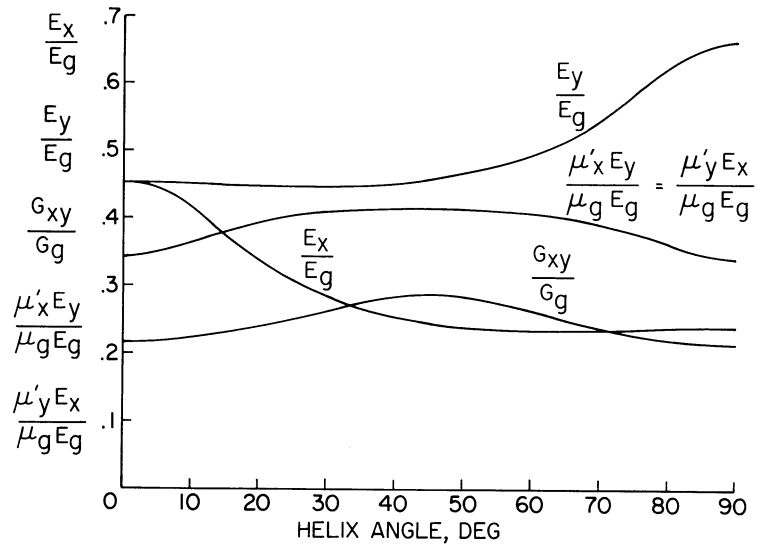


Figure 3

COMPARISON BETWEEN CALCULATED AND MEASURED BUCKLING LOADS FOR GLASS-EPOXY CYLINDERS

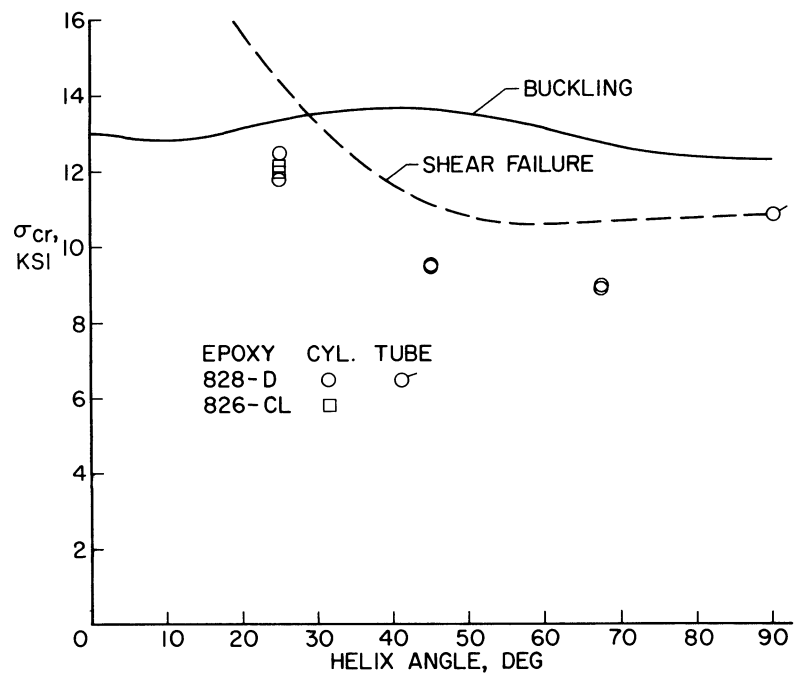


Figure 4

GENERAL INSTABILITY OF ORTHOGONALLY
STIFFENED CYLINDRICAL SHELLS

By Arie van der Neut

Technological University, Delft (Netherlands)
Aeronautical Department

SUMMARY

Earlier research at the National Aeronautics Research Institute (N.L.R.), Amsterdam, which forms the basis of recent work is reviewed. This early work refers to 2 schemes: the orthotropic shell and, in view of buckling modes where the half wave length is of the order of the ring distance, the shell with continuously distributed stringers and discrete rings. Linear theory is considered to be adequate for these structures, where the imperfections are small in comparison to the height of the ring sections. Recent developments account for pressure difference in addition to axial compression, for the correct stiffness matrix of skin panels in the post-buckling stage and for stringer bending due to hoop stresses in the skin, which are of importance as has been shown by the investigation of the post-buckling behaviour. Numerical data for the stiffness matrix of skin panels have been established. Numerical evaluation of the stability equation has not been performed as yet.

INTRODUCTION

The general instability of cylindrical shells received attention in a former period in view of its importance for fuselages of large diameter. The critical condition then originates from fuselage bending. The complexity of the problem, caused by the large number of structural parameters, was a good reason for avoiding the complexity of the non-uniform load condition presented by bending. It might be expected that the easier problem of axial compression would yield valuable information for the actual fuselage problem in those cases where the circumferential half wave length of the critical mode would be much smaller than the radius of the cylinder. With certainty the critical bending stress would be greater than the critical stress in axial compression.

The occurrence of similar structures in missiles has given new impetus to the problem. Here again bending is the critical condition.

However with pressurized fuel tanks the effect of the pressure difference should not be disregarded.

In former calculations the way in which the lateral stiffness and the shear rigidity of buckled skin panels was accounted for was mainly a matter of guessing. The application to missile structures where thin skins are used calls for alleviation of this lack of knowledge. On the basis of earlier work by the N.L.R. on post-buckling behaviour the data needed for stability research have been established.

Another shortcoming of the former work on general instability has emerged recently from knowledge obtained on the tangential stiffness of buckled panels. In contrast to former opinions this stiffness proved to be quite great. It follows then however that the effect of deflection of the stringers caused by the hoop stresses of the skin should also be accounted for.

The present report reviews the various facets of the problem.

SYMBOLS

a	radius of the cylinder
$ a $	stiffness matrix of the skin panel
b	ring pitch
c	$= c_s + c_r$
c_s	distance of centroid of stringer to skin, positive for inside stiffeners
c_r	distance of centroid of ring section to skin, positive for rings inside
e	ϵ/ϵ^*
s	$\sigma/(E\epsilon^*)$
t	skin thickness
w	panel width
A_r	area of ring section, including effective skin width

E	Young's modulus of elasticity
I_r	moment of inertia of ring section, including effective skin width
I_s	moment of inertia of stringer section, including effective skin width
ϵ	strain increment by buckling
ϵ^*	$\pi^2 [3(1 - \mu^2)]^{-1} (t/w)^2$, critical longitudinal compression
μ	Poisson's ratio
ν	average number of rings per half wave length
σ	increment of average stress by buckling

ADEQUACY OF LINEAR THEORY

The effect of imperfections with respect to the true cylindrical shape causes large discrepancies between the actual critical load of unstiffened cylindrical shells and the critical load predicted from linear theory. Finite deflections have to be considered and consequently non-linear equations are required to restore harmony between theory and test. The essential reason for this behaviour of the cylindrical shell is that the imperfection - expressed as the difference between the local radial coordinate and the average radius - is of the same order of magnitude as the wall thickness t , or better the radius of gyration $t/2\sqrt{3}$. Correspondingly, if internal pressure is applied - which restores the circular cross section and prevents buckling modes with circumferential waves - the critical load as predicted by linear theory proves to be correct.

In the case of the stiffened cylinder the necessity to account for non-linearity would exist likewise if the imperfections would have the same order of magnitude as the radius of gyration of the ring section. However, since the imperfections of ring geometry can be kept small in comparison to the height of the ring section, it may be expected that imperfections have no major effect upon the critical load. Therefore it is considered that linear theory is adequate for the investigation of general instability of stiffened shells.

REVIEW OF EARLIER WORK

Structural Schemes

Applying linear theory the National Aeronautical Research Institute (N.L.R.), Amsterdam has analyzed the general instability of stiffened cylindrical shells under axial compression (ref.1). This investigation consisted of 2 phases. In the 1st phase the shell was assumed to be orthotropic, due to continuous distribution of the stiffnesses of the stringers and of the rings. In the 2nd phase the stringers were again continuously distributed, but the rings were discrete at constant pitch.

The reason to investigate this second scheme was that the longitudinal half wave length, as obtained from the orthotropic case, might well be about equal to or a small multiple of the ring pitch. So it seemed doubtful whether the orthotropic scheme would yield reliable results. No necessity existed to criticize the continuous distribution of stringers since the circumferential half wave length comprises a number of stringers.

The investigation took the following characteristics of the structural elements into account:
stringers and rings: longitudinal stiffness, bending stiffness in the plane normal to the shell, torsional stiffness, ring pitch and the excentricity of the center of gravity of the stiffenersections with respect to the skin;
skin: shear rigidity and effective width, which was added to the sections of stringers and rings.

In this way the buckling load parameter was a function of 7 structural parameters and 2 parameters for the buckling mode. The 7 structural parameters are characteristic for respectively shear stiffness of the skin, bending stiffness of the 2 systems of stiffeners, torsional stiffness of the 2 systems of stiffeners, ring pitch and excentricity of the stiffeners, the latter of which proved to be a combined parameter for the 2 systems of stiffeners. In the case of the orthotropic shell the 2 torsional stiffnesses combine into 1 parameter and since ring pitch has been removed 5 structural parameters remain.

Results for Orthotropic Shells

The formula for the buckling load parameter is rather involved with its 5 + 2 parameters and minimization of this parameter with respect to the 2 mode parameters, so as to establish the critical load, is in general impossible.

Simplified expressions could be obtained by considering 5 classes of buckling modes, characterized by the various orders of magnitude of the ratio between the longitudinal and the circumferential wave lengths. Explicit formula for the critical load could be given for 4 of the 5 classes. Out of these 4 2 referred to short longitudinal wave length and small numbers of circumferential waves and 2 referred to long longitudinal waves and again small numbers of circumferential waves. Between these 2 groups the class of short longitudinal and circumferential wave lengths occurs. In this case, which usually is critical, the number of structural parameters reduces to 4, but an explicit formula for the critical load could not be given. However a rapidly converging procedure for the numerical determination of the critical load could be given.

An interesting result is that the effect of stiffener excentricity with respect to the skin is of major importance. Compared to the case where the centroid of stiffeners falls in the plane of the skin outside stiffening increases the buckling load and reversely inside stiffening yields a reduction. In some cases the buckling load reduced to as low as $1/3$ of the value for the case without excentricity.

Results for Shells with Discrete Rings

The investigation of the structure with discrete rings could obviously be confined to those classes of modes in which the longitudinal wave length is short.

It should be remembered that the capacity of the skin to carry hoop stresses has been expressed as an effective width working together with the rings. Accounting for discrete rings the actual structure as far as the rings are concerned is fully reckognized. However the behaviour of the skin is violated in that the distributed tangential force of the skin is concentrated at the rings. A more sophisticated scheme, where the concentrated effective skinwidth was replaced by an "effective skin thickness", was attempted but was cancelled because of the inherent analytical complexity.

For the infinitely long cylinder a formula could be obtained giving the relation between the 6 structural parameters (1 parameter vanished due to the restriction to short waves), 2 mode parameters (governing the displacements at the rings) and the buckling load parameter. A semi-graphical procedure could be evolved for establishing the critical load pertaining to a given set of structural parameters.

A result of major interest is that the solution obtained from orthotropic shell theory is surprisingly accurate. Figure 1 shows for

the case of axially symmetrical buckling the reduction of the buckling load by the small average number ν of rings per half wave length. For $\nu > 2$ the error by assuming orthotropy is less than 1%. Therefore two rings on the half-wave length is mechanically equivalent to "many" rings. Only for $\nu < 1,5$ the critical load is affected more than 5% by ring spacing. In the case of axially non-symmetrical buckling modes the results are similar. The error by orthotropy depends now also on the other structural parameters, but remains of the same order. A numerical example yielded for $\nu = 2$ 4% error and for $\nu = 1,6$ 6%.

Another result is that by increasing the ring stiffness the longitudinal half wave length decreases gradually until it reaches the value $\nu = 1$. Then general instability has degenerated into column failure of the stringers between the rings and the rings, though having finite stiffness, are equivalent to infinitely stiff rings. The ring stiffness required for the exclusion of general instability can be expressed by a simple formula as far as axially symmetrical buckling modes are concerned

$$A_r \geq 4\pi^2 (a/b)^2 \cdot (b/w) \cdot (I_s/b^2).$$

The prevention of general instability in axially non-symmetrical buckling requires unpractically large ring bending stiffness. Therefore in practice general instability is more critical than column failure of the stringers.

RECENT WORK

Scope

Recent developments on the basis of ref. 1 are meant to include load pressure difference, to improve the way in which the post-buckling behaviour of the skin panels is accounted for and to account for bending of the stringers due to hoop stresses of the skin.

Post-buckling Panel Stiffness

In ref. 1 the post-buckling behaviour of the skin panels was accounted for by introducing effective widths for longitudinal and lateral stiffness and an effective shear rigidity. At the time when the investigation was done - 1942 - data existed only on the effective width in longitudinal compression; no data were available on effective width under arbitrary two-axial compression nor on the effective shear rigidity. These data have been established only recently and with the

aim to be used for studying general instability; they have not been published as yet.

The object is to know the stiffness matrix of skin panels in the post-buckling state with regard to incremental deformation,

$$\begin{Bmatrix} s_1 \\ s_2 \\ s_3 \end{Bmatrix} = \begin{bmatrix} a_{11} & a_{12} & a_{13} \\ a_{21} & a_{22} & a_{23} \\ a_{31} & a_{32} & a_{33} \end{bmatrix} \cdot \begin{Bmatrix} e_1 \\ e_2 \\ e_3 \end{Bmatrix}$$

where the indexes 1, 2, 3 denote longitudinal direction, lateral direction and shear respectively. In the subcritical state the matrix is

$$|a| = \frac{1}{1-\mu} \begin{vmatrix} 1 & \mu & 0 \\ \mu & 1 & 0 \\ 0 & 0 & \frac{1-\mu}{2} \end{vmatrix}$$

In view of the limitation to general instability for load conditions without panel shear in the prebuckling state, we confine ourselves to panels where shear is absent in the initial state. Then symmetry considerations yield immediately $a_{13} = a_{23} = 0$. Further from Maxwell's principle $a_{ij} = a_{ji}$. So 4 elements remain to be established: a_{11} , a_{12} , a_{22} , a_{33} .

This has been done on the basis of a theoretical investigation by Koiter on the shear field of flat panels (ref.2). Koiter assumes the deflection pattern, given in fig.2, where f , L , m and α are parameters depending on the magnitude of the 3 overall strain components. The relations between the 4 parameters, the 3 overall strain components and the 3 average stress components have been evaluated in ref.3. When dealing with stability problems we need to know the stiffness matrix valid for small strain increments, with respect to a given initial state of strain. This matrix has been established recently. The results obtained will be discussed briefly.

Fig.3 shows a_{33} as a function of the total strains e_1 , e_2 . The value for the unbuckled state $a_{33} = [2(1 + \mu)]^{-1} = 0,3846$ is approached when the lateral strain e_2 is a large positive number. When lateral compression is added to longitudinal compression the shear rigidity decreases more and more and can even become negative. Conditions where e_2 is a large negative number will not occur in cylindrical shells.

However when e_2 is around zero the shear rigidity can have been reduced to $1/3$ of the initial value. a_{11} cannot present surprising results after what is known on the effective width. a_{12} is usually a small negative number in the order of $-0,05$. As could be expected the lateral stiffness a_{22} increases with increasing positive lateral strain. For e_2 in the order of 5 a_{22} is in the order of $0,9$, whereas a_{22} is $1,10$ in the unbuckled state. It is remarkable that with small negative e_2 in the order of -1 a_{22} does not drop below $0,5$ and even more surprising is that a_{22} increases when the compression $-e_1$ increases under constant e_2 . All this means that the lateral panel stiffness is an important factor to be considered in general instability investigations.

The foregoing results apply to initially flat panels, whereas the shell panels are shallow. Koiter (ref.4) established the relation between compressive strain and load in the initial post-buckling stage of curved panels. The parameter

$$\theta = (2\pi)^{-1} [12(1-\mu^2)]^{1/4} w(at)^{1/2} = 0,289 w/(at)^{1/2}$$

proves to govern the initial stage of post-buckling behaviour. For $\theta < 0,64$ the slope of the load-strain curve is positive. However for a narrow panel like $w/a = 1/15$ (94 panels in the cylinder) and $w/t = 100$ θ amounts already to $0,75$, where the slope is distinctly negative. The critical strain of the curved panel is however $1 + \theta^4$ times the critical strain of the flat panel of equal w/t and Koiter states: (see also fig.4) "it would appear to be not too bold a conjecture that the behaviour of a narrow curved panel in the advanced postbuckling stage approaches the behaviour of a flat panel of equal width". This conjecture finds support in the consideration, that the tendency to keep the extensional strain energy down has the effect of making the bulge towards the inside deeper than the bulge towards the outside. In the limit the buckling pattern approaches the symmetrical configuration with respect to the chord plane. Then the incremental deformation starts from an initial state not different from the initial state of the flat panel. Consequently results obtained for flat panels may be used for analysis of general instability.

In one respect allowance should be made for the initial curvature. In determining the state of stress preceding general instability the stress-strain relations should account for the amount of lateral strain $(\epsilon_2)_0 = w^2/(24a^2)$, which stretches the curved panel and which is not accompanied by membrane stresses.

Bending of Stringers by Hoop Stresses of the Skin.

General instability creates incremental hoop stresses s_2 , proportional to the local deflection, which are not balanced by pressure difference and which result in a radial load q of the stringer. Therefore (when $s_2 > 0$) the stringer deflects towards the inside, thereby reducing e_2 and consequently s_2 . This means that the flexibility of the stringers reduces the effect of the large lateral stiffness of the panel and that this flexibility has to be accounted for. A rigorous analysis would require that the discrete ring scheme should be adopted. Already, in the development of ref.1, the complexities encountered were such that the lateral stiffness of the skin was added to the discrete rings. Therefore at the present stage -where the addition of pressure difference and the true stiffness matrix of the skin panels have already increased the complexity of the equations- no attempt is being made to account rigorously for stringer flexibility. The analysis has been confined to the orthotropic shell, however with the introduction of a correction for stringer bending by hoop stresses. The way in which this correction has been introduced is as follows.

When bending by hoop stresses is neglected the radial displacement of the stringer is (in the orthotropic scheme) in any point equal to the deflection of the ring. Allowance should however be made for a difference in stringer and ring deflection due to stringer bending. This difference is nil at the points where the actual rings and the stringer intersect; the difference is maximal somewhere midway between the rings. Now this variable difference is replaced by its average value between 2 successive rings. This idea can be translated into a mechanical system, where the stringers are connected to the rings by springs and the stringers are assumed to be infinitely rigid with respect to q . With this scheme there is still a linear variation of q from one ring to the next one because of the change of ring and spring deflections from one ring to the next one. This difference is being neglected so that q is assumed to be constant throughout one bay. Before the average deflection can be established one further assumption has to be made with respect to the continuity of slope at the supports. When the half wave length of the buckling mode is much greater than the ring distance, the difference between the average q 's of successive bays is small and the stringer is at its support practically clamped. Then the equivalent spring stiffness is $720 (n-1)EI_s / (nwb^4)$ per unit of area, where $n/n-1$ is the Vianello-correction accounting for combined bending and compression. The stiffness thus obtained is correct if the half wave length is very large in comparison to the ring distance. However in the other extreme case, where the half wave length is equal to the rib distance, the coefficient 720 has to be replaced by 120; moreover the Vianello

correction is greater. So the clamped end assumption may underestimate the flexibility of the stringers quite considerably. This problem needs further consideration and a method will have to be devised by which instead of the coefficient 720 one is introduced which is a function of the wave length to ring pitch ratio.

General Instability Equations.

The stability equations for the orthotropic scheme just discussed contain 4 displacements functions, 2 for displacements in the plane of the shell and 2 radial displacements of which one for the rings and one for the stringers. There are 4 equations available: 3 in the usual way from the equilibrium of an element of the orthotropic shell and one for the deflection of the spring between rings and stringers.

The solution of these equations for the infinitely long cylinder yields the buckling load parameter as a function of 2 mode parameters (for the 2 wave lengths) and 12 structural parameters: stiffness of the ring to extension, bending stiffness of stringers and of rings, torsional stiffness of stringers and of rings, excentricity of stringers and of rings, 'spring' stiffness and 4 elements of the stiffness matrix of the skin panel. The complexity could be somewhat reduced by neglecting the torsional stiffnesses, which usually are not important, and the small matrix element A_{12} . Then still 9 structural parameters remain. This means that there is no hope to find as a result of much algebraic diligence an explicit formula for the critical load. There is however no difficulty to compute the critical load for a given set of numerical values of the structural parameters.

FUTURE RESEARCH

Work still to be done is:

1. To find a better expression for the deflection of the stringers by hoop stresses, which takes into account the ratio between wave length and ring pitch.
2. To carry out numerical calculations for axial load and various pressure differences in order to study the effects of pressurization, of post-buckling behaviour of the skin and of stringer deflection by hoop stresses. Preferably these numerical calculations should be applied to structures and load conditions for which test results are available.
3. To investigate the possibility for analysis of the discrete ring scheme.

REFERENCES

1. van der Neut, A.: The general instability of stiffened cylindrical shells under axial compression. Rep. S314, National Aeronautical Research Institute, Amsterdam; in Reports and Transactions Vol XIII, 1947, pg. S57-S84.
2. Koiter, W.T.: Het schuifplooiveld bij grote overschrijdingen van de knikspanning (The post-buckling behaviour of flat rectangular panels in shear and compression). Rep. S295, Nat. Aer. Res. Inst., Amsterdam, 1944, 86 pgs. (in Dutch).
3. Floor, W.K.G. and Burgerhout, T.J.: Evaluation of the theory on the post-buckling behaviour of stiffened flat rectangular plates subjected to shear and normal loads. Rep. S370, Nat. Aer. Res. Inst., Amsterdam; in Reports and Transactions Vol XVI, 1951, pg S9-S36.
4. Koiter, W.T.: Buckling and post-buckling behaviour of a cylindrical panel under axial compression. Rep. S476, Nat. Aer. Res. Inst., Amsterdam; in Reports and Transactions Vol XX, 1955, pg 71-84.

AXIALLY SYMMETRICAL BUCKLING EFFECT OF FINITE RING PITCH

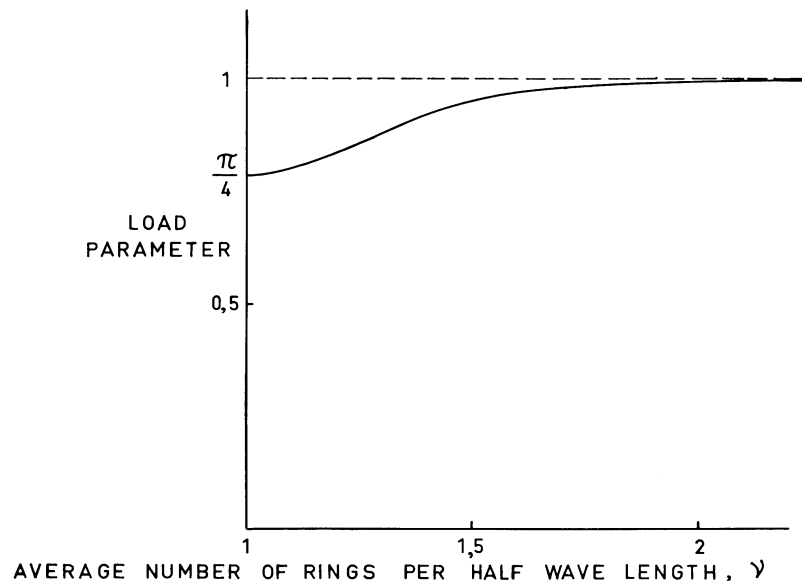


Figure 1

ASSUMED DEFLECTION PATTERN OF BUCKLED SKIN PANEL PARAMETERS f, L, m, α

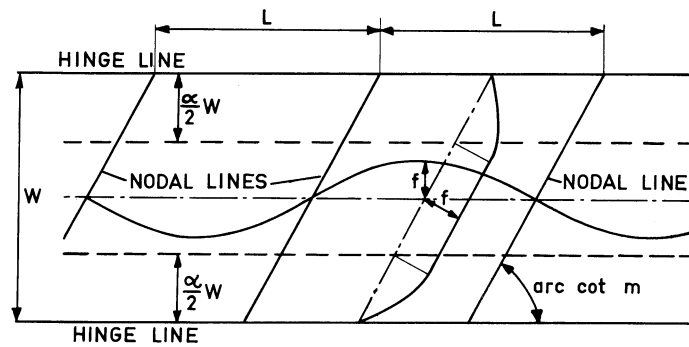


Figure 2

POST-BUCKLING PANEL RIGIDITY TO INCREMENTAL SHEAR

$$a_{33} = E^{-1} \partial \sigma_3 / \partial \varepsilon_3 \quad (\text{UNBUCKLED } a_{33} = 0,3846)$$

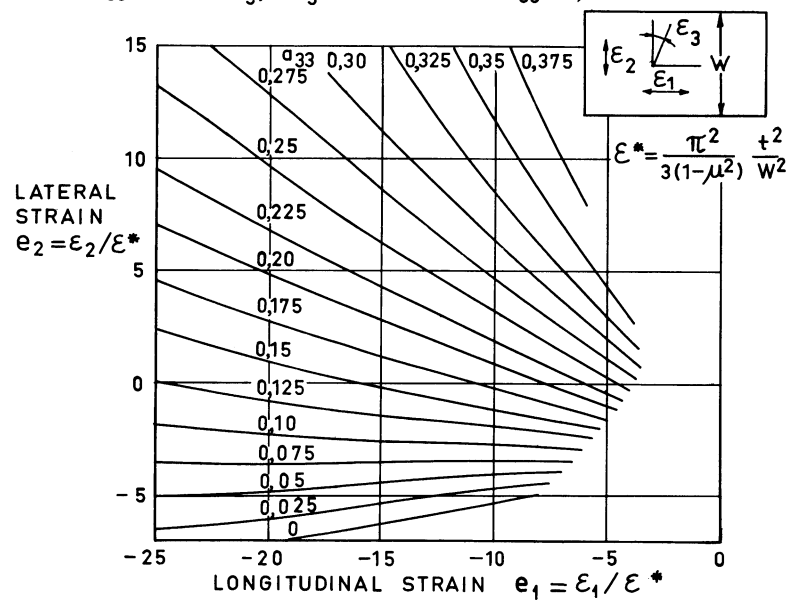


Figure 3

CONJECTURED POST-BUCKLING CURVES OF SHALLOW PANELS

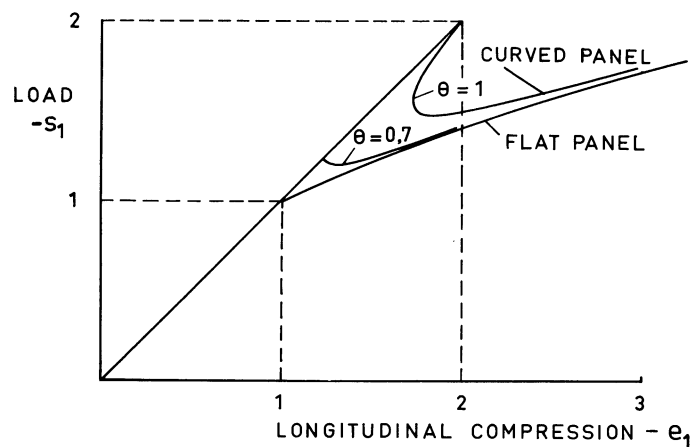


Figure 4

BUCKLING OF LAYERED ORTHOTROPIC AND SANDWICH
CYLINDRICAL SHELLS IN AXIAL COMPRESSION

By Edward W. Kuenzi

U.S. Forest Products Laboratory

SUMMARY

Results of modifications of large-deflection theory for isotropic materials to shells constructed of orthotropic layers and sandwich are presented. Experimental evaluation of the buckling of a rather extensive series of plywood cylinders and of a few curved panels of sandwich construction shows reasonably good agreement with buckling predicted by theory.

INTRODUCTION

It has long been recognized that the buckling of long, thin-walled, cylindrical shells of isotropic material under axial compression is not predictable by the classical small-deflection theory which assumes buckling of the cylinder walls with a radial displacement of the form (ref. 1):

$$w = F \sin n\theta \sin \frac{m\pi x}{L}$$

Buckling stresses about 40 percent of those given by the classical theory were predicted by von Karman and Tsien (ref. 2) who assumed buckling in diamond-shaped waves with an inward deflection in the interior of each diamond. Their analysis was based on large-deflection theory and an energy method.

In this paper, the results of applying the method of von Karman and Tsien to shells of layered orthotropic and sandwich construction are compared with experimental evaluation of plywood cylinders and curved panels of sandwich construction. The inward radial deflection of the cylinder wall, w , was chosen to be of the diamond-shaped form (ref. 3):

$$\frac{w}{r} = g + \delta \cos^2\left(\frac{\pi y}{b} - \frac{\pi x}{a}\right) \cos^2\left(\frac{\pi y}{b} + \frac{\pi x}{a}\right)$$

and appropriate modifications were included in the analyses to account for orthotropic layers and for low shear modulus in the sandwich core.

LAYERED ORTHOTROPIC CYLINDERS

The analysis of plywood cylinders under axial compression by March (ref. 3) was applied to layered orthotropic materials in general. From this the buckling stress of such a cylinder under axial compression is given by the formula

$$p_{cr} = K \sqrt{E_b E_1} \frac{h}{R} \quad (1)$$

where h is cylinder wall thickness, R is radius of neutral axis of cylinder wall, and

$$K = \frac{1}{12\sqrt{3}} (M_4 Q)^{1/2} \quad (2)$$

$$Q = 4M_3 - 9 \frac{M_2^2}{M_1} \quad (3)$$

Values of M_1 , M_2 , M_3 , and M_4 are dependent on the elastic properties of the shell wall and the buckle aspect ratio (ratio of circumferential dimension to axial dimension). It was found by computation that relative minimum values of K were very closely approximated by assuming the buckle aspect ratio to be $(E_2/E_1)^{1/4}$. Introduction of this simplification and introduction of nondimensional elastic parameters similar to those used by Thielemann (ref. 4) results in

$$\left. \begin{aligned} M_1 &= 1 + A^2 + \frac{8A^2}{A^2 + 9AB + 81} + \frac{8A^2}{81A^2 + 9AB + 1} + \frac{34A^2}{A^2 + AB + 1} \\ M_2 &= 1 + \frac{16A^2}{A^2 + AB + 1}, \quad M_3 = 1 + M_2, \quad M_4 = 6 + 2C \end{aligned} \right\} \quad (4)$$

where

$$A = \left(\frac{E_a E_2}{E_b E_1} \right)^{1/2}, \quad B = \left(\frac{1}{G_{ab}} - \frac{2\mu_{ba}}{E_b} \right) (E_a E_b)^{1/2}, \quad C = \left(E_1 \mu_{21} + 2\lambda G_{12} \right) (E_1 E_2)^{-1/2} \quad (5)$$

and

$$E_a = \frac{1}{h} \int_{-h/2}^{h/2} \frac{E_x}{\lambda} dr, \quad E_b = \frac{1}{h} \int_{-h/2}^{h/2} \frac{E_y}{\lambda} dr, \quad G_{ab} = \frac{1}{h} \int_{-h/2}^{h/2} G_{xy} dr$$

$$E_1 = \frac{12}{h^3} \int_{-h/2}^{h/2} \frac{E_x}{\lambda} r^2 dr, \quad E_2 = \frac{12}{h^3} \int_{-h/2}^{h/2} \frac{E_y}{\lambda} r^2 dr, \quad G_{12} = \frac{12}{h^3} \int_{-h/2}^{h/2} G_{xy} r^2 dr$$

$$\mu_{ba} = \frac{1}{hE_a} \int_{-h/2}^{h/2} E_x \mu_{yx} dr \text{ (approx.)}, \mu_{21} = \frac{12}{h^3 E_1} \int_{-h/2}^{h/2} E_x \mu_{yx} r^2 dr \text{ (approx.)}$$

$$\lambda = 1 - \mu_{yx} \mu_{xy}$$

where E is modulus of elasticity, G is modulus of rigidity associated with shear distortion of the plane of the shell wall or layer, μ is Poisson's ratio, x is axial direction of cylinder, and y is circumferential direction. Poisson's ratio, μ_{yx} , is defined as the ratio of contraction in the x direction to extension in the y direction associated with tension in the y direction.

Computation of Q values for three B values and a range of values in A produced the curves shown in figure 1. The point for isotropic cylinders is also shown on figure 1 and the buckling stress formula for the isotropic cylinders reduces to

$$p_{cr} = 0.242 E \frac{h}{R} \quad (6)$$

Formula (1) was solved for previously reported experimental determination of the buckling stresses of plywood cylinders (ref. 5) of several constructions of yellow birch and yellow-poplar veneers. The data considered were limited to the linear elastic range by selecting only the shells that buckled at stresses no greater than 90 percent of the compressive proportional limit stress of the plywood. Measured elastic properties were used to compute the stiffness parameters A, B, and C and these values substituted into expressions (4) to obtain K values. The computed stresses are compared with the experimental values in figure 2. Although there is considerable scatter of individual points, the agreement between experiment and theory can be regarded as reasonably close for the type of problem considered.

SANDWICH CYLINDERS

The analysis for sandwich cylindrical shells in axial compression was carried out by March and Kuenzi (ref. 6) by applying the analysis for plywood cylinders (ref. 3) and accounting for effects of shear deformation in the core of a sandwich by an approximate "tilting" method as used by Williams, Leggett, and Hopkins in their analysis of flat sandwich panels (ref. 7). The analysis of reference 6 includes sandwich with orthotropic facings and cores and presents buckling

coefficients for sandwich with isotropic facings on certain orthotropic cores. Buckling coefficients have also been determined for sandwich with certain orthotropic facings (ref. 8).

The facing stress at axial buckling load of a sandwich cylinder of thin isotropic facings of equal thickness on an isotropic core is given by the formula

$$p_{Fcr} = \frac{4N}{5Q_1} E \frac{h}{R} \quad (7)$$

where h is the sandwich thickness, R is the mean radius of the cylinder, E is the modulus of elasticity of the facings and

$$N = \frac{5M_1Q_1}{4\eta} + \frac{5}{6Q_1(1+Q_2)} \left[\frac{M_2\eta + M_3\eta^2V}{1 + M_4\eta V + M_5\eta^2V^2} + Q_2M_2\eta \right] \quad (8)$$

$$Q_1 = 2 \left[\frac{3(1-\mu^2)}{\frac{c^2}{h^2} + \frac{c}{h} + 1} \right]^{1/2}, \quad Q_2 = \frac{1}{3} \left(\frac{1 - \frac{c}{h}}{1 + \frac{c}{h}} \right)^2$$

$$V = \frac{ctE}{3(1-\mu^2)hRG_c}, \quad \eta = n^2 \frac{h}{R}$$

$$M_1 = \frac{1}{12z^2} + \frac{2z^2}{3(1+z^2)^2} - \frac{3 \left[\frac{1}{64z} + \frac{z^3}{4(1+z^2)^2} \right]^2}{\frac{1+z^4}{128} + \frac{z^4}{16(z^2+9)^2} + \frac{z^4}{16(9z^2+1)^2} + \frac{17z^4}{64(1+z^2)^2}}$$

$$M_2 = 3z^2 + 2 + \frac{3}{z^2}, \quad M_3 = \frac{1}{8} (9z^4 + 70z^2 + 9) \left(\frac{1}{z^2} + 1 \right)$$

$$M_4 = \frac{27}{8} (z^2 + 1), \quad M_5 = \frac{1}{8} (9z^4 + 70z^2 + 9)$$

where c is core thickness, t is facing thickness, μ is Poisson's ratio of facings, G_c is modulus of rigidity of core, n is number of buckles in a circumference, and z is buckle aspect ratio. Minimization of formula (8) for N with respect to η and z results in curves presented in figure 3. The value of $N = 1$ at $V = 0$ represents a cylinder wall with a "shear-rigid" core that has no extensional stiffness and reduces to the buckling stress of an isotropic shell with spaced facings. The curve for $c/h = 1$, extending from the short straight line toward the lower right,

represents the shear instability of the sandwich wall and resultant buckling load per unit circumference of hG_c (approx.).

Theoretical values of N were computed by formula (8) for previously reported experimental determination of the buckling of sandwich curved panels under axial compression (ref. 6). It was found by calculation that the panels were larger than the size of one theoretical buckle and therefore may represent the performance of a complete cylinder. The sandwich was of aluminum facings on end-grain balsa wood cores and on soft cork board cores. Core modulus of rigidity values ranged from 15,000 psi. to 320 psi. Facing stresses at buckling were well below compressive proportional limit stresses. Experimental values of N were computed by solving formula (7) equated to the experimental facing stress at buckling. The experimental and theoretical values of N are compared in figure 4. Although many of the points are on the lower portion of the line, thus representing sandwich with "soft" cores, there is reasonably close agreement between experimental and theoretical values of N .

CONCLUDING REMARKS

Comparison of experimental and theoretical results indicates that a large-deflection theory incorporating buckles of diamond-shape describes the behavior of long, thin-walled, cylindrical shells of layered orthotropic and sandwich construction in axial compression.

Application of the theory for layered orthotropic shells to general buckling of stiffened shells would be of interest. Further experimental evaluation of complete sandwich cylindrical shells is necessary.

REFERENCES

1. Timoshenko, S.: Theory of Elastic Stability. McGraw-Hill Book Co., Inc., 1936, p 455.
2. von Karman, Th. and Tsien, H. S.: The Buckling of Thin Cylindrical Shells under Axial Compression. Jour. of the Aero. Sciences, 8, 303, 1941.
3. March, H. W.: Buckling of Long, Thin, Plywood Cylinders in Axial Compression. U.S. Forest Products Laboratory Rept. 1322-A, 1943.
4. Thielemann, W. F.: New Developments in the Nonlinear Theories of the Buckling of Cylindrical Shells. Aeronautics and Astronautics, 1960.

5. Norris, Charles B., and Kuenzi, Edward W.: Buckling of Long, Thin, Plywood Cylinders in Axial Compression, Experimental Treatment. U.S. Forest Products Laboratory Rept. 1322-B, 1943.
6. March, H. W., and Kuenzi, Edward W.: Buckling of Cylinders of Sandwich Construction in Axial Compression. U.S. Forest Products Laboratory Reprt. 1830, 1952 (revised 1957).
7. Williams, D., Leggett, D. M. A., and Hopkins, H. G.: Flat Sandwich Panels under Compressive End Loads. British Royal Aircraft Establishment Rept. A.D. 3174, 1941.
8. Norris, Charles B., and Zahn, John J.: Compressive Buckling Curves for Sandwich Cylinders Having Orthotropic Facings. U.S. Forest Products Laboratory Rept. 1876, 1960.

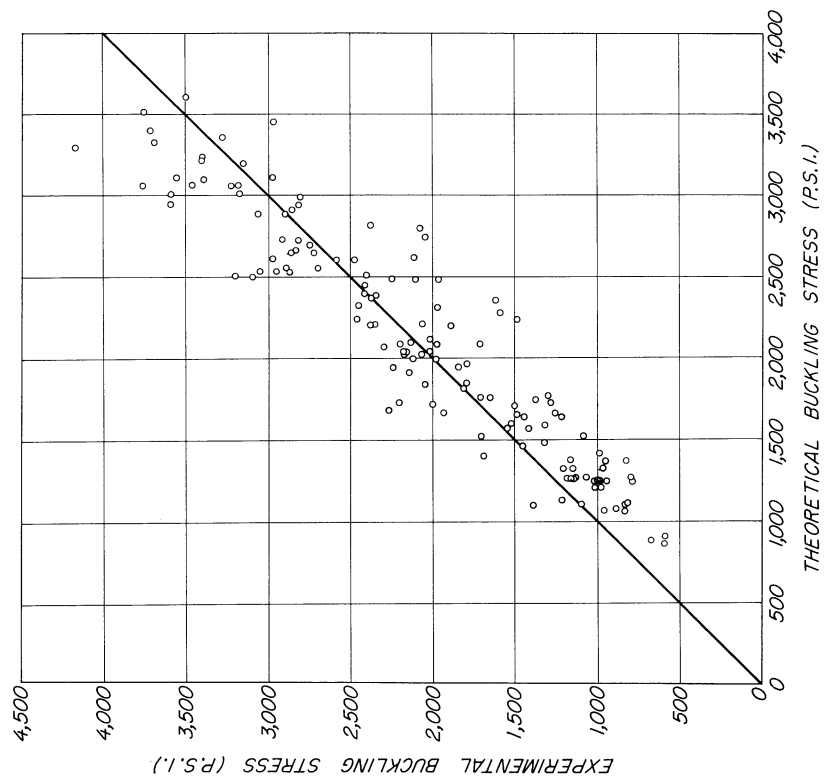


FIGURE 2.- COMPARISON OF EXPERIMENTAL AND THEORETICAL BUCKLING STRESSES OF LONG, THIN-WALLED, CYLINDRICAL SHELLS OF PLYWOOD IN AXIAL COMPRESSION.

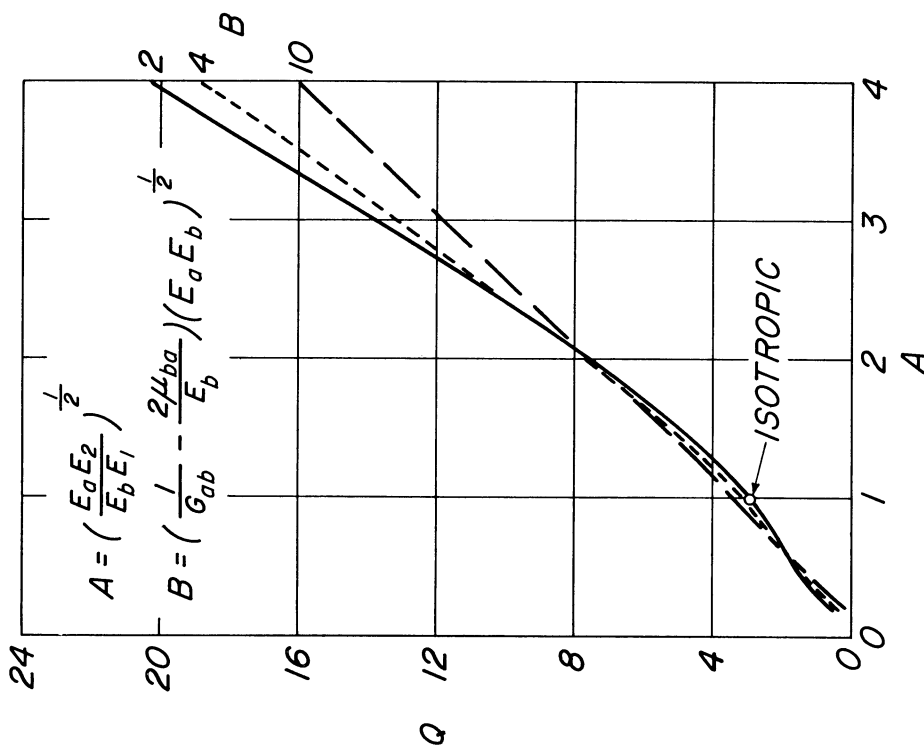


FIGURE 1. - VARIATION OF Q WITH A AND B FOR LAYERED, ORTHOTROPIC, CYLINDRICAL SHELLS IN AXIAL COMPRESSION.

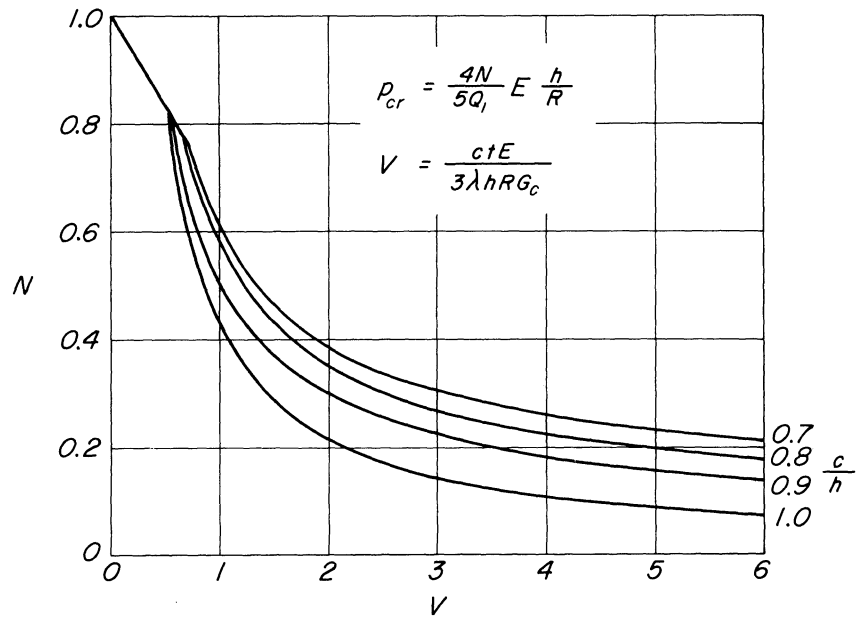


FIGURE 3. - N VALUES FOR BUCKLING OF THIN - WALLED, CYLINDRICAL SHELLS OF ISOTROPIC SANDWICH IN AXIAL COMPRESSION.

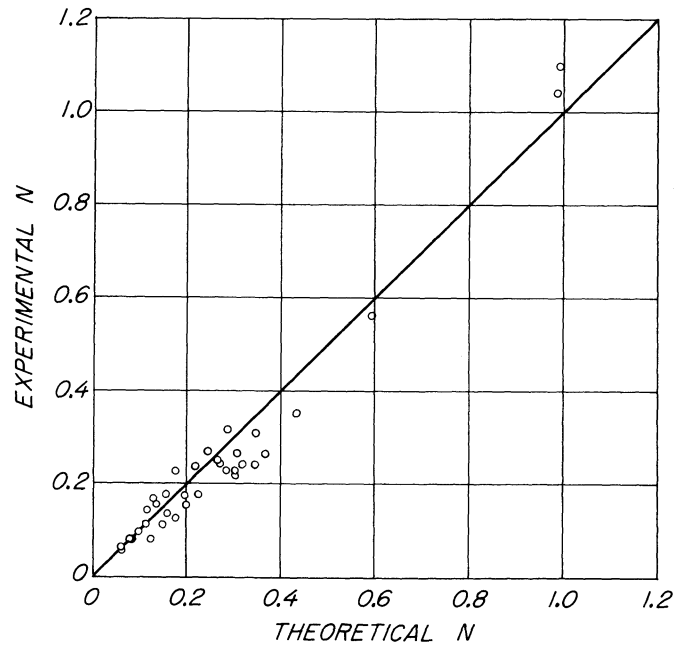


FIGURE 4. - COMPARISON OF EXPERIMENTAL VALUES OF N WITH THEORETICAL VALUES FOR BUCKLING OF SANDWICH CYLINDRICAL SHELLS IN AXIAL COMPRESSION

ELASTIC STABILITY OF SIMPLY SUPPORTED CORRUGATED CORE SANDWICH CYLINDERS

By Leonard A. Harris and Edward H. Baker
North American Aviation, Inc.
Space and Information Systems Division

SUMMARY

Theoretical buckling coefficients are obtained for the general instability of simply supported, corrugated core sandwich circular cylinders under combined loads with the core oriented parallel to the longitudinal axis of the cylinder. Buckling curves are presented for axial compression, external lateral pressure, torsion, and some typical interactions. The differential equations of equilibrium used to obtain the buckling equations were derived from the small deflection equations of Stein and Mayer which include the effect of deformation due to transverse shear. These equations are solved by Galerkin's equation. Remarks are made concerning the probable validity of the results of the small deflection theory for sandwich shells.

INTRODUCTION

The solution for the general instability of corrugated core sandwich circular cylinders with the core oriented parallel to the axis of the cylinder is performed in a manner similar to the solution by Batdorf^{1,2} for the general instability of homogeneous isotropic thin walled cylinders. In the solution presented in this report, and in Batdorf's solution, a differential equation obtained from small deflection theory is solved by Galerkin's³ method. In the present report, the differential equations which were solved by Galerkin's method were obtained from the small deflection theory for curved sandwich plates by Stein and Mayer⁴. The elastic constants for corrugated core sandwich were derived from the basic corrugated sandwich geometry and material properties by Libove and Hubka⁵. The previous Stein and Mayer⁶ solution for the general instability of corrugated core sandwich cylinders loaded under axial compression was performed in a similar manner. This report takes into consideration lateral internal and external pressure and torsion as well as axial compression.

The basic element of the idealized corrugated core sandwich consists of relatively thin isotropic facings which have negligible flexural rigidities about their own centroidal axes and a highly orthotropic core

for which shear distortions are assumed to be admissible only in the plane perpendicular to the corrugation (circumferential). Furthermore, the bending rigidity of the core is assumed to be negligible in the transverse direction. Both the facings and the core are assumed to be elastic.

DERIVATION OF BUCKLING EQUATION

It was assumed that the shear stiffness in the plane parallel to the corrugations (longitudinal) is infinite. The governing differential equations are given by equations (8) and (14) of reference 4. These equations include the influence of the transverse shear, Q_y . For simply supported edges, the boundary conditions on w and Q_y are

$$w = \frac{\partial^2 w}{\partial x^2} = 0, \quad \frac{Q_y}{G_c} = 0: \quad x = 0, L$$

These conditions are satisfied by the assumed orthogonal functions

$$w = \sin \frac{ny}{2r} \sum_{s=1}^{\infty} a_s \sin \frac{s\pi x}{L} + \cos \frac{ny}{2r} \sum_{s=1}^{\infty} b_s \sin \frac{s\pi x}{L} \quad (1)$$

and

$$Q_y = \cos \frac{ny}{2r} \sum_{s=1}^{\infty} c_s \sin \frac{s\pi x}{L} + \sin \frac{ny}{2r} \sum_{s=1}^{\infty} d_s \sin \frac{s\pi x}{L} \quad (2)$$

where n is restricted to even positive integers equal to or greater than 4 and s is restricted to positive integers equal to or greater than 1.

The solution to the governing equations are obtained by use of Galerkin's method as described in reference 3. The Galerkin equations are:

$$\int_0^{2\pi r} \int_0^L Q_1 w V_1 dx dy = 0 \quad (3a)$$

$$\int_0^{2\pi r} \int_0^L Q_1 w V_2 dx dy = 0 \quad (3b)$$

$$\int_0^{2\pi r} \int_0^L Q_2 w V_1 dx dy = 0 \quad (3c)$$

$$\int_0^{2\pi r} \int_0^L Q_2 w V_2 dx dy = 0 \quad (3d)$$

where:

$$V_1 = \sin \frac{n y}{2r} \sin \frac{m \pi x}{L}, \quad V_2 = \cos \frac{n y}{2r} \sin \frac{m \pi x}{L}$$

The expression for $Q_1 w$ is obtained by substituting each term of equations 1 and 2 into equation 8 of reference 6 and that for $Q_2 w$ is obtained by substituting each term of equations 1 and 2 into equation 14 of reference 6. After the proper substitution and integration has been performed on equations (3a) and (3d), equation (3d) is solved for c_m , which is substituted into equation (3a). In a similar manner, after the proper substitution and integration has been performed on equations (3a) and (3c), equation (3c) is solved for d_m which is substituted into equation (3b). With extensive simplification these equations become

$$A a_m - K_s \frac{8 \beta n}{\pi m^2} \sum_s b_s \frac{m s}{m^2 - s^2} = 0 \quad (4)$$

$$A b_m + K_s \frac{8 \beta n}{\pi m^2} \sum_s a_s \frac{m s}{m^2 - s^2} = 0 \quad (5)$$

where

$$A = \left\{ m^2 \frac{D_c}{D} + \frac{(m^2 + \beta^2 n^2)^2 [2J + m^2(1-\mu)]}{[2J + m^2(1-\mu) + 2\beta^2 n^2] m^2} + \frac{4 Z^2 m^2}{\pi^4 (\delta_1 m^4 + 2\delta_2 n^2 m^2 \beta^2 + \delta_3 \beta^4 n^4)} - K_c - K_p \beta^2 \frac{n^2}{m^2} \right\}$$

$$K_p = \frac{p r L^2}{\pi^2 D}$$

$$K_c = \frac{N_c L^2}{\pi^2 D}$$

$$K_s = \frac{N_s L^2}{\pi^2 D}$$

$$D = \frac{E t h^2}{2(1-\mu^2)}$$

$$J = \frac{G_c c L^2}{\pi^2 D}$$

$$\beta = \frac{L}{2\pi r}$$

$$\delta_1 = 1 - \mu^2 \frac{1}{1 + \frac{EA}{E_c A_c}}$$

$$\delta_2 = \frac{1 + \mu}{1 + \frac{1 + \mu}{1 + \mu_c} \left(\frac{t_0}{A_c} \right)^2 \frac{E_c A_c}{EA}} - \mu \frac{EA}{EA + E_c A_c}$$

$$\delta_3 = \frac{1}{1 + \frac{E_c A_c}{EA}}$$

$$Z = \frac{L^2}{r h} (1 - \mu^2)^{1/2}$$

Equations (4) and (5) can be solved explicitly for K_c and K_p for each value of m and n . The minimum is determined by trial and error. In the case of the buckling coefficient K_p , it can be shown that the minimum

occurs when m is one. The buckling coefficients for external pressure and for axial compression are shown in figures 2 and 3, respectively. Figure 4 shows the interaction between axial compression and lateral pressure for $Z = 10^3$.

Solution for K_s ; K_p and K_c Known

Each of equations (4) may be expressed in the form

$$A a_m - \lambda^{-1} B b_{sn} = 0 \quad (6)$$

Each of equations (5) may be expressed in the form

$$A b_m + \lambda^{-1} B a_{sn} = 0 \quad (7)$$

where n s are odd integers and

A is defined above

$$B = \frac{8\beta n}{\pi m^2} \sum_s \frac{ms}{m^2 - s^2}$$

$$\lambda^{-1} = K_s$$

In matrix form, these equations become

$$\lambda |a| = [A]^{-1} [B] |a| = [G] |a| \quad (8)$$

where λ is a scalar, $|a|$ is a column matrix (the Fourier coefficients), and $[G]$ is a nonsymmetrical square matrix. The solution for λ by matrix iteration is complicated by the fact that the cylinder will buckle at a load level which is independent of the direction of the applied shear. Therefore, the buckling coefficients and corresponding eigenvalues occur in pairs which are equal in magnitude but opposite in sign. When the matrix $[G]$ is formed, the upper right quadrant, $[G_1]$, and the lower left quadrant, $[G_2]$, are non-zero matrices; whereas the other two quadrants are null matrices. The matrix $[G]$ is also simplified by the fact that $[G_1]$ is equal to $[-G_2]$. Making use of these relationships,

$$\lambda^2 |a_2| = [-G_2] [G_2] |a_2| = [G_3] |a_2| \quad (9)$$

The matrix $[G_3]$ can be formed from either of equations (6) or (7). An 8 x 8 matrix was formed and iterated to obtain the eigenvalue λ^2 . The

iteration continued until the scalar λ^2 , remained constant to six significant figures. The buckling coefficient K_s is the square root reciprocal of the eigenvalue λ^2 .

For a given set of numerical values of the sandwich parameters, buckling coefficients are obtained for single values of n until the minimum value of the buckling coefficients is found. Figure (5) is a plot of K_s as a function of Z for the special case of K_c and K_p equal to 0. Figure 5 is a plot of K_s as a function of K_c for Z equal to 10^3 . Figure 6 is a plot of K_p as a function of K_s for Z equal to 10^3 .

COMPARISON WITH SOLUTION FOR HOMOGENEOUS ISOTROPIC THIN WALL SHELLS

The method of solution used for the corrugated sandwich cylinders is the same as the method of solution used for homogeneous isotropic cylinders in references (1) and (2). Therefore, if the parameters for a sandwich which is the equivalent of homogeneous sheet are substituted into the sandwich cylinder stability equations, the resulting equations should be the same as the equations presented in references (1) and (2). A sandwich with $G_c = \infty$ and $t = h$ is the equivalent of homogeneous sheet. For the case of $t = h$, the moment of inertia of the facing sheets about their own centroid cannot be neglected so that I is equal to $2/3 t^3$. With this correction, the equation becomes

$$\left[\frac{(m^2 + \beta_o^2)^2}{m^2} + \frac{12 Z_o^2 m^2}{\pi^4 (m^2 + \beta_o^2)^2} - K_c - K_p \frac{\beta_o^2}{m^2} \right] a_m - K_s \frac{\delta \beta_o n}{\pi m^2} \sum_s b_s \frac{m s}{m^2 - s^2} = 0 \quad (10)$$

where β_o and Z_o refer to the thin sheet parameters. This equation is the same as the equations given in references (1) and (2) for cylinders of homogeneous, isotropic thin sheet.

VALIDITY OF RESULTS

The results of this analysis agree with the special case of the homogeneous isotropic thin wall shell. The considerable discrepancy between test data and the linear small deflection theory for the particular loading condition of axial compression has been reported frequently in the literature. In this case, test data may be on the order of only 15% of that predicted by the small deflection theory. Analysis of test data indicates that the buckling coefficient is a function of r/t , whereas the small deflection theory does not indicate this dependence. The consequence of this comparison of data from unstiffened shells must on the surface lead to the conclusion that the small deflection theory does not

accurately predict the behavior of sandwich shells for those cases in which the core shear distortion has a negligible effect. There is, however, some argument that the disagreement between theory and test should not be so great as for thin wall shells. This argument is that the sandwich shell behaves as if it had a relatively low r/t . That is, the effective thickness of the sandwich is relatively large and it might be supposed that the effects of initial imperfection are relatively small because of the rigidity of the wall. Although data are limited, this does not appear to be the real case. For example, March and Kuenzi⁸, in their report of a large deflection theory for axial compression, show some test data. These data show relatively small scatter and the data fall within $\pm 30\%$ of the large deflection predicted buckling loads.

For the case in which shear distortion becomes predominate, it is likely that the small deflection theory will provide good agreement with test data. In this case, the mode of failure (called a crimp) is one which has a very short wave length.

The above statements are relative to the specific case of axial compression. For the cases of external pressure and torsion, agreement between linear theory and test data is closer. Investigations of the interaction buckling coefficients from linear theory for thin wall shells indicates that the shape of the interaction agrees well with test data provided the non-dimensional buckling ratios are used instead of the buckling coefficients themselves.

The probable consequence of the comparisons with thin wall shell behavior are that the linear theory used herein will provide satisfactory solutions for a shell under torsion, will be reasonably accurate for external pressure, and will provide the correct shapes for interaction curves. In contrast, however, the theory will be inadequate for shells under axial compression when the shear distortion effects are negligible. This leads to a very real lack of data for sandwich shells under axial compression loads and under bending. In order to effectively describe the behavior of sandwich shells in axial compression, it will be necessary to perform an extensive series of tests in a systematic fashion. Very little of these data are available.

REFERENCES

1. Batdorf, S. B.: A Simplified Method of Elastic-Stability Analysis for Thin Cylindrical Shells. NACA Rep. 874, 1947. (Formerly included in NACA TN's 1341 and 1342.)
2. Batdorf, S. B., Stein, Manuel, and Schildcrout, Murry: Critical Stress of Thin-Walled Cylinders in Torsion. NACA TN 1344, 1947.
3. Duncan, W. J.: Galerkin's Method in Mechanics and Differential Equations. R. & M. No. 1798, British A.R.C., 1937.
4. Stein, Manuel, and Mayers, J.: A Small-Deflection Theory for Curved Sandwich Plates. NACA Rep. 1008, 1951. (Supersedes NACA TN 2017.)
5. Libove, Charles, and Hubka, Ralph E.: Elastic Constants for Corrugated-Core Sandwich Plates. NACA TN 2289, 1951.
6. Stein, Manuel, and Mayers, J.: Compressive Buckling of Simply Supported Curved Plates and Cylinders of Sandwich Construction. NACA TN 2601, 1952.
7. Harris, Leonard A., Suer, Herbert S., Skene, William T., and Benjamin, Roland J.: The Stability of Thin-Walled Unstiffened Circular Cylinders Under Axial Compression Including the Effects of Internal Pressure. Jour. Aero. Sci., vol. 24, no. 8, Aug. 1957, pp. 587-596.
8. March, H. W., and Kuenzi, Edward W.: Buckling of Cylinders of Sandwich Construction in Axial Compression. Forest Products Laboratory Report No. 1830, 1957.

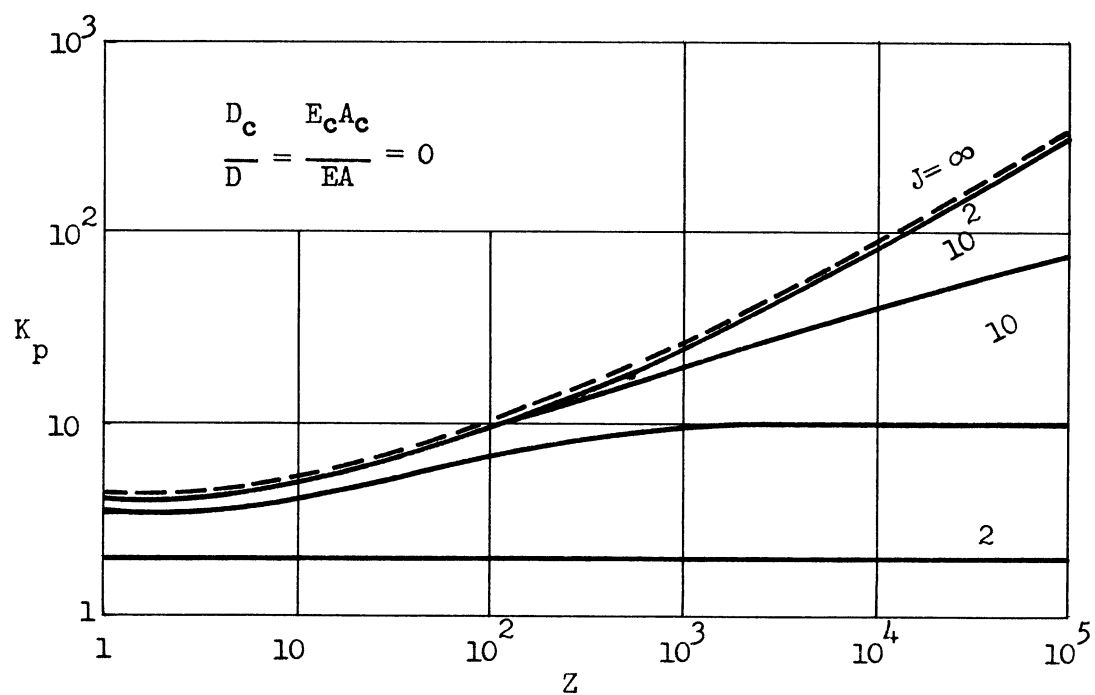


Figure 1.- Buckling coefficients for lateral pressure.

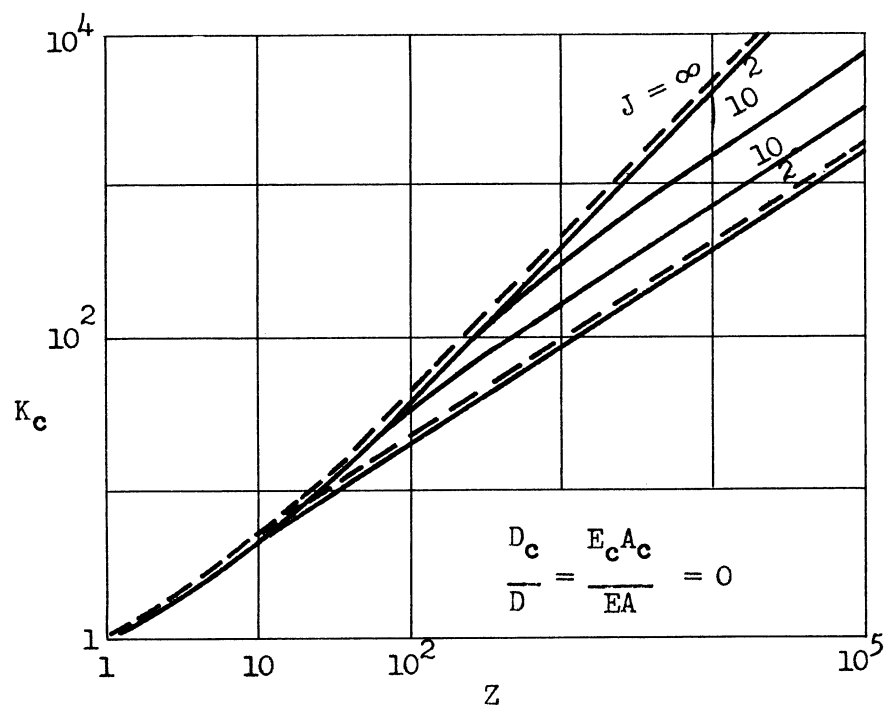


Figure 2.- Buckling coefficients for axial compression.

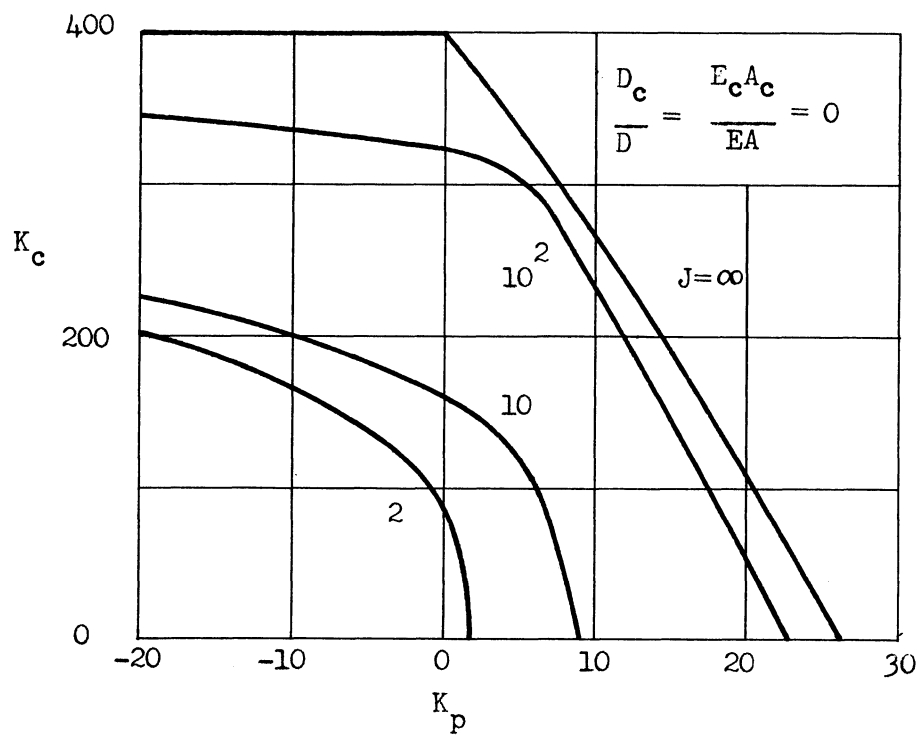


Figure 3.- Combined lateral pressure and axial compression ($Z = 10^3$).

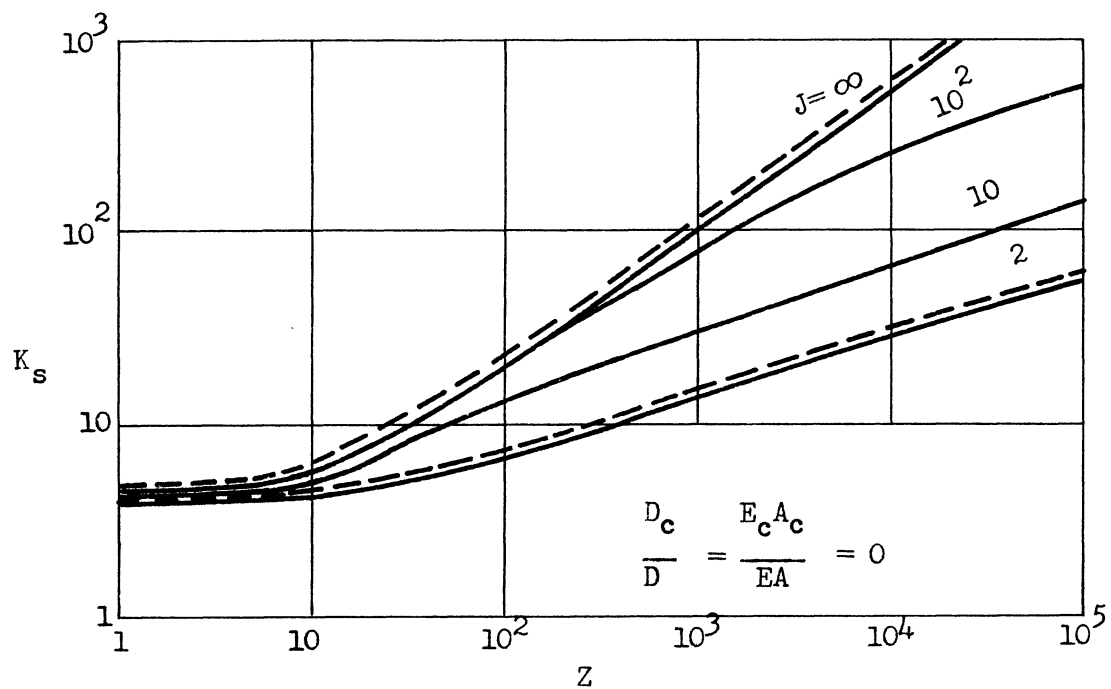
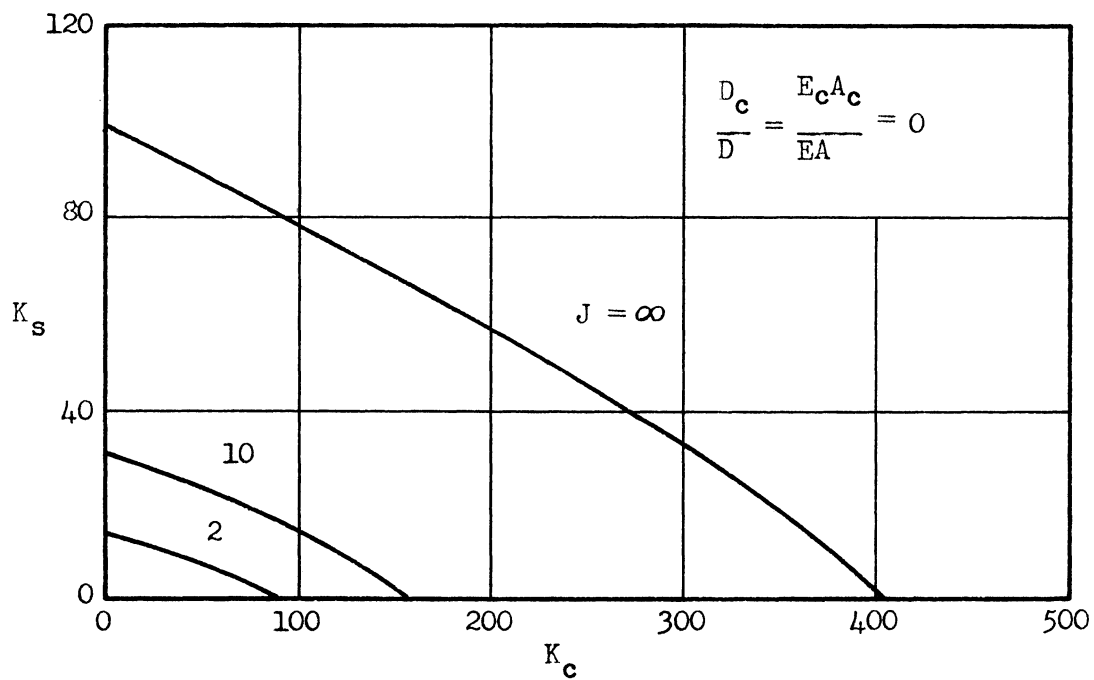
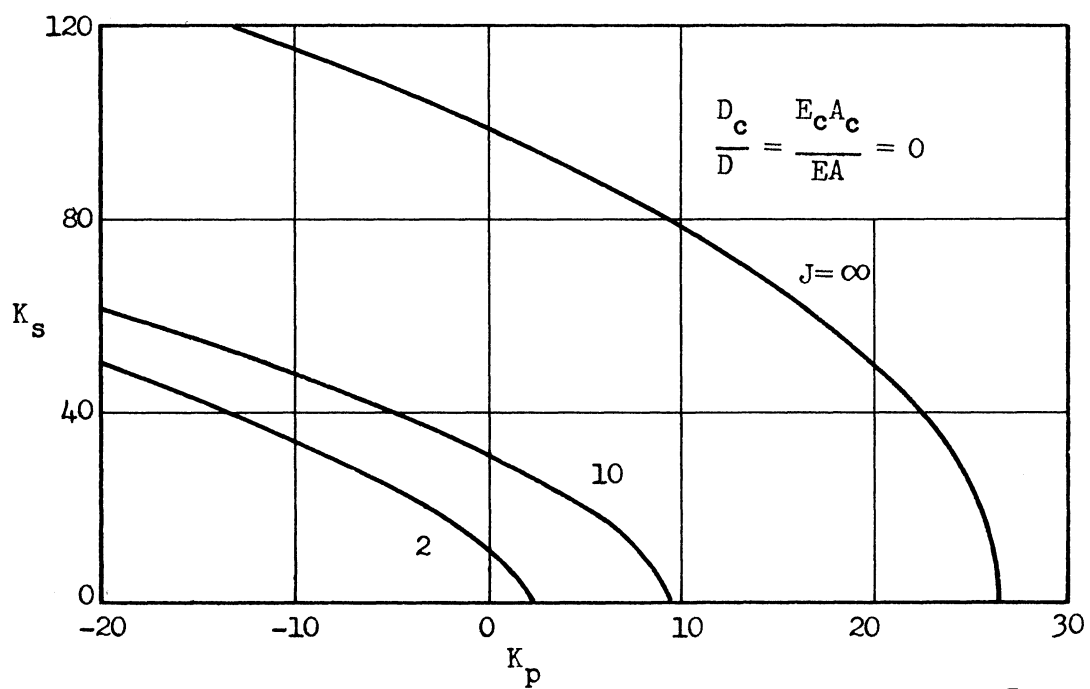


Figure 4.- Buckling coefficients for torsion.

Figure 5.- Combined axial compression and torsion ($Z = 10^3$).Figure 6.- Combined lateral pressure and torsion ($Z = 10^3$).

DESIGN AND TESTING OF
HONEYCOMB SANDWICH CYLINDERS UNDER AXIAL COMPRESSION

By

John H. Cunningham

and

Marcus J. Jacobson

Douglas Aircraft Company, Inc., Missile Structural Systems Section,
Missile and Space Division, Santa Monica, California

SUMMARY

Experimental results for 36" diameter honeycomb cylinders fabricated with thin (0.010") aluminum faces and cores prove that it is quite feasible to stabilize thin faces so they can be loaded beyond the yield point. The effect of initial imperfections and the various modes of failure are discussed.

INTRODUCTION

A recent series of tests by the Douglas Aircraft Company on 36" diameter cylinders has established that with proper design and manufacturing techniques, it is possible to stabilize very thin (0.010") metal skins so that they will carry compressive loads well into the inelastic region. After a brief development period no trouble was experienced at joints, and failures occurred in the middle of the cylinders. The failures occurred by wrinkling of the faces rather than by general instability.

SYMBOLS

A_0	amplitude of imperfection
d	diameter of a circle inscribed in a honeycomb cell
E	Young's modulus of elasticity of face
E_t	tangent modulus of face
E_{sec}	secant modulus of face

E_c	Young's modulus of elasticity of core
F_c	ultimate strength of core
G_c	shear modulus of core in a plane normal to the faces and parallel to the load
I	moment of inertia
K	constant
k	spring constant
L	length of column
N_{cr}	axial compressive buckling load (#/in)
R	mean radius of curvature of cylinder
T	thickness of core
t	thickness of monocoque cylinder
t_f	thickness of one face of sandwich
ϵ	strain
η	plasticity reduction factor ($\eta = 1$ in elastic region)
ρ	radius of gyration
σ	stress
σ^*	stress from stress-strain diagram
σ_{cr}	face buckling stress
σ_f	predicted failing stress with imperfection
σ_{mc}	face monocell buckling stress
σ_{wr}	face wrinkling stress

MODES OF FAILURE

Review of Theoretical Analyses

In the literature, several solutions are presented for buckling of sandwich cylinders under axial compression (Ref. 1). Adequate analyses exist for most modes of failure including small and large deflection theories with, and without initial imperfections.

Solutions to the governing partial differential equations are obtained by assuming a particular mode of failure and then solving for the critical load corresponding to that particular mode of failure. For sandwich cylinders, many modes of failure are possible, each corresponding to a certain critical load. The designer must proportion the shell to obtain the minimum weight construction for a given load by choosing the proper combination of face thickness, core cell size, depth, and shear rigidity for a given cylinder diameter and axial load. The role of initial imperfections and their effects on the different possible modes of failure must be understood. The initial imperfections which occur during manufacturing, especially near end fittings and openings, will in most practical applications limit the efficiency attainable from sandwich constructions.

GENERAL INSTABILITY

General instability corresponds to over-all buckling of the shell. For sandwich construction the effect of shearing rigidity of the core may be extremely important. The small deflection theoretical buckling load of a cylinder with transverse shear deflections included (Ref. 2) is compared to predicted loads obtained by neglecting shear effects in Figure 1. The postbuckling load predicted by a large deflection theory (Ref. 3) is also plotted (Figure 2). For low core shear moduli, initial buckling occurs by the faces sliding with respect to each other (crimping). As the core modulus is increased, buckling strength increases until the core is sufficiently rigid to prevent the faces from sliding and then the classic over-all buckling occurs. The core rigidity required to force buckling in this "rigid core" region is a function of the Et_p/R of the cylinder. Many experiments have yielded unsatisfactory information because the radius (R) and face thickness (t_p) have been scaled down causing the cylinder to be in the soft core region where only a small fraction of the expected strength could be obtained. Obviously, for maximum strength, the cylinder must be designed to be in the rigid core region.

The classic small deflection critical buckling stress (Ref. 4) is,
when $G_c \geq \frac{Et_f}{R}$,

$$\sigma_{cr} = \frac{N_{cr}}{2t_f} = \frac{\eta_{ET}}{R} \left[1.05 - \frac{\eta_{Et_f}}{1.8 RG_c} \right] \quad (1)$$

with

$$\eta = \frac{\sqrt{E_t E_{sec}}}{E} \quad (2)$$

The plasticity reduction factor η for cylinders under axial compression is obtained from Gerard (Ref. 5).

When the core shear modulus is low, i.e., $G_c \leq Et_f/R$, failure occurs by shear instability and the critical load is

$$N_{cr} = T G_c. \quad (3)$$

ROLE OF IMPERFECTIONS IN SMALL DEFLECTION THEORY

Assuming an imperfection consisting of sine waves around the circumference of a cylinder and considering small deflection theory, the effect of imperfections in monocoque cylinders is determined by a factor of the form

$$1 / \sqrt{1 + K \frac{R}{t} \frac{A_o}{t}}$$

while for sandwich cylinders the equivalent expression is

$$1 / \sqrt{1 + K \frac{R}{T} \frac{A_o}{T}} .$$

It is significant that for general instability, the effect of initial imperfections in sandwich construction is related to the total thickness, T . Sandwich thicknesses are much greater than monocoque thicknesses and

the same magnitude of imperfection is much less serious in sandwich construction.

LARGE DEFLECTION THEORY

Large deflection theories are more complete and predict not only the initial buckling load (Figure 2, point A) but also the maximum post-buckling load a cylinder can sustain (Figure 2, point B). The non-linear behavior of monocoque cylinders has been extensively studied (Ref. 6) and it is generally recognized that the minimum point B in Figure 2 corresponds to radial displacements of the cylinder of approximately five sheet thicknesses. If initial imperfections of this magnitude exist, as they often do for foil gages, failure will indeed occur at these low loads. Donnell and Wan (Ref. 7) have described the failure mechanism as a function of the magnitude of the assumed initial imperfection and as expected higher loads are obtained for more nearly perfect cylinders. Often designers choose the postbuckling stress (point B) rather than the initial buckling stress (point A). This may be exceedingly conservative for monocoque cylinders of low R/t and for sandwich cylinders.

LOCAL BUCKLING

In attempting to stabilize a thin foil gage so that it will accept loads stressing it up to the yield point, one must consider ways in which the sheet may fail by local buckling.

MONOCELL BUCKLING

A form of local buckling is monocell buckling, namely, buckling of individual cells within the honeycomb core. Norris and Komers (Ref. 8) give the monocell buckling criterion

$$\sigma_{mc} = 0.9 \eta E \left(\frac{t_f}{d} \right)^{3/2} \quad (4)$$

In the inelastic range, the plasticity reduction factor for flat plates (Ref. 9) is used, and is given by

$$\eta = \frac{E_{\text{sec}}}{E} . \quad (5)$$

The designer must choose a core cell size to prevent monocell buckling. This can be accomplished without difficulty by choosing from the wide variety of commercially available cores.

WRINKLING

With a cell size chosen to prevent monocell buckling, the faces can be considered to be continuously supported by an elastic medium, i.e., the core. Local failures of the faces can occur independent of the dimensions of the cylinder if the core does not have sufficient ability to stabilize the faces. Since the failures will be highly localized, curvature effects can be neglected and analyses developed for flat plates can be utilized.

Non-symmetric failure can occur if the core does not have sufficient shear rigidity to force the two faces to act as an integral unit. The analysis presented previously for general instability included failure by shear instability (crimping) but neglected the flexural resistance of the individual faces about their own neutral axes. Hoff and Mautner's (Ref. 10) analysis for flat plates using energy techniques shows that thin sandwich panels may buckle in the "skew-ripple" unsymmetric mode. The critical load per inch for sandwiches with thin cores is

$$N_{\text{cr}} = 2 t \sigma_{\text{cr}} = 1.18 t_f \sqrt{\frac{E E_c}{T}} + .774 T G_c \quad (6)$$

This should be compared to the expression obtained before for the "soft" core region by neglecting the resistance of the faces to flexure, namely

$$N_{\text{cr}} = T G_c . \quad (7)$$

As the core modulus approaches zero, the only load carrying capability is obtained from the flexural resistance of the faces.

For some material properties and dimensions, symmetrical wrinkling may occur at lower loads. Depending on the assumptions made, one can obtain a variety of expressions for critical loads. The simplest approach neglects the shear effects of the core and treats the faces as a beam on an elastic foundation (Ref. 11). The spring constant is obtained by considering the midplane of the core as an axis of symmetry and then treating the core material as an elastic spring. Upon substitution into the expression for buckling of a beam on an elastic foundation,

$$N_{cr} = 2 \sqrt{k EI} ,$$

one obtains

$$N_{cr} = 1.73 t_f^{3/2} \sqrt{\frac{E E_c}{T}} \quad (8)$$

This indicates that lower loads are obtained for thicker cores. As the core thickness is increased, other factors must be considered.

Upon examining Figure 3, one realizes that neighboring core strips move different distances. Since the strips are physically attached, shear stresses develop and cause the displacements to die off with increasing core depth. Assuming that the displacements die off linearly with depth, Hoff (Ref. 9) using energy techniques obtained

$$N_{cr} = 1.82 t_f \left[E E_c G_c \right]^{1/3} \quad (9)$$

Williams (Ref. 12) assumed an exponential decay of displacements and in Equation (9) obtained 0.85 instead of 0.91. Hoff's solution (Ref. 10) by a theory of elasticity approach gave lower values which were functions of the core depth to face thickness ratio. For thick cores, the coefficient was $(0.873)(0.91) = 0.794$. Many authors have recommended using a coefficient of 0.50 as it gives reasonable agreement with experimental data, but it should be realized that this implies symmetrical wrinkling.

The references mentioned provide criteria for determining whether a given sandwich is "thick" or "thin," but the criteria have been left out of this brief summary. To recapitulate, unsymmetrical "skew-ripple" occurs for cores with low shear moduli, whereas symmetrical wrinkling occurs for cores with high shear rigidity and/or thick cores.

For inelastic wrinkling, a suitable plasticity reduction formula is applied. Since curvature effects are neglected, it is reasonable to use the flat plate reduction factor,

$$\eta = \sqrt{\frac{E_t}{E}} . \quad (10)$$

For large plastic strains, the tangent modulus, E_t , changes so rapidly with increasing load that the same value of critical load is obtained from Equation (9) independent of the coefficient assumed.

EFFECT OF INITIAL IMPERFECTIONS ON WRINKLING

The equations derived for buckling predict the critical load in terms of the elastic constants and provide no information on the strength properties required. The required core compressive strength and the adhesive strength depends on the initial imperfections formed during manufacture or induced in service. Knowing the type and magnitude of the imperfection, one can determine the required strengths. However, by assuming various imperfection values, one obtains a good appreciation for the serious effects produced by small imperfections. One also realizes the importance of using high strength cores and adhesives to insure that the failures occur by buckling before the local stresses exceed the allowable values. Since imperfections are always present, especially around joints, openings, closing members, etc., it is imperative to understand their significance and to minimize their importance by using high strength adhesives and cores.

Yuseff's (Ref. 11) analysis of wrinkling assumes imperfections having the same shape and wave length as the wrinkle pattern. The reduction in strength due to imperfections is easily visualized by comparing the results to the theoretical wrinkling stress without imperfection. Yuseff's equation 22 may be written

$$\frac{\sigma_f}{\sigma_{wr}} = \frac{1}{1 + 1.39 \frac{(E_c G_c)^2}{\eta E F_c} \frac{A_0}{t_f}} \quad (11)$$

Using the properties of the test cylinders Figure 4 shows the reduction in predicted failing stress as a function of the amplitude of the initial imperfection for an elastic failure ($\eta = 1$).

The reduction in wrinkling strength due to the presence of an initial imperfection can be minimized by using a sandwich core with high compressive strength and a high strength adhesive.

COMPARISON BETWEEN TEST AND THEORY

Axial compression tests were run on eight 7075-T6 aluminum sandwich cylinders with faces 0.010 inches thick (Ref. 13). The outside cylinder diameters were 36 inches and the length of each was 30 inches. The cores in each case were aluminum Hexcel Al 3/16-5052 .001 P oriented with the ribbon direction parallel to the load. The core thicknesses were 0.125 inches, 0.188 inches, and 0.400 inches. Table I and Figures 5 and 6 show test results.

The first three cylinders fabricated were unsatisfactory and failed at low stress levels. This was due to poor detail design of the end doublers and unbonded regions. The original doubler was not scalloped and acted as a constraint preventing the cylinder from expanding laterally when loaded axially. This constraint caused local bending, introducing an initial imperfection, and caused wrinkling type failure at low stress levels ($\approx 30,000$ psi). Scalloping the doubler relieved the problem by preventing highly localized bending. One can easily obtain an appreciation of the problem by computing the free radial expansion of the cylinder. The hoop strain is caused by Poisson's ratio

$$\epsilon_h = \mu \epsilon_L$$

and the radial displacement δ

$$\delta = R \epsilon_h = R \mu \epsilon_L .$$

At 62,000 psi the axial strain is 0.0068 in/in. and the radial expansion is 0.0408 inches. If this expansion is prevented by a rigid ring, premature failure occurs due to highly localized bending.

In order to prevent localized bending, a 0.010 inch scalloped doubler was used in subsequent tests. It is apparent that the failures occurred by wrinkling.

To visualize the comparison of the test results to the theoretical buckling stresses predicted by various formulas, one can place the concepts on an elementary level. Consider the buckling of a perfect pin-ended column. The critical buckling stress is

$$\sigma_{cr} = \frac{\pi^2 E_t}{\frac{L^2}{\rho^2}} = K E_t$$

At a given tangent modulus (i.e., at a given strain in the column), the column can support a stress without a stability failure provided that the stress is less than $k E_t$. In Figure 7, $\sigma = k E_t$ represents resistance to buckling instability failure. Also plotted in Figure 7 is σ^* vs. E_t where σ^* and E_t are obtained from a conventional stress-strain diagram of a uniaxial tension specimen. The curve σ^* vs. E_t represents the ability to carry load assuming no instability failure. As the column is loaded, the strain in the unbent column determines the tangent modulus and the stress. As loading increases from zero, the strain increases, the stress increases, and the tangent modulus decreases. Eventually the stress reaches a level where an instability failure occurs, namely, the intersection of the two curves. Hence, the intersection represents the predicted buckling load.

The principle outlined above for obtaining the critical stress of a pin-ended column also applies for finding the critical stress of a sandwich cylinder for each of the various assumed modes of failure. Thus, one can compute for each cylinder (assuming no imperfections) the predicted buckling stress according to the various theories. The results are shown in Figures 8, 9, and 10. The predicted buckling stresses and the actual failing stresses are given in Table II. The predicted buckling stress from small deflection theory and from wrinkling theory were calculated for $G_c = 20,000$ psi and for $G_c = 40,000$ psi and showed only a very slight effect of a variation of core shear modulus in the rigid core region. A conventional stress-strain curve (Figure 11) was obtained from coupons cut from the sheets used to fabricate the cylinders.

The predicted buckling loads from the small deflection general instability equation and the wrinkling equation (assuming no initial

waviness of the faces) are in close agreement with each other. One can not expect exact agreement with test values as some uncertainty is introduced in the inelastic range. Also, the stress-strain curve used is for tension rather than compression as it was not feasible to conduct compression tests on the .010" thick coupons cut from the facing sheets. Note that one of the compression failing stresses (78,800 psi) actually exceeds the ultimate strength in tension (77,000).

Various wrinkling equations corresponding to symmetrical and unsymmetrical failure modes were examined. The equation for symmetrical buckling predicted the minimum critical loads and was used for theoretical predictions (Equation 9). The thin specimen actually failed by unsymmetrical wrinkling, probably due to some slight imperfection.

In summary, the thin 0.010" faces were stabilized well into the inelastic region and failures occurred at stresses much higher than predicted by the large deflection theory.

REFERENCES

1. Arnold, L. H.: Design of Sandwich Cylinders Under Axial Compressive Load, Douglas Aircraft Co., TM-18, April 1960.
2. Cunningham, J. H.: An Engineer's Conceptual Approach to the Buckling of Cylindrical Shells (Axial Loading), Douglas Aircraft Co., Engineering Paper No. 1279, revised May 15, 1962, IAS Paper No. 62-106, June 1962.
3. March, H. W. and Kuenzi, E. W.: Buckling of Cylinders of Sandwich Construction in Axial Compression, Forest Products Laboratory Report No. 1830, revised December 1957.
4. Stein, M. and Mayers, J.: Compressive Buckling Stress of Simply Supported Curved Plates and Cylinders of Sandwich Construction, NACA TN 2601, January 1952.
5. Gerard, G.: Compressive and Torsional Buckling of Thin-Wall Cylinders in the Yield Region, NACA TN 3726, 1956.
6. Kempner, J.: Postbuckling Behavior of Axially Compressed Circular Cylindrical Shells, Journal of Aeronautical Sciences, Vol. 21, May 1954, pp. 329.
7. Donnell, L. H. and Wan, C. C.: Effect of Imperfections on Buckling of Thin Cylinders and Columns Under Axial Compression, Journal of Applied Mechanics, Vol. 17, No. 1, March 1960, pp. 73-88.

8. Norris, C. B. and Komers, W. J.: Short-Column Compressive Strength of Sandwich Construction as Effected by the Size of the Cells of Honeycomb Material, Forest Products Laboratory Report No. 1817, August 1950.
9. Gerard, G.: Introduction to Structural Stability, McGraw-Hill Book Co., 1962.
10. Hoff, N. J. and Mautner, S. F.: The Buckling of Sandwich Type Panels, Journal of the Aeronautical Sciences, Vol. 12, No. 3, July 1945, p. 285.
11. Yuseff, S.: Face Wrinkling and Core Strength in Sandwich Construction, Journal of the Royal Aeronautical Society, March 1960.
12. Williams, D.: An Introduction to the Theory of Aircraft Structures, Edward Arnold (Publishers) Ltd., 1960.
13. Eakin, E. C.: Honeycomb Cylinder Tests, Douglas Aircraft Company, Report No. SM-37719, January 18, 1962.

TABLE I

Specimen Number	Core Thickness Inches	Buckling Load Pounds	Face Stress Psi	Type of Failure
1	0.125	137,600	61,000	Wrinkle About 6" from End
2	0.188	156,000	69,000	Wrinkle At Center of Cylinder
3	0.188	141,400	62,500	Wrinkle at Center of Cylinder
4	0.400	168,500	74,000	Wrinkle at Center of Cylinder
5	0.400	178,000	78,800	Wrinkle at Edge of Doubler

TABLE II

Specimen Number	Predicted Buckling Stresses (psi)				Actual Failing Stress (Psi)
	Wrinkling	Monocell	General Instability		
			Small Deflection	Large Deflection	
1	74,800	70,000	57,000	31,000	61,000
2	74,800	70,000	64,800	45,400	69,000
3	74,800	70,000	64,800	45,400	62,500
4	74,800	70,000	69,000	64,000	74,000
5	74,800	70,000	69,000	64,000	78,800

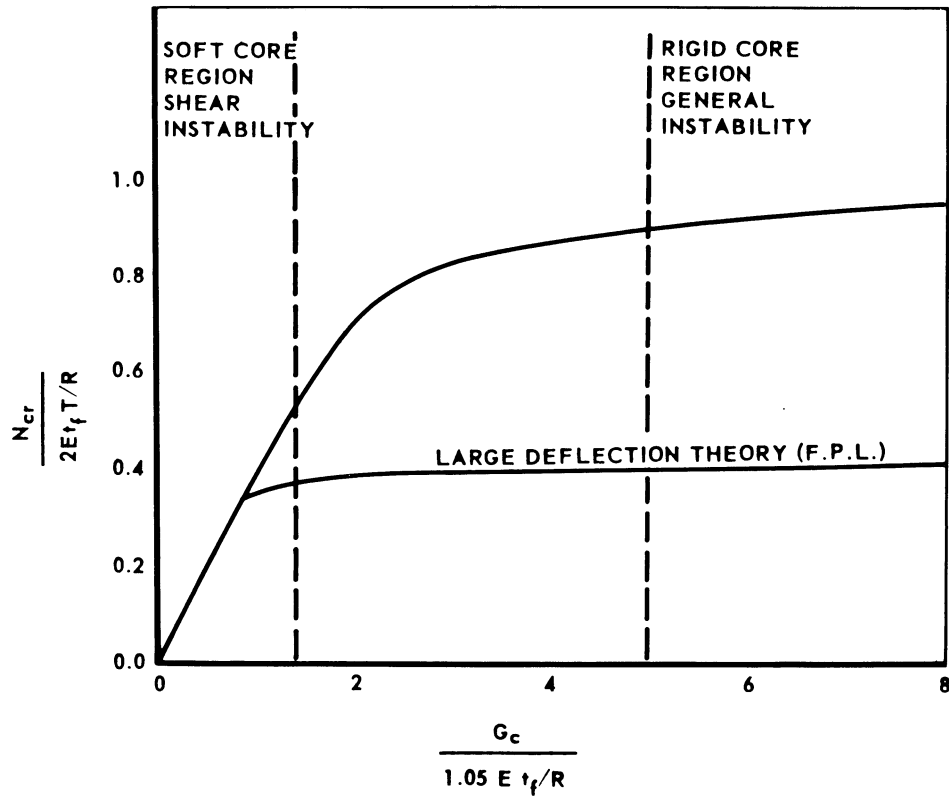


Figure 1.- Effect of shear rigidity on critical buckling of cylinder.

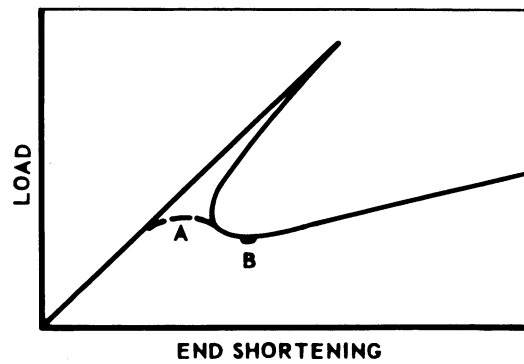


Figure 2.- Load carrying capacity by large deflection theory.

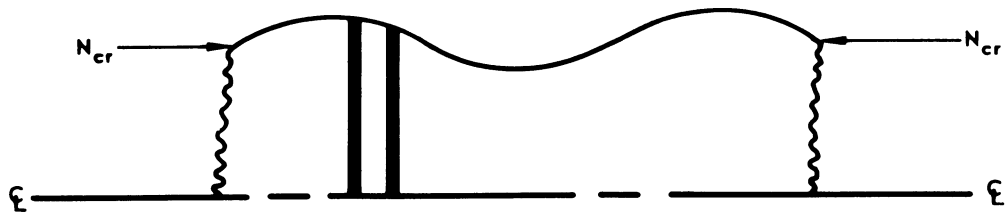
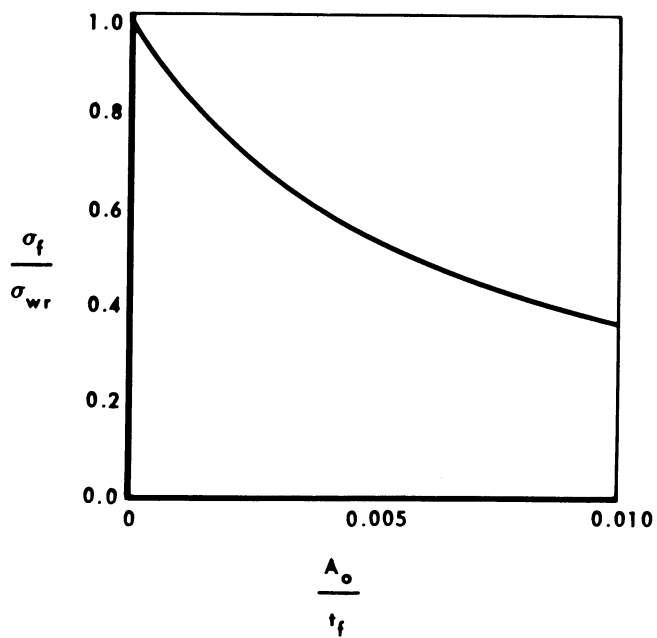


Figure 3.- Wrinkling of sandwich construction.



$$\begin{aligned}
 E &= 10.6 \times 10^6 \text{ PSI} \\
 E_c &= 1.885 \times 10^5 \text{ PSI} \\
 G_c &= 40,000 \text{ PSI} \\
 F_c &= 285 \text{ PSI} \\
 \frac{\sigma_f}{\sigma_{wr}} &= \frac{1}{1 + 183.8 \frac{A_o}{t_f}}
 \end{aligned}$$

Figure 4.- Reduction of buckling strength due to imperfections.

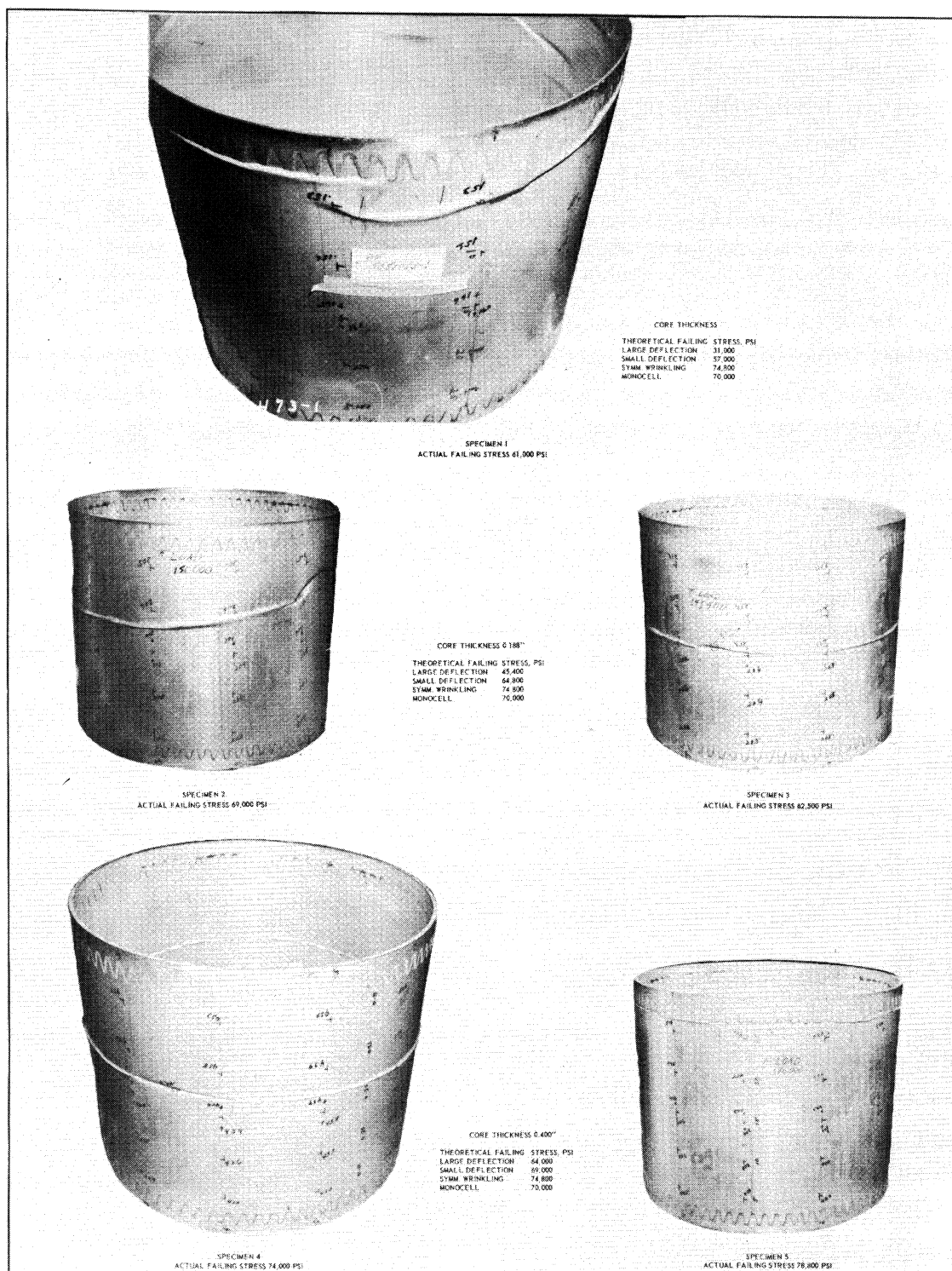


Figure 5.- Test results of buckled cylinders.

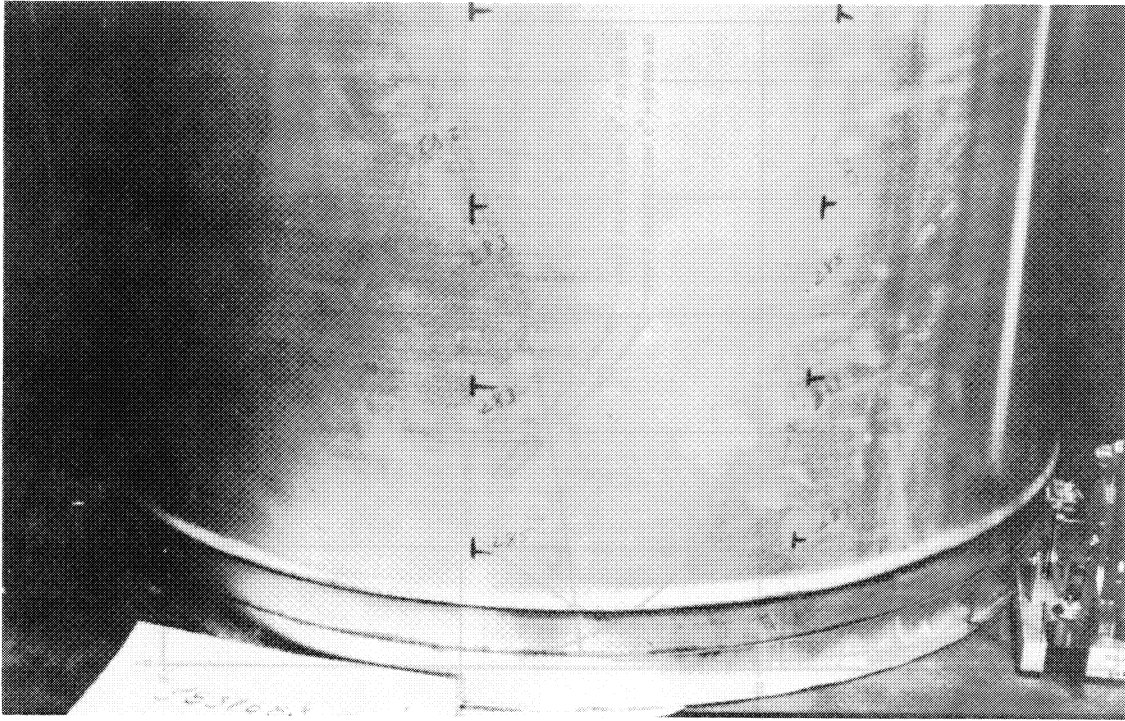


Figure 6.- Premature failure at unscalped doubler.

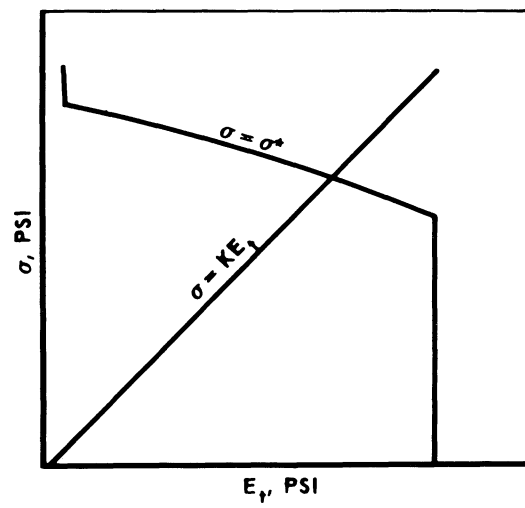


Figure 7.- Instability criterion.

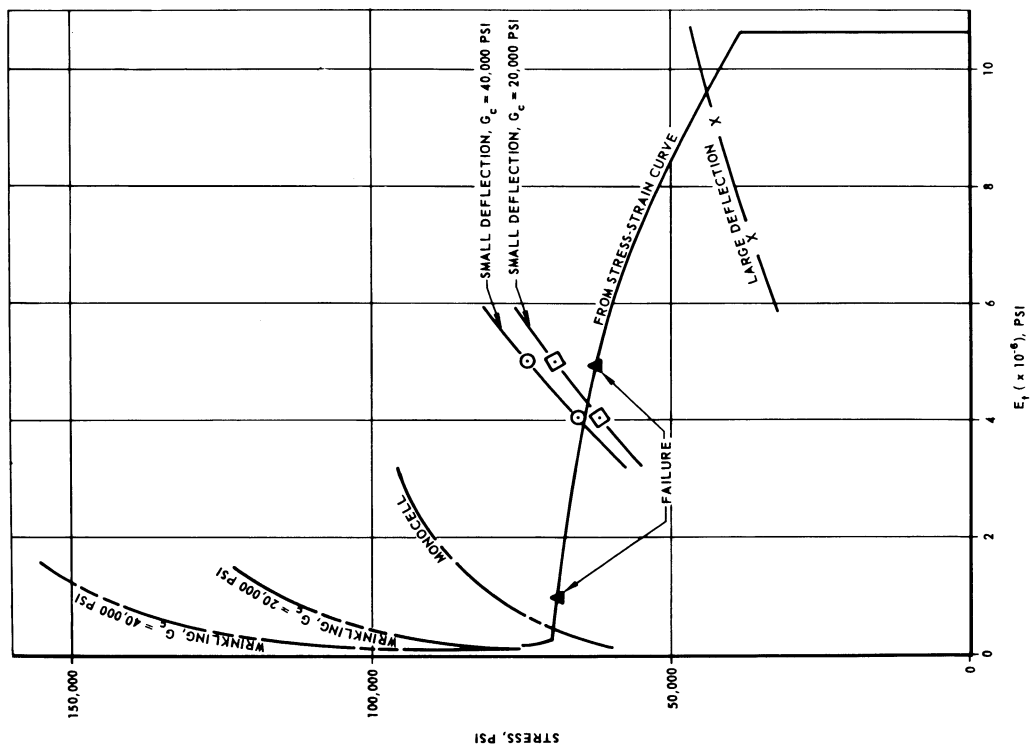


Figure 9.- Instability criteria with core thickness of 0.1875 inch.

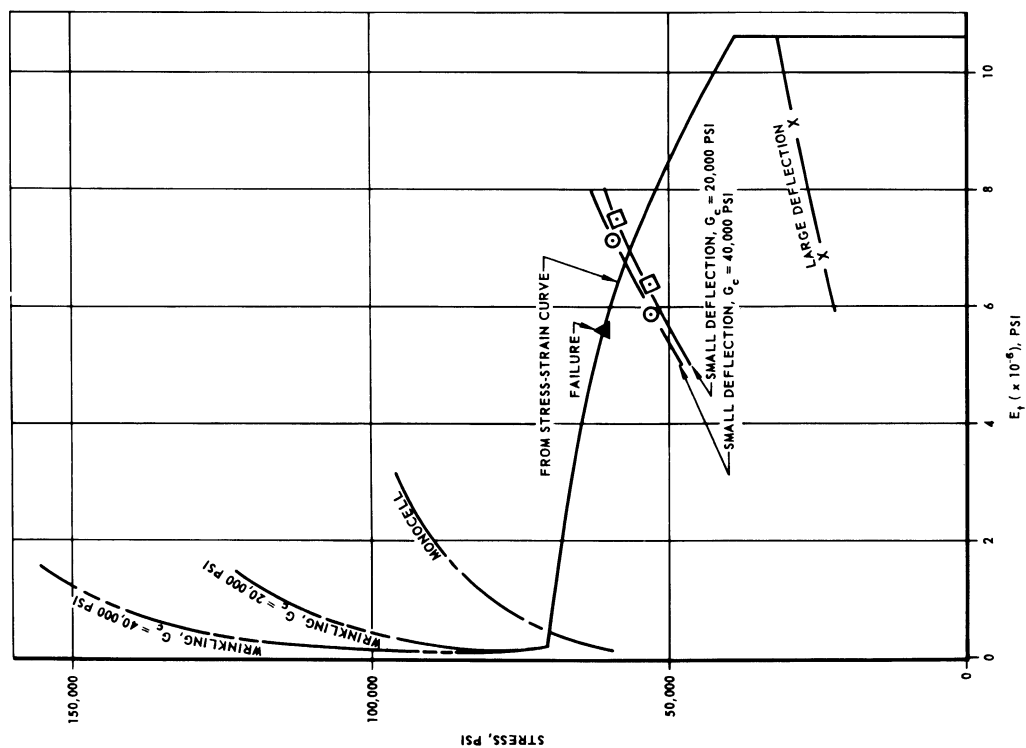


Figure 8.- Instability criteria with core thickness of 0.125 inch.

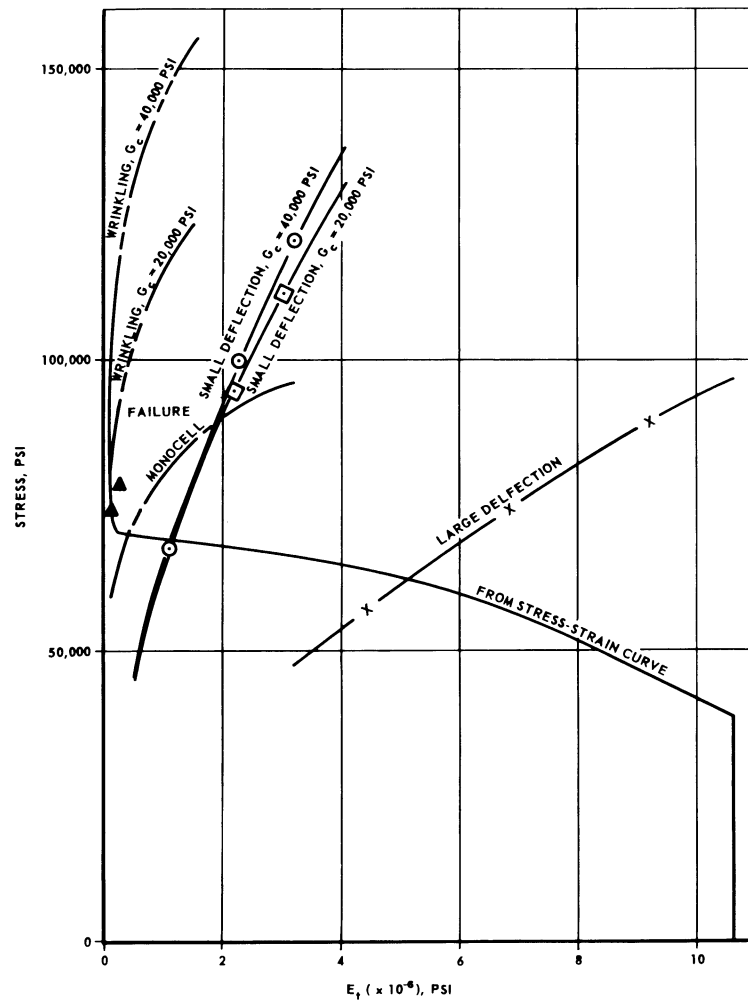


Figure 10.- Instability criteria with core thickness of 0.400 inch.

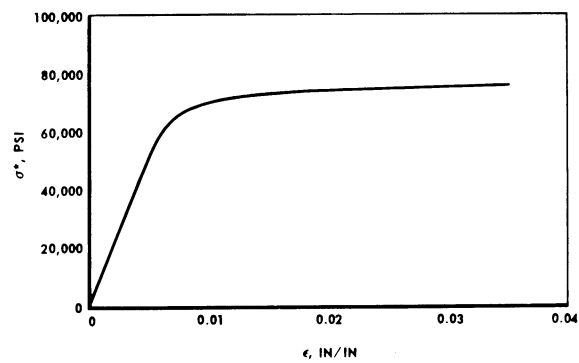


Figure 11.- Stress-strain curve of 7075-T6 aluminum.

THE BUCKLING OF CIRCULAR CYLINDRICAL SHELLS
SUBJECT TO AXIAL IMPACT

By Anthony P. Coppa

Space Sciences Laboratory
Missile and Space Division
General Electric Company

SUMMARY

Early experimental results on the buckling of circular cylindrical shells subject to axial impact are described. A hypothesis for the mechanism of buckling which was based on these experiments is described. The results of further experiments which were designed to test predictions from the hypothesis and which appear to verify it in several aspects are then described.

INTRODUCTION

The work which this paper describes was undertaken several years ago in order to gain an understanding of the behavior of shell structures subject to axial impact. The motivation for this effort was the need to predict the forces which a shell structure, say of a missile or space vehicle, experiences when it suffers a collision with the ground. In many cases, payloads containing shock-sensitive components are mounted in such structures and must function during and/or after impact. In order to assure that the loading tolerances of these components are not exceeded, it is necessary to know in some detail what force pulses can be transmitted by the shell to these components throughout the phases of initial loading, buckling, and collapse.

The results of some early experiments are first discussed and a hypothesis for the mechanism of buckling due to axial impact presented. Later experiments which were designed to test predictions resulting from the hypothesis are then discussed and the results compared with the anticipated magnitudes and trends.

LIST OF SYMBOLS

$c = \sqrt{\frac{E}{\rho}}$	speed of compression waves
D	mean diameter of cylindrical shell
E	Young's Modulus
h	shell thickness
$K = \frac{l_y}{l_x}$	aspect ratio of buckles
l	length of cylinder
l_x, l_y	axial and circumferential half wave lengths of buckles
l_{cr}	critical length
l_f	collapse length
M	impacting mass
m	mass of cylindrical shell
n	number of circumferential buckles
r	mean radius of cylindrical shell
$T = \frac{2l}{c}$	longitudinal period of compression wave
t	time
V, V_o	impact velocity
\bar{V}_r	velocity of contraction of buckle during postbuckling
$\alpha = \frac{m}{M}$	
δ	axial displacement of the cylinder end

δ_o, δ_i	maximum outer and inner lateral displacements of the polygon with respect to the initial circular cross section
ϵ	strain, unit axial shortening
ϵ_{cr}	critical strain
ϵ^*	initial strain
ν	Poisson's ratio
ρ	mass density of shell material
σ	stress
σ_{cr}	critical stress
σ^*	initial stress

EARLY RESULTS

Early experiments by the writer in which open ended thin cylindrical and conical shells were impacted longitudinally showed that buckles of the familiar diamond form occur in an orderly fashion at the impacted end. The characteristic of these buckles is that they allow an almost total axial shortening of the shell surface with very little extensional strain. The materials used included paper, brass, steel, aluminum and the impact velocities ranged up to 35 ft/sec. In all cases, the buckle patterns were of essentially similar form for similar large ratios of the shell radius/thickness. Especially in the case of thin paper shells, the buckle patterns were notably orderly. Examples of such patterns obtained from experiments are shown in figure 1. The specimens, originally cylindrical shells of paper ($r/h = 190$, fig. 1a) and 2024 Aluminum alloy ($r/h = 125$, fig. 1b), are shown after having been expanded axially and, by virtue of this, flattened circumferentially. The axial and circumferential lengths are shown in the vertical and horizontal directions respectively and the impacted edge is at the top. The patterns consist of an array of folded triangular planes which in the fully collapsed configuration of the cylinder lie in the cross section plane. Two triangular planes which share a common base in the circumferential (horizontal) direction form the familiar diamond pattern. In figure 1a, the diamond patterns by and large are pointed at the four corners, at which adjacent patterns occur. The circumferential or inner folds are situated along a straight line. The diagonal or outer folds also lie along straight lines, these being inclined to the axial direction by the angle whose tangent is $K = \ell_y/\ell_x$, the aspect ratio of the individual buckles. In the fully collapsed form, that in which the shell is after the impact, the inner folds form essentially a regular polygon of n sides whose perimeter is equal to the initial circumference of the cylinder. In figure 1b the patterns are quite similar except that the horizontal points of adjacent diamonds do not touch precisely but rather, form the ends of short circumferential line segments. This latter property is characteristic of metal shells and becomes more pronounced for smaller r/h ratios. It is due primarily to the flexural rigidity of the shell wall which prevents sharp folding in the region of corners.

From the early experiments it was clearly evident that buckling occurs at the impacted end and progresses in discrete stages at the velocity of the impacting head. During the entire process there is a

region of collapsed material, folded in the manner described above, adjacent to the impacting head and an undisturbed region of the shell which extends from there to the other end. This observation was based on the appearance of specimens after impact and substantiated by high speed motion pictures. This phenomenon, that is, the localization of the buckling and collapse, occurs even when the end opposite the impacted end is merely placed on the base of the test apparatus with no other attachment or support.

Buckling and collapse progresses in the manner described over substantial percentages of the initial length, 90% not being uncommon for thin shells. An example of the sharp separation between the collapsed and undisturbed regions is given in figure 2 which shows a cylinder of 2024 Aluminum alloy before and after an impact at a velocity of about 21 ft/sec. having the following initial dimensions in inches: $l = 27$, $D = 4.50$, $h = .004$. The shell was dropped (together with a weight attached at the upper end) with no guidance of any sort against a flat base. Impact occurred, therefore at the bottom end.

The manner of testing was to impact the free edge of the shell vertically with a flat surface, either by dropping the shell (with a weight attached at the end opposite the impact) against a flat base or by dropping a flat plate on the edge of the stationary specimen. Initially there was no pressure differential across the shell wall, but as the shell collapsed, the pressure of the internal air increased, this being limited by an air vent. The internal pressure was sufficient to maintain roundness in the portion of the shell beyond the buckled region during the collapse process and hence contributed to the orderliness of the buckle deformations, especially for shells having high r/h ratios.

Due to the fact that the collapse configuration of the shell is a system of folded plane surfaces, it was asked whether this configuration could be described essentially by an inextensional deformation process. It was assumed therefore that the initial circumference of the cylinder has the same length as the perimeter of the polygon formed by the inner (horizontal) folds of the collapse pattern. The following procedure was used: Consider a circular cylinder of diameter D . Cross-section A which is initially circular becomes a regular polygon of n sides as it moves axially from A to C. (fig. 3a) The perimeter of the polygon equals the circumference. Now consider the circular cross-section which was in the undeformed cylinder at B. It becomes a polygon of n sides as it moves to C, this polygon being rotated about the cylinder

axis by the angle θ with respect to the former polygon. In fig. 3b the cross-section of the buckled cylinder at C is shown (for $n = 5$) in which both polygons are shown in their true relative positions when stations A and C are axially coincident. Cross-sections A and B which in the undeformed cylinder were circular are given by the polygons, $A_1A_2A_3A_4A_5A_1$ and $B_1B_2B_3B_4B_5B_1$ respectively. The cross-section at C has deformed into a polygon $C_1C_2C_3C_4C_5C_1$ which is coincident with $A_1A_2A_3A_4A_5A_1$. The originally cylindrical surface between stations A and C is reduced to $4n$ triangular plane surfaces: $A_1B_1A_2$, $A_2B_2A_3$, $A_3B_3A_4$, $A_4B_4A_5$, $A_5B_5A_1$, $B_1A_2B_2$, $B_2A_3B_3$, $B_3A_4B_4$, $B_4A_5B_5$, $B_5A_1B_1$, $B_1C_2B_2$, $B_2C_3B_3$, $B_3C_4B_4$, $B_4C_5B_5$, $B_5C_1B_1$, $C_1B_1C_2$, $C_2B_2C_3$, $C_3B_3C_4$, $C_4B_4C_5$, and $C_5B_5C_1$.

The dimensions of these triangles can be calculated easily. In figure 4 a plan view of a portion of the collapsed configuration is shown together with the arcs $PQRST$ and $Q^1R^1S^1T^1U^1$ respectively of the original cross sections A and B (see fig. 3a). In the collapsed configuration the arc $PQRST$ becomes the straight line segments B_1B_2 and B_2B_3 while the arc $Q^1R^1S^1T^1U^1$ becomes the segments A_2A_3 and A_3A_4 . The segments form the congruent triangles $B_1A_2B_2$, $A_2B_2A_3$, $B_2A_3B_3$, and $A_3B_3A_4$ which, of course, lie in the cross section plane. The altitude of these triangles is determined as follows:

$$l_x = (r - \delta_i) \frac{(1 - \cos \theta)}{\cos \theta}$$

From the assumption of inextensionality

$$\delta_i = r(1 - \theta \cot \theta)$$

$$\text{Hence } l_x = r \frac{\pi}{n} \tan \frac{\pi}{2n} \quad (1)$$

and since $l_y = r \frac{\pi}{n}$, the aspect ratio, $K = \frac{l_y}{l_x}$, of the collapse pattern is:

$$K = \frac{1}{\tan \frac{\pi}{2n}} \quad (2)$$

The quantities l_x and l_y can be shown to be the axial and circumferential half waves of the collapsed configuration. According to eqn. (2), as the number of circumferential waves in the collapse pattern increases, the triangular planes become more slender in the circumferential direction.

The pattern shown in fig. 1a has an average of five circumferential waves over the surface. The aspect ratio of the buckles is 3.0.

By comparison the aspect ratio derived from eqn. (2) (for $n = 5$) is 3.08.

The above relations, therefore, follow directly from the assumptions that the initial circumferential length of the cylinder is equal to the perimeter of the regular polygon of the collapsed configuration and that the axial length of the collapsed region is zero. They apply strictly to cylinders having zero wall thickness. Collapse patterns were constructed according to equation (2) and compared with patterns obtained from experiments. One such comparison may be seen in figure 5 which shows a partially expanded collapse pattern of seven circumferential waves obtained from a 2024 Aluminum cylinder of .004 in. wall thickness and an initial diameter of 4.50 in. The constructed pattern, also of $n = 7$ waves, agrees closely in overall appearance.

The orderliness of the experimentally derived collapse patterns stimulated the effort toward gaining an understanding of the process of buckling due to impact. An hypothesis, developed in an attempt to explain the mechanism of buckling, is given in reference 1. Because of the limited availability of this work, it is discussed in the following sections.

MECHANISM OF BUCKLING

The problem considered was the response of a thin circular cylindrical shell to an axially symmetric impact of a rigid mass against one end (see fig. 6). At the other end, the cylinder is supported longitudinally by a plane rigid surface. Both ends of the shell are assumed to be unrestrained against lateral displacement.

Loading due to Impact

The axial loading introduced into an elastic cylindrical shell by an axial impact prior to the initiation of instability may be taken, at least to a first approximation, from the solution of the longitudinal impact on an elastic bar. Donnell (Ref. 2) gives the solution for the stresses produced when a rigid mass of finite magnitude M strikes the end of an elastic bar which is supported rigidly at the other end. The total compression stress, $\sigma_n(t)$, at the impacted end is given by

$$\sigma_n(t) = \overset{\rightarrow}{\sigma_n(t)} + \overset{\leftarrow}{\sigma_{n-1}(t-T)}, \quad nT < t < (n+1)T \quad (3)$$

where the arrows indicate the sense of the wave motion, \rightarrow being away and \leftarrow toward the impacted end. $\vec{\sigma}_n(t)$ is given by

$$\vec{\sigma}_n(t) = \sigma^* \sum_{m=0}^{m=n} e^{Z_m} \sum_{h=0}^{h=m} \frac{m!}{h!} \frac{(2Z_m)^h}{2(m-h)} \quad (4)$$

where $Z_m = 2\alpha \left(m - \frac{t}{T}\right)$ and $\alpha = \frac{\text{cylinder mass}}{\text{Impacting mass}}$.

$\leftarrow \sigma_{n-1}(t-T)$ is obtained from $\rightarrow \sigma_n(t)$ by taking $n-1$ and substituting $(t-T)$ for t . According to this solution, the initial stress σ^* produced at the instant of impact travels at the sonic velocity as the front of a system of waves which increase in magnitude instantaneously by σ^* at each reflection from the ends.

When the mass M is infinite ($\alpha = 0$), its velocity is constant throughout the impact. Hence, the stress distribution in the bar is rectangular and its magnitude at any position (or time) is an integral multiple of the initial stress σ^* . This behavior is illustrated in Figure 7, which shows the variation of stress with time at each end of the bar. At the struck end, the stress is always an odd multiple of the initial stress: σ^* , $3\sigma^*$, $5\sigma^*$, etc., and at the other end, an even multiple: 0 , $2\sigma^*$, $4\sigma^*$, etc., each value remaining for a time $\frac{2\ell}{c}$.

Impact by an Infinite Mass ($\alpha = 0$)

a) Initiation of Instability

At the instant of impact, a stress wave of magnitude $\sigma^* = \frac{V}{c} E$ propagates from the impacted end at a velocity $c = \sqrt{E/\rho}$. When the front of the wave has moved a distance $x = \ell_{cr}$ from the impacted end, instability will initiate during the first passage of the stress wave if σ^* is sufficiently large (see Figure 8). Instability occurs over this region because there is a geometrical configuration other than the cylindrical one which accommodates the axial displacement $\delta = \frac{V}{c} \ell_{cr}$ of the striking mass with a reduction in the axial strain. For regions of length $x < \ell_{cr}$, the cylindrical form is stable because other geometrical configurations which can contract by an amount δ cannot be generated by the imposed axial stress. Once instability has

started, the region $x = l_{cr}$ is not able to transmit the high level of axial stress which caused instability and, hence, the stresses transmitted to the remainder of the cylinder are insufficient to produce instability over that region. As a result, further axial displacement of the impacted end is accommodated by suitable displacements of the shell wall within the region $x = l_{cr}$, whereas the cylinder beyond the critical length remains relatively undisturbed.

In Figure 9, the variation of the total axial strain in the buckling part as anticipated by this mechanism is indicated. For the time from zero to $t = \frac{l_{cr}}{c}$, the strain remains at the value $\frac{V}{c}$. Instability occurring at $t = \frac{l_{cr}}{c}$ is accompanied by a rapid reduction in the axial strain in the unstable region. As the impacted end is continually displaced, the strain decreases due to the formation of other geometrical configurations in the buckling part, which have continually decreasing axial resistance. This is discussed under the section on post-buckling behavior.

Consider now an impact at a velocity which produces a stress wave of insufficient magnitude to cause instability in the first passage of the wave from $x = 0$ to l . At $x = l$ and thereafter at every reflection from the rigid boundaries at each end, the stress abruptly increases by σ^* as was shown before in Figure 7.

In this manner, an initially low stress can increase to a value sufficient to cause instability. Since the stress increases by σ^* at each reflection, however, instability can occur at either end, depending on where the additional increment σ^* due to reflection makes the total stress sufficiently large to initiate instability over the region l_{cr} adjacent to the particular end. If an even number ($N = 0, 2, 4, \dots$) of reflections produces the critical stress σ_{cr} , instability must occur at the impacted end whereas for the case of an odd number ($N = 1, 3, 5, \dots$) of reflections, instability must initiate at the end opposite the impacted end (see Figure 10).

Thus, the critical stress and time are given by the following relations:

$$\sigma_{cr} = (N + 1) \frac{V}{c} E \quad (5)$$

$$t_{cr} = \frac{l}{c} N + \frac{l_{cr}}{c} \quad (6)$$

Inextensional Buckling

A cylindrical shell subjected to axial loading buckles at a particular value of axial compression strain at which a geometrical configuration other than cylindrical provides the same axial shortening but with lower axial strain. Although such behavior can be called typical of all structures under axial compression loading, the cylindrical shell is singularly prominent in this respect. This is because its axial rigidity in the initial state is largely a result of its cylindrical form. However, even small lateral displacements from the cylindrical form cause large reductions in axial resistance. Yoshimura (Ref. 3) has shown that a cylindrical shell subjected to an end shortening can be developed into a surface which accommodates the axial shortening or displacement with a minimum of extensional strain. It is readily shown that if the trigonometric terms for the inextensional cross sections are retained instead of the approximations as used in reference 3, pp 6, 7, the unit end shortening is given exactly by

$$\epsilon = 1 - \sqrt{1 - K^2 \tan^2 \frac{\pi}{2n}} \quad (7)$$

Eqn. (7) applies only to a cylindrical membrane ($h = 0$), but is useful for studying the buckling forms of actual shells having large r/h ratios.

According to eqn. (7), for a given value of ϵ , there exists an infinitude of surfaces each defined by a particular combination of K and $n(2, 3, 4, \dots)$. Now suppose that a region of the shell a distance x from the end has an elastic axial strain of magnitude ϵ prior to buckling. Then if the surface assumes any one of the surfaces (defined by eqn. 7) corresponding to the given value of ϵ , the same amount of shortening will now be realized with no axial membrane strain. These surfaces consist of a system of plane triangles, the planes of which are inclined to the axis of the cylinder. The cross section of the inextensional surface is a regular polygon of n sides.

It is to be noted that when $\epsilon = 1$, which applies to total axial shortening, eqn (7) reduces to eqn (2) which was derived previously for the collapse configuration.

Because the edges of the cylinder were assumed to be free to move laterally, it was considered that the edge could suddenly change from a circle to a regular polygon when buckling was initiated.

Furthermore, construction of inextensional patterns showed that patterns consisting of one row of axial half waves were sufficient to accommodate any admissible value of ϵ and would have a lower density of fold line per unit axial length of surface. The density of fold line was taken as an indication of the bending strain energy that would be present in an actual shell. It was assumed, therefore, that the initial buckle pattern consists of a single row of axial half waves, that is, a single row of triangular planes.

A plot of some of these configurations is given in Figure 11, which shows curves of constant circumferential wave number. The unit axial shortening ϵ is plotted against the ratio ℓ_x/D of the axial half-wave length to the cylinder diameter. For a given ϵ , the configurations have the property that the smaller the axial half-wave length, the higher the number of circumferential waves. This property is illustrated in Figure 12, which shows several configurations corresponding to $\epsilon = .001$ in/in.

The ratio ℓ_x/D may be considered to be the initial dimensionless length of a region of the cylinder adjacent to one of its ends. If a given compressive strain, $\epsilon = \frac{V}{C} (N + 1)$ is imposed over the cylindrical region of a particular dimensionless length, there is one inextensional configuration which can provide an equal unit axial shortening with no axial compression strain over a region of the same initial length. This configuration is defined by a particular value of circumferential wave number n (2, 3, 4, ...) and aspect ratio K .

Instability as defined herein is the change from the cylindrical form to an inextensional form having a particular n and K which provide, by inextensional deformation, the same unit axial shortening as the axial compression strain which existed in the cylindrical form.

In order to define a criterion for instability, reference is made to the previously stated relationship that for a given imposed unit axial shortening $\epsilon = \frac{V}{C} (N + 1)$, the shorter the axial wave length, the higher the number of circumferential waves. This suggests that cylindrical regions of small ℓ_x/D should require higher axial loading to become unstable than regions of larger ℓ_x/D . A further assertion is that the variation of axial resistance with ℓ_x/D should be increasingly stronger as ℓ_x/D approaches zero since the rate of rise of n and the fold-line density become increasingly greater as ℓ_x/D becomes very small. If ϵ_{cr} is the axial strain required to initiate instability, then instability will occur when the actual strain $\frac{V}{C} (N + 1)$ over a

region of length ℓ_x equals or exceeds the critical strain corresponding to that region. The criterion for instability is therefore

$$\frac{V}{c} (N + 1) \geq \epsilon_{cr} \quad (8)$$

This criterion is illustrated in Figure 13 in which the critical strain is plotted against the ratio ℓ_x/D . Let a strain wave of magnitude ϵ proceed from the end of the cylinder designated by $\ell_x/D = 0$. As the wave travels along the cylinder, there is, at any instant, an inextensional configuration corresponding to the imposed value of ϵ . Since the critical value of axial strain of these configurations varies inversely with their axial length, the cylinder remains stable until the wave front has moved to the value of ℓ_x/D , at which the first configuration whose critical strain is equal to or less than the imposed strain exists. Then the cylindrical form becomes unstable over this length ℓ_x/D . This new configuration is the critical configuration.

Postbuckling Behavior

The postbuckling range is defined as the interval of buckling beginning with the critical configuration and ending with the collapse configuration. The collapse configuration corresponds to a unit axial shortening of unity and is defined by eqn. 2.

$$K = \frac{1}{\tan \frac{\pi}{2n_{cr}}}$$

An examination of the critical configuration shows that, at the vertices, an infinite curvature in the circumferential direction exists while all other locations along the cross section of the buckled surface have zero curvature (see Figure 14). This applies to the idealized inextensional surface in which the sides of the triangles are sharp folds formed by the intersections of adjacent plane triangles. In an actual cylinder, that is, one having a non-zero wall thickness, the initially buckled surface (see Figure 14) consists of alternating convex A and concave B surfaces (with respect to the initially circular cross section). The concave and convex surfaces correspond to the plane triangles of the ideal inextensional surface. The curvature in the circumferential direction of the convex surfaces is greater than that of the concave surface. Also, by considering the ideal inextensional

form, it may be seen that the displacement δ_o of the vertex from the initial cross section (outward in direction) is smaller than the displacement δ_i of the midpoint of the side of the polygon (inward). The ratio δ_i / δ_o of these displacements is given by

$$\frac{\delta_i}{\delta_o} = \frac{\sin \pi/n - \pi/n \cos \pi/n}{\pi/n - \sin \pi/n} \quad (9)$$

and varies from a maximum value of 2.75 ($n = 2$) to a minimum value of 1 ($n \rightarrow \infty$). The generators of the cylinder, therefore, are more bent in the vicinity of the plane surfaces corresponding to the concave surfaces of the real shell than in the vicinity of the vertices. Because of these properties, the axial rigidity varies around the cross section of the critical surface in such a way that greater axial loading is concentrated in the region of the convex surfaces than near the concave surfaces. Thus, there is a preference to maintain the circumferential wave number of the critical configuration n_{cr} , throughout the postbuckling range.

The critical configuration must change in order to accommodate the further motion of the impacting mass of velocity V . Assuming that the shell maintains inextensional configurations having n_{cr} circumferential waves throughout the postbuckling range, it may be observed from Equation 7 that it is necessary for the aspect ratio K to increase continually since n_{cr} is fixed and ϵ depends on the displacement of the mass. The aspect ratio varies according to

$$K = \frac{\sqrt{2\epsilon - \epsilon^2}}{\tan \frac{\pi}{2n_{cr}}} \quad (10)$$

Since $K = \frac{\ell_y}{x}$ and $\ell_y = \frac{\pi D}{2n_{cr}}$ remain constant, ℓ_x , the axial half-wave length of the buckling region, must decrease as ϵ increases. K can be related to the axial displacement of the mass by

$$K = \frac{2 \frac{\delta}{\ell_f}}{1 + \left(\frac{\delta}{\ell_f} \right)^2} \cdot \frac{1}{\tan \frac{\pi}{2n_{cr}}} \quad (11)$$

which is plotted in Figure 15. Referring to Figure 15, K rises rapidly and with decreasing rate as δ increases. The initial rate of increase of K is greater the higher the number of circumferential waves in the critical configuration. The reduction of ℓ_x is

produced by the axial displacement of the vertices of the inextensional configuration (initially located at a distance ℓ_{cr} from the end at which buckling takes place.) This behavior is illustrated in Figure 16. The configuration corresponding to $\epsilon = .001$ in/in may be considered as the critical configuration and those corresponding to $\epsilon = .01, .1$, and 1 representing various stages of postbuckling. These constructions result from Equation 10. It is interesting to note how the boundary between the buckling region and the remainder of the cylinder, a regular polygon of n_{cr} sides, approaches the end as greater axial shortening is imposed on the buckling region. The velocity \bar{V}_r at which this boundary approaches the particular boundary adjacent to which buckling takes place is related to the impact velocity V by the relation

$$\frac{\bar{V}_r}{V} = \frac{1}{2} \left[1 + \left(\frac{\delta}{\ell_f} \right)^2 \right], \quad \frac{\delta_{cr}}{\ell_f} \leq \frac{\delta}{\ell_f} \leq 1 \quad (12)$$

This applies to buckling at either the impacted end, where the end of the cylinder is displaced at velocity V , or at the opposite end which is stationary. Equation 12 is plotted in Figure 17. This relative approach velocity, which is the velocity of axial contraction of the buckling surface, is much greater than V for small values of $\frac{\delta}{\ell_f}$ and becomes

equal to V when $\frac{\delta}{\ell_f} = 1$. In terms of the unit axial shortening, the ratio $\frac{\bar{V}_r}{V}$ is given by

$$\frac{\bar{V}_r}{V} = \frac{1}{\epsilon} \quad (11)$$

and, specifically for $\epsilon = \epsilon_{cr} = \frac{V}{c} (N + 1)$, the approach velocity is

$$\bar{V}_{r_{cr}} = \frac{c}{N + 1} \quad (12)$$

d) Secondary Buckling

When the axial displacement δ of the striking mass is equal to the collapse length ℓ_f where

$$\ell_f = \frac{\pi D}{2n_{cr}} \tan \frac{\pi}{2n}$$

the axial length of the buckled region is zero (see Figure 16, $\epsilon = 1$). When the axial length equals the collapse length, the cylinder has

shortened by an amount ℓ_f and the previously moving vertices of the inextensional surface are coincident with the rigid boundary adjacent to which the instability took place. The approach velocity \bar{V}_r at the instant when $\delta = \ell_f$ is V . Thus, independent of the end at which the buckling has taken place, a new impact of the longitudinally rigid boundary at velocity V against the new end of the cylinder takes place. This new end is, of course, a regular polygon having n_{cr} sides. The secondary impact, therefore, is against a cylinder whose impacted end has the form of a regular polygon in contrast to the initial impact against a circular end. The geometry of the surface adjacent to the end is the same as that described under the previous section, that is, the surface has varying axial rigidity around the cross section. Since the axial rigidity is higher near the vertices of the polygon than elsewhere, the major axial loading due to the new impact is introduced into the shell at the vertices. This latter set of vertices is displaced circumferentially from the corresponding vertices of the critical configuration by one-half circumferential wave length. Thus, there is a strong tendency for the same number of circumferential waves, and hence the overall geometry, as the previously developed buckled surface to form in all subsequent stages of buckling. Each stage of buckling contributes another row of triangular planes to the fully collapsed pattern formed in the preceding stages. Due to the aforementioned circumferential displacement of the vertices with each new stage of buckling, the overall collapse pattern has the appearance of regular parallelograms folded along their major diagonal. These diagonals form the sides of the regular polygon of the cross section plane. This is the familiar "diamond" configuration common to the buckling of thin-cylinder-like shells under axial compression.

Since each stage of secondary buckling is initiated by the collision of the impacting mass or the rigid base of the opposite end against the end of the stable part of the cylinder, collapse progresses along the cylinder at the velocity V .

Extensional Buckling

Buckling of the symmetrical or "ring" type is another mode of deformation other than axial strain which can accommodate the axial displacement. Indeed, from the viewpoint of the axial symmetry of geometry, loading, and constraint (since in actual practice, a truly free edge cannot be realized), it is to be asked whether this is not the mode of buckling which should occur initially over a wide

range of shell geometry and impact velocity. Even for the free edge condition, which implies no friction present between the edge of the shell and the impacting mass, there is an axially symmetric lateral displacement of the shell wall of the amount $\nu r \frac{V}{c}$ present at the front of the compression wave. This displacement can be a significant fraction of the shell wall, and not only introduces bending of the wall but also an axially symmetric circumferential compression strain in the region of the wave front. Both these factors can induce buckling. If lateral constraint of the shell wall is present as well, another axially bent and circumferentially strained (compression) region exists in the shell wall adjacent to the edge. The smaller the impact velocity, the smaller are all these effects, so it is to be expected that the symmetrical buckling mode is more likely (at least initially) for higher impact velocities.

e) Effect of Internal Pressure

It has long been apparent that the random nature of the initial imperfections of a cylindrical shell and the strong dependence of the axial rigidity on the cylindrical form produce large scatter and poor reproducibility in the experimental behavior of thin cylindrical shells subject to axial compression. Since the buckling behavior described herein is affected not only by the initial imperfections but also by their subsequent variation and magnification throughout the postbuckling range, a degree of disorder (although less than in static tests) is to be expected in experimental behavior. This is especially true for shells having large ratios of radius to thickness. In the experimentation, therefore, it has been necessary to allow a certain amount of internal pressure differential to be produced by the collapse of the internal volume of the buckling cylinder in order to reduce the effect of these random influences. This has been found to be of decreasing importance for thicker shells (i. e., those having relatively lower ratios of radius thickness).

EXPERIMENTAL TESTING OF PREDICTIONS

Predictions from the Theory

Several predictions follow from the mechanism described above. These are stated as follows:

1. The initial axial strain due to the impact rapidly rises to a value given by $\epsilon = \frac{V}{c}$.

2. If the velocity is sufficiently high this strain, after being sustained for a time, $t < \ell/c$, will rapidly decrease to a value which is small compared to the initial value, thereby indicating buckling. This buckling will occur at the impacted end.

3. If the velocity is smaller than the above value, but the momentum of the impacting sufficient, then the strain will rise in jumps due to reflections from the boundaries to a magnitude given by

$$\epsilon = \frac{V}{c} (N + 1)$$

until buckling, indicated by the first substantial reduction in strain, occurs. The time between discrete jumps in strain will be $t = \frac{2\ell_1}{c}$, for odd N and $t = \frac{2\ell_2}{c}$ for even N , where ℓ_2 and ℓ_1 are the distances from the strain measurement point to the impacted end and the opposite end respectively.

4. If the velocity is insufficient to cause buckling on the first passage of the compression wave, it is possible for buckling to occur at the end opposite the impacted end.

5. The critical buckling pattern, if it is of the inextensional form will be in the form of a row of triangular buckles whose aspect ratio is given approximately by eqn. (10). This is provided that the edge at which buckling occurs is free to move laterally.

6. During post buckling, the buckle size shortens axially from its initial form until the aspect ratio is as given by eqn. (2). The rate of shortening of the buckle pattern is initially much higher than the impact velocity and rapidly decreases as the collapse configuration is attained.

Experiments were conducted to test the hypothesis according to the above predictions.

Apparatus

The experimental apparatus used was the Precision Drop Tester,

located at the General Electric Company Space Sciences Laboratory (See Figure 18). This device consists of a hardened steel shaft 40 feet in length which is attached under tension between two vertically aligned points. A carriage situated concentrically with the shaft by means of two ball bushings rides along the shaft. The impact head, a hardened and ground steel disc, 10 inches in diameter is mounted to the carriage. The carriage assembly (drop head) is hoisted to the drop height by means of an electric winch which is attached to the carriage by an electro-magnet. A hardened and ground steel base, 8 inches thick and 20 inches in diameter is mounted at the bottom end of the shaft and situated concentrically with it. The base is mounted on three adjustable screws for the accurate positioning of the base in the horizontal plane. The carriage can also be adjusted with respect to the shaft so that the final alignment of the head with the impact end of the shell specimen can be accurately accomplished.

The drop head assembly contains ports for venting the air rapidly from the cylinder as it is collapsing. By means of this venting system, the buildup of internal pressure is prevented. The vent area can be decreased or completely closed according to specific requirements.

The specimen and its retainer are mounted on the base concentrically with the shaft. In order to do this the shaft must be raised clear of the base. This is accomplished by a manually operated winch.

Specimens

The specimens used in the experiments were cylindrical shells having the following dimensions: 5.70 in. inner diameter, 22.8 in. length and wall thicknesses of .004, .008, .016 and .019 inches. These correspond to a length to diameter ratio (l/D) of 4 and diameter to thickness ratios of 1425, 712, 356 and 300. The materials used were the aluminum alloys 2024 F, 2024 T3, and 5052 H-38 and 301 $\frac{1}{2}$ H stainless steel.

The specimens were fabricated from flat sheet by simply rolling

the sheet into a cylinder and making a longitudinal joint. Both rubber based and epoxy adhesives were used as bonding agents for the joints and both lap and double butt strap configurations were employed.

The specimens were simply cylindrical, containing no stiffeners. In most cases, the shells were mounted on a rigid circular base. The impacted end was initially free of support and was unconstrained from radial displacement during the impact except by friction forces at the impact interface.

Experimental Results

Initial Strain

Cylindrical shells of 2024 H-19 Aluminum alloy ($D = 5.700$ in., $h = .008$, $l = 22.8$ in.) were impacted at velocities of 11.5, 25, and 46 ft/sec. Strain gages were mounted to the cylinders in a back-to-back manner (except where noted) at several circumferential locations and two axial stations, one at an inch behind the impacted end and the other at two inches from the opposite end. Tektronix oscilloscopes, triggered simultaneously by a common source, were used with Poloroid cameras to record the strain.

Typical strain records are reproduced in Figures 19, 20 and 21. These show the resultant compression strain near (one inch behind) the impacted end. The impact velocities are 46, 11.5, and 25 ft/sec. for Figures 19, 20 and 21 respectively. Figure 19, the short time record, has time and compression strain along the horizontal and positive vertical axes respectively. The time scale is 10 microseconds per unit grid spacing and the strain scale is .00196 in/in per unit spacing. A zero strain base is established (at the extreme left) by triggering the trace immediately prior to impact. It is seen that the strain rises within 10 microseconds to a peak strain of .00214 in/in and is sustained thereafter at an average level of .00194 in/in for 40 microseconds after initiation of the pulse (+85 μ sec. after impact) the strain has decreased to zero. The time required for the initial elastic stress wave to return to the forward gage position is 216 μ sec. It is apparent from this that buckling has been initiated during the first passage of the stress wave.

The axial compression strain produced by an impact at a velocity of 11.5 ft/sec. is shown in fig. 20. The pertinent scales are 50 μ sec. per grid spacing (horizontal axis) and .000783 in/in strain per unit

spacing (vertical axis). As before, the trace begins at the extreme left. The strain rises within 20 μ seconds to a value of .000802 in/in and after remaining at an average level of about .000622 in/in rises to a peak strain of approximately twice the initial peak. Thereafter, it decreases steadily and becomes equal to zero at 345 μ sec. after impact. It is interesting to note that the time at which the strain begins to rise to attain twice the initial value is slightly greater than 200 μ sec. after initiation of the signal. According to the loading mechanism in the theory a rapid rise in strain to twice the initial value is expected at 216 μ sec. when the compression wave reflected forward from the rear end arrives at the forward gage position.

The strain recorded for the test at a velocity of 25 ft/sec, shown in fig. 21 initially rises rapidly to a value of .00146 in/in. Thereafter the strain fluctuates about a similar mean value and then drops off rapidly. Only the initial portion of the trace, however, is offered as evidence since the measurement is due to a single axial gage. Bending strain components, therefore, may be present in the later portions of the trace.

Table 1

Impact Velocity ft/sec.	Measured Strain in/in	Predicted Strain in/in	Error %
46	.00214	.00274	-22%
25	.00146	.00149	-2%
11.5	.000802	.000684	+17%
	.000622*		-9%

*Average Strain during first passage of compression wave.

After buckling has been initiated, as indicated by the first reduction of axial strain, relatively small strains were measured during the entire long time trace. This was expected as previously discussed. In addition to the low total compression strain during this interval the measurements showed a considerable amount of bending of the shell wall. This is shown in Figures 22a and 22b which pertain to the test conducted at 11.5 ft/sec. These traces are from a pair of axial strain gages mounted back-to-back and wired to read separately. The time scale (horizontal axis) is 500 μ sec. per grid spacing and the strain scales (vertical) are

.000785 in/in (Fig. 22a) and .000783 in/in (Fig. 22b). After impact begins (at the extreme left) both traces show the compression strain pulse which is associated with the initiation of buckling. At about 400 μ sec. the traces run opposite each other, one reading tension and the other compression, thereby demonstrating axial bending of the wall. The bending strains run off the scale but the magnitude appears to be about .002 in/in or 2.5 times the maximum compression strain in the initial pulse. A composite plot of Figures 22a and 22b is shown in Figure 23, which reveals that the total compression strain present simultaneously with the bending strains is relatively low during the entire time trace.

The results described above appear to be in substantial agreement with predictions 1, 2, and 3 stated previously.

Buckling away from Impacted End

Buckling was obtained near the end opposite the impacted end with no buckling deformations present at the impacted end. This resulted from an impact at a velocity of 1.8 ft/sec. on a $\frac{1}{2}$ H 301 stainless steel cylinder ($D = 2.50$ in., $h = .010$ in., $l = 10$ in.). This test was qualitative in nature and no measurements of strain were made. The buckle pattern that was present in the specimen after the test was very well formed and consisted of eight circumferential waves. The pattern went around the entire circumference and exhibited three rows of triangular buckles having an aspect ratio of about one. Other experiments of a more quantitative nature must be conducted to study the response of shells to impacts at such low velocity in more detail, but the test described seems to bear out prediction no. 4 to some degree.

Initial Buckling Configuration

High speed motion pictures were examined to study the initial buckling configuration. It was found that the initial deformation, which occurred almost immediately after impact, was rather axially symmetric over a very small axial length. Examination of the shell ($r/h = 356$) impacted at 46 ft/sec. (discussed previously) after the test showed that about .080 in. of the shell at the impacted end had bent through an angle of 90° into the cross section plane. This was followed by buckling in the triangular form. Another example in which the initial buckling mode was symmetrical is given in the sequence of photographs in fig. 24. The photographs show the behavior of a stainless steel cylinder ($D = 5.70$ in.,

$h = .019$ in., $l = 22.8$ in.) impacted at 23 ft/sec. The pictures begin shortly after impact and show buckling initiating in the symmetrical form (plate 1). This buckle progresses through full collapse in one wave length. As full collapse is almost complete, the circular cross section at the rear end of the buckle changes into a polygon (plate 2). The probable reason for this is that a state of circumferential compression exists at the rear of the buckle due to radial inward displacement of the shell wall. As the inward radial displacement increases and with it the magnitude of circumferential compression, the circular section snaps into the shape of a polygon; thereby generating deformations of the quasi-inextensional form. Thereafter the triangular planes continue to rotate inward (plate 3) until they are almost in the cross section plane, at which time another row of triangular buckles are formed (plates 4, 5). The process continues as these latter buckles rotate into the cross section plane (plate 6).

It has been observed that formation of the initial symmetrical buckling is more pronounced for high velocities and lower friction coefficients at the impact interface.

Symmetrical deformation appears to be the initial form of response of a cylindrical shell to an axial impact, especially when the impacted edge is held circular and the velocity is high. When the shell is sufficiently thick, as, for example, fig. 24, the symmetrical buckling deformation serves as a transition between the circular constraint and a quasi-inextensional mode which dominates the further history of buckling and collapse. If the shell is quite thick, symmetrical buckling is the dominating mode for the entire history.

If the shell is thin, the symmetrical mode, although it is initiated quickly gives way to a quasi-inextensional mode that serves as a transition to the other (but lower) quasi-inextensional mode. Once this latter mode is produced, it dominates the further history of buckling and collapse.

From experiments on thin shells ($r/h = 356 - 718$), it appears that the observed patterns in this latter mode are similar to the initial patterns anticipated by the theory described herein. The patterns have the very low aspect ratios which the theory predicts for the given strain level and the observed number of circumferential waves. In addition these patterns exhibit the large and initially rapid shortening effect predicted the theory. This will be discussed later.

Due to the presence of friction at the impact interface, the experiments have imposed a constraint of possible lateral displacements of the shell wall, even though the shell is initially unsupported. The theory on the other hand considers an edge which is totally unrestrained in the lateral direction. Due to this difference, comparison of initial patterns between experiment and theory are not possible.

On the other hand, the fact that the patterns that dominate the longer history of post buckling are similar to the prediction of the theory and that these patterns occur when buckling has progressed sufficiently away from the edge, suggests that these patterns may be those which would be generated initially if the edge were unrestrained in the experiments.

Axial Shortening of Postbuckling Pattern

This phenomenon has been observed in high speed motion pictures. An example of this is given in fig. 25 which shows a cylindrical shell ($D = 4.50$ in., $h = .004$ in.) after its bottom end has impacted on a flat rigid surface at a velocity of about 18 ft/sec. The grid lines are one inch apart. In plate A, the triangular buckle which is very elongated in the axial direction is seen. In subsequent plates the buckle shortens axially by virtue of the downward motion (toward the impacted end) of the upper vertex. At the same time, the relatively small downward motion of the cylinder against the impacted surface is evident. Considerably superior photographic results have been obtained from a recent experiment with a thin conical shell having a semi-vertex angle of 5° . These photographs, which are presently not available in published form, demonstrate clearly the shortening phenomenon. The initial rate of shortening of the buckle pattern has been measured to be greater than 1000 ft/sec for an impact velocity of only 25 ft/sec.

For thicker shells, like that shown in fig. 24, the axial shortening of triangular patterns is much less than that described above. This is to be expected since the greater flexural rigidity interferes with the formation of highly elongated buckles in axial direction. It also is instrumental in maintaining substantial axial strength of the shell even in the late stages of postbuckling. As a result the buckling and collapse of thicker shells is accompanied by significant extensional strains.

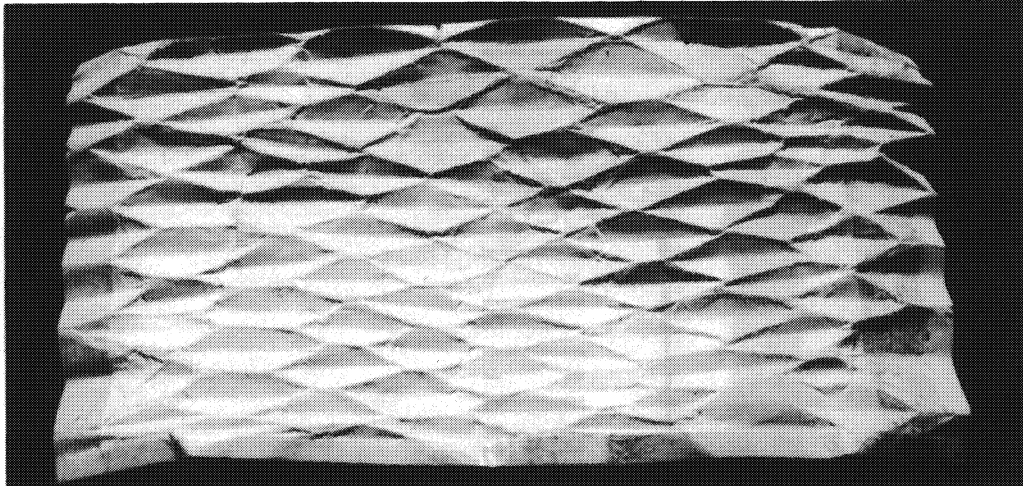
ACKNOWLEDGEMENTS

The contributions to the experimental effort made by Mr. S. A. Cimorelli, Specialist, Experimental Stress Analysis, General Electric Company, are gratefully acknowledged.

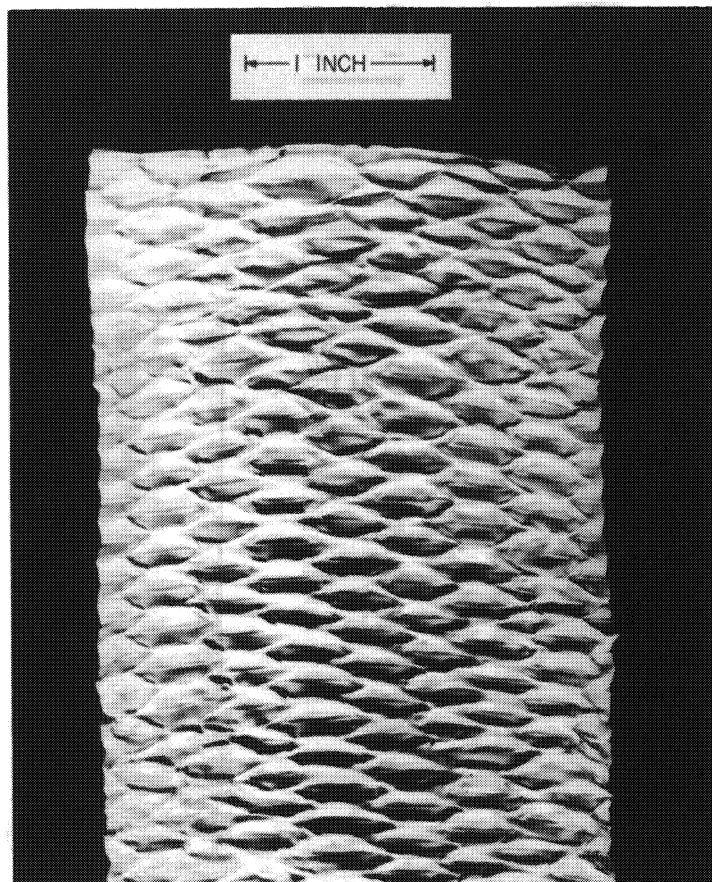
The writer also acknowledges the support of the Aeronautical Systems Division, United States Air Force, which partially sponsored the investigations.

REFERENCES

1. Coppa, A. P., "On the Mechanism of Buckling of a Circular Cylindrical Shell Under Longitudinal Impact", General Electric Company TIS Rep. No. R60SD494, presented at Tenth International Congress of Applied Mechanics, September, 1960, published in Mechanics (USSR) - Periodical Selection of Translations of Foreign Articles, No. 6, 1961.
2. Donnell, L. H., "Longitudinal Wave Transmission and Impact", Transactions of the ASME, 1930.
3. Yoshimura, Y., "On the Mechanism of Buckling of a Circular Cylindrical Shell Under Axial Compression", NACA TM 1390, July, 1955.



(a) Paper ($r/h = 190$).



(b) Aluminum ($r/h = 125$).

Figure 1.- Collapse patterns in thin cylindrical shells.

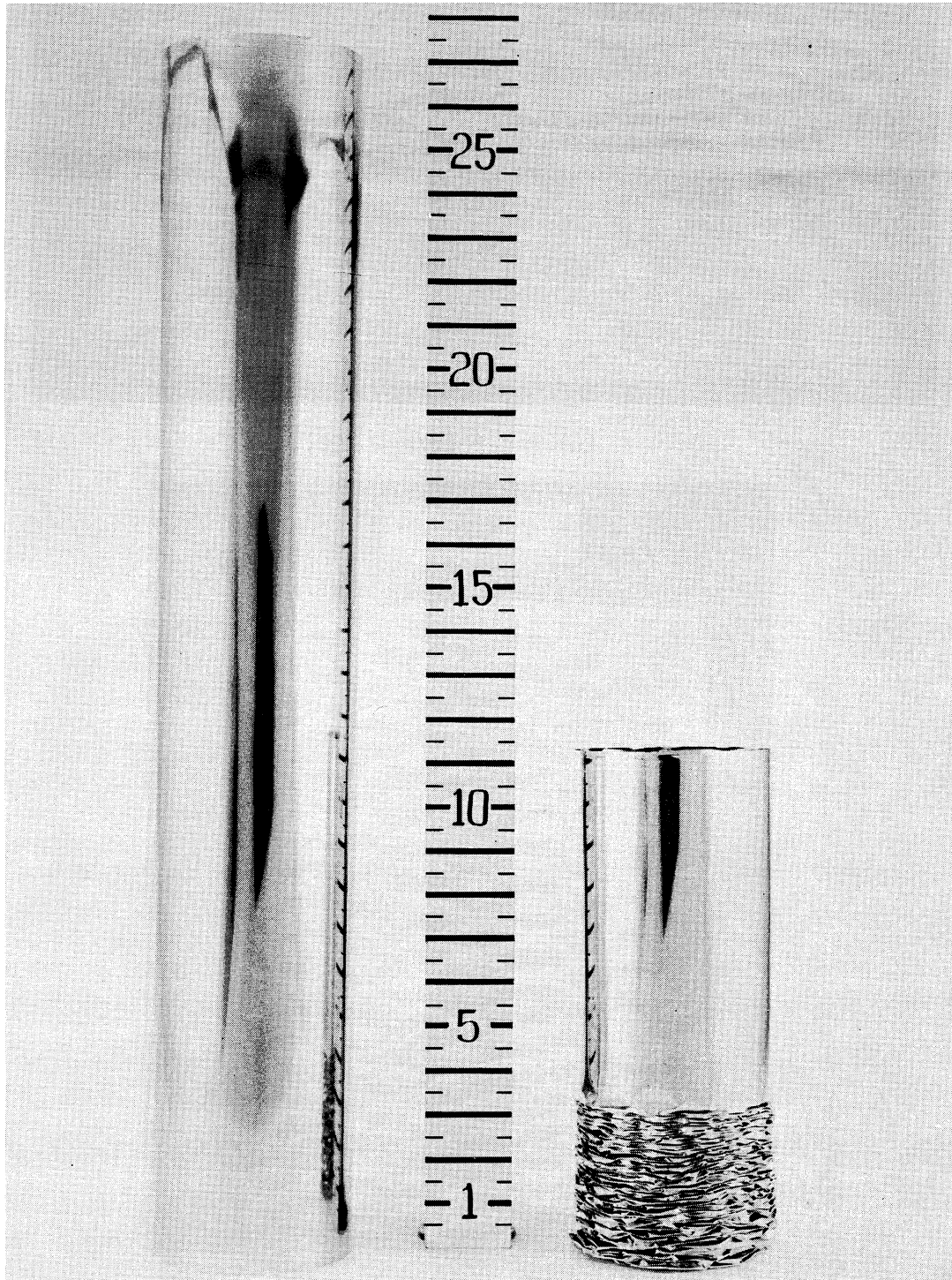


Figure 2.- Cylindrical shell before and after impact ($V_0 = 21$ ft/sec).

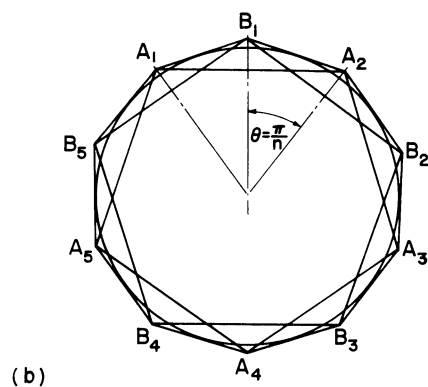
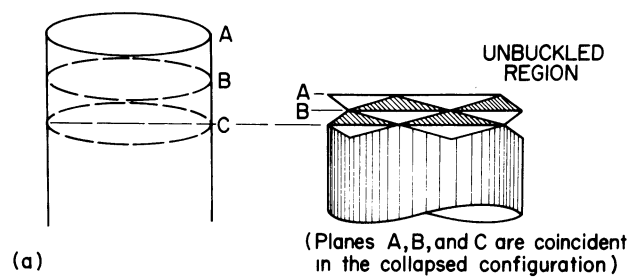


Figure 3.- Geometry of collapse - cross section.

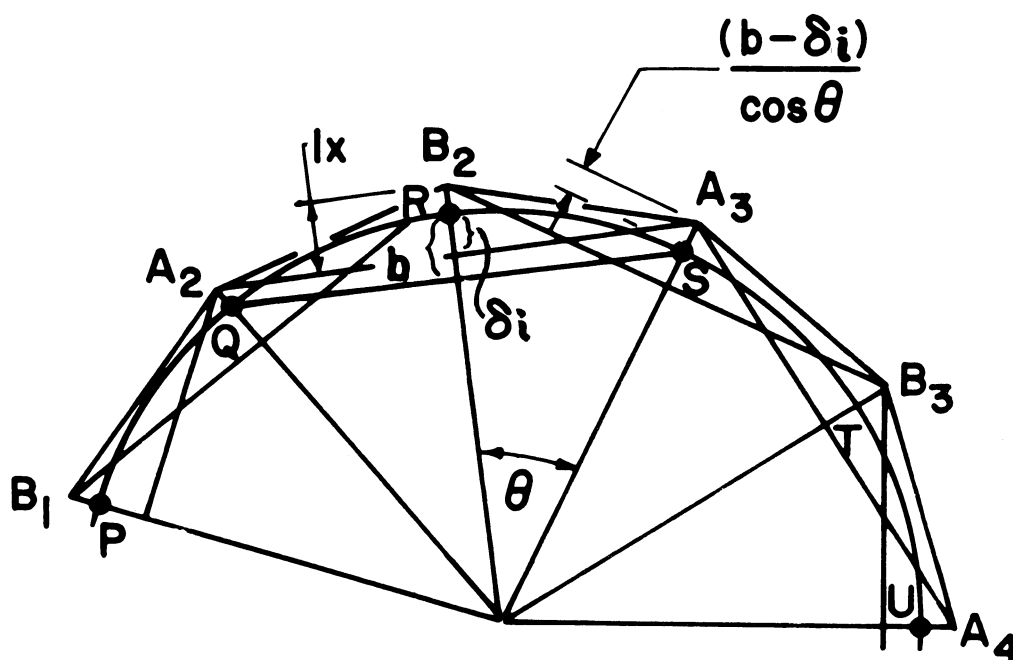


Figure 4.- Geometry of collapse - cross section.

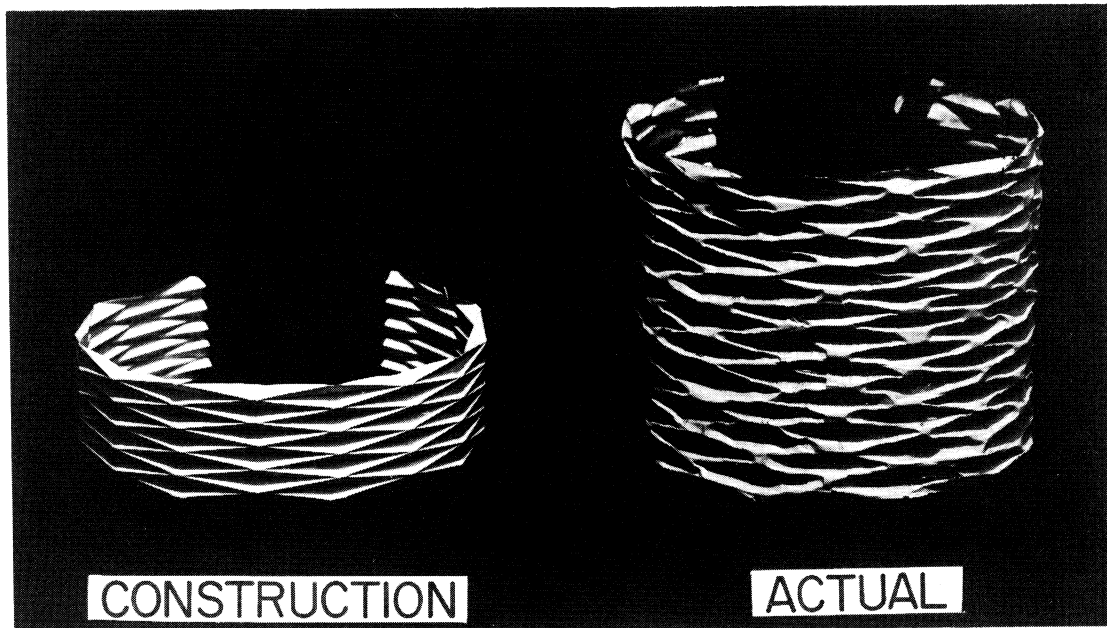


Figure 5.- Comparison of ideal inextensional and actual collapse patterns ($n = 7$).

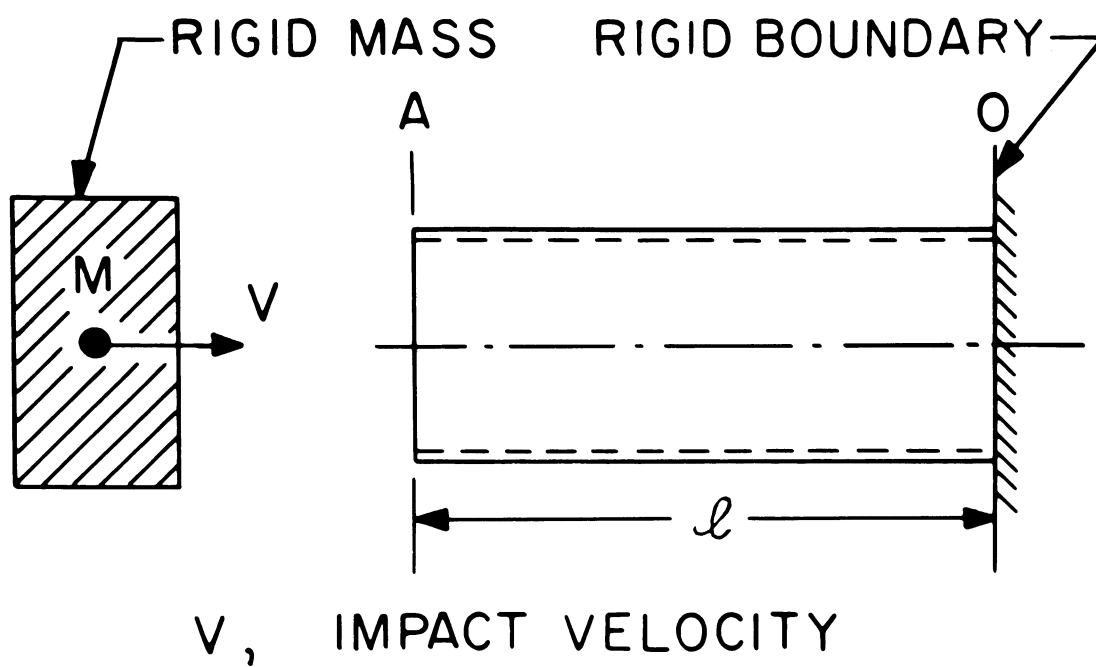


Figure 6.- Impact on a cylindrical shell.

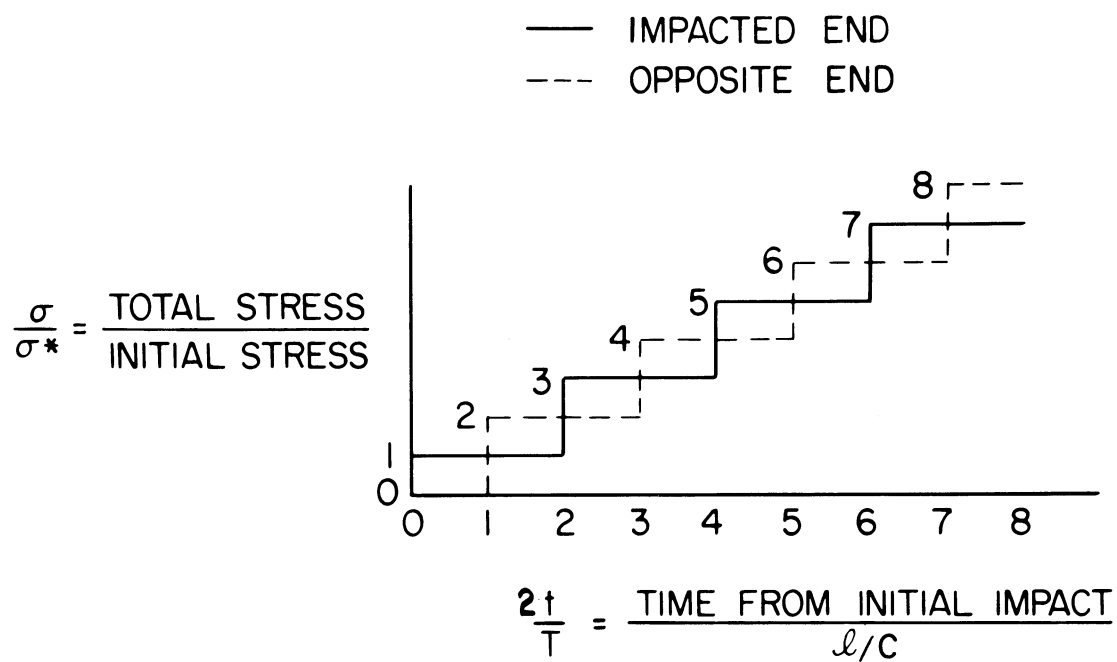


Figure 7.- Increase of stress due to reflections.

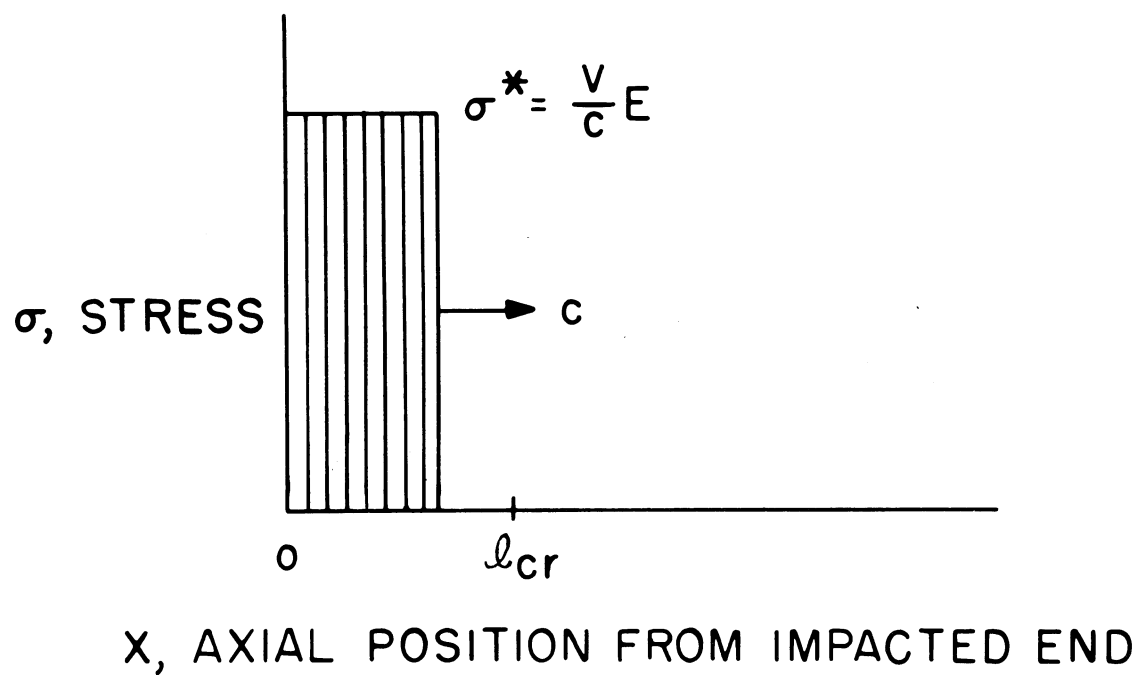


Figure 8.- Motion of the stress wave.

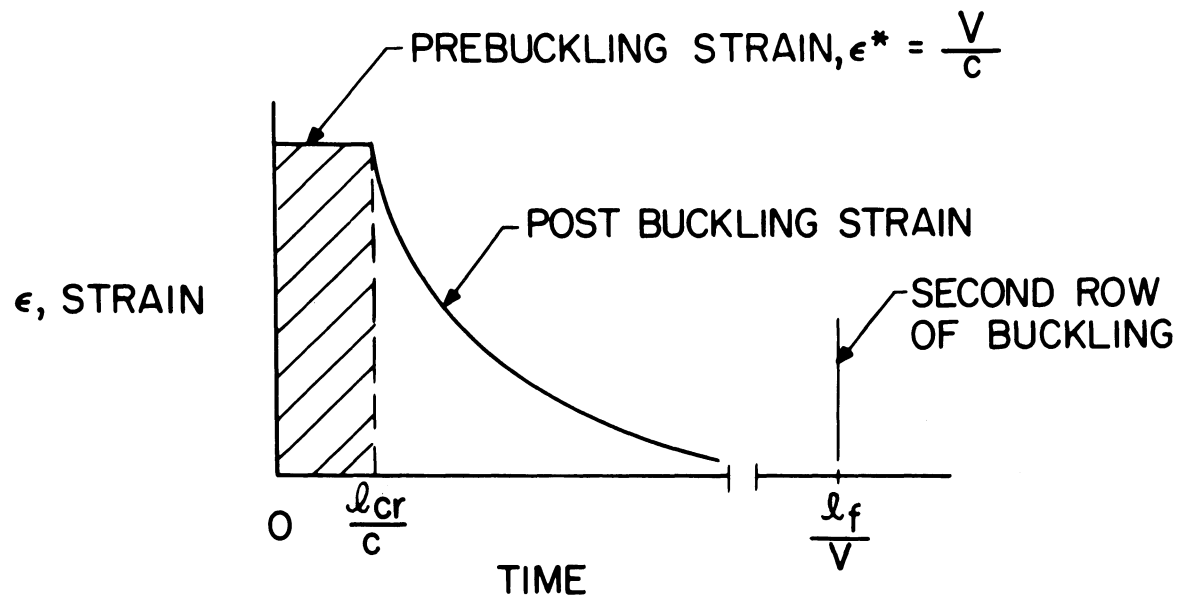


Figure 9.- Resultant axial strain in the buckling part.

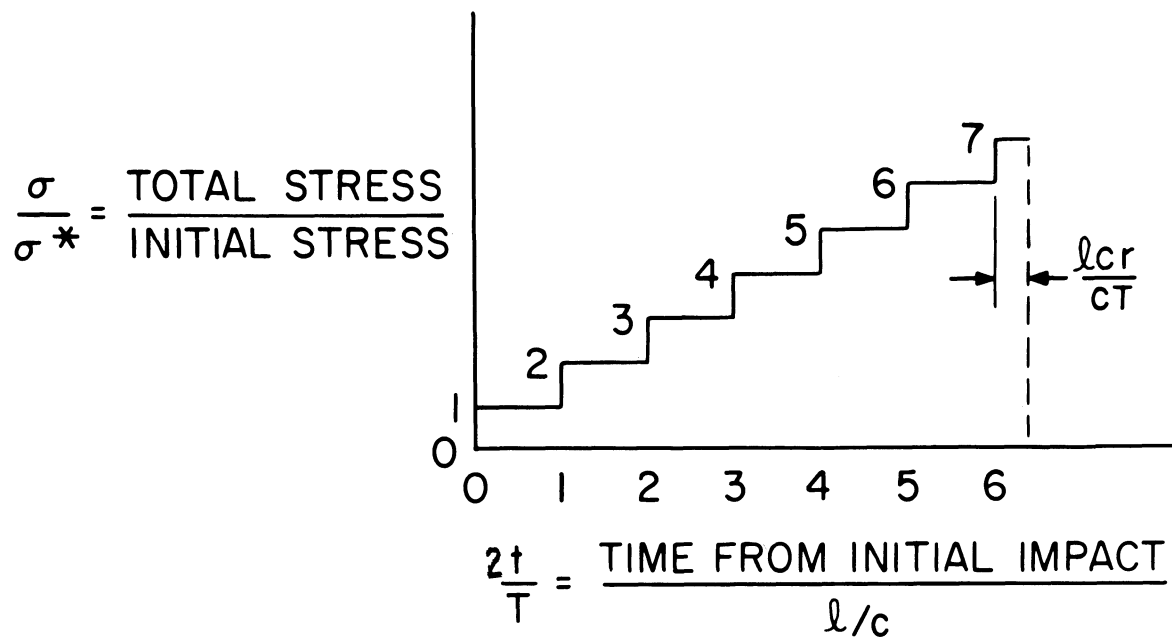


Figure 10.- Buckling resulting from reflections.

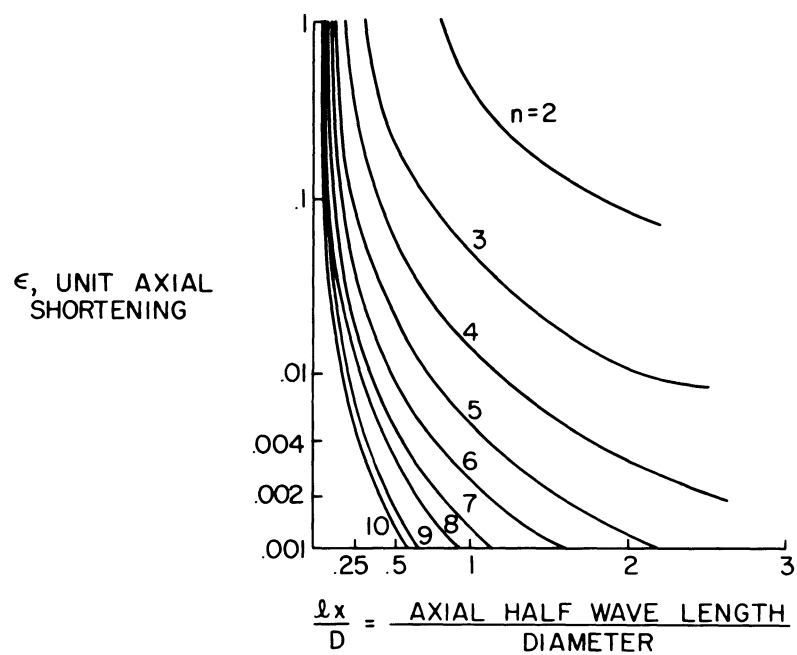
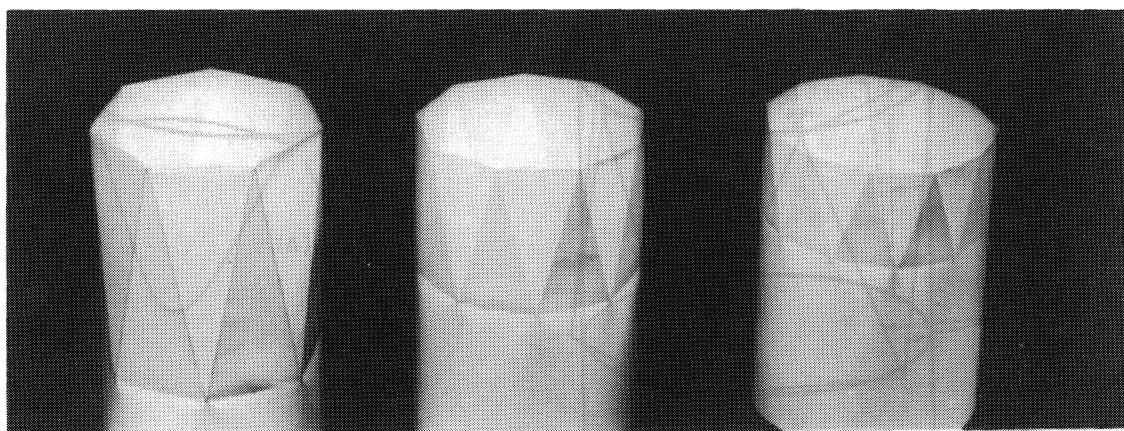


Figure 11.- Inextensional buckling configurations.



$n=7$
 $l_x=5.02$ in.

$n=9$
 $l_x=3.1$

$n=11$
 $l_x=2.06$

Figure 12.- Inextensional buckle patterns ($\epsilon = \frac{1}{1000}$).

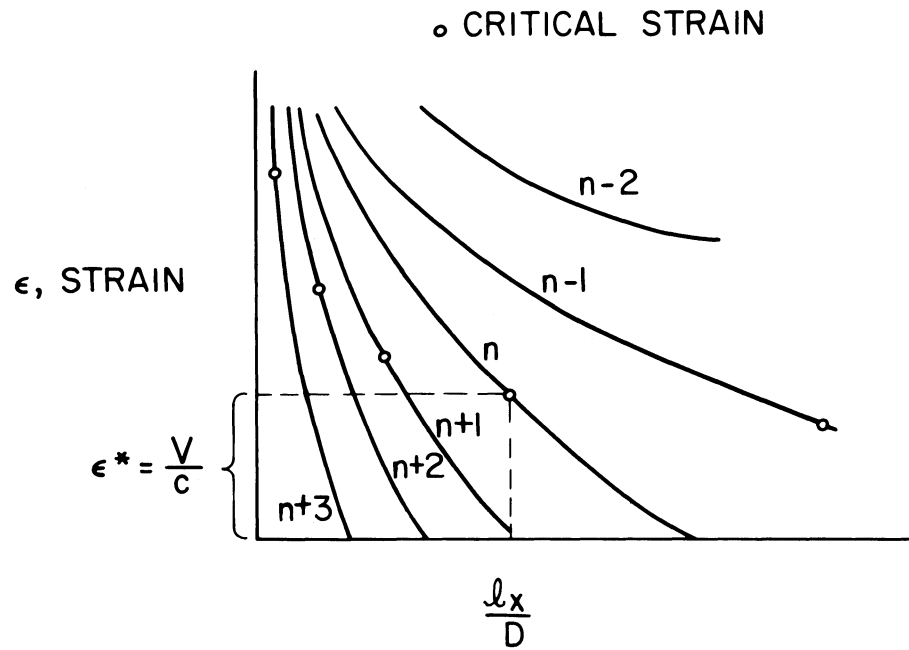


Figure 13.- Critical buckling configuration.

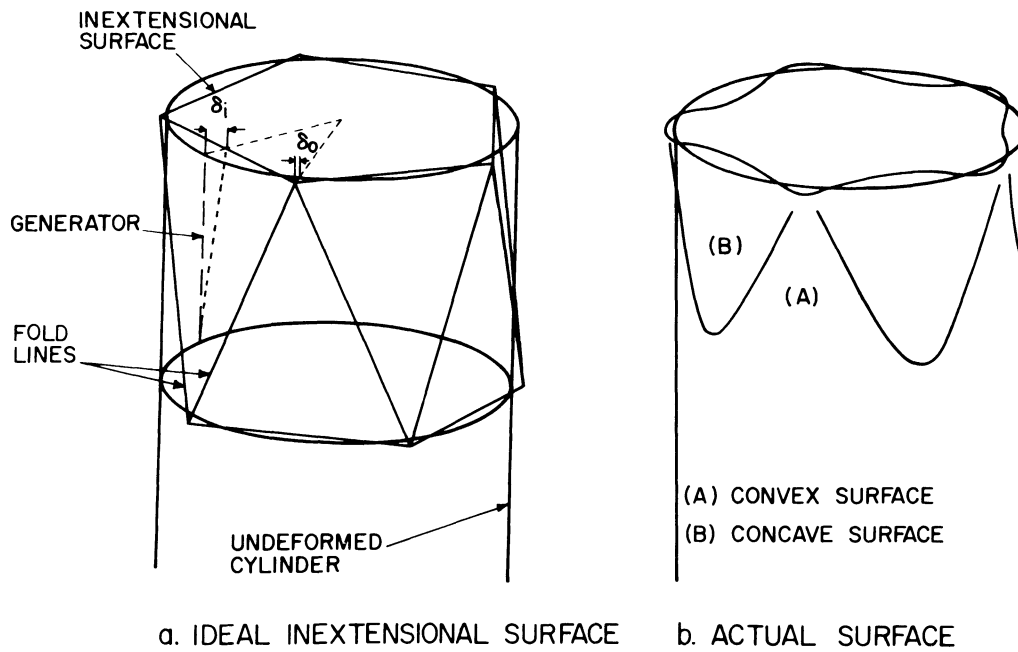


Figure 14.- Comparison of ideal and actual buckle surfaces.

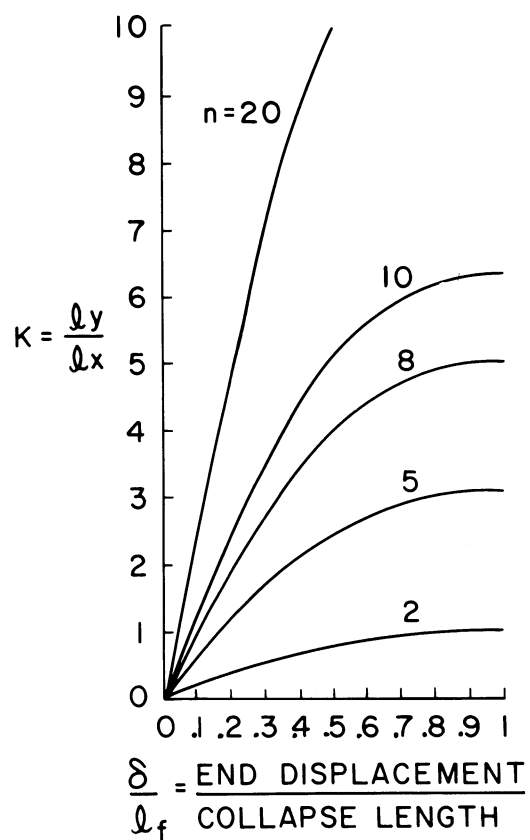


Figure 15.- Change of aspect ratio, K , during postbuckling.

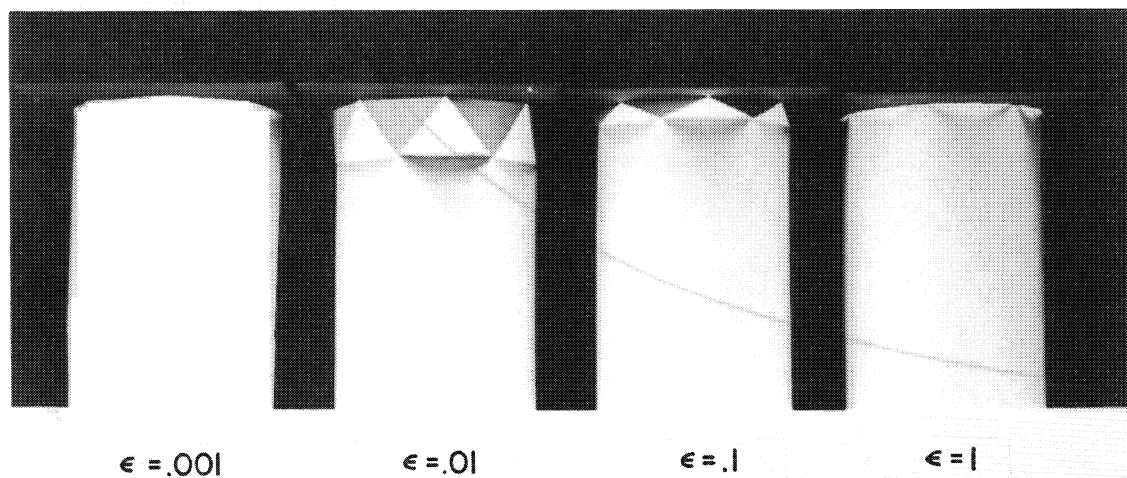


Figure 16.- Change of buckle pattern during postbuckling ($n = 7$).

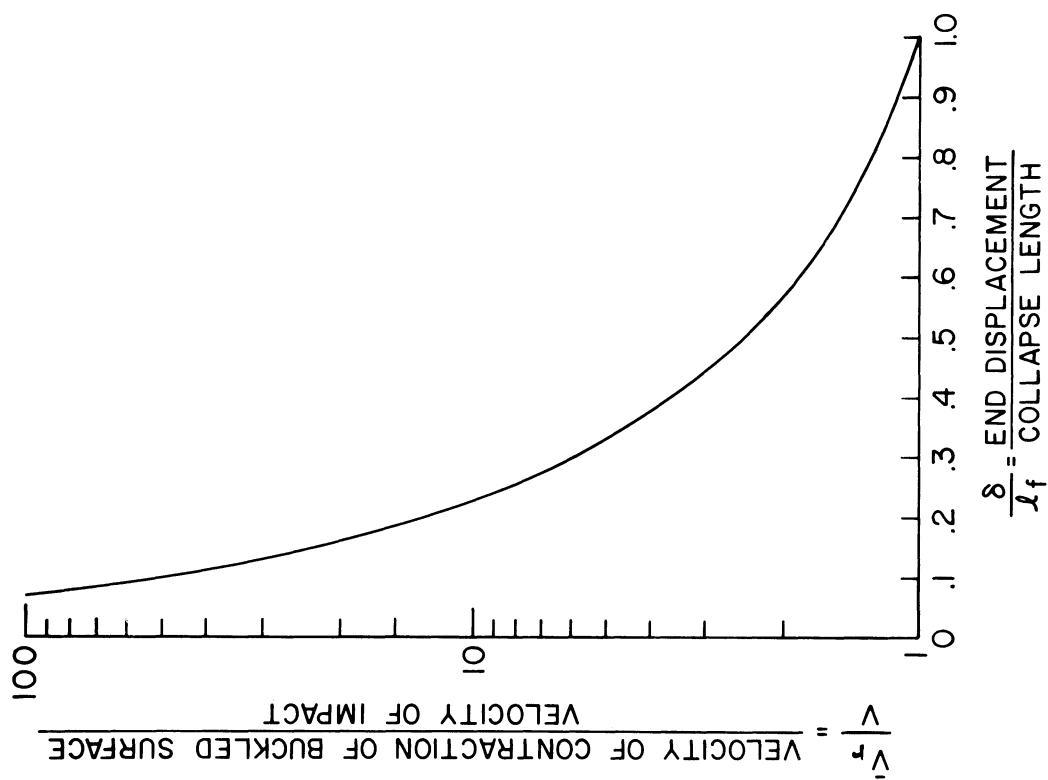


Figure 17.- Axial shortening of the buckling region vs. end displacement.

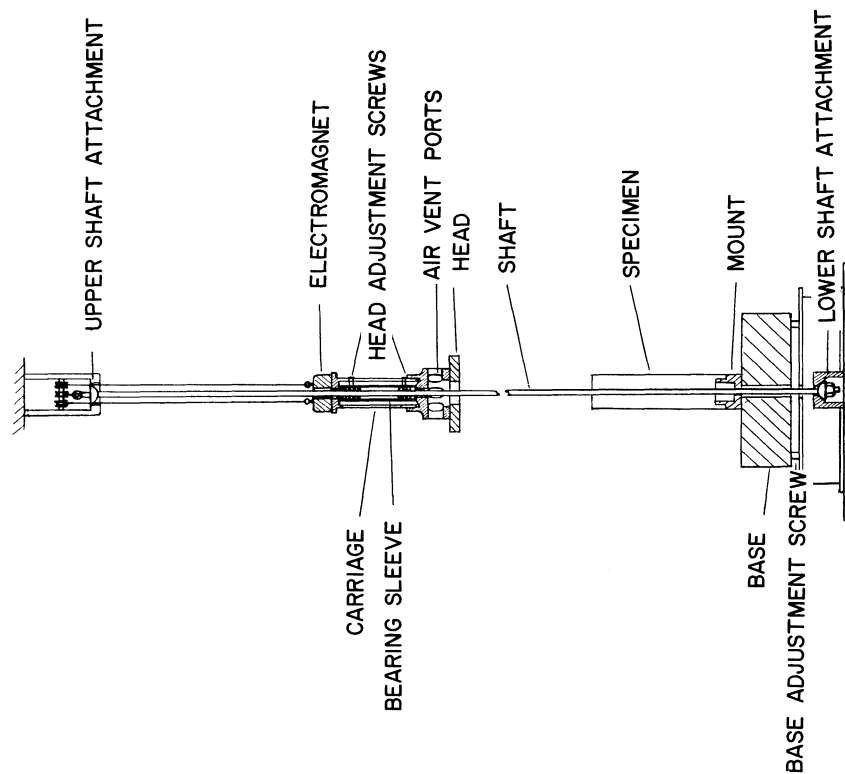


Figure 18.- Impact test apparatus.

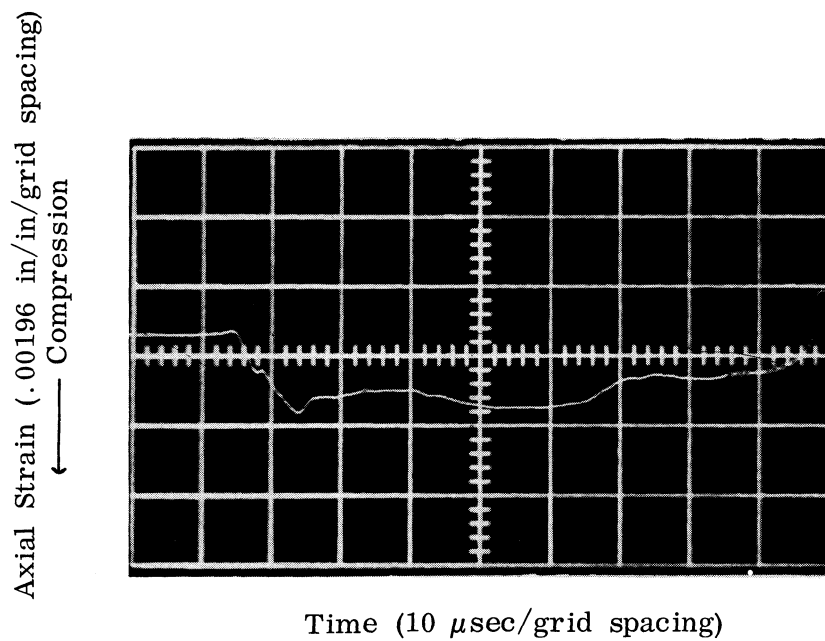


Figure 19.- Initial strain after impact ($V_0 = 46$ ft/sec).

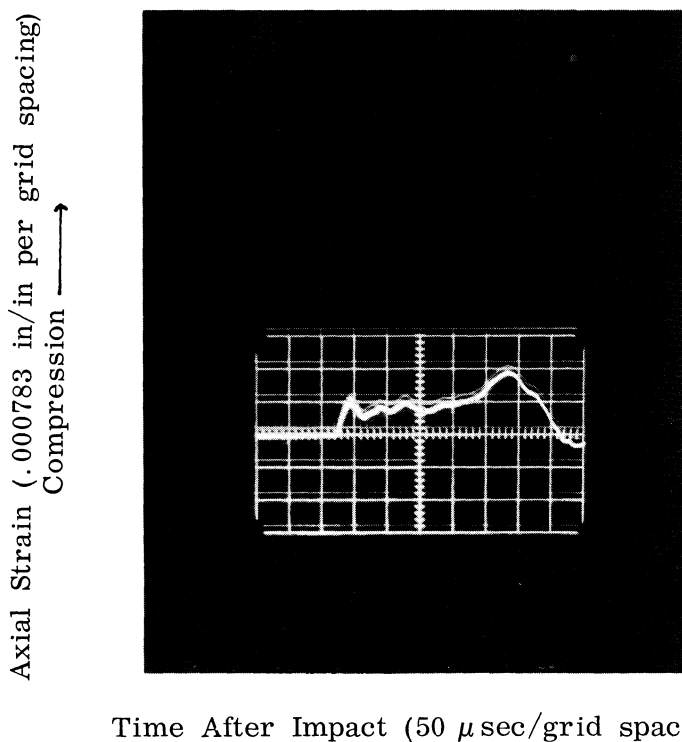


Figure 20.- Initial strain after impact ($V_0 = 11.5$ ft/sec).

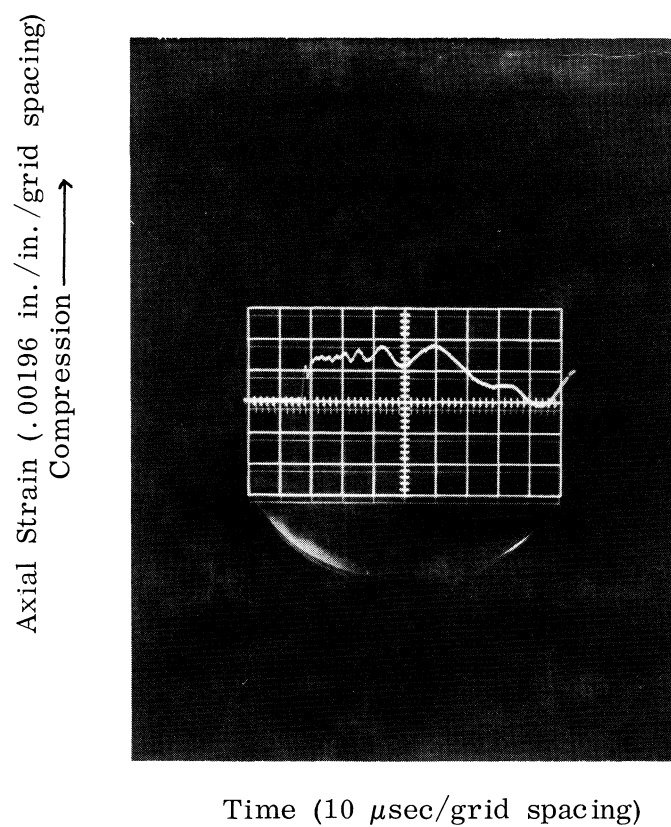
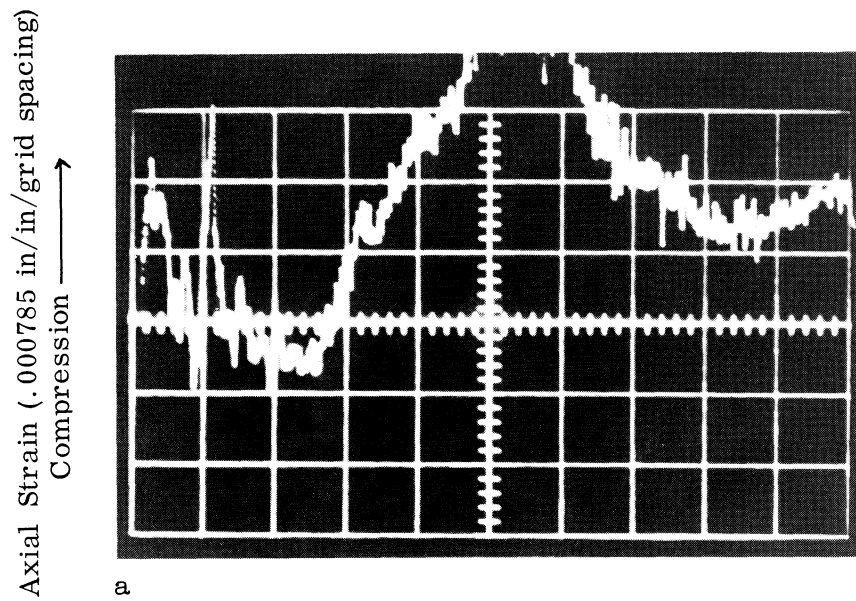
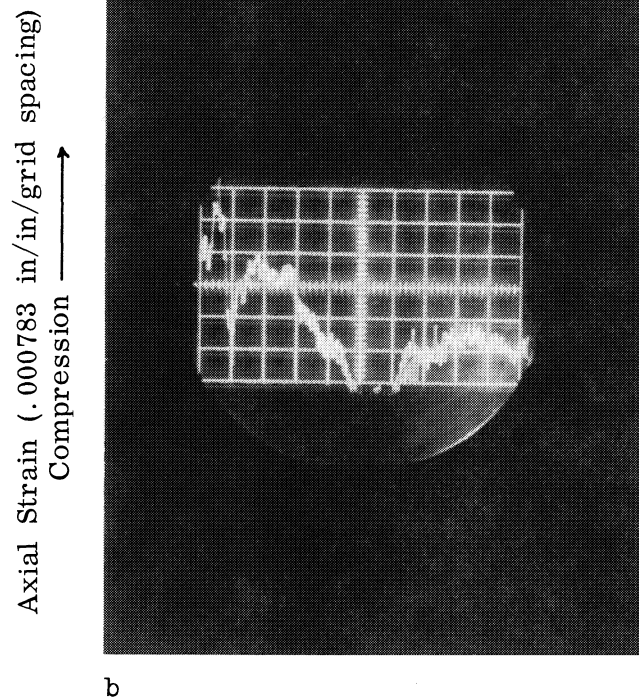


Figure 21.- Initial strain after impact ($v_o = 25$ ft/sec).



Time After Impact ($500 \mu\text{sec}/\text{grid spacing}$)



Time After Impact ($500 \mu\text{sec}/\text{grid spacing}$)

Figure 22.- Strain after impact ($V_0 = 11.5 \text{ ft/sec}$).

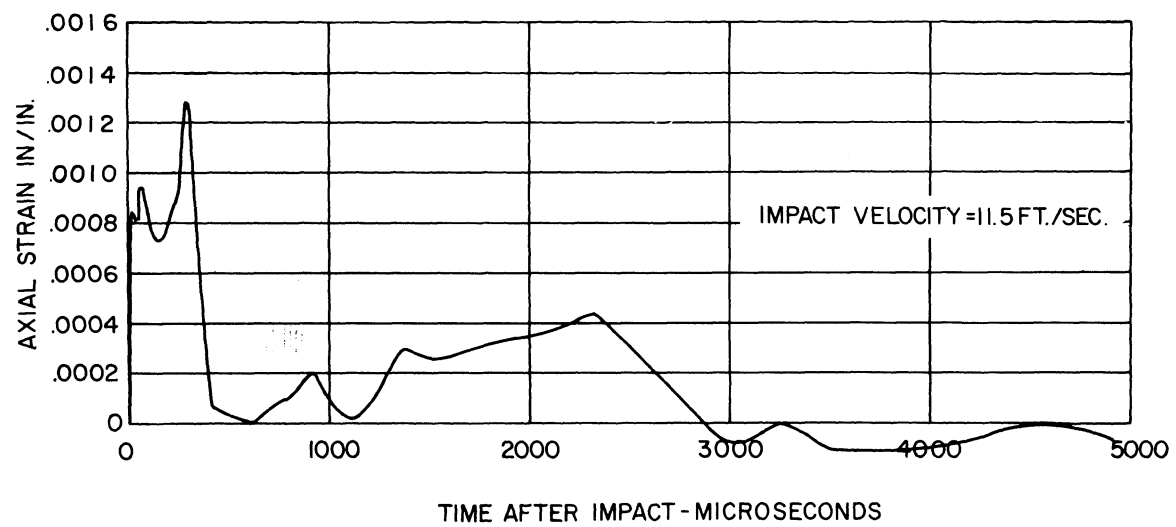


Figure 23.- Strain after impact ($V_0 = 11.5 \text{ ft/sec}$).

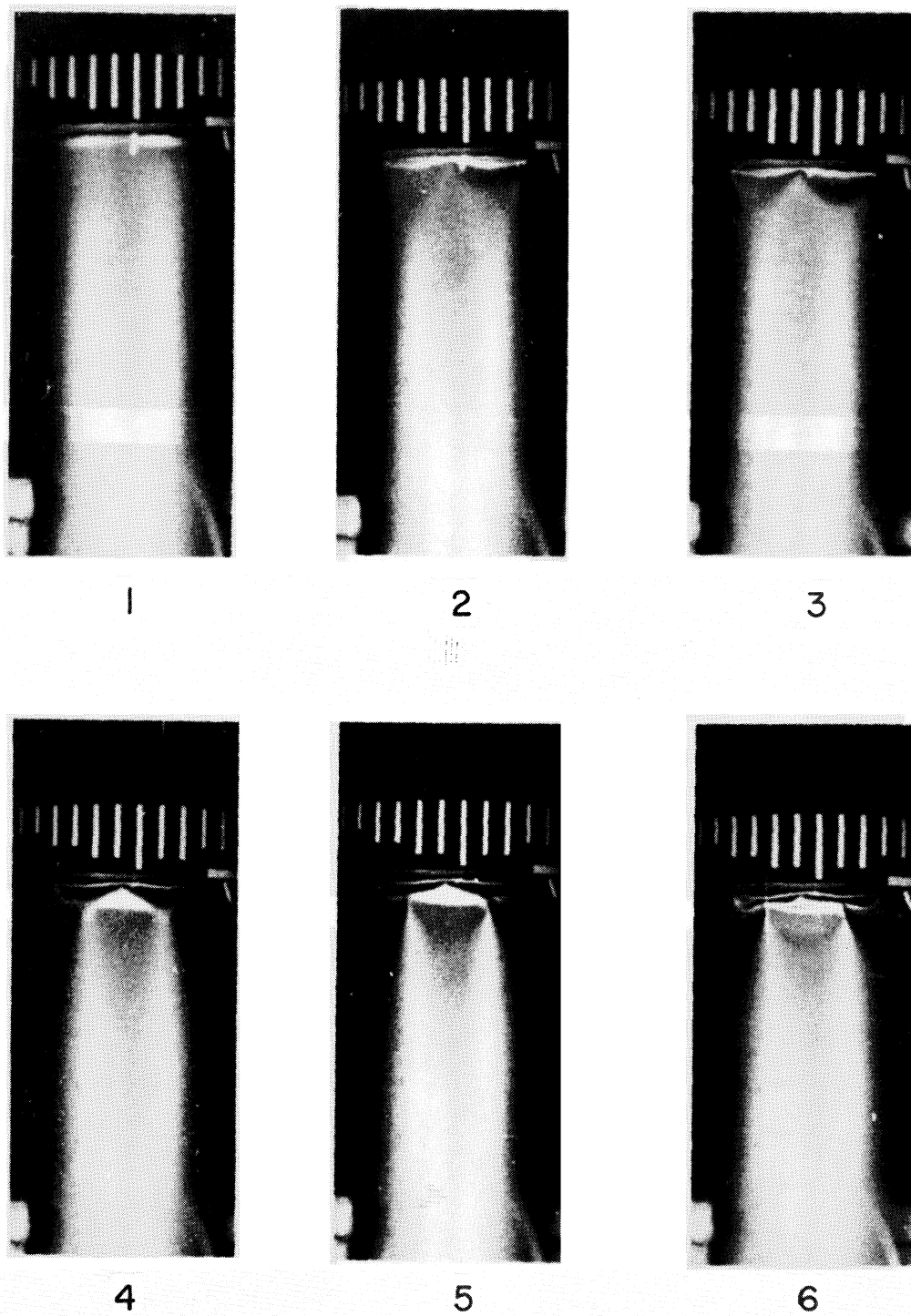


Figure 24.- Buckling sequence ($v_0 = 23$ ft/sec).

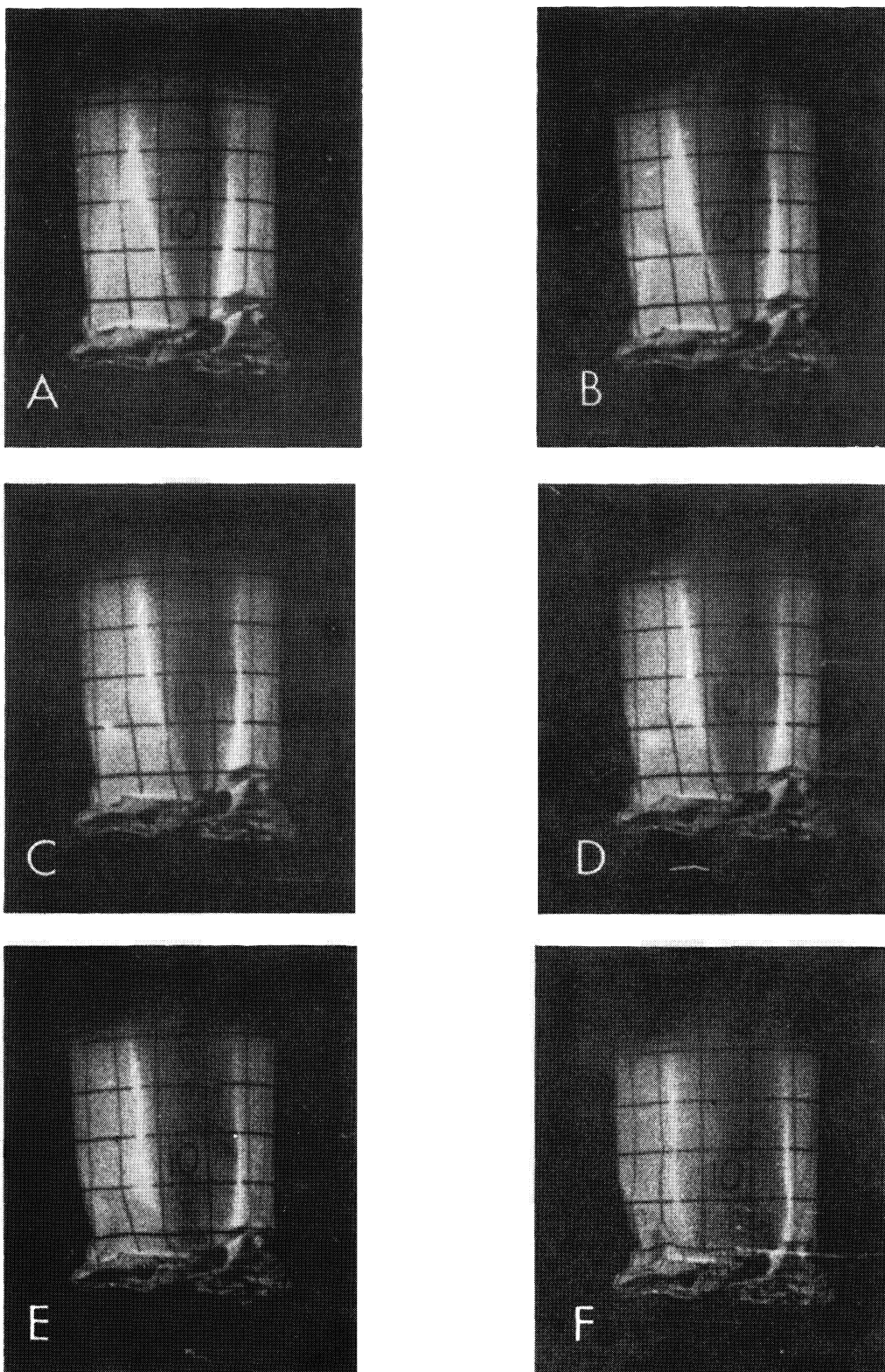


Figure 25.- Axial contraction of the buckled surface (from Fastax motion pictures).

III CONICAL SHELLS

A SURVEY OF BUCKLING THEORY AND EXPERIMENT FOR
CIRCULAR CONICAL SHELLS OF CONSTANT THICKNESS

By Paul Seide

Aerospace Corporation

SUMMARY

A survey of the state-of-the-art for the stability of thin-walled conical shells is presented. Known theoretical results are summarized and compared with experiment. The shortcomings of present knowledge and recommended work for the future are discussed.

INTRODUCTION

Only four years ago, in 1958, the state of knowledge of the elastic stability of conical shells was described (ref. 7) as being "quite unsatisfactory at the present time". In the ensuing period, however, a considerable amount of work has been done so that although not all of the desired information is available, conical shells can be designed somewhat more intelligently to withstand many of the loading conditions of interest. The purpose of the present paper is to review, as concisely as possible, the available theoretical and experimental knowledge, to indicate the gaps in the present state-of-the-art, and to suggest additional problems that should be studied.

A reasonably complete bibliography of papers on the stability of circular conical shells is included. The entries consist of those in "Bibliography on Shells and Shell-Like Structures" and the 1954-56 Supplement (both by William A. Nash*), "Structural Mechanics in the U.S.S.R., 1917-1957" (edited by I. M. Rabinovich⁺) and ref. 25, and of other papers that have come to the author's attention.

* David W. Taylor Model Basin Report 863, Nov. 1954, and Dept. of Eng. Mechanics University of Florida, Report for Office of Ordnance Research (Contract DA-01-009-ORD-404), respectively.

⁺ Translation published by Pergamon Press, 1960.

SYMBOLS

D	Bending stiffness of cone wall $\left[\frac{Et^3}{12(1-\nu^2)} \right]$
E	Young's modulus of cone material
L, ℓ	axial and slant length of cone, respectively
M	bending moment
P, P_o	applied and critical axial compressive forces, respectively.
P_{cr}	theoretical critical axial compressive force $\left[\frac{2\pi}{\sqrt{3(1-\nu^2)}} E (t \cos \alpha)^2 \right]$
P^l	axial compressive collapse force
p, p_o	applied and critical external uniform hydrostatic pressure, respectively; internal uniform hydrostatic pressure
p_{cr}	theoretical critical external uniform hydrostatic pressure
\bar{p}	theoretical critical external uniform hydrostatic pressure for "equivalent" cylinder
p^*	internal pressure parameter $\left[\sqrt{12(1-\nu^2)} \frac{p}{E} \left(\frac{R_1}{t \cos \alpha} \right)^2 \right]$
R_1, R_2	radius of small and large cone cross sections, respectively
T_{cr}	critical torque
t	cone wall thickness
α	semi-vertex angle of cone
ζ	geometry parameter $\left[\sqrt{12(1-\nu^2)} \frac{R_1}{t \cos \alpha} \cot^2 \alpha \right]$
ν	Poisson's ratio of cone material

ρ_1, ρ_{av}	cone radius of curvature at small end and center of cone generator, respectively
	$\left(R_1 / \cos \alpha, \frac{R_1 + R_2}{2 \cos \alpha} \right)$
σ_b^1 / σ_c	ratio of net compressive stress due to bending and critical axial compressive stress
	$\left(\sqrt{3(1-\nu^2)} \frac{\frac{2M}{R_1} - \pi p R_1^2}{2\pi E (t \cos \alpha)^2} = \frac{\sqrt{3(1-\nu^2)}^M}{\pi E R_1 (t \cos \alpha)^2} - \frac{1}{4} p^* \right)$
τ_{max}	maximum critical torsional stress $\left[T_{cr} / (2\pi R_1^2 t) \right]$

SMALL DEFLECTION THEORY

The only load conditions for which theoretical small deflection solutions are reasonably well established are some of those for which the stress distribution prior to buckling is independent of position around the circumference of the conical shell. The problem of the buckling of conical shells under axial compression has been studied in refs. 40 and 49. Both investigations are of the axisymmetric form of buckling and indicate that the critical axial compression load for a simply supported conical shell is given approximately by the simple formula:

$$P_{cr} = \frac{2\pi}{\sqrt{3(1-\nu^2)}} E (t \cos \alpha)^2 \quad (1)$$

a value which should be relatively good for cones with clamped edges as well. Investigation of the axisymmetric state of buckling is extended to the combined case of axial compression and internal pressure in ref. 45. The results are not given by any simple expression, but can be represented by a series of curves for the variation of an axial load parameter as a function of a pressure parameter for various values of a geometry parameter for the small end of the cone. The results are not very dependent on cone length, but do depend strongly on the boundary conditions at the small end of the conical shell. Values for a particular kind of simply supported edge and a particular kind of clamped edge are shown in Fig. 1.

For other types of loading, more general modes of deformation have to be taken into account. Many sets of equations have been derived for this task, with the rigorous theory of ref. 28 at one end of the spectrum and the Donnell-type theory of refs. 23, 41 and 53 at the other. Success in obtaining reasonably accurate, but simple, solutions appears to depend, however, on the use of a high speed digital computer and a combination of luck and educated guesswork to correlate the resulting mass of data depending on at least three independent parameters. The correlation process has been carried out for simply supported conical frustums under external hydrostatic pressure in ref. 43 where the critical pressure is shown to be given approximately by the expression

$$p_{cr} \approx \bar{p} f(1 - R_1/R_2) \quad (2)$$

where \bar{p} is the critical pressure of the "equivalent" cylinder having a length equal to the slant length of the cone, a radius equal to the average radius of curvature of the cone, and the same thickness, and $f(1 - R_1/R_2)$ is given by the solid curve of Fig. 2. The pressure \bar{p} can itself be approximated by

$$\bar{p} \approx \frac{0.92 E}{\left(\frac{l}{\rho_{av}}\right) \left(\frac{\rho_{av}}{t}\right)^{5/2}} \quad (3)$$

The same problem has been studied in numerous other papers (refs. 3, 8, 9, 11, 14, 26, 27, 28, 30, 31, 32, 35, 38, 50, 55, 56 and 59) which give similar results. Some results for external pressure which varies along the generator but is uniform around the circumference are given in ref. 50 and for thermal buckling of conical shells under axisymmetric temperature distributions in ref. 52.

Investigations have also been carried out for simply supported cones under torsion (refs. 29 and 44) and combined external hydrostatic pressure and axial load (refs. 26 and 46). For the latter loading conditions, the interaction curves appear to be a function of the taper ratio $1 - R_1/R_2$ and are shown in ref. 46 to lie between the limiting curves shown in Fig. 3. For the former loading condition, an approximate expression for the critical torque is given in ref. 44 by

$$\frac{T_{cr}}{\pi D} \approx 16.2 \left(\frac{t}{L}\right)^{\frac{1}{2}} \left\{ \left[1 + \left(\frac{1 + R_2/R_1}{2}\right)^{\frac{1}{2}} - \left(\frac{2}{1 + R_2/R_1}\right)^{\frac{1}{2}} \right] \frac{R_1 \cos \alpha}{t} \right\}^{5/4} \quad (4)$$

It is obvious that much work remains to be done to complete small deformation investigations of only the loading conditions which yield axisymmetric stress distributions, let alone such asymmetric cases as pure bending. In all of the investigations, membrane theory has been used to define the stress state prior to buckling. For those cases involving internal pressure, it would be desirable to know if consideration of bending effects changes the results to any great extent, since buckling is confined to the immediate vicinity of the small end of the cone where the pre-buckling stress distribution may differ considerably from the membrane state. Large deformation investigations are known to be necessary and have been attempted in refs. 10, 37, and 39. Present knowledge of both small deflection results and test buckle patterns indicate, however, that these analyses are probably quite inaccurate, so that this area of stability theory remains to be explored.

COMPARISON OF THEORY AND EXPERIMENT

Axial Compression and Internal Pressure

As is usual for the stability of thin shells, experimental results are in qualitative, but not quantitative, agreement with theoretical results. In Fig. 4, the available experimental load coefficients (refs. 19 and 47) for conical shells in axial compression are shown as a function of the small radius of curvature-thickness ratio, together with a lower bound curve for cylinders. The agreement between theory and experiment appears to be about the same as for cylinders, possibly a little better. It would appear that the usual empirical cylinder formulas, with the substitution of the small radius of curvature of the cone for the cylinder radius, can be used to design conical shells under axial compression. More test data is needed, however, to establish the effect of cone length and to verify the conjecture that no other parameters are important.

When internal pressure is added to cones under axial compression, the critical compressive loads tend to approach those predicted theoretically. The results of refs. 4, 20, and 47 for clamped cones (see Figs. 5(a) to 5(e)) indicate, however, that discrepancies may exist between theory and experiment at all pressure levels. For low values of internal pressure these discrepancies are most likely due to the decreasing effects of initial imperfections as for cylindrical shells and parameters other than those shown should be investigated. For large values of internal pressure, the discrepancy between theory and experiment is suspected to be due to plastic yielding at the small clamped edge which makes the results fall closer to those for cones with simply supported edges. Thus, more test data is needed to establish design

curves for cones of various materials as well as for those of various geometries and end conditions.

External Pressure

Considerable test data is available in refs. 12, 13, 15, 16, 22, 34, 47, 48, 54 and 57 for cones subjected to uniform external hydrostatic pressure. While it is almost gospel that theory and experiment compare favorably for this loading condition, the comparison shown in Fig. 6 indicates that such is actually not the case for either cylinders or cones since the scatter is considerable, with experimental values ranging from 60% to 140% of the values predicted for simply supported ends. Some of the scatter is due to the fact that the end conditions are not the same for all of the test specimens, a good many being clamped rather than simply supported. Since it is known that clamping theoretically increases the critical pressure of a cylinder by 40%, it may be presumed that clamped cones will, on the average, have higher critical pressures than simply supported cones. Initial imperfections are very likely another cause of scatter since they undoubtedly differ from specimen to specimen. Still another cause of scatter is the difficulty of determining the so-called buckling load. Buckling under external pressure is not a collapse phenomenon defined by a maximum load, as is the case for axial compression, but a phenomenon usually defined by the visual perception of large skin deformations and as such, depends on the variable judgement of the observer. It is obvious, therefore, that further investigation of the problem of buckling under external pressure is required.

Axial Compression and External Pressure

For cones under combined external pressure and axial compression, some data is available in ref. 47. If the results are plotted as ratios of applied external pressure to critical external pressure and critical axial compression to critical axial compression in the absence of pressure, as in Fig. 7(a) and 7(b), the various interaction curves are seen to closely agree with the theoretical curves. Such behavior indicates that the ratio of experimental to theoretical critical compressive loads is relatively independent of pressure, a result which differs from that obtained for cylinders under combined axial compression and external pressure. Cones also exhibit an elastic phenomenon which does not appear to be obtainable for cylinders, the non-coincidence of axial buckling and collapse loads for external pressures near the critical value. As indicated in Fig. 7, cones can withstand additional axial load after buckles appear in the shell wall and continue to do so at external pressures considerably larger than the critical value. The behavior seems to depend on the semi-vertex angle of the cone. Since the axial load carrying capacity of a buckled cone can be signi-

ficant, about 40% of the critical compressive load for a 60° cone buckled at the critical external pressure, this aspect should be investigated further.

Torsion

Experiments on conical shells in torsion are reported in refs. 21 and 47. While the cone of ref. 21 did not differ enough from a cylinder to test the theory of ref. 44, the results of ref. 47 (see Table 1) indicate that the agreement between theory and experiment for cones in torsion is about as good as for cylinders in torsion. On the average the 10 clamped shell specimens buckled at about 95% of the torque predicted by the theory for simply supported conical shells, with individual specimens buckling at torques ranging from 68% to 122% of the theoretical values. Thus it would appear that eq. (4), multiplied by the same reduction factor as for cylinders, may be used to determine critical torques of cones with the same degree of confidence as for cylinders.

ADDITIONAL EXPERIMENTAL RESULTS

Some additional load conditions, for which no theoretical results are available, have been investigated experimentally in ref. 47. Although the number of tests is small, enough is available to allow some tentative conclusions to be drawn.

Pure Bending

The results for clamped conical shells in pure bending are expressed in terms of a moment coefficient

$$\frac{M}{\pi E R_1 (t \cos \alpha)^3}$$

and the ratio of the small radius of curvature to the wall thickness,

$\frac{\rho}{t}$. The moment parameter is a constant times the ratio of the maximum membrane compressive stresses due to bending and to axial compression, the reasoning being that a theoretical solution for the problem would very likely yield the same result as for cylinders, that buckling occurs when the maximum compressive stress due to bending is equal to the critical axial compressive stress. When corresponding values of the parameters are plotted (Fig. 8), the resulting chart is similar to that for cylindrical shells in bending, for which a suggested lower bound curve is also shown.

Despite the success in correlating the data, it is entirely possible that additional parameters, such as semi-vertex angle and length, may be important. In addition, the effect of the type of edge restraint should be significant. The data available is insufficient or lacking, however, to permit any decision to be made concerning these questions.

Bending and Internal Pressure

The addition of internal pressure to conical shells causes the bending moment carrying capacity to increase by a very significant amount, as is the case for cylinders. The data is given in terms of a net membrane compressive stress parameter σ_b/σ_c which is plotted in Fig. 9 as a function of a pressure parameter p^* . Elsewhere in the present compilation⁺, collapse of pressurized cylindrical shells in bending is explained in terms of collapse of cylindrical membranes and the test results are shown to fall between the limits, expressed in the notation of the present paper,

$$2 + \frac{1}{4} p^* > \frac{\sigma_b^1}{\sigma_c} > \frac{1}{4} p^* \quad (5)$$

where the lower limit corresponds to the theoretical membrane collapse load and the upper limit to a modified membrane collapse load. The same upper and lower bound lines are plotted in Fig. 9 and are seen to bound the data for cones as well. Thus, at high pressures the bending collapse of conical shells can very likely also be explained in terms of a membrane collapse theory.

For cylinders, a good lower bound to the available data is shown in the cited paper to be given for the entire pressure range, by

$$\frac{\sigma_b^1}{\sigma_c} = \frac{1}{2} + \frac{1}{4} p^* \quad (6)$$

This does not, however, appear to suffice for conical shells since results for some of the specimens lie below this bound, closer to the membrane collapse moment. For pressurized cones in the intermediate range of pressure values, therefore, additional testing is needed to establish important parameters and values of collapse moments suitable for design purposes.

⁺ McComb, Harvey, G., Jr, Zender, George W., and Mikulas, Martin M., Jr.: The Membrane Approach to Bending Instability of Pressurized Cylindrical Shells.

Bending, Axial Compression, and Internal Pressure

The final set of data is for a single 30° conical shell subjected to combined bending, axial compression, and internal pressure. The results, are shown in Fig. 10 in the form of combined values of the moment divided by the critical moment for no net axial force at the small end and the net axial force at the small end divided by the critical net axial force for no moment. The data for zero internal pressure and two other values of pressure indicate that there is a single interaction relation between three loads which is very similar in appearance to that obtained theoretically for combined axial compression and uniform external hydrostatic pressure. When the net axial force is compressive, this relation may be approximated by

$$\frac{M}{M_{(P-\pi p R_1^2 = 0)}} + \frac{P - \pi p R_1^2}{(P - \pi p R_1^2)_{M=0}} = 1 \quad (7)$$

More data is needed, of course, to firmly establish this relationship and to indicate other parameters that may be significant for other cone geometries.

CONCLUDING REMARKS

Although a good deal of territory has been covered in trying to establish design and analysis criteria for the buckling of conical shells, the number of unanswered and bypassed questions is still considerable. Many elastic small deflection problems remain to be investigated as well as large deformation and plastic stability problems which appear to be necessary for our understanding of the experimental results for several loading conditions. The large number of parameters in all of the problems makes it necessary for theory and experiment to proceed together. Thus far the theory has been necessary to provide correlation parameters for the experimental data. In many of the problems that should be considered, however, the theoretician will need experimental data to guide him in making his analyses.

BIBLIOGRAPHY ON STABILITY OF CIRCULAR CONICAL SHELLS

1. Alfutov, N. A.: Stability of Reinforced Cylindrical and Conical Shells Loaded by External Pressure. Avtoref. Kand. diss., Mosk. vyssh. tekhn. uch., 1956.
2. Alfutov, N. A., and Razumeyev, V. F.: Dynamic Stability of a Conical Shell Supported at One Edge and Subjected to Axially Symmetric Pressure. Izv. Akad. Nauk SSSR, otdel. tekhn. nauk, no. 10, 1955.
3. Bijlaard, P. P.: Critical External Pressure of Conical Shells that are Simply Supported at the Edges. Bell Aircraft Corp., Technical Report No. 02-941-027, February 1953.
4. Brown, J. K., and Rea, R. H.: The Elastic Stability of Thin-Walled Pressurized Conical Shells under Compression and Compression-Bending Interaction. M.S. Thesis, Institute of Technology (Air University) Wright-Patterson Air Force Base. August 1960.
5. Dill, E. H.: General Theory of Large Deflections of Thin Shells with Special Applications to Conical Shells. NASA TN D-826, March 1961.
6. Esslinger, M.: Über das Ausbeulen von Kegelschalen. Der Stahlbau (Supplement to Bautechnik), Berlin, vol. 22, no. 11, 1953, pp. 254-257.
7. Fung, Y. C., and Sechler, E. E.: Instability of Thin Elastic Shells. Structural Mechanics, Pergamon Press, 1960, pp. 115-168.
8. Grigolyuk, E. I.: The Elastic Stability of Orthotropic and Layered Conical and Cylindrical Shells. Gosizdaten Structures and Architecture, collection "Space Systems", vol. 3, 1953.
9. Grigolyuk, E. I.: On the Stability of a Closed Two-Layered Conical Shell Subjected to Uniform Normal Pressure. Inzhenerny Sbornik, vol. 19, 1954, pp. 73-82. (Also available in English as David W. Taylor Model Basin Translation 265, March 1956).
10. Grigolyuk, E. I.: Loss of Stability in the Case of Finite Deflections of a Closed Laminated Conical Shell Subject to the Action of Uniform Pressure Normal to the Surface. Inzh. Sb, vol. 22, Moscow, izd. Akad. Nauk. SSSR, 1955.

11. Hakansson, A.: Calculation of Cylindrical and Conical Shells Under External Overpressures. Teknisk Tidskrift, Stockholm, Sweden, vol. 81, no. 13, 1951, pp. 261-263.
12. Harris, L. A., and Whinery, R. O.: Buckling of Conical Shells Under Uniform External Pressure. North American Aviation Inc., Structures Technical Report no. 28, October 1955.
13. Harris, W. F., and Leyland, J.: The Strength of Conical Vessels Subject to External Pressure. Transactions of the Institute of Chemical Engineers, vol. 30, 1952.
14. Hoff, N. J., and Singer, J.: Buckling of Circular Conical Shells Under External Pressure. Proceedings of the IUTAM Symposium on the Theory of Thin Elastic Shells, Delft, Holland, Aug. 24-28, 1959, North-Holland Publishing Co., Amsterdam, 1960, pp. 389-414.
15. Homewood, R.H., Brine, A. C., and Johnson, A. E.: Buckling Instability of Monocoque Shells. AVCO Technical Report RAD-TR-9-59-20, August 1959.
16. Jordan, William D.: Buckling of Thin Conical Shells under Uniform External Pressure. Technical Report, Bureau of Engineering Research, College of Engineering, University of Alabama, February 1955.
17. Kempner, Joseph: Stability Equations for Conical Shells. Journal of the Aeronautical Science, vol. 25, no. 2, February 1958, pp. 137-138.
18. Kurzweil, A. C.: The Bending and Buckling of Shells with Special Reference to Truncated Cones. Ph.D Dissertation, Stanford University, 1939.
19. Lackman, L. and Penzien, J.: Buckling of Circular Cones Under Axial Compression, Jour. Appl. Mech., vol. 27, no. 3, Sept. 1960, pp. 458-460.
20. Lofblad, R. P.: Stability of Thin-Walled Cylinders and Cones with Internal Pressure under Axial Compression. Massachusetts Institute of Technology, Technical Report No. 25-29, May 1959.
21. Lundquist, E. E., and Schuette, E. H.: Strength Tests of Thin-Walled Truncated Cones of Circular Section. NACA WR L-442, December 1942.

22. Magula, A. W.: Structural Test-Conical Head Assembly, Test No. 815. North American Aviation, Inc., Downey, Missile Test Lab. Report MTL-531, 1954.
23. Mushtari, Kh. M.: Some Generalizations of the Theory of Thin Shells with Applications to the Analysis of Problems of the Stability of Elastic Equilibrium. *Prikladnaya Matematika i Mekhanika*, Moscow, vol. 2, no. 4, 1939, pp. 439-456.
24. Mushtari, Kh. M.: The Approximate Solution of Certain Problems of Stability of a Thin-Walled Conic Shell with a Circular Cross Section. *Prikladnaya Matematika i Mekhanika*, vol. 7, no. 3, 1943, pp. 155-166.
25. Mushtari, Kh. M., and Galimov, K. Z.: Non-Linear Theory of Thin Elastic Shells. Academy of Sciences, USSR, Kazan Branch, 1957, pp. 287-307. (Translated and available as NASA-TT-F62, 1961).
26. Mushtari, Kh. M. and Sachenkov, A. V.: Stability of Cylindrical and Conical Shells of Circular Cross Section, with Simultaneous Action of Axial Compression and External Normal Pressure. *Prikladnaya Matematika i Mekhanika*, vol. 18, no. 6, November-December 1954, pp. 667-674. (Also available in English as NACA TM 1433, April 1958).
27. Niordson, F. I. N.: Buckling of Conical Shells Subjected to Uniform External Lateral Pressure. *Transactions of the Royal Institute of Technology*, Stockholm, Sweden, no. 10, 1947, pp. 1-21.
28. Pflüger, A.: Stabilität dünner Kegelschalen. *Ingenieur Archiv*, vol. 13, no. 2, 1942, pp. 59-72.
29. Pflüger, A.: Zur Stabilität der dünnen Kegelschale. *Ingenieur Archiv*, vol. 13, no. 2, 1942, pp. 59-72.
30. Pittner, E. V., and Morton, F. G.: Stress and Stability Analysis of Cylindrical and Conical Shells, Final Report.
 - a) Volume I, An Infinitesimal-Buckling Analysis for Truncated Conical Shells Subjected to External Pressure.
 - b) Volume II, A Method of Analysis for Buckling of Monocoque Conical Shells Subjected to Hydrostatic Pressure. Lockheed Aircraft Corp., Report No. LMSD-894808, May 1961.

31. Radkowski, P. P.: The Stability of Truncated Cones. Proceedings of the Second Conference on the Mechanics of Elasticity and Plasticity, Washington D.C., Feb. 1957, pp. 121-157.
32. Radkowski, P. P.: Buckling of Thin Single- and Multi-Layer Conical and Cylindrical Shells with Rotationally Symmetric Stresses. Proceedings of the Third U. S. National Congress of Applied Mechanics, Providence, R.I., June 11-14, 1958, pp. 443-449.
33. Radkowski, P. P., and Johnson, D. R.: Buckling of Single- and Multi-Layer Conical and Cylindrical Shells Subjected to Axial Loads and Lateral Pressure. AVCO Corp., Technical Report RAD-TR-61-36, Dec. 1961.
34. Reed, G. W., and Pipes, E. J.: Structural Reliability Methods for Cylinders and Cones. Lockheed Aircraft Corp., Report no. LMSD-4507, May 1959.
35. Ryayamet, R. K.: Stable Equilibrium of Elastic Conical Shells Subjected to Uniformly Distributed External Pressure. Trud. Tallinsk. Politekh. Inst., no. 65, 1955.
36. Sachenkov, A. V.: Some Problems of the Stability of Conical Shells Within the Elastic Limit. Avtoref. Kand. Diss., Mosk. Aviats. Inst., 1954.
37. Sachenkov, A. V.: Approximate Determination of the Lower Bounds of the Critical Loads of Thin Conical Shells Subjected to Axial Compression. Izv. Kazansk. fil. Akad. Nauk SSSR, Seriya fiz.-mat. i. tekhn. nauk, no. 7, Kazan, Tatknigoizdat, 1955.
38. Saranti, Y.: Theoretical Investigation Concerning the Collapse of Round Conical Shells by Pressure. Thesis, Kyushu Imperial University, Japan, 1942.
39. Schnell, Walter: Die Dünwandige Kegelschale unter Axial- und Innendruck. Dissertation Rheinisch-Westfälischen Technischen Hochschule, Aachen, 1960.
40. Seide, Paul: Axisymmetric Buckling of Circular Cones Under Axial Compression. Jour. Appl. Mech., vol. 23, no. 4, Dec. 1956, pp. 625-628.
41. Seide, Paul: A Donnell-Type Theory for Asymmetrical Bending and Buckling of Thin Conical Shells. Jour. Appl. Mech., vol. 24, no. 4, Dec. 1957, pp. 547-552.

42. Seide, Paul: Note on Stability Equations for Conical Shells. JAS, vol. 25, no. 5, May 1958, p. 342.
43. Seide, Paul: On the Buckling of Truncated Conical Shells Under Uniform Hydrostatic Pressure. Proc. IUTAM Symposium on the Theory of Thin Elastic Shells, Delft, Holland, Aug. 24-28, 1959, North-Holland Publishing Co., Amsterdam, Holland, 1960. pp. 363-388.
44. Seide, Paul: On the Buckling of Truncated Conical Shells in Torsion. Jour. Appl. Mech., vol. 29, no. 2, June 1962, pp. 321-328.
45. Seide, Paul: On the Stability of Internally Pressurized Conical Shells Under Axial Compression. (to be published in Proc. 4th. U.S. National Congress of Appl. Mech., University of California, Berkeley, Calif, June 18-21, 1962).
46. Seide, Paul: Calculations for the Stability of Thin Conical Frustums Subjected to External Uniform Hydrostatic Pressure and Axial Loads. (To be published in Journal of the Aero-Space Sciences).
47. Seide, Paul, Weingarten, V. I., and Morgan, E. J.: Final Report on the Development of Design Criteria for Elastic Stability of Thin Shell Structures. Space Technology Laboratories, Inc., Report No. STL/TR-60-0000-19425, EM 10-26, AFBMD/TR-61-7, Dec. 31, 1960.
48. Shroeder, F. J., Kusterer, E. T., and Hirsch, R. A.: An Experimental Determination of the Stability of Conical Shells. Aircraft Armaments, Inc., Cockeysville, Md., Report ER-1361, May 1958.
49. Shtayerman, I. Ya.: Stability of Shells. Sb. trud. Kazanak. aviats. Inst, no. 1, 1936.
50. Singer, Josef: Buckling of Circular Conical Shells under Axisymmetric External Pressure. Israel Institute of Technology, Haifa, Israel, Technical Note #1, November 1960.
51. Singer, Josef: The Effect of Axial Constraint on the Instability of Thin Conical Shells under External Pressure. Israel Institute of Technology, Haifa, Israel, Technical Note no. 2, December 1960.

52. Singer, Josef: Buckling of Thin Circular Conical Shells, Subjected to Axisymmetrical Temperature Distributions and External Pressure. Israel Institute of Technology, Haifa, Israel, Technical Note no. 3, July 1961.
53. Singer, Josef: A Donnell Type Theory for Bending and Buckling of Orthotropic Conical Shells. Israel Institute of Technology, Haifa, Israel, Technical Note no. 5, December 1961.
54. Singer, Josef, and Eckstein, Abraham: Experimental Investigations of the Instability of Conical Shells under External Pressure. The Bulletin of the Research Council of Israel, vol. 11C, no. 1, April 1962, pp. 97-122.
55. Taylor, C. E.: Elastic Stability of Conical Shells Loaded by Uniform External Pressure. Proceedings of the Third Midwestern Conference on Solid Mechanics, University of Michigan, 1958, p. 443.
56. The Staff of the Applied Mechanics Branch, Watertown Arsenal Laboratories, under the direction of Oscar L. Bowie, Burton S. Parker, Peter P. Radkowski, and Joseph I. Bluhm: A Study of the Buckling of the IRBM (Jupiter) Bulkheads. WAL 880/54, August 31, 1956.
57. Tokugawa, T.: Experiments on the Elastic Stability of a Thin-Wall Cone under Uniform Normal Pressure on All Sides, and an Approximate Method for Computing its Collapsing Pressure. Applied Mechanics League, Congress Shipbuilding Association, Japan (Zosen Kiokai), Miscellaneous Publication no. 125, 1932, pp. 151-169.
58. Tokugawa, Takesada: Approximate Method of Calculating the Collapsing Pressure of Thin Cylindrical Conical, and Spherical Shells under Uniform External Pressure. Journal of the Society of Naval Architects, Japan (Zosen Kiokai), vol. 66, 1940, pp. 231-240.
59. Trapezin, I. I.: Stability of Conical Shells Subjected to Hydrostatic Pressure. Collection "Analysis of Strength, Stiffness, Stability and Vibration", Moscow, Mashgiz, 1955.
60. Trapezin, I. I.: On the Stability of a Thin Walled Conical Shell of a Circular Section under Loads Symmetrical about its Axis. Trudy Mosk. aviats. instituta, no. 17, 1952.
61. Westmoreland, R. T.: Model Test of Conical Bulkhead, Test No. 1098. North American Aviation, Inc., Downey, Missile Test Lab. Report MTL-652, 1955.

Table 1. Comparison of Theory and Experiment for Steel Cylinders and Cones in Torsion (Ref. 47).

t (in.)	R ₁ (in.)	R ₂ (in.)	L (in.)	τ_{\max} (experimental) psi	τ_{\max} (computed) psi	$\frac{\tau_{\exp}}{\tau_{\text{comp}}}$
$\alpha = 30^\circ$						
0.010	4	10	10.39	11650	11100	1.05
0.010	4	10	10.39	11490	11100	1.03
0.020	4	10	10.39	32400	26570	1.22
0.020	4	10	10.39	23400	26570	0.88
$\alpha = 60^\circ$						
0.010	2	10	4.62	14300	21030	0.68
0.010	2	10	4.62	14300	21030	0.68
0.010	3	10	4.04	10800	12460	0.87
0.010	3	10	4.04	13600	12460	1.09
0.010	5	10	2.89	8390	7850	1.07
0.010	5	10	2.89	6900	7850	0.88

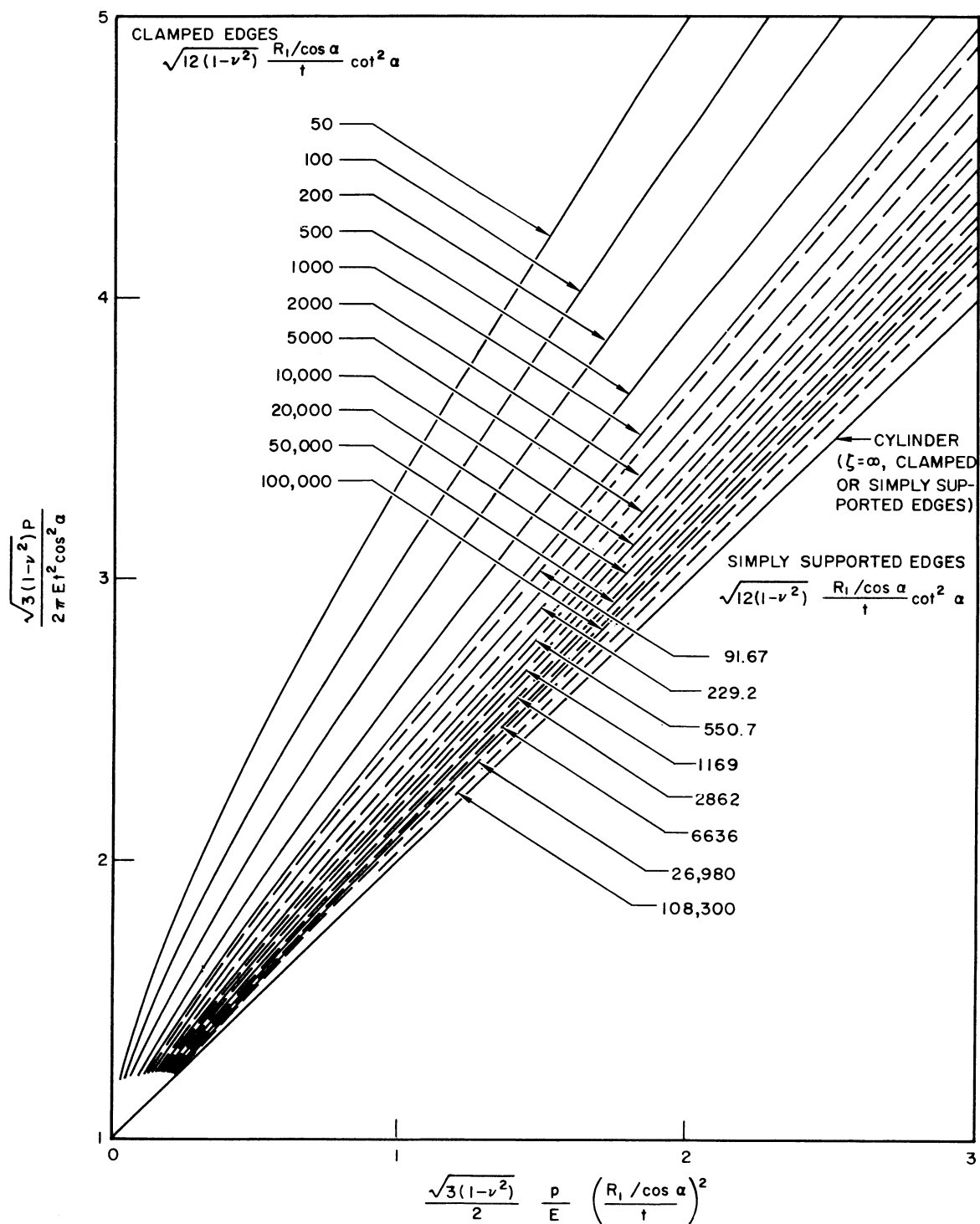


Figure 1.- Theoretical variation of axial load parameter with internal pressure parameter for conical shells with clamped or simply supported edges ($\nu = 0.3$).

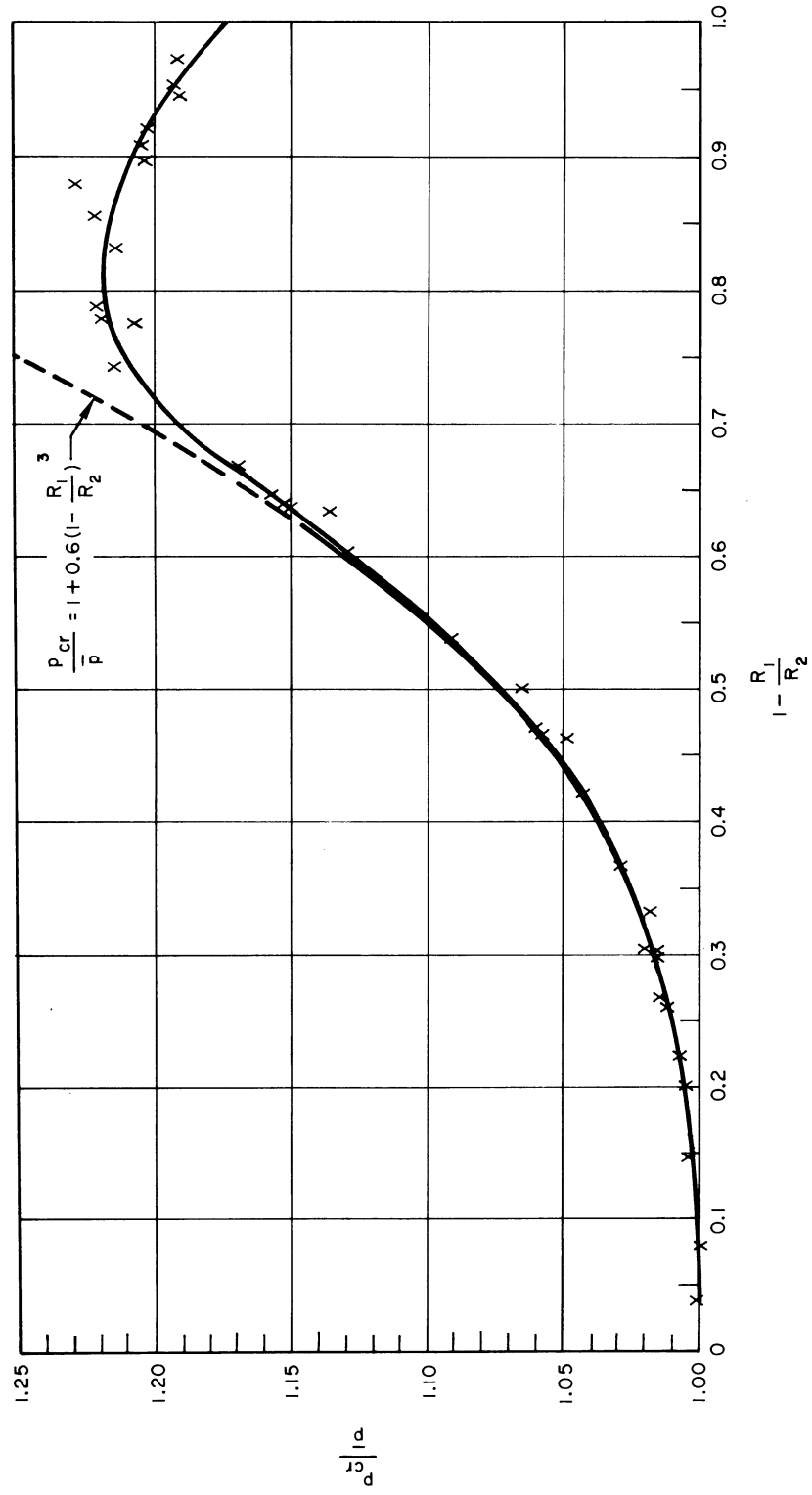


Figure 2.- Theoretical variation of buckling pressure ratio with taper ratio for simply supported cones.

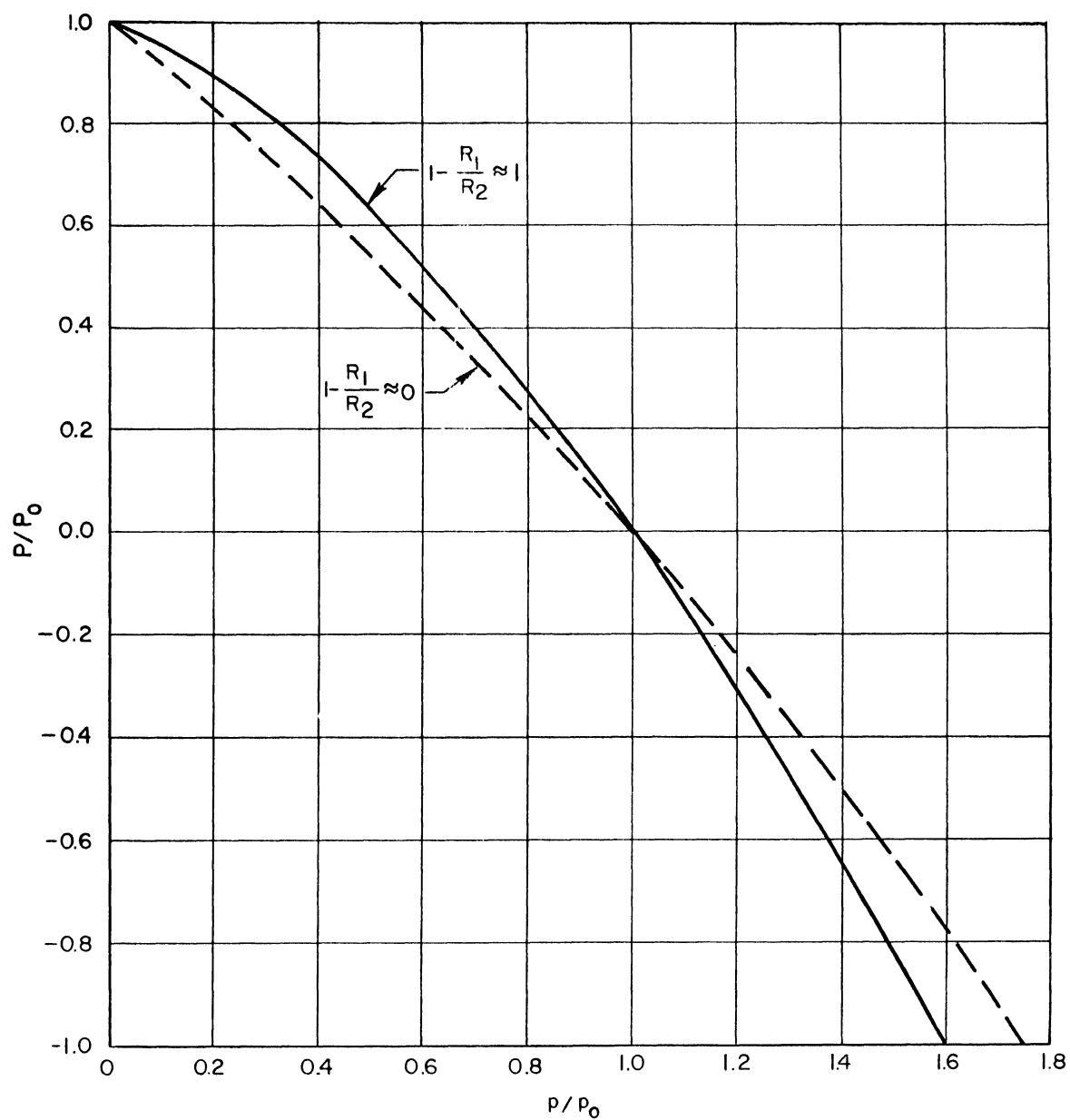


Figure 3.- Theoretical interaction curves for cones under combined axial load and external uniform hydrostatic pressure.

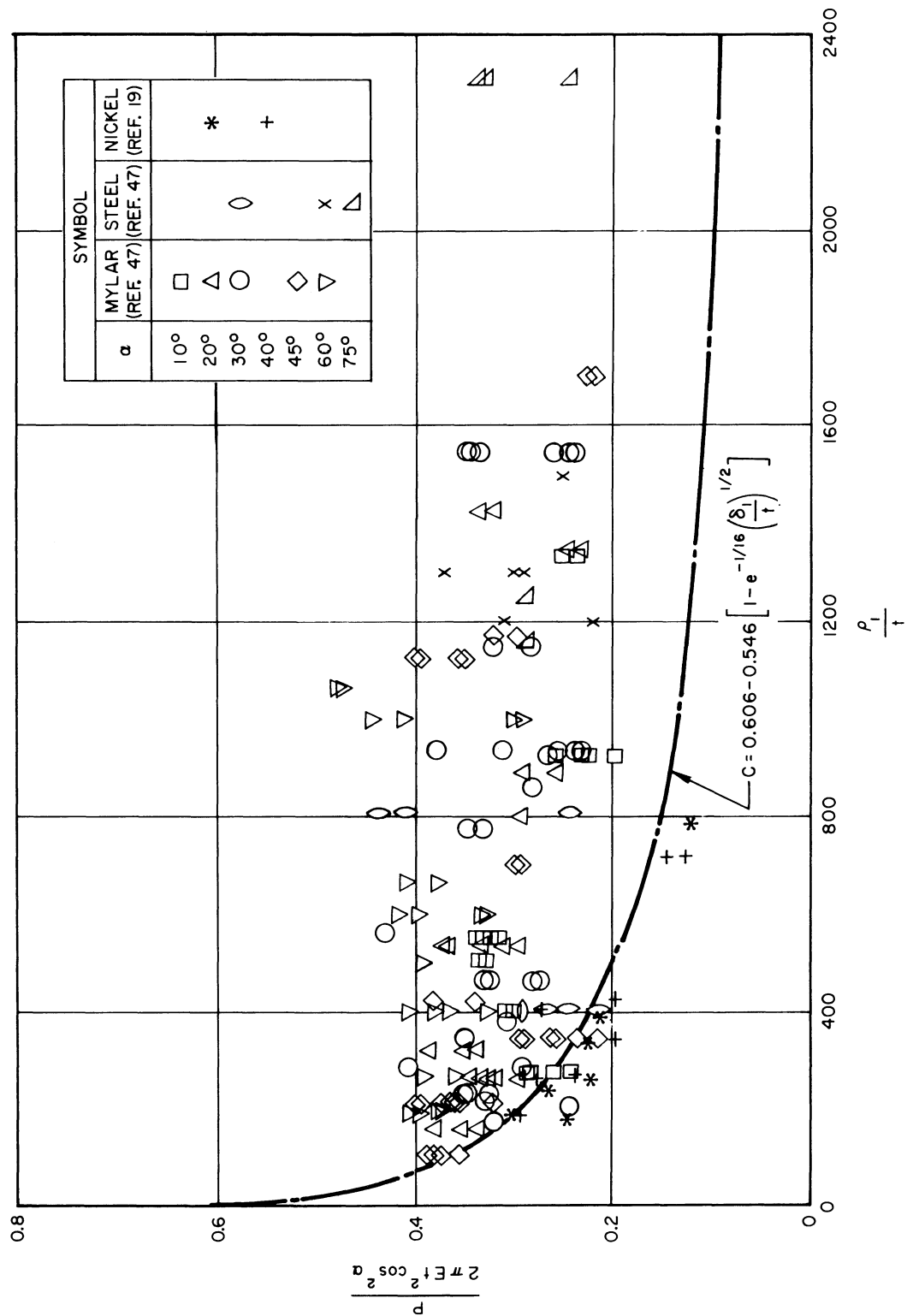


Figure 4.- Comparison of axial compression coefficients for conical shells with lower bound curve for cylinders.

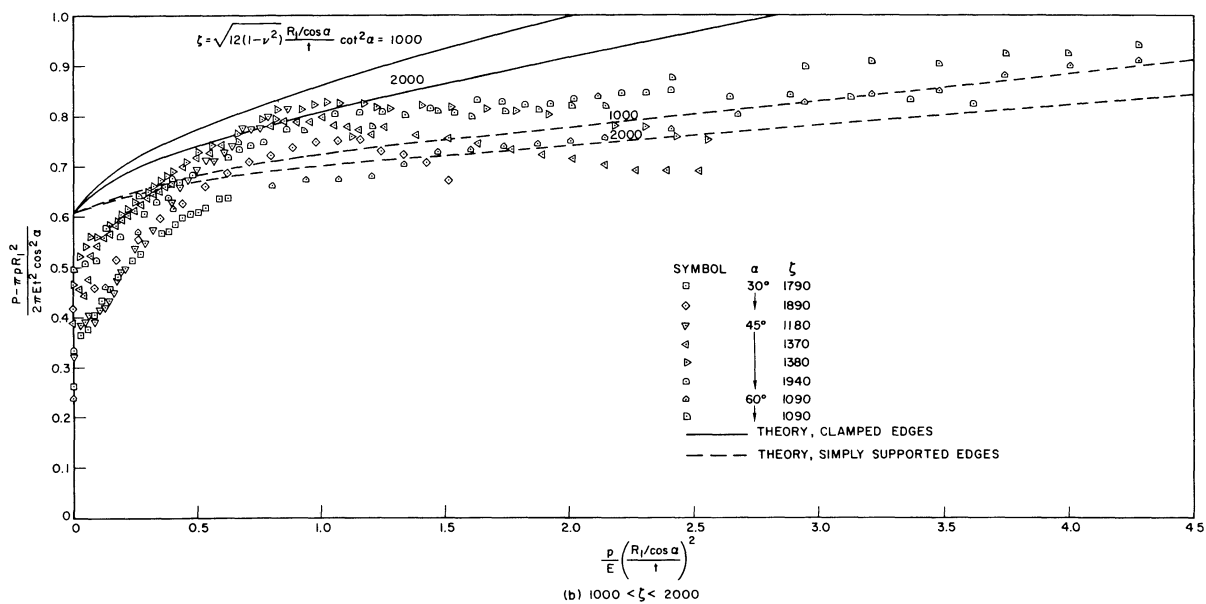
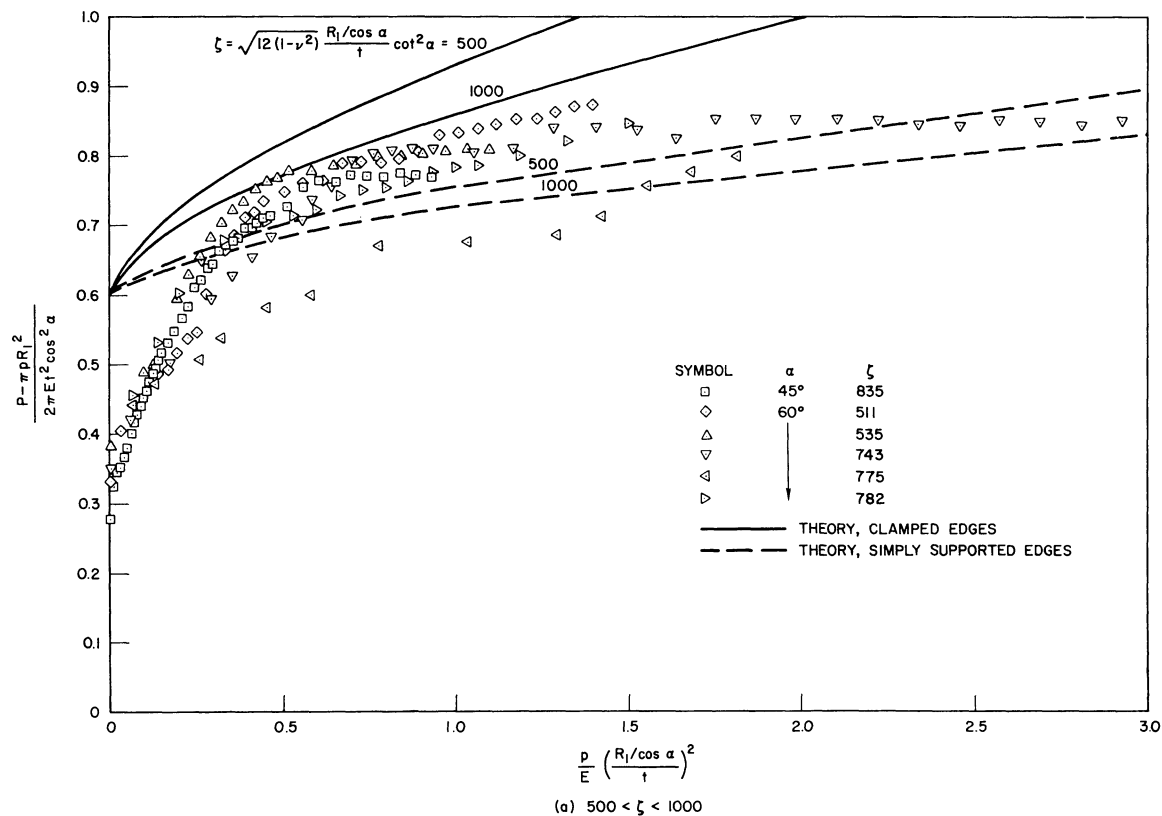


Figure 5.- Comparison of theory and experiment for pressurized conical shells under axial compression.

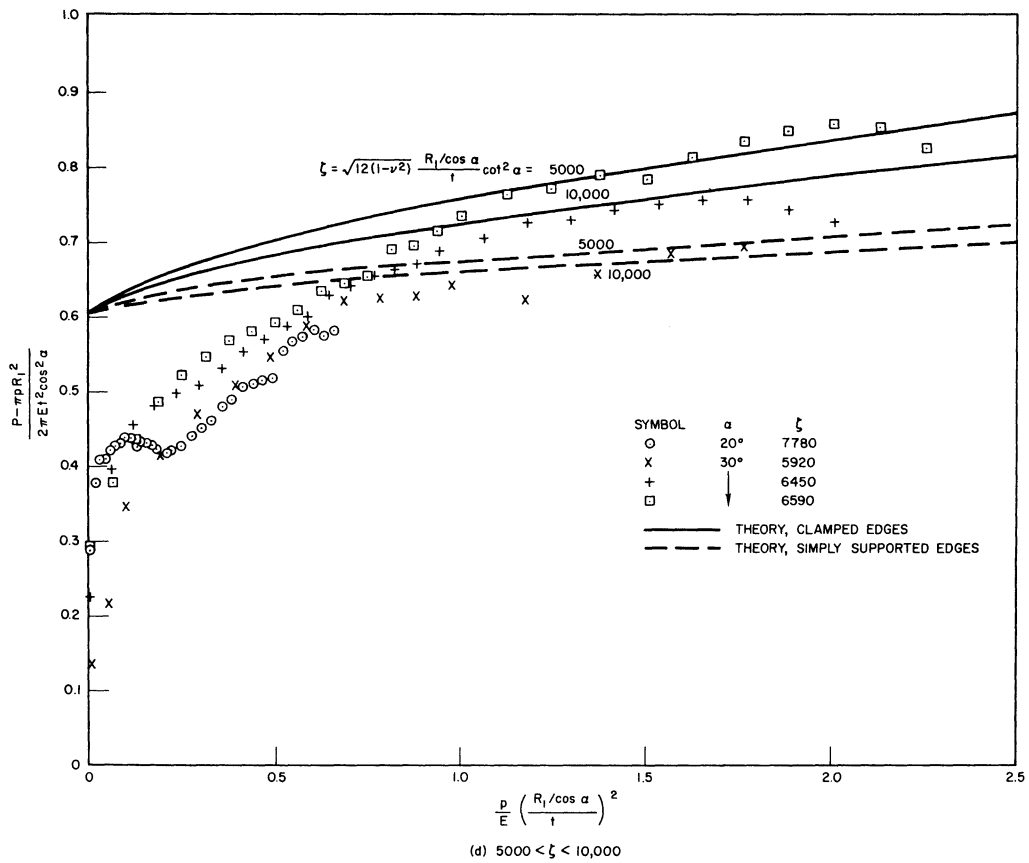
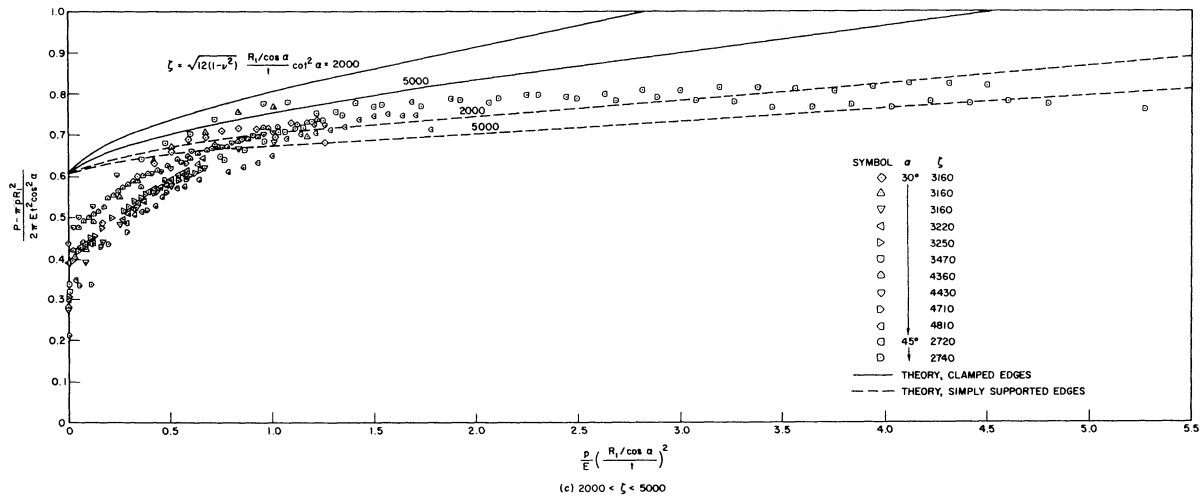


Figure 5.- Continued.

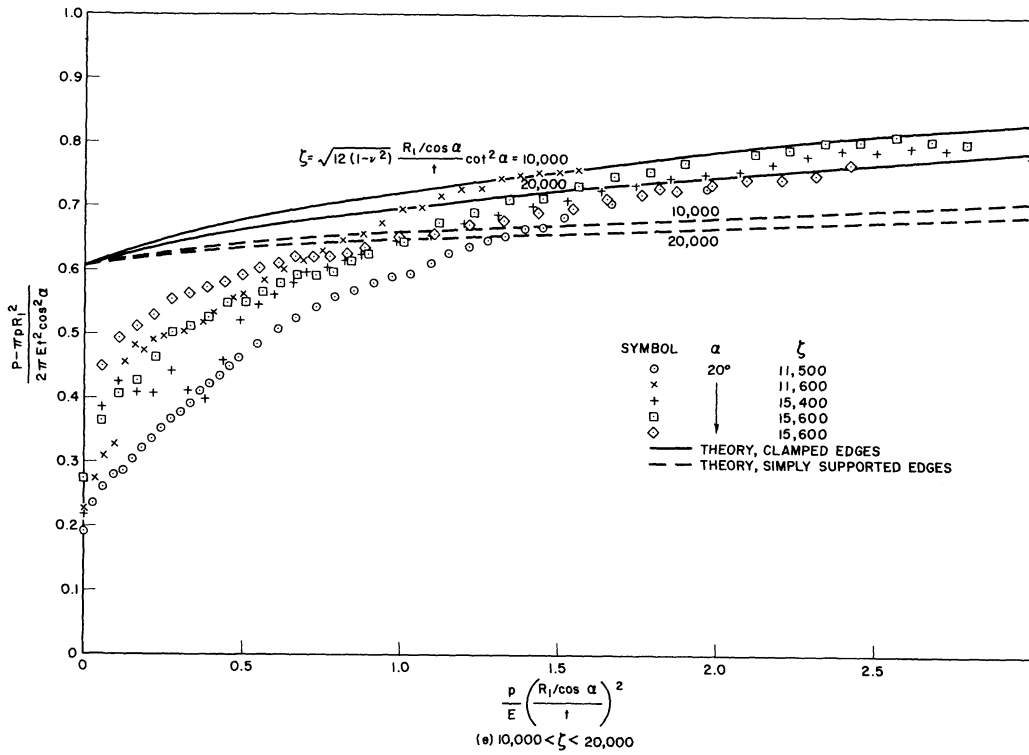


Figure 5.- Concluded.

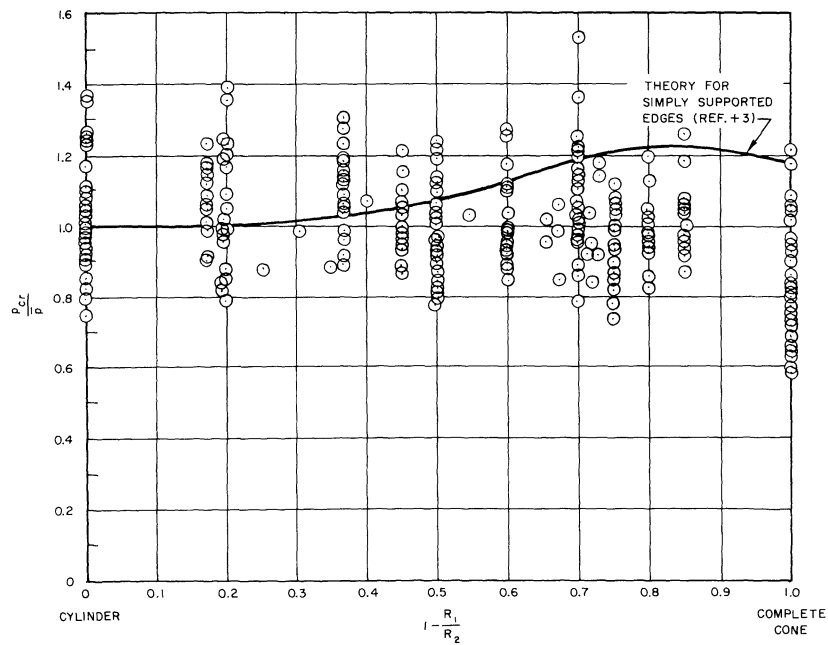


Figure 6.- Comparison of theory and experiment for conical shells under external hydrostatic pressure.

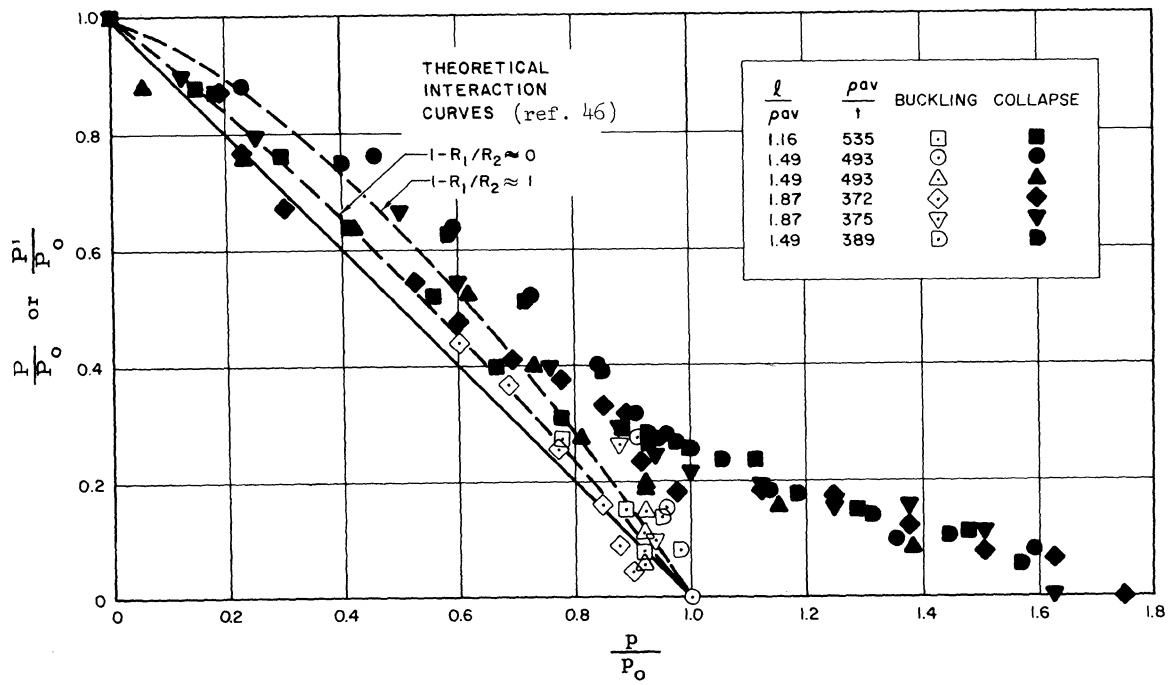
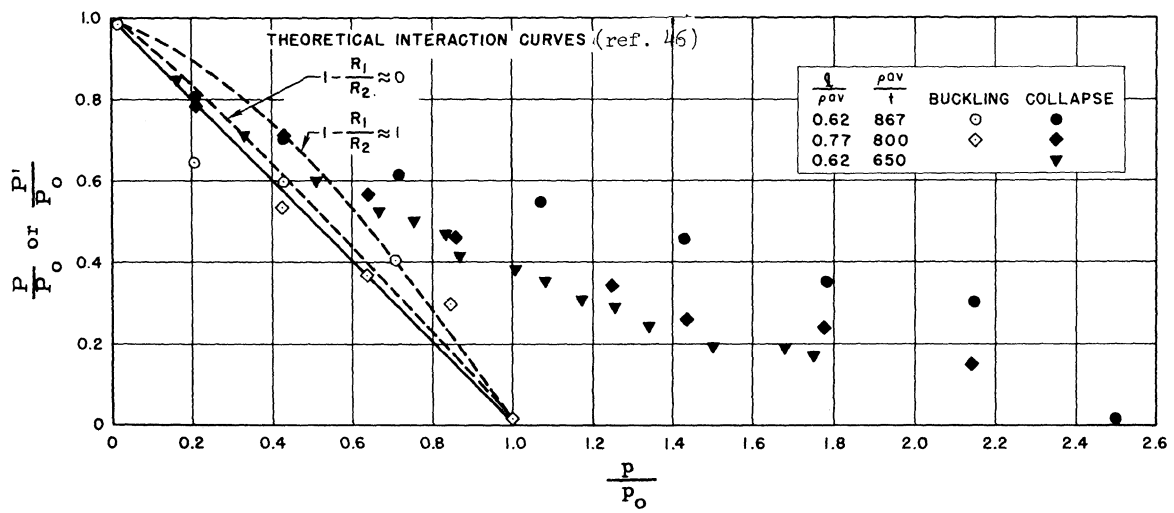
(a) $\alpha = 30^\circ$.(b) $\alpha = 60^\circ$.

Figure 7.- Interaction curves for cones under axial compression and external uniform hydrostatic pressure.

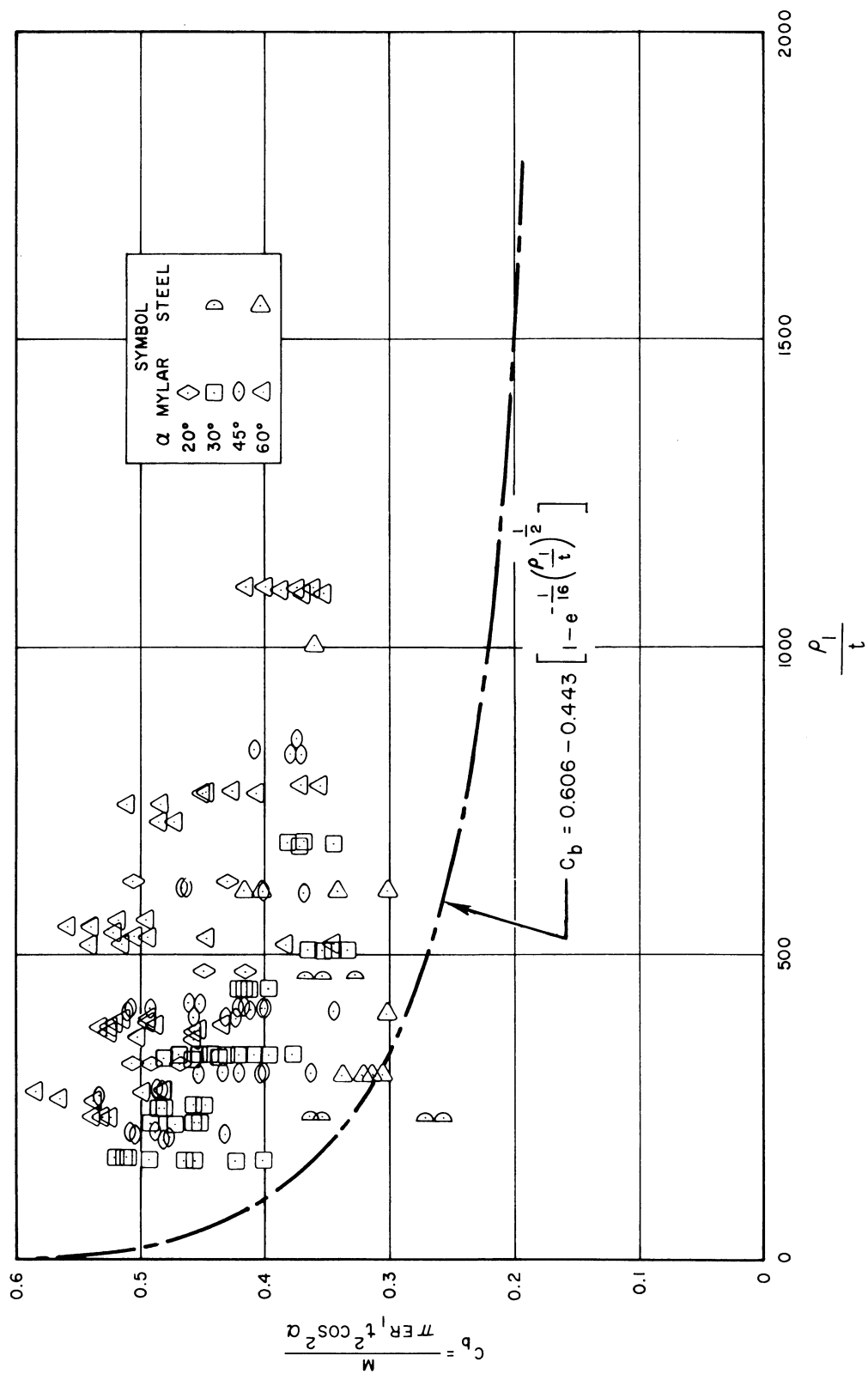


Figure 8.- Comparison of bending moment coefficients for conical shells with lower bound curve for cylinders (data from ref. 47).

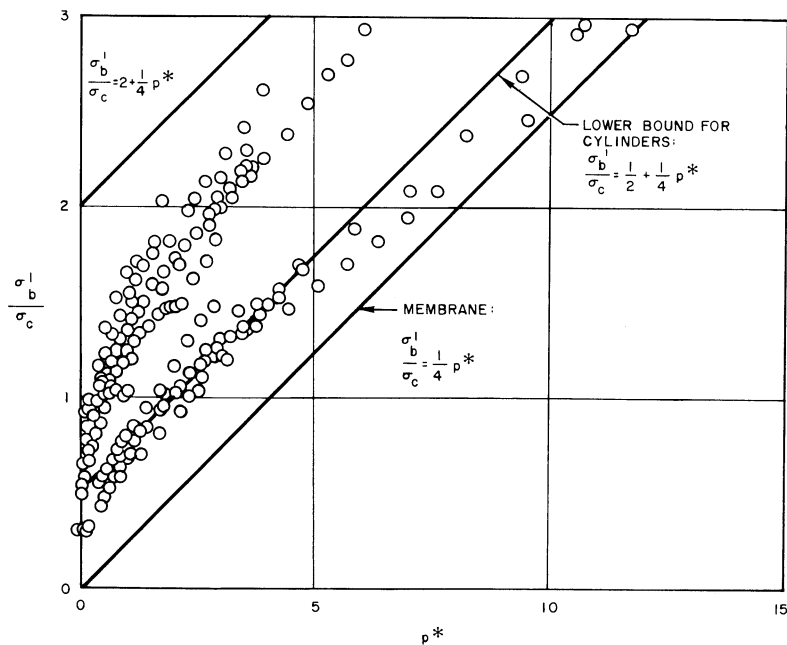


Figure 9.- Variation with internal pressure parameter of net bending stress ratios for 30° and 60° cones under uniform hydrostatic pressure.

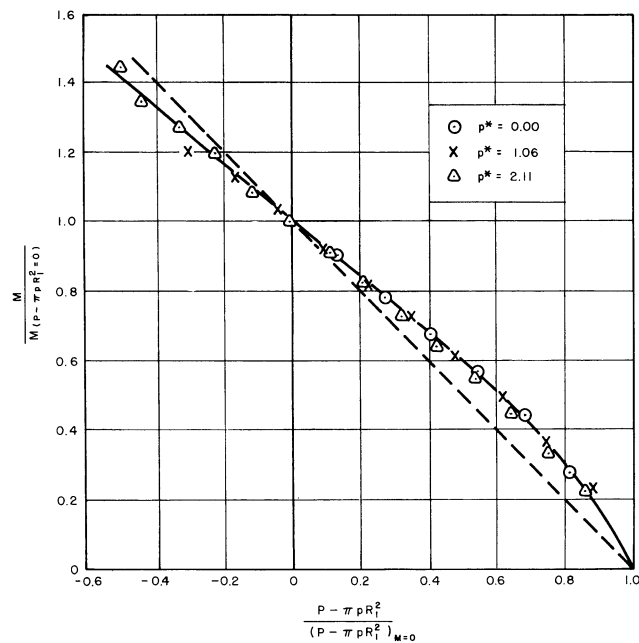


Figure 10.- Interaction curve for a pressurized cone under bending and axial compression ($\alpha = 30^\circ$, $\frac{\rho_1}{t} = 670$).

ELASTIC INSTABILITY OF CONICAL SHELLS UNDER COMBINED LOADING

by P. P. Radkowski

Avco Research and Advanced Development Division

SUMMARY

1. Criteria are presented for the elastic instability of thin single and multilayer conical and cylindrical shells under combined axial load and external pressure. These criteria, used in design analysis, are based on theoretical results and the correlation of these results with readily available experimental data.

2. A summary is included of the studies at Avco RAD of shells under static or dynamic loads.

INTRODUCTION

In designing vehicles for space and/or re-entry environments, many interrelated parameters must be considered. Overall optimization of a design can best be achieved by studies showing the tradeoff between the various parameters which are chosen. One of the most critical problems in achieving this optimization is to obtain more reliable information on the instability of conical shells under combined lateral pressure and axial loading.

The analytical results of reference 1 have been extended and correlated with readily available experimental data; a relatively simple formula may now be used for an elastic instability analysis of conical and cylindrical shells. This report shows that further analysis is required for correlation and interpretation of analytical and experimental results for design purposes.

SYMBOLS

B = effective extensional modulus,

D = effective bending modulus,

E = Young's modulus,

$$K = \frac{(1 - \nu^2) \ell^2 B}{\pi^2 k^2 D (\bar{k}_1 - 1)^4} ,$$

L = total axial load (positive in compression),

$$\bar{M} = \frac{L \ell}{2\pi^2 k^2 D (\bar{k}_1 - 1)^2 \sin^2 \alpha}$$

$$P = - \frac{\ell^2 B k_2 P_{cr}}{\pi^2 D (\bar{k}_1 - 1)} ,$$

a = largest base radius,

h = thickness of shell,

$$k = \frac{\pi a (1 - \beta/2)}{\ell \sin \alpha} ,$$

$$\bar{k}_1 = \frac{\beta (1 - (2/3)\beta)}{2(1 - \beta/2)^2} ,$$

$$k_2 = \frac{k \ell}{\pi B} ,$$

ℓ = slant length,

P_{cr} = critical lateral pressure,

α = base angle

β = $(l/a) \cos \alpha$,

ρ = $\frac{a(1 - \beta/2)}{\sin \alpha}$ = average radius of curvature, and

ν = Poisson's ratio.

DISCUSSION

Theoretical Buckling Criteria

The equation, derived in reference 2,

$$\frac{P}{|P_{\text{int}}|_T} = -\frac{2}{13} \left(\frac{\bar{M}}{|M_{\text{int}}|_T} \right)^2 + \frac{5}{6} \left(\frac{\bar{M}}{|M_{\text{int}}|_T} \right) + 1 \quad (1)$$

is a relation approximating the theoretical buckling criteria for single and multilayer conical and cylindrical shells subjected to axial load and lateral pressure. This relation is a reasonable approximation to the theoretical relation for $10 < \sqrt{K} < 10,000$. Here,

$$|\bar{M}_{\text{int}}|_T = 2\sqrt{K} \quad \text{and} \quad |P_{\text{int}}|_T = \frac{4}{3} \left[1 + (3K)^{1/4} \right] \quad (2)$$

are the theoretical intercepts of the curve with the \bar{M} and P axes respectively. For design purposes, these intercept relations will be replaced by relations based upon theoretical and experimental results.

Experimental results and correlation with theoretical results. -

The experimental results are divided into two categories, i.e., hydrostatic and lateral pressure, and axial load. The data is then correlated with theoretical results for an interaction curve for combined loading. Many test results exist for either axial load or hydrostatic loading of cylinders, but only a limited number of test results exist for combined loading.

Hydrostatic loading. - Figure 1 shows only a small portion of the available experimental data and the scatter is considerable. Several years ago a systematic evaluation of the available data was initiated. Some of the conclusions are shown in figure 2; a more extensive set of

results with the tabulation of readily available experimental data are given in reference 3. Here, we consider the base angle $\alpha = 30$ degrees and plot $p_{cr} 10^6/E$ versus l/a for various values of h/a . A plot of p_{cr}/E versus α is given in figure 3 for a fixed value of h/a and l/a .

It is extremely difficult to evaluate all of the experimental results, because some of the experimenters chose the buckling pressure when the first buckle or lobe appeared, while others chose the pressure when all the lobes appeared. The ideal case, as assumed, would be when all lobes appeared simultaneously at one pressure. Some of the tests observed and listed in reference 3 showed that when the first lobe appeared, e. g., at pressure p_1 the pressure dropped, and as the pressure was increased again the remaining lobes appeared but at a pressure less than p_1 . However, in other tests listed in reference 4 the reverse was the case, i. e., after the first lobe appeared the pressure dropped, and as the pressure was increased again the remaining lobes appeared but at a pressure greater than p_1 . Probably, the appearance of the first lobe distorted the remaining structure so as to render the resulting configuration weaker in one case and stronger in the other. Except for reference 4, all of the data reported used the pressure when the first lobe appeared as the critical pressure. The experimental data reveals some scatter as expected. This scatter is probably due to test techniques, physical properties of the material, imperfection and variation in geometry, different edge restraints, and possible nonuniform edge restraints.

To determine the data used in plotting the banks of curves, the theoretical curves were used as a basis of study and then modified to conform to the experimental results listed in reference 3. The modifications were accomplished in the horizontal portion of the typical curve given in figure 2. In almost every case the horizontal portion remained horizontal for h/a of the order of 10^{-3} , and as h/a increased towards 10^{-2} the slope increased negatively. Where the curve is nearly horizontal the theoretical and the limited experimental results agreed remarkably well. However, in the region where the horizontal portion of the curve was modified and h/a was of the order of 10^{-2} , the difference between the experiments and the predicted theoretical values could be as high as a factor of two for a nontruncated cone, e. g., when $\alpha = 70$ degrees and $h/a = 10.6 \times 10^{-3}$. Although, in general, relatively good correlation exists between the limited number of experimental and theoretical results, the designer should use his own discretion.

In figure 3 p_{cr} pressure versus α is plotted. A maximum appears for a base angle between 70 to 80 degrees. Only 18 experimental data points for α less than 30 degrees and various l/a and h/a were available at this time and the curve for this range might have to be modified.

To summarize the hydrostatic loading analysis, very little experimental data exists for (1) $\alpha < 30$ degrees, (2) $l/a < 1$ for all angles, (3) h/a of the order 5×10^{-3} , and (4) multilayer cones. Interestingly, the critical buckling pressure could vary by a factor of 2 or more for a variation of α within 10 degrees.

Axial load. - The data for axial load, shown in figure 4, is somewhat scattered as it was for the lateral pressure case; this scattering could be due to the factors similar to those for the hydrostatic case. Data from reference 4 is somewhat higher than the other results shown in figure 4, from references 5 and 6. Probably, this is due to the fact that the load which gave the first buckle was considered the critical load in most experiments, while reference 4 gives the load which gave all the buckles as the critical load. From a design viewpoint the critical load which gives all of the buckles may be considered, i.e., where the buckles do not affect the load carrying capacity of the structure. However, in re-entry vehicles a single buckle, or lobe, may cause the thermal protection system to fail and then the whole system fails. Consequently, the curve beneath all of the experimental data would normally be used for design studies of re-entry vehicles.

The experimental data for axial loading should be analyzed to determine the effect of angle, length, thickness, radius, and materials (among other factors) on the critical load applied to conical and cylindrical shells. Studies of this type have been initiated and results should be published as soon as they are available.

A criterion for combined loading. - In certain cases of designing conical shells, equation 1 is not sufficient. In general, equation 1 is an upper bound for the combined loading case; a lower bound should be used. Several methods of determining a lower bound suggest themselves. To determine a lower bound for P_{int} (lateral pressure only), refer to figure 1. Curve C is plotted through the two lowest experimental curves, and for most purposes, is a reasonable value for the lower bound. The equation for curve C can be written as,

$$p^4 = K \quad (3)$$

Consequently, the new P_{int} for equation 1 can be

$$P_{int} = 4\sqrt{K} \quad (4)$$

As an alternative, the results of reference 3 may be used, typified by figure 2, for determining a more refined P_{int} .

For the lower bound of \bar{M}_{int} (axial load only), one proceeds as in determining P_{int} , which is given in equation 4. Here,

$$\begin{aligned} |\bar{M}_{int}| &= \frac{5}{8} \sqrt{K}, \quad \frac{\rho}{h} \leq 450, \\ |\bar{M}_{int}| &= \frac{1}{2} \sqrt{K} \quad 450 < \frac{\rho}{h} \leq 600, \\ |\bar{M}_{int}| &= \sqrt{\frac{2}{5}} K, \quad 600 \leq 900 \\ |\bar{M}_{int}| &= K^{2/5}, \quad 900 < \frac{\rho}{h} \leq 2000 \\ |\bar{M}_{int}| &= \frac{5}{3} K^{1/3} \quad 2000 < \frac{\rho}{h} \leq 3000 \end{aligned} \quad (5)$$

The expressions in equation 5 are comparable to those of reference 6.

Figure 5 illustrates the use of equation 3. Experimental Avco RAD* combined loading data are plotted, and their relationship to the curve of equation 1 is shown. The choice of \bar{M}_{int} and P_{int} will depend upon geometrical considerations (in this case, see equation 5 for \bar{M}_{int} , and reference 3 for P_{int}). It is apparent that further refinements are necessary for \bar{M}_{int} .

Summary of studies on instability due to static loading. - The instability of isotropic shells of revolution has been completed and will be presented in a forthcoming report, reference 7. This report gives a simplified energy relation based on Donnell-type assumptions. A set

*These experiments were conducted by R. H. Homewood and are as yet unpublished

of displacement functions are used which are slightly more general than those used for noncylindrical shells. The instability of toroidal shells subject to internal or external loading is presented as a relatively simple formula; an energy solution for a truncated spherical shell subject to compressive loading is also presented. Very few experimental or analytical results are available for shells other than the cone, cylinder and shallow sphere.

Very little experimental data appear to be available for any type of multilayer shell of revolution subject to compressive loading.

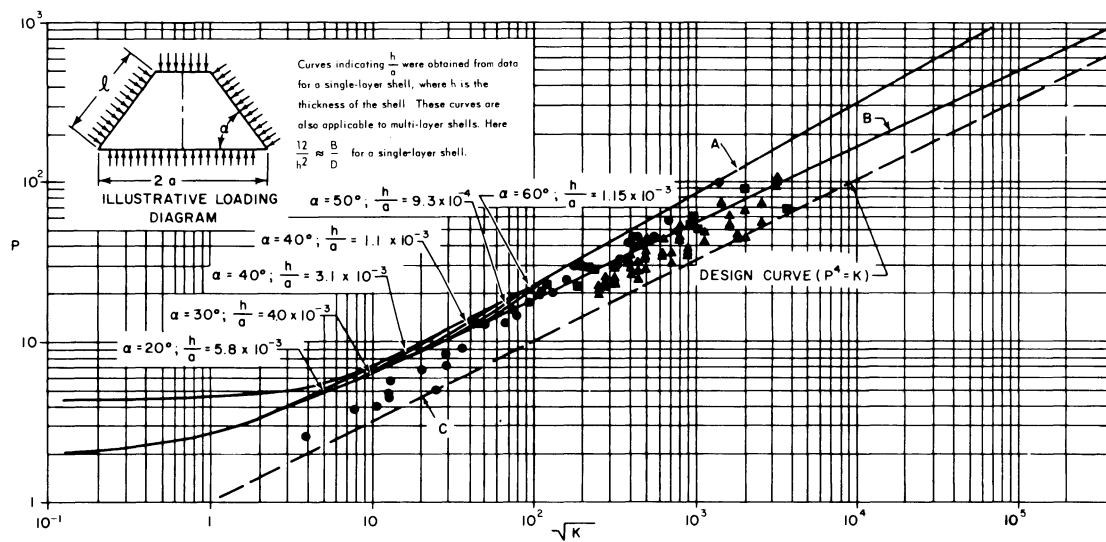
Several experiments are being carried out at Avco RAD for a pressure distribution varying linearly over the slant length of a conical shell.

Summary of studies on instability due to a pressure pulse. - For several years studies have been made of the dynamic response of shell structures and materials subjected to a pressure pulse. This problem could be characterized (1) by shell-fluid interaction, such as water entry of a shell-like structure, and (2) by applying a sheet explosive over a portion of a cylinder with results as illustrated in figures 6 and 7. This application of a sheet explosive over a portion of a cylinder is characterized by very high pressures for very short times, which presents a dynamic boundary condition not often treated in recently published literature. The problem of the behavior of cylindrical and spherical shells under such conditions have been approached from two extremes; ideal elastic buckling and ideal rigid-plastic collapse (reference 8). The work on elastic buckling of cylinder and sphere is for a pressure time history. The analysis of a shallow sphere is presented at this symposium by Professor B. Budiansky.

As in the case of buckling of shells under static loading, considerably more analytical and experimental work is necessary for a truly definitive understanding of the problem of dynamic response of shell-like structures. Experimental and analytical investigations have been undertaken at several universities and by private industry. These efforts should help to provide the means of corroborating the present theoretical understanding and the basis for additional analytical and experimental work.

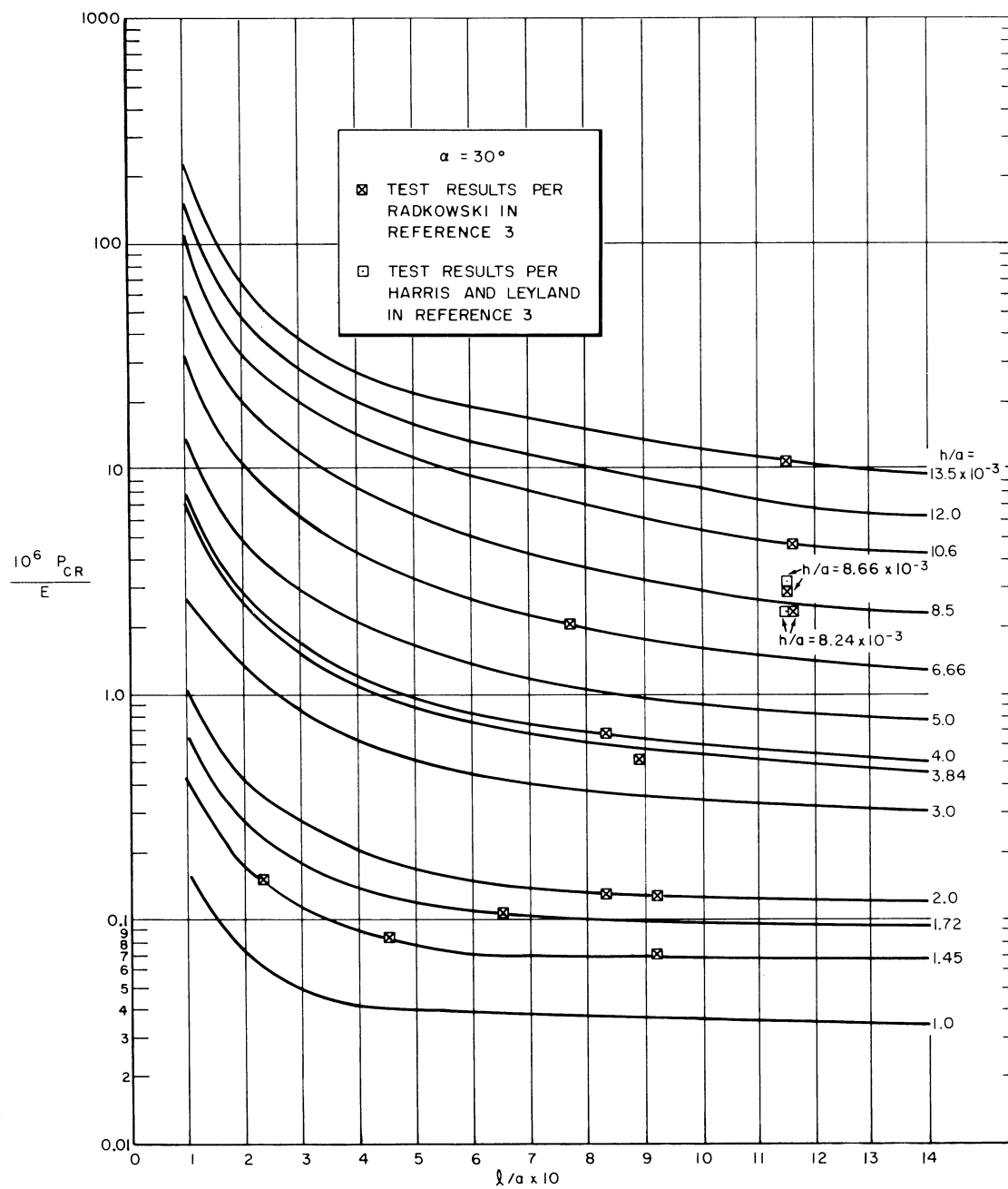
REFERENCES

1. Radkowski, P. P.: Buckling of Single- and Multi-Layer Conical Cylindrical Shells with Rotationally Symmetric Stresses. Proceedings of the Third U.S. National Congress of Applied Mechanics, ASME, June 11-14, 1958.
2. Radkowski, P. P.: Buckling of Single- and Multi-layer Conical and Cylindrical Shells Subjected to Axial Loads and Lateral Pressure. Avco RAD TR-61-36, Dec. 1961.
3. Radkowski, P. P.: Correlation of Analytical and Experimental Results of the Instability of Conical Shells under Hydrostatic Pressure. Avco RAD (in preparation).
4. Weingarten, V. I., Morgan, E. J., and Seide, P.: Development of Design Criteria for Elastic Stability of Thin Shell Structures. STL/TR 60-0000-19425, Dec. 31, 1960.
5. Lockman, L. and Penzien, J.: Buckling of Circular Cones under Axial Compression. Jour. Applied Mech., vol 27, Sept. 1960, pp. 458-460.
6. Batdorf, S. B., Schildcrout, M., and Stein, M.: Critical Stress of Thin-walled Cylinders in Axial Compression. NACA Report 887, 1947.
7. Radkowski, P. P.: Buckling of Thin Single- and Multi-Layer Shells of Revolution with Rotationally Symmetric Stresses. Avco RAD TR-62-1, Dec. 1961.
8. Radkowski, P. P., Humphreys, J. S., Payton, R. G., Bodner, S. R., and Budiansky, B.: Studies on the Application of X-ray as a Lethal Mechanism on Decoy Discrimination Technique (vol. 2) Studies on the Dynamic Response of Shell Structures and Materials to a Pressure Pulse. Avco RAD TR 61-31, July 1961.



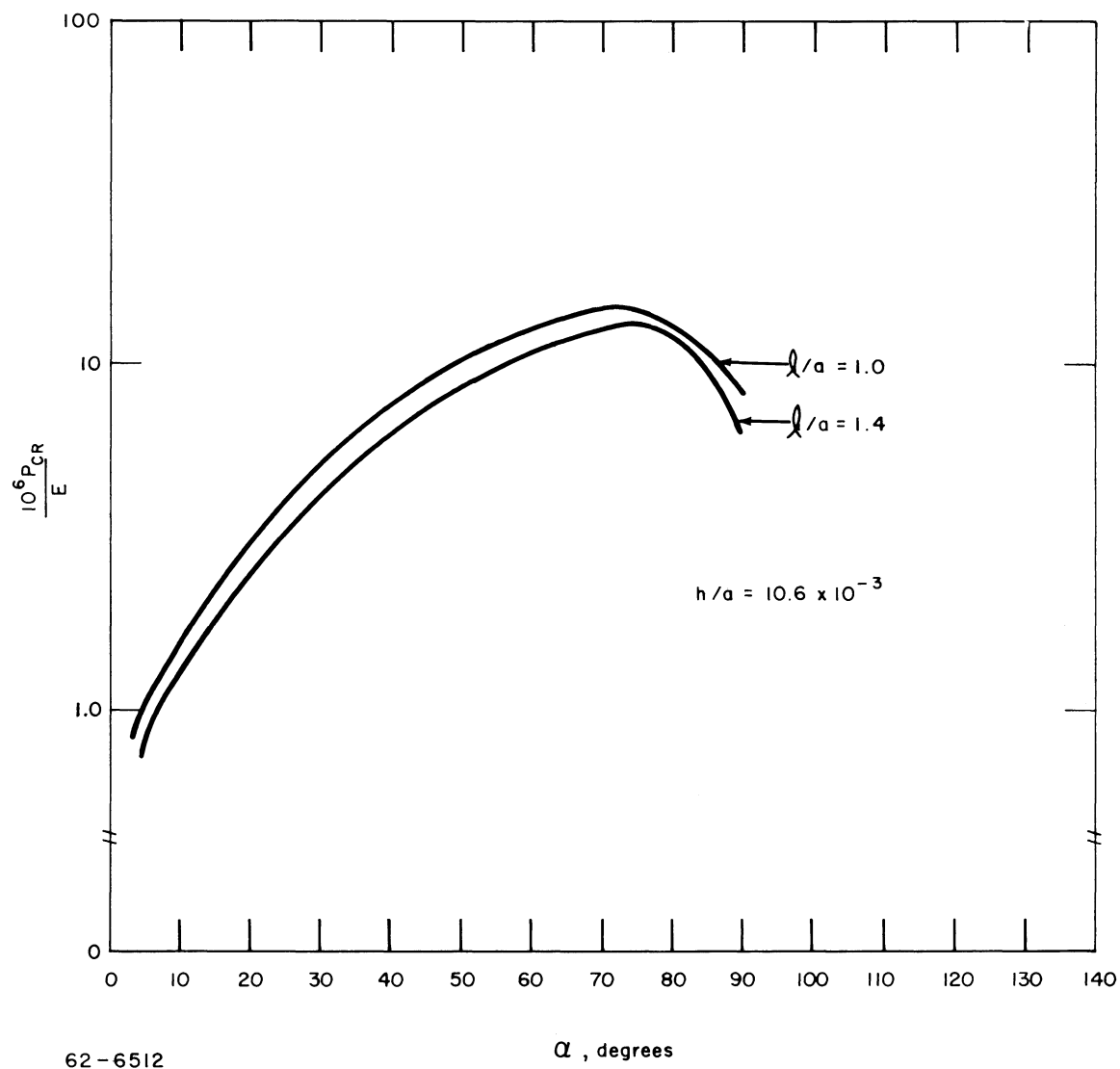
59-458

Figure 1. - Critical pressure curves for thin single- and multi-layer conical and cylindrical shells.



61-2622

Figure 2. - Instability of conical shells subjected to hydrostatic pressure.



62-6512

Figure 3. - Effect of cone angle on the buckling of conical shell subjected to hydrostatic pressure.

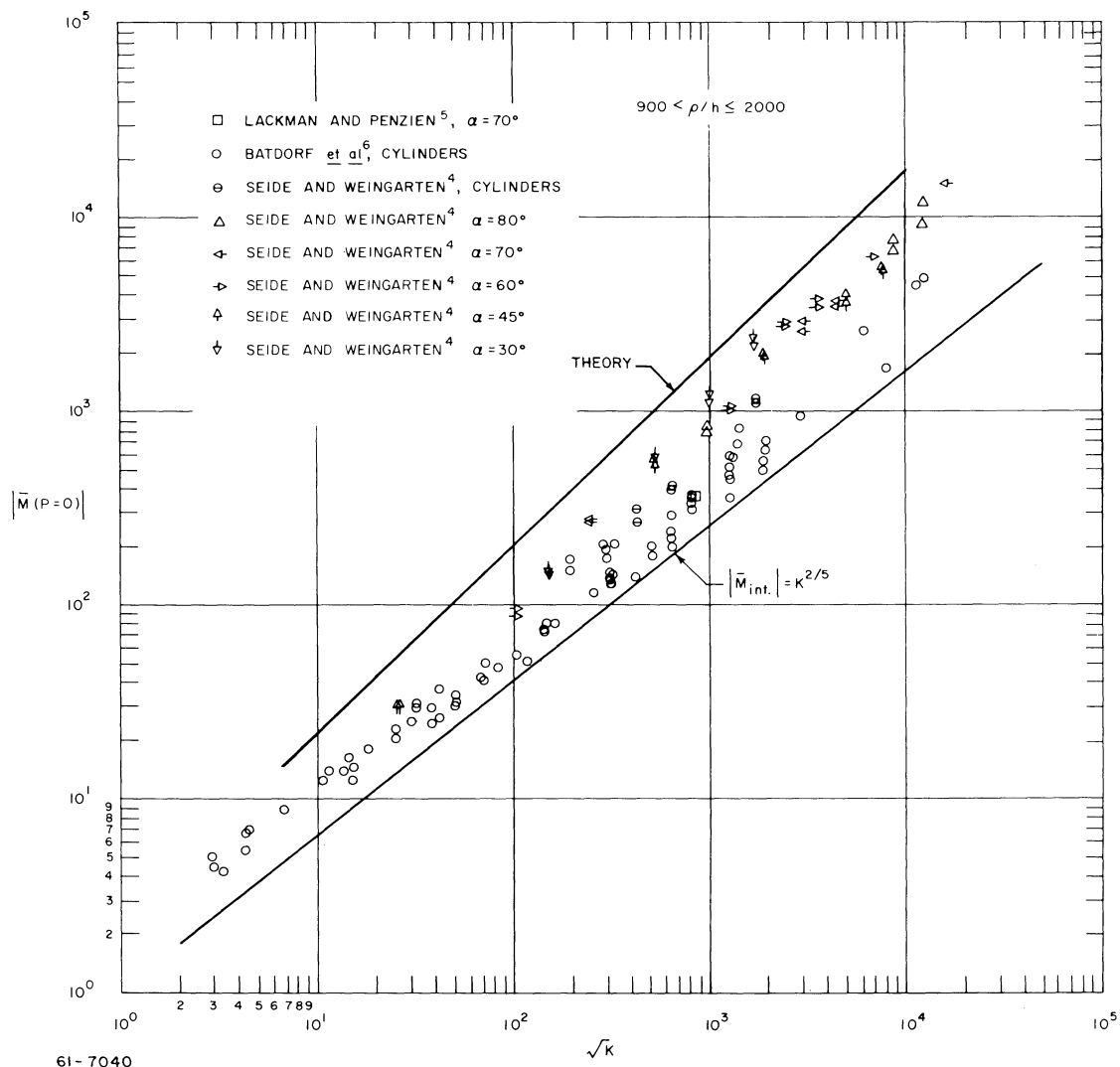


Figure 4. - Axial loading curves for thin single- and multi-layer conical and cylindrical shells.

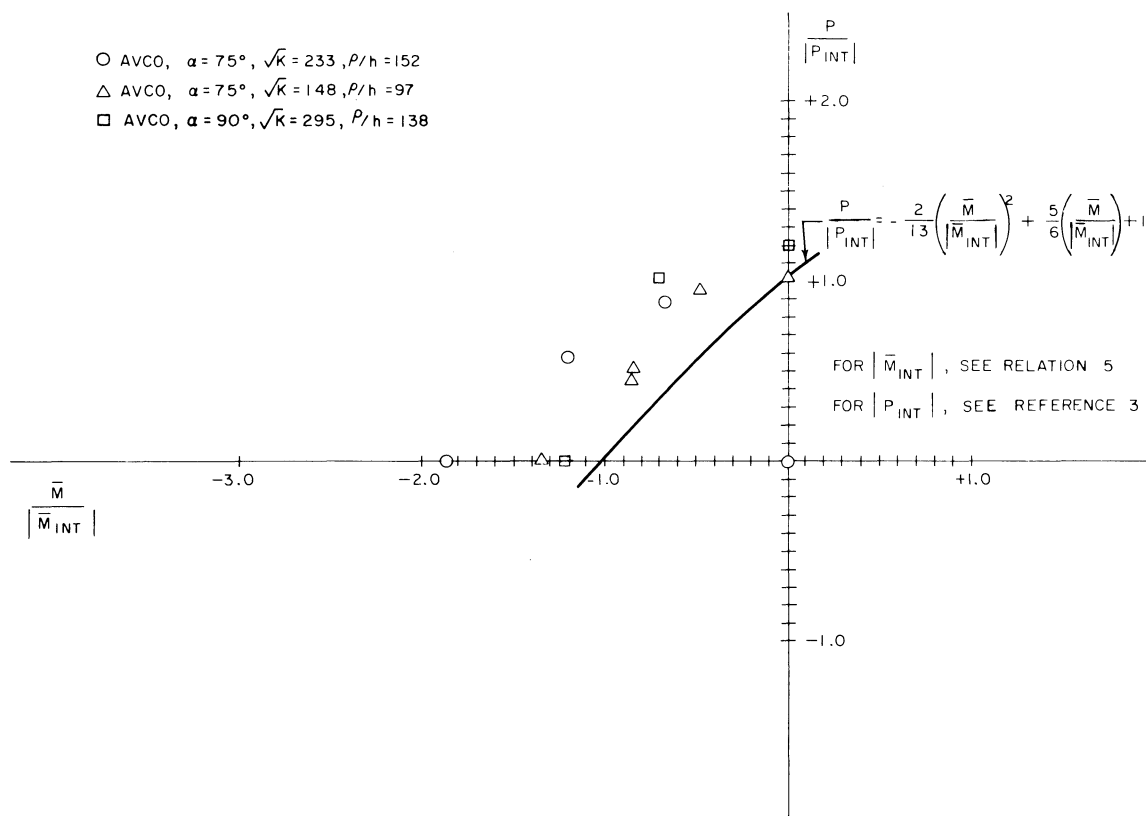


Figure 5. - Combined loading design curve for thin single- and multi-layer conical and cylindrical shells.

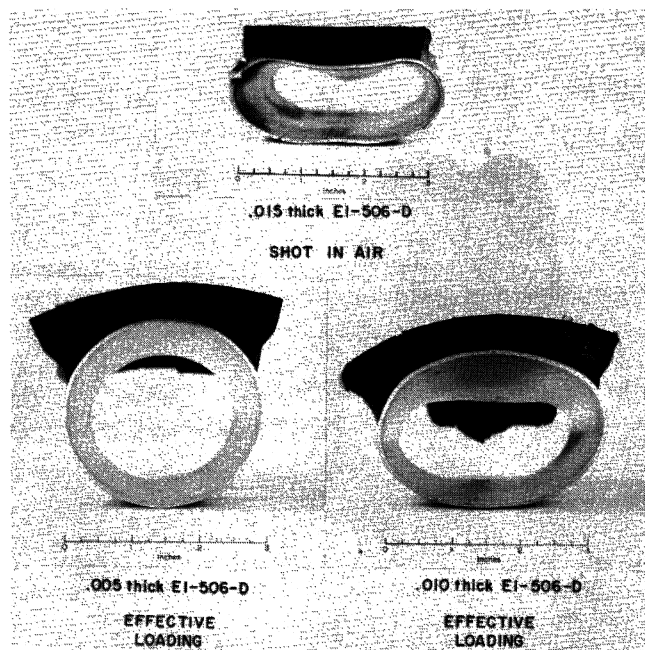


Figure 6.- Final configuration of magnesium cylinder series (courtesy S.R.I.).

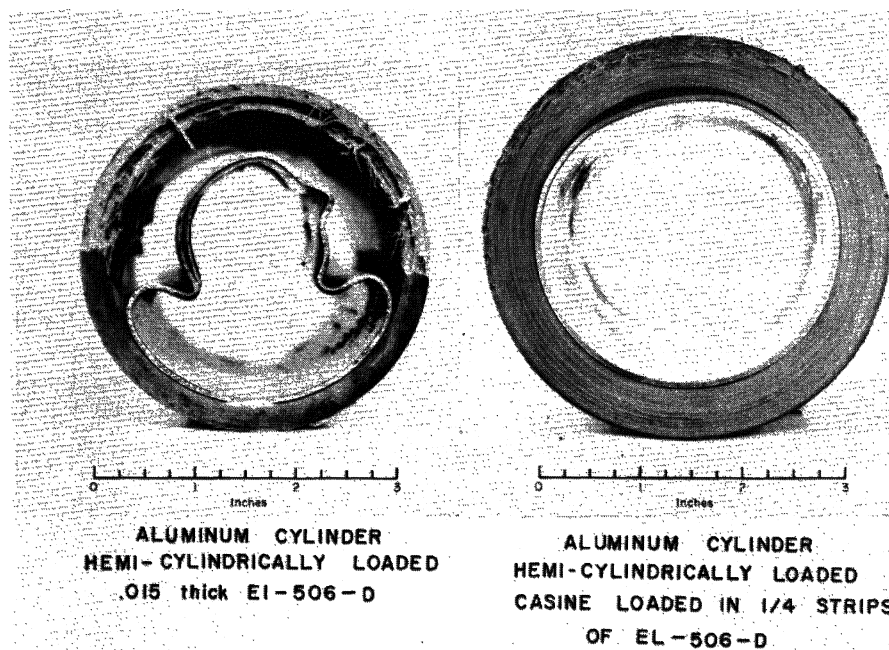


Figure 7.- Final configuration of cylinders with stiff outer layer after explosive test (courtesy S.R.I.).

BUCKLING OF CONICAL SHELLS UNDER EXTERNAL PRESSURE

By P. P. Bijlaard

Cornell University and Bell Aerosystems Company

SUMMARY

It is shown that the initial and the buckled shapes of a certain element of a conical shell can be considered as similar to those of an element of a cylindrical shell of which the radius and length are conservatively determined. It is concluded that therefore the buckling pressure of the conical shell is equal to that of the comparable cylindrical shell. A simple method for finding the buckling pressure if it varies along a generatrix is also given.

INTRODUCTION

The buckling pressure of simply supported conical shells has been the subject of several recent papers on theoretical as well as experimental investigations. Several of these papers (refs. 1 through 6) refer to an unpublished company report of 1953 (ref. 7) in which the present author conservatively derived the buckling pressure of complete or truncated conical shells under uniform or non-uniform external pressure. The background of this derivation will be more elaborately explained here.

BUCKLING UNDER UNIFORM EXTERNAL PRESSURE

For design purposes a reliable estimate of the buckling pressure of simply supported conical shells was required. At that time (1952) insufficient information was available. The problem had been dealt with in references 8 and 9, both assuming uniform pressure and using small deflection theory. However, also within the limitations of this theory the results obtained in these references were open to question. The differential equation derived in reference 8 could be solved only by assuming radial deflection

$$w = C r^m \cos n\theta \quad (1)$$

and at the same time assuming the thickness t to be proportional to

the radii r of latitudinal cross sections (Figs. 1 and 2). The angle θ is measured in the circumferential direction. For a minimum buckling load m has to be equal to 2. It is evident that at edges where r differs from zero, w from equation (1) is not zero, so that it does not satisfy the geometric boundary conditions of simple support. From this relaxation of restraints, reference 8 will underestimate the buckling stresses for simply supported shells.

In reference 9 an energy method was used, assuming radial displacements

$$w = C \sin \lambda x \cos n\theta \quad (2)$$

where $\lambda = \pi/\ell$, so that w is assumed to vary as a half sine wave in the direction of a generatrix. Obviously, for a complete conical shell this is far from reality, since for that case at the apex equation (1) satisfies the geometrical boundary condition $w = 0$ for a simply supported edge, so that the deflection of a generatrix near the apex actually approximates that of a clamped beam. Hence assumption of a deflection as in equation (2), that differs substantially from the real one, will lead to a too high buckling pressure. Apart from that, several approximations were made in reference 9 of which the effect was difficult to assess.

In order to find a more reliable solution it was reasoned as follows: One can imagine that for a cylindrical shell, where for free edges w is constant with varying axial coordinate x , the simply supported buckling mode, as given by equation (2), is obtained by multiplication of this constant deflection with $\sin \lambda x$. Hence, for a conical shell, of which for free edges the buckling mode is given by equation (1), with $m = 2$, that for simply supported edges can be approximately obtained by multiplying w from equation (1) with $\sin \lambda x$, whence

$$w = C r^2 \sin \lambda x \cos n\theta. \quad (3)$$

This deflection is shown by the solid curves in Figs. 1b and 2b. It may be pointed out that equation (1) and therefore equation (3) actually applies for a shell of which the wall thickness t is proportional to r . Therefore, for uniform wall thickness, as considered here, the deflection w for smaller r values will be relatively somewhat smaller than would follow from equations (1) or (3). As explained later on, this will make the results obtained by using equation (3) somewhat conservative.

Using the energy method, equation (3) and accessory displacements in the other two directions, could be expected to yield lower buckling

pressures than equation (2), since the former may be expected to approximate the actual buckling mode better. However, since equation (3) could not be expected to be the real mode, it would overestimate the real buckling pressure by an unknown amount, which was undesirable. Therefore, since no time was available for other lengthy methods, a simple reasoning was used, which led more directly and much quicker to a result and also afforded an opportunity to remain sufficiently at the safe side to account for the lowering of the buckling stress due to snap-through, which was estimated at not more than 25% (see ref. 10). This method will now be described.

If an equivalent cylindrical shell can be found for which, at a given point, the initial shape and loading and also the deflection function and its derivatives are the same as those at a point of the conical shell, it is evident that for elements at these corresponding points the same equilibrium equations apply. Therefore the critical pressures for these corresponding elements and hence for the entire shells will be equal.

From Fig. 1b, an element near the lower edge of the conical shell will have the same initial shape and loading as an element of a cylindrical shell with equal thickness t and with radius $\rho = r_2/\sin\alpha$. Indeed, with the same all sided pressure p , at the lower edge also the compressive membrane stresses σ_θ and $\sigma_x = \sigma_\theta/2$ are equal. The simply supported length of the equivalent cylindrical shell, buckling in a half sine wave along a generatrix, can be chosen such that near the lower edge this half sine wave coincides with the buckling deflection of the conical shell. From Fig. 1b, where $r_1/r_2 = 0$, this simply supported length is

$$(l_{eq})_{r_1/r_2 = 0} = (0.5 \text{ to } 0.55)l \quad (4)$$

Hence, for both shells the buckling pressure will be the same function of the number of lobes. For a frustrum of a conical shell, where $r_1/r_2 = 0.5$ (Fig. 2), the length of the equivalent cylinder is, from Fig. 2b,

$$(l_{eq})_{r_1/r_2 = 0.5} = (0.75 \text{ to } 0.80)l \quad (5)$$

Conservatively, using the higher values in equations (4) and (5), this leads to an equivalent cylindrical shell with length

$$l_{eq} = \frac{r_1 + 1.2r_2}{2.2r_2} l \quad (6)$$

and radius $\rho = r_2/\sin\alpha$, with, of course, the same thickness t as the

conical shell. It should be pointed out that by assuming the radius of the equivalent cylindrical shell as $r_2/\sin\alpha$ again some conservatism is introduced. Actually the point where the buckling modes will coincide will be above the lower edge, since equation (3) only satisfies the geometric boundary condition that $w = 0$ for $x = l$, but not the natural one that the second derivative with respect to x is zero, which the half sine wave does. Hence the radius ρ of the equivalent cylinder is actually smaller than $r_2/\sin\alpha$. Moreover, as stated in the foregoing, the actual buckling deflection of the conical shell for smaller values of x will be relatively somewhat smaller as compared with that for larger values of x . From Figs. 1b and 2b this would slightly decrease l_{eq} , so that also the assumed buckling mode tends to lead to conservative results if this method is used, although it would be unconservative if using the energy method, since it need not be the real buckling mode. In connection with all this built-in conservatism it was judged that the actual buckling pressure, if equated to that of a cylindrical shell with length l_{eq} and radius $\rho = r_2/\sin\alpha$, could be considered to include the influence of snap-through and thus would be reliable for design purposes. Hence, using a formula given in reference 11, the buckling pressure is

$$p_b = \frac{0.92E(t/\rho)^2}{(l_{eq}/\rho)(\rho/t)^{1/2} - 0.636} \quad (7)$$

As derived in reference 12 the same formula applies for a clamped cylindrical shell of length l and radius ρ , with $l_{eq} = (2/3)l$.

BUCKLING UNDER NON-UNIFORM EXTERNAL PRESSURE

To find the effect of non-uniform external pressure, it is observed that the curvature changes of the conical shell depend mainly on the radial deflection w and can be expressed as

$$\chi_\theta = (w/r^2) \sin^2\alpha + \partial^2 w / (r^2 \partial \theta^2) \quad \text{and} \quad \chi_x = \partial^2 w / \partial x^2 \quad (8)$$

The radial deflecting forces dD acting upon an element $r d\theta dx$ exert an amount of work upon a ring of the conical shell of length dx that can be expressed as

$$dV = \frac{1}{2} \int_0^{2\pi} w dD = -\frac{1}{2} t dx \int_0^{2\pi} (\sigma_\theta \chi_\theta + \sigma_x \chi_x) wr d\theta \quad (9)$$

Neglecting the relatively small influence of $\sigma_x \chi_x$, with uniform external pressure p , where $t\sigma_\theta = pr/\sin\alpha$, using equations (3) and (8) in

(9) yields

$$dV = \frac{\pi}{2} p \left(\frac{n^2}{\sin \alpha} - \sin \alpha \right) C_1^2 r^4 \sin^2 \lambda x dx = C_1^2 r^4 \sin^2 \lambda x dx \quad (10)$$

where C_1 is proportional to p and independent of x . Presenting this graphically for ratios r_1/r_2 of 0 and 0.5, it is observed that if p varies linearly with x , from p_1 at the upper edge ($r = r_1$) to p_2 at the lower edge ($r = r_2$), where $2 > p_2/p_1 > 0.5$ as happened to be the case, the deflection surfaces will not differ appreciably from that of equation (3). For example, for a simply supported long plate, subjected to compressive stresses in its plane that vary from σ_1 at one edge to $\sigma_2 = 2\sigma_1$ at the other edge, from page 173 of reference 13 the buckling stress coefficient k for σ_2 is 5.32, while, assuming the same buckling mode as for constant compressive stress, one would find $k = 4$ for the average stress and hence, $k = 5.33$ for σ_2 , so practically no difference. Hence, from equation (10), where C_1 is proportional to p , the work done by the variable pressure p is found by multiplying the ordinates of the curves presenting dV from equation (10) by a constant times p . From a simple calculation it followed that the result can be approximated very well by assuming that the varying pressure is equivalent to a constant pressure p_{eq} equal to the pressure p at the center of the length l_{eq} of the equivalent half sine wave, so that

$$p_{eq} = p_2 + \frac{l_{eq}}{2l} (p_1 - p_2) \quad (11)$$

CONCLUDING REMARKS

When these results were reported in reference 7 no tests were available to check them. In the meantime, however, several experimental results were published. These were compiled for complete conical shells in reference 2, from which Fig. 3 has been copied. It shows that the method of reference 7 as reviewed here leads indeed to a reliable design formula, since it forms the lower bound to the test results. Fig. 4 was copied from Fig. 11 of reference 4, adding the curve according to reference 7 and the present note, and gives the results for truncated shells, where p_N is the buckling pressure from reference 9. Figs. 3 and 4 also present several theoretical results. For low taper ratios (nearly cylinders) where equation (7) was not meant for, the conservatism in determining l_{eq} and ρ vanishes, so that it is understandable that there in Fig. 4 some test results are below the line according to reference 7. As stated in the foregoing, equation (2), used in reference 9, could be expected to overestimate the buckling pressure. Assuming that reference 2 gave the correct buckling pressure from small deflection theory this is not revealed in Fig. 3. Apparently the lower buckling stress found in reference 9 is due to

additional approximations. Reference 6 also uses equation (2) and indeed gives higher values than reference 2. It is interesting that, as mentioned in reference 2, reference 14 later used the same mode, according to equation (3), as reference 7. From Fig. 3 its results are lower than those from reference 6, so that indeed equation (3) gives a better approximation than equation (2). It also shows that the method of reference 7 using the same equation (3), although very simple, served better for attaining its aim, which was not a formal computation, but a reliable design formula. Using the energy method would have led, with much more effort, to the unconservative results of reference 14.

After reference 7 was distributed the author was informed about an earlier paper that compares a conical shell to an equivalent cylindrical one (reference 15). From a partial translation only the case of a complete conical shell is considered there. Strips along a generatrix are considered as beams, clamped at the apex and simply supported at the base, so that their maximum deflection occurs at about $0.6l$ from the top. Therefore the radius of the equivalent shell was assumed as the radius of curvature of the conical shell at $0.6l$ from the top, that is, in the present notation, equal to $0.6 r_2 / \sin \alpha$, with a length equal to the total slant length l of the cone. This leads to smaller buckling stresses than the present method and is not based on the same principles.

It should be realized that for many problems, that require extremely elaborate computations for exact or even approximate solutions, often good results can be obtained by a simple reasoning. In several cases this will even yield exact solutions (see for example refs. 12, 16, 17, and 18).

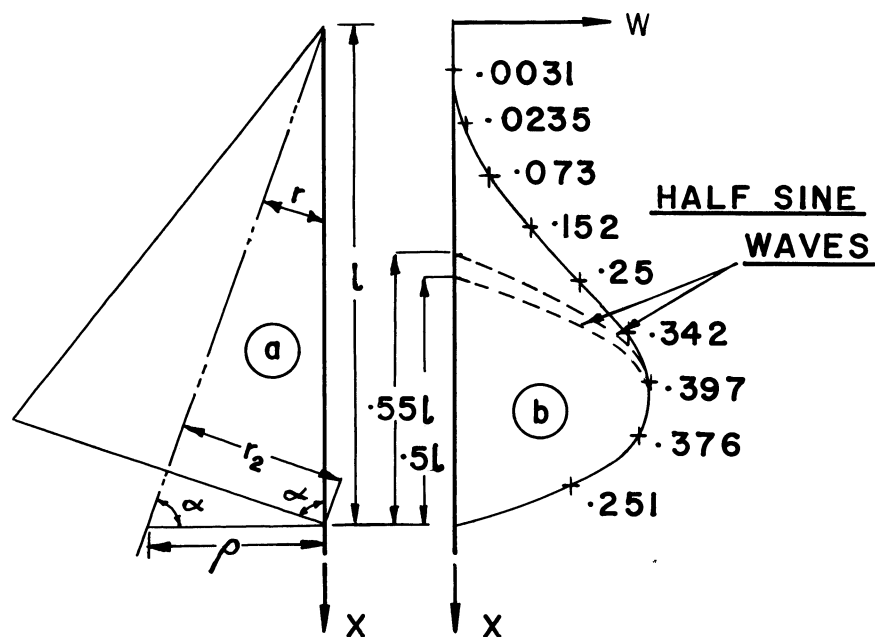
The author wishes to thank Bell Aerosystems Company for permission to publish these results and Messrs. Arthur Schnitt and R. E. Wong, formerly with Bell Aircraft Corporation, for their helpful discussions.

REFERENCES

1. Taylor, E. C., Elastic Stability of Conical Shells Loaded by Uniform External Pressure, Third Midwestern Conference on Solid Mechanics, 1957, p. 86.
2. Seide, P., On the Buckling of Truncated Conical Shells under Uniform Hydrostatic Pressure, Proceedings of the Symposium on the Theory of Thin Elastic Shells, Delft, 1959, p. 363, also Space Technology Laboratories, Inc., Report No. EM 9-9, 1959.

3. Hoff, N. J. and Singer, J., Buckling of Circular Conical Shells under External Pressure, Proc. of the Symposium on the Theory of Thin Elastic Shells, Delft, 1959, p. 389.
4. Singer, J. and Eckstein, A., Experimental Investigations on the Instability of Conical Shells under External Pressure, The Bulletin of the Research Council of Israel, Vol IIC, No. 1, April 1962.
5. Jordan, W. D., Buckling of Thin Conical Shells under Uniform External Pressure, Bureau of Engineering Research, College of Engineering, University of Alabama, February 1955.
6. Radkowski, P. P., Buckling of Thin Single and Multi-layer Conical and Cylindrical Shells with Rotationally Symmetric Stresses, Proc. Third U.S. National Congress of Applied Mechanics, 1958, p. 443.
7. Bijlaard, P. P., Critical External Pressure of Conical Shells that are Simply Supported at the Edges, Bell Aircraft Corporation, Techn. Rep. No. 02-941-027, February 1953.
8. Pflüger, A., Stabilität dünner Kegelschalen, Ing. Archiv, Vol. 8, No. 3, 1937, p. 151.
9. Niordson, F. I. N., Buckling of Conical Shells Subjected to Uniform External Lateral Pressure, Transactions Royal Institute of Technology, Sweden, No. 10, 1947.
10. Bijlaard, P. P., Buckling under External Pressure of Cylindrical Shells Evenly Stiffened by Rings only, Journal of the Aeronautical Sciences, Vol. 24, June 1957, p. 437.
11. Windenburg, D. F., and Trilling, C., Collapse by Instability of Thin Cylindrical Shells under External Pressure, Trans, ASME, Vol. 56, 1934, p. 819.
12. Bijlaard, P. P., Buckling Stress of Thin Cylindrical Clamped Shells Subjected to Hydrostatic Pressure, Journal of the Aeronautical Sciences, Vol. 21, December 1954, p. 852.
13. Kollbrunner, C. F. and Meister, M., Ausbeulen, Springer-Verlag, Berlin, 1958.
14. Grigolyuk, E. I., On the Stability of a Closed Two-Layered Conical Shell Subjected to Uniform Normal Pressure, Inzhenernyi Sbornik, Vol. 9, 1954, p. 73.

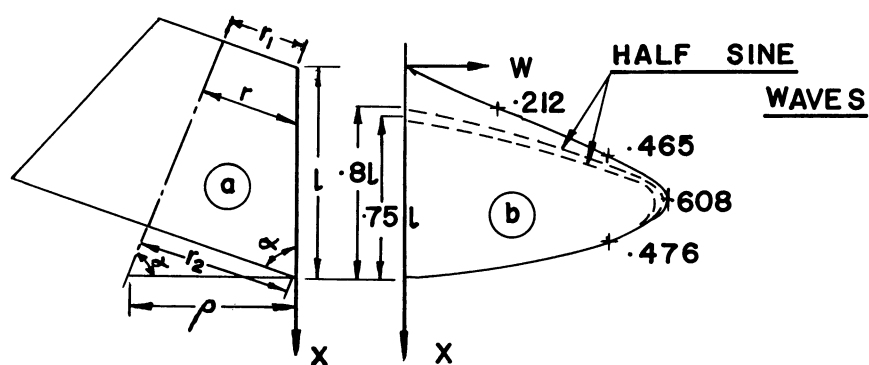
15. Tokugawa, T., Approximate Method of Calculating the Collapsing Pressure of Thin Cylindrical, Conical and Spherical Shells under Uniform External Pressure, Society of Naval Architects, Japan, Vol. 66, 1940, p. 231.
16. Bijlaard, P. P., Stability of Alclad Plates, Journal of the Aeronautical Sciences, Vol. 17, No. 4, 1950, p. 252.
17. Bijlaard, P. P., Discussion of paper "Buckling of Sandwich Cylinders under Combined Compression, Torsion and Bending Loads", by C. T. Wang, R. J. Vaccaro, and D. R. DeSanto, Journal of Applied Mechanics, Vol. 23, No. 1, March 1956, pp. 157.
18. Bijlaard, P. P., Method of Split Rigidities and Its Application to Various Buckling Problems, NACA TN 4085, July 1958.



(a) Complete conical shell.

(b) Buckling mode of shell according to eq. (3).

Figure 1.



(a) Frustum of conical shell.

(b) Buckling mode of frustum according to eq. (3).

Figure 2.

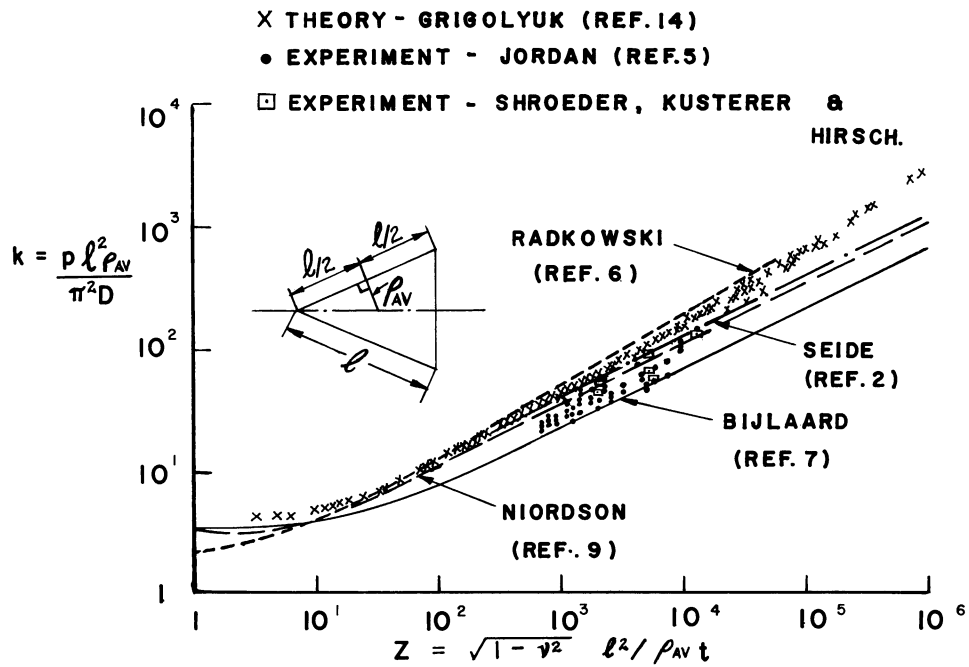


Figure 3.- Comparison of theoretical buckling pressures (curves and crosses) of complete conical shells with experiments (from 2nd ref. 2).

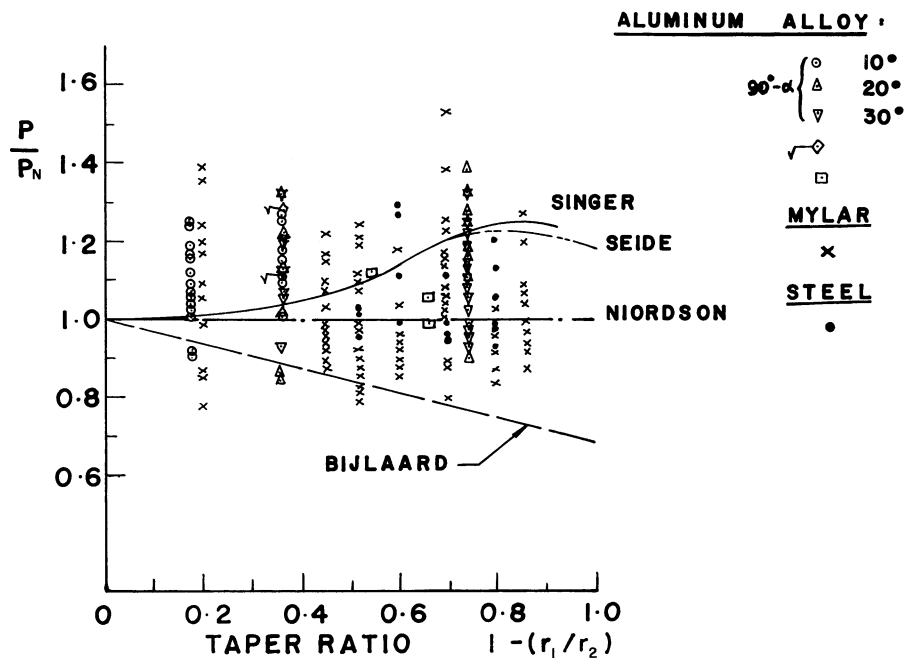


Figure 4.- Comparison of theoretical buckling pressures (curves) of truncated conical shells with experiments (from ref. 4).

AXISYMMETRIC SNAP BUCKLING OF CONICAL SHELLS

By Malcolm Newman and Edward L. Reiss*

Republic Aviation Corporation and New York University

SUMMARY

The authors give a brief account of some of their recent analytical and numerical studies of cone buckling, limiting the discussion to axisymmetric deformations.

Pertinent numerical results for the relaxation buckling of full cones subjected to uniform external pressure and Belleville springs deformed by axial edge loads are presented. In addition, bifurcation buckling problems are discussed. For a specific case, the existence of Friedrichs' intermediate buckling load, P_m , as applied to cones, is established. Upper and lower bounds for its value are given.

INTRODUCTION

The buckling of conical shells is, in many cases, characterized by a snapping phenomenon. Thus, at some critical load value, the shell suddenly jumps from a slightly deformed equilibrium state into a non-adjacent one with relatively large deformations. If the cone is initially shallow it may buckle axisymmetrically, as in spherical cap snapping. However, for slender cones experimentally observed buckling modes are asymmetrical and appear to be related to those of cylinder buckling.

The principal unresolved buckling problem for conical shells, as well as for cylindrical and spherical shells, is to determine the mechanism which "triggers" the sudden snapping and to estimate the load at which it occurs. Some investigators[†] have sought to determine this "critical" load by using classical linearized buckling theory or variants thereof. However, to obtain a deeper insight into the buckling phenomenon it is essential to employ a non-linear theory.

In this paper we briefly describe some of our recent analytical and numerical investigations of axisymmetric cone buckling.[‡] We first present the

*The work of the second author was supported by a grant from the U. S. Army Research Office (Durham) to the Courant Institute of Mathematical Sciences, New York University.

[†]See the review articles of refs. 1-2 and ref. 3 for detailed accounts of previous work.

[‡]The authors are currently preparing a paper which describes this work in greater detail.

results of a numerical study pertaining to the buckling of simply supported full cones subjected to uniform external pressure. We also indicate some numerical results obtained for the buckling of shallow truncated cones, sometimes called Belleville springs, deformed by axial edge loads. In both of these problems the shell undergoes small deformations from its initial conical shape immediately upon application of load. With increasing load, compressive membrane stresses are developed which essentially reduce the "stiffness" of the shell. Thus the shell "softens" with increasing load. After snapping, the membrane stresses tend to become tensile thereby increasing the "stiffness." Hence a "hardening" effect is observed yielding, at least for a limited range of parameters, deformations which increase with load at a decreasing rate (see fig. 1). In analogy to the discussion in reference 4 for spherical caps, we call the buckling phenomenon associated with this behavior relaxation buckling.

In our final example, a full cone subjected to external pressure is again considered. However, the pressure is no longer uniform. Instead, the pressure and boundary conditions are prescribed such that a membrane state of uniform compression is a solution (unbuckled) of the nonlinear problem. We then conjecture that bifurcation buckling will occur by branching from the unbuckled solution, yielding a load deflection characteristic similar to that shown in figure 2. For this problem, analytical studies are facilitated by our precise knowledge of the unbuckled solution. We are thus able to prove the existence of Friedrichs' intermediate buckling load, P_m (ref. 5), for which the potential energies of the buckled and unbuckled states are equal; we also establish upper and lower bounds on its value.

1. RELAXATION BUCKLING OF A COMPLETE CONE

Formulation of the Boundary Value Problem

We consider a complete conical shell of thickness t , base angle θ and slant length s_1 (fig. 3) subjected to a uniform external pressure p which is counted positive when directed inward. Assuming that the shell deforms axisymmetrically, the non-vanishing middle surface displacements u and w (see fig. 3) are functions of s only. Here s is the distance along a generator of the conical middle surface measured from the apex. The base of the cone is rigidly pinned, i.e., the meridional bending moment and horizontal displacement vanish at $s = s_1$.

We assume that the shell is constructed of a homogeneous, isotropic, elastic material for which Hooke's law is valid. Employing the usual assumptions of thin shell theory, we have derived the following nonlinear boundary value problem which describes the small finite deformations of the cone:

$$Ly(x) - Kz(x) [y(x) + 1] = Px^2 \quad (1a)$$

$$Lz(x) = -\frac{K}{2} [y^2(x) + 2y(x)] \quad (1b)$$

$$y(0) = z(0) = 0 \quad (2a)$$

$$\frac{dy(1)}{dx} + \nu y(1) = \frac{dz(1)}{dx} - \nu z(1) = 0. \quad (2b)$$

The differential operator L in (1) is defined by

$$L \equiv x \frac{d}{dx} \frac{1}{x} \frac{d}{dx} x$$

and the following dimensionless variables are employed:

$$x \equiv \frac{s}{s_1}, \quad y(x) \equiv \cot \theta \frac{dw(s)}{ds}$$

$$P \equiv \frac{6(1-\nu^2)s_1^3}{t^3 \tan \theta} \frac{P}{E}, \quad K \equiv \left[12(1-\nu^2) \right]^{\frac{1}{2}} \frac{s_1}{t} \tan \theta.$$

Here E is Young's modulus and ν is Poisson's ratio which we henceforth take as $\nu = .30$. The stress function $z(x)$ is defined in terms of the membrane (or middle surface) stresses $\sigma_\theta^0(s)$ and $\sigma_\phi^0(s)$ by the relations

$$\left[\frac{12(1-\nu^2)}{Et \tan \theta} \right]^{\frac{1}{2}} s_1 \sigma_\theta^0(s) = \frac{z(x)}{x},$$

$$\left[\frac{12(1-\nu^2)}{Et \tan \theta} \right]^{\frac{1}{2}} s_1 \sigma_\phi^0(s) = \frac{dz(x)}{dx}.$$

Equations (1), in which we refer to K as the geometric parameter and P as the loading parameter, can also be obtained by specializing the work of previous authors (references 6-8). In addition, a special case of equations (1) has previously been given by Grigoliuk (reference 9) in connection with his work on shallow cones.

The conditions (2a) are obtained from the assumption of regularity at the apex. However, in a sufficiently small neighborhood of the apex the shell is not "thin" and hence equations (1) may be invalid in this neighborhood. To circumvent this difficulty we define our boundary value problem for the complete cone as the limit of a sequence of boundary value problems for truncated cones (with the same values of K and P) as the slant length approaches that of the complete cone.

Presentation and Analysis of Numerical Results

We suppose that for a limited range of parameters the relation between P and deflection is similar to that shown in figure 1. The indicated curve implies that for $P < P_L$ and $P > P_U$ only one equilibrium state is possible. In the former case the equilibrium state is represented by a point on the unbuckled branch IOU, while in the latter case the equilibrium state corresponds to a point on the buckled branch LN. For P in the range $P_L < P < P_U$ there are three equilibrium states, represented by points on the unbuckled and buckled branches and the unstable branch UL. Friedrichs' energy buckling criterion (reference 5) as applied to cones implies the existence of an intermediate load P_m in the range $P_L < P_m < P_U$. For $P < P_m$ the potential energy of the unbuckled state is less than that of the buckled state and conversely for $P > P_m$.

We have obtained, for a range of K and P , numerical solutions* of the nonlinear boundary value problem defined by eqs. (1) and (2). The numerical method employed consists in solving, by iteration, a finite difference approximation of the boundary value problem. Essentially, the technique is similar to that previously employed in studies of the nonlinear bending and buckling of circular plates (references 11 - 13) and spherical caps (reference 10). Details of the method and extensive results will appear in a subsequent paper.

In the present paper, we give some of the numerical results directly concerned with the evaluation of P_U , P_m , and P_L . Figure 4 shows the variation of dimensionless base slope $y(1)$ vs. load for several values of K . We note that for $K = 2$ and 3.5 the cones are nonbuckling since the base slopes are single valued functions of load. Buckled branches are first discernible at $K = 4$. Thus, the transition between nonbuckling and buckling cones occurs in the interval $3.5 < K < 4$.

In figure 5, the variations of P_U , P_m , and P_L with K are shown. We note that when $K > 7.5$, then $P_L < 0$. This indicates the existence of buckled equilibrium states for $P \leq 0$, i.e., for unpressurized or internally pressurized cones. The numerical results, however, indicate that for these pressures the buckled states possess greater potential energy than the unbuckled states. For $P = 0$ this can be proven analytically. Thus, in this sense, the buckled solutions for $P \leq 0$ are unstable.

The dashed curve in figure 5 is obtained from a linearized approximation. The "critical" load value, $P = P_0$, thus determined, gives an exceptionally close approximation to P_m for the range of K considered.

*All computations were performed on the IBM 7090 computer at the Republic Aviation Corporation. The authors are indebted to B. Sackaroff and M. Gershinsky of the Applied Math. Section, Digital Computing Division for their aid in programming and running the computer code.

2. THE BELLEVILLE SPRING

Belleville springs are shallow truncated conical shells for which $x_0 \leq x \leq 1$, where x_0 is the dimensionless distance from the imagined apex to the plane of truncation.

We have applied our numerical procedure to a specific problem wherein the edges are subjected to compressive axisymmetric axial loads F . The edges are free to rotate and move radially. The differential equations describing the axisymmetric deformations are the same as equations (1) if the right side of equation (1a) is replaced by R , where

$$R \equiv \left[\frac{12(1-\nu^2)s_1}{\pi Et^3 \sin 2\theta} \right] F.$$

The boundary conditions are

$$\frac{dy(x_0)}{dx} + \frac{\nu}{x_0} y(x_0) = \frac{dy(1)}{dx} + \nu y(1) = 0, \quad (3a)$$

$$z(x_0) = z(1) = - \frac{\sin^2 \theta}{K} R. \quad (3b)$$

In figures 6 and 7, some results of the numerical computations are given for two buckling cone configurations. These are compared with the experimental results of Almen and Laszlo (ref. 14). The graphs show fair agreement between the calculated and measured axial shortening. However, Almen and Laszlo do not give a description of their testing technique and boundary conditions.

Stresses and deflections for several other cone configurations have been calculated. These have been compared with the results of approximate formulas and computer calculations given by Wempner (refs. 15-16), and Schmidt and Wempner (ref. 17). The agreement of results for the cases considered was found to be good.

3. BIFURCATION BUCKLING

We now consider a full cone subjected to an external pressure distribution which varies inversely with x . The appropriate differential equations are the same as equations (1) if Px^2 is replaced by Px in equation (1a). The edge $x = 1$ is assumed to be restrained against rotation but free to expand or contract horizontally. It is then easy to show that

$$y(x) \equiv 0, \quad z(x) = - \frac{P}{K} x \quad (4)$$

is a solution (unbuckled) of the nonlinear boundary value problem for all K and P . We conjecture* that additional solutions (buckled) will appear by branching from equation (4) at an infinite number of discrete values $P = P_i$, $i = 1, 2, \dots$. The P_i are the eigenvalues of the linearized shell buckling theory obtained by omitting nonlinear terms in the differential equations. The load deflection curves are then similar to those shown in figure 2.

It is assumed that for each K and P the potential energy functional possesses a minimum. We can then prove the existence of an intermediate buckling load P_m . Furthermore, we have obtained upper and lower bounds for P_m given by,

$$\omega^2 \leq P_m < \bar{P}(K),$$

where ω is the first zero of the Bessel function $J_1(x)$ and $\bar{P}(K) = \text{g.l.b. } P_i$. The quantity ω^2 is also the dimensionless buckling load, HR^2/D of a radially compressed clamped circular plate, where H , R , and D are the critical edge thrust, plate radius and flexural rigidity, respectively. As in the case of spherical caps (ref. 4) we refer to this as the "equivalent" flat plate problem.

Upper bounds for P_m which are lower than \bar{P} have also been obtained by a minimization procedure.

CONCLUDING REMARKS

We are currently extending our numerical calculations for the relaxation buckling problems discussed in Sections 1 and 2 to include a larger range of parameter values. In addition, numerical solutions for other cone problems are being considered. In particular, we plan to obtain accurate numerical approximations of P_m for the bifurcation problem discussed in the previous section.

It appears likely that some of the analysis briefly outlined in Section 3 can be extended, with suitable modification, to unsymmetric bifurcation buckling of cones.

There are, to the authors' knowledge, no experimental results available for the problems and ranges of parameters considered in Sections 1 and 3. Carefully performed experiments for these cases may give valuable insight into the buckling mechanism.

*Similar conjectures have been proved for circular plates (ref. 18) and spherical caps (ref. 4)

REFERENCES

1. Nash, W.A., "Recent Advances in the Buckling of Thin Shells," Applied Mechanics Reviews, Vol. 13, No. 3, pp. 161-164, (1960).
2. Fung, Y.C., and Sechler, E.E., "Instability of Thin Elastic Shells," Proc. of the First Symposium on Naval Structural Mechanics, Stanford University, California, Pergamon Press, pp. 115-168, (1960).
3. Seide, P., "On the Buckling of Truncated Conical Shells Under Uniform Hydrostatic Pressure," Proc. of the Symposium on the Theory of Thin Elastic Shells, I. U. T. A. M., Delft, pp. 363-386, (1959).
4. Reiss, E. L., "Birurcation Buckling of Spherical Caps," to appear.
5. Friedrichs, K.O., "On the Minimum Buckling Load for Spherical Shells," von Kármán Anniversary Volume, California Institute of Technology, Pasadena, pp. 258-272, (1941).
6. Chien, W.Z., "The Intrinsic Theory of Thin Shells and Plates," Quart. of Appl. Math., Vol. II, No. 2, pp. 120-135, (1944).
7. Reissner, E., "On Axisymmetrical Deformations of Thin Shells of Revolution," Proc. Symp. Appl. Math., Vol. III, pp. 27-52, (1950).
8. Mushtari, Kh.M., and Galimov, K.Z., Nonlinear Theory of Thin Elastic Shells, Tatknigoizdat, Kazan, p. 304, (1957). Now available in English as NASA-TT-F62, (1961).
9. Grigoliuk, E.I., "On the Instability with Large Deflections of a Closed Laminated Conical Shell Subject to Uniform Normal Surface Pressure," Institute of Mech. of the Academy of Sciences, USSR, Vol. XXII, pp. 111-119, (1955).
10. Keller, H.B., and Reiss, E. L., "Spherical Cap Snapping," Jour. Aero/Space Sciences, Vol. 26, No. 10, pp. 643-652, (1959).
11. Keller, H.B., and Reiss, E. L., "Iterative Solutions for the Non-Linear Bending of Circular Plates," Comm. on Pure and Appl. Math, Vol. XI, No. 3, pp. 273-292, (1958).
12. Keller, H.B. and Reiss, E. L., "Non-Linear Bending and Buckling of Circular Plates," Proc. Third U.S. Nat'l. Cong. of Appl. Mech., Providence, R.I., pp. 375-385, (1958).

13. Newman, M. and Forray, M., "Axisymmetric Large Deflections of Circular Plates Subjected to Thermal and Mechanical Load," Proc. of the Aerospace Forum I Session, S.M.F. Fund Paper No. FF-30, pp. 56-67, presented at the IAS 30th Annual Meeting, New York, (1962).
14. Almen, J.O., and Laszlo, A., "The Uniform-Section Disk Spring," Trans. ASME, Vol. 58, No. 4, pp. 305-314, (1936).
15. Wempner, G.A., "The Conical Disk Spring," Proc. Third U.S. Nat'l. Congress of Appl. Mech., Providence, R.I., pp. 473-478, (1958).
16. Wempner, G.A., "Axially Symmetric Deformations of a Shallow Conical Shell," Ph.D. Thesis, University of Illinois, (1957).
17. Schmidt, R., and Wempner, G.A., "The Nonlinear Conical Spring," Trans. ASME, 81E (J. Appl. Mech.), 4, pp. 681-682, (1959).
18. Keller, H.B., Keller, J.B., and Reiss, E.L., "Buckled States of Circular Plates," Quart. Appl. Math., Vol. XX, No. 1, pp. 55-65, (1962).

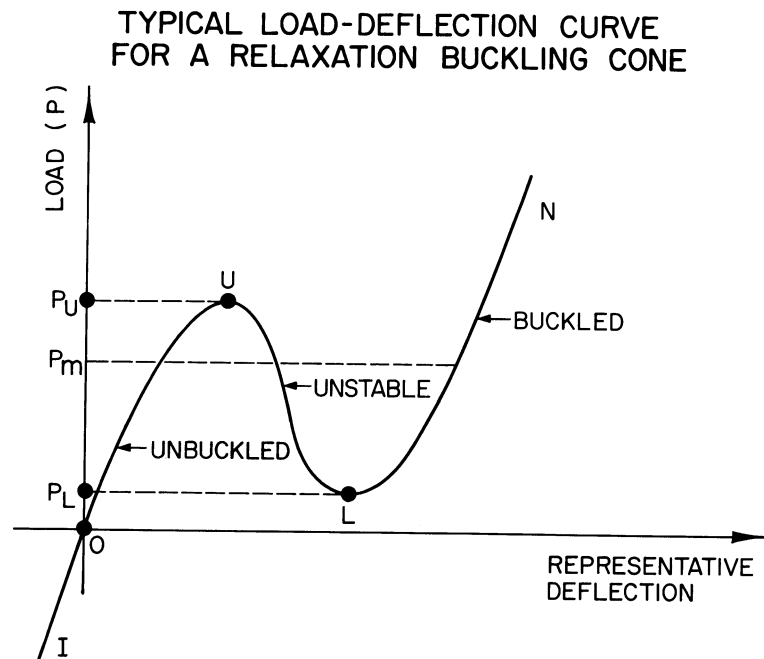


Figure 1

**LOAD-DEFLECTION CHARACTERISTIC FOR
BIFURCATION BUCKLING (CONJECTURED)**

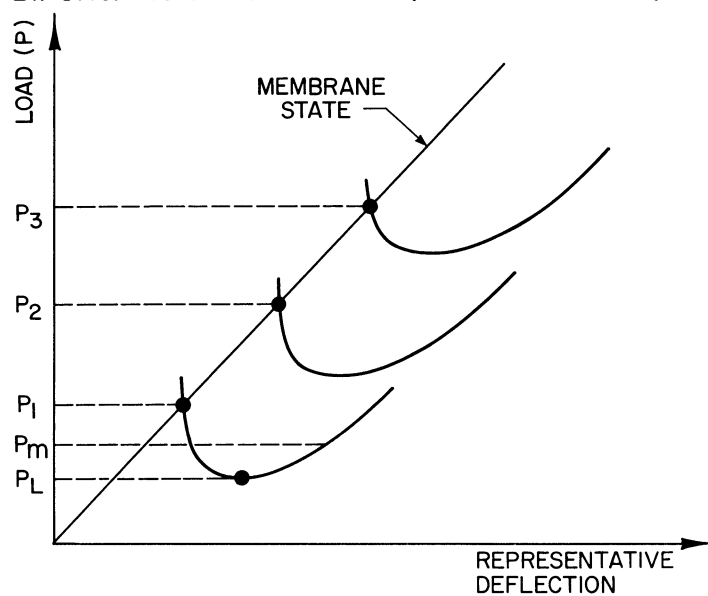


Figure 2

CONE GEOMETRY AND DISPLACEMENTS

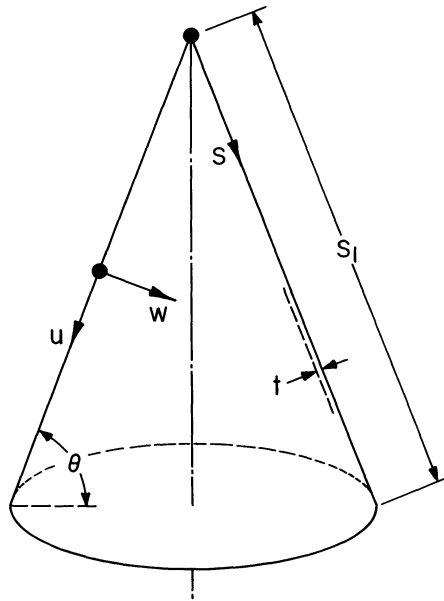


Figure 3

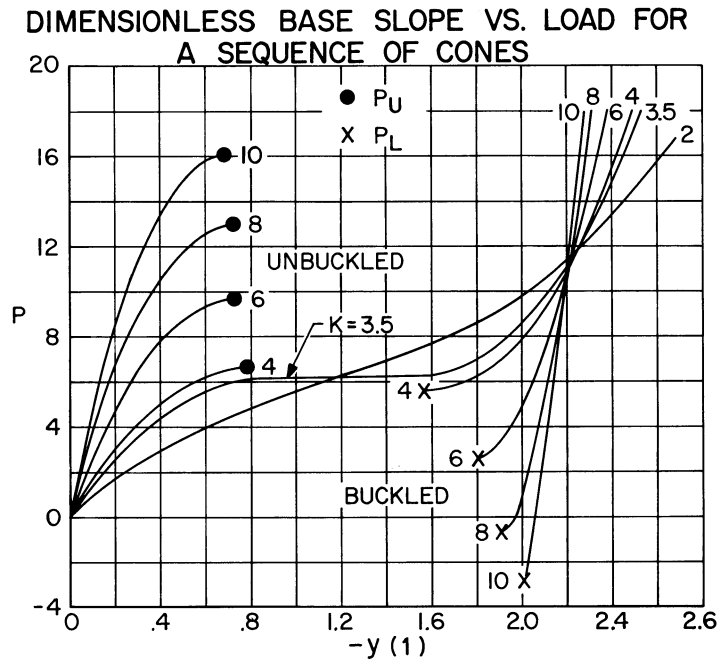


Figure 4

BUCKLING LOADS VS. K

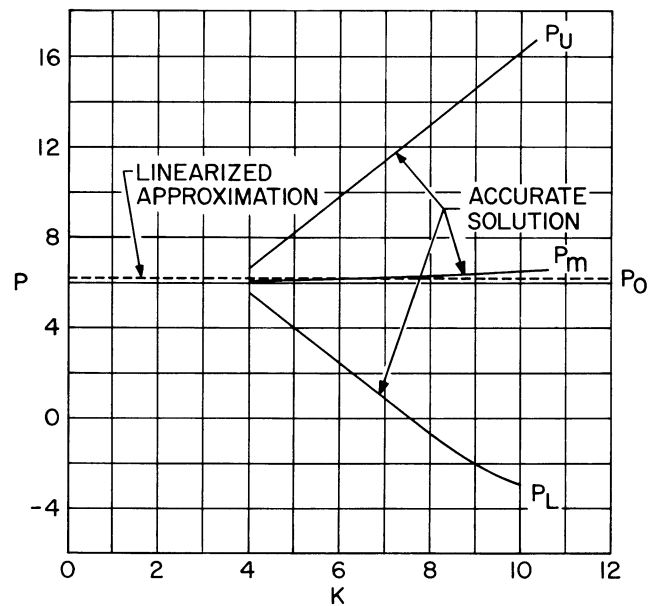


Figure 5

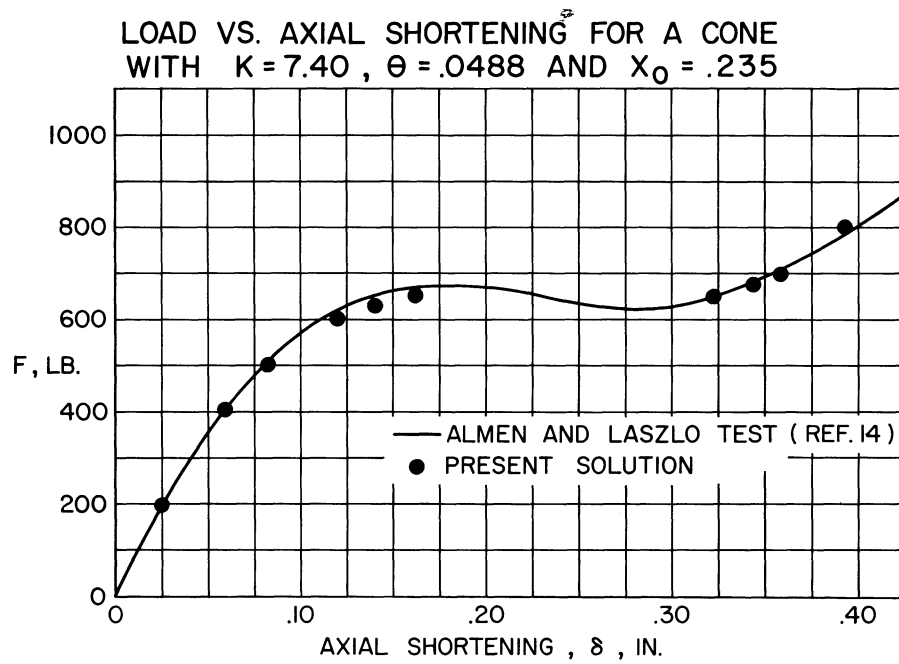


Figure 6

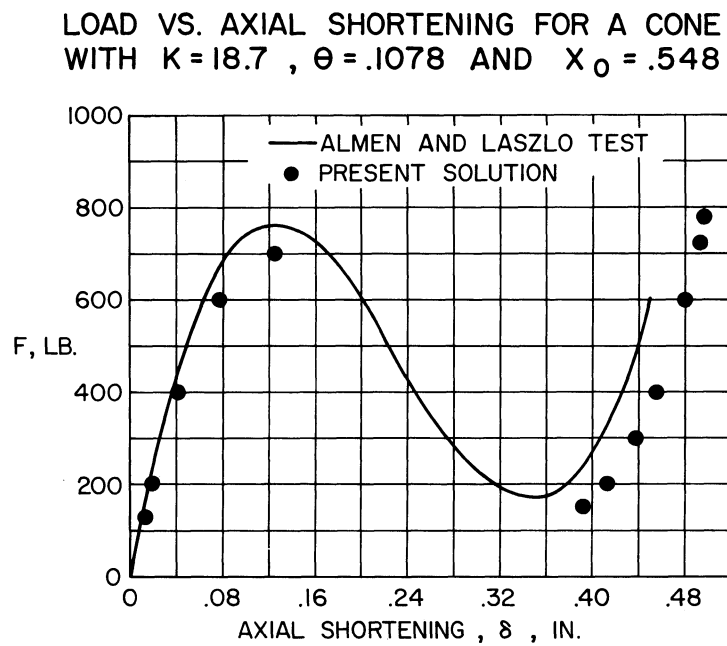


Figure 7

BUCKLING OF ORTHOTROPIC AND STIFFENED CONICAL SHELLS*

By Josef Singer

Technion, Israel Institute of Technology.

SUMMARY

Donnell type stability equations for thin circular orthotropic conical shells are presented and solved for external pressure, axial compression and combined loading. The solution is likewise applied to stiffened conical shells. Correlation with equivalent cylindrical shells yields a simple approximate stability analysis for orthotropic or ring-stiffened conical shells under hydrostatic pressure. The general instability of stiffened conical shells under hydrostatic pressure is also analysed by a more accurate approach. Preliminary experimental results for buckling of ring-stiffened conical shells under hydrostatic pressure are presented and discussed.

INTRODUCTION

Most aerospace shell structures are orthotropic or stiffened shells. The increasing use of new constructional materials, such as reinforced plastics, fiber reinforced materials etc., which have orthotropic elastic properties, have focussed attention on orthotropic shell theory and the corresponding stability analysis. Buckling of orthotropic cylinders has been subject to extensive investigations (See refs. 1 - 4), and the general instability of stiffened cylindrical shells has likewise been analysed by consideration of an equivalent orthotropic shell (refs. 5 - 6), as well as by other approaches (See, for example, ref. 7). In this report, the investigations are extended to orthotropic and stiffened conical shells.

The method developed in reference 8 for isotropic conical shells is applied to the solution of Donnell type stability equations for orthotropic conical shells, derived in reference 9, for external pressure loading. The solution is then used to analyse the general instability of ring-stiffened conical shells under external pressure by consideration of an equivalent orthotropic shell. Typical cases of orthotropic and ring stiffened conical shells are computed and correlated with equivalent cylindrical shells. The comparison brings out again the taper ratio as the most significant factor representing the conicity in

*This work was supported in part by the U.S. Air Force under Grant No. AF-EOAR-62-61 and monitored by the European Office, Office of Aerospace Research.

the case of buckling under uniform external pressure, as shown for isotropic shells by Seide (ref. 11) and reconfirmed by the author for slightly different boundary conditions (ref. 8). A relatively simple approximate analysis for the buckling of any orthotropic or ring-stiffened conical shell under uniform external pressure is obtained from the correlation.

As for isotropic conical shells (ref. 12), the same linear analysis is extended to the case of axial compression and combined axial compression and external or internal pressure. On the basis of results for cylindrical shells (ref. 1), the linear orthotropic theory may be expected also to yield fairly realistic buckling loads for conical shells with closely spaced stiffeners.

The more accurate method of separate "distributed stiffness" of rings and stringers is then employed to show the effect of eccentricity of stiffeners on the general instability of stiffened conical shells under external pressure.

Preliminary experimental results for 3 machined ring-stiffened conical shells verify in general the theoretical analysis for buckling under hydrostatic pressure.

The analysis referred to is written in non-dimensional form, and the coordinates and displacements are non-dimensionalized through division by a , the distance along a generator of the top of a truncated cone from the vertex. (See fig. 1).

SYMBOLS

D	$= [Eh^3/12 (1 - \nu^2)], \text{ in. lb.}$
E_x, E_ϕ, E, E_1, E_2	$= \text{moduli of elasticity of orthotropic shell, and of stiffened shell and its stringers and rings respectively, psi}$
G	$= \text{shear modulus, psi}$
h	$= \text{thickness of shell, in.}$
K^4	$= 12 \mu (a/h)^2$
p	$= \text{hydrostatic pressure or critical hydrostatic pressure, psi}$
\bar{p}	$= \text{critical hydrostatic pressure or equivalent cylindrical shell, psi}$
P	$= \text{axial compressive load, lb.}$
t	$= \text{number of circumferential waves}$

u	$= (u^*/a) =$ non-dimensional displacement of shell middle surface along a generator
v	$= (v^*/a) =$ non-dimensional circumferential displacement of shell middle surface
w	$= (w^*/a) =$ non-dimensional radial displacement of shell middle surface
x	$= (x^*/a) =$ non-dimensional axial coordinate, along a generator
x_2	$=$ ratio of distance of the bottom of a truncated cone from the vertex to that of the top.
α	$=$ cone angle
$\alpha_1 = (h E_x / \mu)$, lb./in.
$\alpha_2 = (h E_\phi / \mu)$, lb./in.
$\alpha_3 = G h$, lb./in.
γ	$= (1 - \nu_{\phi x})/2$ for orthotropic, or $(1 - \nu)/2$ for isotropic shells
μ	$= 1 - \nu_{x\phi} \nu_{\phi x}$
$\nu_{x\phi}, \nu_{\phi x}, \nu$	$=$ Poisson's ratios for orthotropic and isotropic shells
$\bar{\sigma}_x, \bar{\sigma}_\phi, \bar{\tau}_{x\phi}$	$=$ membrane stresses of prebuckling state, psi
ϕ	$=$ circumferential coordinate

Subscripts following a comma indicate differentiation.

ORTHOTROPIC THEORY

Buckling of Orthotropic Conical Shells Under External Pressure

The stability equations for thin circular orthotropic conical shells employed in the analysis are presented (in non-dimensional form) in Appendix A. These equations are derived in reference 9 and reduce to Seide's equations (ref.10) for the case of isotropic shells or to Bodner's equations for orthotropic cylindrical shells (ref.5) when the cone angle approaches zero. The third equation, in the radial direction, is however a Batdorf type modified equation, instead of the usual eighth order equation, to facilitate its solution by the Galerkin method. It reduces therefore to the modified equation of reference 8 for the case of

isotropic shells, instead of the corresponding equation of reference 10.

The problem is solved for a cone supported in a manner approximating conventional simple supports. The conditions for the radial displacement are therefore

$$w = 0 \quad \text{at} \quad x = 1, x_2 \quad (1)$$

and

$$w_{,xx} \quad (v_{\phi x} / x) w_{,x} = 0 \quad \text{at} \quad x = 1, x_2 \quad (2)$$

The circumferential axial displacements (along the generators) are assumed to be resisted by elastic supports instead of the usual requirements that $v = 0$ and u is unrestrained. These elastic supports, however, approximate the usual conditions fairly closely as in the case of isotropic shells (ref. 8).

Now, since an orthotropic shell may be expected to buckle in a mode similar to that of an isotropic one, the same solution is assumed for the displacement functions

$$u = I_m \sum_{n=1}^{\infty} A_n x^s \sin t\phi$$

$$v = I_m \sum_{n=1}^{\infty} B_n x^s \cos t\phi \quad (3)$$

$$w = I_m \sum_{n=1}^{\infty} C_n x^s \sin t\phi$$

where C_n and t are real (t is the number of circumferential waves of the buckling deformations), s is the complex number

$$s = \gamma + i\eta \beta \quad (4)$$

n is an integer and the symbol I_m indicates the imaginary part of the solution.

The detailed analysis is carried out in reference 13, and only the salient features are given here. Substitution of the complex functions of equations (26) into the first two stability equations (eqs. (A1) and

(A2) of Appendix A) yields A_n and B_n in terms of C_n , and thence the spring constants representing the elastic restraints. Since these restraints arise from the non-compliance of the assumed solutions with the u and v boundary conditions, their effect may be expected to be of the same order of magnitude for isotropic and orthotropic conical shells, and this is confirmed by calculations for a typical shell (ref. 13). Hence the effect of the elastic restraints is very small and may be neglected (see refs. 14 and 8). The boundary conditions on w , equations (1) and (2), are enforced rigorously, and hence β and γ are determined as

$$\beta = \pi/l g_e x_2 \quad (5)$$

and

$$\gamma = (1 - \nu_{\phi x})/2 \quad (6)$$

With the assumption that the membrane stresses represent the prebuckling stress state satisfactorily, the third stability equation, eq. (A3), is then solved by the Galerkin method, as in reference 8. The critical pressure is obtained from the resulting set of linear equations, which are for uniform hydrostatic pressure

$$\sum_{n=1}^{\infty} C_n \left\{ [(-1)^{m+n} x_2^{2\gamma-2} - 1] G_1(n, m) + K^4 (\alpha_2/\alpha_1) \cos^2 \alpha [(-1)^{m+n} x_2^{2\gamma} - 1] G_2(n, m) \right. \\ \left. + K^4 [(-1)^{m+n} x_2^{2\gamma+1} - 1] G_3(n, m) (p/E_x) (a/h) \tan \alpha \right\} = 0 \quad (7)$$

where the symbols $G(n, m)$ denote values of the G functions (algebraic expressions given in ref. 13) for the particular n and m .

The critical pressures, for the case of uniform hydrostatic pressure loading, were computed for some typical orthotropic shells, and compared with those for similar isotropic shells (see table 1). The results confirm Hess's conclusions (ref. 2), about the desirability of $(E_x/E_\phi) < 1$ and the general weight saving potential in the use of orthotropic material, also for conical shells.

The analysis can readily be applied to the case of external pressure varying in the axial direction. Since the orthotropy does not affect the load terms (the G_3 terms of equations (7) are identical to those of ref. 8), one has only to replace them by the corresponding terms for axially varying external pressure derived for isotropic shells (ref. 8) and proceed as before.

General Instability of Stiffened Conical Shells Under External Pressure

The above analysis is now applied to the investigation of the general instability of stiffened conical shells under external pressure by consideration of an equivalent orthotropic shell. Though the method may be used for longitudinal stiffening (stringers) as well as for circumferential stiffening (rings or frames), the former is omitted on account of the marked inferiority of stringers as stiffeners against general instability under external pressure, and since the orthotropic approach would be limited only to stringers which increase in area, or number, in accordance with the cone diameter.

The ring-stiffened conical shell is correlated to an equivalent orthotropic one in the manner proposed by Bodner for cylindrical shells (ref. 5). Essentially, the equivalent orthotropic shell is an isotropic one with a larger effective thickness in the circumferential direction to account for the contribution of the rings to the circumferential extensional rigidity, and having also a larger bending rigidity in the circumferential direction due to the marked increase in the effective moment of inertia of the ring and shell combination. The increase in extensional rigidity is represented by the parameter

$$k = 1 + (A_2/a_0 h) \quad (8)$$

where A_2 is the cross sectional area of the ring, and a_0 its spacing; and the increase in bending rigidity is represented by f a second parameter

$$f = I_\phi / [a_0 h^3 / 12 (1-\nu^2)] \quad (9)$$

where I_ϕ is the effective moment of inertia on the ring and shell combination,

$$I_\phi = I_{22} + A_2(e_2 - \bar{z}_2)^2 + [a_0 h^3 / 12 (1-\nu^2)] + [a_0 h \bar{z}_2^2 / (1-\nu^2)] \quad (10)$$

where I_{22} is the moment of inertia of the ring cross section about its centroid and the other geometrical quantities are shown in fig. 1.

Once the equivalent orthotropic shell has been defined, the orthotropic theory can be applied (see ref. 13). It should be noted that Bodner's approximation of unity for k (ref. 5) is verified, with an error of much less than one percent, also by calculations for conical shells. In Table 1, the critical pressures for typical ring-stiffened conical shells are again compared with those for corresponding isotropic shells.

Correlation with Equivalent Cylindrical Shells

For isotropic conical shells under hydrostatic pressure, Seide (ref. 11) showed that the critical pressures can be correlated to those of equivalent cylindrical shells, bringing out the taper ratio, $\psi = 1 - (R_1/R_2)$, as the significant parameter of conicity. The equivalent cylindrical shell is taken on the basis of Niordson's results (ref. 15) as one having a length equal to the slant length of the cone, l , a radius equal to its average radius of curvature, ρ_{av} , and the same thickness h , where

$$\begin{aligned}
 l &= a (x_2 - 1) \\
 \rho_{av} &= [a(1 + x_2) \tan \alpha/2] = (R_1 + R_2)/2 \cos \alpha \\
 \psi &= 1 - (1/x_2) = 1 - (R_1/R_2)
 \end{aligned}
 \tag{11}$$

The correlation yielded an approximate curve for the ratio of the critical pressure of conical shells to that of their equivalent cylindrical shells versus the taper ratio

$$(p/\bar{p}) = g(\psi) \tag{12}$$

(fig. 2 of ref. 15). A very similar curve was obtained in reference 8 for conventional simple supports (which differ slightly from Seide's boundary conditions) verifying the significance of the taper ratio as the main geometrical parameter of the conicity in the case of external pressure loading.

It is therefore reasonable to expect that also for the case of orthotropic and ring-stiffened conical shells under external pressure the taper ratio will be the significant parameter of conicity. The orthotropy and ring-stiffening will probably affect cylindrical and conical shells in the same manner and hence the ratio of (p/\bar{p}) should be very nearly the same as for isotropic shells.

In order to investigate this hypothesis, the critical pressures for the equivalent cylindrical shells were computed by Bodner's method (ref. 5) for all the typical conical shells given in Table 1, which include orthotropic shells of fiberglass reinforced epoxy and plywood, and ring stiffened shells of steel. The ratios (p/\bar{p}) are plotted in fig. 2 and compared with the curve $g(\psi)$ taken from reference 8, since the present analysis is for the same simple supports assumed there. The comparison in fig. 2 verifies the hypothesis and yields a very convenient approximate method for the determination of the critical uniform external pressure of any orthotropic, or ring-stiffened, conical

shell.

The procedure involves: (a) calculation of the dimensions of the equivalent cylindrical shell, using equations (11); (b) computation of the critical pressure \bar{p} for this equivalent shell by Bodner's method (ref. 5), and (c) reading the correct g from fig. 2. Finally p_{cr} for the conical shell is obtained from $p = \bar{p} g$.

Buckling Under Axial Compression and Under Combined Axial Load and External or Internal Pressure

In reference 12, the solution of reference 8, is applied to a linear analysis of the asymmetrical buckling of thin isotropic conical shells under uniform axial compression, after the effect of axial constraint has been shown to be small also for this type of loading (ref. 16). Calculations for a typical isotropic conical shell yielded a slightly lower buckling load than by the corresponding linear axisymmetrical analysis (ref. 17). The analysis is now extended to orthotropic shells, and can then be applied directly to stiffened shells by consideration of an equivalent orthotropic shell.

The final set of linear equations of the stability analysis eqs. (7) have separate load terms which are not affected by the orthotropy and are hence identical to those for isotropic shells. Provided the same form of buckling displacement is possible, only this load term has to be changed, if instability under a different type of loading has to be investigated. For uniform axial compression the third term of equations (7) is therefore replaced, as for isotropic conical shells, by

$$K^4 [(-1)^{m+n} x_2^{2n-1} - 1] G_4(n, m) (P/E_x) (1/\pi a h \sin 2\alpha) \quad (13)$$

where $G_4(n, m)$ is an algebraic expression given in reference 12.

It should be noted that though the same form of deflection functions is assumed as solutions in case of buckling under external pressure and under uniform axial compression, the calculations differ slightly, since the basic buckling mode has, instead of $n = 1$, a number of axial waves of the same order as t (see ref. 12).

As the analysis is linear, combinations of load terms may be added, subject to the above mentioned proviso of admissibility of displacement functions. Hence for combined axial compression and external or internal pressure the final simultaneous equations would be obtained directly by adding expression (13) to equation (7), changing the sign of p in the case of internal pressure or that of P in the case of a tensile axial load.

Insofar as linear theory can represent actual buckling shapes, it may be expected from similar analyses for isotropic conical and cylindrical shells, that asymmetrical modes will predominate for combinations of external pressure and axial compression, or tension, whereas in the

presence of internal pressure symmetrical modes will appear (ref. 18).

MORE ACCURATE ANALYSIS FOR STIFFENED CONICAL SHELLS

Stress-Strain Relations

The instability of ring- or stringer- stiffened conical shells may be analysed more accurately by consideration of the separate distributed stiffness of the rings and stringers. The circumferential or longitudinal stiffeners are assumed each to be distributed evenly along one spacing (one half spacing each side), the middle surface of the shell being chosen as reference line. This approach is valid for closely spaced stiffeners which need not be necessarily evenly spaced and equal, and permits detection of differences in the critical load caused by their eccentricity.

The theory sets out with the formulation of stress-strain relations of the shell together with stiffeners. The stiffeners may have different elastic properties, and the strains are assumed to be identical at the contact surface of stiffeners and shell.

For the shell the stress and strain relations are

$$\sigma_x(z) = [E/(1-\nu^2)] [\epsilon_x + \nu\epsilon_\phi - (z/a)(\kappa_x + \nu\kappa_\phi)] \quad (14)$$

$$\sigma_\phi(z) = [E/(1-\nu^2)] [\epsilon_\phi + \nu\epsilon_x - (z/a)(\kappa_\phi + \nu\kappa_x)]$$

while for the stiffeners they are

$$\begin{aligned} \sigma_x(z) &= E_1 [\epsilon_x - (z/a) \kappa_x] \\ \sigma_\phi(z) &= E_2 [\epsilon_\phi - (z/a) \kappa_\phi] \end{aligned} \quad (15)$$

Hence the forces and moments acting on an element become

$$\begin{aligned} N_x &= [Eh/(1-\nu^2)] [\epsilon_x(1+\mu_1) + \nu\epsilon_\phi - \chi_1 \kappa_x] \\ N_\phi &= [Eh/(1-\nu^2)] [\epsilon_\phi(1+\mu_2) + \nu\epsilon_x - \chi_2 \kappa_\phi] \end{aligned} \quad (16)$$

$$N_{x\phi} = N_{\phi x} = [Eh/2(1+\nu)] \gamma_{x\phi}$$

and

$$\begin{aligned} M_x &= - (D/a) [\kappa_x(1+\eta_{o1}) + \nu\kappa_\phi - \zeta_1 \epsilon_x] \\ M_\phi &= - (D/a) [\kappa_\phi(1+\eta_{o2}) + \nu\kappa_x - \zeta_2 \epsilon_\phi] \\ M_{x\phi} &= (D/a) [(1-\nu) + \eta_{t1}] \kappa_{x\phi} \\ M_{\phi x} &= - (D/a) [(1-\nu) + \eta_{t2}] \kappa_{x\phi} \end{aligned} \quad (17)$$

where μ_1 and μ_2 are the increases in effective cross sectional area of the shell due to stringers and rings respectively, χ_1 and χ_2 are the changes in extensional stiffness caused by the eccentricities of stringers and rings, η_{o1} , η_{o2} , η_{t1} , η_{t2} are the increases in bending and twisting stiffness of the shell due to stringers and rings, and ζ_1 and ζ_2 are the changes in bending stiffness caused by the eccentricities of stringers and rings.

With the aid of these relations the stability equations are obtained in terms of displacements. These equations are similar to those for isotropic shells, before uncoupling, though more complicated.

Buckling Under External Pressure

General instability under external pressure is analysed with the aid of the same solution employed for isotropic and orthotropic conical shells, equations (3). However, since the more accurate stiffened shell equations are not amenable to the direct solution, coupled with the Galerkin method for the third equation, employed for isotropic and orthotropic shells, a modified solution using successive correction factors and a variational approach, that is basically an extension of the Galerkin method, has been applied by M. Baruch in his unpublished doctoral dissertation under the guidance of the author. Since the successive correction factors converge rapidly, the method is not too laborious. The extended Galerkin approach also permits direct estimates and correction of the error involved in the partial compliance only with the boundary conditions for u and v . When the stiffeners have no eccentricity, or the eccentricity is neglected, the method reduces to the orthotropic analysis discussed above.

The Effect of Eccentricity of Stiffeners

By an analysis similar to that outlined above, Baruch and the author investigated the effect of eccentricity of stiffeners on the general instability of stiffened cylindrical shells under hydrostatic pressure. For typical shells with rings on the inside, the critical pressures were found to be 11.5 percent to 13.5. percent above those obtained with the identical rings on the outside. For typical conical shells similar magnitudes are obtained. For example, for two ring stiffened conical shells of the following properties

$$\begin{aligned} \alpha &= 30^\circ & a &= 57.59 \text{ in.} & (A_2/a_o h) &= 0.1471 & (e_2/h) &= 1.653 \\ \nu &= 0.3 & h &= 0.1 \text{ in.} & [I_{22}/(a_o h^3/12)] &= 0.7819 & (\bar{z}_2/h) &= 0.2119 \end{aligned}$$

one obtains

x_2	Taper Ratio $\psi = 1 - (1/x_2)$	(ρ_{av}/h)	p/p _{no eccentricity}		$\left(\frac{p_{\text{inside rings}}}{p_{\text{outside rings}}} \right)$
			inside rings	outside rings	
1.5	0.333	415	1.021	0.963	1.061
5.0	0.800	995	1.058	0.965	1.093

It may be concluded that from a buckling point of view the placing of stiffening rings (or frames) on the inside of the shell is advantageous. Further it should be noted that the effect of eccentricity of stiffening rings is of sufficient magnitude to require care in the interpretation of experimental results.

For stringers the effect of eccentricity is smaller and opposite: outside stringers yield higher instability pressures than inside ones, as has also been shown for cylindrical shells.

EXPERIMENTAL INVESTIGATION

The first phase of an experimental program on the instability of orthotropic and stiffened conical shells initiated at the Technion, is concerned with the general instability of ring stiffened shells under hydrostatic pressure. The test rig (fig.3) is similar to that used in previous investigations of isotropic shells (ref. 19), except that it is smaller and designed for higher pressures. The specimens (see fig.4a) are of mild steel, have rings on the outside, and are fabricated by careful machining (a tolerance of ± 0.001 in. was obtained on thickness of shell and rings). The specimens are clamped at the edges. As in reference 20, strain gages are installed around the circumference and opposite a stiffening ring near the estimated position of maximum buckling deflection. On the first test cone, an additional row of strain gages was installed opposite the centre of the bay between two stiffening rings, to detect early panel instability. No panel instability appeared before failure by general instability, and the fact that the strain values of the two rows did not differ appreciably during the whole test, seems to justify the assumption of effectiveness of complete bay length, a_0 , implied in the theoretical analyses.

Three conical shells of similar geometry ($R_1 = 1.77$ in., $R_2 = 5.67$ in., and $\alpha = 20^\circ$) were tested. All failed by general instability. The strain gage readings indicated clearly the embryonic lobe formation discussed in references 19 and 20, and the cones buckled by a sudden formation of one large general instability wave in place of one of those embryonic lobes (see fig.4b). Since the buckling stress was not far from the yield stress of the material, the elastic buckling transformed immediately into plastic deformation. Attempts to raise the pressure again resulted in growth of the wave (and appearance of one further wave in two tests) with additional small plastic panel buckles.

Theoretical buckling pressures which would appear for perfect cones

were determined from strain gage readings of the 3 tests by the extension of Southwell's method given in reference 21. The intercept and the slope methods, suggested there, yielded nearly similar perfect cone buckling pressures, which were about 8 percent higher than the observed ones, as follows:

Specimen no.	1	2	3
Theoretical buckling pressure (psi)	106.1	96.2	95.8
Observed failing pressure (psi)	99.2	94.0	84.6
Perfect cone buckling pressure (psi)	106	103	92

The ratios of observed failing pressure and perfect cone buckling pressure to the equivalent cylinder buckling pressure (\bar{p}) is also plotted in figure 2. These preliminary results are in good agreement with the theory. It should be noted, however, that the test specimens were clamped while the theory is for simple supports. However, the effect of clamped edges should be rather small for ring stiffened shells due to their relatively large circumferential stiffness (for cylindrical shells it is usually neglected - see ref. 20).

FUTURE RESEARCH

Both the orthotropic theory and the more accurate theory for stiffened shells should be extended to torsion and combined loading and verified experimentally. Further experimental investigation of the buckling under external pressure of orthotropic and ring-stiffened conical and cylindrical shells is required. The tests should also aim at verifying the effect of eccentricity of stiffeners postulated by the theory. The effect of clamped edges should also be further clarified. Extensive tests of cylindrical and conical shells with closely spaced stiffeners under axial compression are needed to confirm the remarkable agreement with linear theory pointed out by Becker and Gerard (ref. 1) in the case of a recent test by Pugliese. Research along these lines is planned at the Technion.

APPENDIX A

STABILITY EQUATIONS FOR ORTHOTROPIC CONICAL SHELLS

For orthotropic conical shells the uncoupled Donnell type stability equations of reference 9 can be written in non-dimensional form (for zero surface forces) as

$$L_{10}(u) = \cot \alpha \left\{ (L_5 + L_9) [x \nu_{\phi x} w_{,x} - (\alpha_2/\alpha_1) w] - (1/\sin \alpha) (\alpha_2/\alpha_1) (\alpha_2/\alpha_3) L_7(w, \phi) \right\} \quad (A1)$$

$$L_{10}(v) = (\alpha_2/\alpha_3) \cot \alpha \left\{ -L_8 [x \nu_{\phi x} w_{,x} - (\alpha_2/\alpha_1) w] + (1/\sin \alpha) [L_5 + (\alpha_2/\alpha_1) L_6] (w, \phi) \right\} \quad (A2)$$

and

$$\begin{aligned}
& (1/x)L_1(w) - K^4 \left\{ (\bar{\sigma}_x/E_x)w_{,xx} + (\bar{\sigma}_\phi/E_x)[(w_{,\phi\phi}/x^2 \sin^2 \alpha) + (1/x)w_{,x}] \right. \\
& \left. + 2(\bar{\tau}_{x\phi}/E_x)[(w_{,x\phi}/x \sin \alpha) - (w_{,\phi}/x^2 \sin \alpha)] \right\} \\
& + (1/x^3)(\alpha_2/\alpha_1) K^4 \cot^2 \alpha L_4^{-1} [(1/x)(x^3 w_{,xx})_{,xx}] = 0 \quad (A3)
\end{aligned}$$

where the operators L_1 to L_{10} are defined in reference 9 or 13, and the inverse operator L_4^{-1} is defined by

$$L_4 [L_4^{-1}(z)] = z \quad (A4)$$

It should be noted that the radial stability equation, eq. (A3), is not the usual eighth order equation, which is a higher derivative of the radial equilibrium equation, but a Batdorf type modified equation which is more convenient for solution by the Galerkin method, since it ensures monotonic decrease of the approximate buckling loads with increase in number of terms of approximation.

REFERENCES

1. Becker, H., and Gerard G.: Elastic Stability of Orthotropic Shells, Jour. Aerospace Sci., vol. 29, no. 5, May 1962, pp. 505-512.
2. Hess, T. E.: Stability of Orthotropic Cylindrical Shells Under Combined Loading. ARS Jour., vol. 31, no. 2, Feb. 1961, pp. 237-246.
3. Thielemann, W. F.: New Developments in the Nonlinear Theories of the Buckling of Thin Cylindrical Shells. Aeronautics and Astronautics, Proc. Durand Cent. Conf., Stanford Univ., 1958, Pergamon Press 1960.
4. March, H. W.: Buckling of Long Thin Plywood Cylinders in Axial Compression - Mathematical Treatment, Rep. 1322-A, Forest Prod. Lab., U.S. Dept. of Agriculture, Madison, Wisconsin, 1956.
5. Bodner, S. R.: General Instability of a Ring Stiffened Circular Cylindrical Shell Under Hydrostatic Pressure. Jour. App. Mech., vol. 24, no. 2, June 1957, pp. 269-277.
6. Becker, H.: General Instability of Stiffened Cylinders. NACA TN 4237, July, 1958.
7. Becker, H.: Handbook of Structural Stability, Part VI-Strength of Stiffened Curved Plates and Shells. NACA TN 3786, July, 1958.
8. Singer, J.: Buckling of Conical Shells Under Axisymmetrical External Pressure. Jour. Mech. Eng. Science, vol. 3, no. 4, Dec. 1961, pp. 330-339. Also, Technion Res. and Dev. Found. (Israel) AFOSR TN 60-711, Nov. 1960.
9. Singer, J.: A Donnell Type Theory for Bending and Buckling of Orthotropic Conical Shells. TAE Rep. 18, Technion Res. and Dev. Found. (Israel) Dec. 1961.

10. Seide, P.: A Donnell Type Theory for Asymmetrical Bending and Buckling of Thin Conical Shells. *Jour. App. Mech.*, vol. 24, no. 4, Dec. 1957, pp. 547-552.
11. Seide, P.: On the Buckling of Truncated Conical Shells Under Uniform Hydrostatic Pressure. *Proc. IUTAM Symposium on the Theory of Thin Elastic Shells*, Delft, 1959, North-Holland Publ. Co. Amsterdam, pp. 363-386.
12. Singer, J., Eckstein, A., and Baruch, M.: Buckling of Conical Shells Under External Pressure, Torsion and Axial Compression. TAE Rep. 19, Tech. Rep. (Final) Contract AF 61 (052)-339, Technion Res. and Dev. Found. (Israel), Sept. 1962.
13. Singer, J. and Fersht, R.: Buckling of Orthotropic Conical Shells Under External Pressure. TAE Rep. 22, Technion Res. and Dev. Found. (Israel), Sept. 1962.
14. Singer, J.: The Effect of Axial Constraint on the Instability of Thin Conical Shells Under External Pressure. *Jour. App. Mech.* vol. 29, no. 1, March, 1962, pp. 212-214.
15. Niordson, F. I. N.: Buckling of Conical Shells Subjected to Uniform External Lateral Pressure. *Trans. Royal Inst. of Technology, Sweden*, no. 10, 1947.
16. Singer, J.: The Effect of Axial Constraint on the Instability of Thin Circular Cylindrical Shells Under Uniform Axial Compression. *International Jour. Mech. Sciences*, vol. 4, no. 2, 1962, pp. 253-258.
17. Seide, P.: Axisymmetrical Buckling of Circular Cones Under Axial Compression. *Jour. Appl. Mech.*, vol. 23, no. 4, Dec. 1956, pp. 625-628.
18. Seide, P., and Weingarten, V. I.: On the Stability of Internally Pressurized Conical Shells Under Axial Compression. Rep. no. TDR-930(2570-30) TN-1, Aerospace Corp., Sept. 1961.
19. Singer, J., and Eckstein, A.: Experimental Investigations of the Instability of Conical Shells Under External Pressure. *Proc. 4th Annual Conf. Aviation and Astronautics*, Feb. 1962. *Bull. Res. Council of Israel*, vol. 11C, no. 1, April 1962, pp. 97-122.
20. Galletly, G. D., and Reynolds, T. E.: A Simple Extension of Southwell's Method for Determining the Elastic General Instability Pressure of Ring Stiffened Cylinders Subject to External Hydrostatic Pressure. *Proc. Soc. Exp. Stress Analysis*, vol. 13, no. 2, 1956, pp. 141-151.
21. Galletly, G. D.; Slankard, R. C., and Wenk, E.: General Instability of Ring Stiffened Cylindrical Shells Subject to External Hydrostatic Pressure - A Comparison of Theory and Experiment. *Jour. App. Mech.*, vol. 25, no. 2, June 1958, pp. 259-266.

T A B L E 1

CRITICAL PRESSURES OF TYPICAL ORTHOTROPIC AND RING-STIFFENED
CONICAL SHELLS(a) Orthotropic Shells (Cone angle 30°)

No	Material	Taper Ratio $1-(1/x_2)$	$\left(\frac{\rho_{av}}{h}\right)$	$\frac{E_x}{E_\phi}$	$\nu_{\phi x}$	$(p/E_x) \times 10^6$		
						Ortho- tropic Shell	Equivalent Cylinder	Iso- tropic Shell
1	Plywood	0.333	415	20.0	0.022	0.0412	0.0402	0.4050
2	Fibreglass	0.333	415	2.59	0.090	0.2041	0.2003	0.4050
3	Reinforced	0.500	499	0.386	0.234	0.3048	0.2841	0.1538
4	Epoxy(143)	0.600	582	2.59	0.090	0.0418	0.0373	0.5340
5		0.800	995	0.386	0.234	0.0307	0.0246	0.0159

(b) Ring Stiffened Shells (Material: steel;
Cone angle: Nos. 6,7; - 30° No.8 - 20°)

No	Taper Ratio $1-(1/x_2)$	$\left(\frac{\rho_{av}}{h}\right)$	$\left(\frac{A_2}{a_o h}\right)$	$\left(\frac{12 I_{22}}{a_o h^3}\right)$	$\frac{e_2}{h}$	$(p/E) \times 10^6$		
						Stiff- ened Shell	Equiv- alent Cylinder	Iso- tropic Shell
6	0.333	415	0.1471	0.7819	1.653	1.263	1.234	0.4050
7	0.800	995	0.1471	0.7819	1.653	0.0557	0.0450	0.0159
8	0.678	98.4	0.152	0.590	1.325	3.54	3.02	1.297

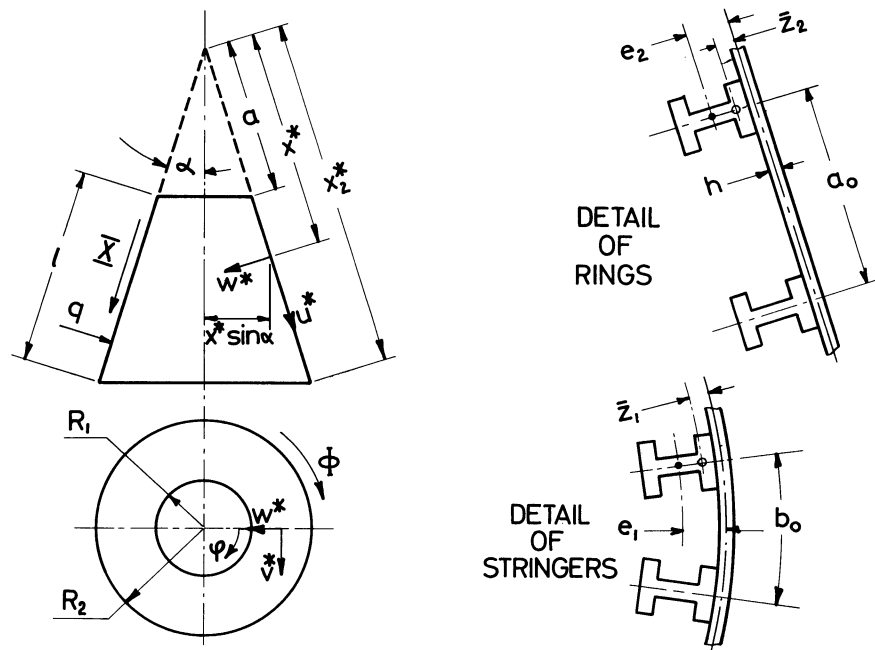


Figure 1.- Notation.

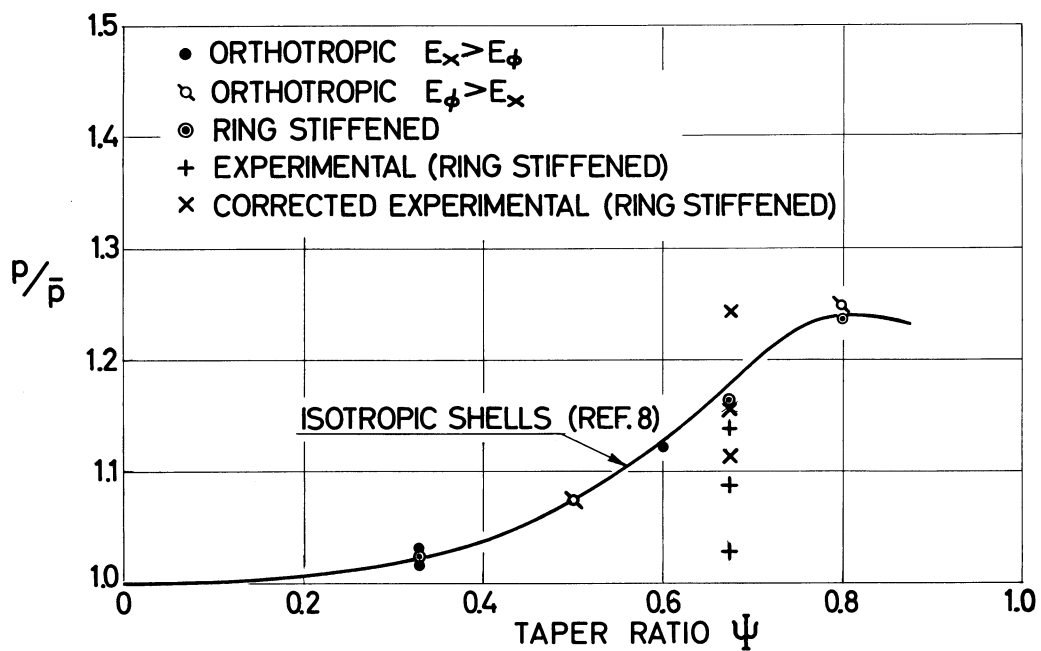


Figure 2.- Ratios of the buckling pressure of orthotropic and ring stiffened conical shells to that of equivalent cylindrical shells.

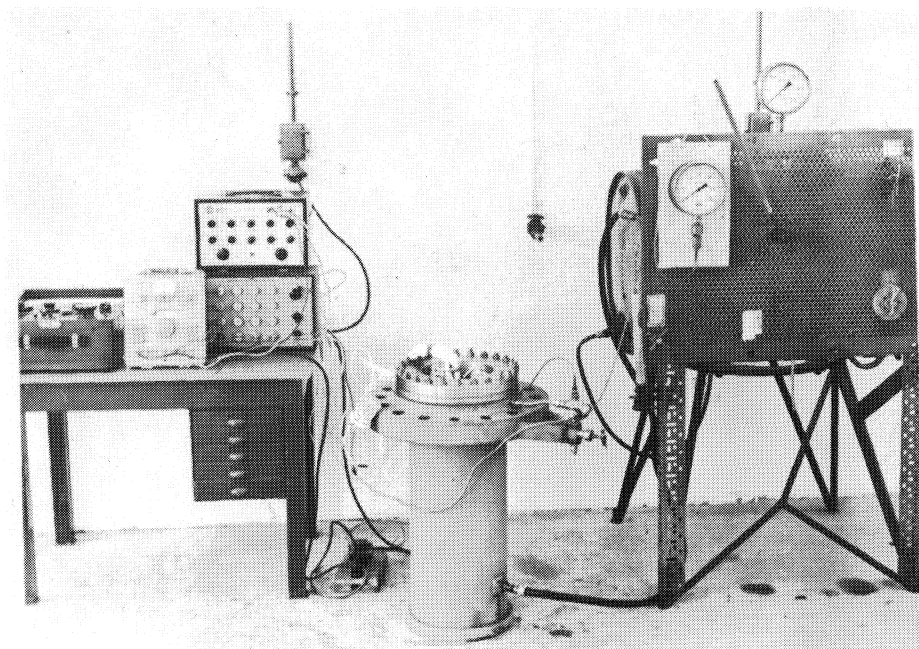


Figure 3.- Experimental set-up.

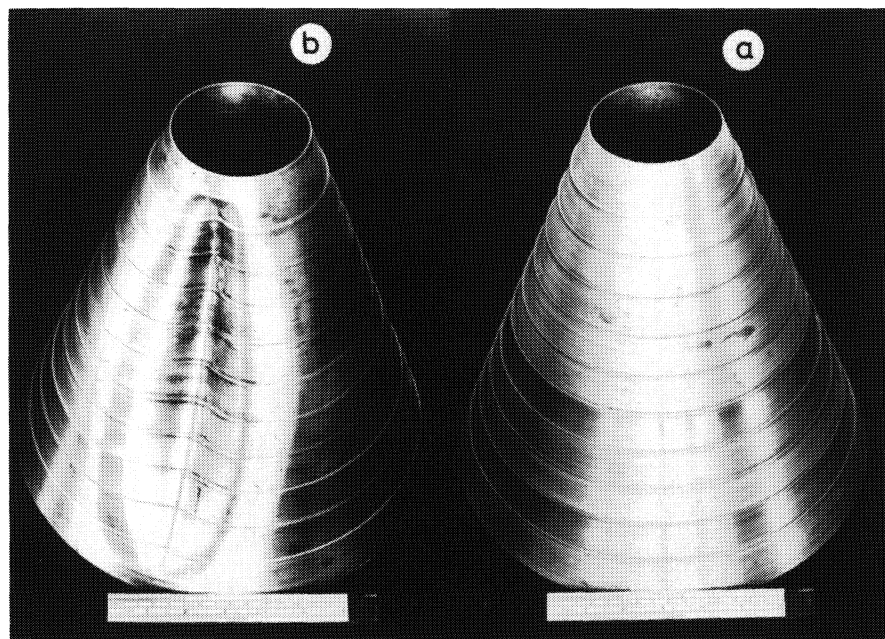


Figure 4.- Test specimen: (a) prior to test, (b) after failure by general instability.

IV SPHERICAL SHELLS

ASYMMETRIC BUCKLING OF CLAMPED SHALLOW SPHERICAL SHELLS*

By Hubertus J. Weinitschke

Hughes Aircraft Company, Ground Systems Group

SUMMARY

The problem of buckling of clamped shallow spherical shells has recently been considered in several theoretical investigations. Buckling loads under uniform external pressure were obtained in these investigations which show a surprisingly good agreement with each other, but show a marked disagreement with available experimental values. In all previous studies it has been assumed that the shell deformations are rotationally symmetric. In this paper, the buckling problem is re-examined by introducing asymmetric modes of deformation. The approach is to superimpose small asymmetric deflections on finite axisymmetric deflections, and to show that the symmetric states of deformation are unstable over certain ranges of load and geometry parameter. Numerical results are obtained by means of a digital computer and are compared with previous theoretical and experimental results.

INTRODUCTION

Problems of elastic stability of thin shells that require a large deflection analysis have been of considerable interest lately. In some well-known examples, approximate theoretical results are in reasonably good agreement with available experimental information; but the author does not know of a single problem that has yielded to a mathematically satisfactory and accurate solution, which at the same time is in good agreement with experiments. This unsatisfactory situation holds true even for the problem of buckling under uniform pressure of a shallow spherical shell, which is in a sense the simplest of shell stability problems and which is the subject of this paper. A reason for this situation may be found in the fact that the majority of theoretical large deflection analyses of stability problems have been carried out by means of Rayleigh-Ritz type approximations, whose accuracy is in

*This work was carried out at the Massachusetts Institute of Technology, supported by the Office of Naval Research. The author is indebted to Prof. E. Reissner whose help and encouragement was of great value to him. The calculations were carried out at M. I. T. Computation Center.

general difficult to assess in nonlinear problems. Frequently, shells exhibit deflection patterns that are difficult to represent in terms of such approximations. (For instance, using a one- or two-term Ritz approximate solution of the axisymmetric buckling of a spherical cap, one finds increasingly incorrect buckling loads with increasing shell heights.) It seems that at the present state of knowledge, recourse to numerical methods of well-defined accuracy should be considered as a powerful (if temporary) alternate approach in theoretical studies of shell instability. In view of the complexity of large deflection equations, such an approach may involve extensive calculations on a high speed digital computer; however, a more detailed understanding of the buckling mechanism which one may gain from such calculations may render this approach worth-while. The problem treated in the present paper is believed to give some support to this point of view.

The buckling under uniform pressure of a shallow spherical shell, clamped along its boundary, has generally been considered to be of the snapping type. On the basis of a theory of finite axisymmetric deflections, one obtains a nonlinear load deflection curve which shows a local maximum of the pressure, except for extremely shallow shells which do not buckle. This maximum pressure p_c determines the critical load at which snapping occurs, provided that the classical buckling criterion is assumed to be valid. What is of particular interest is the stability curve that shows how p_c varies with the shell geometry parameter μ defined below. Several recent investigations have been concerned with the calculation of this stability curve (refs. 1 to 4). The results of these studies, which were obtained by entirely different techniques, show good agreement with each other. They were all based on a system of nonlinear differential equations for finite axisymmetric deformations. However, experimental results are generally in serious disagreement with the results of the axisymmetrical buckling theory. For some time, it has been believed that these discrepancies might be due to imperfections in geometrical shape. Recent results of Budiansky (see ref. 1) for certain types of imperfections of reasonable magnitudes tend to discourage such speculations.

The present analysis is based on the assumption that asymmetrical deflection modes are significant in the process of buckling. The buckling of spherical caps appears then to be a bifurcation rather than a snapping phenomenon: axisymmetric deformation takes place until a critical value is reached, at which point, bifurcation of solutions of the basic equations occurs. One branch of solutions corresponds to axisymmetric states of equilibrium, other branches correspond to asymmetric states, which in the vicinity of the bifurcation point differ from the axisymmetric states by infinitesimal amounts. The axisymmetric states are therefore unstable for pressures above the critical

value, hereafter referred to as the asymmetrical buckling load. The main result of this paper is a new stability curve, based on asymmetric deflections of the form $w = w(r)\cos n\theta$. Two different techniques are employed; one amounts to calculation of the second variation of an appropriate potential energy functional, the other reduces the stability problem to a nonlinear eigenvalue problem.

BASIC EQUATIONS

The basic equations for finite bending of shallow shells have been derived by Marguerre (ref. 5) under the traditional assumptions of thin shell theory, that is, neglect of transverse shear deformability and of tangential displacement components u , v in the nonlinear terms. These equations, when written in polar coordinates and specified to a spherical cap, can be put in the form

$$\begin{aligned} A^{-1} \nabla^4 F + 2H \nabla^2 w + \frac{1}{2} K[w, w] &= 0 \\ D \nabla^4 w - 2H \nabla^2 F - K[F, w] &= pb^4 \end{aligned} \quad (1)$$

where b is the base radius of the shell, H is the shell "rise", p is the external pressure, A and D are stretching and bending stiffness factors respectively and ∇^2 is the Laplace operator in the polar coordinates r and θ . Stress resultants and couples are related to the stress function F and the axial displacement w by the formulas

$$\begin{aligned} N_r &= r^{-2} F_{\theta\theta} + r^{-1} F_{,r}, & N_\theta &= F_{,rr}, & N_{r\theta} &= r^{-2} F_{,\theta} - r^{-1} F_{,r\theta} \\ Q_r &= -D(\nabla^2 w)_{,r}, & Q_\theta &= -Dr^{-1}(\nabla^2 w)_{,\theta} \\ M_r &= -D(w_{,rr} + \nu Tw), & M_\theta &= -D(Tw + \nu w_{,rr}) \end{aligned}$$

where $Tw = r^{-1} w_{,r} + r^{-2} w_{,\theta\theta}$, $D = D(1 - \nu)$ and ν is Poisson's ratio. A comma followed by subscripts indicates differentiation with respect to the subscripted variable(s). The nonlinear terms in Eqs. (1) are expressed in terms of the differential operator K as follows

$$\begin{aligned} K[F, w] &= \varrho^{-1} F_{,\varrho\varrho} (w_{,\varrho} + \varrho^{-1} w_{,\theta\theta}) + w_{,\varrho\varrho} (F_{,\varrho} + \varrho^{-1} F_{,\theta\theta}) + 2\varrho^{-2} \cdot \\ &\quad [\varrho^{-1} (F_{,\varrho\theta} w_{,\theta} + F_{,\theta} w_{,\varrho\theta}) - F_{,\varrho\theta} w_{,\varrho\theta} - \varrho^{-2} F_{,\theta} w_{,\theta}] \end{aligned}$$

where $\varrho = rb^{-1}$.

The boundary conditions corresponding to a clamped edge are

$$u = v = w = w_{,r} = 0 \quad \text{at} \quad r = b(\varrho = 1). \quad (3)$$

In order to express the first two conditions in terms of F and w , consider the stress-strain relations

$$A_1 F \equiv N_r - \nu N_\theta = A(u, r + rw, r R^{-1} + \frac{1}{2} w, r^2)$$

$$A_2 F \equiv N_\theta - \nu N_r = A r^{-1}(u + v, \theta + \frac{1}{2} r^{-1} w, \theta^2)$$

$$A_3 F \equiv 2(1+\nu)N_{r\theta} = A[v, r - r^{-1}(v - u, \theta) + R^{-1}w, \theta + r^{-1}w, r w, \theta]$$

Expressing N_r , N_θ , and $N_{r\theta}$ in terms of F as indicated by the differential operators A_1 , A_2 , A_3 , it can be verified that conditions (3) are equivalent to

$$A_2 F \equiv (r A_2 F), r - A_1 F - (A_3 F), \theta = w = w, r = 0 \quad \text{at } r = b. \quad (4)$$

The boundary value problem (1) and (4) constitutes the basis for the present analysis.

A convenient dimensionless form of Eqs. (1) is obtained by introducing the functions $g(\varphi, \theta) = D^{-1}F$ and $h(\varphi, \theta) = m t^{-1}w$, and the relevant geometry and load parameters $\mu^2 = 2mHt^{-1}$ and $\gamma = pb^4m(4Dt)^{-1}$ (t = shell thickness, $m^2 = 12(1 - \nu^2)$). With this, we have the following equations for g and h

$$\nabla^4 g + \mu^2 \nabla^2 h + \frac{1}{2}K[h, h] = 0, \quad \nabla^4 h - \mu^2 g - K[g, h] = 4\gamma \quad (5)$$

For convenience of describing the buckling process, a dimensionless deformed volume is introduced by $V = \iint h(\varphi, \theta) \varphi d\varphi d\theta$, and a load parameter by $P = \gamma\mu^{-4}$

RESULTS OF PREVIOUS WORK

In all previous theoretical studies, the assumption was made that deformations are rotationally symmetrical (except in ref. 6). In that case, Eqs. (5) can be simplified considerably. With $p = g'(\varphi)$, $q = h'(\varphi)$, where the primes denote differentiation with respect to φ , it can be shown that Eqs. (5) reduce to the following ordinary differential equations:

$$(p' + \varphi^{-1}p)' = \mu^2 q - \frac{1}{2} \varphi^{-1} q^2, \quad (q' + \varphi^{-1}q)' = \mu^2 p + 2\gamma\varphi + \varphi^{-1}pq. \quad (6)$$

The corresponding boundary conditions are

$$p(0) = q(0) = 0, \quad p(1) = q'(1) - \nu q(1) = 0. \quad (7)$$

A great deal of effort has been devoted to solving Eqs. (6) and (7) and calculating the resulting stability curve $P_c(\mu)$. If the curve $P = P(V)$ is plotted for a fixed shell geometry, the variation of P with increasing V is roughly as

follows: P increases until it reaches a local maximum P_C , then decreases to a local minimum P_ℓ (unstable states of equilibrium), and then increases again (stable post-buckling states of equilibrium).

In some recent papers, buckling criteria have been discussed that are based on a finite-jump buckling mechanism according to which the minimum load P_ℓ is to be considered as the actual collapse load of the shell. The shortcomings of these criteria, which have no logical basis, have been pointed out, e.g., see the comprehensive review article on shell instability by Fung and Sechler (ref. 7). It has further been shown (ref. 8) that for simply supported spherical caps under uniform pressure, P_ℓ is negative for certain shell geometries. Similar difficulties are encountered in the application of so-called energy buckling criteria to the spherical cap problem (see ref. 7). In the following, the term "buckling load" is to be understood in the classical sense.

The results of the earlier studies of Eqs. (6) and (7) which were obtained by Ritz-type approximations, perturbation techniques, and power series methods are generally in disagreement with each other (see refs. 1 and 2 for a more complete discussion and additional references). The power series approach proved promising; however, convergence difficulties for larger values of μ^2 made it impossible to obtain solutions for values of γ up to the critical load $\gamma_C = \mu^4 P_C$.

The results of the more recent investigations are based on iterative numerical solution of the above differential equations. A number of entirely different techniques have been used successfully to overcome the difficulties in the numerical solution, which are related to the increasing waviness of the normal deflection w with increasing shell parameter μ^2 . A modified power series approach, expanding the solutions of Eqs. (6) in both powers of φ and powers of $1 - \varphi$ was employed by Weinitschke (ref. 2). In the work of Budiansky (ref. 1), the problem was formulated in terms of two nonlinear integral equations which were solved by means of matrix approximations. A different integral equation formulation was employed by Thurston (ref. 3), and a finite difference solution of Eqs. (6) and (7) was given by Archer (ref. 4). The stability curves based on the results of refs. 1 and 4 are in almost perfect agreement with each other (see curve S in Figure 1). However, except for the range $\mu \leq 5.5$, the experimental values shown in Figure 1 are in serious disagreement with the axisymmetric buckling theory.

It is interesting to note that the range $\mu \leq 5.5$ corresponds to the simple deflection mode: $w(\varphi)$ has its maximum at the apex ($\varphi = 0$) and is monotonically decreasing towards the edge. For larger shell rises, $\mu \geq 5.5$, the shell deforms according to axisymmetric theory into a deflection pattern of a higher degree of waviness before it snaps through at large values of P . However, in view of the results discussed below, the more wavy axisymmetric states become unstable in the asymmetric buckling theory.

THE BIFURCATION PROBLEM

The results discussed in the previous section lead to the conclusion that the low experimental values of P_c cannot be explained on the basis of axisymmetric deformations. The strong increase of the ratio $|N_\theta/N_r|$ for increasing P and for $\mu \geq 5.5$ observed in ref. 2 indicates the possibility of wrinkling in the circumferential direction of the cap. Furthermore, there is strong experimental evidence (see ref. 1) for asymmetrical buckling. Recently, buckling loads have been calculated by Gjelsvik and Bodner (ref. 6) using a Rayleigh-Ritz procedure, where $w(r, \theta)$ is assumed to be nonsymmetrical involving one free parameter. The resulting numerical values of P_c are larger than the values of axisymmetric theory (curve S in Figure 1); therefore, it is not evident from their work whether asymmetric deflection theory is able to explain the low experimental values.

A new approach to the buckling problem will now be outlined which takes into account asymmetrical deflection modes of the type $W(r)\cos n\theta$. It is assumed that axisymmetric deformation takes place until a critical value P^* is reached at which point bifurcation of solutions of the basic equations (6) occurs. The branch of axisymmetric solutions becomes unstable for pressure parameters $P \geq P^*$, and the shell deforms in an unsymmetrical mode. In other words, the smallest load for which bifurcation occurs is considered as the limit of stability, in accordance with general principles of elastic stability theory. However, the possibility must be admitted that the loss of stability represented by points of bifurcation on the axisymmetric load deflection curve $P = P(V)$ may be rather localized. Further investigation of the branches of asymmetrical states of equilibrium is necessary in order to determine the complete behavior of the shell.

In order to obtain the stability curve on the basis of this approach, small asymmetrical deflections $w(r, \theta)$ must be superimposed on finite axisymmetrical deflections. Since the latter are known, the equations for $w(r, \theta)$ and for the stresses are linear. Two ways of formulating the present approach analytically are described below which are at the same time suitable for obtaining numerical results.

VARIATIONAL METHOD

The potential energy of a shallow shell subject to uniform pressure can be written as follows

$$E_1[\epsilon_{ik}, w] = \frac{1}{2} A(1 - \nu^2)^{-1} \iint [(\epsilon_{xx} + \epsilon_{yy})^2 - 2(1 - \nu)(\epsilon_{xx}\epsilon_{yy} - \epsilon_{xy}^2)] dx dy + \frac{1}{2} D \iint [\nabla^2 w^2 - 2(1 - \nu)(w_{,xx}w_{,yy} - w_{,xy}^2)] dx dy + \iint p w dx dy \quad (8)$$

where the quantities ϵ_{ik} denote the midsurface strains of the shell. Eqs. (1) and (4) are now equivalent to the variational problem: minimize E_1 with respect to all (smooth) functions u, v, w satisfying $u = v = w = w' = 0$ along the edge $r = b$. The above integrals are to be taken over the projection of the shell midsurface on the x, y -plane. Using the stress strain relations as constraints, one can transform this variational problem into an equivalent one where u and v are eliminated. This leads to a new functional $E_2[w, F]$, where E_2 is to be minimized with respect to all functions w satisfying $w = w' = 0$. Here the function F is given in terms of w by the first of Eqs. (1) subject to the boundary conditions (4).

The details of this transformation and of the subsequent solution of the stability problem are too lengthy to be reproduced here and will be given in a future paper. Briefly, the procedure is as follows. Let $F_0(r), W_0(r)$ refer to a given axisymmetric solution and define \bar{f}, \bar{w} by $F = F_0 + \bar{f}, w = W_0 + \bar{w}$. In order to show that the solutions F_0, W_0 become unstable for values of the pressure exceeding a certain limit, one has to calculate the second variation $\delta^2 E_2[w, F]$ of the functional E_2 and show that it can be made negative for suitably chosen functions $w(r, \theta)$. The application of this method is thus reduced to numerical evaluation of certain double integrals and to solving a linear biharmonic equation to find the \bar{f} corresponding to a given \bar{w} .

DIFFERENTIAL EQUATIONS METHOD

Assume the dimensionless stress g and displacement h in the form

$$g = g_0(\varphi) + \epsilon g_1(\varphi, \theta) + O(\epsilon^2), \quad h = h_0(\varphi) + \epsilon h_1(\varphi, \theta) + O(\epsilon^2) \quad (9)$$

where g_0, h_0 denote the axisymmetric solution, ϵ is a small parameter and $O(\epsilon^2)$ stands for terms of order ϵ^2 . Substituting (9) into (5), noting that g_0, h_0 satisfy Eqs. (6), and collecting terms of order ϵ , one obtains the desired equations for small asymmetric deflections. These deflections, represented by g_1, h_1 are

$$\begin{aligned} \nabla^4 g_1 + \mu^2 \nabla^2 h_1 + K[h_0, h_1] &= 0 \\ \nabla^4 h_1 - \mu^2 \nabla^2 g_1 - K[g_0, h_1] - K[h_0, g_1] &= 0 \end{aligned} \quad (10)$$

A similar process leads to appropriate boundary conditions for the functions g_1, h_1 . These conditions together with Eqs. (10) constitute the basic 8th order eigenvalue problem to be solved. Although Eqs. (10) are linear in g_1, h_1 , the problem is nonlinear insofar as the eigenvalue γ enters via the functions g_0, h_0 , which depend on γ through the nonlinear equations (6).

In view of the periodicity in θ , we set $g_1 = G(\varphi)\cos n\theta, h_1 = H(\varphi)\cos n\theta$.

This leads to the following equations for G and H

$$\begin{aligned} LLG + \mu^2 LH + M[h_0, H] &= 0 \\ LLH - \mu^2 LG - M[g_0, H] - M[h_0, G] &= 0 \end{aligned} \quad (11)$$

where

$$\begin{aligned} L &= (\dots)'' + \varphi^{-1}(\dots)' - n^2 \varphi^{-2}(\dots) \\ \varphi M[X, Y] &= X''(Y' - n^2 \varphi^{-1} Y) + X' Y''; \quad X = X(\varphi), \quad Y = Y(\varphi) \end{aligned}$$

The boundary conditions for G, H can be written in the form

$$\begin{aligned} H = H' = G'' - \nu(G' - n^2 G) &= 0 \\ G''' + G'' + (\nu n^2 + 2\nu n + 2n - 1)(G' - G) &= 0 \end{aligned} \quad \text{at } \varphi = 1 \quad (12)$$

In addition, G, H, G', H' must be regular at $\varphi = 0$.

As mentioned above, the solution of the axisymmetric problem has been obtained in ref. 2 in terms of power series in φ and $1 - \varphi$; therefore, it is indicated to calculate the solutions G, H also in this form, that is,

$$G(\varphi) = \varphi^\lambda \sum_{k=0}^{\infty} G_k \varphi^{2k}, \quad H(\varphi) = \varphi^\lambda \sum_{k=0}^{\infty} H_k \varphi^{2k} \quad (13)$$

and similar expansions with respect to $1 - \varphi$. Substitution of (13) into (11) leads to the fourth degree indicial equation for the roots λ and to recurrence relations for the coefficients G_k, H_k from which four regular linear independent solutions can be constructed. Satisfaction of the boundary conditions (12) by an appropriate linear combination of these solutions leads to the condition of vanishing of a certain determinant $I(\mu, n; P)$, where $P = \gamma \mu^{-4}$, which determines a smallest eigenvalue $P^*(n)$ for each n . For a fixed parameter μ , the asymmetric buckling load parameter P_c is therefore determined by the smallest of the $P^*(n)$, that is, $P_c(\mu) = \min_n P^*(n)$.

RESULTS AND DISCUSSION

In the application of the procedure outlined in the preceding section it is important to obtain sufficiently accurate solutions of Eqs. (11) because of the loss of some accuracy in the evaluation of the determinant $I(\mu, n, P)$. The roots of $I = 0$ were found by plotting I versus P keeping μ and n fixed. The use of a digital computer (IBM-7090) was essential in calculating I for sufficiently large ranges of the three parameters μ, n , and P .

The results of these calculations are shown in Fig. 1. The critical loads corresponding to a fixed circumferential wave number n are plotted versus μ , from which the scalloped asymmetric stability curve $P_c(\mu)$ (labeled A in Fig. 1)

is obtained as the lower envelope. It is seen that axisymmetric snap-buckling prevails only over the narrow range $3.4 \leq \mu \leq 4$. For $\mu > 4$, there is bifurcation-buckling caused by asymmetric deflection modes showing an increasing number of circumferential waves with increasing μ . Although no attempt has been made to extend the stability curve beyond $\mu = 10$, it is significant that the calculated buckling loads are in reasonably good agreement with the observed data, thus essentially closing the large gap between theory and experiment that has hitherto existed.

In conclusion, it must be admitted that although a bifurcation phenomenon seems to determine the onset of buckling, the process of buckling at large may well appear as a snap-through phenomenon, that is, the asymmetric modes may become unstable with increasing deformation so that the final (post-buckled) state is again axisymmetrical. A theoretical confirmation would involve finite asymmetric post-buckling deflections and would be of great value for a more detailed understanding of the buckling process.

REFERENCES

1. Budiansky, B.: Buckling of Clamped Shallow Spherical Shells. IUTAM Symposium on the Theory of Thin Elastic Shells (Delft), 1959, pp. 64-94.
2. Weinitschke, H. J.: On the Stability Problem of Shallow Spherical Shells, Jour. Math. Phys., vol. 38, 1960, pp. 209-231.
3. Thurston, G. A.: A Numerical Solution of the Non-linear Equations for Axisymmetric Bending of Shallow Spherical Shells. Jour. Appl. Mech., vol. 28, 1961, pp. 557-568.
4. Archer, R. R.: On the Numerical Solution of the Nonlinear Equations for Shells of Revolution. Jour. Math. Phys., to appear.
5. Marguerre, K.: Zur Theorie der gekrümmten Platte grosser Formänderung. Proc. 5th. Int. Congress Appl. Mech. (Cambridge), 1938, pp. 93-101.
6. Gjelsvik, A., and Bodner, S. R.: The Non-symmetrical Snap-Buckling of the Clamped Spherical Cap. Tech. Report No. 30, Brown Univ. (Providence), 1962.
7. Fung, Y. C., and Sechler, E. E.: Instability of Thin Elastic Shells. Proc. 1st. Sympos. Naval Struct. Mechanics (Stanford), 1960, pp. 115-168.
8. Weinitschke, H. J.: On the Nonlinear Theory of Shallow Spherical Shells. Jour. Soc. Ind. Appl. Math., vol. 6, 1958, pp. 209-232.

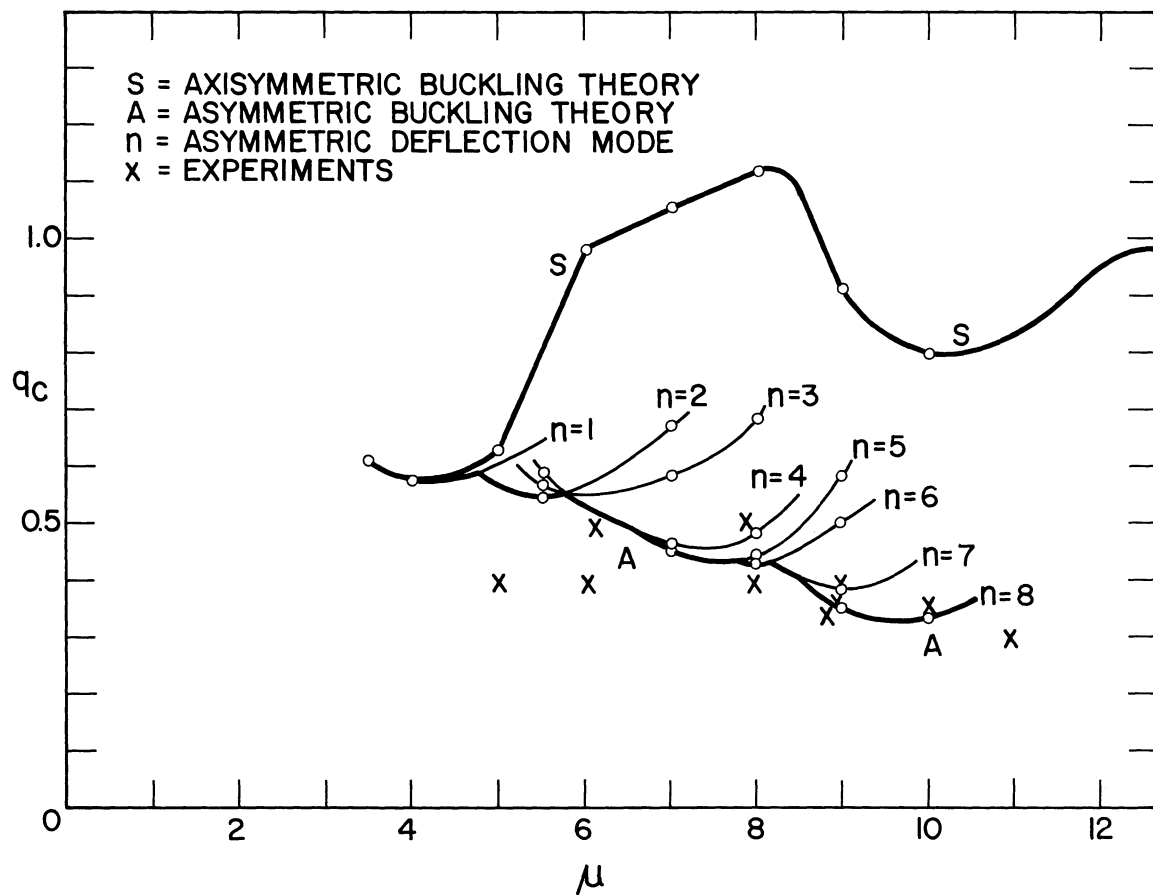


Figure 1.- Theoretical buckling pressures for clamped shallow spherical shells and experimental data.

ON THE INFLUENCE OF NON-SYMMETRICAL MODES ON THE BUCKLING OF SHALLOW SPHERICAL SHELLS UNDER UNIFORM PRESSURE

By R. R. Parmerter and Y. C. Fung
CALIFORNIA INSTITUTE OF TECHNOLOGY

SUMMARY

In view of the wide discrepancy between theoretical and experimental results that still exists, the problem of buckling of shallow spherical shells under uniform external pressure is reexamined with the introduction of non-symmetrical deflection modes. The basic idea is that, for a symmetrical shell under gradually increasing symmetrical loading, the deformation will be symmetrical up to and after buckling, but it is feasible that a non-symmetrical mode participates in the snap-through process. Including this possibility in the governing equations may lower the theoretical buckling load. Some analytical results are presented and compared with experiment.

SYMBOLS

$$\lambda^2 = \sqrt{12(1-\mu^2)} \frac{b^2}{at} = \text{geometrical shell parameter}$$

b = radius of shallow spherical segment

a = radius of sphere

t = shell thickness

μ = Poisson's ratio

p = pressure

$$q = p\left(\frac{a}{t}\right)^2 \frac{\sqrt{3(1-\mu^2)}}{2E} = \text{non-dimensional pressure}$$

s = inplane radial displacement (symmetrical)

z = inplane radial displacement (non-symmetrical)

y = inplane tangential displacement

$w(r, \theta) = u(r) + v(r) \cos n\theta$ = assumed displacement perpendicular to shell

$$\bar{u}(r) = \left(\frac{\lambda}{b}\right)^2 a u(r) = \text{non-dimensional displacement}$$

E = Young's Modulus

INTRODUCTION

The problem of oil-canning or snap-through buckling of shallow spherical shells is one of considerable practical and theoretical interest. The initial investigation (Ref. 5) was undertaken to see if the classical continuous deformation concept of buckling would work if the non-linear, rather than linear equations were used, or whether it is necessary to follow Tsien's suggestion (Ref. 2) and introduce an artificial "energy criterion" for jumping, or distinguish and evaluate the "upper" and "lower" buckling loads as advocated by Friedrichs (Ref. 3) with the concomitant necessity of assessing any real shell buckling load to be somewhere in between. Several theoretical investigations followed (Refs. 7-15), but the theoretical program has not yet been satisfactorily completed. Considerable differences between theoretical predictions and experimental measurements (Refs. 4, 5, 16, 17) still exist and remain unexplained.

Taking a cue from the similar, but much simpler, problem of shallow arches (Ref. 6), we propose to investigate the influence of non-symmetrical modes and non-symmetrical initial imperfections on the snap-through buckling of shallow spherical shells. The idea is that for a symmetrical shell under a symmetrical loading, the deflection will be symmetrical before buckling, and symmetrical after buckling; but during the buckling process, or in initiating the buckling process, a non-symmetrical mode may participate. In the case of arches, the participation of non-symmetrical modes lowers the critical buckling load considerably when the arch-rise parameter λ is sufficiently large. We would like to see if the same is true for spherical shells. Furthermore, in arches, any small initial imperfection of the non-symmetrical type has large effect toward lowering the critical buckling load; the same might be true for spherical shells.

Grigolyuk (Ref. 18) has presented some formulas for the non-symmetrical deformation of spherical shells, but no results with respect to buckling were given. Recently, Gjelsvik and Bodner (Ref. 19) investigated the same problem by a single term approximation. Although interesting features are demonstrated, the solutions are numerically unreliable. The work to be presented herein was initiated in 1960, and is not yet completely finished. However, in

demonstrating (see Fig. 1) that for relatively small values of λ good agreement is obtained with Weinitzschke and Budiansky's theoretical results (Ref. 13) and with the experimental deformation pattern of Kaplan and Fung (Ref. 5), some confidence is gained as to the correctness of the approach: for this reason it is thought worthwhile to present this progress report. Only initially perfect spherical shells will be discussed herein.

THE MATHEMATICAL PROBLEM

We consider a shallow portion of a spherical shell, clamped along a circular boundary, (Fig. 2), and subjected to uniform pressure on its top. We assume that the shell is so shallow that von Kármán's large deflection equations for slightly curved plates are applicable. These equations are given in Ref. 18 for cylindrical coordinates. We assume that the shell is initially a perfect spherical cap, and that the deflection is symmetrical except during buckling. In other words, as the symmetrical load deflection path is traced, we look for bifurcation points involving non-symmetrical states. If such a point can be found, it represents a possible way of initiating a non-symmetrical transition mode which can carry the shell into the buckled state. The existence of these points can be discovered by considering small non-symmetrical disturbances about the symmetrical, large deflection solution. In other words, the equations can be linearized with respect to the non-symmetrical terms.

We assume that the deflection can be represented by a function of the form

$$w(r, \theta) = u(r) + v(r) \cos n\theta \quad (1)$$

where $v(r) \ll u(r)$. When this assumption is inserted into von Kármán's equations we find that the stress function $F(r, \theta)$ should be represented in the form

$$F(r, \theta) = G(r) + H(r) \cos n\theta \quad (2)$$

Neglecting second order terms in $v(r)$ and $H(r)$, von Kármán's equations reduce to:

$$D \nabla^4 u = p + \frac{1}{r} (G_{rr} u_r + G_r u_{rr}) + \frac{1}{a} (G_{rr} + \frac{1}{r} G_r) \quad (3a)$$

$$\frac{\nabla^4 G}{Et} = -\frac{1}{r} (u_r u_{rr} + \frac{1}{a} u_r) - \frac{1}{a} u_{rr} \quad (3b)$$

$$\frac{D\nabla^4(v \cos n\theta)}{\cos n\theta} = \frac{1}{r} (u_r H_{rr} + v_r G_{rr} + H_r u_{rr} + v_{rr} G_r + \frac{1}{a} H_r) - \frac{n^2}{r^2} (G_{rr} v + H u_{rr} + \frac{1}{a} H) + \frac{1}{a} H_{rr} \quad (3c)$$

$$\frac{\nabla^4(H \cos n\theta)}{Et \cos n\theta} = -\frac{1}{r} (u_r v_{rr} + u_{rr} v_r + \frac{1}{a} v_r) + \frac{n^2}{r^2} (u_{rr} v + \frac{1}{a} v) - \frac{1}{a} v_{rr} \quad (3d)$$

$$\text{where } \nabla^4 = \frac{\partial^4}{\partial r^4} + \frac{2}{r} \frac{\partial^3}{\partial r^3} - \frac{1}{r^2} \frac{\partial^2}{\partial r^2} + \frac{1}{r^3} \frac{\partial}{\partial r} + \frac{4}{r^4} \frac{\partial^2}{\partial \theta^2} - \frac{2}{r^3} \frac{\partial^3}{\partial r \partial \theta^2} + \frac{2}{r^2} \frac{\partial^4}{\partial r^2 \partial \theta^2} + \frac{1}{r^4} \frac{\partial^4}{\partial \theta^4}$$

and u , G , H , v are functions of r only.

Equations 3a, 3b are the usual non-linear symmetric equations, while 3c, 3d are the equations of a linearized non-symmetrical perturbation on the symmetrical solution. If the boundary conditions are symmetrical, equations 3c, 3d have the solution $v = H = 0$, i.e., the solution is symmetrical. However, for certain values of the load intensity q , with its corresponding functions $u(r)$, $G(r)$, Eqs. 3c, 3d may admit non-trivial solutions. We seek the condition on $u(r)$, $G(r)$ for eigensolutions to exist. The non-symmetrical buckling pressure p can then be determined from eq. 3a.

By treating the problem in this manner we have uncoupled the symmetrical equations from the non-symmetrical terms. Thus the symmetrical problem can be solved independently. We begin by solving 3a and 3b. The existing satisfactory solutions to these equations are all numerical, and have been used only to predict the buckling pressure. For our purpose we need expressions for $u(r)$ and $G(r)$ which can be used in the solution of 3c and 3d. We use Galerkin's method to obtain these functions.

Previous attempts to solve 3a, b by Galerkin's method have not proven too successful. We have attempted to pick a two term expression for $u(r)$ which is capable of reproducing the experimental

mode shapes reported by Kaplan and Fung. For values of $\lambda < 8$ a satisfactory representation can be given by

$$u = u_1 \left(1 + \cos \frac{\pi}{b} r\right) + u_2 \left(1 - \cos \frac{2\pi}{b} r\right) \quad (4)$$

The assumed form of u satisfies the clamped boundary conditions $\frac{\partial u}{\partial r} = u = 0$ at $r = b$, and the symmetry condition $\frac{\partial u}{\partial r} = 0$ at $r = 0$.

Using Eq. 4 we can solve Eq. 3b for G . Three constants of integration arise which are determined by the conditions of finite stress at $r = 0$ and zero radial displacement in the plane of the edge of the cap, at $r = b$. We now substitute G and u into Eq. 3a, which will not in general be exactly satisfied, but can be satisfied approximately in the Galerkin sense. This leads to two algebraic equations which determine u_1 and u_2 as a function of q . The resultant equations are

$$\begin{aligned} &7.111 \bar{u}_1^3 + 8.191 \bar{u}_1^2 \bar{u}_2 + 35.79 \bar{u}_1 \bar{u}_2^2 + 10.47 \bar{u}_2^3 \\ &- 7.217 \lambda^2 \bar{u}_1 \bar{u}_2 - 4.659 \lambda^2 \bar{u}_1^2 - 9.349 \lambda^2 \bar{u}_2^2 \\ &+ (.6984 \lambda^4 + 36.38) \bar{u}_1 + (1.005 \lambda^4 + 32.40) \bar{u}_2 \\ &- 1.189 \lambda^4 q = 0 \end{aligned} \quad (5a)$$

$$\begin{aligned} &5.488 \bar{u}_1^3 - 13.09 \bar{u}_1^2 \bar{u}_2 + 17.11 \bar{u}_1 \bar{u}_2^2 - 50.63 \bar{u}_2^3 \\ &+ 3.903 \lambda^2 \bar{u}_1 \bar{u}_2 - 2.513 \lambda^2 \bar{u}_1^2 + 5.006 \lambda^2 \bar{u}_2^2 \\ &+ (.1010 \lambda^4 + 17.11) \bar{u}_1 - (.03610 \lambda^4 + 235.87) \bar{u}_2 = 0 \end{aligned} \quad (5b)$$

for $\mu = 1/3$.

Beginning at $\bar{u}_1 = \bar{u}_2 = 0$, equation 5b defines a continuous sequence of pairs u_1, u_2 which describe a series of neighboring equilibrium positions for the shell, which begins at the unloaded state. Equation 5a is used to calculate the value of q corresponding to a given pair. Tracing the u_1, u_2 curve from $u_1 = u_2 = q = 0$ we find q increases, reaches a maximum, and then decreases. This maximum value of q obviously defines the symmetrical buckling pressure, as there is no neighboring equilibrium position corresponding to $q = q_{\max} + dq$. Following the shell beyond q_{\max} we

find a minimum value of q and then the pressure again increases. This is the post buckling regime. The u_1, u_2, q curves for $\lambda = 5.5$ and $\lambda = 6$ are shown in Figs. 3 and 4. The $\lambda = 5.5$ curve is typical of the curves for $\lambda \leq 5.5$, while the $\lambda = 6$ curve is typical of the curves for $\lambda \geq 6$. The rapid transition between $\lambda = 5.5$ and $\lambda = 6$ is very striking, and in agreement with the sudden change of mode shape observed by Kaplan and Fung in this region.

The u_1, u_2 curves can be used in conjunction with Eq. 4 to plot the mode shapes as a function of q . This has been done for $\lambda = 5.5$ in Figure 5. The curves are in good agreement with the experimental measurements of Kaplan and Fung. The symmetrical buckling pressures (Fig. 1) agree very well with Budiansky for $\lambda \leq 5.5$, but diverge from his values for $\lambda \geq 6$. This is probably due to the increased importance of the third mode, $(1 + \cos \frac{3\pi}{b} r)$, for larger λ .

NON-SYMMETRICAL SOLUTION

The solution of the non-symmetrical equations is carried out in a similar manner. The function $v(r)$ is assumed in the form

$$v(r) = v_1 r (r-b)^2 \quad (6)$$

This function satisfies the clamped condition $dv/dr = v = 0$ at $r = b$. Substituting this along with $u(r)$ and $G(r)$ from the symmetrical solution, in the right hand side of (3d) we can solve for $H(r)$. The four constants of integration in $H(r)$ are evaluated from the conditions of finite stress at $r = 0$ and zero inplane displacement, $z = y = 0$, at $r = b$. $H(r)$, $G(r)$, $u(r)$, $v(r)$ are now substituted into Eq. 3c and the equation is satisfied in the mean according to Galerkin's method. Since the equations are homogeneous, v_1 is a factor in every term of the resultant equation, so we obtain an equation of the form

$$v_1 [f(u_1, u_2)] = 0 \quad (7)$$

where $f(u_1, u_2)$ is a quadratic in u_1, u_2 , whose coefficients depend on n . The desired condition for the existence of eigensolutions is the vanishing of the bracket.

The coefficients of $f(u_1; u_2)$ have been found for $n = 1$, and the resultant solution curve plotted in the u_1, u_2 plane for various λ . Intersections of this curve with the u_1, u_2 curve defined by the symmetrical solution represent bifurcation points in the symmetrical solution involving a branch with a non-symmetrical component approximated by $v(r) \cos \theta$. We find that no intersections occur between $q = 0$ and the symmetrical buckling pressure for $\lambda \leq 5.5$ (Fig. 3).

However, intersections do occur for $6 \leq \lambda \leq 8$ (Fig. 4) at a pressure of about 90% of our symmetrical buckling pressure. No conclusions can be drawn for $\lambda > 8$ because of limitations on the validity of the solutions for large λ .

Buckling pressure vs. λ according to our equations, and according to Budiansky, are shown in Fig. 1. Although our non-symmetrical, $n = 1$, buckling pressures fall below our symmetrical pressures, they are somewhat above the symmetrical buckling pressures of Budiansky. Improvements in both our non-symmetrical and symmetrical solutions will be required before any positive statements about the magnitude of the non-symmetrical buckling pressure can be made. However, the argument that non-symmetrical modes may participate in buckling at higher values of λ has been considerably strengthened by this work.

Our present efforts to improve our solutions are concentrated in three areas: a) Finding $f(u_1, u_2)$ for $n > 1$, b) finding non-symmetrical solutions for improved functions $v(r)$, c) extending the validity of our symmetrical solution to larger values of λ .

CONCLUSIONS

A two term Galerkin solution to the symmetrical, non-linear shallow spherical shell equations has been found which compares very well with experimental load deflection results and the buckling loads of Budiansky, for small values of λ . The results break down for larger λ because of the increased importance of higher modes in the deflection pattern. The effect on the buckling load of allowing non-symmetrical deflections has been investigated and found to be important at values of $\lambda > 5.5$. Work along these lines is being continued, with more positive results expected in the near future.

ACKNOWLEDGEMENT

This work was supported in part by the United States Air Force, through a grant from the Office of Scientific Research.

REFERENCES

1. von Karman, Th., and Tsien, Hsue-Shen: The Buckling of Spherical Shells by External Pressure. Jour. Aero. Sci., vol. 7 no. 2, Dec. 1939, pp. 43-50.
2. Tsien, Hsue-Shen: A theory for the Buckling of Thin Shells. Jour. Aero. Sci., vol. 9, no. 10, Aug. 1942, pp. 373-384.
3. Friedrichs, K. O.: On the Minimum Buckling Load for Spherical

- Shells. Theodore von Karman Anniversary Volume, C.I.T. (Pasadena), 1941, pp. 258-272.
4. Klöppel, K. V., and Jungbluth, O.: Beitrag zum Durchschlag Problem dünnwandiger Kugelschalen. *Der Stahlbau*, vol. 22, 1953, p. 121.
 5. Kaplan, A., and Fung, Y. C.: A Nonlinear Theory of the Bending and Buckling of Thin Elastic Shallow Spherical Shells. NACA TN 3212, Aug. 1954.
 6. Fung, Y. C., and Kaplan, A.: Buckling of Low Arches or Curved Beams of Small Curvature. NACA TN 2840, 1952.
 7. Archer, R. R.: Stability Limits for a Clamped Spherical Shell Segment under Uniform Pressure. *Quarterly of Applied Mathematics*, vol. 15, Jan. 1958, p. 355.
 8. Reiss, E. L., Greenberg, H. J., and Keller, H. B.: Nonlinear Deflections of Shallow Spherical Shells. *Jour. Aero. Sci.*, vol. 54, Jul. 1957, p. 533.
 9. Weinitschke, H. J.: On the Nonlinear Theory of Shallow Spherical Shells. *Jour. Soc. Ind. and App. Math.*, vol. 6, Sept. 1958, p. 209.
 10. Chen, W. L.: Effect of Geometrical Imperfection on the Elastic Buckling of Shallow Spherical Shells. Sc.D. Thesis, Dept. of Civil and Sanitary Engineering, M.I.T., Jan. 1959.
 11. Von Willich, G.P.R.: The Elastic Stability of Thin Spherical Shells. *Jour. Eng. Mech. Div., Proc. ASCE*, vol. 185, no. EM 1, Jan. 1959.
 12. Budiansky, B.: Buckling of Clamped Shallow Spherical Shells. *Proc. of I.U.T.A.M. Symposium on the Theory of Thin Elastic Shells*, North Holland Pub. Co., 1960, pp. 64-94.
 13. Budiansky, B., and Weinitschke, H.: On Axisymmetrical Buckling of Clamped Shallow Spherical Shells. *Jour. Aero. Sci. (Readers Forum)*, vol. 27, Jul. 1960, pp. 545-6.
 14. Reiss, E. L., and Keller, H. B.: Spherical Cap Snapping. *Jour. Aero. Sci.*, vol. 26, Oct. 1959, pp. 643-652.
 15. Thurston, G. A.: A Numerical Solution of the Nonlinear Equations for Axisymmetric Bending of Shallow Spherical Shells. *J. Ap. Mech.*, vol. 28, no. 4, Dec. 1961, p. 557.
 16. Homewood, R. H., Brine, A. C., and Johnson, A. E., Jr.: Buckling Instability of Monocoque Shells. SESA Paper no. 547, vol. 18, no. 1, 1961.

17. Bellinfante, R. J.: Buckling of Spherical Caps under Uniform External Pressure. Douglas Report, Jan. 1962.
18. Grigolyuk, E. I.: On the Unsymmetrical Snapping of Shells of Revolution. Proc. of the I.U.T.A.M. on the Theory of Thin Elastic Shells, North Holland Pub. Co., 1960, pp. 112-121.
19. Gjelsvik, A., and Bodner, S. R.: The Non-Symmetrical Snap Buckling of the Clamped Spherical Cap. Technical Report No. 30, Engineering Div., Brown University, March 1962.

BUCKLING PRESSURE VS λ

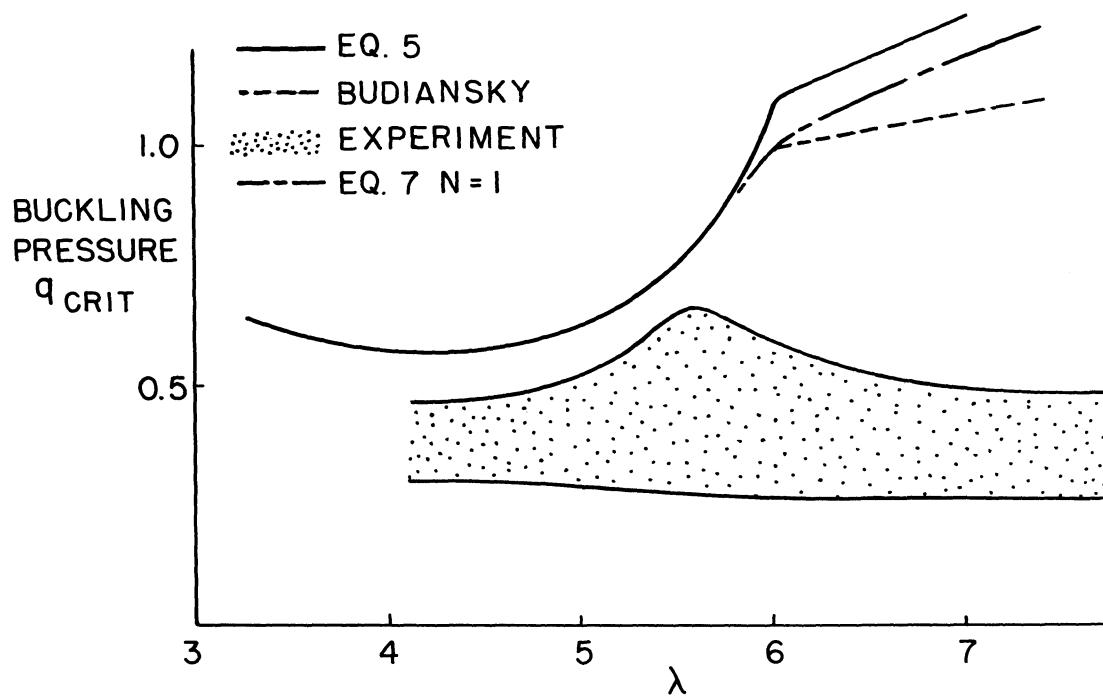


Figure 1

SHELL GEOMETRY AND COORDINATE SYSTEM

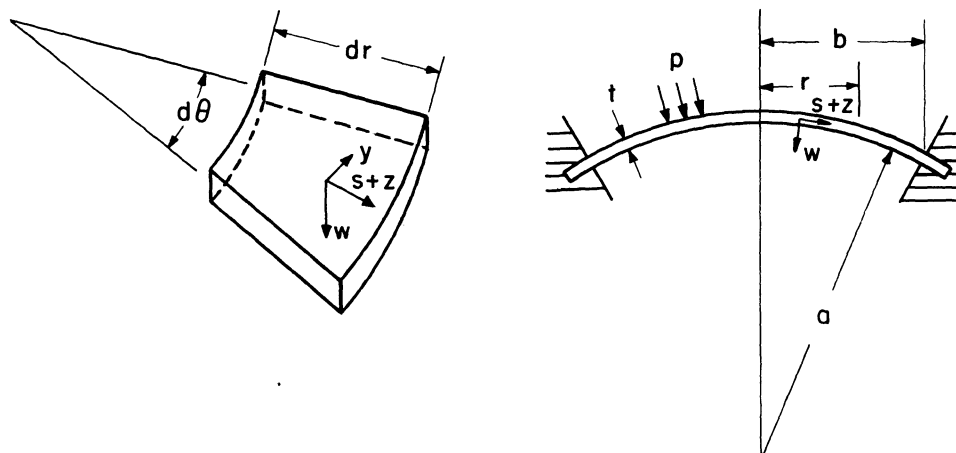


Figure 2

SOLUTIONS TO EQ. 5b AND EQ.7 FOR $\lambda = 5.5$

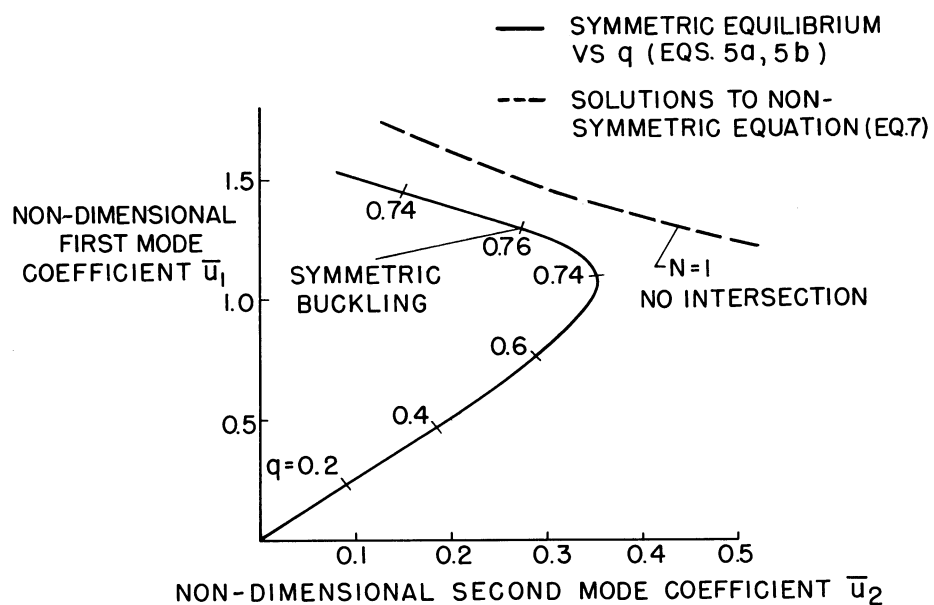


Figure 3

SOLUTIONS TO EQ. 5b AND EQ. 7 FOR $\lambda = 6.0$

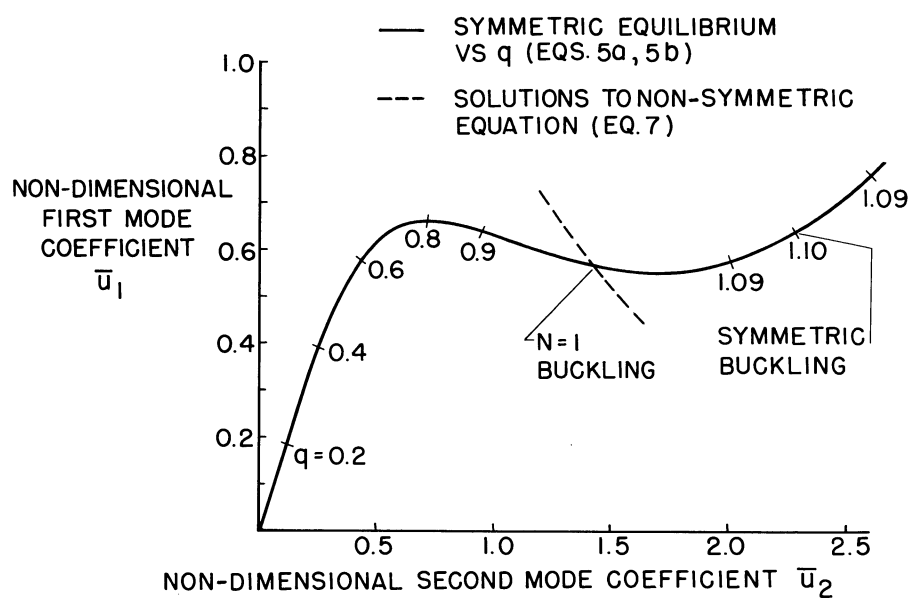


Figure 4

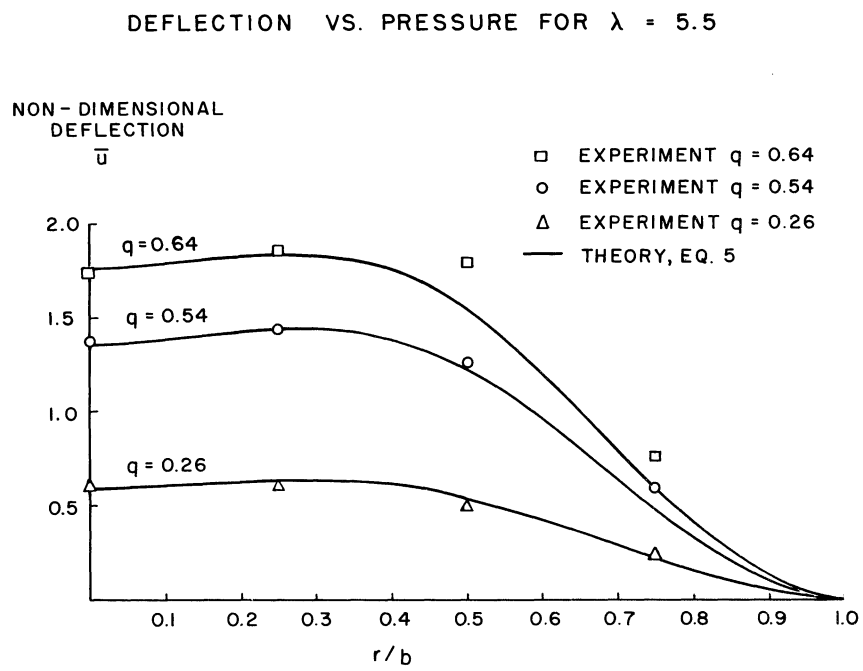


Figure 5

SOME RECENT RESULTS ON THE BUCKLING MECHANISM OF SPHERICAL CAPS*

By Herbert B. Keller and Edward L. Reiss

New York University

1. INTRODUCTION

The curve of pressure versus deformation for a spherical cap subjected to external pressure is frequently assumed to be similar to that of Fig. 1. Here P is a loading parameter and $D(P)$ is a measure of the deformation (e.g. maximum displacement). This curve implies that for $P > P_U$ and for $P < P_L$ there is only one equilibrium state. For each P in $P_L < P < P_U$ there are three equilibrium states and the cap must buckle at some P in this interval. We call P_L and P_U , respectively, the upper and lower buckling loads. Points on the branch OU correspond to unbuckled equilibrium states, those on the branch LN to buckled states and those on UL to unstable states.

The buckled and unbuckled equilibrium states are not "adjacent". Therefore when buckling occurs at some value of P the shell snaps from an unbuckled state to a buckled one. Of course, the buckling process is dynamic and a complete understanding of it requires a corresponding analysis. However, we believe that a static analysis can yield a description of the mechanism which initiates or "triggers" the dynamic process and can also yield the theoretical value, say $P = P_A$, at which this occurs.

Several ways of defining P_A are based on the curve of Figure 1. First von Kármán and Tsien [1], who proposed this figure, assumed that P_L should be the buckling load. Later Kaplan and Fung [2] applied the classical buckling criterion

* The research presented in this paper was supported by a grant from the U.S. Army Research Office (Durham) to the Courant Institute of Mathematical Sciences.

to conclude that P_U might be the appropriate value. All attempted calculations of P_U and P_L do not in general show agreement with the experimentally determined buckling loads, P_E .

Two other proposals for defining P_A introduce additional considerations. One assumes that "initial imperfections" are always present in the shell specimen and that they serve to change the corresponding value of P_U , say to P'_U . Then applying the classical criterion to such a shell yields different values for P_A . However, some rough calculations [3,4] with special forms of initial imperfection in the undeformed shape do not account for the discrepancy between P_U and P_E . Of course imperfection theory requires a more complete investigation.

The second proposal [5] assumes the existence of an intermediate load, P_M , in the interval $P_L < P_M < P_U$ such that for all P in $P_L \leq P < P_M$ the unbuckled states have less potential energy than the corresponding buckled states and conversely for P in $P_M < P \leq P_U$. It is further assumed that a shell will not snap to a state of higher energy and thus P_M is a lower bound on P_A . However, this theory does not at present define a precise value for P_A . Calculations for clamped caps [6] show that P_E is close to P_M for a specific range of caps and then they deviate sharply.

Recent analytical and theoretical results of the authors indicate that the curve of Figure 1 is usually not correct for clamped and other spherical shells. In fact a much more complicated behavior is found, allowing more than three equilibrium states for various loads. Consequently the previously described buckling criteria cannot be valid in general. In the remainder of this paper we shall present modifications of these criteria and some of our results which suggest them.

2. BUCKLING MECHANISMS

In analogy with the usual precise mathematical definition of stability we may say that an equilibrium state of a shell is stable at a given load if it depends continuously on the load. Thus if $D(P)$ is an appropriate measure of the deformation at load P then no buckling is possible if $D(P)$ is a continuous function of P . We therefore define "stability-loss" pressures as those values of P at which $D(P)$ becomes discontinuous.

In all buckling problems known to us the discontinuities occur by virtue of $D(P)$ becoming multivalued. Thus the stability-loss pressures are those values of P at which the equilibrium problem loses uniqueness. In analogy with our previous discussion we define P_L , the lower buckling load, as the least such pressure (i.e. there are unique solutions for all $P < P_L$ but nonunique ones for $P = P_L$). Similarly P_U is defined as the greatest stability-loss pressure (i.e. unique solutions exist for all $P > P_U$ but not for $P = P_U$). Both P_L and P_U need not exist in all problems (in fact we know of no case in which both have been proven to exist).

The sense of the inequalities is arbitrary in the above definitions. We could let $Q = -P$ in the formulation and then $Q_U = -P_L$ and $Q_L = -P_U$. Indeed this should be the case — for if the load on an elastically buckled shell is relaxed it will eventually unbuckle. We do not distinguish this unbuckling phenomenon from what is usually called buckling. In fact we shall later propose some experiments, based on this observation, to measure various critical pressures. (Such unbuckling experiments may eliminate some of the effects of initial imperfections.)

In addition to P_U and P_L we define as critical pressures all values of P at which the multiplicity of solutions of the equilibrium problem changes. The critical pressures thus defined need not include the load P_A . That is, the appearance of several equilibrium states at a given P does not insure that the shell will snap from one such state to another. However by extending Friedrichs' idea [5] we may define an order or preference of the equilibrium states for a fixed P

as follows. Let $S_1(P), S_2(P), \dots, S_n(P)$ denote the equilibrium states (note that n depends upon P) and let $E_1(P)$ denote the potential energy of the state $S_1(P)$. Then we order these states according to the magnitude of E . Thus $S_1(P)$ is "preferred" to $S_k(P)$ or has lower order if $E_1(P) < E_k(P)$. We now define the "intermediate" critical pressures as those P for which $E_1(P) = E_k(P)$ for some $1 \neq k$. The load (or loads) P_A may be "close" to one of the intermediate critical pressures.

We assume that it is always possible for a shell to snap from any state to a preferred state. If the shell is in $S_k(P)$ and jumps to $S_1(P)$ which is preferred, we must still invoke some mechanism to initiate the jump. "Small" disturbances which are always present could trigger the snapping provided that $S_k(P)$ and $S_1(P)$ are reasonably close states, say nearly similar deformations, stresses, etc. However, if there is some intermediate state $S_j(P)$ preferred to $S_k(P)$ (i.e. $E_1 < E_j < E_k$) and sufficiently close to $S_k(P)$ then a small disturbance would enable the shell to jump or rather start to jump from $S_k(P)$ to $S_j(P)$. Once this snapping is initiated the problem becomes dynamic and it is possible to end in the non-neighboring lower state $S_1(P)$. Thus, roughly speaking, we may say that the intermediate states such as $S_j(P)$ furnish some internal degrees of freedom to enable small disturbances to initiate a large snap through. Of course this mechanism allows asymmetric equilibrium states to play a role even though the buckling may be between symmetric states. Thus if these intermediate states actually exist the cap has essentially a "built-in" triggering mechanism.

The load at which buckling occurs in the above theory depends upon the "initial" state $S_k(P)$ and the "final" state $S_1(P)$. Thus if S_1 and S_k are "close" no intermediate state may be required. However, if these states are no longer close, then snap through becomes more difficult. Furthermore with changing geometric parameter intermediate states may appear or disappear between S_1 and S_k either enhancing or retarding the ability to buckle.

To apply the above considerations we must investigate the existence of non-unique equilibrium states and the energies of these states. We will indicate below several results which have been obtained for a variety of spherical cap problems. Only axisymmetric deformations are considered in these studies.

3. BIFURCATION BUCKLING

The radially symmetric equilibrium equations for a shallow spherical cap have been formulated in terms of $\alpha(x)$, a slope of the deformed midsurface, and $\gamma(x)$, a stress function [6]. These equations are

$$(1) \quad L\alpha = \rho(\alpha\gamma + Px^2) , \quad L\gamma = \rho(x^2 - \alpha^2) ,$$

where P is the dimensionless loading parameter, ρ is a geometric parameter and $L \cdot = x \frac{d}{dx} (\frac{1}{x} \frac{d}{dx} x \cdot)$. Assuming regularity and symmetry at the center of the cap, $x = 0$, implies the boundary conditions:

$$(2) \quad \alpha(0) = 0 , \quad \gamma(0) = 0 .$$

At the edge of the cap, $x = 1$, we now consider two types of boundary conditions which are such that the uniformly compressed spherical cap (i.e. $\alpha(x) = x$, $\gamma(x) = -Px$) is a solution of the equilibrium problem:

$$(3) \quad \begin{array}{ll} \text{A)} & \alpha(1) = 1 , \quad \gamma(1) = -P ; \\ \text{B)} & \alpha(1) = 1 , \quad \gamma'(1) - \nu\gamma(1) = -(1-\nu)P . \end{array}$$

These edge conditions are physically reasonable, the first in each case implying no rotation and the second implying no transverse shear force and that the meridional membrane stress in case A or the meridional displacement in case B is proportional to the external pressure.

The precise knowledge of the unbuckled state permits us, in these cases, to rigorously establish certain properties of the non-unique solutions. (The mathematical proofs and a detailed discussion of these results will be presented else-

where.) We prove, using the bifurcation theory of Poincaré, [7] that for each ρ and all P in a sufficiently small neighborhood of each eigenvalue of an appropriate linearized problem there exists a solution of the full nonlinear problem. Furthermore the curve of $D(P)$ versus P for each ρ can be shown to have the form of the solid portion of the curve in Figure 2. Some of the dotted portions of this figure are determined by numerical calculations. Assuming the potential energy expression to have a minimum we can establish the existence of an intermediate buckling load P_M (see Fig. 2) at which the unbuckled and "first" buckled states have equal energy. Upper and lower bounds on P_M have been determined as:

$$\frac{\omega_1^2}{\rho} \leq P_M < \underline{P}(\rho) .$$

Here $\underline{P}(\rho)$ is the lowest of the eigenvalues $P_k = \frac{\omega_k^2}{\rho} + \frac{2\rho}{\omega_k^2}$ of the linearized problem and ω_k is the k -th zero of the Bessel function $J_1(x)$. By using a minimization procedure rigorous upper bounds have been obtained which are considerably lower than \underline{P} and which for a limited range of ρ , serve to closely bracket P_M . In addition we have extended our previously employed finite difference method [6] to the bifurcation problems and have determined accurate numerical approximations of P_M and P_L . These numerical results will be reported in detail elsewhere. We have, as yet, been unsuccessful in establishing the existence of any intermediate buckling loads at which the potential energies of two buckled solutions are equal. It seems likely that some of the bifurcation analysis can be extended with suitable modification to the unsymmetric bifurcation buckling of spherical caps.

4. RELAXATION BUCKLING

Shallow spherical shells clamped and fixed along the edge have been studied in a number of recent papers. The nonlinear boundary value problem is the same as in case B of the previous section if we set $P = 0$ in the γ boundary condition (3B).

We have extended the previous finite difference calculations [6] to obtain results for larger values of ρ . The new results obtained in this way agree in many respects with those of [3,8,9]. However they cover a larger range and we do not interpret them in the same manner.

Another set of calculations based on initial value problems, which are the most extensive yet known to us, clarifies many of the previous results. This method has also been used by Murray and Wright [10] in more limited calculations. Although these two calculations were initiated independently we have benefited from private communications with Murray and Wright before embarking on extensive numerical work. The details of the techniques employed will be published elsewhere and we shall summarize here only some preliminary results relating to multiplicity of solutions and energy loads.

In Figure 3 we show curves, in the $P - \sqrt{\rho}$ plane, which separate regions of different numbers of solutions. For example consider the line $\rho = \rho_1$. As P increases along this line it represents a particular clamped cap subjected to increasing uniform external load. From $P = 0$ to A_1 there we find a unique, "unbuckled", solution. At the load corresponding to point A_1 more equilibrium states are possible, hence P_{A_1} is apparently the lower buckling load. Between A_1 and B_1 only three equilibrium states were found and only one was found above B_1 (up to pressures of 3.6). If there are only unique solutions above B_1 then P_{B_1} is an upper buckling load and the cap must snap between P_{A_1} and P_{B_1} . Two of the solutions in this interval were found to have equal energy at point a_1 . These solutions correspond to the unbuckled solution and what we term the "buckled" solution. The deformation of the buckled state is similar in shape to that of the unbuckled state but has a considerably larger amplitude. The third solution found here always has more energy than the buckled and unbuckled solutions (we call it an "unstable" state). Thus only one intermediate critical pressure can be defined for this value of ρ . This entire situation was observed in the approximate interval $2.8 < \sqrt{\rho} < 5$.

It was also observed that in this interval the experimentally determined buckling loads were quite close to the equal energy load. All of these results have also been obtained previously, by the finite difference calculations [6].

The situation changes at about $\rho = 25$. Consider the cap $\rho = \rho_2 > 25$ of Figure 3. Again we find a lower buckling load at P_{A_2} , three solutions above and an intermediate critical pressure at P_{a_2} . However the "buckled" and "unbuckled" states are much less similar than they were previously. Furthermore as P increases above P_{B_2} a new pair of solutions is found, for a total of five equilibrium states. One of these new solutions has energy between the "buckled" and "unbuckled" states at load P_{b_2} and a deformation closer to the unbuckled state. This state could function as the "trigger state" discussed in section 2. However the loads at which these solutions have been found are considerably above P_E . [Our calculations can only indicate existence and hence, of course, do not preclude the existence of other equilibrium states at lower pressures. In fact asymmetric states have not been included in our study but even other symmetric states could be present. See also the remarks in the next section.]

Having found the above solutions a closer study of the results of finite difference calculations revealed that they had actually "jumped" to one of the intermediate solutions at some $P > P_{B_2}$. For still higher pressures around P_{C_2} the solution jumped to the final buckled state.

The calculations are being continued and as many as nine non-unique solutions have recently been determined.

5. CONCLUDING REMARKS

To facilitate a comparison between theoretically and experimentally determined buckling loads extensive numerical results are required for a variety of other boundary conditions. The experiments of Kaplan and Fung and others were

conducted for nominally clamped edges. However this condition cannot be precisely realized in practice. The crucial dependence of the solutions on the boundary conditions is illustrated by the bifurcation buckling problem discussed in section 3.

The results described in the preceding sections indicate the need for a series of carefully controlled experiments on accurately fabricated specimens subject to a variety of boundary conditions. If it is feasible, an experimental study of bifurcation buckling would be of great interest. It is particularly important to design experiments which will explore the mechanisms of buckling. For example, many of the effects of initial imperfections in the specimen could be eliminated by conducting an unbuckling test. In such a test the specimen is allowed to buckle elastically and the pressure is increased slightly above the buckling load. Then the pressure is lowered until the shell snaps back to an unbuckled equilibrium position. A comparison of the experimentally determined snap-back load with the appropriate critical pressures may give an indication of the buckling mechanism.

REFERENCES

1. von Kármán, T. and Tsien, H. S.: The Buckling of Spherical Shells by External Pressure. Jour. Aero. Sci., vol. 7, 1939, pp. 43-50.
2. Kaplan, A. and Fung, Y. C.: A Nonlinear Theory of Bending and Buckling of Thin Elastic Shallow Spherical Shells. NACA TN 3213, 1954.
3. Budiansky, B.: Buckling of Clamped Shallow Spherical Shells. Symp. on Theory of Thin Elastic Shells, Delft, 1959, pp. 64-94.
4. Donnell, L. H.: Shell Theory. Proc. 4th Midwestern Conf. on Solid Mech., 1959, pp. 1-17.
5. Friedrichs, K. O.: On the Minimum Buckling Load for Spherical Shells, v. Karman Anniv. Vol., 1941, pp. 258-272.
6. Keller, H. B. and Reiss, E. L.: Spherical Cap Snapping. Jour. Aero. Sci., vol. 26, 1959, pp. 643-52.
7. Keller, H. B., Keller, J. B. and Reiss, E. L.: Buckled States of Circular Plates. Quart. Appl. Math., vol. 20, 1962, pp. 55-65.
8. Weinitschke, H. J.: On the Stability Problem for Shallow Spherical Shells. Jour. Math. and Phys., vol. 38, 1960, pp. 209-31.
9. Thurston, G. A.: A Numerical Solution of the Nonlinear Equations for Axisymmetric Bending of Shallow Spherical Shells. Jour. Appl. Mech., vol. 28, 1961, pp. 557-62.
10. Murray, F. J. and Wright, F. W.: The Buckling of Thin Spherical Shells. Jour. Aerospace Sci., vol. 28, 1961, pp. 223-36.

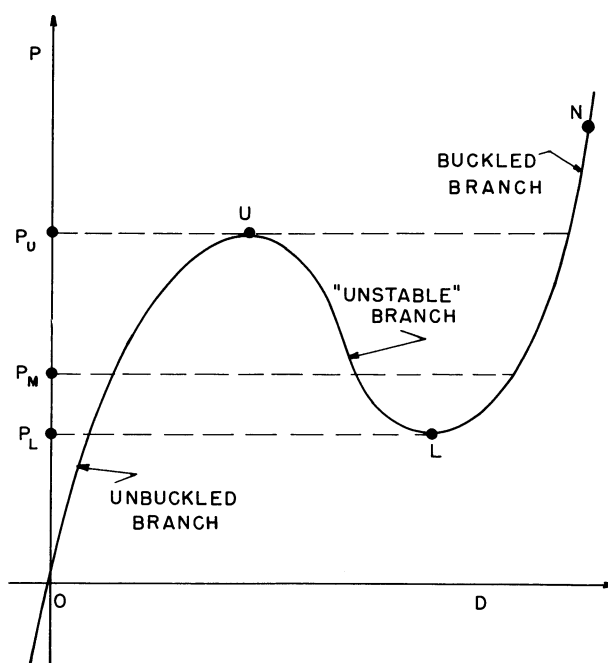


Figure 1.- Load deformation curve proposed by v. Kármán and Tsien.

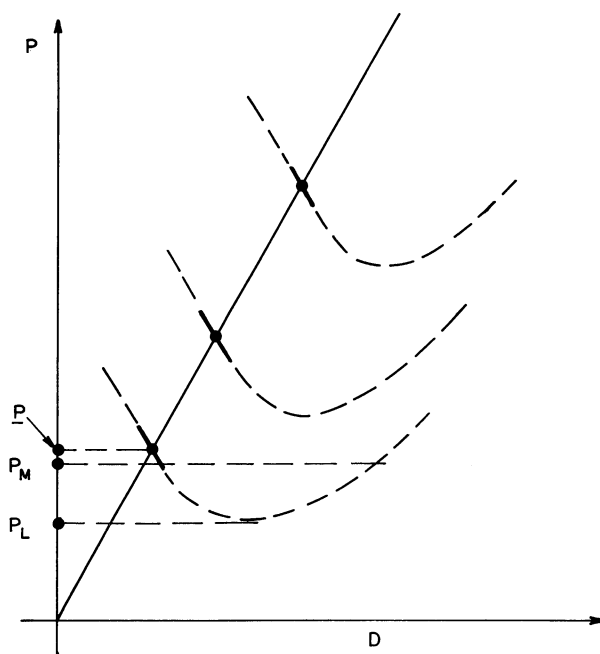


Figure 2.- Load deformation curve for bifurcation buckling (sketch).

COMPARISON OF EXPERIMENTAL AND
THEORETICAL BUCKLING PRESSURES FOR
SPHERICAL CAPS

By Gaylen A. Thurston
General Electric Company

SUMMARY

Theoretical buckling pressures for shallow spherical caps are compared with results of various experimental investigations. Classical theory for shells with an initial imperfection gives good agreement with experimental pressures. The results cast serious doubt on the validity of the equal potential energy buckling criterion for "dead-weight" loading.

INTRODUCTION

The problem of the buckling of a clamped shallow spherical cap subject to external pressure shows a large discrepancy between the pressures predicted by finite-deflection theory (refs. 1-4) and experimental results (refs. 5-8). Among other theoretical approaches to this problem are applying the energy criterion of buckling (refs. 8 and 9), computing the effect of initial axisymmetric imperfections in the shell shape, and extending the analysis to include non-axisymmetric imperfections and buckling modes. The first two alternatives are considered here.

The numerical results were obtained from a digital computer program* which solves Reissner's finite-deflection equations (ref. 10, Eqs. I and II) for any shell of revolution with continuous second derivatives of the parametric equations of the shell middle surface. The nonlinear ordinary differential equations of the finite-deflection theory are solved by an extension of Newton's method for calculating roots of algebraic equations. Bellman, Juncosa, and Kalaba (ref. 11) credit the method to Chaplygin (ref. 12) and give an extensive bibliography.

*Mr. H. Rowan programmed the numerical solution.

The strain energy in the shell and the potential energy of the shell and load system at each equilibrium state are computed by numerical integration over the shell surface using the stress resultants and deflections from the solution of the finite-deflection equations.

SYMBOLS

a	radius of curvature of spherical cap
E	Young's Modulus
h	shell thickness
L	rise of shell center above plane through the edge
P	buckling pressure parameter, q/q_{cr}
P_u, P_v, P_m, P_i, P_k	values of P from classical theory for a perfect shell, energy criterion for "constant-volume" buckling, equal potential energy criterion, classical theory for an imperfect shell and the lower buckling pressure from classical theory, respectively
q	external pressure
q_{cr}	classical buckling pressure of complete spherical shell, $2Eh^2/a^2 (3(1-\mu^2))^{1/2}$
r_o, z_o	radial and axial coordinates of point on shell mid-surface
λ	geometrical parameter, $2(3(1-\mu^2))^{1/4} (L/h)^{1/2}$
μ	Poisson's ratio
ϕ_o	angle from shell centerline to normal of the undeflected shell
$\bar{\phi}_o$	value of ϕ_o at shell edge

NUMERICAL RESULTS

The numerical results are summarized by the stability curves shown in Figs. 1 and 2. These curves show how the buckling pressures from the different theories vary with the geometrical shell parameter λ . The computations were based on the spherical cap with nominal dimensions of Specimen No. 10 of Kaplan and Fung (ref. 5), and λ was varied by changing the thickness h while holding the rest of the dimensions constant.

Fig. 1 shows the experimental buckling pressures for air pressure loading and oil loading reported by Kaplan and Fung. The post-buckled pressures for oil-loading are also shown. According to the energy criterion as defined by Tsien (ref. 8), there is a large difference between "constant-volume" buckling (approximated experimentally by the oil loading) and "dead-weight" loading (approximated by the air pressure loading).

In order to compute the buckling loads for the energy theory, it is necessary to solve the finite-deflection equations for the three separate equilibrium states which can exist at each pressure above the lower buckling pressure. There is the pre-buckled equilibrium state, the post-buckled equilibrium state where the shell is nearly inverted from its original shape except near the clamped edges, and there is an intermediate unstable equilibrium position.

Results from Energy Theory

The "constant-volume" buckling pressure is defined as the pressure at which the strain energy of the pre-buckled shell becomes as large as the strain energy of the unstable state at the same volume displaced by the pressure. It is assumed that the volume does not change during the jump between the two equilibrium states. On the other hand, the assumption of "dead-weight" loading is that the pressure is held constant during buckling. The buckling pressure is the pressure at which the potential energy of the shell and load system for the pre-buckled state is equal to the potential energy of the post-buckled state.

It can be seen from Fig. 1 that the "dead-weight" buckling curve P_m falls considerably below the experimental data for air pressure loading. Also, the experimental buckling pressures show no marked difference between the two types of loading. Although it must be admitted that it is impossible to duplicate the two idealized loading conditions experimentally, it also seems clear that the results of Kaplan and Fung contradict those of the energy criterion for "dead-weight" loading.

The buckling curve P_V for "constant-volume" buckling is unconservative for most of the experimental results in Figs. 1 and 2. However, this criterion cannot be excluded because of the possibility that unsymmetrical equilibrium states exist with lower levels of strain energy than those computed for the axisymmetric case.

Results for an Imperfect Shell

The stability curve P_i from the classical theory for an imperfect shell shape is in relatively good agreement with the experimental buckling pressures. In this case, the pressure vs. volume curve from the solution of the finite-deflection equations has a horizontal tangent at the buckling pressure. The computer solution solves the nonlinear finite-deflection equations as a sequence of nonhomogeneous linear "variational" equations (see ref. 3). The numerical solution transforms these into a sequence of linear algebraic equations. At the buckling pressure, the determinant of these algebraic equations vanishes. In practice, this buckling pressure must be determined by extrapolating the curve of the determinant vs. pressure to zero, since the numerical solution fails to converge at this point.

The parametric equations for the middle surface of the imperfect shell were taken as

$$\begin{aligned} r_o &= a \sin \phi_o \\ z_o &= a(1 - \cos \phi_o) + (.0458L)e^{-10(\phi_o/\bar{\phi}_o)^2} \\ L &= a(1 - \cos \bar{\phi}_o) \end{aligned}$$

with dimensions

$$a = 19.7 \text{ in.}, L = .41 \text{ in.}, a \sin \bar{\phi}_o = 4.0 \text{ in.}, \text{ and } h = 6.5639L/\lambda^2$$

This choice of shell shape puts an inward dimple at the apex of the shell. The amplitude of the imperfection of $.0458L$ is in the range of values measured on their specimens by Kaplan and Fung. The maximum derivative of the imperfection with respect to arc length is roughly $.012$ which is also in the measured range.

Budiansky (ref. 1) used a smoother imperfection shape with a smaller derivative and found a much smaller effect on the calculated buckling pressures.

The good correlation between the stability curve P_i for the imperfect shell and the experimental buckling pressures of Kaplan and Fung is encouraging in view of the fact that the imperfect shape is consistent with the measured imperfections. The numerical calculations also agree with the pressure-deflection curves of ref. 5 much better for the imperfect shell than for the perfect one.

For higher values of λ , the apparent correlation in Figs. 1 and 2 between the stability curves for the imperfect shell and the experimental data is somewhat misleading for two reasons. First, the imperfection amplitude becomes on the order of magnitude of the shell thickness for $\lambda > 10$ and there is no assurance that the experimental specimens have such large imperfections. Second, many of these shells buckled in asymmetric mode shapes contrary to the assumption used in the computations reported here.

Homewood, Brine, and Johnson (ref. 6) report buckling modes with an asymmetric dimple near the clamped edge. A check of their measured stresses before buckling for Specimen No. 9 reveals compressive circumferential stresses near the edge which are much higher than the calculated stresses for a perfect cap. This indicates that any analysis for asymmetric buckling modes should also include the effect of initial imperfections.

CONCLUDING REMARKS

Considering the effect of initial axisymmetric imperfections has done much to explain the discrepancy between theory and experiment for the buckling pressures for shallow spherical caps. Whether extending the analysis to allow asymmetric buckling modes and/or asymmetric imperfections will further clarify this problem remains to be seen.

The results from the energy criterion of buckling do not appear to agree with experiment. More experiments would be desirable to test the assumption of this theory that there is a difference in the buckling load depending on whether the load or the deflections are held constant during the buckling process.

REFERENCES

1. Budiansky, B.: Buckling of Clamped Shallow Spherical Shells. Proceedings of IUTAM Symposium on the Theory of Thin Elastic Shells, Delft, August, 1959, pp. 64-85.
2. Weinitschke, H.: On the Stability Problem for Shallow Spherical Shells. Journal of Mathematics and Physics, Vol. 38, No. 4, January, 1960, pp. 209-231.
3. Thurston, G.A.: A Numerical Solution of the Nonlinear Equations For Axisymmetric Bending of Shallow Spherical Shells. Journal of Applied Mechanics, Vol. 28, December 1961, pp. 557-562.
4. Keller, H.B. and Reiss, E.L.: Spherical Cap Snapping. Journal of the Aero-Space Sciences, Vol. 26, 1959, pp. 643-652.
5. Kaplan, A. and Fung, Y.C.: A Nonlinear Theory of Bending and Buckling of Thin Elastic Shallow Spherical Shells. NACA TN 3212, August, 1954.
6. Homewood, R.H., Brine, A.A., and Johnson, A.E., Jr.: Experimental Investigation of the Buckling Instability of Monocoque Shells. Experimental Mechanics, Vol. 1, March 1961, pp. 88-96.
7. Kloppel, K. Von, and Jungbluth, O.: Beitrag zum Durchschlag Problem dünnwandiger Kugelschalen. Der Stahlbau, Vol. 22, p. 121, 1953.
8. Tsien, H.S.: A Theory for the Buckling of Thin Shells. Journal of the Aeronautical Sciences, Vol. 9, August, 1942, pp. 373-384.
9. Friedrichs, K.O.: On the Minimum Buckling Load for Spherical Shells. Theodore Von Karman Anniversary Volume, California Institute of Technology, 1941, pp. 258-272.
10. Reissner, E.: On Axisymmetrical Deformation of Thin Shells of Revolution. Proceedings of Symposia in Applied Mathematics, Vol. III, McGraw-Hill, New York, 1950, pp. 27-52.
11. Bellman, R., Juncosa, M.L., and Kalaba, R.: Some Numerical Experiments Using Newton's Method for Nonlinear Parabolic and Elliptic Boundary - Value Problems. Comm. of Association for Computing Machinery, Vol. 4, No. 4, April, 1961, pp. 187-191.
12. Chaplygin, S.A.: A New Method for Approximate Integration of Differential Equations. 1905, recently printed under Classics of the Natural Sciences, Moscow, 1950.

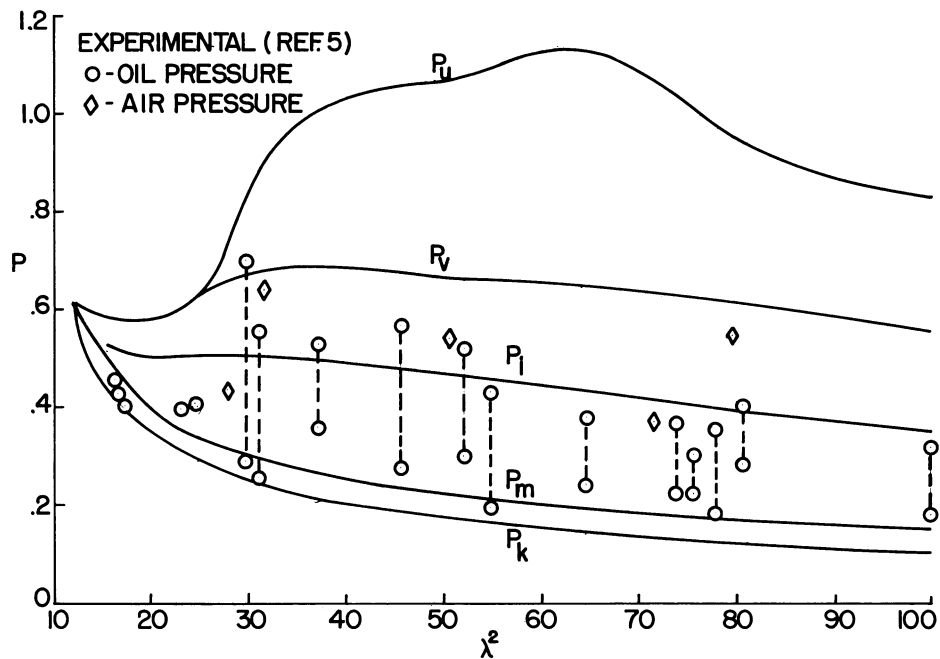


Figure 1.- Stability curves compared with experimental data of Kaplan and Fung.

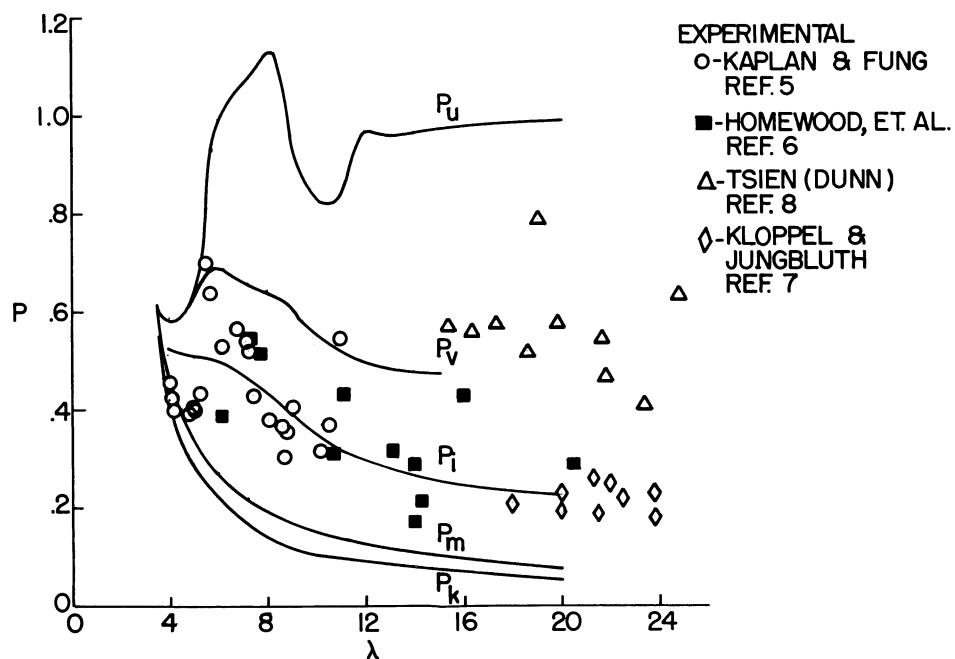


Figure 2.- Stability curves compared with experiment.

LOWER BOUNDS FOR THE BUCKLING PRESSURE
OF SPHERICAL SHELLS*

By Nicholas J. Hoff and Tsai-Chen Soong

Stanford University

SUMMARY

An approximate large-deflection theory is developed for the calculation of the hydrostatic pressure under which a thin-walled spherical shell buckles. The theory is based on the assumptions that the buckle has the shape of a spherical cap and that a yield hinge develops along the circumference of the cap. The effect of the test arrangement on the buckling pressure is taken into account. In spite of the rough approximate nature of the analysis reasonable numerical values are obtained for the buckling pressure.

INTRODUCTION

In a review of the state of knowledge regarding the buckling of thin elastic shells, Fung and Sechler¹ ** noted that "a complete spherical shell buckles in the form of a small inward dimple of small solid angle at some point on the surface of the shell; a fact entirely at variance with the linear theory of buckling". The non-linear theories developed to explain the discrepancies have all dealt with shallow spherical caps rather than with complete spheres and almost all the experimental effort related to spherical shells was made with spherical caps supported along their edge. The only known test with a complete spherical shell was carried out by Sechler and Bollay and was reported by Tsien.² In this test a brass shell buckled under approximately one-quarter the critical value of the external pressure of the linear theory. More recently, Thompson³ published the results of two experiments carried out with polyvinyl chloride shells of a radius to thickness ratio of approximately 20. Buckling occurred after about three-quarters of the classical value of the buckling pressure was reached. The paper also contains a large-deflection strain energy analysis which yielded satisfactory agreement with the results of the experiments.

*The work here described was carried out under NASA Grant NsG-93-60.

**Superscript numbers indicate entries under References at the end of the paper.

In a recent paper⁴ the senior author developed a rough approximate theory of the buckling of axially compressed thin-walled circular cylindrical shells on the basis of the assumption that plastic hinges form along the ridges when the shell snaps into the large-deflected shape. Since reasonable agreement was found between available experimental data and the results of the approximate theory, it appears worth while to apply the same method of analysis to the spherical shell. The absence of noticeable permanent deformations after the pressure is released does not prove that yielding had not taken place in the material. If a sufficient amount of elastic energy is stored in the buckled shell, the shell can snap back into a shape that appears to be the same as the initial one. Nevertheless some damage is always done because the buckling experiment cannot be repeated many times with the same specimen.

Since the details of the loading machine were found to influence significantly the buckling load in the case of the cylindrical shell, the loading apparatus to be used with the spherical shells is carefully defined in the present paper. The numerical values obtained for a special case and plotted in two figures appear to be reasonable. Nevertheless no claim is made for the accuracy of the theory because it is based on rather far-fetched assumptions. It obviously cannot yield more than approximate lower bounds on the buckling pressure because it consists of equating energy quantities before and after buckling. The relative success of the present approach may, however, indicate that the yield stress is one of the physical factors to be taken into account in more rigorous analyses of the large-deflection buckling process. It was included in the empirical formula proposed by Donnell⁵ twenty-eight years ago.

SYMBOLS

C	correction factor for influence coefficient (see Eq. 23)
d	radial components of displacement
h	wall thickness of specimen
H	wall thickness of container
E	Young's modulus
k	influence coefficient (see Eqs. 21 and 22)
K	Baker-Cline multiplier (see Eq. 23)

M	moment resultant
N	edge moment resultant
p	pressure
P	radial component of force resultant
q	non-dimensional quantity defined in Eq. 25
r	radius of specimen
R	radius of container
v	volume inside specimen
V	volume between spheres
W	work
x	non-dimensional quantity defined in Eq. 24
α	semi-vertex angle of bulge
β	multiplier defined in Eq. 62
γ	ratio of specific heats of air (= 1.4)
Δ	lack of fit defined in Eq. 20
κ	curvature
ν	Poisson's ratio
σ	stress
χ	rotation

In addition, the following subscripts are used:

a	atmospheric
ad	adiabatic
c	inside specimen after loading; also refers to cap
cc	inside specimen after buckling

cr	critical (refers to classical theory)
edge	refers to edge of buckle
el.b	elastic bending
f	final
i	initial after loading (before buckling)
o	initial before loading
out	refers to work done by outside atmosphere
pl	plastic
r	remainder
y	yield

BUCKLING ANALYSIS

Assumptions Regarding the Buckling Process

It is assumed that the thin-walled spherical test specimen is enclosed in a larger spherical container as shown in Fig. 1. The space between the two spheres is filled with water and at the beginning of the test the air outside the container, the water between the spheres and the air inside the test specimen are at the same atmospheric pressure p_a . In the first phase of the test the pressure of the water is increased to $p_a + p_i$ through the use of a pump provided with a no-return valve. The increase in the pressure expands the large sphere and compresses the small sphere; the effective pressure on the test specimen is therefore $p_i - p_c$ if the notation of Fig. 2 is employed. As the pressure in the water should be increased very slowly, it can be assumed that the compression inside the test specimen takes place isothermally. Thus the pressure inside the specimen before and after the compression is related to the volume inside the specimen before and after the compression through the equation

$$p_a v_o = (p_a + p_c) v_i \quad (1)$$

if the notation of Fig. 2b is used.

Under the conditions just described, the specimen is assumed to be in a neutral equilibrium. It suddenly jumps over into a buckled shape characterized by a dimple of a semivertex angle α (see Fig. 1). The dimple is again spherical and it has the same radius as the original spherical specimen would have if it were subjected to the prevailing pressure difference. The deformations during the buckling process consist therefore of a uniform expansion corresponding to the change in the pressure difference and an inextensional reversal of the curvature of the buckled portion of the median surface of the spherical specimen.

After buckling the water pressure is $p_a + p_f$ (see Fig. 2c), the pressure inside the specimen is $p_a + p_{cc}$, and the effective pressure on the spherical specimen is $p_f - p_{cc}$. The volume between the two spheres does not change during buckling as the water is incompressible. The change in the pressure inside the specimen is governed by the adiabatic law

$$\frac{p_a + p_{cc}}{p_a + p_c} = \left(\frac{v_i}{v_f} \right)^\gamma \quad (2)$$

where for air the value of γ is

$$\gamma = 1.4 \quad (2a)$$

Strain Energy in Unbuckled State

If the letters R and r denote the median surface radii of the outer and inner shells, and the letters H and h the uniform wall thicknesses of the outer and inner shells, the uniform normal stresses in the shell walls are

$$\begin{aligned} \sigma &= p_i R / 2H && \text{in the outer shell} \\ \sigma &= (p_i - p_c) r / 2h && \text{in the inner shell} \end{aligned} \quad (3)$$

The elastic strain energy stored in the outer shell is

$$U = (\sigma^2 / 2E) 4\pi R^2 H = (2\pi R^2 H / E) (p_i R / 2H)^2 = (\pi / 2) p_i^2 R^4 / EH$$

The total energy stored initially in the two shells is therefore

$$U_i = \frac{\pi p_i^2 R^4}{2 E H} + \frac{\pi (p_i - p_c)^2 r^4}{2 E h} \quad (4)$$

Elastic Membrane Strain Energy after Buckling

After buckling the final pressure $p_a + p_f$ prevails between the two shells. Even though part of the inner shell is now concave, the absolute magnitude of the membrane stress is the same throughout the inner shell as the magnitude of the curvature is the same everywhere. The total membrane strain energy stored in the system is

$$U_f = \frac{\pi}{2} \frac{p_f^2}{E} \frac{R^4}{H} + \frac{\pi}{2} \frac{(p_f - p_{cc})^2}{E} \frac{r^4}{h} \quad (5)$$

Elastic Energy of Bending of Cap

After buckling the portion of the shell, called the cap, that jumped over into a position of opposite curvature, is under the action of bending moments. The magnitude of the elastic strain energy stored because of bending can be evaluated approximately if the energy necessary to bend a flat circular plate of a radius $r \sin \alpha$ into a spherical cap of radius r is calculated and multiplied by 2. The curvature κ caused by uniform bending moment resultants N distributed along the entire circular edge of the plate and acting perpendicularly to the edge is

$$\kappa = [12(1 - \nu)/Eh^3]N \quad (6)$$

Since the curvature sought is $1/r$, Eq. 6 can be solved for N and $\kappa = 1/r$ can be substituted in the result obtained:

$$N = \frac{Eh^3/r}{12(1 - \nu)} \quad (7)$$

Since the edge of the plate must rotate through the angle 2α , and since the work done by the edge moment resultant N is $(1/2)N2\alpha$ per unit length of the circumference, the total work W done is

$$W = [12(1 - \nu)]^{-1} (Eh^3/r)\alpha 2\pi r \sin \alpha$$

As the work done is equal to the energy stored, the following expression is obtained for the energy $U_{el.b}$ of elastic bending:

$$U_{el.b} = \frac{\pi E}{6(1 - \nu)} h^3 \alpha \sin \alpha \quad (8)$$

Plastic Work Performed

In agreement with the assumptions the edge of the buckled cap deforms as a yield hinge. When a yield hinge forms in a ideally rigid-plastic material, half the thickness of the sheet is subjected to the tensile yield stress, and the other half to the compressive yield stress as indicated in Fig. 3. If the two yield stresses are equal numerically, the bending moment per unit length is

$$M_{pl} = \sigma_y (h/2)^2 \quad (9)$$

This moment is constant during the deformations because no plastic deformations can take place in a rigid-plastic solid until the bending moment reaches the value given in Eq. 7. Hence the total plastic work done amounts to

$$W_{pl} = M_{pl} 2\alpha 2\pi r \sin \alpha$$

where 2α is the total angle of rotation and $2\pi r \sin \alpha$ is the length of the yield hinge. Substitution yields

$$W_{pl} = \pi \sigma_y h^2 r \alpha \sin \alpha \quad (10)$$

Changes in Volume of the Two Shells

The volume between the two shells in their natural state is

$$V_o = (4\pi/3)(R^3 - r^3) \quad (11)$$

After the water between the two shells is brought to the pressure $p_a + p_i$, the outer shell expands and the inner shell is compressed with the result that the volume increases. Since the strains in the outer and inner shells are

$$\epsilon = (1 - \nu)(\sigma/E) = [(1 - \nu)/2](p_i R/Eh) \quad \text{in the outer shell}$$

$$\epsilon = -(1 - \nu)(\sigma/E) = -[(1 - \nu)/2](p_i - p_c)(r/Eh) \quad \text{in the inner shell} \quad (12)$$

the volume of air just before buckling is

$$V_i = \frac{4\pi}{3} \left\{ R^3 \left[1 + \frac{1-\nu}{2} \frac{p_i R}{Eh} \right]^3 - r^3 \left[1 - \frac{1-\nu}{2} \frac{(p_i - p_c)r}{Eh} \right]^3 \right\} \quad (13)$$

The volume V_f after buckling can be calculated in a similar manner but in addition the volume of the buckle itself must also be taken into account.

The volume of the cap is

$$V_c = (1/3)\pi r^3 (\cos^3 \alpha - 3 \cos \alpha + 2) \quad (14)$$

Hence the volume V_f after buckling is

$$V_f = \frac{4\pi}{3} \left\{ R^3 \left[1 + \frac{1-\nu}{2} \frac{p_f R}{Eh} \right]^3 - r^3 \left[1 - \frac{1-\nu}{2} \frac{(p_f - p_{cc})r}{Eh} \right]^3 \right\} + (2\pi/3)r^3 (\cos^3 \alpha - 3 \cos \alpha + 2) \quad (15)$$

The volume of the test sphere immediately before buckling is

$$v_i = \frac{4\pi}{3} r^3 \left[1 - \frac{1-\nu}{2} \frac{(p_i - p_c)r}{Eh} \right]^3 \quad (16)$$

and after buckling

$$v_f = \frac{4\pi}{3} r^3 \left[1 - \frac{1-\nu}{2} \frac{(p_f - p_{cc})r}{Eh} \right]^3 - (2\pi/3)r^3 (\cos^3 \alpha - 3 \cos \alpha + 2) \quad (17)$$

Work Done by the Air

The air outside the container remains at the atmospheric pressure during the buckling process. Hence the work done by the outside air is

$$W_{out} = \frac{4\pi}{3} R^3 p_a \left\{ \left[1 + \frac{1-\nu}{2} \frac{p_i R}{Eh} \right]^3 - \left[1 + \frac{1-\nu}{2} \frac{p_f R}{Eh} \right]^3 \right\} \quad (18)$$

The work necessary to compress adiabatically the air inside the test specimen is

$$W_{ad} = \frac{(p_a + p_c)v_i}{\gamma - 1} \left[-1 + \left(\frac{p_a + p_{cc}}{p_a + p_c} \right)^{\frac{\gamma-1}{\gamma}} \right] \quad (19)$$

Elastic Strain Energy in Edge Zone

It is easy to see that the deformations of the cap and the remainder in the state of membrane stress existing after the buckle was formed are not compatible. The remainder is in compression and the cap is in tension. The relative displacement Δ between cap and remainder can be easily calculated with the aid of Figs. 1 and 2:

$$\Delta = (1 - \nu)(r^2/h) \sin \alpha [(p_f - p_{cc})/E] \quad (20)$$

In order to reestablish continuity, edge forces P (perpendicular to the axis of the cap) and edge moments M must develop. These can be calculated with the aid of formulas derived in Reference 6. The displacement d perpendicular to the axis of the cap and the rotation χ of the end tangent are given by

$$\begin{aligned} d &= k_{dM} M + k_{dP} P \\ \chi &= k_{\chi M} M + k_{\chi P} P \end{aligned} \quad (21)$$

with the sign convention shown in Fig. 4. For the cap, the influence coefficients can be given as

$$\begin{aligned} k_{dM} &= -k_{\chi P} = 2[3(1-\nu^2)]^{\frac{1}{2}} (1/E)(r/h^2) \sin \alpha C_{12} \\ k_{dP} &= -2[3(1-\nu^2)]^{1/4} (1/E)(r/h)^{3/2} \sin^2 \alpha C_{11} \\ k_{\chi M} &= 4[3(1-\nu^2)]^{3/4} (1/E)(r^{1/2}/h^{5/2}) C_{22} \end{aligned} \quad (22)$$

where the factors C are defined as

$$\begin{aligned}
c_{11} &= (K_{11}/\sqrt{2}) \frac{(1 + R^*)^{1/2}}{1 + 2R^*} \\
c_{22} &= (K_{22}/\sqrt{2}) \frac{(1 + R^*)^{1/2}}{1 + 2R^*} \\
c_{12} &= K_{12} \frac{1}{1 + 2R^*}
\end{aligned} \tag{23}$$

The coefficients K were derived by Baker and Cline⁷; they are tabulated in the reference quoted.⁶ It is of interest to note that they vary little with α but change more rapidly with the quantity

$$x = q \alpha \tag{24}$$

where

$$q = \sqrt{2} [3(1 - \nu^2)]^{1/4} (a/b)^{1/2} \tag{25}$$

As the ratio h/a approaches zero, the values of K_{11} , K_{22} , and K_{12} approach the values $\sqrt{2}$, $\sqrt{2}$, and 1, respectively. Moreover

$$R^* = \sigma/\sigma_{cr} \tag{26}$$

with the classical critical stress

$$\sigma_{cr} = [3(1 - \nu^2)]^{-1/2} E(h/a) \tag{27}$$

The influence coefficients for the remainder are given by the same expressions except for the sign: In the expression for k_{ap} the right-hand member is positive and in the expression for $k_{\chi M}$ the right-hand member is negative. Equations 23 remain unchanged but the values of the Baker-Cline coefficients must be taken from the table established for the remainder, and not for the cap. The value of R^* also changes sign; it is positive for the cap where the stress is tensile and negative for the remainder where the stress is compressive.

With the sign convention used

$$P_c = P_r = P \qquad M_c = -M_r = -M \tag{28}$$

One condition of compatible deformations is that the lack of fit Δ must be equal in magnitude to the difference in the radial edge displacement d of the remainder and the cap:

$$\Delta = d_r - d_c \quad (29)$$

Finally, the sign convention for the rotation of the edge tangent is such that

$$\chi_c + \chi_r = 0 \quad (30)$$

Solution of these equations yields

$$M = -(1/2)[3(1-\nu^2)]^{-1/2} E(h^2/r) \operatorname{cosec} \alpha \frac{c_{12c} + c_{12r}}{2(c_{22c} + c_{22r})(c_{11c} + c_{11r}) - (c_{12c} + c_{12r})^2} \Delta$$

$$P = [3(1-\nu^2)]^{-1/4} E(h/r)^{3/2} \operatorname{cosec}^2 \alpha \frac{c_{22c} + c_{22r}}{2(c_{22c} + c_{22r})(c_{11c} + c_{11r}) - (c_{12c} + c_{12r})^2} \Delta \quad (31)$$

Since the work done by the edge moment resultants is zero as the relative rotation between the edges of cap and remainder is zero, work is done only by the edge force resultants P . This work is

$$W_{el} = (1/2) 2\pi r \sin \alpha P \Delta$$

This work is equal to the elastic energy stored in the edge zone. Substitutions yield

$$U_{edge} = \pi \frac{(1-\nu)^2}{[3(1-\nu^2)]^{1/4}} \frac{(p_f - p_{cc})^2}{E} \frac{r^{7/2}}{h^{1/2}} \sin \alpha \frac{c_{22c} + c_{22r}}{2(c_{22c} + c_{22r})(c_{11c} + c_{11r}) - (c_{12c} + c_{12r})^2} \quad (32)$$

It is of interest to note that the value of the last fraction approaches $1/2$ as the final pressure $p_f - p_{cc}$ (and thus R^*) decreases and as the ratio h/r decreases and approaches zero.

Buckling Condition

Obviously buckling cannot occur unless the energy stored in the system before buckling plus the potential of the external loads is at least as large as the energy stored in the system after buckling plus the work done in an irreversible manner and transformed into heat. Hence

a lower limit on the buckling pressure p_i can be obtained by solving the energy equation

$$U_i + W_{out} = U_f + U_{el.b} + U_{edge} + W_{pl} + W_{ad} \quad (33)$$

In addition the geometric constraint

$$V_f = V_i \quad (34)$$

must be satisfied and the conditions connecting the changes in volume of the air contained in the test specimen with the changes in pressure (Eqs. 1 and 2) must be observed. The equations contain the nine unknowns p_i , p_f , p_c , p_{cc} , V_i , V_f , v_i , v_f and α . For their solution there are available four equations of geometry (Eqs. 13, 15, 16, and 17), two equations of change of state of the air (Eqs. 1 and 2), one equation of incompressibility of the water (Eq. 34) and one energy equation (Eq. 33). If a value of α is arbitrarily selected, the eight equations suffice to determine all the remaining unknowns. One can plot then p_i as a function of α and consider the minimal value of p_i as the lower bound on the buckling pressure.

Numerical Values

The calculations outlined in the preceding sections were programmed for the Burroughs 220 digital computer in order to obtain some numerical results. For prescribed values of α , the semivertex angle of the buckle, the gauge pressure p_i in the container was calculated and plotted. Figure 5 contains six such curves corresponding to different ratios of the radius R of the container to the radius r of the specimen. The six values are 1.1, 1.2, 1.3, 1.6, 2.0, and 2.2. The other parameters of the problem are fixed in the following manner:

$$E = 15 \times 10^6 \text{ psi} \quad \sigma_y = 30,000 \text{ psi}$$

$$h/H = 0.1 \quad r/h = 500 \quad \nu = 0.3$$

It is to be expected that buckling will occur at the minimal value of the gauge pressure. Hence the test arrangement corresponding to $R/r = 1.1$ yields a buckling pressure p_i which is about 24.5 percent of the classical value. This is in good agreement with the test results obtained by Sechler and Bollay with the brass shell mentioned in the Introduction. The semivertex angle is about 11 degrees according to Fig. 5.

As the volume enclosed between test specimen and container is increased, the semivertex angle increases slowly and the pressure ratio decreases slowly. For $R/r = 2.2$ the values obtained are $\alpha = 13$ degrees and $p_i/p_{cr} = 0.17$.

The effect of a change in the material of the specimen (and of the container) is illustrated in Fig. 6. When $R/r = 1.2$, the minimal values of the gauge pressure at buckling amount to approximately 22, 24 and 39 percent of the classical values of the critical pressure for carbon steel, brass and an aluminum alloy, respectively. The corresponding semivertex angles are about 10.5, 11, and 12.5 degrees.

To illustrate details of the buckling process, the following data are given:

Characteristics of brass test specimen and container:

$$R/r = 1.2 \quad h/H = 0.1 \quad r/h = 500$$

$$E = 15 \times 10^6 \text{ psi} \quad \sigma_y = 30,000 \text{ psi}$$

$$\text{Semivertex angle of buckle} \quad \alpha = 11 \text{ degrees}$$

$$\text{Gauge pressure before buckling} \quad p_i = 17.30 \text{ psi}$$

$$\text{Gauge pressure after buckling} \quad p_f = 5.30 \text{ psi}$$

$$\text{Gauge pressure inside specimen after buckling} \quad p_{cc} = 0.011 \text{ psi}$$

The relative importance of the various energy quantities can be seen from the following data:

$$(1/\pi r^3)(U_i - U_f) = 5.436 \times 10^{-3} \text{ in. lb per in.}^3$$

$$(1/\pi r^3)U_{el.b} = 1.044 \times 10^{-3} \text{ in. lb per in.}^3$$

$$(1/\pi r^3)U_{edge} = 1.255 \times 10^{-6} \text{ in. lb per in.}^3$$

$$(1/\pi r^3)W_{out} = 1.695 \times 10^{-3} \text{ in. lb per in.}^3$$

$$(1/\pi r^3)W_{pl} = 4.399 \times 10^{-3} \text{ in. lb per in.}^3$$

$$(1/\pi r^3)W_{ad} = 1.692 \times 10^{-3} \text{ in. lb per in.}^3$$

Simplified Solution

If use is made of the observation that the changes in volume caused by the elastic strains are small compared to the initial volumes, and that the semivertex angle α of the bulge is likely to be small, and if in addition the container is assumed to be rigid

$$H = \infty \quad (35)$$

the expressions presented simplify considerably. In particular

$$\cos^3 \alpha - 3 \cos \alpha + 2 = (3/4) \alpha^4 \quad (36)$$

and the volumes of interest become

$$v_i = \frac{4\pi}{3} r^3 \left[1 - \frac{3(1-\nu)}{2} \frac{(p_i - p_c)r}{Eh} \right] \quad (37)$$

$$v_f = \frac{4\pi}{3} r^3 \left[1 - \frac{3(1-\nu)}{2} \frac{(p_f - p_{cc})r}{Eh} \right] - \frac{\pi}{2} r^3 \alpha^4 \quad (38)$$

$$V_i = \frac{4\pi}{3} (R^3 - r^3) + 2\pi(1-\nu)(p_i - p_c) \frac{r^4}{Eh} \quad (39)$$

$$V_f = \frac{4\pi}{3} (R^3 - r^3) + 2\pi(1-\nu)(p_f - p_{cc}) \frac{r^4}{Eh} + \frac{\pi}{2} r^3 \alpha^4 \quad (40)$$

From Eq. 1

$$v_i = \frac{p_a}{p_a + p_c} \frac{4\pi}{3} r^3 \quad (41)$$

Equation 2 can be re-written as

$$\frac{p_a + p_c}{p_a + p_{cc}} = \left(\frac{v_f}{v_i} \right)^\gamma \quad (42)$$

and the incompressibility condition becomes

$$p_i - p_c = p_f - p_{cc} + \frac{E}{4(1-\nu)} \frac{h}{r} \alpha^4 \quad (43)$$

These equations suffice to express all the quantities of interest in terms of the geometric and physical constants of the problem and of the initial pressure p_i and the angle α . Consideration of the energy equation yields then p_i as a function of α .

The energy terms become:

$$U_i = \frac{\pi}{2} \frac{(p_i - p_c)^2}{E} \frac{r^4}{h} \quad (44)$$

$$U_f = \frac{\pi}{2} \frac{(p_f - p_{cc})^2}{E} \frac{r^4}{h} \quad (45)$$

$$U_{el.b} = \frac{\pi E}{6(1 - \nu)} h^3 \alpha^2 \quad (46)$$

$$W_{pl} = \pi \sigma_y h^2 r \alpha^2 \quad (47)$$

$$W_{ad} = \frac{(p_a + p_c) v_i}{\gamma - 1} \left[\left(\frac{v_i}{v_f} \right)^{\gamma-1} - 1 \right] \quad (48)$$

$$W_{out} = 0 \quad (49)$$

Moreover, in a first approximation, U_{edge} can be disregarded. Two immediate consequences of the incompressibility condition and Eq. 42 are

$$v_i = v_f \quad p_c = p_{cc} \quad (50)$$

and it follows from Eq. 48 that

$$W_{ad} = 0 \quad (51)$$

From Eqs. 44 and 45 it follows that

$$U_i - U_f = (\pi/2)(r^4/Eh)(p_i - p_f)(p_i + p_f - 2p_c) \quad (52)$$

But the condition

$$v_i = v_f$$

implies

$$2\pi(r^4/Eh)(1 - \nu)(p_i - p_f) = (\pi/2)r^3\alpha^4 \quad (53)$$

while the first of Eqs. 50 leads to the same requirement. Hence, Eq. 33 becomes simply

$$U_i - U_f = U_{el} \cdot b + W_{pl} \quad (54)$$

or

$$\frac{\pi}{2} \frac{r^4}{Eh} (p_i - p_f)(p_i + p_f - 2p_c) = \frac{\pi E}{6(1-\nu)} h^3 \alpha^2 + \pi \sigma_y h^2 r \alpha^2 \quad (55)$$

Eq. 55 together with Eq. 53, can be solved for $(p_i - p_c)$:

$$p_i - p_c = \frac{4(1-\nu)}{\alpha^2} \left[\frac{E}{6(1-\nu)} \left(\frac{h}{r} \right)^3 + \sigma_y \left(\frac{h}{r} \right)^2 \right] + \frac{E}{8(1-\nu)} \frac{h}{r} \alpha^4 \quad (56)$$

From Eqs. 41 and 37 one obtains

$$\frac{p_a}{p_a + p_c} = 1 - \frac{3}{2} (1-\nu) \frac{(p_i - p_c)r}{Eh} \quad (57)$$

that is

$$\frac{1}{1 + (p_c/p_a)} = 1 - \frac{3}{2} (1-\nu) \frac{(p_i - p_c)r}{Eh}$$

or approximately,

$$\frac{p_c}{p_a} = \frac{3}{2} (1-\nu) \frac{(p_i - p_c)r}{Eh}$$

that is

$$p_c = \frac{(3/2)(1-\nu)(r/Eh)}{(1/p_a) + (3/2)(1-\nu)(r/Eh)} p_i \quad (58)$$

Substitution in Eq. 56 yields

$$p_i \left[1 - \frac{(3/2)(1-\nu)(r/Eh)}{(1/p_a) + (3/2)(1-\nu)(r/Eh)} \right] = \frac{4(1-\nu)}{\alpha^2} \left[\frac{E}{6(1-\nu)} \left(\frac{h}{r} \right)^3 + \sigma_y \left(\frac{h}{r} \right)^2 \right] + \frac{E}{8(1-\nu)} \frac{h}{r} \alpha^4$$

or

$$P_i \left[\frac{1}{1+(3/2)(1-\nu)(r/Eh)p_a} \right] = \frac{4(1-\nu)}{\alpha^2} \left[\frac{E}{6(1-\nu)} \left(\frac{h}{r} \right)^3 + \sigma_y \left(\frac{h}{r} \right)^2 \right] + \frac{E}{8(1-\sigma)} \frac{h}{r} \alpha^4 \quad (59)$$

This can also be written as

$$\beta p_i = \frac{4(1-\nu)}{\alpha^2} \left[\frac{E}{6(1-\nu)} \left(\frac{h}{r} \right)^3 + \sigma_y \left(\frac{h}{r} \right)^2 \right] + \frac{E}{8(1-\nu)} \frac{h}{r} \alpha^4 \quad (60)$$

where β is the expression in brackets multiplying p_i in Eq. 59; its value is almost exactly equal to unity. To obtain $p_{i\min}$ set $dp_i/d\alpha$ equal to zero and solve for α :

$$\alpha_m^6 = \frac{16(1-\nu)^2}{E} \frac{h}{r} \left[\frac{E}{6(1-\nu)} \frac{h}{r} + \sigma_y \right] \quad (61)$$

Substitution in Eq. 60 yields

$$p_{i\min} = \frac{3}{8} \frac{Eh}{(1-\nu)r} \alpha_{\min}^4 (1/\beta) \quad (62)$$

A numerical example will show the accuracy of the approximate formula. If a brass sphere is characterized by the values

$$\begin{aligned} E &= 15 \times 10^6 & h/r &= 1/500 \\ \sigma_y &= 30,000 & \nu &= 0.3 \end{aligned}$$

one obtains from Eq. 61

$$\alpha^6 = 38.9 \times 10^{-6} \quad \alpha = 0.1842 = 10^\circ 30'$$

and from Eq. 62

$$p_i = 18.39 \text{ psi} \quad p_i/p_{cr} = (18.39/72.3)100 = 25.4\%$$

SIMPLE BUCKLING FORMULAS

If the assumptions of the last section are maintained, namely that the container is perfectly rigid, and in addition ν is taken as 0.3, the results of the analysis can be presented in the following simple formulas:

$$\alpha_{\min} = 1.31 \left(\frac{\sigma_{cr}}{E} \right)^{1/6} \left(\frac{\sigma_{cr}}{E} + 2.54 \frac{\sigma_y}{E} \right)^{1/6} \quad (63)$$

$$\alpha_{\min} = 1.11 \left(\frac{h}{r} \right)^{1/6} \left(\frac{h}{r} + 4.2 \frac{\sigma_y}{E} \right)^{1/6} \quad (64)$$

$$p_{i\min} = 2.62 \sigma_{cr} \left(\frac{\sigma_{cr}}{E} \right)^{2/3} \left(\frac{\sigma_{cr}}{E} + 2.54 \frac{\sigma_y}{E} \right)^{2/3} \quad (65)$$

$$p_{i\min} = 0.814 E \left(\frac{h}{r} \right)^{5/3} \left(\frac{h}{r} + 4.2 \frac{\sigma_y}{E} \right)^{2/3} \quad (66)$$

$$\sigma_{i\min} = 0.407 E \left(\frac{h}{r} \right)^{2/3} \left(\frac{h}{r} + 4.2 \frac{\sigma_y}{E} \right)^{2/3} \quad (67)$$

where σ_{cr} is the critical stress defined in Eq. 27.

The last equation shows that for comparatively thick shells with a low value of the yield stress the buckling stress decreases more rapidly with decreasing h/r ratio than is predicted by the classical small-deflection formula, while for comparatively thin shells with a high value of the yield stress the opposite is true.

REFERENCES

- (1) Fung, Y. C., and Sechler, E. E., Instability of Thin Elastic Shells, Structural Mechanics, Proceedings of the First Symposium on Naval Structural Mechanics, edited by J. N. Goodier and N. J. Hoff, Pergamon Press, Oxford, England, p. 115, 1960.
- (2) Tsien, Hsue-Shen, A Theory for the Buckling of Thin Shells, Journal of the Aeronautical Sciences, Vol. 9, No. 10, p. 373, 1942.
- (3) Thompson, J. M. T., The Elastic Instability of a Complete Spherical Shell, The Aeronautical Quarterly, Vol. 13, Part 2, p. 189, May 1962.
- (4) Hoff, N. J., Buckling of Thin Shells, Theodore von Kármán 80th Anniversary Lecture, SUDAER No. 114, Department of Aeronautics and Astronautics of Stanford University, August 1961.
- (5) Donnell, L. H., A New Theory for the Buckling of Thin Cylinders under Axial Compression and Bending, Transactions of the American Society of Mechanical Engineers, Report AER-56-12, Vol. 56, p. 795, 1934.

- (6) Hoff, N. J., Elastic Analysis of Motor Case Shells, Lockheed Missiles and Space Division Report LMSC-3-80-61-7, August 1, 1961.
- (7) Baker, B. R., and Cline, G. B., Jr., Influence Coefficients for Thin Smooth Shells of Revolution Subjected to Symmetric Loads, Journal of Applied Mechanics, Vol. 29, Series E, No. 2, p. 335, June 1962.

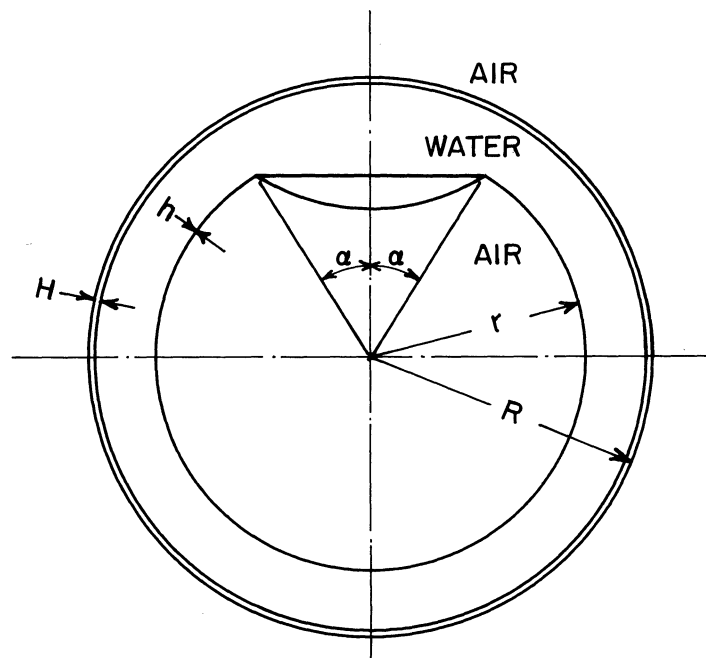


FIG.1. BUCKLED SPHERICAL TEST SPECIMEN IN SPHERICAL CONTAINER.

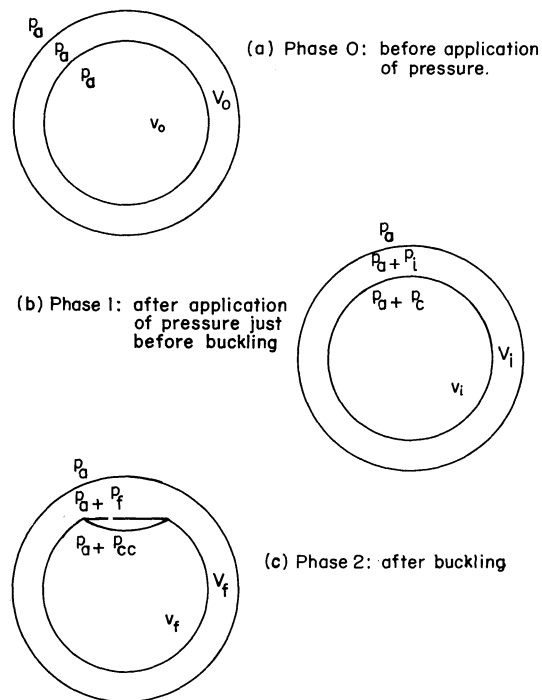


FIG. 2. THREE PHASES OF BUCKLING TEST.

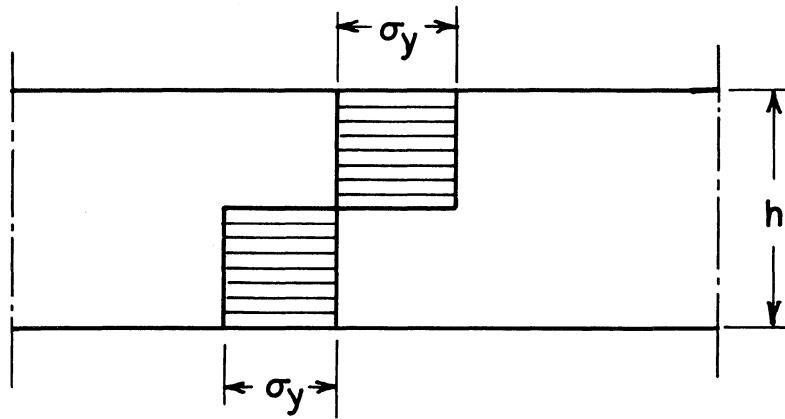


FIG. 3. STRESS DISTRIBUTION IN WALL OF SHELL CORRESPONDING TO PLASTIC HINGE.

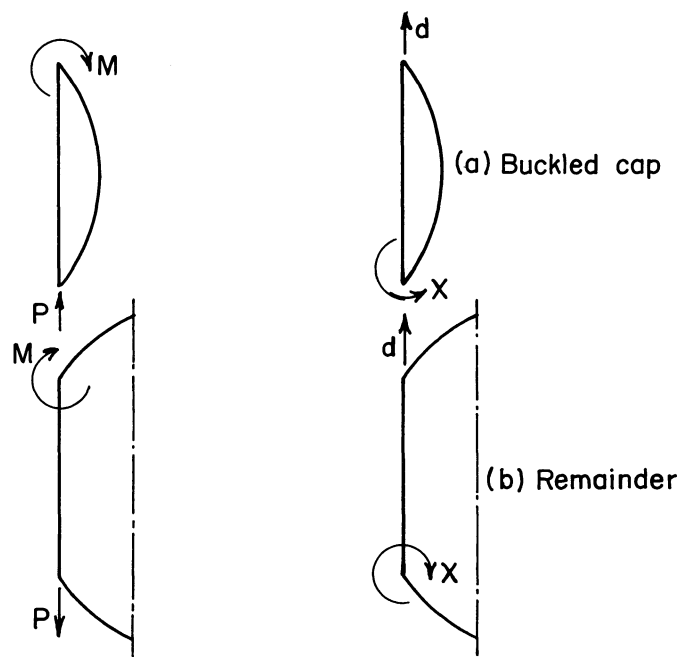


FIG. 4. CONVENTION FOR EDGE DISPLACEMENTS AND STRESS RESULTANTS.

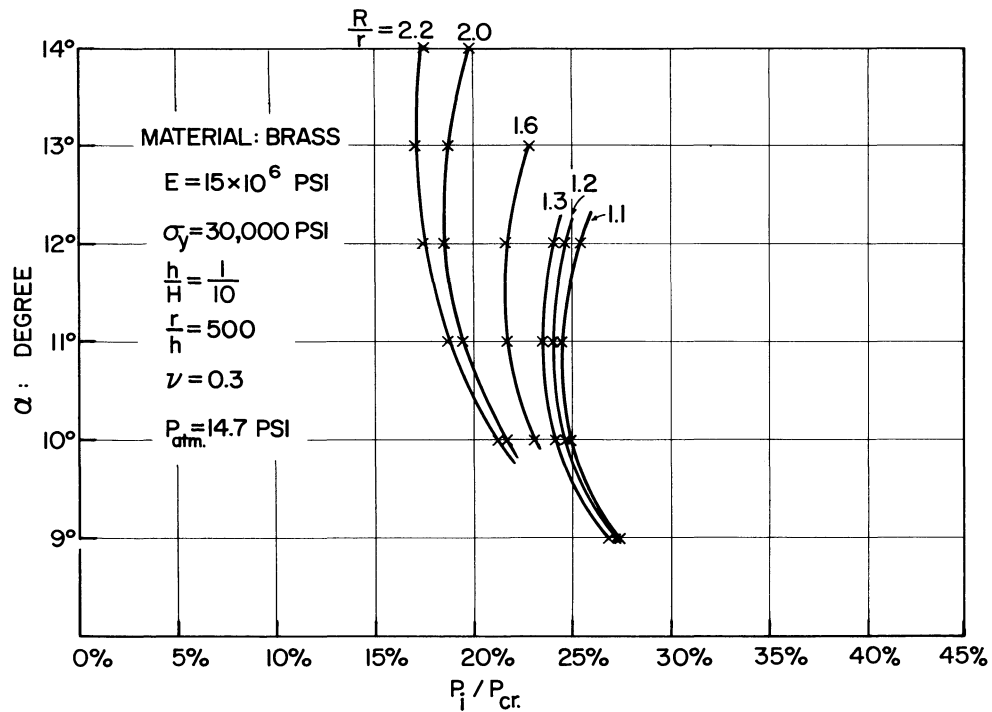


FIG. 5. EFFECT OF VOLUME OF CONTAINER ON BUCKLING PRESSURE.

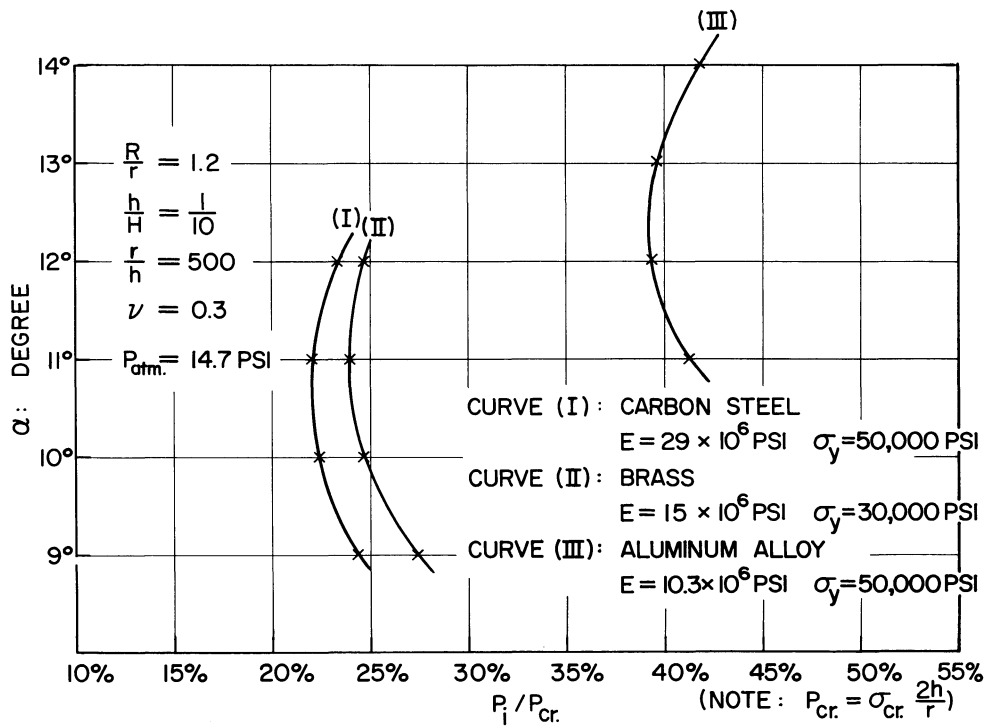


FIG. 6. EFFECT OF MATERIAL OF SPECIMEN ON BUCKLING PRESSURE.

A SURVEY OF RESEARCH ON THE STABILITY OF HYDROSTATICALLY-
LOADED SHELL STRUCTURES CONDUCTED AT
THE DAVID TAYLOR MODEL BASIN

By Thomas E. Reynolds

David Taylor Model Basin

SUMMARY

Experimental and theoretical studies have been carried out to investigate the stability of ring-stiffened cylinders and hemispherical shells under hydrostatic pressure. The use of accurately machined models has been found extremely valuable in improving the quality of experimental data, thereby permitting a more careful examination of theory. As a result, the effects of boundary conditions and other factors usually masked by the influence of structural imperfections have been clarified.

So far these studies have caused the investigators to regard classical small-deflection theory with increasing confidence.

INTRODUCTION

As the major structural element in a submersible, the ring-stiffened cylinder has long been of prime interest to the naval architect. It is likely that future vehicles attaining greater operational depths may also make extensive use of spherical shells for the main pressure hull as well as for terminating closures. This paper is concerned with recent studies of the buckling characteristics exhibited by these two shell types when subjected to hydrostatic pressure.

RING-STIFFENED CYLINDERS

The basic buckling configuration to be considered is the antisymmetric or lobar mode. It has been convenient to investigate separately two distinct classes: general instability, wherein both rings and shell deflect radially (figure 1), and shell instability, in which the rings do not deflect radially and buckles appear between them (figure 2).

General Instability

Considerable work has been directed toward an experimental

evaluation of Kendrick's small-deflection solution (reference 1, second solution) for the elastic instability of a cylinder with simply-supported ends. Tests of a variety of small, externally-stiffened cylinders machined from high-strength steel tubing have revealed that buckling pressures can be obtained with remarkable accuracy using Southwell's nondestructive technique (references 2 and 3). It has also been established that variations in end restraint, even for cylinders as long as five diameters, can have an appreciable influence on buckling strength (reference 4).

As an example of the investigations being conducted, a recent study by W.F. Blumenberg is cited. The objective was to obtain buckling pressures by Southwell's method as a function of cylinder length with boundary conditions held constant. The test arrangement is shown in figure 3. The length of the central test section was varied by rearranging the pairs of movable discs whose rounded edges were in contact with the inner wall of the cylinder. The outer discs were maintained at one frame space from the inner ones as an approach to isolating the central section from variations in conditions of support resulting from changes in the lengths of the end sections. The maximum test pressure attained averaged about 98 per cent of the Southwell buckling pressure. The maximum measured stress was about 43,000 psi compared with a value of 85,000 psi for the yield strength.

Since it was not expected that this arrangement would closely approximate the condition of simple support, it was not surprising that the experimental pressures were somewhat higher than those given by Kendrick's solution. However, a plot of the results is instructive. In figure 4 the circles represent the experimental pressures and the solid curve is Kendrick's solution for a nominal Young's modulus of 30×10^6 psi. The abscissa is N , the number of frame spaces separating the inner discs. These results suggest the possibility that, so far as buckling is concerned, a cylinder of length L (N frame spaces) whose ends are arbitrarily restrained behaves as if its length were L_{eff} (N_{eff} frame spaces) and its ends simply-supported, where

$$L_{\text{eff}} = kL \quad (N_{\text{eff}} = kN) \quad (1)$$

k is a constant whose value depends on the degree of restraint - being less than unity where the restraint is more restrictive than simple support and greater than unity where the opposite is true. This would mean that for a given cylinder any degree of restraint can be represented on a single plot of buckling pressure versus L_{eff} or N_{eff} and that the transition from one circumferential mode to another must occur at the same pressure regardless of the boundary

conditions.

In figure 4 the slight difference between the theoretical and experimental pressures for the transition from 2 lobes to 3 could easily result from a small disparity between the actual and assumed values of Young's modulus. If the corresponding transition values for N are substituted into equation (1) the resulting value for k is 0.725. Using this number the experimental points were replotted with N_{eff} as the new abscissa and with the appropriate adjustment in Young's modulus. These points are the triangles in figure 4.

This approach has been used with data from a variety of tests to obtain values of k ranging from 0.71 to 0.94, and corresponding pressure variations of as much as 65 per cent. The results to date have strengthened the investigators' belief that Kendrick's solution will give reliable predictions when appropriate adjustments are made for the degree of restraint.

Shell Instability

To summarize very briefly, small-deflection solutions for elastic shell instability have not been entirely satisfactory when applied to shells with closely-spaced stiffeners. Von Mises' solution (reference 5), for example, does not account for the effect of the stiffeners on buckling strength, hence is not strictly applicable. Von Sanden and Tölke (reference 6) considered the stiffeners as they affect the deflections prior to buckling, but neglected their influence on the buckling deformations. Experimental results in many cases have not been particularly illuminating. Because of inadequate yield strengths and fabrication imperfections, elastic shell instability has seldom been observed with closely-spaced stiffeners. In cases where the Von Mises pressure has not been attained "snap-through" buckling has sometimes been offered as the explanation.

A small-deflection solution recently developed by the author accounts for the influence of the stiffeners on deformations occurring both before and during buckling by expressing all deflections as trigonometric series. The solution is obtained using the Ritz procedure and includes the resistance of the stiffeners to deformations in and out of their planes. To evaluate this solution data are available from collapse tests of four machined cylinders where again elastic buckling was achieved through the use of high-strength steel tubing. Two of these tests are reported in reference 7. The results are shown in table 1. It appears that the performances of the cylinders are adequately explained by the new small-deflection

solution. This is supported by the fact that the buckling strength in one case was accurately determined using Southwell's method, which is only successful where small-deflection theory applies. It is further indicated, by comparing the Von Mises pressures with the collapse pressures, that the influence of the stiffeners can be appreciable. It is only partially accounted for by the solution of Von Sanden and Tölke.

SPHERICAL SHELLS

In spite of a long history of investigation it appears that the buckling of spherical shells is not yet properly understood. The elastic buckling pressure given by the classical small-deflection analysis of Zoelly (reference 8) is far in excess of anything that has been observed experimentally, and various attempts to explain these vast discrepancies on the basis of finite deflection theory have been less than satisfactory (reference 9). Furthermore, most work has been devoted to the study of shallow spherical caps whereas the interest of the pressure vessel designer is in deep and complete spherical shells.

Krenzke (reference 10) has recently completed tests of a series of machined hemispherical shells about 1.6 inches in diameter which were designed to study both elastic and inelastic buckling. One group of shells was machined from 6061-T6 aluminum (yield strength of 43,000 psi), another from 7075-T6 aluminum (80,000 psi). Each hemisphere was terminated by a stiffened cylinder which, in all but three cases, was designed so that no bending stresses could develop in the hemisphere prior to buckling. The three exceptions were cases in which the cylinders had to be made somewhat more rigid to provide them with adequate buckling strength. Accurate machining assured nearly perfect sphericity in all cases.

Figure 5 shows a few of the observed failures. The three shells having the more rigid boundaries buckled well within the elastic range. It appeared that the buckling strengths of these shells were not adversely affected by the boundary conditions since, in each case, the portion immediately adjoining the cylinder was undamaged. Their buckling pressures are compared in table 2 with the theoretical values given by the small-deflection solution of Zoelly:

$$p_e = \frac{1.154 E}{\sqrt{1 - \nu^2}} \left(\frac{h}{R} \right)^2 = 1.21 E \left(\frac{h}{R} \right)^2 \text{ for } \nu = 0.3, \quad (2)$$

where E is Young's modulus, ν is Poisson's ratio, h is the shell

thickness and R is the mean radius. The ratios of experimental pressures to p_e , although less than one, are much larger than have been observed for shells formed from flat plates, indicating the sensitivity of buckling strength to imperfections and residual stresses. The tests also show that the minimum buckling pressures defined by large-deflection theory can be greatly exceeded. From the results of table 2 Krenzke has proposed an empirical buckling formula for the elastic range:

$$p_e' = \frac{0.80 E}{\sqrt{1 - \nu^2}} \left(\frac{h}{R_0} \right)^2 = 0.84 E \left(\frac{h}{R_0} \right)^2 \text{ for } \nu = 0.3, \quad (3)$$

where the use of the outer radius, R_0 , is dictated by simple load equilibrium.

The rest of the shells collapsed in the yield region at pressures ranging from 6 to 46 per cent of p_e . For this range Krenzke has suggested the following formula to represent p_c , the inelastic collapse pressure:

$$p_c = \sqrt{\frac{E_s E_t}{E^2}} p_e' = 0.8 \sqrt{\frac{E_s E_t}{(1 - \nu^2)}} \left(\frac{h}{R_0} \right)^2 \quad (4)$$

E_s and E_t are the secant and tangent moduli which can be determined from the stress-strain diagram for the material under uniaxial loading. The quantity under the radical which multiplies p_e' is a simplified plasticity reduction factor based on theoretical studies by Bijlaard and Gerard (references 11 and 12). In the elastic range equation (4) reduces to equation (3). Figure 6 shows how well this formula fits the experimental data. The abscissa is the ratio of p_c to p_e , the elastic buckling pressure according to equation (2), and the ordinate is the ratio of the experimental pressure, p_{exp} , to p_e .

Despite the consistency of these results it is not necessarily conclusive that they represent the maximum buckling strength attainable. Each of the shells had small deviations in thickness which presumably had some weakening effects. Future studies will include tests of larger machined shells in which such deviations can be further reduced. Other tests are presently underway with spun and pressed hemispheres and with machined spherical shells having central angles greater than as well as less than 180° . The benefits of stiffening are also being studied.

REFERENCES

1. Kendrick, S.: The Buckling under External Pressure of Circular Cylindrical Shells with Evenly Spaced Equal Strength Circular Ring Frames - Part III. N.C.R.E./R. 244, Sept. 1953.
2. Galletly, G. D., and Reynolds, T. E.: A Simple Extension of Southwell's Method for Determining the Elastic General Instability Pressure of Ring-Stiffened Cylinders Subject to External Hydrostatic Pressure. Proc. SESA, vol. XIII, no. 2, 1956, p. 141.
3. Galletly, G. D., Slankard, R. C., and Wenk, E., Jr.: General Instability of Ring-Stiffened Cylindrical Shells Subject to External Hydrostatic Pressure - A Comparison of Theory and Experiment. Jour. Appl. Mech., vol. 25, Trans. ASME, vol. 80, June 1958, pp. 259-266.
4. Reynolds, T. E., and Blumenberg, W. F.: General Instability of Ring-Stiffened Cylindrical Shells Subject to External Hydrostatic Pressure. DTMB Report 1324, June 1959.
5. Von Mises, R.: The Critical External Pressure of Cylindrical Tubes under Uniform Radial and Axial Load. EMB Report 366, Aug. 1933.
6. Von Sanden, K., and Tölke, F.: On Stability Problems in Thin Cylindrical Shells. DTMB Translation 33, Dec. 1949.
7. Hom, K., and Couch, W. P.: Hydrostatic Tests of Inelastic and Elastic Stability of Ring-Stiffened Cylindrical Shells Machined from Strain-Hardening Steel. DTMB Report 1501, Dec. 1961.
8. Timoshenko, S.: Theory of Elastic Stability. McGraw-Hill Book Co., Inc., 1936, p. 491.
9. Fung, Y. C., and Sechler, E. E.: Instability of Thin Elastic Shells. Proc. First Symposium on Naval Structural Mechanics, 1960, p. 115.
10. Krenzke, M. A.: Tests of Machined Deep Spherical Shells under External Hydrostatic Pressure. DTMB Report 1601, May 1962.
11. Bijlaard, P. P.: Theory and Tests on the Plastic Stability of Plates and Shells. Jour. Aero. Sci., vol. 9, no. 10, Aug. 1942.
12. Gerard, G.: Plastic Stability Theory of Thin Shells. Jour. Aero. Sci., vol. 24, no. 4, April 1957.

Table 1 - Results of Elastic Shell Buckling Studies

$\frac{A_f}{L_f h}$	Flexibility Parameter $\sqrt[4]{\frac{3(1-\nu^2)}{R^2 h^2}} L_f$	Experimental Buckling Pressure, psi	Theoretical Buckling Pressures, psi		
			New Solution	von Sanden and Tolke (ref. 6)	Von Mises (ref. 5)
0.418	4.13	803(14)*	811(11)	693(16)	665(15)
0.526	4.75	725(13)	744(13)	665(14)	654(14)
0.650	5.26	475(14)	460(14)	386(16)	387(14)
0.228	6.80	633(11)**	633(11)	599(11)	600(10)
<p>*Number of circumferential lobes in parentheses **Southwell method gave 637 psi A_f = cross-sectional area of stiffener L_f = stiffener spacing h = shell thickness R = mean radius All cylinders had external rectangular stiffeners</p>					

Table 2 - Comparison of Collapse Pressures from the Classical Theory with Experimental Values

$\frac{h}{R}$	Buckling Pressures, psi		$\frac{P_{exp}}{P_e}$
	Experiment, P_{exp}	Equation (2), P_e	
0.0095	800	1180	0.68
0.0096	830	1210	0.69
0.0120	1230	1875	0.66

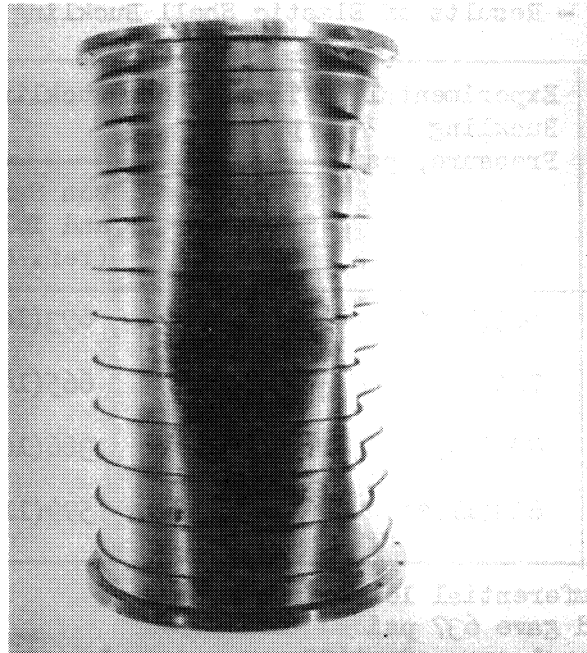


Figure 1.- General instability type of collapse.

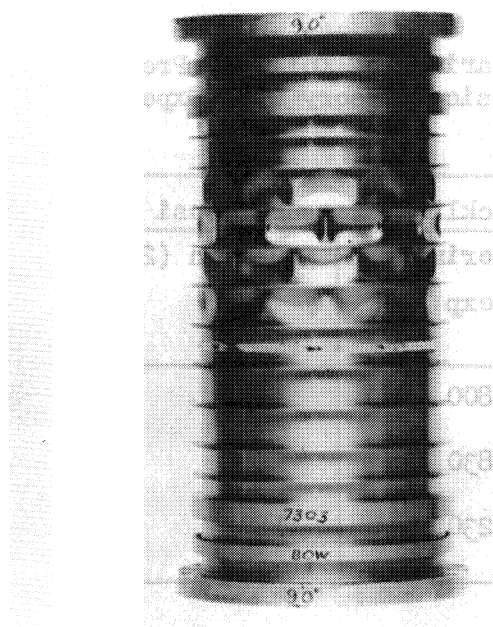


Figure 2.- Shell instability type of collapse.

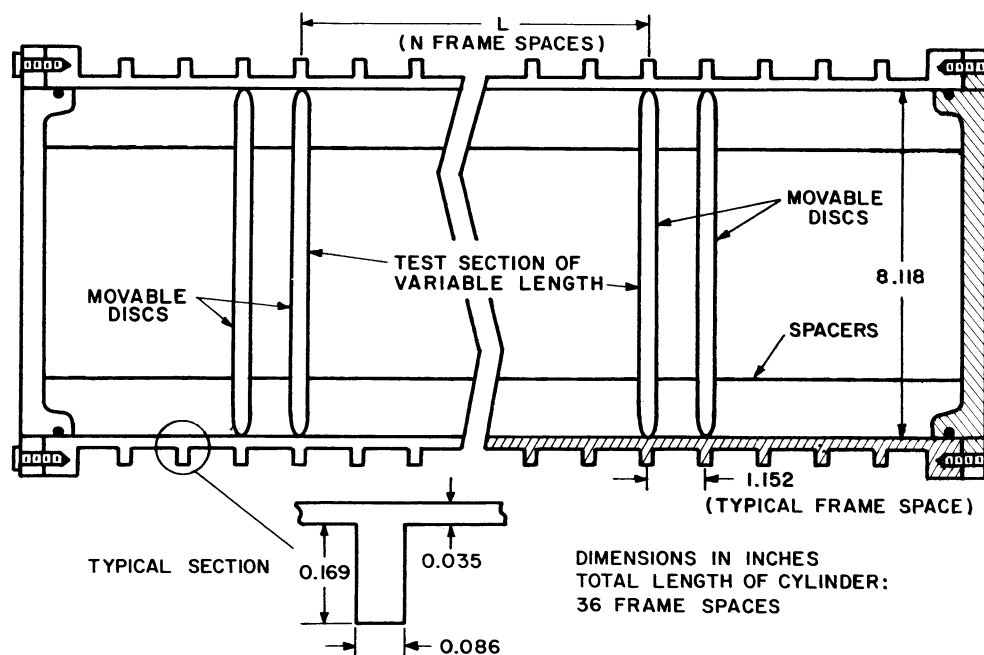


Figure 3.- General instability test arrangement.

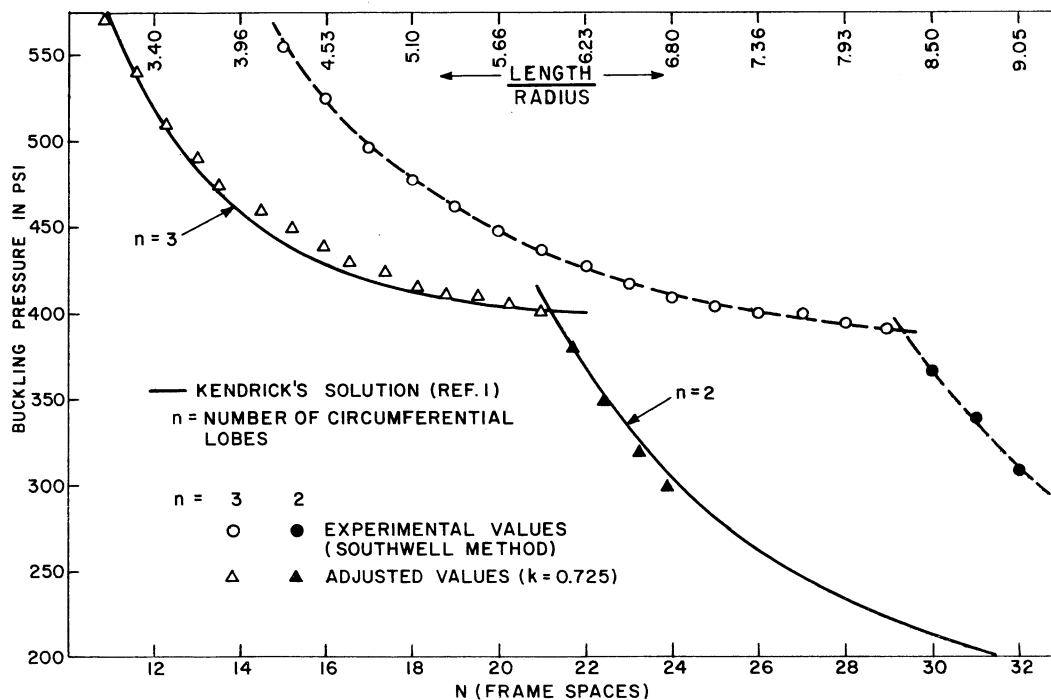


Figure 4.- Stiffened cylinder - elastic general instability results.

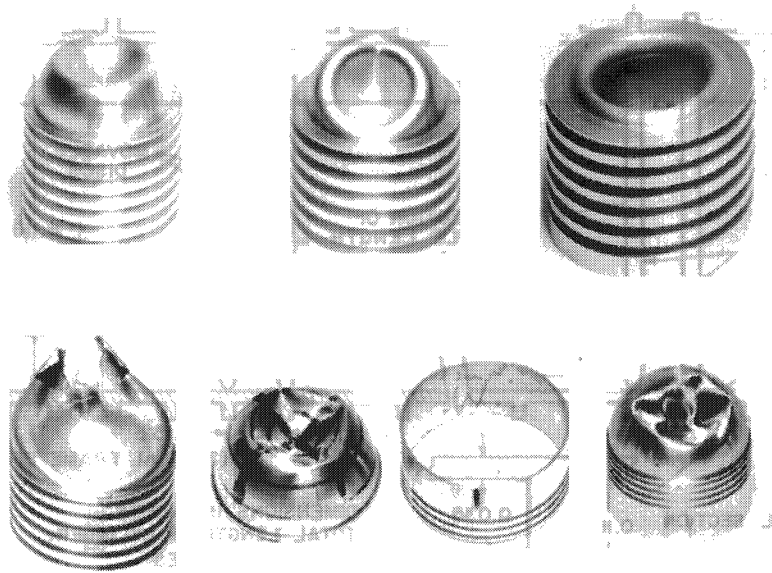


Figure 5.- Examples of collapsed hemispheres.

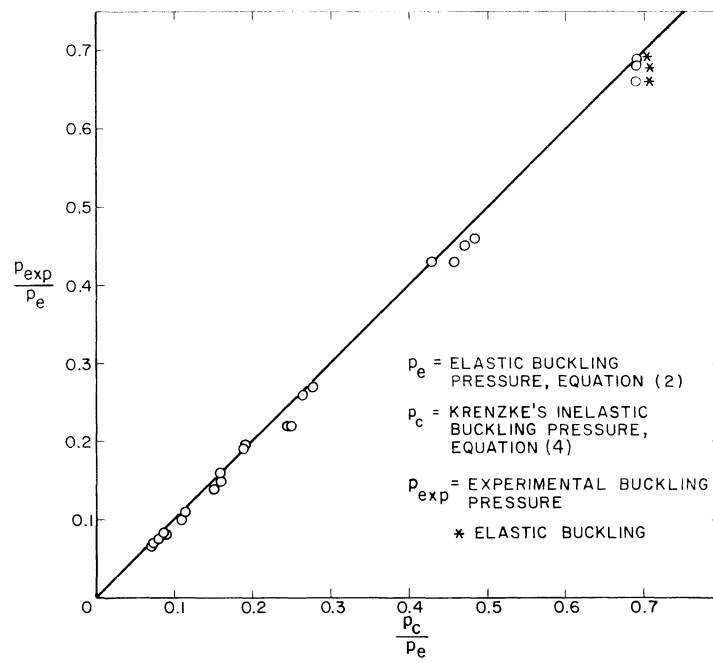


Figure 6.- Buckling data for hemispheres.

BUCKLING OF A SPHERE OF EXTREMELY HIGH
RADIUS-THICKNESS RATIO

By Harvey G. McComb, Jr., and Wilbur B. Fichter

NASA Langley Research Center

SUMMARY

Some buckling experiments on a complete spherical shell having a radius-thickness ratio of about 85,000 are discussed. Extremely small pressure differentials and many relatively large local imperfections were involved in these experiments. In spite of these drawbacks, the results obtained are consistent and well defined. The test results indicated that the local initial imperfections were not as significant in their influence on the shell behavior as were such effects as overall nonuniformity of construction and loading.

INTRODUCTION

Proposed passive communications satellites are ultrathin-walled spherical shells which may experience buckling from external pressure due to solar radiation or atmospheric drag. Large buckling deformations of such a satellite are undesirable because they seriously reduce the satellite's performance as a reflector. At present, shell buckling technology is lacking in several respects with regard to design of spherical shells subjected to external pressure. Large discrepancies exist between theoretical and experimental buckling pressure; therefore, the designer must be guided primarily by experimental data. However, very little experimental data on complete spheres are available; the primary research effort has been concerned with shallow spherical caps. All available experimental data are for radius-thickness ratios several orders of magnitude smaller than that for the proposed satellites. In order to provide a basis for estimating the buckling strength of these satellites, therefore, buckling experiments were conducted on a complete spherical shell having a radius-thickness ratio of about 85,000. This value is much higher than that of any spherical cap or complete sphere used in previously reported experiments.

SYMBOLS

D	plate flexural stiffness of shell wall material, 51.2×10^{-5} lb-in. for test specimen
K	extensional stiffness of a unit width beam of shell wall material, 4,140 lb/in. for test specimen
N	stress resultant, lb/in.
Δp	differential pressure, pressure outside sphere minus pressure inside, psi unless otherwise noted
r	radius of spherical shell, in.
Subscripts:	
cl	classical linear theory
o	associated with initial inflation pressure

SPECIMEN

The specimen tested is illustrated in figure 1. It was a spherical shell 12.5 feet in diameter fabricated of material similar to that used in the 135-foot-diameter Echo A-12 rigidized sphere. The material is a three-layer laminate composed of Mylar sheet with an aluminum face layer bonded on either side. The aluminum in the face layers is 99.8-percent pure and is designated as 1080 aluminum. The faces are intended to provide flexural stiffness in the laminate; they also add some strength.

The specimen was composed of 23 meridional gores bonded together in butt, single-strap splices. The straps were 1-inch-wide strips of the same three-layer laminate used in the gores and were bonded on the outside of the specimen. A stem at one pole provided access to the specimen for inflation and for control and measurement of internal pressure. Thickness measurements made on the specimen indicated that the thickness of the Mylar lamina was 0.00049 inch and thickness of each aluminum face was 0.00019 inch as shown in figure 1(b).

The full-scale Echo A-12 sphere is folded for the launch phase and deployed by inflation after being injected into orbit. Depending on the magnitude of internal pressure used for deployment, the sphere

may have various imperfections in shape after deployment. There may be many small wrinkles caused by routine handling and distributed at random all over the surface. In addition, there may be a regular pattern of creases resulting from the folding. In order to simulate imperfections due to folding of the Echo A-12 sphere, the specimen was folded in a manner similar to that of the full-scale sphere. Finally, there may be some overall distortions due to inaccuracies in gore dimensions or slight mismatching of the splices. All these imperfections were present in the test specimen.

TEST PROCEDURE AND EQUIPMENT

The procedure followed in the experiments was to inflate the specimen to a small value of internal pressure, release the internal pressure, and then draw a slight vacuum in the specimen until buckling occurred. This procedure was then repeated for progressively higher values of initial internal pressure in order to shed some light on the possible influence of initial inflation pressure on the buckling strength of the sphere.

Testing such a flimsy specimen in a 1 g environment required considerable care. In order to counteract the effect of gravity and minimize localized support loads on the specimen, it was inflated with a mixture of air and helium. The specimen was mounted on scales which were counterweighted to balance the weight of the mounting fixture and inlet tubes. Then, the proportion of air and helium was adjusted until the weight of the specimen was balanced by the buoyancy of the inflating gas. Photographs of the specimens made during two of the tests are shown in figures 2 and 3. In each test, photographs were made at the differential pressure associated with initial inflation pressure (figs. 2(a) and 3(a)), at zero differential pressure (figs. 2(b) and 3(b)), and after buckling (figs. 2(c) and 3(c)). The series in figure 2 is for a test with a low initial inflation pressure, and the series in figure 3 is for a high initial inflation pressure. Thus, the pattern of imperfections due to folding is more pronounced in figure 2 than in figure 3.

Differential pressure between the inside and outside of the sphere was measured with two instruments - a micromanometer having a least count of 0.001 inch of water and a differential-pressure indicator having a least count of 0.0001 inch of water. The micromanometer was used to measure the maximum inflation pressure, but the more sensitive differential-pressure indicator was necessary to measure buckling pressures.

RESULTS AND DISCUSSION

Results of this investigation are summarized in table 1. The column under the heading Δp_0 gives the differential pressure to which the specimen was initially inflated. The column under the heading N_0 gives the stress resultant in the wall developed by this initial pressure. In the column headed "Folding imperfection depth" are listed estimates, where practical, of the peak-to-valley distance of the imperfections due to folding after the initial inflation pressure was released. In the next column is listed the excess buoyant force on the specimen which in all cases was less than 5 percent of the weight of the specimen. The columns headed "Buckling" give the pressure differential at buckling in inches of water, pounds per square inch, and finally as a ratio of measured buckling pressure differential to a theoretical buckling pressure differential calculated by classical linear theory. The theoretical buckling pressure differential for the laminated shell wall was taken as

$$\Delta p_{cl} = \left(\frac{2}{r}\right)^2 \sqrt{DK}$$

where the calculated values of D and K are those for a smooth, wrinkle-free wall.

Because of the difference in densities of the gas inside the specimen and of the surrounding atmosphere, the pressure differential between the inside and outside of the specimen varied with vertical location. At buckling, the largest pressure differential was at the bottom of the specimen. In addition, any excess buoyant force was balanced by a downward concentrated force at the stem. As a result of these factors, buckles invariably appeared first in the lower hemisphere. It was necessary to take into account the variation in differential pressure in evaluating the data. The data reported represent the differential pressure at approximately the height of the center of the buckles which appeared. Also, small corrections have been made, where significant, for the effects of differences in height of the stem and the micromanometer. The data from the final column in table 1 are plotted in figure 4 as a function of wall stress resultant due to initial inflation pressure. These buckling pressures represented in each case the maximum value of differential pressure on the specimen which could be attained under essentially static loading.

The primary effect of increasing N_0 is to reduce the magnitude of the initial imperfections due to random wrinkles and the regular folding pattern. The results in figure 4 show that large reductions in

these imperfections increase the buckling pressure significantly. The two points at the highest values of N_0 , however, show a decrease in buckling pressure. A simple calculation indicated that at the values of N_0 associated with these points, the aluminum face layers had very likely yielded significantly. Also, since at the splices the material is heavier than in the gores, the specimen tended to stretch more in the gores than at the splices. This permanent deformation in the gores apparently induced premature buckling.

The results shown in figure 4 suggest that further increases in N_0 would not result in large increases in buckling pressure even if the shell wall remained elastic. Thus, it would seem that effects other than the random wrinkles and the folding pattern imperfections must play a large role in causing buckling to occur below the classical value. Possible other effects are overall distortions due to seam misalignment and discrepancies in gore dimensions, nonuniform loading due to variation in differential pressure with height and due to any concentrated force at the stem, and nonuniform properties of the shell wall material.

CONCLUDING REMARKS

Buckling experiments on a complete spherical shell having a radius-thickness ratio of about 85,000 are discussed. Results are given for buckling under external pressure after the sphere was pressurized to progressively higher values of initial internal pressure. Although the specimen was very flimsy, it was found that well-defined and consistent buckling loads could be obtained by inflating the sphere with the proper mixture of air and helium to counteract the effects of the 1 g environment and to minimize support loads. Local folding and handling imperfections influenced the buckling pressures but apparently could account for only a small part of the deviation from classical theory.

TABLE 1.- BUCKLING DATA FOR 12.5-FOOT-DIAMETER SPHERICAL SHELL
FABRICATED OF THREE-LAYER ALUMINUM-MYLAR-ALUMINUM LAMINATE

Test	Δp_o , in. H ₂ O	N_o , lb/in.	Folding imperfection depth, in.	Excess buoyant force, lb	Buckling		
					Δp , in. H ₂ O	Δp , psi	$\frac{\Delta p}{\Delta p_{cl}}$
1	-0.019	0.026	1	0.10	0.0035	1.26×10^{-4}	0.122
2	-.049	.066	1/2	.05	.0035	1.26	.122
3	-.074	.10	1/4	.10	.0037	1.34	.129
4	-.10	.14	---	.20	.0037	1.34	.129
5	-.20	.27	---	.10	.0040	1.45	.140
6	-.30	.41	---	.15	.0044	1.59	.154
7	-.40	.54	---	.10	.0045	1.63	.157
8	-.50	.68	---	.10	.0045	1.63	.157
9	-.75	1.0	---	.05	.0050	1.81	.175
10	-1.0	1.4	---	.10	.0052	1.88	.182
11	-1.5	2.0	---	.10	.0045	1.66	.157
12	-2.0	2.7	---	.10	.0047	1.70	.164

SPHERICAL SHELL SPECIMEN

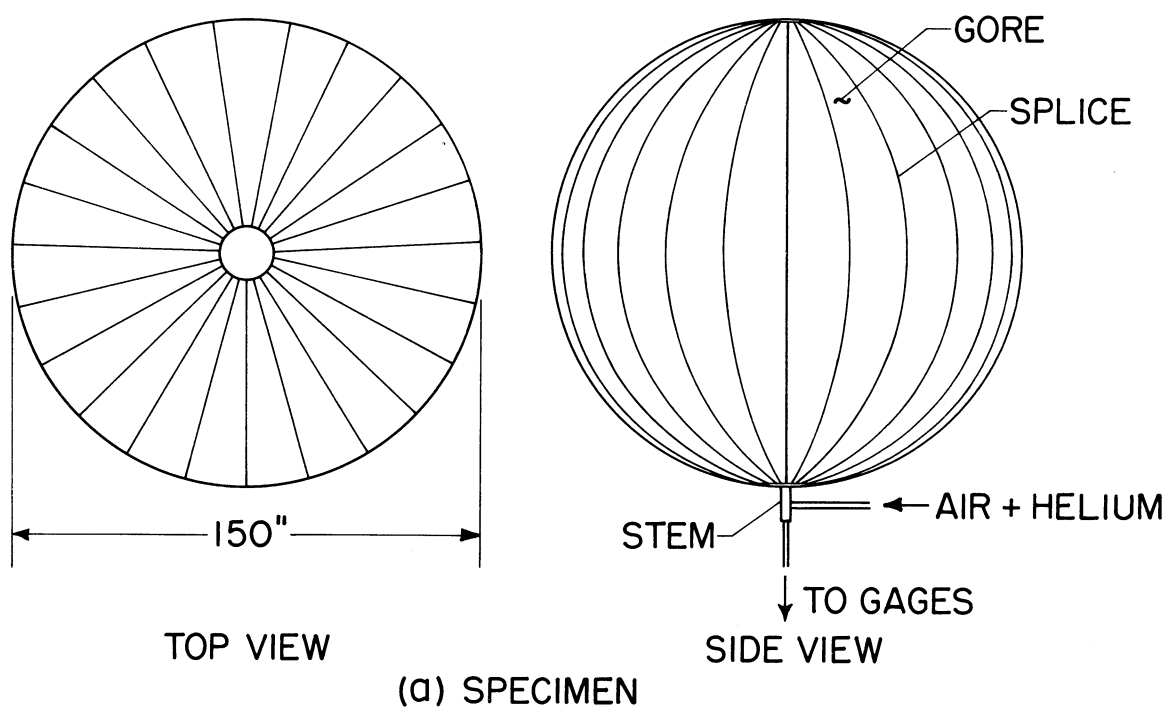
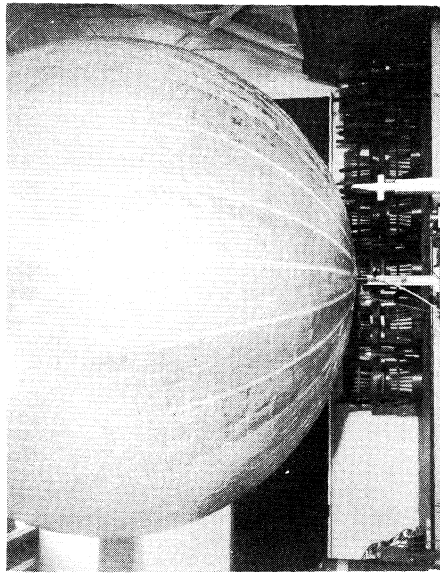
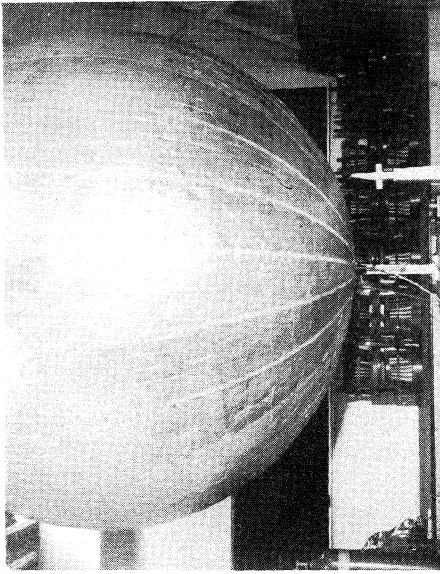


Figure 1

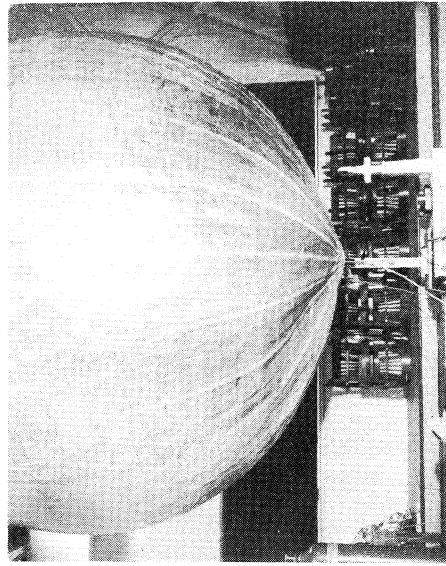
SPHERICAL SHELL SPECIMEN AT VARIOUS VALUES OF DIFFERENTIAL PRESSURE DURING TEST NO. 2



(a) $\Delta p_0 = -0.049$ IN. H₂O



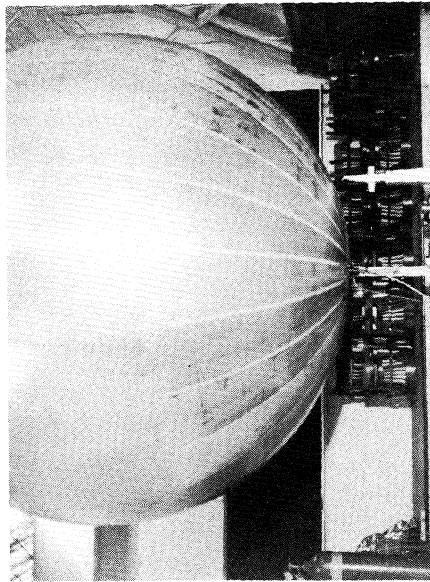
(b) $\Delta p = 0$



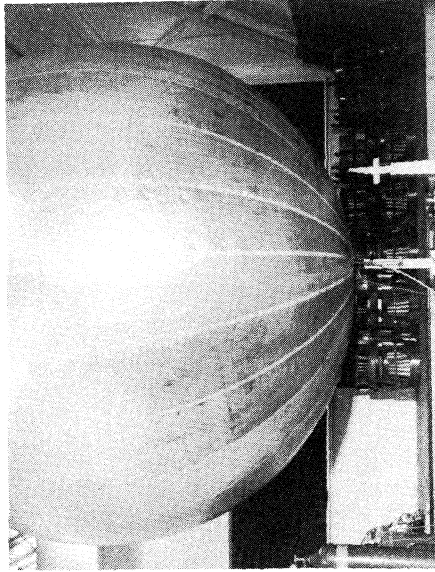
(c) AFTER BUCKLING
(AT BUCKLING $\Delta p = 0.0035$ IN. H₂O)

Figure 2

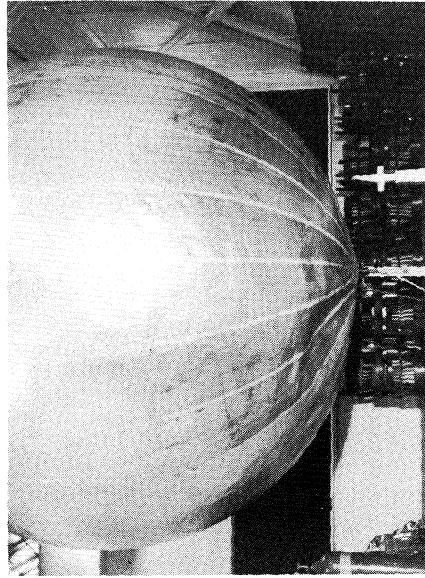
SPHERICAL SHELL SPECIMEN AT VARIOUS VALUES
OF DIFFERENTIAL PRESSURE DURING TEST NO. 9



(a) $\Delta p_0 = -0.75$ IN. H_2O



(b) $\Delta p = 0$



(c) AFTER BUCKLING
(AT BUCKLING $\Delta p = 0.0050$ IN. H_2O)

BUCKLING PRESSURES FOR 12.5-FOOT-DIAMETER SPHERICAL SHELL
FABRICATED OF THREE-LAYER ALUMINUM-MYLAR-ALUMINUM LAMINATE
RADIUS-THICKNESS RATIO $\approx 85,000$

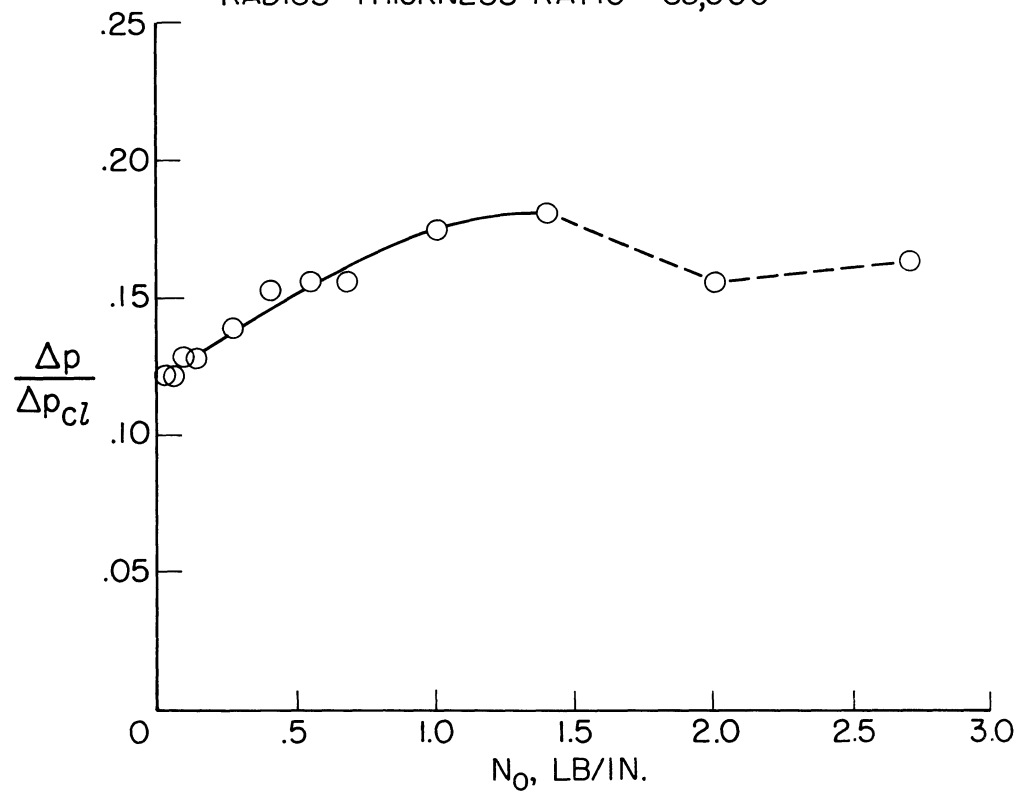


Figure 4

DEFORMATIONS AND STABILITY OF SPHERICAL SHELLS SUBJECTED TO
THE ACTION OF ASYMMETRICAL LOADINGS - EXPERIMENTAL STUDY¹

by R. M. Evan-Iwanowski²

Syracuse University Research Institute

SUMMARY

This paper presents the results of an experimental investigation of the deformations and stability of spherical shallow shells subjected to asymmetrical loadings consisting of normal concentrated eccentric loads; and of normal concentrated eccentric loads superimposed upon uniform pressure in varying magnitude and order.

New phenomena are observed for simply supported and free edge conditions under concentrated loading. There exist three ranges of position of an eccentric load between the apex of a shell and its edge along the meridional lines within which a distinct behavior of a shell is manifested. The first limiting range is the apex itself, point D_0 in figure 1. The resultant type of buckling has been discussed in reference 3. Loading in the range D_0D_1 results in a single mode buckling. Loading in the range D_1D_2 results in two mode buckling; the first mode is apparently related to the discontinuity of the radius of curvature and the thickness at the boundary, and may be considered to be "local buckling."³ Loading in the third range D_2D_3 results again in single mode buckling. When the concentrated loads are applied in the range $D_3D_4 = D_3D_e$ no buckling takes place. The lengths of the ranges, or what is the same, the values of the eccentricities, e , depend upon shell geometry and material constants. The end points of two of these ranges, i.e. points D_1 and D_2 are well defined and reproducible. Point D_3 is not as well defined. However, all three points are clearly transitional points from one type of buckling to another.

¹Research Program sponsored by AROD (Durham)

²Professor, Syracuse University, Mechanical Engineering Department

³The phenomenon of local buckling induced by a system of loadings such as ring loads and two-point loads is being investigated by the author. The results will be published elsewhere.

It has been observed in references 3 and 5 that shells with clamped edges subjected to concentrated loads do not buckle. When, however, concentrated loads are superimposed on uniform pressure buckling may occur depending on the amount of pressure and geometry of the shell. The critical asymmetrical concentrated loads are higher than the symmetrical loads for the same magnitudes of pressure. Moreover, uniform critical pressures are higher when applied after asymmetrical concentrated loads have been applied, than they are after symmetrical concentrated loads. This circumstance is somewhat puzzling in view of a common belief that asymmetrical buckling modes are responsible for lower experimental buckling pressures when compared with theoretical calculations for the symmetrical case. Perhaps, the relative positions of imperfections and boundary discontinuities have to be considered in order to account for low experimental critical pressures.⁴

Membrane and bending stresses are presented for one eccentricity.

INTRODUCTION

Previous theoretical and experimental investigations on deformations and stability of spherical shells were conducted exclusively for loadings symmetrical about the apex, such as uniform pressure, normal concentrated loads at the apex, and ring loads. A bibliography on this subject may be found in reference 3.

Asymmetrical loadings are of considerable interest, however, for several reasons. Firstly, such loads are most probable under actual service conditions, and thus the obtained results may serve as a guide to design criteria for such situations. Secondly, eccentric concentrated loads form "imperfections" for the superimposed uniform pressure. This situation provides, to some degree, controlled imperfections and permits the assessment of their qualitative and quantitative influence on the deformation and stability of shells. Thirdly, asymmetrical loadings are necessarily connected with asymmetrical deformations. Thus, the effects of initial asymmetrical deformations must be reflected in the history of deformations and in the critical values of the loads when combined with the application of uniform pressure.

Since the edge support conditions for shallow spherical shells play a considerable role in their stability, various boundary supports have been used, such as clamped, simply supported, and free edge conditions.

⁴This subject is discussed more fully in reference 6.

Two types of concentrated loads were used: constant displacement and constant load (dead weight).

EXPERIMENTAL PROGRAM

An experimental program was carried out on a series of plastic and metallic shells. Metallic shells, supplied by the Oak Ridge National Laboratory, were made by the hydroform process. Plastic shells which could be fabricated in the laboratory were die-pressed.

The selected plastic was rigid vinyl polyethylene. This material was found to have consistent Young's modulus in tension. In addition, the moduli in tension and bending were found to be nearly equal. Poisson's ratio also was found to have consistent values. As a result of the high ratio of yield stress to Young's modulus, an extensive range of elastic behavior in the pre- and post-buckling regimes could be studied. Due to the nature of the plastic, precautions were taken to correct the material constants to actual temperature recorded during the tests.

In this phase of the investigation uniform air pressure,⁵ constant displacement and constant load (or dead weight) type loadings were used. Vertical deformations of shells around the load point at various stages of the loading were measured by means of a specially designed fixture. For clamped edge conditions, contoured rigs were used. Care was exercised to machine the profiles of the clamping rigs so that they would match the curvatures of the shells, and thus avoid any extraneous bending at the boundary.

The following experiments were conducted:

- (a) simply supported shells subjected to eccentric constant displacement loads;
- (b) free supported shells subjected to eccentric constant displacement loads;
- (c) clamped shells subjected to uniform pressure and eccentric constant displacement concentrated loads;
- (d) clamped shells subjected to uniform pressure and eccentric dead weight concentrated loads;
- (e) clamped shells subjected to eccentric dead weight concentrated loads and uniform pressure.

⁵This is in effect a dead weight type of loading, as contrasted with a constant displacement type of loading which would be afforded by the use of an incompressible fluid.

RESULTS AND DISCUSSION

Pertinent parameters used in the presentation of the experimental results are: $\lambda^4 = a^4 \{12(1-\nu^2)/(Rh)^2\}$, where a is the base radius, R the radius and h the thickness of the shell; H/a , where H is the rise of a shell; $e = d/a$, eccentricity of the load, where d is the distance from the apex; δ the deflection of a shell at the load point (see also figure 1). The observed critical values are designated by an asterisk. Other notations are standard. The deformation curves or the plots of load parameter versus deformation parameter are noted (P, δ) .

Figure 2 indicates the influence of the eccentricity e , of the constant displacement load on the behavior and critical loads for the simply supported shell. The behavior of the shell in different ranges is seen from this figure. It was observed in reference 3 that for the loads at the apex, or for the loads slightly off the apex there is only one mode of buckling. Point D_1 , figure 1, or the point where the first two-mode buckling occurs, corresponds to the eccentricity $e = 0.192$. The values of the eccentricities $e = 0.315$ and $e = .385$ are the values about the point D_2 , since for $e = 0.315$ two-mode buckling is still observed, and for $e = 0.385$ only single-mode buckling takes place. The eccentricity $e = 0.402$ corresponds to a point between the points D_2 and D_3 . The point D_3 is somewhat difficult to establish exactly in the elastic range. As to the critical loads two interesting observations are made. First, the critical loads corresponding to $e = 0.192$ and $e = 0.402$ are identical; moreover, both critical loads in two-mode buckling ($e = 0.192$) are also identical. In other words, the same critical loads can be obtained through different deformation paths. Second, the lowest of all critical loads is the "local critical load" corresponding to $e = 0.315$. In the "local buckling" for $e = 0.192$, there is a substantial reduction of the load, characterized by a jump, or escape deformation.

A very similar situation is observed for the shells with free edge conditions, figure 3, except that the subsequent buckling loads are higher than "local buckling loads."

Another interesting conclusion may be derived from figure 4, which represents effects of thickness on the behavior of shallow spherical shells. All geometry, material, and loading conditions were kept the same, and only the thickness h was varied. It is seen, that a shell with $h = 0.015$ has markedly different behavior from the other two

shells. In general, the following effects can be attributed to the variation in thickness.

From reference 3 it was found that the thinner the shell the smaller was the radius of the symmetrical deformation. From figures 2 and 3 it may be seen that the thinner the shell the larger the range $D_2 D_3$.

It must be emphasized that the limiting points of various ranges ($D_i D_j$) are well defined (with some exception in the range $D_3 D_4$) and have good consistency and reproducibility. The ranges apparently constitute a set of parameters, which is equivalent to the set of geometrical and material parameters. To put it another way, given $D_i D_j$ one may infer the values of λ , h , E or ν of a given shell.

The history of the deformations at various stages of the loading (or what is the same, for various δ), or so-called profile curves, are shown in figures 5 and 6. The deformations were measured along the meridional line passing through the apex and the load-point, and the curve perpendicular to it. It seems that the effects on the deformation imposed by the localization of the loads is felt in the early stages of the loading, but the effects of initial imperfections, if any, are soon erased.

Another series of tests were conducted on clamped shells with asymmetrical concentrated loads superimposed on uniform pressures. The critical values of these asymmetrical dead-weight type concentrated loads superimposed on uniform pressures are shown in figure 7. Corresponding plots (not shown) were made for uniform pressures superimposed on the concentrated loads. It was noted that critical combinations of dead-weight and pressures were independent of the order in which these loadings were applied. Also, the concentrated loads for any given critical load combination represented in figure 7, increase with increasing eccentricity for the same λ . But, what is more interesting, all of these values are considerably higher than the values obtained for the symmetrical loadings, viz., for the concentrated loads at the apex superimposed on uniform pressure, cf. reference 4. These results seem to be surprising in one respect. The asymmetrically applied concentrated loads cause asymmetrical deformations, figures 5 and 6, and yet the critical combinations of dead weight and uniform pressure are higher than for the symmetrical case, viz., when concentrated load is applied at the apex. This is somewhat disturbing in view of the commonly accepted notion that the asymmetrical deformations are responsible for the fact that the experimental critical pressures are lower than predicted by theory, cf. reference 2 or 3.

The experimental observations made on clamped shells subjected to

uniform pressure and then asymmetrical constant displacement concentrated loads are shown in figures 8-11, and the critical loads plotted in figure 12.

It may be seen that the greater the eccentricity, e , the higher are the critical concentrated loads for the same pressure, p , and the geometry parameter λ . The general shape of the deformation curves, (P, δ) remains, however, unchanged. As expected, the cut-off value of λ (i.e., the value above which no buckling occurs) depends upon the magnitude of applied pressure.

Figure 12 gives critical combinations of uniform pressures and constant displacement concentrated loads. Comparison with figure 7 shows that here, as in the symmetrical case, reference 4, critical displacement concentrated loads are higher than dead weight for the same values of e , P and λ .

Bending and membrane stresses measured by strain gages are given in figures 13-16 for an aluminum shell with an eccentric loading at $e = \frac{1}{8}$.

CONCLUDING REMARKS

The material presented in this paper constitutes part of the data obtained in the course of the current research program, and only a portion of the complete spectrum of the problem of stability of spherical shells under asymmetrical loading. Such areas as those pertaining to deep shells, effects of the reversed application of uniform pressure and constant displacement concentrated loads; and, certainly, analytical work are still open. A broad program to cover such areas has been developed by the author and his associates, and work is currently proceeding.

The phenomenon of two-mode buckling, and associated with it "local buckling" may shed some light on the mechanism of buckling, but, perhaps more directly may be utilized for programming and distribution of reinforcing elements such as ribs and rings. For instance, figure 1 tells us that if a shell is reinforced around the region corresponding to $e = 0.125$, "local buckling" may be avoided even when a shell is loaded in this region by normal concentrated loads.

The question of how or whether at all the phenomena observed for the concentrated loads are related to other types of loading is also unanswered. But, at least, we become aware of the very whimsical

behavior of spherical shells when certain asymmetries are introduced, and the problem must be treated with great care.

REFERENCES

1. Biezeno, C. B.: Über die Bestimmung der Durchschlagkraft einer schwachgekrümmten, Kreisförmigen Platte. ZAMM., Vol. 15, 1935, pp. 10-22.
2. Kaplan, A., and Fung, Y. C.: A Nonlinear Theory of Bending and Buckling of Thin Elastic Shallow Spherical Shells. NACA TN 3212, 1954.
3. Evan-Iwanowski, R. M., Cheng, H. S., and Loo, T. C.: Deformations and Stability of Spherical Shells under Action of Concentrated Loads. SURI. TR 834-2, 1961.
4. Evan-Iwanowski, R. M., and Loo, T. C.: Deformations and Stability of Spherical Shells under Action of Concentrated Loads and Uniform Pressure. SURI. TR 834-4, 1962.
5. Evan-Iwanowski, R. M., Cheng, H. S., and Loo, T. C.: Experimental Investigations on Deformations and Stability of Spherical Shells Subjected to Concentrated Loads at the Apex. To be published at the Proceedings of the Fourth U. S. National Congress of Applied Mechanics, Berkley, California, June 18-21, 1962.
6. Evan-Iwanowski, R. M., and Loo, T. C.: Local Buckling of Shells, Experimental Study. To be published.
7. Loo, T. C., and Evan-Iwanowski, R. M.: Deformations and Collapse of Spherical Domes. To be presented at the World Conference on Shell Structures, San Francisco, California, October 1-4, 1962.

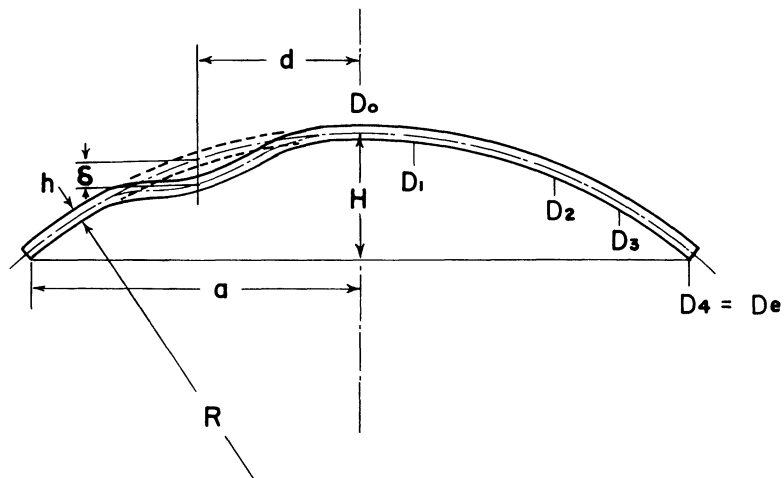


Figure 1.- Shell geometry.

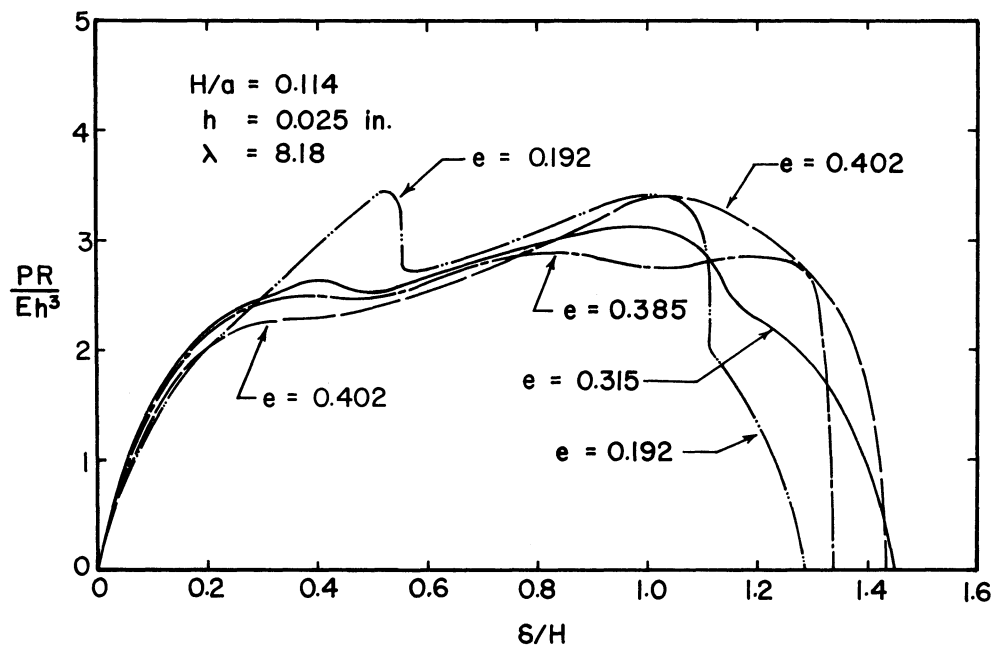


Figure 2.- Load-deflection curves for simply supported spherical shells under constant displacement concentrated loadings with varying eccentricity.

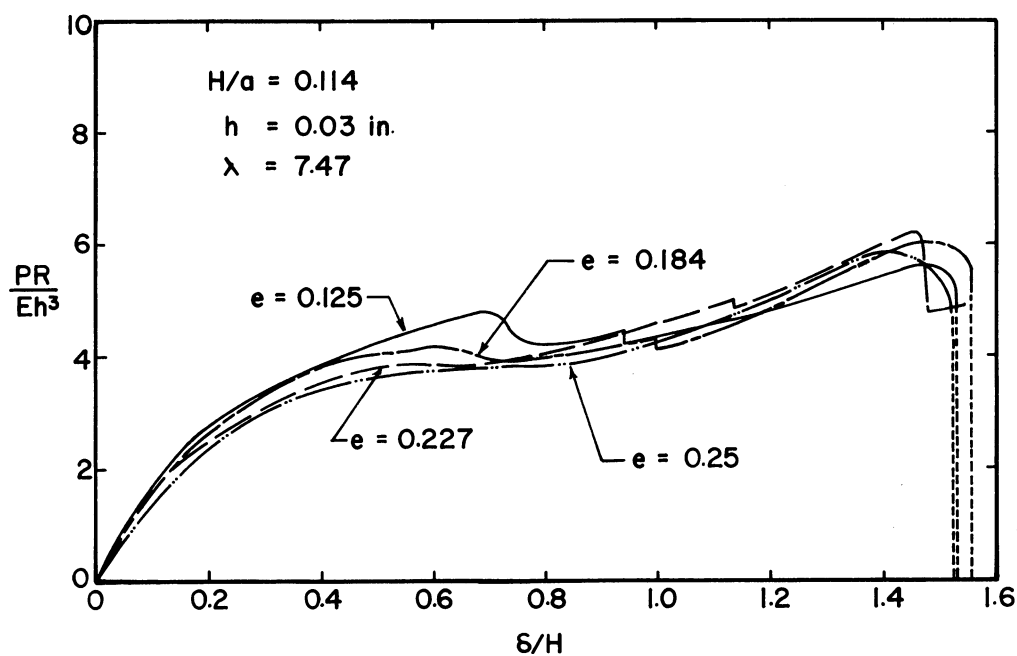


Figure 3.- Load-deflection curves for free edge spherical shells under constant displacement concentrated loadings with varying eccentricity.

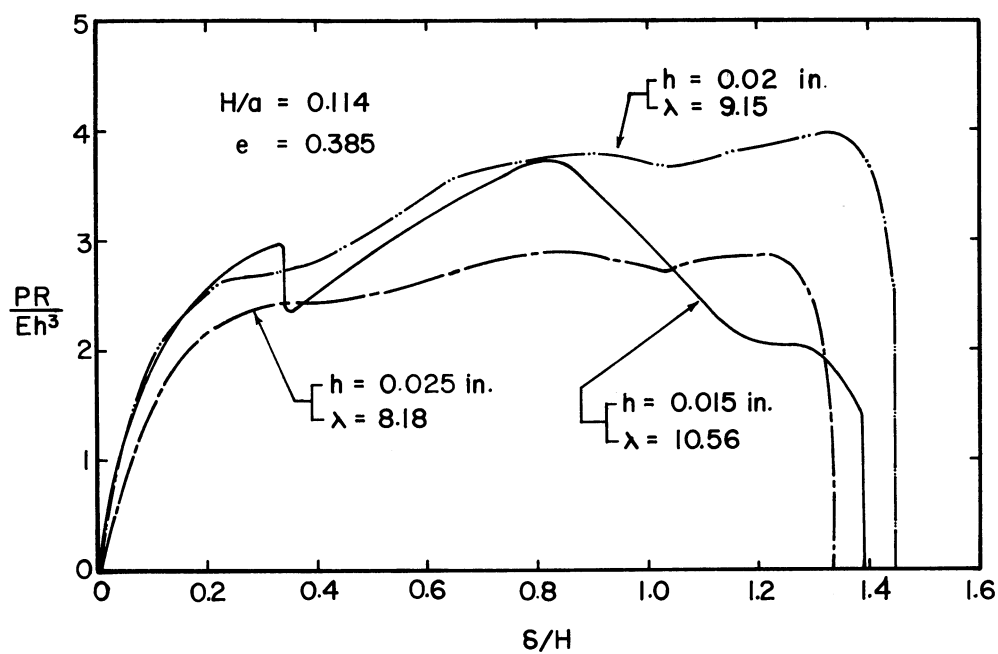


Figure 4.- Load-deflection curves for simple supported spherical shells of varying thickness under constant displacement concentrated loadings with fixed eccentricity.

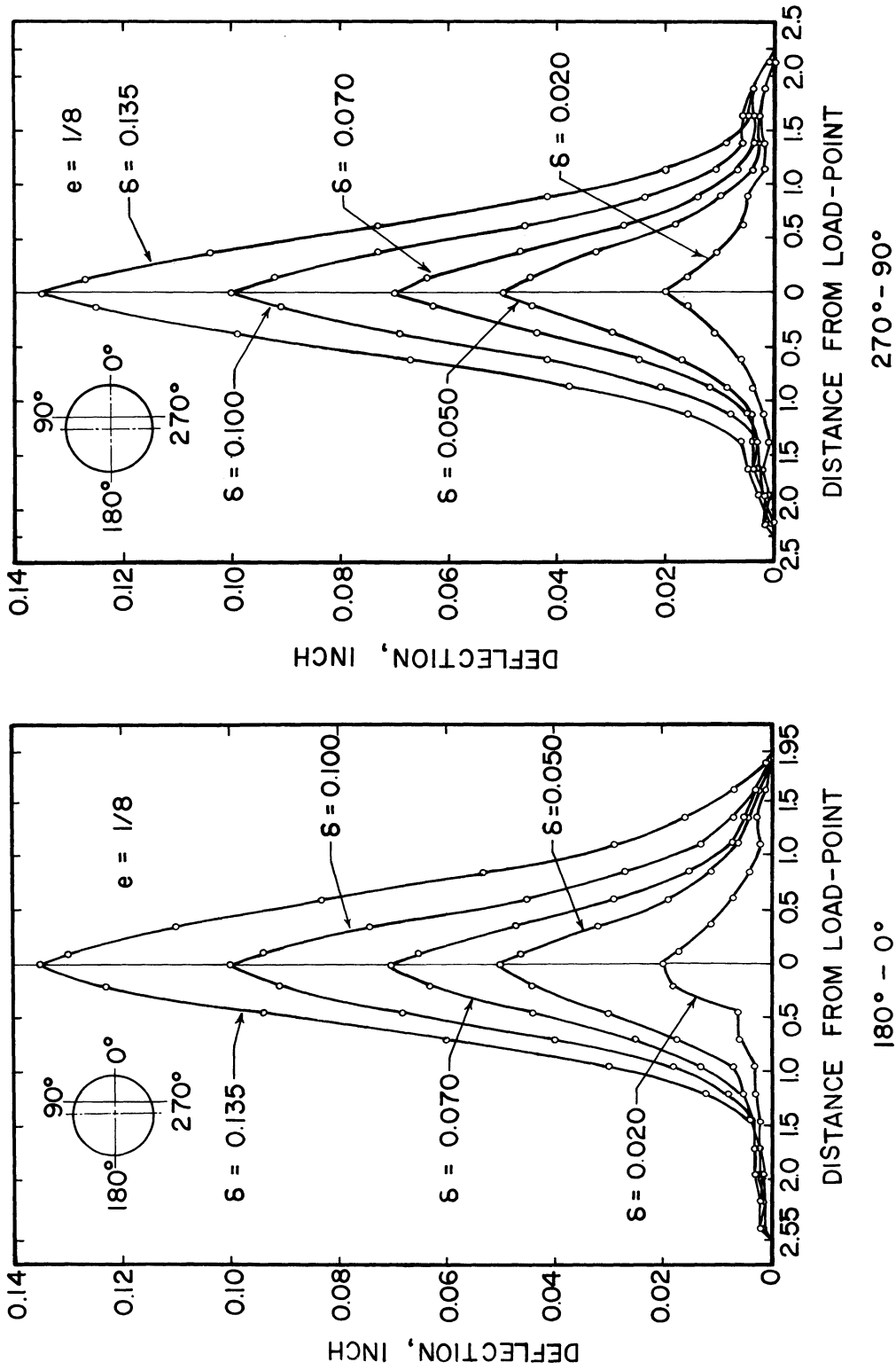


Figure 5.- Deflection profile curves for simply supported spherical shells under constant displacement concentrated loading with 1/8 eccentricity: 180°-0° meridian.

Figure 6.- Deflection profile curves for simply supported spherical shells under constant displacement concentrated loading with 1/8 eccentricity: 270°-90°, $e = 1/8$ displacement.

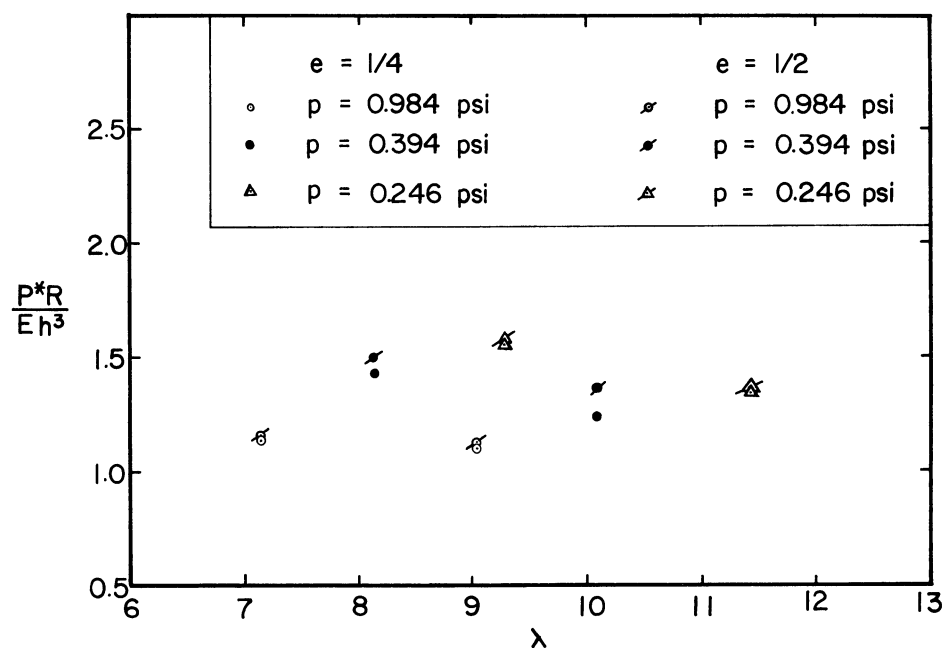


Figure 7.- Critical loads on clamped spherical shells with three uniform pressures superimposed on concentrated dead weight loading, with $e = 1/4$ and $e = 1/2$.

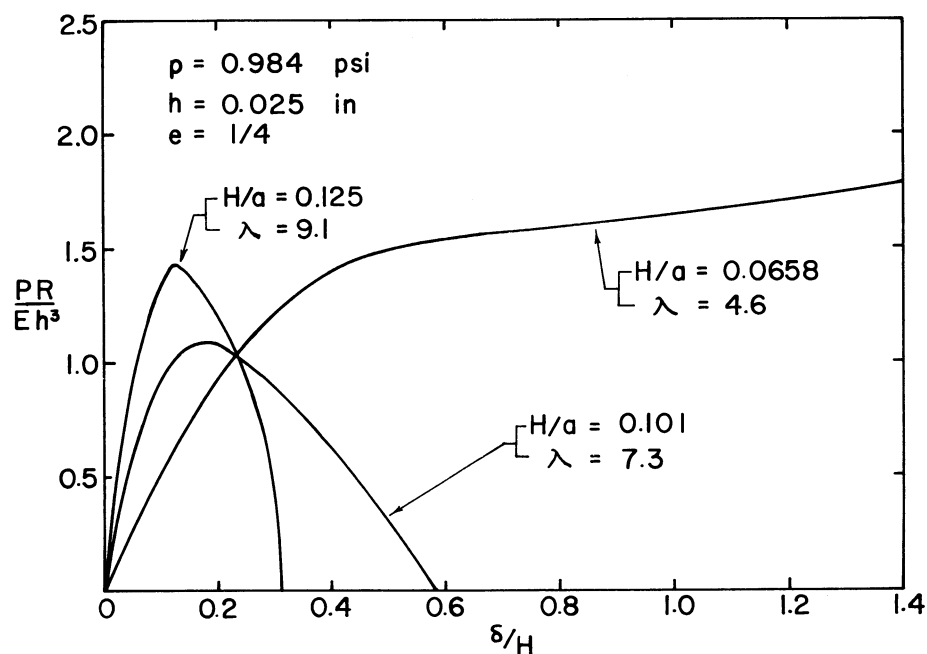


Figure 8.- Load deflection curves for clamped spherical shells with varying geometry parameter under constant displacement concentrated loading superimposed on uniform pressure: $p = 0.984$, $h = 0.025$, and $e = 1/4$.

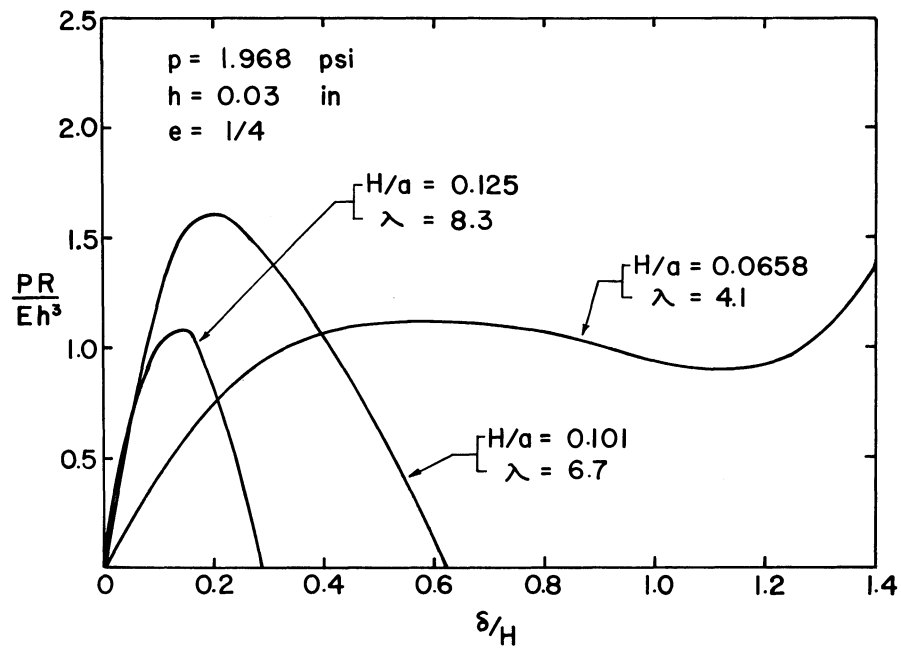


Figure 9.- Load deflection curves for clamped spherical shells with varying geometry parameter under constant displacement concentrated loading superimposed on uniform pressure: $p = 1.968$, $h = 0.03$, and $e = 1/4$.

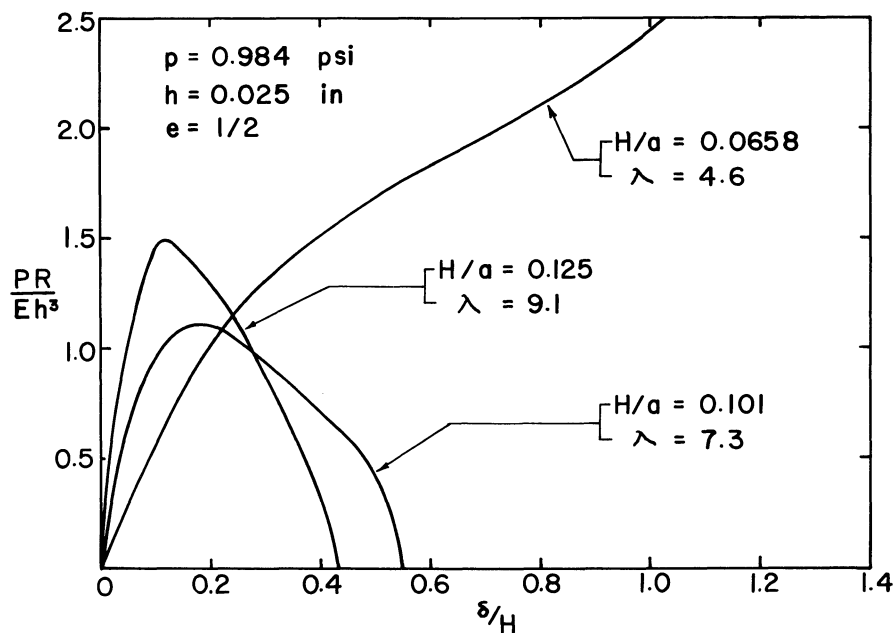


Figure 10.- Load deflection curves for clamped spherical shells with varying geometry parameter under constant displacement concentrated loading superimposed on uniform pressure: $p = 0.984$, $h = 0.025$, and $e = 1/2$.

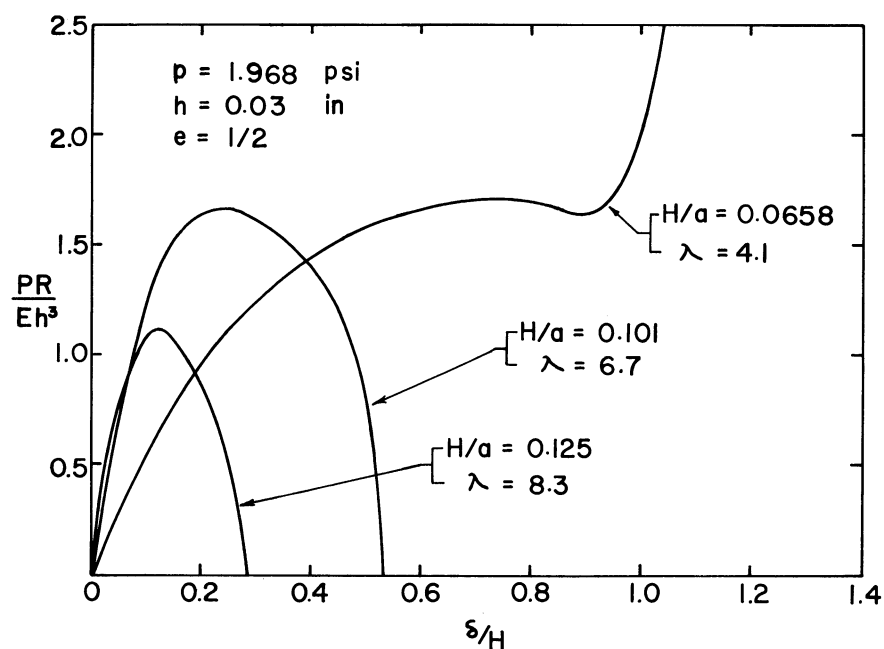


Figure 11.- Load deflection curves for clamped spherical shells with varying geometry parameter under constant displacement concentrated loading superimposed on uniform pressure: $p = 1.968$, $h = 0.03$, and $e = 1/2$.

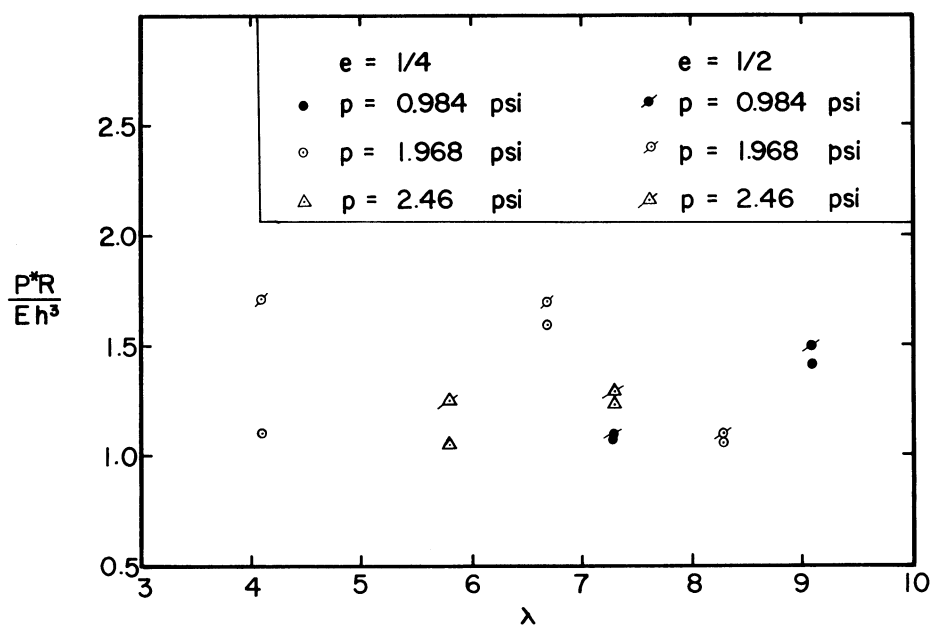


Figure 12.- Critical loads on clamped spherical shells with concentrated constant displacement loading with $e = 1/4$ and $e = 1/2$ superimposed on three uniform pressures.

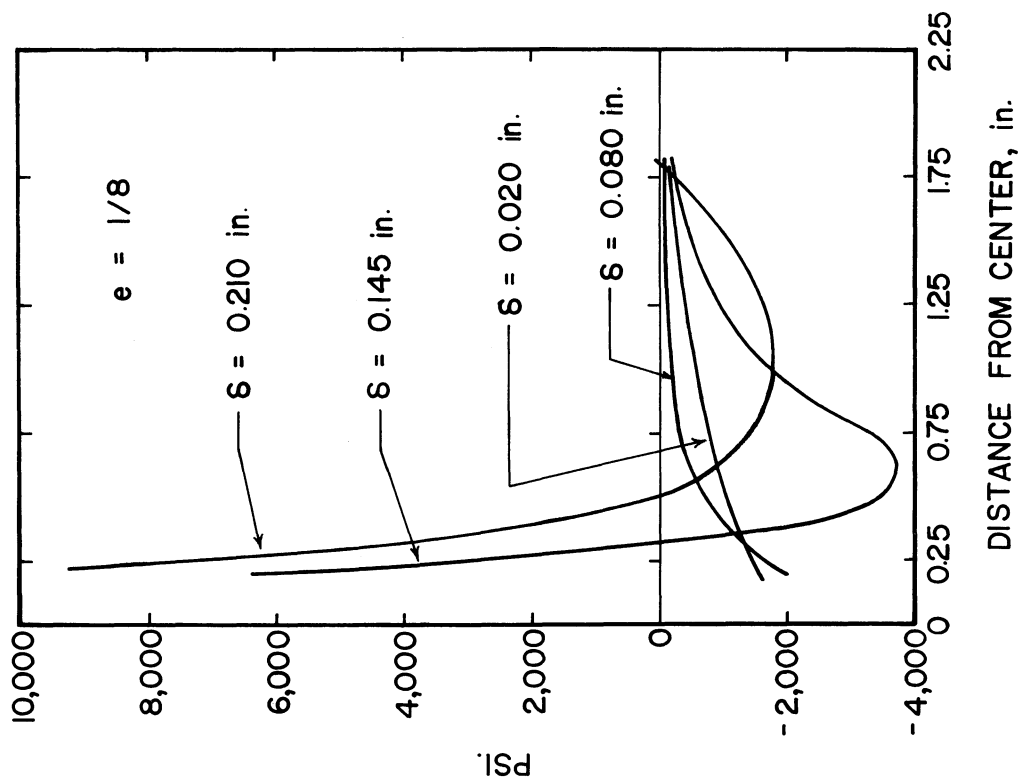


Figure 13.- Membrane meridional stress in a spherical shell with an eccentric constant displacement concentrated loading at $e = 1/8$.

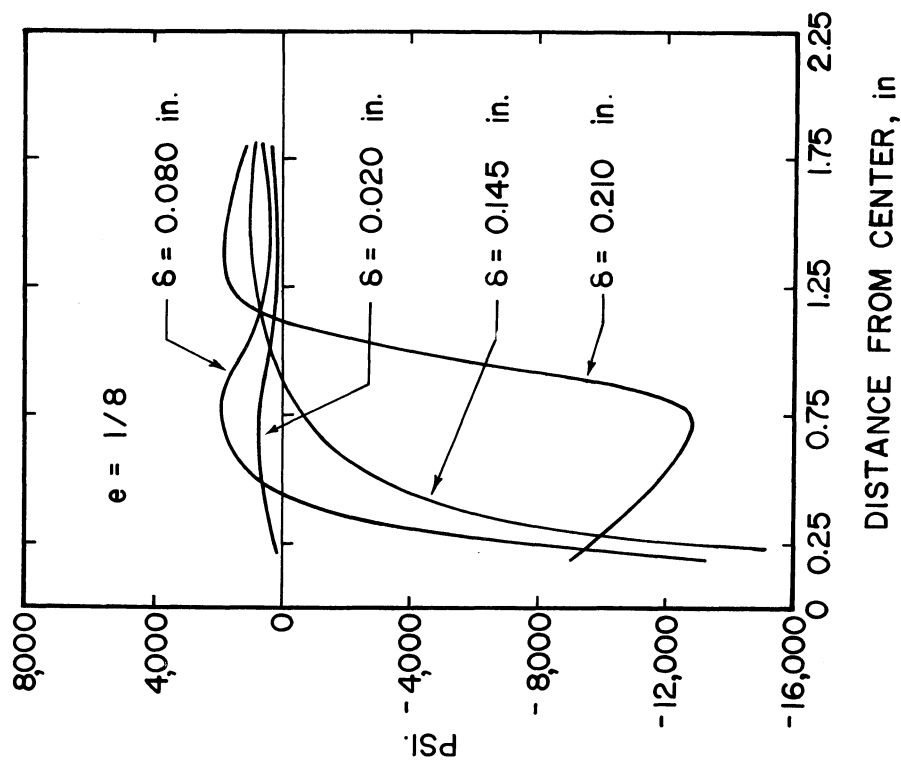


Figure 14.- Membrane circumferential stress in a spherical shell with an eccentric constant displacement concentrated loading at $e = 1/8$.

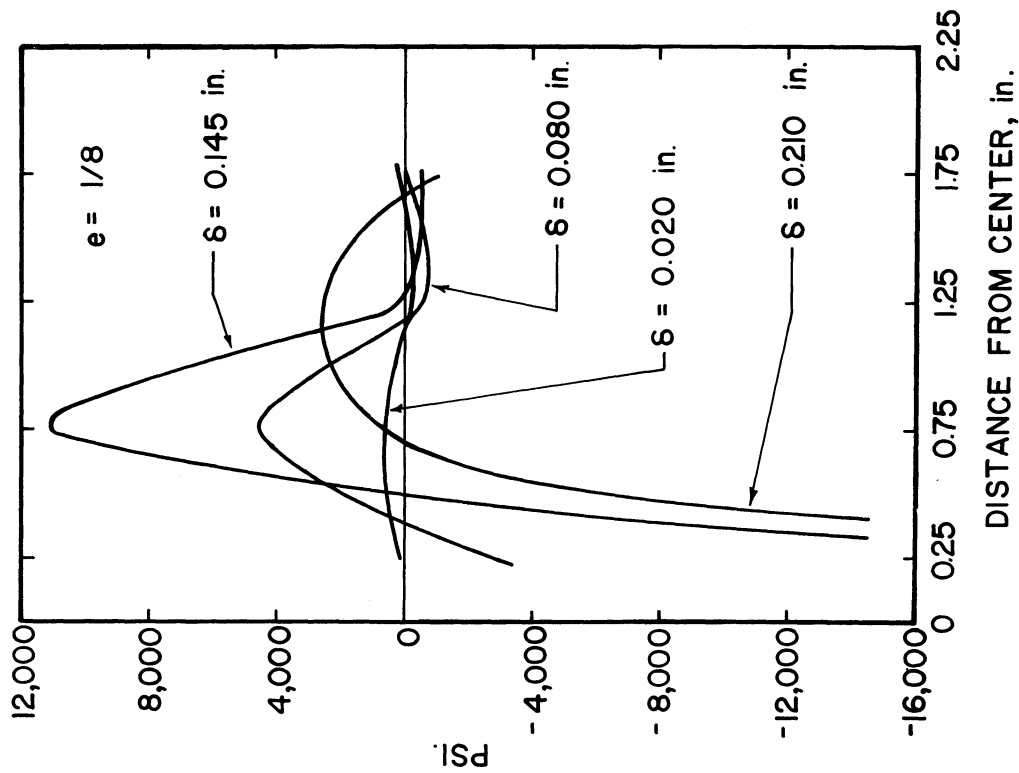


Figure 15.- Bending meridional stress in a spherical shell with an eccentric constant displacement concentrated loading at $e = 1/8$.

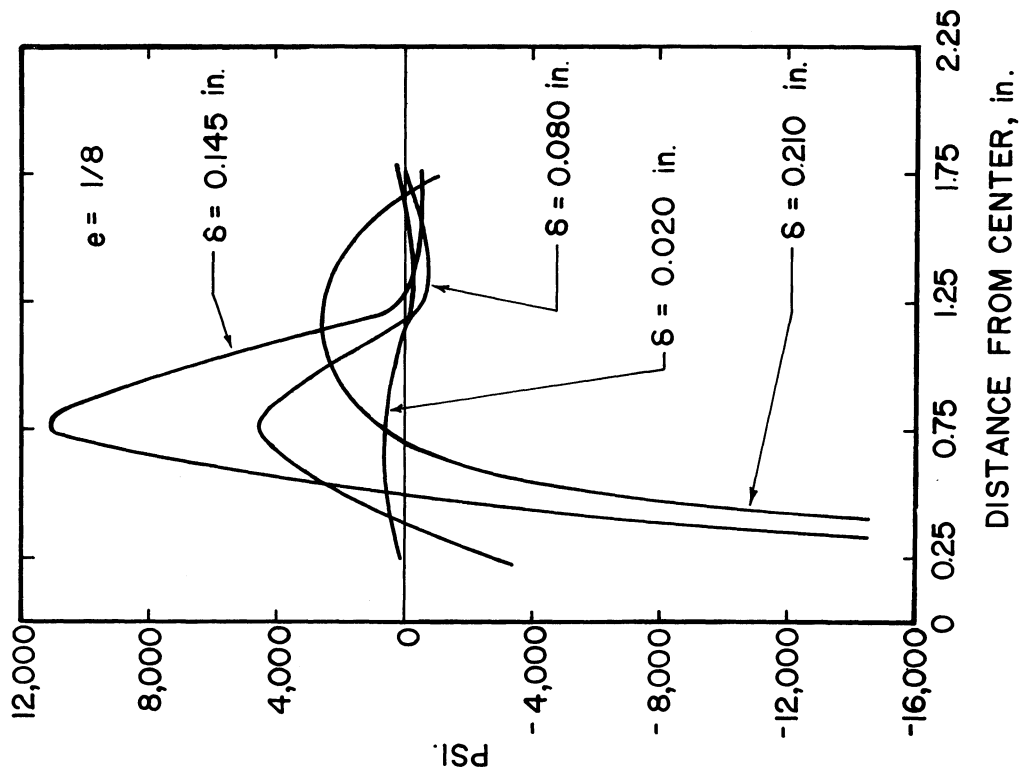


Figure 16.- Bending circumferential stress in a spherical shell with an eccentric constant displacement concentrated loading at $e = 1/8$.

EXPERIMENTAL OBSERVATIONS ON CREEP BUCKLING OF SPHERICAL SHELLS

by
K. N. Tong
Syracuse University

and
B. L. Greenstreet
Oak Ridge National Laboratory

SUMMARY

Creep buckling experiments were performed on hemispherical shells and spherical dishes of lead, copper, and aluminum to study the mechanism of failure. The results indicate that for thin shells under moderately high external pressure the failure mechanism is essentially that of static instability of a configuration that is arrived at through creep.

INTRODUCTION

In certain designs of nuclear power reactors, thin hemispherical shells are to be subjected to an external pressure at an elevated temperature. Because of creep it is certain that the shell will collapse after a certain period of time. It is not clear, however, what is the nature of the instability mechanism itself. Consider for the moment a hemisphere subjected to a uniform external pressure and supported at its equator in some manner. The stress distribution in the shell is predominantly that of a uniform membrane compression except at regions near the support and near some unavoidable imperfections in the shell. There the stress state deviates from being a uniform compression. This deviation in stress state causes a progressive deviation of the shell geometry from being a hemisphere through creep. The question now is when or how this process terminates into a failure.

The failure mechanisms usually associated with the creep buckling of columns and of thin-walled tubes subjected to external pressure are not applicable to shells of non-developable surfaces. With such shells the formation of a few "plastic hinges" having infinite strain rate is not by itself sufficient to cause collapse. Two possible mechanisms suggest themselves in the case of creep buckling of spherical shells. In the first mechanism it is conceived that, through creep, a small dimple having a negative curvature is eventually formed and enlarged with increasing rate. The kinematics of the phenomenon is similar to the turning over of a spherical membrane inside out through a process of continuous application. In the second, one visualizes that after the shape of the shell has been sufficiently altered by creep there is

a time when the configuration of the shell structure is no longer in a state of stable equilibrium in relation to the applied load and the process terminates abruptly by either elastic or plastic buckling.

The distinction between the two mechanisms described is, of course, only conceptual in nature. Any collapsing process can take place only in a finite amount of time. But, as a practical matter, a feasible analysis of the phenomenon will require certain simplifications, and the construction of an appropriate model demands a qualitative knowledge of what happens in reality. A number of experiments were thus performed to study the phenomenon of creep buckling of spherical shells. Although certain quantitative data were taken, the interest at first was mostly in the qualitative nature of the creep buckling process.

EXPERIMENTS

Test on Lead Shells

Because of the ease with which lead specimens can be formed and made to creep at room temperatures, a series of experiments were first performed using hemispheres and spherical dishes with nominal radius of 5.5 in. and nominal wall thickness of 0.500 in. The specimens were, however, not very accurately made and they were very susceptible to mishandling. Therefore no quantitative results will be given here and the following observations are offered instead.

(1) The buckling of hemispheres initiated from a small region. A dimple of about 2 in. diameter first appeared and was quickly followed by collapsing of the shell. Measurements of radial displacement of the shell surface in one experiment confirmed that the initiation of the instability is localized.

(2) Not until very late in the process was the location of the buckle predictable from a radial displacement survey which had a resolution of 0.001". Once the existence of a "flat spot" became discernible, a dimple formed shortly thereafter. In one experiment brittle lacquer coating was used. When the creep of the specimen became sufficiently fast, cracking of the coating began at a small annular region. It took about a minute for the shell to dimple. Figure 1 depicts roughly the rate of progress of the overall process.

(3) The buckled shapes of spherical dishes were always asymmetrical. The dimples in hemispherical shells were likely to be formed anywhere.

Test on Copper Dishes

A number of tests were performed on shallow copper spherical dishes of different geometries. Figure 2 shows the data from one of the test series. The specimens used in this series had the following geometry.

Radius of curvature	11.82 ± 0.30 in.
Thickness	0.032 ± 0.0005 in.
Base circle diameter	5.946 in.
Rise	0.38 in.
Half angle	14.6°

The rim of the dish was soldered to a copper plate with a circular recess which fits the base rim. A 95 - 5 tin-lead solder was used. The data for 200°F are perhaps not very significant. The delayed buckling might be entirely due to the relaxation of the edge constraint offered by the soldering. At 300°F, however, soldering will creep sufficiently fast so that the edge condition was probably very close to being simply supported.

The following observations may be made of this test.

- (1) There is a significant difference between the "instantaneous" buckling load and the load causing buckling in a few hours.
- (2) The shells failed by snap-through. The final buckling process was not exactly axisymmetrical.

Test on Copper Hemispherical Shells

Specimens and Test Procedure. - The specimens used in this series of experiments were manufactured by "Hydroforming" from commercially pure copper sheets. A steel sheet was used as an outer wrap in forming. The finished shell consisted of a 12.625 in. diameter hemisphere with a 1/2 in. cylindrical section attached to the equator. Material beyond the cylindrical section was machined off from the shell as formed. Trial tests using several arrangements of clamping along the equator invariably resulted in a failure initiated at the clamping. Subsequently, the following arrangement was used. A steel ring of 12.63" O. D. and 11.75" I. D. was machined out of 3/8" plate. It also contained a saw cut of about 1/16" width. This ring was then squeezed and inserted into the cylindrical portion of the specimen. The shell thus stiffened, was placed on a hardened steel plate and lapped until a metal-to-metal seal

was formed between the rim of the shell and the plate. The assembled test rig is shown in figure 3.

Spot check of the shells found that the variation in the wall thickness was within 0.001 in., the same variation in the starting sheet stock. The radius was within 0.005 in.

After the specimen was placed in the rig it was heated in the rig to 400°F for about 2 hours. Subsequently, the temperature was adjusted to the test temperature. By adjusting the currents in the different heaters, the temperature variation in the specimen could be limited to $\pm 1^\circ\text{F}$. The rig was then pressurized to the desired pressure. Time to failure, which automatically shut down the rig, was recorded by an hour meter.

Test Results. - The results of this test are given in figure 4. It is a log-log plot of pressure versus life. In spite of the scatter, there appeared to be a consistent tendency for the curves to level off at a certain pressure. The leveling off seems to be earlier with thicker shells. Note that, because of the logarithm scale used, the shapes of the curves would be the same if membrane stresses instead of pressures were used for the ordinates.

Data on failures taking place within a few hours after loading were not included here. There was a considerable amount of scatter in this group of data. Two reasons may be offered for this scatter. The buckling pressure of thin hemispheres was known to be extremely sensitive to geometrical imperfections. Any defect due to chance mishandling in the entire process from making the shell to placing it in the rig was likely to cause a significant though varied amount of loss in life. In other words, by disregarding data from short time failures, most of the defective specimens were removed from the population under test. The second reason is that previous tests with spherical dishes have indicated that the buckling failure at 300°F was quite sensitive to loading rate. With the test setup used, this loading rate cannot be easily controlled.

The buckled shells had varied shapes. Some were nearly axisymmetrical as shown in figure 5a. Others were definitely not symmetrical as those in figure 5b. The great majority of shells failed in a way similar to one of these shells. A few odd failures are shown in figure 5c. No correlation was discernible between the mode of failure and the life.

Tests on Aluminum Shells

This series of tests have not yet been completed. As a comparison, partial results are presented in figure 6. The tests were carried out

in the same manner as those on copper shells.

CONCLUSION AND DISCUSSION

The experiments performed showed that, within the ranges of parameters used, the creep buckling of hemispherical shells is essentially a process of creep followed by buckling. Furthermore, the buckling process is initiated from a rather localized region provided that the edge condition does not produce unduly high localized stresses. The following remarks are offered in support of these contentions.

(1) The varied shapes of buckled shells showed that buckling originates from some imperfections. A few tests were also made in which an inner support was placed inside the hemispherical specimen so that when it buckled only a small dimple could form without inducing a complete collapse of the shell. The shell surface away from the dimple showed no grossly measurable deviation from being spherical.

(2) The collapsing of the shell was usually very violent. It was always accompanied by an audible bang and a quick release of pressure.

(3) A few shell specimens contained barely measurable flat spots caused perhaps by mishandling. The buckling pressures of these shells were found to be drastically lower. Similar flat spots could very well be produced by creep deformation.

(4) The data from spherical copper caps at 300°F shown in figure 2 fitted in well with those from copper hemispheres of nearly equal wall-thickness-to-radius ratio. This indicates that the buckling of hemispheres was a local phenomenon.

In view of the experimental evidence obtained, it is suggested that an analytical treatment of the phenomenon may well utilize the following simplified model. First, assume a complete spherical shell with two identical axisymmetric flat spots located diametrically opposite to each other. These flat spots consist of regions where the curvature is only slightly different from the rest of the sphere. Using membrane stress distribution and an appropriate creep law, one may analyze the change in the geometry of the shell with time by a stepwise integration procedure. To terminate the process, one must determine when the current shape is no longer in stable equilibrium with the applied load. This analysis will require the finding of buckling pressure for a nearly spherical shell of arbitrary shape taking into account bending stress and perhaps finite deformation. Knowledge on this problem is currently still lacking, but is being added daily by various workers. The fact that, until buckling takes place, the shell is essentially spherical allows the ignoring of bending stress in creep analysis

and thus simplifies the picture. The main difficulty now is the solution of elastic or plastic buckling problems.

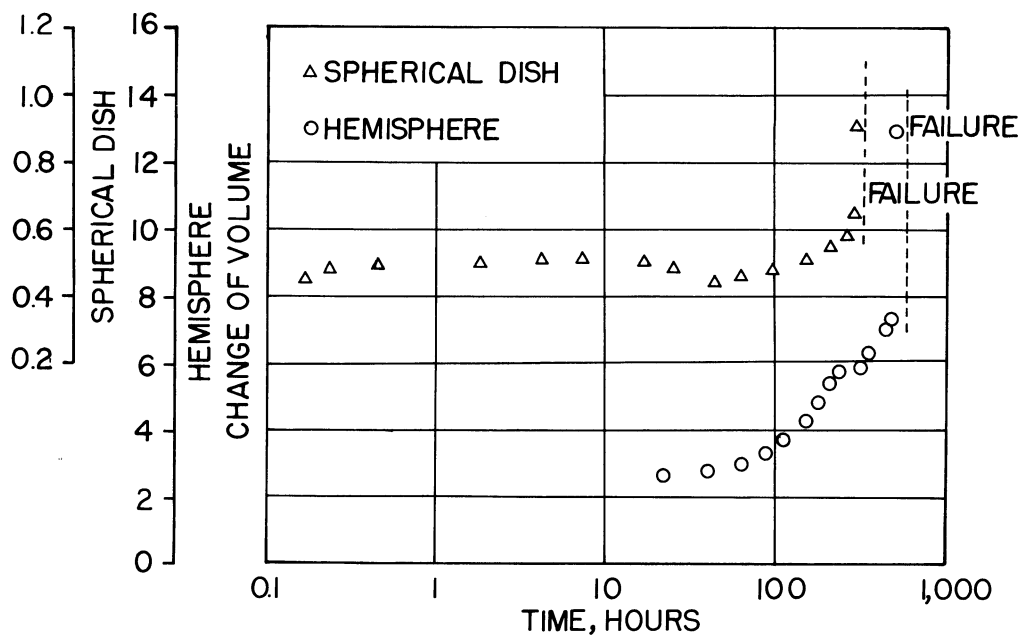


Figure 1.- Change of internal volume with time of lead shells under creep.

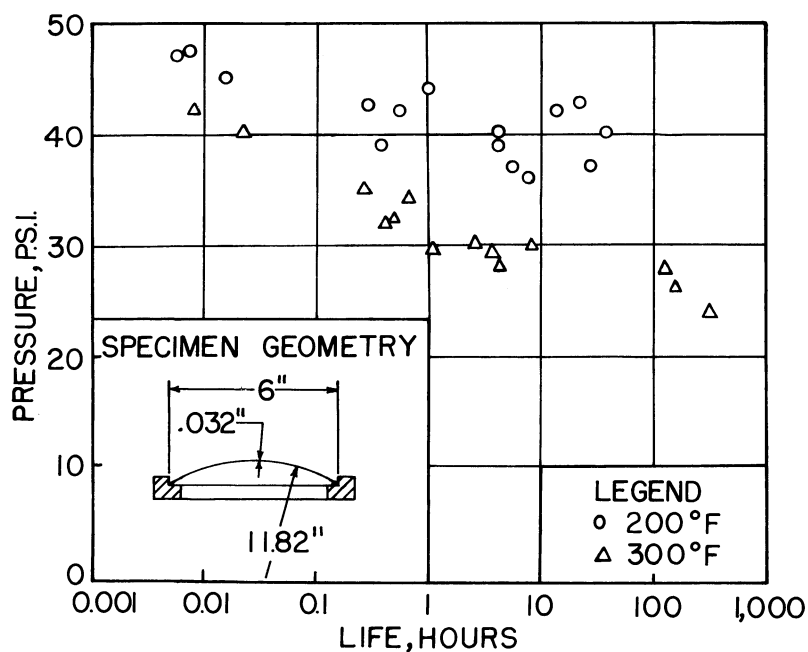


Figure 2.- Pressure versus creep life of a copper spherical cap under external pressure.

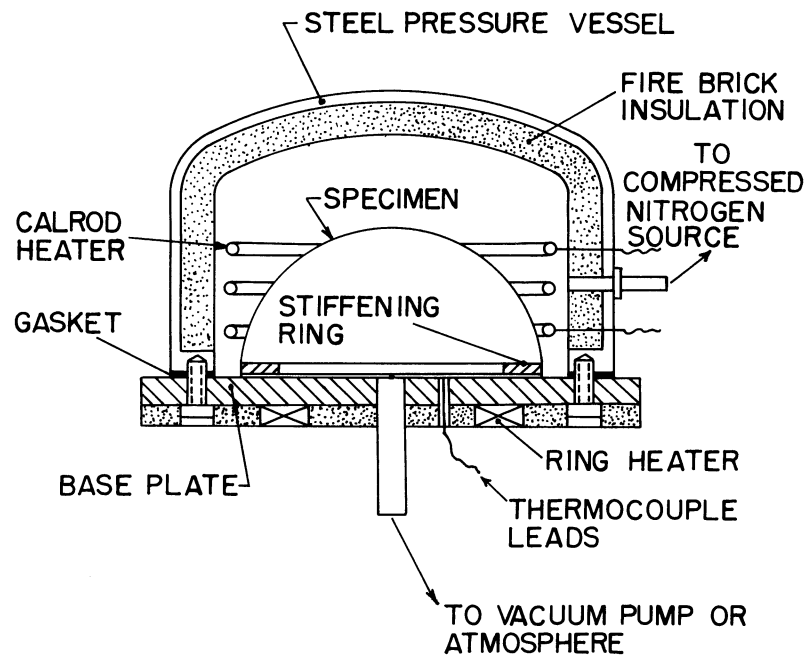


Figure 3.- Schematic diagram of the apparatus for creep test of hemispherical shells under external pressure.

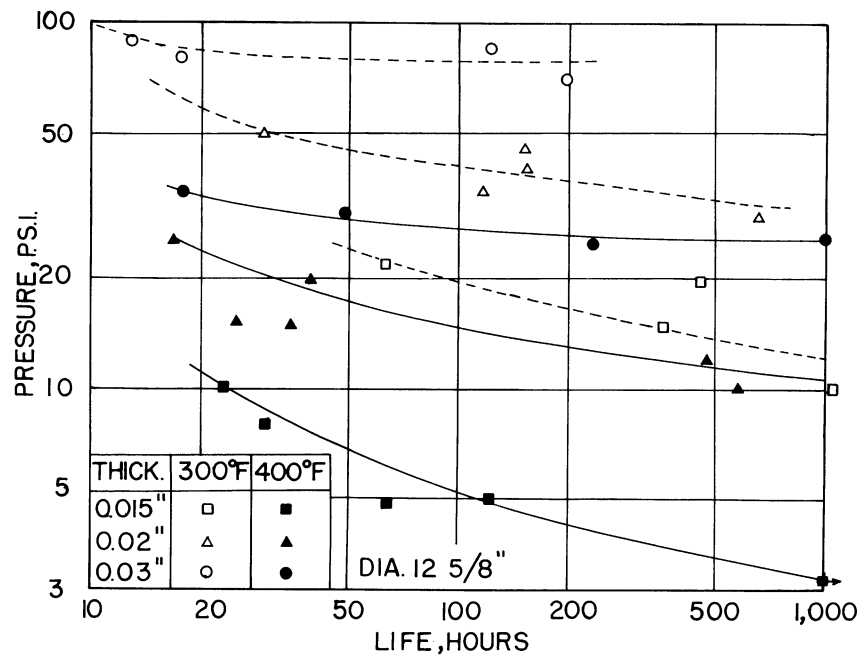


Figure 4.- Pressure versus creep life of copper hemispheres.

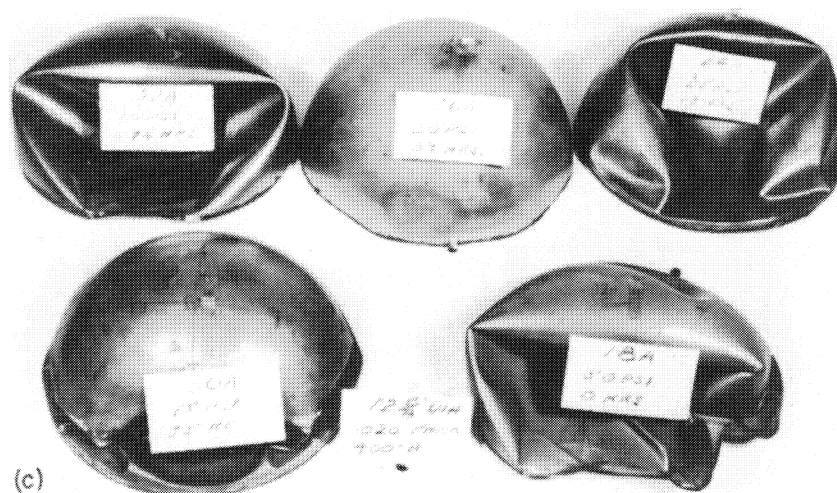
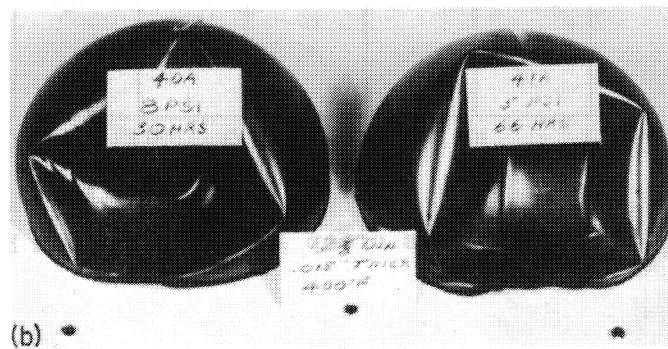
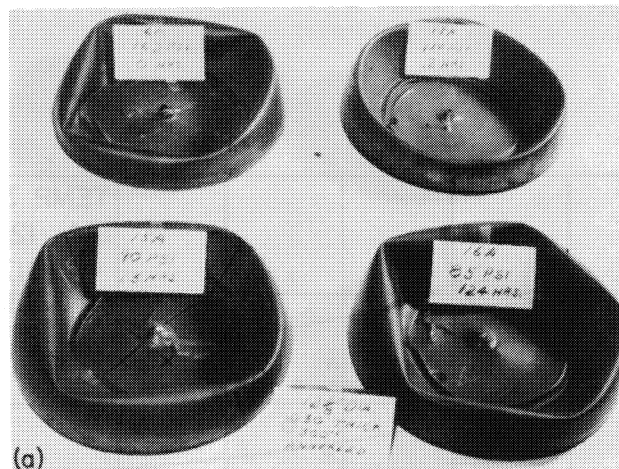


Figure 5.- The buckled shapes of some of the specimens.

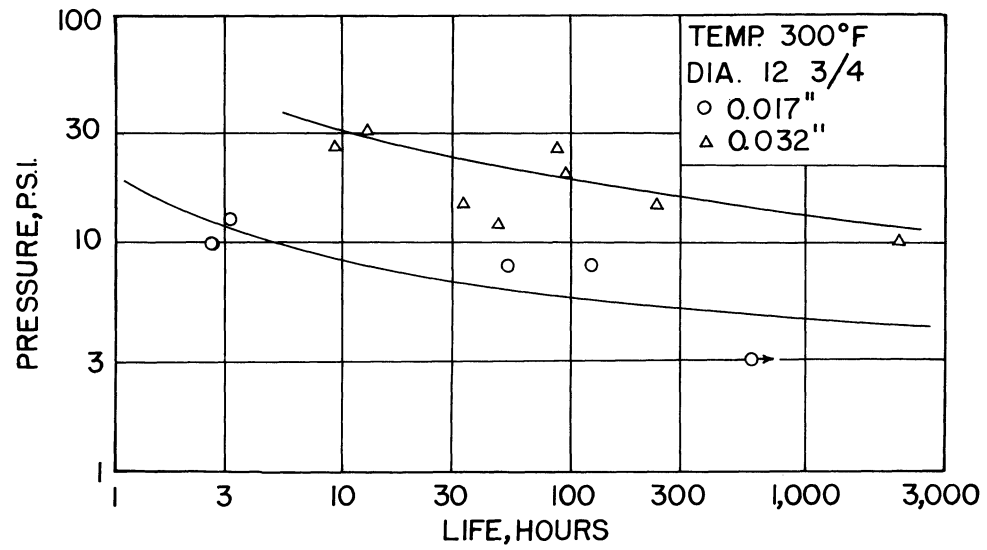


Figure 6.- Pressure versus creep life of aluminum hemispheres.

AXISYMMETRIC DYNAMIC BUCKLING OF CLAMPED SHALLOW SPHERICAL SHELLS

By Bernard Budiansky and Robert S. Roth
Harvard University and AVCO Corporation

SUMMARY

On the basis of non-linear theory, the axisymmetric deformations produced in a clamped shallow spherical shell by a transient pressure loading are calculated. A criterion for dynamic buckling is suggested and used to determine critical pressures as a function of duration of loading. The results are limited to shell geometries for which axisymmetric, rather than unsymmetric, deformations control the buckling phenomenon.

INTRODUCTION

The response to a uniform transient pressure loading of a clamped, shallow, spherical cap of constant thickness will be studied on the basis of non-linear elastic shallow shell theory. Numerical results will be used to obtain critical loads for "dynamic buckling" according to a qualitative, but fairly well defined, criterion.

PROBLEM STATEMENT AND METHOD OF SOLUTION

A meridional cross-section of the shell and the pertinent geometrical dimensions are shown in figure 1. Because of the shallowness assumption, the initial spherical shape is defined adequately by the parabolic relationship

$$z_0 = H [1 - (r/a)^2] \quad (1)$$

and the shell radius R , the base radius a , and the central rise H are related approximately by $a^2 = 2RH$. The problem under consideration is to calculate the time variation of the axisymmetric downward vertical displacement $W(r, t)$ produced by a prescribed history of uniform pressure on the convex surface.

The governing non-linear differential equations, taking into account moderately large rotations as well as inertial loads, are presented in the Appendix, together with a general procedure for their approximate

solution. This solution, based on the Galerkin method, requires the calculation of the time variation of a finite number of coefficients a_n in the expansion

$$W(r, t) = \sum a_n(t) W_n(r) \quad (2)$$

wherein the functions $W_n(r)$ are chosen proportional to the natural modes of axisymmetric vibration of a circular clamped flat plate of radius a .

RESULTS AND DISCUSSION

Numerical results have been obtained for "rectangular" loadings characterized by the sudden application of a pressure q at time $t = 0$ which is held constant for a time duration \bar{t} and then suddenly removed. The limiting case of an impulsive loading for which $\bar{t} = 0$ but $q\bar{t}$ remains finite has also been considered.

The results may be displayed in terms of the following non-dimensional parameters.

$$\text{Geometrical parameter: } \lambda = 2 [3 (1-\nu^2)]^{1/4} \left(\frac{H}{h}\right)^{1/2} \quad (3)$$

$$\text{Pressure parameter: } p = \frac{q}{q_0}, \quad (4)$$

$$\text{where } q_0 = \frac{2E}{[3 (1-\nu^2)]^{1/2}} \left(\frac{h}{R}\right)^2 \quad (5)$$

$$\text{Time parameter: } \tau = \frac{ct}{R}, \quad (6)$$

$$\text{where } c = \sqrt{\frac{E}{\rho}} \quad (7)$$

In these definitions E is Young's modulus, ν is Poisson's ratio, and ρ is the material density. The reference pressure q_0 is the classical, small-deflection-theory, buckling pressure of a complete spherical shell. The parameters λ and p have been used previously in static analyses (see, for example, ref. 1).

The overall downward deflection of the shell is conveniently characterized by the quantity

$$\Delta = \frac{(W)_{\text{ave}}}{(Z_0)_{\text{ave}}} \quad (8)$$

which is the ratio of the average downward deflection to the average value of the initial shell height.

A "rectangular" history of p is illustrated in figure 2(a) for the value $\bar{\tau} = 5$ of the non-dimensional load duration parameter; figure 2(b) shows, for the case of the shell characterized by $\lambda = 5$, the corresponding early histories of $\Delta(\tau)$ calculated for various values of p on the basis of five terms in the expansion (2). The most striking feature of these results (which are typical of those obtained for other values of $\bar{\tau}$) is illustrated in figure 2(c) which shows the variation with p of $(\Delta)_{\max}$, the largest positive value of Δ occurring during the early history of the response. It is seen that a very steep rise in $(\Delta)_{\max}$ occurs for a very small change in p in the vicinity of $p = .5$. Somewhat arbitrarily, then, a value $p_{cr} = .52$ in the middle of this region of rapid change is selected as the critical pressure for "dynamic buckling". It should be noted that the values of $(\Delta)_{\max}$ for p greater than .55 are "large", since $\Delta > 1$ indicates that the deflected shell has moved, on the average, below the plane of its boundary. On the other hand, the values of $(\Delta)_{\max}$ for p less than .5 can be considered moderate. Thus, the critical pressure corresponds, qualitatively, to a transition from moderate to severe deformations.

Very similar results have been obtained for other values of $\bar{\tau}$ (ref. 2) and in each case there is little uncertainty in picking a critical value for p on the same basis. The results for p_{cr} versus $\bar{\tau}$, still for $\lambda = 5$, are shown by the solid curve in figure 3. As expected, p_{cr} decreases as the duration of loading increases, but eventually, at about $\bar{\tau} = 10$, p_{cr} becomes constant. This is so because for $\bar{\tau} < 10$, the peak deflections occur after the removal of loading, whereas for $\bar{\tau} \geq 10$ the maximum deflections determining p_{cr} occur for $\tau < \bar{\tau}$, and so the continued application of pressure for $\tau > \bar{\tau}$ becomes irrelevant.

The dotted horizontal line shows the static buckling pressure parameter $(p)_{static}$ found in ref. 1 for $\lambda = 5$. It is interesting to note that whereas the dynamic (p_{cr}) exceeds $(p)_{static}$ for short durations of loading (as it should), the limiting value for long durations is somewhat less than $(p)_{static}$. Presumably this is due to the suddenness of the application of pressure in the present dynamic problem and the consequent occurrence of a "dynamic overshoot" effect.

The dotted curve in figure 3 shows the variation of the impulse parameter $\alpha_{cr} = (p_{cr} \bar{\tau})$ with $\bar{\tau}$, faired into a point for $\bar{\tau} = 0$ found from a separate calculation for impulsive loading (ref. 3). For very small durations of loading, it is evident that the impulse rather than the pressure is the important loading parameter.

Calculations have also been made (ref. 3) for impulsive loading for other values of λ , with the results shown in figure 4 as given by five-degree-of-freedom solutions. But, for two reasons, these results must not be taken seriously for λ larger than 5 or 6. First, whereas convergence with 5 terms in Eq. (2) appears satisfactory for $\lambda < 6$, it is progressively less so as λ increases; this is due to the in-

creasing "waviness" of the axisymmetric deformations for larger λ 's, as in the static case (ref. 1). Second, and more important, it is probable that for $\lambda > 6$ non-axisymmetric deformations will control the situation in both the static and dynamic buckling cases. For the same two reasons, the one-degree-of-freedom solution of ref. 4, shown dotted in fig. 4, must also be discounted for $\lambda > 6$.

CONCLUDING REMARK

The qualitative criterion presented for the establishment of critical parameters for dynamic buckling has a physically significant basis, and analogous criteria, based on the rapid change of response with loading parameters, may be useful in other dynamic buckling problems.

APPENDIX

ANALYSIS

The governing differential equations in non-dimensional form (see refs. 1, 3) are

$$(\xi w'')'' - \left(\frac{w'}{\xi}\right)' - \lambda^2 (\xi \emptyset)' + \lambda^4 (\xi \ddot{w}) = (\emptyset w')' + 4\lambda^4 p \xi \quad (A1)$$

$$(\xi \emptyset')' - \frac{\emptyset}{\xi} + \lambda^2 (\xi w') = -\frac{1}{2} (w')^2 \quad (A2)$$

where primes denote differentiation with respect to $\xi = r/a$, and dots denote differentiation with respect to τ . The non-dimensional displacement w is defined as $w = (w/h) [12(1-\nu^2)]^{1/2}$. The quantity \emptyset is a non-dimensional stress function defined in terms of the dimensional stress function ψ by $\emptyset = \psi [12(1-\nu^2)a] / [\lambda E t^3]$, where ψ is related to the meridional and circumferential membrane forces per unit length N_r and N_θ by $N_r = \psi/r$ and $N_\theta = (d\psi/dr)$. The equations (A1) and (A2) express, respectively, equilibrium in the vertical direction and compatibility of membrane strains.

The boundary conditions for the clamped edge at $\xi=1$ are

$$w = w' = 0 \quad (A3)$$

$$\text{and} \quad \emptyset' - \nu \emptyset = 0 \quad (A4)$$

The substitution (2), non-dimensionalized, is

$$w(\xi, \tau) = \sum a_n(\tau) w_n(\xi) \quad (A5)$$

where

$$w_n(\xi) = \frac{I_0(\Omega_n \xi)}{I_0(\Omega_n)} - \frac{J_0(\Omega_n \xi)}{J_0(\Omega_n)} \quad (A6)$$

where J is the Bessel function of the first kind, I is the modified Bessel function of the first kind, and the Ω_n are the roots of

$$\frac{I_1(\Omega_n)}{I_0(\Omega_n)} + \frac{J_1(\Omega_n)}{J_0(\Omega_n)} = 0 \quad (A7)$$

Substituting (A5) into (A1) and following Galerkin's procedure gives

$$\Omega_m^4 a_m + \lambda^4 \ddot{a}_m = \lambda^2 \int_0^1 (\xi \emptyset)' w_m d\xi + \int_0^1 (\emptyset w')' w_m d\xi + 4\lambda^4 p N_m \quad (A8)$$

($m = 1, 2, 3, \dots$)

where

$$N_m = \int_0^1 \xi w_n d\xi = - \frac{2J_1(\Omega_m)}{\Omega_m J_0(\Omega_m)} \quad (A9)$$

and use has been made of the orthonormality condition for the flat plate vibration modes

$$\int_0^1 \xi w_m w_n d\xi = \delta_{mn}$$

where δ_{mn} is the Kronecker delta (0 for $m \neq n$, 1 for $m = n$).

Now let $\emptyset = \emptyset_0 + \emptyset_1$, where

$$(\xi \emptyset_0)' - \frac{\emptyset_0}{\xi} = -\lambda^2 (\xi w') \quad (A10)$$

and

$$(\xi \emptyset_1)' - \frac{\emptyset_1}{\xi} = -\frac{1}{2} (w')^2 \quad (A11)$$

and both \emptyset_0 and \emptyset_1 satisfy the boundary condition (A4). The solution of (A10), regular at $\xi = 0$, is

$$\phi_o = -\frac{\lambda^2}{\xi} \int_0^\xi \eta w(\eta) d\eta - \lambda^2 \left(\frac{1+\nu}{1-\nu} \right) \xi \int_0^1 \eta w(\eta) d\eta \quad (A12)$$

$$\text{Then } \int_0^1 (\xi \phi_o)' w_m d\xi = -2\lambda^2 \left(\frac{1+\nu}{1-\nu} \right) N_m \sum_n a_n - \lambda^2 a_m \quad (A13)$$

can be used directly in (A8).

Next, following ref. 5, write

$$\phi_o = A_o \xi + \sum b_n^{(o)} J_1(\lambda_n \xi) \quad (A14)$$

$$\phi_1 = A_1 \xi + \sum b_n^{(1)} J_1(\lambda_n \xi) \quad (A15)$$

where the λ_n are the roots of $J_1(\lambda_n) = 0$. Then use of (A13), (A14), and (A15) in (A8) gives

$$\begin{aligned} & \ddot{a}_m + \left[1 + \left(\frac{\Omega_m}{\lambda} \right)^4 + 2 \left(\frac{1+\nu}{1-\nu} \right) N_m^2 \right] a_m + 2 \left(\frac{1+\nu}{1-\nu} \right) N_m \sum_n a_n (1 - \delta_{mn}) \\ &= \frac{1}{\lambda^2} \left[2A_1 N_m - \sum_{mn} C_{mn} b_n^{(1)} \right] - \frac{1}{\lambda^4} \left[(A_o + A_1) \sum_{mn} D_{mn} a_n + \sum_n \sum_p E_{mnp} a_n (b_p^{(o)} + b_p^{(1)}) \right] \\ &+ 4 \sum_p N_m \quad (m = 1, 2, 3, \dots) \quad (A16) \end{aligned}$$

$$\text{where } C_{mn} = \int_0^1 \xi J_1(\lambda_n \xi) w_m' d\xi = \frac{\Omega_m^4 N_m \lambda_n J_o(\lambda_n)}{\lambda_n^4 - \Omega_m^4}$$

$$\begin{aligned} D_{mn} &= \int_0^1 \xi w_m' w_n' d\xi = -(\Omega_m \Omega_n)^2 \left(\frac{N_m - N_n}{\Omega_m^2 - \Omega_n^2} + \frac{N_m + N_n}{\Omega_m^2 + \Omega_n^2} \right) (m \neq n) \\ &= \frac{\Omega_m^4 N_m^2}{4} + \frac{\Omega_m^2 N_m}{2} \quad (m = n) \end{aligned}$$

$$\text{and } E_{mnp} = \int_0^1 w_m' w_n' J_1(\lambda_p \xi) d\xi,$$

which must be found by numerical integration.

Finally, A_0 , A_1 , $b_n^{(0)}$, and $b_n^{(1)}$ must be expressed in terms of the a_n 's. Substitution of (A14) into (A10), and use of the Galerkin method again gives

$$b_n^{(0)} = \frac{2\lambda_n^2}{\lambda_n^2 J_o^2(\lambda_n)} \sum_m C_{mn} a_m \quad (A17)$$

and a similar calculation with (A15) and (16) gives

$$b_n^{(1)} = \frac{1}{\lambda_n^2 J_o^2(\lambda_n)} \sum_r \sum_s E_{rsn} a_r a_s \quad (A18)$$

By the boundary condition (A4)

$$A_1 = -\left(\frac{1}{1-\nu}\right) \sum b_n^{(1)} \lambda_n J_o(\lambda_n) \quad (A19)$$

On the other hand, A_1 is most conveniently found from (A12) as

$$A_0 = \phi_o(1) = -\frac{2\lambda_n^2}{1-\nu} \sum N_n a_n \quad (A20)$$

The constants Ω_n , λ_n , N_n , C_{mn} , D_{mn} , and E_{mnp} are tabulated in ref. 3, up to $m = n = p = 5$.

For a prescribed $p(\tau)$, equations (A16) now constitute a well-defined set of non-linear, second-order equations for the response coefficients a_n , and they have been solved numerically for the various cases discussed in the body of this report. The initial conditions are generally $a_n(0) = \dot{a}_n(0) = 0$; but in the case of impulsive loading, the last term in (A16) does not appear, and instead the initial (dimensional) velocity $(q\bar{t}) / (\rho h)$ must be imposed. Then, non-dimensionally,

$$\dot{w}(\xi, 0) = \sum \dot{a}_n(0) w_n = 4 \alpha$$

where

$$\dot{a}_n(0) = 4 N_n \alpha$$

for the impulsive loading case. Finally, Δ is found as

$$\Delta = \frac{(w)_{ave}}{(z_o)_{ave}} = \frac{8}{\lambda^2} \sum N_n a_n$$

with results typified by fig. 2.

REFERENCES

1. Budiansky, Bernard: Buckling of Clamped Shallow Spherical Shells, Proceedings of IUTAM Symposium, Theory of Thin Elastic Shells, Delft (1959), North Holland Publishing Co.
2. Roth, Robert S.: Dynamic Instability of Shallow Spherical Shells Subjected to Pressure Pulse Loadings. Technical Memorandum RAD-TM-62-24, AVCO RAD, May 1962.
3. Radkowski, P.P., Humphreys, J.S., Bodner, S.R., Payton, R.G., and Budiansky, B.: Studies on the Dynamic Response of Shell Structures to a Pressure Pulse. AFSWC-TR-61-31 (II) AVCO RAD, July 1961.
4. Humphreys, J.S., and Bodner, S.R.: Dynamic Buckling of Shells under Impulsive Loading. Journal of the Engineering Mechanics Division, ASCE, April 1962.
5. Archer, R.R.: Stability Limits for a Clamped Spherical Shell Segment under Uniform Pressure. Quarterly of Applied Mathematics, vol. XV (1958) p. 355.

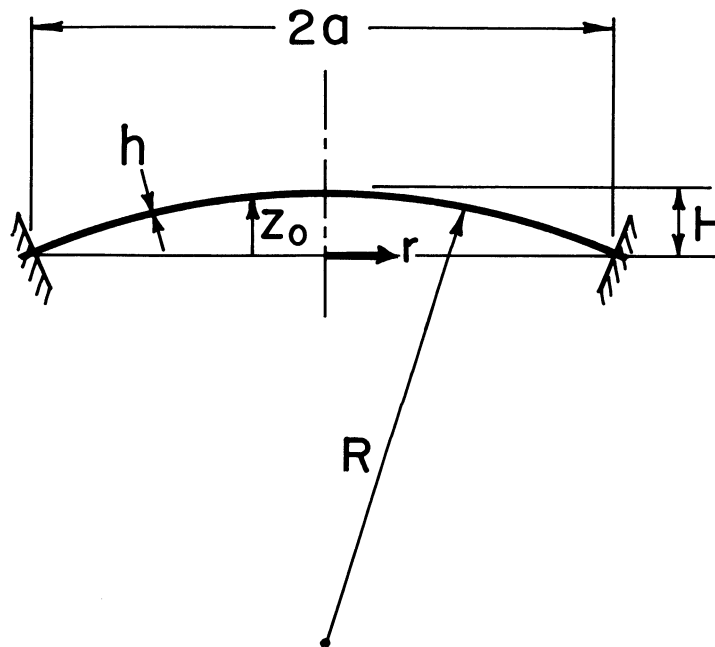


Figure 1.- Clamped shallow spherical shell.

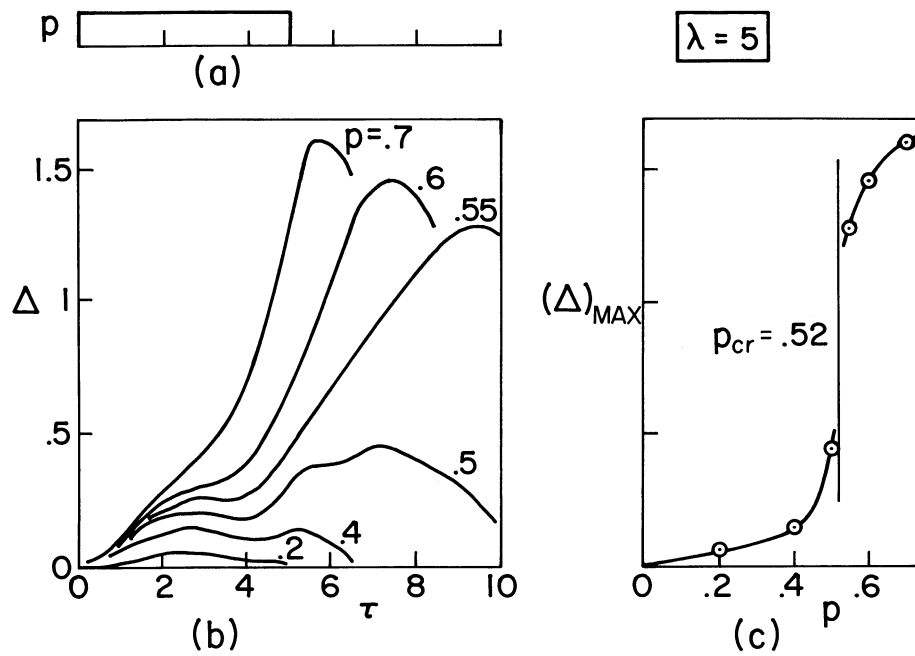


Figure 2.- (a) Rectangular pressure history; (b) response histories for various pressures; (c) variation of maximum response with pressure.

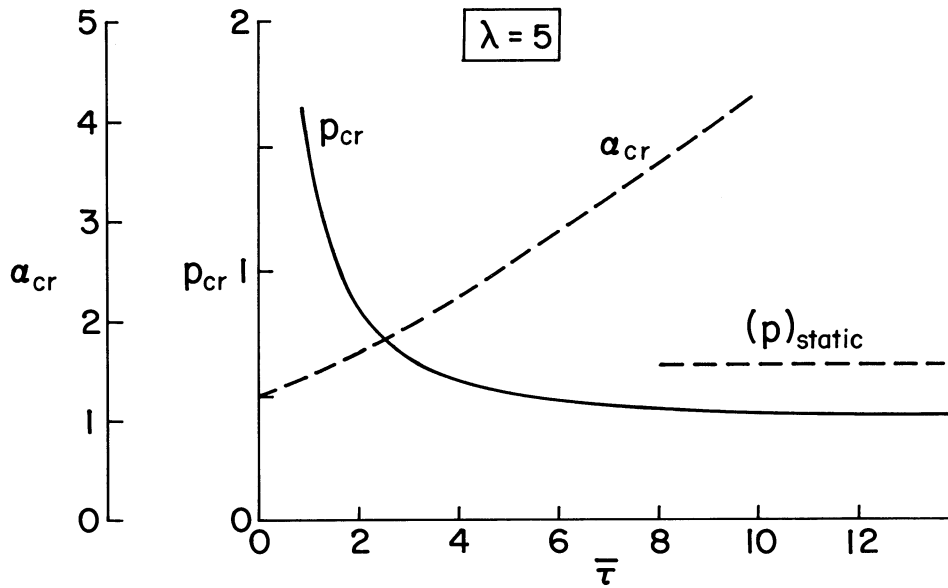


Figure 3.- Variation with load duration of critical pressure and critical impulse parameter.

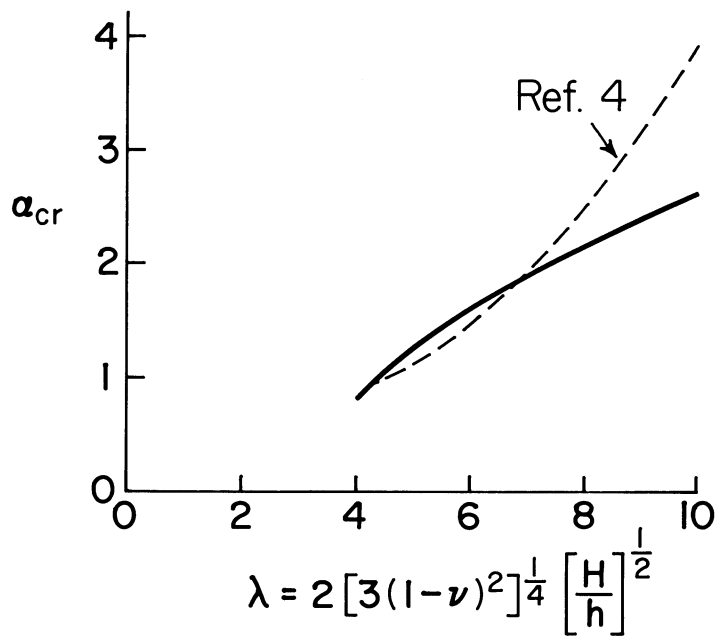


Figure 4.- Calculated variation of critical-impulsive-load parameter with shell-geometry parameter.

DYNAMIC DEFORMATION AND BUCKLING OF SPHERICAL
SHELLS UNDER BLAST AND IMPACT LOADING

By Emmett A. Witmer, Theodore H. H. Pian,
and Hans A. Balmer

Massachusetts Institute of Technology

SUMMARY

Two types of dynamic tests on spherical shells have been conducted. One involved blast-induced dynamic buckling and permanent deformation of the shell; the other involved producing permanent deformation of hemispherical shells by projectile impact coincident with the axis of symmetry of the shell. An analysis which predicts only the axisymmetric response of the shell has been formulated. The analysis which takes into account large deflections and plastic deformations is employed to predict and compare with the experimentally-observed results.

INTRODUCTION

This paper presents the results of some recent studies conducted at the Aeroelastic and Structures Research Laboratory, M.I.T., on buckling of thin spherical shells under dynamic loadings. Both experimental and theoretical results are included. The experimental program pertains to shells under blast loading in a shock tube and shells impacted by projectiles. The objective of the theoretical program is to develop a numerical method for predicting the response and permanent plastic deformation of shells under general dynamic loading conditions. The analysis given in the present paper is limited entirely to the axisymmetric motion of shells.

EXPERIMENTS

Test Specimens

Spherical shells of nominal 4-inch diameter and uniform thickness ranging from 5 to 11 mils were prepared by hydro-forming, spinning, and chemical milling from 6061-0 aluminum alloy. The average of the extreme variations in thickness of a given model ranged from ± 4.1 percent to ± 9.5 percent for shells having nominal radius-to-thickness, R/t , values of 180 and 380, respectively. These specimens were subsequently heat treated to a Rockwell hardness of 74-80, resulting in measured compression yield of 36,000 psi for 0.2 percent offset and a tensile ultimate stress of 42,500 psi. These models were mounted for testing by positioning them such that the base of each, for any chosen H/R conditions, extended well into a 3/8-inch deep circular moat machined into a heavy steel plate. This moat was then filled with liquid cerrobend metal which cools, solidifies, and expands thus firmly clamping the base of the model.

Blast Tests

Blast-test apparatus and procedure. - The experiments involving blast loading on the spherical shells were performed using the MIT-ASD 8 by 24-inch by 98-foot shock tube which provides essentially a step-function blast wave. Using the 24-inch side wall as the base plane for a specimen permits side-on blast impingement wherein the normal to the shock front is perpendicular to the axis of symmetry of the shell. On the other hand, when the 8 by 24-inch end of the shock tube is used as the base plane of the model, the normal to the incident shock front is coincident with or parallel to the axis of symmetry of the shell; this results in axisymmetric blast loading of the specimen. Schematics of the shock tube testing arrangement and of model-shock front orientations together with the associated H/R values employed are shown in figure 1.

From a knowledge of (a) the measured pressure and temperature of the air in the shock tube test section, where the test specimen is located, before the shock arrives, and (b) the velocity of the shock front, the pressure jump across the shock front can be determined readily from the Rankine-Hugoniot shock relations.¹ Also, from the Rankine-Hugoniot shock relations, the density and the material velocity of

the shock-initiated flow can be determined. These relations together with the boundary condition of zero material velocity normal to a solid surface enable a determination of the pressure behind the reflected shock occurring when the incident shock impinges upon a solid surface. The condition for which the plane of the shock front is parallel to the surface against which it impinges is referred to as "head-on" shock reflection, and the associated pressure increase at the wall above that present before shock impingement is often termed simply: the reflected-shock overpressure. This quantity is useful in later discussion.

In the blast loading experiments depicted in parts (b) and (c) of figure 1, each model was subjected to a small shock overpressure and then examined visually and with a template for any evidence of permanent deformation. If none was found, the specimen was subjected to a slightly greater shock overpressure and, once again, was inspected. This procedure was repeated until evidence of permanent damage was found. The shock overpressure at which any evidence of permanent damage is first noted is termed the dynamic-buckling threshold overpressure.

Blast-test results. - In some cases, the first permanent deformation observed was very slight, and very large in others; figure 2, showing first-damage results, serves to illustrate this fact for the cases of side-on and axisymmetric loading. Since increments in incident shock overpressure of about 0.4 to 0.8 psi were employed, it is seen that permanent deformation is extremely sensitive to the amount by which the incident shock overpressure exceeds the actual "threshold" shock overpressure, $\Delta p_{s,cr}$. Accordingly, the threshold shock overpressure was chosen as that with which damage of the type exhibited by specimen 11-13 (figure 2) occurred. For more severe initial damage, the threshold shock overpressure was taken as an appropriate value interpolated between the damage-inflicting value employed and that of the next smallest overpressure to which the specimen was subjected.

At the location on the specimen which was first struck by the shock front, head-on reflection occurs and the head-on reflected shock overpressure Δp_r is produced. The value of $\Delta p_{r,cr}$ corresponding to $\Delta p_{s,cr}$ is a convenient reference value and is employed in figure 3 to denote the dynamic buckling threshold as a function of R/t . Note that for cases involving $H/R = 1.5$, the dynamic-buckling thresholds for cases of side-on blast are indistinguishable

from those for axisymmetric blast. This is not surprising in view of the local nature of dynamic buckling and the rapidity with which it occurs. Motion pictures taken at 10,000 frames per second for a specimen with $R/t = 380$ show clearly that dynamic buckling has proceeded to a significant extent within 100 microseconds, but may have proceeded significantly much earlier than this. By way of contrast, the time for an acoustic signal in the metal to propagate from the crown to the base and back for this specimen is about 33 microseconds. On the other hand, in 100 microseconds the blast shock front has traveled typically only about 1.85 inches; thus, buckling has been initiated before wall effects have influenced the blast loading on the shell.

Only a few dynamic tests were conducted for $H/R = 1.0$ and 0.293. Although not sufficient in number to be definitive, these results are included in figure 3. However, it appears that the expected trend of reduced critical load with reduced H/R is indicated.

It was observed that dynamic buckling for side-on loading was initiated near the region first struck by the blast (i.e., at the nose) in some cases, and adjacent to the clamped base in others. By contrast, hydrostatic tests of 31 specimens with $H/R = 1.5$ and with R/t values ranging from about 180 to 450 exhibited a great preponderance of buckles occurring adjacent to the base. The hydrostatic buckling pressure for all of these base-influenced buckling cases is given by

$$\Delta p_{cr} = 0.35 E \left(\frac{t}{R} \right)^2$$

where E is the elastic modulus, with a mean probable error of 2.2 percent. This relation is the form of the familiar Tsien² equation for static elastic buckling of spherical shells. Tests on spherical shell specimens which were thickness-prepared by chemical milling (as were all of the specimens) so as to provide a slightly thicker region adjacent to the base compared with the remainder of the shell resulted in buckles occurring well away from the base. The buckling pressures for the five cases tested in this manner were significantly larger and may be expressed by

$$\Delta p_{cr} = 0.62 E \left(\frac{t}{R} \right)^2$$

with a mean probable error of 3.8 percent; these are referred to as base-uninfluenced cases.

The hydrostatic test results are in marked contrast with the dynamic buckling results since, as seen from figure 3, the latter show no distinction between "base-influenced" and the "base-uninfluenced" cases. All of the dynamic buckling results of figure 3 for $H/R = 1.5$ may be correlated by

$$\Delta p_{r,cr} = 0.33 E \left(\frac{t}{R} \right)^2$$

where, as before, the elastic modulus E has been taken as 10,400,000 psi, and $\Delta p_{r,cr}$ is in psi units.

Impact Tests

Impact-test apparatus and procedure. - For the projectile-shell impact tests, a hemispherical test specimen was mounted as a bob of a ballistic pendulum. The specimen was then impacted at its crown by a lead projectile. By applying the conditions expressing the conservation of momentum and energy, and by assuming that the energy of deformation of the projectile is negligibly small, the energy ultimately dissipated by the shell through plastic deformation and friction can be computed from

$$E_d = 1/2 \left\{ m' V [2V_o - V(1 + \frac{m'}{m})] \right\}$$

where

V_o = projectile impact velocity

V = maximum velocity acquired by the pendulum

m = mass of the projectile

m' = mass of the pendulum

Further, if it is assumed that the displacement of the pendulum was negligible during the time to complete the deformation of the shell, the maximum velocity V of the pendulum can be found from the maximum side swing, x , of the pendulum:

$$V = x \sqrt{\frac{g}{r}}$$

where r is the length of the pendulum and g is the gravitational constant. Thus, a measurement of V_o and x permits a determination of E_d .

Impact-test results. - The results from eight projectile-shell impact tests are shown in figure 4. The permanent deflection δ/R is given in figure 5 as a function of the shell dissipation energy where δ is the central permanent deflection. Profiles of permanent deformation for two of these cases are shown in figure 6. Detailed data for these tests may be found in reference 3.

NUMERICAL SOLUTION OF DYNAMIC RESPONSE OF AXISYMMETRIC SHELLS

This section presents briefly a step-by-step numerical method that has been developed in reference 5 for predicting the dynamic responses of shells of revolution in axisymmetric deformations.

Part (a) of figure 7 shows a shell of revolution defined by the curvilinear coordinates S and ϕ . The location of any point on the meridian can be determined by the two coordinates r and z . On the element of the shell shown in part (b) of figure 7 there are two tangential stress resultants N_θ and N_ϕ , a transverse stress resultant Q_θ and two stress couples M_θ and M_ϕ . The equations of equilibrium for large deflections of shells are

$$\begin{aligned} \frac{d}{dS} [N_\theta r \sin \theta] + \frac{d}{dS} [Q_\theta r \cos \theta] - mr\ddot{z} &= 0 \\ \frac{d}{dS} [N_\theta r \cos \theta] - \frac{d}{dS} [Q_\theta r \sin \theta] - N_\phi - mr\ddot{r} &= 0 \\ \frac{d(M_\theta r)}{dS} - M_\phi \cos \theta - Q_\theta r &= 0 \end{aligned}$$

where

$$\begin{aligned} m &= \text{mass of the shell per unit area} \\ \theta &= \text{angle of inclination of the element} \\ &\quad \text{with respect to the } r\text{-direction} \end{aligned}$$

For an approximate solution, the meridian of the shell is first divided into a finite number of discrete segments and a set of finite-difference equations is used to replace the above set of differential equations. The difference equations can be represented approximately by a lumped-parameter model consisting of rings connected by weightless

frustums. In determining the symmetrical motion of the shell, a step-by-step numerical procedure is used. At time t_j the stress-resultants N_θ and N_ϕ and stress couples M_θ and M_ϕ , the location z and r of each mass ring, and the angle of inclination θ of each frustum segment have all been previously evaluated. Then, it is possible to calculate the transverse stress resultant Q_θ and to evaluate the two components of acceleration \ddot{r} and \ddot{z} at each ring. By using the central-difference approximation to represent the second derivatives with respect to time, one can determine the coordinates z and r at time $t_j + \Delta t$, i.e., at t_{j+1} . One can then determine the increments in mid-surface^{j+1} strain components and the changes in principal curvatures.

In determining the corresponding increments in stress resultants and stress couples, the shell material is assumed to be concentrated at two layers separated by a material which cannot carry normal stresses but has infinite shear rigidity. Under this simplified assumption, the stress and strain in the shell can be defined by those of the upper and lower layers. For each layer, the stress-strain relations under plane-stress conditions can be used. For the present analysis the material is assumed to be elastic, perfectly plastic. The method can be extended to materials which exhibit strain hardening behavior and for materials whose plastic behaviors are affected by the rate of straining.

CORRELATION AND DISCUSSION

Blast-Loaded Specimens

Preliminary calculation of responses of spherical shells under dynamic loading indicates that the solution is very sensitive to the space-mesh size to be chosen in the analysis and that considerable length of time must be followed in order to obtain an evidence of dynamic buckling. Results obtained so far are not sufficient for the determination of the threshold reflected-shock overpressure for dynamic buckling of spherical shells. There is, however, an indication that the calculated values are higher than the corresponding experimental values. It is reasonable to think that severe constraint imposed by the axisymmetric mode(s) of deformation would tend to result in overestimation of the buckling threshold blast loading. As in static

buckling problems, the admission of asymmetric modes of deformation is expected to result in considerably improved theoretical-experimental agreement. This effect has also been demonstrated theoretically in (a) reference 6, concerning dynamic buckling of impulsively-loaded arches and (b) reference 7, dealing with dynamic buckling of impulsively-loaded spherical shells.

Since the experimental results have indicated that the initiation of dynamic buckling involves only a very small cap angle, it is felt that results obtained using small cap angles may be equally valid for dynamic buckling of spherical shells of large H/R values. Calculations are under way for various H/R values and space-mesh sizes in order to ascertain the minimum of each required to produce responses valid for spherical shells of large H/R values.

Impact-Loaded Specimens

The permanent central deflections predicted by axisymmetric theory employing the two-flange model with a flange separation $h = t/2$ and using 30 segments per quadrant are shown in figure 5 as a function of the energy initially imparted to the shell. Very little difference was found by using 60 and 180 segments per quadrant. It is seen, as expected, that the central deflection is underestimated by this theory. Figure 6 gives a comparison between predicted and measured permanent deformation profiles for impacted specimens 3 and 7. The degree of deformation asymmetry observed in these experiments is indicated by the maximum, mean, and minimum of deformation profiles measured along ten directions across the impact-deformed region of each specimen. The general nature of the asymmetry of these deformations can be seen in figure 4. It is clear that the asymmetric character of the deformation pattern leads to larger central deflections for a given energy input than would occur by axisymmetric deformation.

It is interesting to note that the present theory predicts that 97 percent of the initial energy input has been absorbed by plastic work of shell specimen 7 by about 400 microseconds after impact, with the remaining 3 percent being accounted for by elastic and kinetic energy of the shell.

CONCLUDING REMARKS

The critical buckling load for a deep spherical shell clamped at its base, for the static case, depends upon whether or not the induced buckle occurs adjacent to the base, as it usually does. The dynamic buckling threshold, on the other hand, exhibits no such dependence. With respect to theory, the use of the present highly restrictive axisymmetric calculation tends to overestimate the blast load required to initiate dynamic buckling of spherical shells. A theory admitting both symmetric and asymmetric modes of deformation should yield much-improved results.

For the prediction of permanent deformation of shells under concentrated dynamic loads, the present study shows clearly the necessity for including more than axisymmetric modes in an elastic, plastic dynamic analysis. The present axisymmetric elastic, plastic theory underestimates the central permanent deformation by about 20 percent.

ACKNOWLEDGMENTS

This research was sponsored in part by the Aeronautical Systems Division of the United States Air Force under Contract AF 33(657)-8427 and by the U. S. Army under Air Force Contract AF 19(604)-7400 to the M.I.T. Lincoln Laboratory. The assistance and use of the facilities of the M.I.T. Computation Center are gratefully acknowledged. The authors especially wish to acknowledge Mr. J. W. Leech, Mr. O. E. Wallin, and their associates in the M.I.T. Aeroelastic and Structures Research Laboratory for assistance with the experimental phases of this study.

REFERENCES

1. Courant, R., and Friedrichs, K. O.: Supersonic Flow and Shock Waves. Interscience Publishers, Inc., 1948.
2. Tsien, H. S.: Theory of Buckling of Thin Shells. Journal of the Aeronautical Sciences, vol. 9, no. 10, August 1942.

3. Witmer, E. A., Herrmann, W., Leech, J. W., and Pian, T. H. H.: Response of the Plates and Shells to Intense External Loads of Short Duration. WADD TR 60-433, Massachusetts Institute of Technology, Aeroelastic and Structures Research Laboratory, April 1960.
4. Gallagher, E. V.; Air Blast Loading on Arches and Domes. Final Test Report No. 13, AFSWC-TN-58-26, AFSWP-1108, Armour Research Foundation, September 1958.
5. Leech, J. W., Pian, T. H. H., Witmer, E. A., and Herrmann, W.: Dynamic Response of Shells to Externally-Applied Dynamic Loads. ASD-TDR-62-610, Massachusetts Institute of Technology, Aeroelastic and Structures Research Laboratory, July 1962.
6. Hsu, P. T., and Chen, M. M.: Snapping Phenomena of Elasto-Plastic Curved Beams under Static and Dynamic Loadings, ASRL TR 100-2, AFOSR 2460, Massachusetts Institute of Technology, Aeroelastic and Structures Research Laboratory, January 1962.
7. Radkowski, P. P., Humphreys, J. S., Bodner, S. R., Payton, R. G., and Budiansky, B., Studies on the Dynamic Response of Shell Structures and Materials to a Pressure Pulse, AFSWC-TR-61-31(II), July 1961.

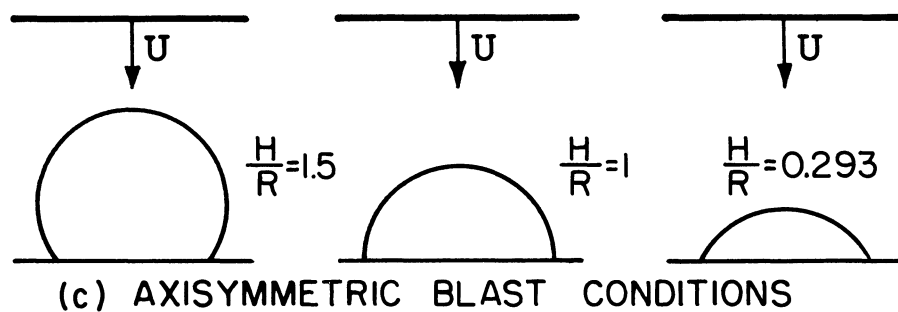
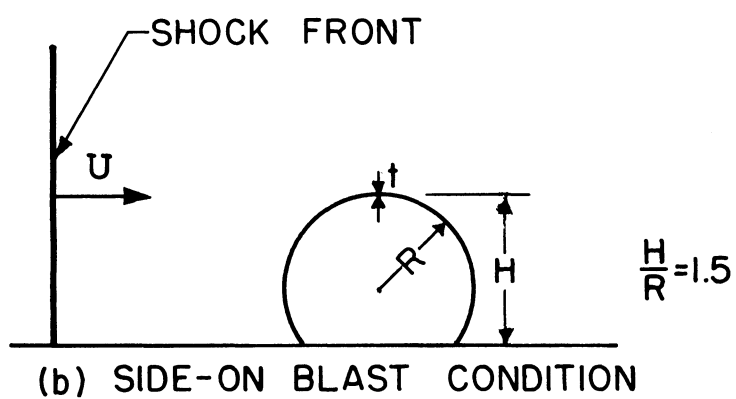
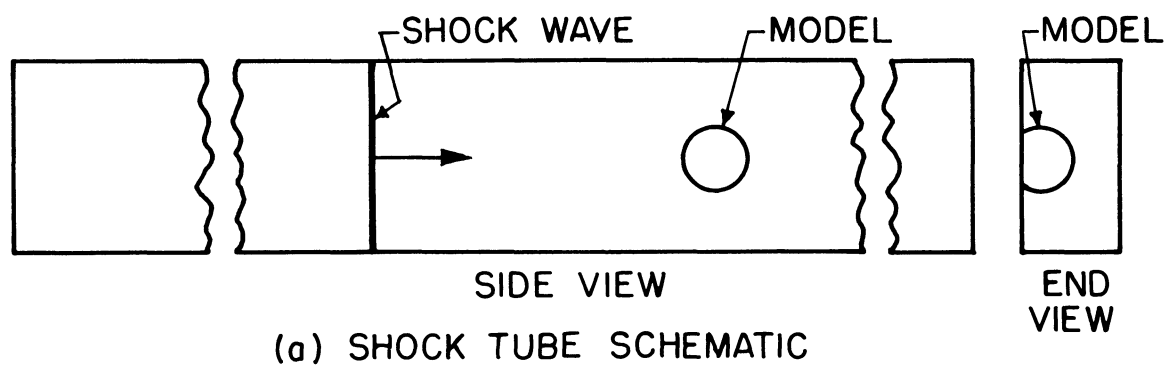
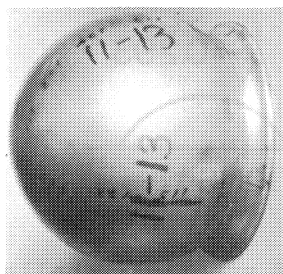
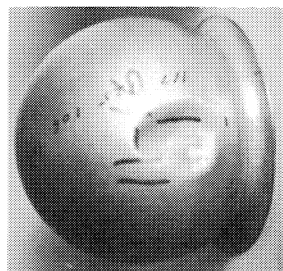


Figure 1.- Configurations for shock tube tests of spherical shells.

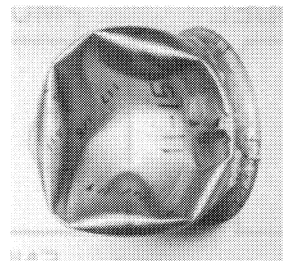


11-13

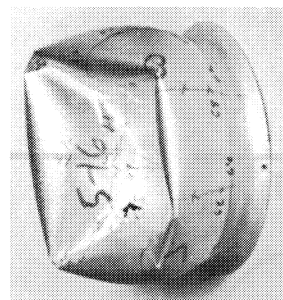


11-16

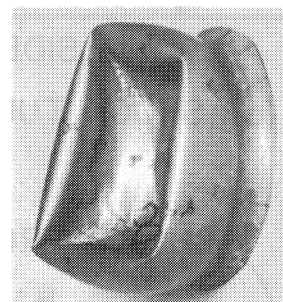
(a) SIDE-ON BLAST



11-15



5-16



8-17

(b) AXISYMMETRIC BLAST

Figure 2.- Typical blast-loaded dynamically-buckled spherical shells.

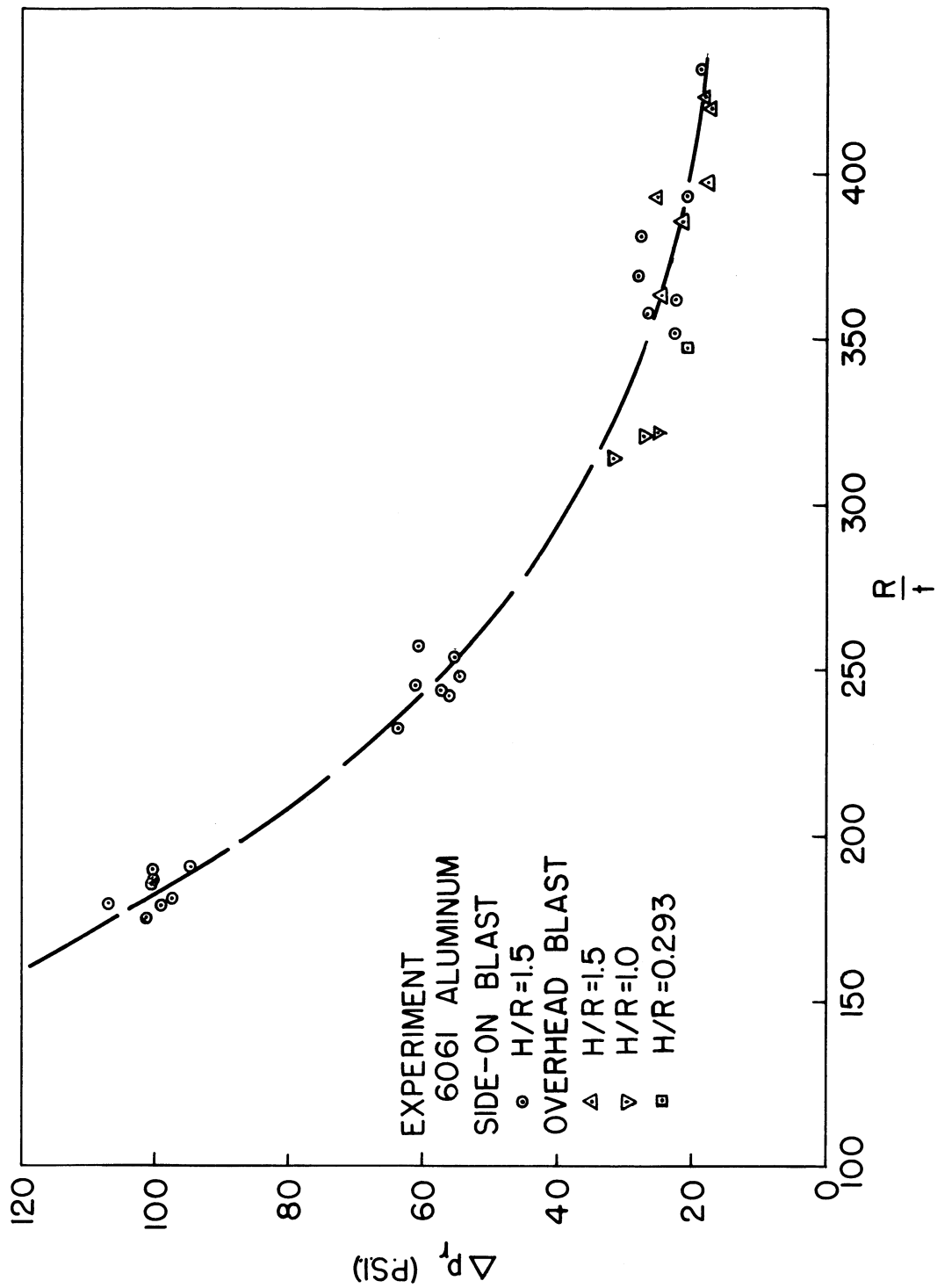


Figure 3.- Peak reflected blast overpressure at the buckling threshold for spherical shells.

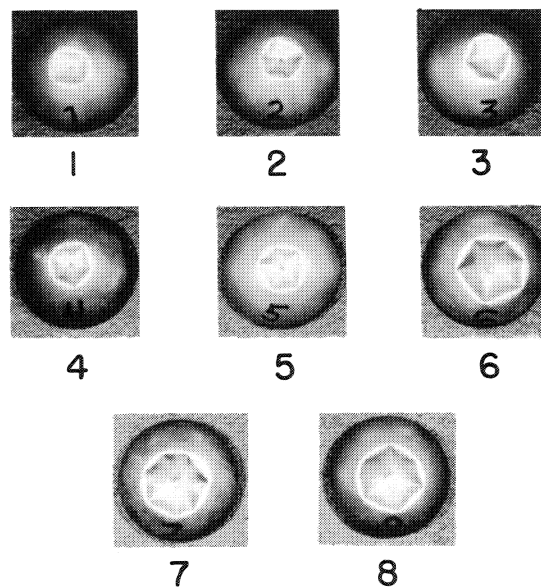


Figure 4.- Projectile-impacted spherical shells.

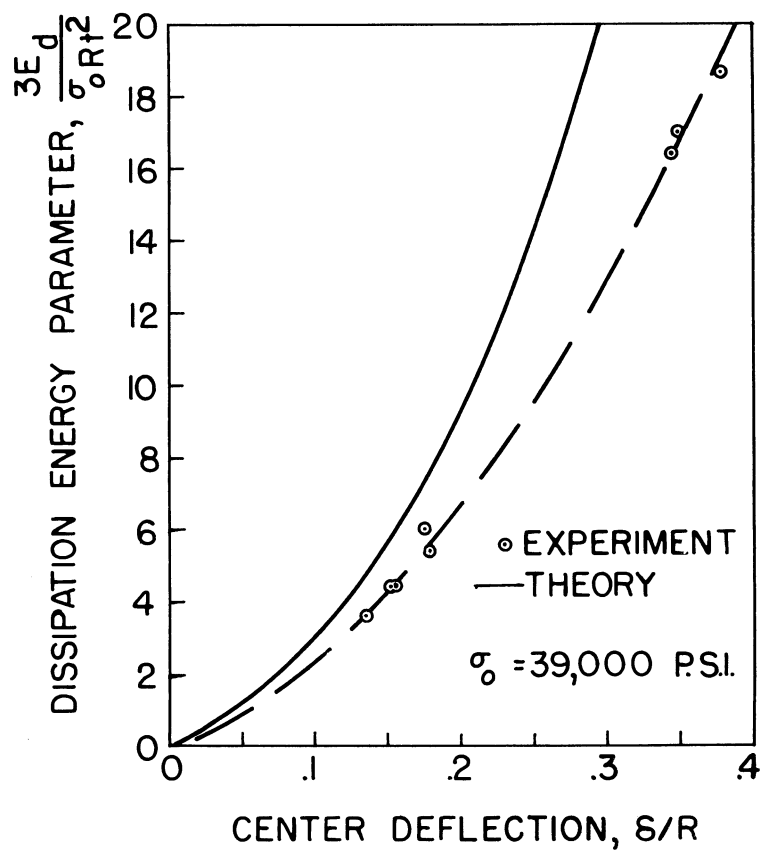
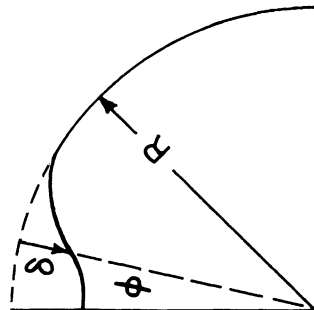
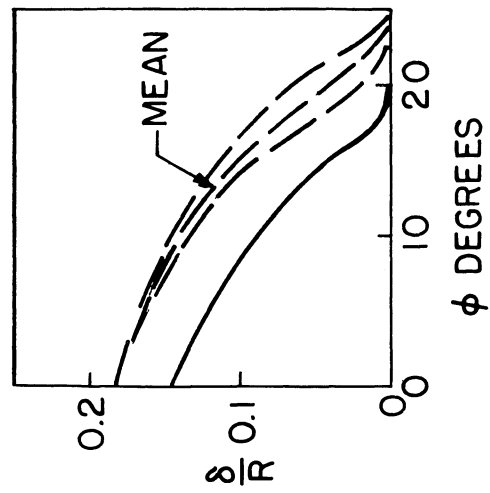


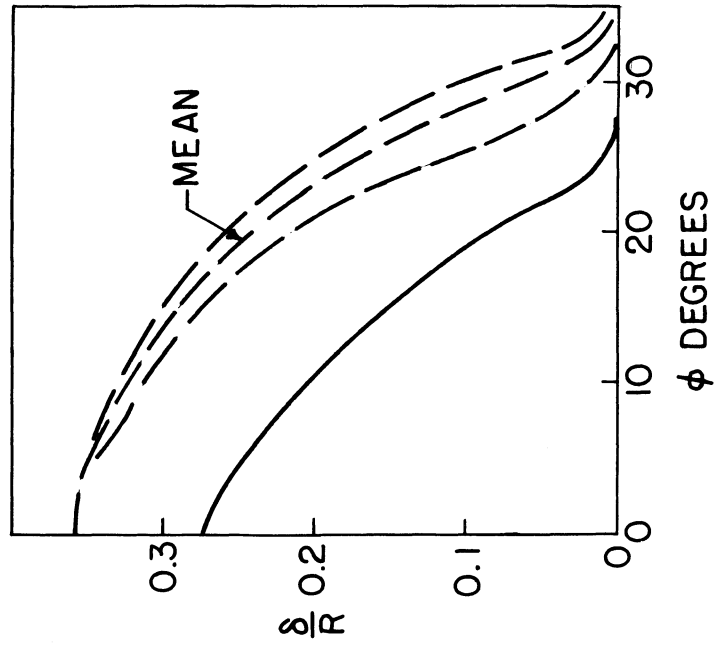
Figure 5.- Permanent deformation of projectile-impacted spherical shells as a function of shell dissipation energy.



(a) NOMENCLATURE

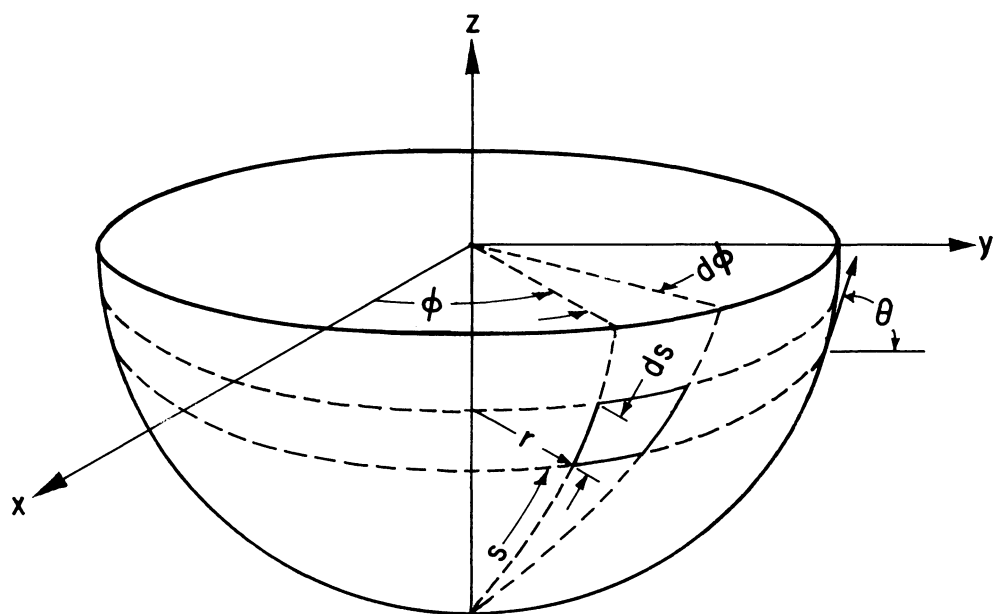


(b) SPECIMEN 3

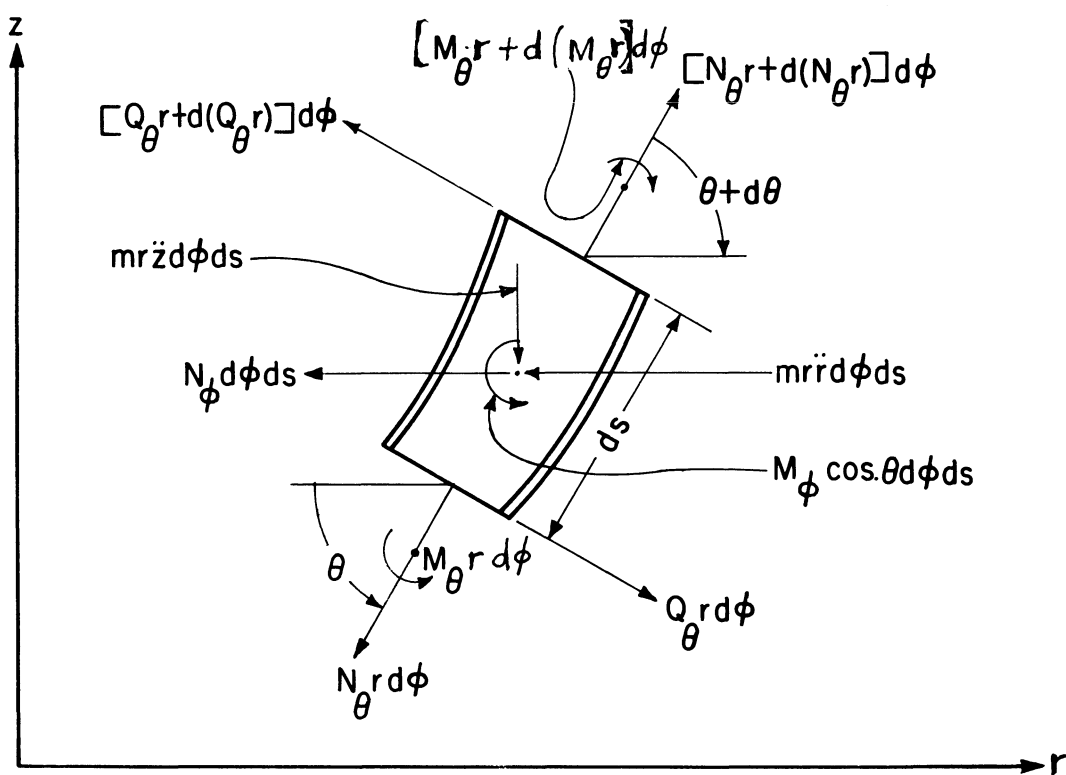


(c) SPECIMEN 7

Figure 6.- Permanent-deformation profiles of projectile-impacted spherical shells.



(a) SHELL OF REVOLUTION



(b) EQUILIBRIUM OF A SHELL ELEMENT

Figure 7.- Nomenclature for a shell of revolution.

NONLINEAR TRANSVERSE AXISYMMETRIC VIBRATIONS
OF SHALLOW SPHERICAL SHELLS

By J. Connor, Jr.

Watertown Arsenal Laboratories

SUMMARY

A system of ordinary differential equations defining the axisymmetric nonlinear dynamic behavior of a shallow shell is obtained by expanding the transverse displacement in terms of the normal modes for the linear case. This system is integrated numerically for a rectangular pulse loading, using one and two mode expansions. Also, a simple two degree of freedom model for a spherical shell is proposed, and its limiting dynamic behavior investigated.

INTRODUCTION

E. Reissner has shown that for primarily transverse linear vibrations of shallow shells, longitudinal inertia can be neglected in comparison to transverse inertia, resulting in an appreciable simplification of the problem⁽¹⁾. Reissner applied this approximation to the case of free axisymmetric transverse vibrations of shallow spherical shells and determined the fundamental frequencies for clamped and free edges⁽²⁾. Recently, an exact analysis for this case was carried out by Kalnins and Naghdi⁽³⁾. Good agreement between the approximate (using Reissner's theory) and exact results for the first two frequencies was found.

In this paper, the nonlinear axisymmetric transverse vibration of shallow spherical shells subjected to uniform external time-dependent normal pressure is investigated. Longitudinal inertia is neglected and the nonlinearity is restricted to the meridional middle surface strain-displacement relation. The normal displacement is expanded in terms of the normal modes for the linear case, and Galerkin's Method is used to obtain a set of nonlinear simultaneous ordinary differential equations relating the generalized coordinates. A simple two degree of freedom nonlinear system which behaves statically similar to a shallow shell is

considered first in order to investigate the nature of dynamic buckling. Then, numerical solutions are obtained for the particular case of a rectangular pressure pulse, using one and also two modes.

NOTATION

The positive directions of the displacement components and coordinates are shown in Figure 1. The notation used in the analysis is listed below for reference:

h = shell thickness

ρ = mass density

E = Young's modulus

ν = Poisson's Ratio

\bar{u}, \bar{w} = meridional, normal displacement components of middle surface

R = spherical radius

\bar{r}_0 = base radius

\bar{r} = radial coordinate

$r = \frac{\bar{r}}{\bar{r}_0}$

$w = \frac{\bar{w}}{h}$

$u = \frac{\bar{r}_0}{h^2} \bar{u}$

\bar{t} = time

$\gamma = R \left(\frac{\rho}{E} \right)^{1/2}$

$t = \frac{1}{\gamma} \bar{t}$ = dimensionless time variable

\bar{p} = external pressure

\bar{p}_{cl} = theoretical elastic buckling pressure for a deep spherical shell $= 2 \left[3(1-\nu^2) \right]^{-1/2} \frac{Eh^2}{R^2}$

p = $\frac{\bar{p}}{\bar{p}_{cl}}$

$\epsilon_\phi, \epsilon_\theta$ = meridional, parallel strains at middle surface

χ_ϕ, χ_θ = meridional, parallel curvatures

T = kinetic energy

U_m, U_B = strain energy due to stretching, bending

PE_s = potential energy of surface forces

α = shallow shell parameter $= \frac{\bar{r}_o}{(Rh)^{1/2}} \left[12 (1-\nu^2) \right]^{1/4}$

$\bar{\alpha}$ = $\frac{\bar{r}_o}{(Rh)^{1/2}}$

$\bar{\omega}_n$ = circular frequency with respect to \bar{t}

μ_n = $\alpha \left[\frac{\bar{\rho} \bar{\omega}_n^2 R^2}{E} - 1 \right]^{1/4}$

ω_n = $\left[1 + \left(\frac{\mu_n}{\alpha} \right)^4 \right]^{1/2} = \gamma \bar{\omega}_n$ = circular frequency with respect to t

$\phi_n(\mu_n, r)$ = characteristic function for linear case

A_n, B_n, C_n = coefficients in expression for $\phi(\mu_n, r)$

$\bar{\phi}_n(\mu_n, r)$ = normalized characteristic function

$\bar{A}_n, \bar{B}_n, \bar{C}_n$ = coefficients in expression for $\bar{\phi}_n$

J_n, I_n = Bessel functions of first kind of real and imaginary arguments

$$\nabla^2 = \frac{\partial^2}{\partial r^2} + \frac{1}{r} \frac{\partial}{\partial r}$$

$$P_n = \frac{1}{\omega_n^2} \left[\frac{2}{3(1-v^2)} \right]^{1/2} \left[\frac{1}{2} \bar{A}_n + \frac{2}{\mu_n} \bar{C}_n J_1(\mu_n) \right]$$

$q_n(t)$ = generalized coordinate

$$\bar{q}_n(t) = \frac{1}{P_n} q_n(t)$$

$$\Theta_{nm} = r \int_0^r \frac{1}{\xi} \bar{\phi}_n' \bar{\phi}_m' d\xi$$

$$\Psi_{nm} = \frac{1}{r} \int_0^r \xi \bar{\phi}_n' \bar{\phi}_m' d\xi$$

$$\gamma_n = \frac{1}{r} \int_0^r \xi \bar{\phi}_n d\xi$$

EQUILIBRIUM EQUATIONS

Lagrangian Functional

The middle surface extensional strains and curvatures are taken as:

$$\begin{aligned}\epsilon_{\theta} &= \frac{\bar{u}}{\bar{r}} - \frac{\bar{w}}{\bar{R}} \\ \epsilon_{\varphi} &= \bar{u}' - \frac{\bar{w}}{\bar{R}} + \frac{1}{2} \bar{w}'^2 \\ \chi_{\varphi} &= -\bar{w}'' \quad \chi_{\theta} = -\frac{1}{\bar{r}} \bar{w}'\end{aligned}\tag{1}$$

where $(\)' = \frac{\partial}{\partial \bar{r}} (\)$

We consider the material to be linear elastic and neglect the strain energy due to transverse shear. Then, the strain energy reduces to:

$$\begin{aligned}U &= U_M + U_B \\ U_M &= \frac{\pi E h}{1-\nu^2} \int_0^{\bar{r}_0} \left[\epsilon_{\varphi}^2 + \epsilon_{\theta}^2 + 2\nu \epsilon_{\varphi} \epsilon_{\theta} \right] \bar{r} d\bar{r} \\ U_B &= \frac{\pi E h^3}{12(1-\nu^2)} \int_0^{\bar{r}_0} \left[\chi_{\varphi}^2 + \chi_{\theta}^2 + 2\nu \chi_{\varphi} \chi_{\theta} \right] \bar{r} d\bar{r}\end{aligned}\tag{2}$$

We neglect the kinetic energy due to the middle surface meridional velocity and also to the rotatory velocity. The first approximation is valid⁽¹⁾ when the frequency of transverse vibration is small compared with the frequency of longitudinal vibration, which is of order $\frac{R}{r_0} \frac{1}{\tau}$

and the second approximation is valid for small h , that is, thin shells. The Kinetic and Potential Energy terms are:

$$T = \pi \rho h \int_0^{\bar{r}_0} \dot{\bar{w}}^2 \bar{r} d\bar{r}\tag{3}$$

$$PE_s = -2\pi \int_0^{\bar{r}_0} \bar{p} \bar{w} \bar{r} d\bar{r} \quad (4)$$

where

$$(\dot{}) = \frac{\partial}{\partial \bar{t}} ()$$

Finally, the Lagrangian Functional is:

$$L = T - U_M - U_B - PE_s \quad (5)$$

Application of Hamilton's Principle

We determine the equilibrium equations by applying Hamilton's Principle, which states that the time integral of the Lagrangian Functional, L , is stationary for variations, $\delta \bar{u}$ and $\delta \bar{w}$, which are arbitrary in the time interval and vanish at the end points. The stationary requirement is:

$$\delta \int_{\bar{t}_1}^{\bar{t}_2} L d\bar{t} = \int_{\bar{t}_1}^{\bar{t}_2} \left[\delta T - \delta U_M - \delta U_B - \delta PE_s \right] d\bar{t} = 0 \quad (6)$$

Substituting for T , U_M , U_B , PE_s , and introducing the dimensionless quantities,

$$\begin{aligned} u &= \frac{\bar{r}_0}{h^2} \bar{u} & w &= \frac{1}{h} \bar{w} & r &= \frac{1}{\bar{r}_0} \bar{r} \\ t &= \frac{1}{\tau} \bar{t} & p &= \frac{\bar{p}}{\bar{p}_{cl}} \end{aligned} \quad (7)$$

the stationary requirement for the case of a clamped shell ($u, w' = 0$ at $r = 0, 1$ and $w = 0$ at $r = 1$) reduces to:

$$\int_{\bar{t}_1}^{\bar{t}_2} \left[\left(\frac{12}{\alpha^4} \right) \int_0^1 \left\{ -\frac{1-\nu}{2} \frac{1}{r} w'^2 + \frac{\partial}{\partial r} \left[(1+\nu) \alpha^2 w \right. \right. \right.$$

$$\begin{aligned}
& - \left(\frac{\beta}{r} + \frac{1}{2} w'^2 \right) \Big] \Big\} r \delta u \, dr \\
& + \int_0^1 \left\{ \ddot{w} + \frac{1}{\alpha^4} \nabla^2 \nabla^2 w + w \right. \\
& + \frac{1}{(1-\nu)\bar{\alpha}^2} \left[(1+\nu) \bar{\alpha}^2 w - \left(\frac{\beta}{r} + \frac{1}{2} w'^2 \right) \right] \\
& + \frac{12}{\alpha^4} \frac{1}{r} \frac{\partial}{\partial r} \left[(1-\nu) u w' + r w' \left((1+\nu) \bar{\alpha}^2 w - \left(\frac{\beta}{r} + \frac{1}{2} w'^2 \right) \right) \right] \\
& \left. - \left[\frac{2}{3(1-\nu^2)^{1/2}} \right] p \right\} r \delta w \, dr \Big] \, dt = 0 \quad (8)
\end{aligned}$$

where $\beta = u + r u' = (ru)'$ (9)

and differentiation is with respect to the dimensionless variables t and r . We do not list the "natural" boundary conditions associated with (8) since we are interested only in the clamped case.

The equilibrium equations for u and w are:

$$\begin{aligned}
& \frac{\partial}{\partial r} \left[(1+\nu) \bar{\alpha}^2 w - \left(\frac{\beta}{r} + \frac{1}{2} w'^2 \right) \right] - \left(\frac{1-\nu}{2} \right) \frac{1}{r} w'^2 = 0 \\
& \ddot{w} + \frac{1}{\alpha^4} \nabla^2 \nabla^2 w + w + \frac{1}{(1-\nu)\bar{\alpha}^2} \left[(1+\nu) \bar{\alpha}^2 w - \left(\frac{\beta}{r} + \frac{1}{2} w'^2 \right) \right] \\
& + \frac{12}{\alpha^4} \frac{1}{r} \frac{\partial}{\partial r} \left\{ (r w') \left[(1-\nu) \frac{u}{r} + (1+\nu) \bar{\alpha}^2 w - \left(\frac{\beta}{r} + \frac{1}{2} w'^2 \right) \right] \right\} \\
& = \left[\frac{2}{3(1-\nu^2)^{1/2}} \right] p \quad (10)
\end{aligned}$$

Solution for u in Terms of w

The D.E. for u is:

$$\begin{aligned} \frac{\partial}{\partial r} \left[(1+\nu) \bar{\alpha}^2 w - \frac{1}{r} (ru)' - \frac{1}{2} w'^2 \right] \\ - \frac{1-\nu}{2} \frac{1}{r} w'^2 = 0 \end{aligned} \quad (11)$$

We integrate (11), multiply by r, and integrate again, obtaining:

$$\begin{aligned} ru = \frac{1}{2} r^2 C_1 + C_2 + (1+\nu) \bar{\alpha}^2 \int_0^r \mathcal{F} w d\mathcal{F} \\ - \frac{1}{2} \int_0^r \mathcal{F} w'^2 d\mathcal{F} - \frac{1-\nu}{2} \int_0^r \mathcal{F} \left[\int_0^r \frac{1}{\mathcal{F}} w'^2 d\mathcal{F} \right] d\mathcal{F} \end{aligned} \quad (12)$$

where \mathcal{F} is a dummy variable.

Now, u must be finite at $r = 0$, and therefore, $C_2 = 0$. We determine C_1 from the requirement that $u = 0$ at $r = 1.0$. The solution for u is:

$$\begin{aligned} u = (1+\nu) \bar{\alpha}^2 \left[\frac{1}{r} \int_0^r \mathcal{F} w d\mathcal{F} - r \int_0^1 r w d r \right] \\ - \left(\frac{1-\nu}{4} \right) \left[r \int_0^r \frac{1}{\mathcal{F}} w'^2 d\mathcal{F} - r \int_0^1 \frac{1}{r} w'^2 d r \right] \\ - \left(\frac{1+\nu}{4} \right) \left[\frac{1}{r} \int_0^r \mathcal{F} w'^2 d\mathcal{F} - r \int_0^1 r w'^2 d r \right] \end{aligned} \quad (13)$$

Substituting for u, the stationary requirement for the clamped case reduces to:

$$\int_{t_1}^{t_2} \left[\int_0^1 \left\{ \bar{w} + \frac{1}{\alpha^4} \nabla^2 \nabla^2 w + w \right. \right.$$

$$\begin{aligned}
& + 2 \left(\frac{1+v}{1-v} \right) \int_0^1 r w \, dr - \left[\frac{2}{3(1-v^2)^{1/2}} \right] p \} r \delta w \, dr \\
& - \frac{2[3(1-v^2)]^{1/2}}{\alpha^2} \int_0^1 \left\{ \left[\frac{1}{2} \left(\frac{1+v}{1-v} \right) \int_0^1 r w'^2 \, dr + \frac{1}{2} \int_0^1 \frac{1}{r} w'^2 \, dr \right. \right. \\
& \quad \left. \left. - \frac{1}{2} \int_0^r \frac{1}{\mathcal{F}} w'^2 \, d\mathcal{F} \right] r \delta w \right. \\
& \quad \left. + \left[\frac{1}{r} w' \int_0^r \mathcal{F} w \, d\mathcal{F} + r w' \left(\frac{1+v}{1-v} \right) \int_0^1 r w \, dr \right] \delta w' \right\} dr \\
& + \frac{3(1-v^2)}{\alpha^4} \int_0^1 \left\{ r w' \left[\int_0^1 \frac{1}{r} w'^2 \, dr + \left(\frac{1+v}{1-v} \right) \int_0^1 r w'^2 \, dr \right. \right. \\
& \quad \left. \left. - \int_0^r \frac{1}{\mathcal{F}} w'^2 \, d\mathcal{F} \right] + \frac{1}{r} w' \int_0^{\mathcal{F}} r w'^2 \, dr \right\} \delta w' \, dr \Big] dt = 0 \quad (14)
\end{aligned}$$

Expansion for w

The normal modes for the linear case are⁽²⁾:

$$w_n(r) = \varphi_n(\mu_n, r) = A_n + J_0(\mu_n r) + B_n I_0(\mu_n r) \quad (15)$$

where

$$B_n = \frac{J_1(\mu_n)}{I_1(\mu_n)}$$

$$A_n = -J_0(\mu_n) - B_n I_0(\mu_n) \quad (16)$$

and μ_n satisfies the following transcendental equation:

$$\mu_n \left\{ 1 - \left(\frac{1-v}{1+v} \right) \frac{\mu_n^4}{\alpha^4} \right\} = - \frac{\mu_n^4 J_1(\mu_n)}{A_n} \quad (17)$$

The normalized characteristic functions are:

$$\bar{\varphi}_n = \frac{1}{C_n} \varphi_n = \bar{A}_n + \bar{C}_n J_0(\mu_n r) + \bar{B}_n I_0(\mu_n r) \quad (18)$$

where

$$\begin{aligned} C_n^2 = \int_0^1 r \varphi_n^2 dr &= \frac{3}{2} A_n \left[\frac{1}{2} A_n + \frac{2}{\mu_n} J_1(\mu_n) \right] \\ &+ \frac{1}{4} \left[J_0(\mu_n) - B_n I_0(\mu_n) \right]^2 \end{aligned} \quad (19)$$

These functions are orthogonal with respect to the weighting function, r ,

$$\begin{aligned} \int_0^1 r \bar{\varphi}_n \bar{\varphi}_m dr &= 0 \quad n \neq m \\ \int_0^1 r \bar{\varphi}_n^2 dr &= 1 \end{aligned} \quad (20)$$

and satisfy the following D.E.:

$$\nabla^2 \nabla^2 \bar{\varphi}_n - \mu_n^4 \bar{\varphi}_n = -\mu_n^4 \bar{A}_n \quad (21)$$

We expand w in terms of the normalized characteristic functions, $\bar{\varphi}_n$.

$$w = \sum_n q_n(t) \bar{\varphi}_n(\mu_n, r) \quad (22)$$

Substituting (22) in (14), and taking $v = 1/3$, we obtain

$$\begin{aligned}
& \int_{t_1}^{t_2} \left[\int_0^1 \left\{ \sum_n \ddot{q}_n \bar{\phi}_n - \frac{(2)^{1/2}}{2} p \right. \right. \\
& \quad \left. \left. + \sum_n q_n \left[\bar{\phi}_n + \frac{1}{\alpha^4} \nabla^2 \nabla^2 \phi_n + \frac{1}{4} \bar{\gamma}_n \right] \right\} r \delta w \, d r \right. \\
& \quad - \left(\frac{32}{3} \right)^{1/2} \frac{1}{\alpha^2} \int_0^1 \left[\left\{ \sum_n \sum_m q_n q_m \left[r \bar{\psi}_{nm} + \frac{1}{2} r \bar{\theta}_{nm} - \frac{1}{2} \theta_{nm} \right] \right\} \delta w \right. \\
& \quad \left. + \left\{ \sum_n \sum_m q_n q_m \left[\gamma_n \bar{\phi}'_m + 2 r \bar{\gamma}_n \bar{\phi}'_m \right] \right\} \delta w' \right] d r \\
& \quad + \frac{8}{3} \frac{1}{\alpha^4} \int_0^1 \left\{ \sum_n \sum_m \sum_p q_n q_m q_p \left[r \bar{\phi}'_p \bar{\theta}_{nm} - \bar{\phi}'_p \theta_{nm} \right. \right. \\
& \quad \left. \left. + \bar{\phi}'_p \bar{\psi}_{nm} + 2 r \bar{\phi}'_p \bar{\psi}_{nm} \right] \right\} \delta w' \, d r \Bigg] d t = 0 \quad (23)
\end{aligned}$$

where

$$\begin{aligned}
\bar{\gamma}_n &= (\gamma_n)_{r=1.0} \\
\bar{\theta}_{nm} &= (\theta_{nm})_{r=1.0} \\
\bar{\psi}_{nm} &= (\psi_{nm})_{r=1.0}
\end{aligned} \quad (24)$$

Equilibrium Equations for Generalized Coordinates

We take $\delta w = \delta q_j \bar{\phi}_j$ and require that the coefficient of δq_j vanish for arbitrary t . The differential equation for \ddot{q}_j has the form

$$\frac{1}{\omega_j^2} \ddot{q}_j + \bar{q}_j - \left(\frac{32}{3} \right)^{1/2} \frac{1}{\omega_j^2} \frac{\mu_j^2}{\alpha^2} \sum_n \sum_m \frac{P_n P_m}{P_j} \bar{q}_n \bar{q}_m \left[\frac{\mu_m}{\mu_j} H_n \bar{Y}_{mj}^* \right]$$

$$\begin{aligned}
& + \frac{\mu_m}{\mu_n \mu_j} Q_{nmj} + \frac{1}{2} H_j \bar{\Psi}_{nm}^* \frac{\mu_n \mu_m}{\mu_j^2} + \frac{1}{2} \frac{\mu_n \mu_m}{\mu_j^3} Q_{jnm} \Bigg] \\
& + \frac{8}{3} \frac{1}{w_j^2} \frac{\mu_j^4}{\alpha^4} \sum_n \sum_m \sum_p \left[\frac{\mu_n \mu_m \mu_p}{\mu_j^3} \right] \left[\frac{P_n P_m P_p}{P_j} \right] \bar{q}_n \bar{q}_m \bar{q}_p \left[S_{nmpj} + 2 \bar{\Psi}_{pj}^* F_{nm} \right] = p \quad (25)
\end{aligned}$$

where

$$\begin{aligned}
q_j &= P_j \bar{q}_j \\
P_j &= \frac{(2)^{1/2}}{2} \frac{\bar{\gamma}_j}{\omega_j} \\
\Psi_{nm}^* &= \frac{1}{\mu_n \mu_m} \Psi_{nm} \\
\Theta_{nm}^* &= \frac{1}{\mu_n \mu_m} \Theta_{nm} \\
F_{nm} &= \bar{\Psi}_{nm}^* + \frac{1}{2} \bar{\Theta}_{nm}^* \\
H_n &= 2 \bar{\gamma}_n + \frac{1}{2} \bar{A}_n \quad (26)
\end{aligned}$$

and

$$\begin{aligned}
Q_{nmj} &= \frac{1}{\mu_j \mu_m \mu_n^3} \int_0^1 \bar{\phi}_j' \bar{\phi}_m' \frac{d}{dr} \nabla^2 \bar{\phi}_n \, dr \\
S_{nmpj} &= \frac{1}{\mu_j \mu_p} \int_0^1 \bar{\phi}_j' \bar{\phi}_p' (\Psi_{nm}^* - \Theta_{nm}^*) \, dr \quad (27)
\end{aligned}$$

Expressions for γ_n and Ψ_{nm} were obtained by integrating the differential equation for $\bar{\phi}_n$; however, Θ_{nm} , Q_{nmj} , and S_{nmpj} must be determined by numerical integration.

The new variable, \bar{q}_j , has been introduced so that the generalized coordinates will be equal for the linear static case, and of order unity for the nonlinear static case. Actually, P_j is the static participation factor and $\bar{\gamma}_j$ is the average deflection or volume change per unit

\bar{q}_j for the j 'th mode. The total decrease in volume under the shell is:

$$\Delta \bar{V} = \frac{V_o - V}{2\pi r_o^2 h} = \sum_n q_n \bar{\gamma}_n = \sum_n P_n \bar{\gamma}_n \bar{q}_n \quad (28)$$

DYNAMIC MODEL

The equilibrium equations for the two degree of freedom system shown in Figure 2 have the same form as (25) when the resistance functions (spring forces) are taken as:

$$\begin{aligned} R_{11} &= a_1 q_1 - a_2 q_1^2 + a_3 q_1^3 \\ R_{12} &= b_1 (q_2 - q_1) + b_2 (q_2 - q_1)^2 \\ &\quad + b_3 (q_2 - q_1)^3 \end{aligned} \quad (29)$$

By studying the behavior of this simple system, we can obtain some indication of the behavior of an actual shell.

Static Behavior

To simplify the analysis, we take $b_2 = b_3 = 0$. The equilibrium conditions are:

$$\begin{aligned} R_{12} &= P_2 \\ R_{11} &= R_{12} \end{aligned} \quad (30)$$

then,

$$P_2 = a_1 q_1 - a_2 q_1^2 + a_3 q_1^3 \quad (31)$$

and

$$q_2 = q_1 + \frac{1}{b_1} P_2 \quad (31)$$

In general, P_2 and q_2 will be single-valued in q_1 . We determine the load-deflection relationship (P_2 vs q_2) by first specifying q_1 , and then computing P_2 and q_2 .

An equilibrium position is unstable with respect to an infinitesimal disturbance when

$$\frac{dP_2}{dq_1} < 0 \quad \text{for a dead weight loading} \quad (32)$$

and

$$\frac{1}{b_1} \frac{dP_2}{dq_1} < -1 \quad \text{for a rigid loading} \quad (33)$$

Then, static instability is possible for a dead weight loading when q_2 is not single valued in P_2 whereas, for a rigid loading, instability will occur when P_2 is not single valued in q_2 or, equivalently, when q_1 is not single valued in q_2 . A typical load-deflection curve for the latter case is shown in Figure 3, and the corresponding Strain Energy - q_2 curve in Figure 4. The segment, A-B, is unstable for a rigid loading and B-C is unstable for a dead weight loading.

Limiting Dynamic Behavior

The D.E.'s for the actual system are:

$$\begin{aligned} m_2 \ddot{q}_2 + b_1 (q_2 - q_1) &= P_2 \\ m_1 \ddot{q}_1 + R_{11} &= b_1 (q_2 - q_1) \end{aligned} \quad (34)$$

where:

$$R_{11} = a_1 q_1 + a_2 q_1^2 + a_3 q_1^3$$

We restrict the analysis to $R_{11} > 0$ for $q_1 > 0$, since the lower buckling pressure for a spherical shell is positive. Also, we consider only the limiting case where $m_1=0$. The D.E.'s reduce to:

$$m_2 \ddot{q}_2 = P_2 - R_{11} \quad (35a)$$

$$q_2 = q_1 + \frac{1}{b_1} R_{11} \quad (35b)$$

Differentiating (35b) with respect to time, and solving for \dot{q}_1 ,

$$\dot{q}_1 = \frac{1}{1 + \frac{1}{b_1} \frac{\partial R_{11}}{\partial q_1}} \dot{q}_2 \quad (36)$$

The velocity, \dot{q}_1 , is infinite at the static stability transition points for a rigid loading (points A and B in Figures 3 and 4).

We can determine \dot{q}_2 as a function of q_2 for the free vibration case using the Principle of Conservation of Energy. The total energy is:

$$E = T + SE = \frac{1}{2} m_2 \dot{q}_2^2 + \frac{1}{2} \frac{1}{b_1} R_{11}^2 + \int_0^{q_1} R_{11}(\xi) d\xi \quad (37)$$

Since the strain energy is multiple valued in q_2 , we must specify q_1 in order to determine \dot{q}_2 . If the initial energy is less than the strain energy for q_{1A} , no discontinuities will occur. However, if the initial energy is greater, a jump will occur when $q_1 = q_{1A}$ and also when $q_1 = q_{1B}$. The total energy and q_2 remain constant⁽⁴⁾ during the jump, $|\dot{q}_2|$ will increase, and q_1 will increase or decrease, depending on whether \dot{q}_2 is positive or negative. A typical integral curve is shown in Figure 5. The path is OAFG for increasing q_2 and GBHO for decreasing q_2 . No jump will occur when q_2 is negative since \dot{q}_1 is always finite.

A jump of this nature cannot occur when m_1 is finite since the velocities and displacements must be continuous. At most, there can only be a discontinuity in acceleration, resulting from a discontinuity in the applied load. The response for an actual system subjected to a

rectangular pulse is shown in Figure 6. The static buckling load for this system is 0.60.

RESULTS

Typical integral curves for $\alpha = 5.0$ and a one mode expansion (first mode) are plotted in Figure 7. Response curves for a rectangular pulse loading, using one and two mode expansions, are plotted in Figures 8 and 9. The latter curves were determined by integrating the Equilibrium Equations numerically. A fourth order Runge-Kutta formula⁽⁵⁾ was employed to start the solution, and a sixth order closed finite difference formula of the Störmer type⁽⁵⁾ to continue the solution. Calculations were carried out on an IBM 1620 digital computer.

A two mode expansion for $\alpha = 7.0$ was also attempted. However, the static behavior for only two modes differed appreciably from the known behavior⁽⁶⁾. The programs are currently being revised to handle a larger number of modes.

REFERENCES

1. Reissner, E., "On Axi-symmetrical Vibrations of Shallow Spherical Shells", Quarterly of Applied Mathematics 13, 279-290 (1955).
2. Reissner, E., "On Transverse Vibrations of Thin Shallow Elastic Shells", Quarterly of Applied Mathematics 13, 169-176 (1955).
3. Kalnins, A., and Naghdi, P.M., "Axisymmetric Vibrations of Shallow Elastic Spherical Shells", Journal of the Acoustical Society of America, Vol 32 (3). 343-347 (1960).
4. Andronow, A.A., and Chaikin, C.E., "Theory of Oscillations", Princeton University Press, 1949.
5. Hildebrand, F., "Numerical Analysis", Mc Graw Hill Book Co., Inc. 1956.
6. Thurston, G.A., "A Numerical Solution of the Nonlinear Equations for Axisymmetrical Bending of Shallow Spherical Shells", Paper presented at Xth International Congress of Applied Mechanics in Stresa, Italy, 1960.

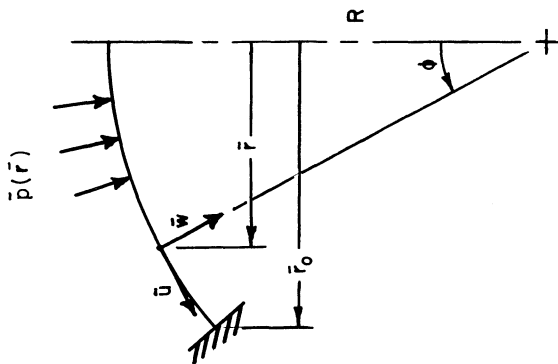


Figure 1.- Notation.

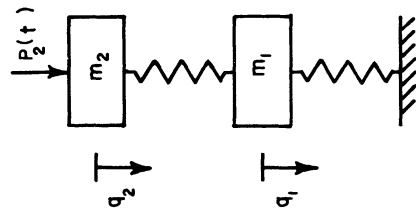


Figure 2.- Model.

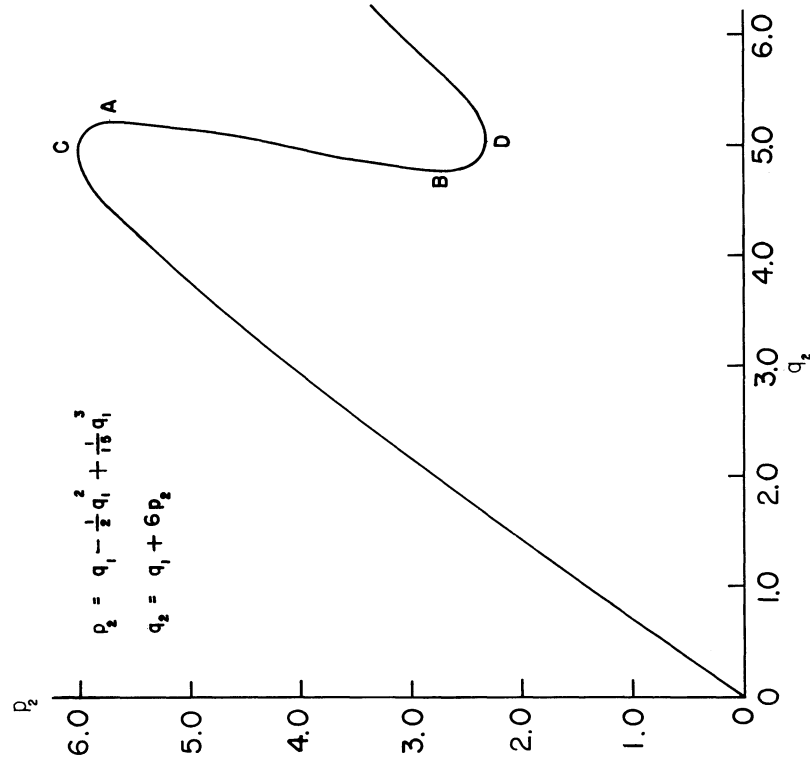
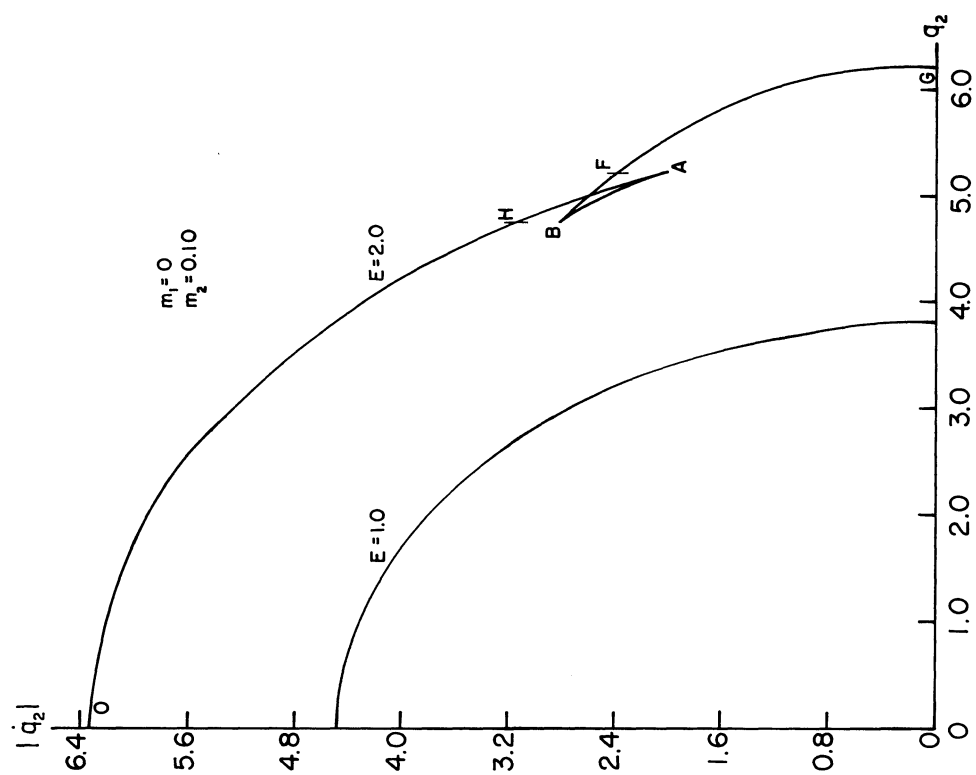
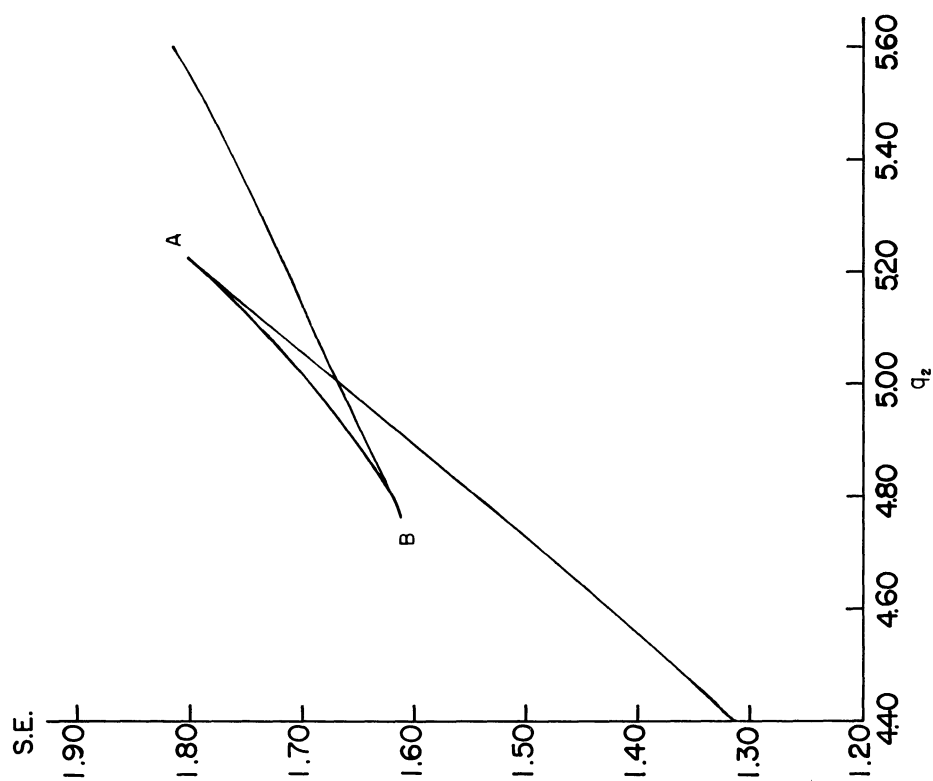


Figure 3.- p_2 versus q_2 , static case.

Figure 5.- Integral curves for q_2 .Figure 4.- Strain energy versus q_2 .

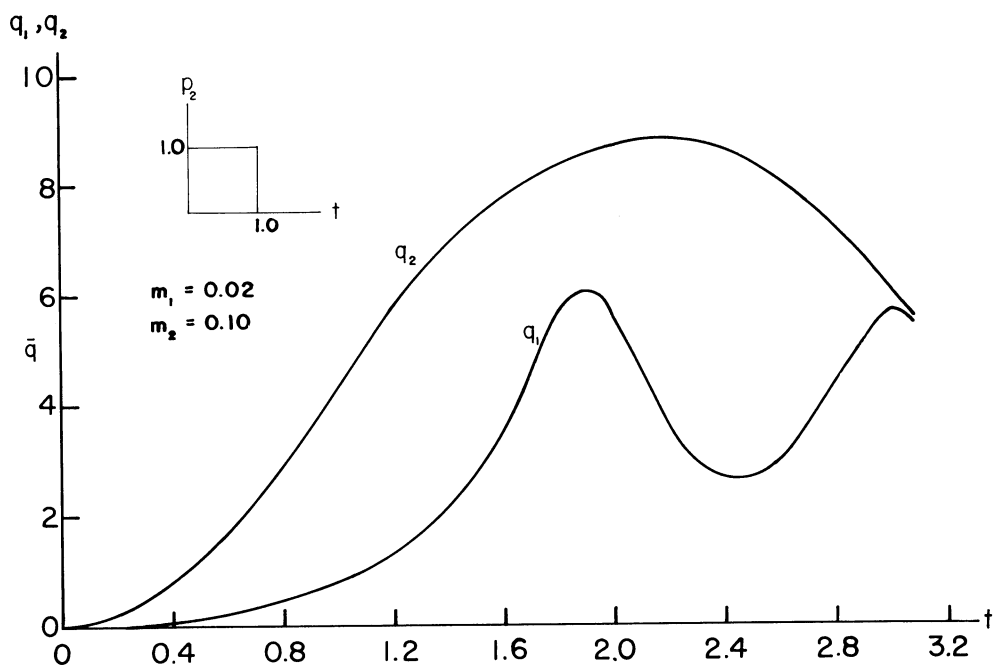


Figure 6.- Response for finite m_1 .

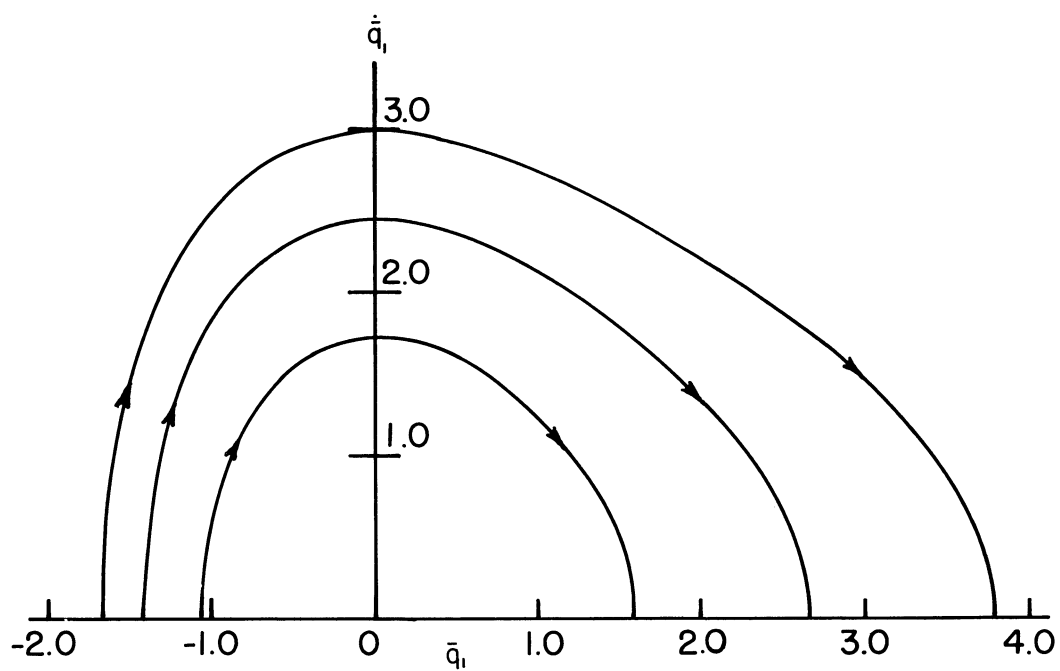
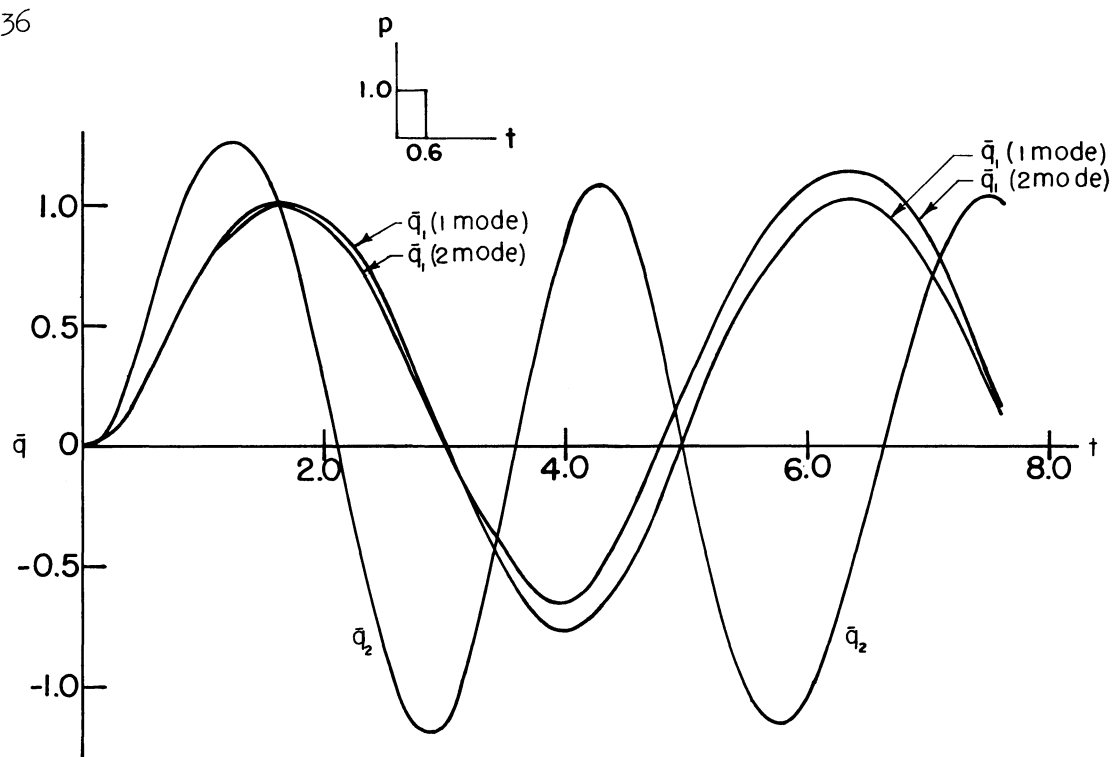
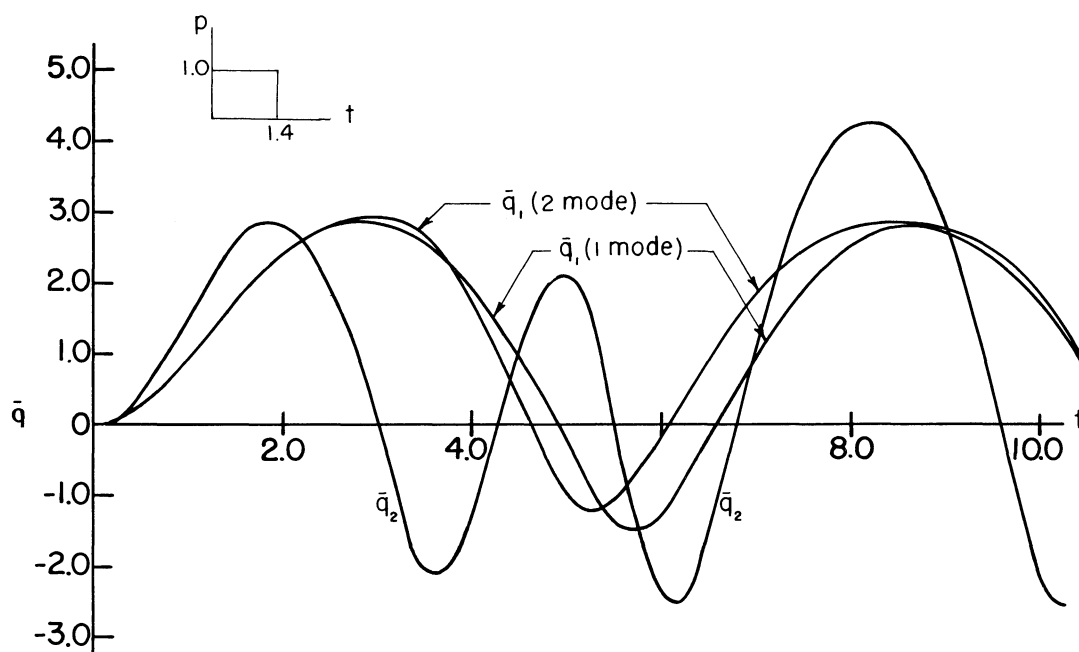


Figure 7.- Integral curves for \dot{q}_1 , $\alpha = 5.0$
(one mode expansion).

Figure 8.- Response for $\alpha = 5.0$.Figure 9.- Response for $\alpha = 5.0$

V OTHER SHELL PROBLEMS

STRUCTURAL INSTABILITY OF SOLID PROPELLANT

ROCKET MOTORS

By Adam R. Zak and Max L. Williams

California Institute of Technology

SUMMARY

A review is made of the literature pertaining to the problem of structural stability of solid propellant rocket motors. Two aspects of this problem, which so far have not received attention, are introduced and discussed. It is shown that the conditions at the ends of the propellant grain can differ sufficiently from those existing in the body of the rocket as to warrant a localized stability analysis. The viscoelastic nature of the real propellant is discussed and the effect of viscoelasticity on the buckling phenomena is illustrated by an example.

INTRODUCTION

The development of the solid propellant rocket motor has brought about many new structural problems associated with the viscoelastic nature of the fuel. In contrast to the well known liquid propellant rocket motor wherein the fuel can exert only a hydrostatic compressive stress on the container, the usual case-bonded solid rocket configuration can transmit both shear and tensile stress across the fuel-to-case interface. The general effect is to stabilize the shell and the general question is to determine by how much and for how long.

Structural loads which promote buckling can occur under a variety of operating conditions, and due consideration must be given to the characteristic sensitivity of the fuel to temperature and strain rate. Some typical properties of the viscoelastic fuel, as determined in constant strain rate uniaxial tension tests, have been published in reference 1 and are shown in figure 1 where the abscissa is the reduced strain rate, Ra_T . This parameter reflects a fortunate occurrence for linear viscoelastic materials in that strain rate and temperature are related in this product quantity when $\log_{10} a_T = \frac{-8.86 (T-297)}{101.6 + T-297}$

with temperature in degrees Kelvin, and a similarity in the glass transition temperatures of the various propellants has been assumed. As to other material characteristics, the fuel is generally assumed incompressible due to the rubberlike composition of the fuel binder,

and the linear coefficient of thermal expansion is typically 5×10^{-5} per deg. F, or an order of magnitude larger than metal.

The incipient buckling situation which suggests itself most obviously is the case when the rocket is subjected to axial compression due to inertia loads, such as when an upper stage, consisting of a solid propellant rocket, is being accelerated by a lower booster. External lateral buckling loads may also be visualized. For example a rocket fired from under water will, for a short time, be subjected to a distributed external lateral pressure. Also a concentrated lateral band of pressure could be produced by the rocket supports during a storage operation or flight carry. Bending moments induced by ground handling or wind shear in flight are also another source of buckling loads.

There are also less obvious sources of buckling loads. For example if the propellant, which is bonded to the case, shrinks during manufacture or curing of the rocket, then resulting compressive stresses arising in the case could produce or help to produce buckling. A similar situation would also arise if the rocket is temporarily exposed to a high temperature environment. The case, which is usually a much better conductor of heat, would then expand faster than the propellant and induce compressive stresses in the case which would be limited by the (radial) tensile strength of the case-bonding.

From the few examples given above it is obvious that a stability analysis can be an important part of the structural design. While the need for such analysis was recognized several years ago, it is just recently that a number of papers dealing with the subject have appeared. It is the purpose of this paper to review the publications in this area and discuss certain aspects of this problem which it is felt need further attention.

REVIEW OF CURRENT WORK

In the simplest idealization, the solid propellant case-bonded rocket is regarded as a cylindrical thin shell filled with a relatively soft elastic core, the core being assumed bonded to the shell and completely or partially filling the cylinder. Under these conditions the theoretical analysis of the structural stability must be carried out for the shell and the core simultaneously. A buckling analysis of empty cylindrical shells is usually difficult, except for most simple configurations and loadings; however, if in addition a simultaneous stability analysis of core is required then the problem becomes considerably more difficult and simplifying assumptions as to the core behavior are mandatory.

The published theoretical analyses of cylindrical shells filled with an elastic core are given in references 2 to 9. Buckling under axial compressive load has received the widest attention and the results of such analysis are given in references 2 to 7. The effects of lateral pressure on stability are analyzed in references 4, 5, 8 and 9, and buckling under combined axial and lateral loads are discussed in references 4 and 5. Buckling under thermal stresses combined with axial compression are treated in references 3 and 6.

Certain experimental buckling investigations have also been conducted and reported in references 10 and 13. References 10, 11 and 12 describe experiments with axially loaded cylinders. Investigation of buckling under combined axial load and uniformly distributed lateral pressure are presented in reference 13, and circumferential band lateral loading is investigated in reference 12.

Experimental results show, see for example reference 12, that the buckling pattern of filled cylinders can be very similar to that of empty shells. Furthermore the snap-through buckling which is a well-known characteristic of cylindrical shell buckling can occur in the presence of a core. This suggests that the large deflection theory, which has been widely used for empty shells, may be necessary to explain buckling of certain core filled shells. Up to the present time all of the theoretical analysis, except for reference 6, have employed small deflection classical buckling theory. Therefore it may prove necessary for further work to be done on the nonlinear aspects of this problem.

The analysis of the core has been treated in various ways with approximations introduced to make the solution tractable. The most complete analysis of the core, treated as a three dimensional body, has been carried out in reference 7 using classical linear elasticity. In order to do an exact analysis it would be necessary to include the nonlinear terms in the strain displacement relations. Such nonlinear terms arise from the fact that the core is bonded to the shell and since the latter undergoes large rotations during buckling, the core would also have undergone similar deformations, at least in the neighborhood of the shell. However a solution to such a nonlinear analysis of the core would most likely be impossible to obtain. A slightly different analysis of the core is given in references 5 and 9, again using a three dimensional analysis. At the boundary between the core and the shell, the radial displacements are matched and the shear is made arbitrarily equal to zero. This treatment of the core, where the shear stresses are taken as zero, apparently gives the same results as the more complete analysis of reference 7. This suggests that shear stress between the case and the core can be neglected in a stability analysis. In turn this suggests that the effect of the core can be represented by an elastic foundation. This type of model was used in

references 4 and 6, although it appears that additional work is necessary to establish how well such a model represents a soft core and how the foundation constant should be calculated.

THE PROBLEM OF END DISCONTINUITIES

In most of the investigations reported in the previous section uniform stress conditions have been assumed in the core and the shell. However in an actual solid propellant rocket there are geometrical discontinuities present which will alter the stress in their neighborhood. If for example we concern ourselves here with a discontinuity of the type which arises at the propellant-case interface at the point where the propellant terminates, the results of a recently completed analysis, reference 14, show that such discontinuities can lead to stress singularities in the propellant. For example the stresses between the propellant, which has the form of a right angle cylinder, and the case have the axial variations shown in figure 2. These curves, which are taken from reference 14, show that, theoretically, an infinite stress will be developed at the end of the grain, and hence, even allowing for finite strain or fillets, high localized stresses might be expected in actual configurations. It should be noted that the constant a in figure 2 is a function of the type of loading which would be applied to the structure. High end stresses in the propellant are also calculated by Parr (reference 15) for a case-bonded rocket subjected to axial acceleration.

High stresses in a propellant will be transferred to the case and if the resultant stresses in the case are compressive then they may produce localized buckling at the ends of the rocket. Hence in such cases it will be necessary to base the stability analysis on the local stress conditions rather than on the average stresses which exist away from the ends and which, if used in the analysis, would lead to incorrect results. For such localized buckling analyses the analytical methods developed in references 6 and 16 would be useful.

THE VISCOELASTIC CORE

Another new area for investigation would explicitly include the character of the solid propellant core. Up to now all the theoretical analyses have assumed an elastic core. The question therefore arises as to the effect on buckling when the actual viscoelastic property is included. In order to obtain some feeling for the time dependent buckling or post buckling behavior we shall investigate the following simple post buckling problem of a cylindrical shell filled with an viscoelastic core.

Consider therefore a cylindrical shell with a case bonded solid core. It is assumed that this shell possesses initial imperfections

which have the same shape as the axisymmetrical buckle pattern produced by axial compression. The problem is to calculate the time dependent deformation history for given values of the load. In passing it is interesting to note that axisymmetric buckling of filled cylindrical shells has actually been observed and reported in reference 10.

For axisymmetric deformation the large deflection strain displacement relations are

$$\epsilon_x = \frac{\partial u}{\partial x} + \frac{1}{2} \left(\frac{\partial w}{\partial x} \right)^2 - z \frac{\partial^2 w}{\partial x^2} \quad (1)$$

$$\epsilon_y = \frac{w}{R} \quad (2)$$

where: x is measured in the axial direction and y in the circumferential, and u is the axial and w the outward radial displacement, z is the distance of any point in the shell from the middle surface.

The stress displacement relations at the middle surface are

$$\sigma_x = \frac{E}{1-\nu^2} \left[\frac{\partial u}{\partial x} + \frac{1}{2} \left(\frac{\partial w}{\partial x} \right)^2 + \nu \frac{w}{R} \right] \quad (3)$$

$$\sigma_y = \frac{E}{1-\nu^2} \left[\frac{w}{R} + \nu \frac{\partial u}{\partial x} + \frac{\nu}{2} \left(\frac{\partial w}{\partial x} \right)^2 \right] \quad (4)$$

where: E is the Young's modulus and ν the Poisson's ratio of the shell material.

The core will be assumed to behave as a simple viscoelastic foundation and therefore there will be no shear stresses acting on the shell. The equilibrium condition in the axial direction gives

$$\frac{\partial \sigma_x}{\partial x} - \sigma_x \frac{\partial w}{\partial x} \cdot \frac{\partial^2 w}{\partial x^2} = 0 \quad (5)$$

Since only the first order terms in u and the second order terms in w have been retained in equations (1) and (2), for consistency the second term in equation (5) must also be neglected and therefore

$$\frac{\partial \sigma_x}{\partial x} = 0$$

and $\sigma_x = -N_x / h = \text{constant}$, where h is the thickness of the shell.

The time dependent relation between the core displacement and the radial force $F(t)$ on the shell can be written as, (see reference 17),

$$F(t) = \int_0^t \frac{\partial w}{\partial \tau} m(t - \tau) d\tau \quad (6)$$

where: t is the time, τ a dummy variable, and $m(t)$ is the relaxation modulus of the core.

The assumption of linear viscoelastic behavior is inherent in equation (6).

Omitting the details, which are similar to those described on page 391 of reference 18, the equilibrium equation for the shell in the radial direction can be written in the following form

$$D \frac{\partial^4 w}{\partial x^4} + N_x \frac{\partial^2 w}{\partial x^2} + \sigma_y \frac{h}{R} + \int_0^t \frac{\partial w}{\partial \tau} m(t - \tau) d\tau = -N_x \frac{\partial^2 w_i}{\partial x^2} \quad (7)$$

where: $D = \frac{Eh^3}{12(1 - \nu^2)}$ and w_i is the initial deformation of the middle surface.

Combining equations (3) and (4) it follows that

$$\sigma_y = E \frac{w}{R} + \nu \sigma_x \quad (8)$$

substituting into equation (7) for σ_y from (8) the radial equilibrium equation becomes

$$D \frac{\partial^4 w}{\partial x^4} + N_x \frac{\partial^2 w}{\partial x^2} + \nu \frac{N_x}{R} + \frac{Eh}{R^2} w + \int_0^t \frac{\partial w}{\partial \tau} m(t - \tau) d\tau = -N_x \frac{\partial^2 w_i}{\partial x^2} \quad (9)$$

The displacement w is now written as

$$w = w_0 + w_1 \quad (10)$$

where: w_0 is an average value of w and w_1 is a periodic component in x . The initial displacement w_1 will be assumed as a periodic function of x and therefore substituting for w from equation (10) into (9) and integrating over the whole length of the cylinder it is easily seen that

$$\sqrt{\frac{N_x}{R}} + \frac{Eh}{R^2} w_0 + \int_0^t \frac{\partial w_0}{\partial \tau} m(t - \tau) d\tau = 0 \quad (11)$$

Subtracting equation (11) from (9) and taking Laplace transforms it follows that

$$D \frac{\partial^4 \bar{w}}{\partial x^4} + N_x \frac{\partial^2 \bar{w}}{\partial x^2} + \frac{Eh}{R^2} \bar{w} (1 + \frac{R^2}{Eh} m(P)) = - \frac{N_x}{P} \frac{\partial^2 w_1}{\partial x^2} \quad (12)$$

where: \bar{w} is the Laplace transform of w_1 and $m(P)$ the transform of $m(t)$, P is the transform variable.

It is now assumed that the initial deformation has the form

$$w_1 = A_1 \sin \lambda x \quad (13)$$

where: A_1 is a constant and λ defines the wavelength of w_1 .

The parameter λ will be chosen so that it corresponds to the lowest axisymmetric buckling load. The classical buckling load has to be calculated using the long time, or the rubbery modulus, of the elastic core. The reason for this is that the classical buckling theory allows only for infinitesimal deflections which can be formed in a very short time with very small rates of strain and therefore will not be affected by viscoelastic properties of the foundation. We can therefore define a critical value of N_x by

$$N_{xcr} = \frac{1}{\lambda^2} \left[D \lambda^4 + \frac{Eh}{R^2} + m_e \right] \quad (14)$$

The value of λ is such that N_{xcr} is a minimum.

Substituting equation (13) into (12) and assuming a solution for w_1 as

$$w_1 = A(t) \sin \lambda x \quad (15)$$

it follows that

$$\bar{A} \left[D \lambda^4 - N_x \lambda^2 + \frac{Eh}{R^2} + m(P) \right] = \frac{N_x A_o \lambda^2}{P} \quad (16)$$

where: \bar{A} is the Laplace transform of $A(t)$.

From (16)

$$\frac{\bar{A}}{A_i} = \frac{N_x \lambda^2}{P} \cdot \frac{1}{D \lambda^4 - N_x \lambda^2 + \frac{Eh}{R^2} + m(P)} \quad (17)$$

By carrying out the inverse transformation of equation (17) the postbuckling displacement w_1 will be obtained. For general viscoelastic materials the form of the function $m(P)$ would be such that the exact inverse of equation (17) would be very difficult to obtain. In such cases approximate inversion techniques could be used, for example the approximate methods developed in reference 19 would be most suitable for this purpose. In this paper, however, we shall assume that the elastic foundation can be represented by a simple viscoelastic model shown in figure 3 and therefore an exact inverse of equation (17) will be possible. For this model

$$m(P) = m_e + \frac{m_1 \tau_1 P}{\tau_1 P + 1} \quad (18)$$

Substituting equation (18) into (17) and rearranging it follows

$$\frac{\bar{A}}{A_i} = \frac{\gamma}{1-\gamma} \left[\frac{1}{P} - \frac{1-\alpha}{P + \frac{\alpha}{\tau_1}} \right] \quad (19)$$

where:

$$\alpha = \frac{1-\gamma}{1-\gamma + \frac{m_1}{N_{xc} \lambda^2}} \quad \text{and} \quad \gamma = \frac{N_x}{N_{xc}}$$

The inverse transform of (19) is obvious

$$\frac{A(t)}{A_i} = \frac{\gamma}{1-\gamma} \left[1 - (1-\alpha) e^{-\alpha \frac{t}{\tau_1}} \right] \quad (20)$$

Equation (20) will now be used to evaluate the variation of displacements with time for a particular shell configuration.

We assume that for this shell:

$$E = 30 \times 10^6 \text{ psi}$$

$$\nu = 0.3$$

$$\frac{R}{h} = 10^3$$

$$\text{and } R = 30 \text{ in.}$$

The core is assumed to be a solid propellant of the type described in reference 20, page 395, and designated in that reference by HA. The relaxation modulus of this propellant at 25°C is shown in figure 4. For the purpose of our calculation this propellant is approximated by a viscoelastic model, similar to the one shown in figure 3, where E_e , E_1 and τ_1 are now the defining parameters of the model. Choosing $E_e = 158$ psi, $E_1 = 17,640$ psi and $\tau_1 = 10$ minutes the approximate curve shown in figure 4 is obtained.

The next step is to obtain the relation between the constant for the viscoelastic foundation m_e and m_1 and the parameters E and E_1 . In order to obtain these relations it will be assumed that plane stress conditions exist in the core. This is a rather conservative assumption since as a result of it the postbuckling deflection will be larger than those which actually exist. We justify making this assumption on the basis that we are interested here in relative effects of viscoelasticity of the core and not exact numerical answers. Using the plane stress condition, and assuming that the Poisson's ratio of the core material is equal to 0.5, it is shown in the Appendix that

$$\bar{\sigma}_r = \frac{2E(P)}{R} \bar{w} \quad (21)$$

where; $\bar{\sigma}_r$ is the Laplace transform of the radial stress between the core and the shell, and $E(P)$ is the transform of the relaxation modulus of the core material.

It now follows from equation (6) that

$$m(P) = \frac{2E(P)}{R}$$

and therefore

$$m_e = \frac{2E_e}{R} = 10.5 \text{ psi/in} \quad (22)$$

and

$$m_1 = \frac{2E_1}{R} = 1177 \text{ psi/in} \quad (23)$$

where: where m_e and m_1 are the spring constants of the model in figure 3.

The value of λ , which makes N_{xcr} a minimum, can now be evaluated and it is equal to 1.915. Using this value of λ , N_{xcr} can be calculated and therefore equation (20) can now be written as

$$\frac{A(t)}{A_i} = \frac{\gamma}{1-\gamma} \left[1 - \frac{0.6}{1.6-\gamma} e^{-\left(\frac{1-\gamma}{1.6-\gamma}\right) \frac{t}{\tau_1}} \right] \quad (24)$$

Equation (24) can now be used to investigate the time history of the radial displacement of the shell for various values of the load parameter γ .

Numerical Results

Recalling that $\gamma = N_x/N_{xcr}$, equation (24) has been evaluated for $\gamma = 0.8, 1.0$ and 1.2 . The results of these calculations are presented in figure 5. The results indicate that if γ is less than one, that is N_x is below the critical value, then the displacement approaches the equilibrium value exponentially with time. In the case when $\gamma = 1$, that is $N_x = N_{xcr}$, the displacement will go to infinity as a linear function of time. When the critical buckling load is exceeded, for example $\gamma = 1.2$, then the displacement will again approach infinite value but now as a positive exponential of time. It should be noted that when $\gamma = 1.6$ then the displacement becomes infinite instantaneously. The reason for this is the load has reached the critical value based on the glassy modulus of the material and corresponding to the value of $\lambda = 1.915$.

The interesting conclusion to be drawn from these calculations is that the displacement is strongly dependent on time, especially in the vicinity of $\gamma = 1$. Furthermore the load can equal or exceed the critical value, based on rubbery modulus, without causing instantaneous infinite deflections which would be predicted if viscoelastic behavior is omitted. It is also interesting to note that the order of magnitude of time t in figure 5 is in terms of minutes. Such times are comparable with times of operation of many rocket systems and therefore viscoelastic effects may sufficiently retard the postbuckling deformations to allow the structure to operate near the buckling point or even above it until the mission has been accomplished. These results suggest that further investigations of buckling of shells with a viscoelastic core could be most fruitful.

ACKNOWLEDGMENT

The preparation of this report was partially supported by the U. S. Army Ordnance under Contract No. DA-04-495-Ord - 1985; GAL-CIT SM 62-41, in conjunction with committee activities of the Physical Properties Panel of the JANAF Solid Propellant Information Agency.

APPENDIX

Relaxation Modulus of the Viscoelastic Foundation

It is assumed that the Poisson's ratio ν of the viscoelastic core is a constant and therefore under plane stress conditions the stress strain relations, in the Laplace transform plane, are

$$\bar{\sigma}_r = \frac{E(P)}{1 - \nu^2} (\bar{\epsilon}_r + \nu \bar{\epsilon}_\theta) \quad (1. A.)$$

$$\bar{\sigma}_\theta = \frac{E(P)}{1 - \nu^2} (\bar{\epsilon}_\theta + \nu \bar{\epsilon}_r) \quad (2. A.)$$

where: the bar indicates the Laplace transform of a quantity and $E(P)$ is the transform of the relaxation modulus, $\bar{\sigma}_r$, $\bar{\sigma}_\theta$, $\bar{\epsilon}_r$ and $\bar{\epsilon}_\theta$ are the stresses and strains in the usual polar coordinate system.

The strain-displacement relations at any radial distance r , also in the transformed plane, have the form

$$\bar{\epsilon}_r = \frac{\partial \bar{w}}{\partial r} \quad (3. A.)$$

$$\bar{\epsilon}_\theta = \frac{\bar{w}}{r} \quad (4. A.)$$

where: w is the radial displacement at any point in the core.

The equilibrium equation is

$$\frac{\partial \bar{\sigma}_r}{\partial r} + \frac{\bar{\sigma}_r - \bar{\sigma}_\theta}{r} = 0 \quad (5. A.)$$

Using equation (1. A.) to (4. A.) the equilibrium equation (5. A.) can be written in terms of \bar{w}

$$\frac{\partial^2 \bar{w}}{\partial r^2} + \frac{1}{r} \frac{\partial \bar{w}}{\partial r} - \frac{\bar{w}}{r^2} = 0 \quad (6. A.)$$

Solution to equation (6. A.) for a solid core is

$$\bar{w} = Ar \quad (7. A.)$$

The radial stress can be written in terms of the solution for w , from equation (1. A.),

$$\bar{\sigma}_r = \frac{E(P)}{1-\nu} A \quad (8. A.)$$

Using equations (7. A.) and (8. A.) the radial stress can now be related to the radial displacement at $r = R$, assuming $\nu = 1/2$,

$$\frac{\bar{\sigma}_r}{\bar{w}}_{r=R} = \frac{2E(P)}{R} \quad (9. A.)$$

Equation (9. A.) defines the relaxation modulus for the viscoelastic foundation in the transformed plane.

$$m(P) = \frac{2E(P)}{R} \quad (10. A.)$$

REFERENCES

1. Williams, M. L., Blatz, P. J. and Schapery, R. A.: Fundamental Studies Relating to Systems Analysis of Solid Propellants. GALCIT SM 61-5. California Institute of Technology, February 1961. p. 88-90.
2. Seide, P.: On the Axisymmetric Buckling Under Axial Load of a Long Thin Cylindrical Shell Containing an Elastic Core. GM-TR-0165-00409 (EM 8-12), 25 June 1958
Space Technology Laboratories, Inc.
3. Zak, A. R., and Bollard, R. J. H.: Buckling of Thin, Short Cylindrical Shells Filled with an Elastic Core. Developments in Mechanics, Vol. 1. Proceedings of the 7th Midwestern Mechanics Conference, September 1961.
4. Brush, D. O., and Almroth, B. O.: Buckling of Core-Stabilized Cylinders Under Axially-Symmetrical External Loads. Lockheed Missiles and Space Co., LMSC 6-90-62-6, January 1962.
5. Seide, P.: The Stability under Axial Compression and Lateral Pressure of Circular-Cylindrical Shells with a Soft Elastic Core. Presented at IAS 30th Annual Meeting, New York, January 1962.
6. Zak, A. R., and Bollard, R. J. H.: Elastic Buckling of Cylindrical Thin Shells Filled with an Elastic Core. ARS Journal, Vol. 32, April 1962.
7. Yao, J. C.: Buckling of Axially Compressed Long Cylindrical Shell with Elastic Core. Journal of Applied Mechanics, Vol. 29, June 1962.
8. Seide, P., and Weingarten, V. I.: The Buckling under Uniform External Pressure of Circular Rings and Long Cylinders Enclosing an Elastic Material. GM - TR - 59-0000-00872 (EM 9-25), November 1959, Space Technology Laboratories, Inc.
9. Seide, P., and Weingarten, V. I.: Buckling of Circular Rings and Long Cylinders Enclosing an Elastic Material under Uniform External Pressure. ARS Journal, Vol. 32, May 1962.
10. O'Neal, A. P.: Preliminary Results of Compression Test-Sustainer Motor Case, DM-15.

(cont.)

Memorandum A 260 - STRE - 214, Missile and Space Systems Engineering, Douglas Aircraft Company. Santa Monica, California, 1959.

11. Kachman, D. R.: Test Report on Buckling of Propellant Cylinders under Compressive Loads.
GM - 59 - 7520. 6-24, November 1959, Space Technology Laboratories, Inc.
12. Goree, W. S., and Nash, W. A.: Elastic Stability of Circular Cylindrical Shells Stabilized by a Soft Elastic Core.
Experimental Mechanics, Vol. 2, May 1962.
13. Fitzgibbon, D. P.: Preliminary Results of Sub-Scale Tests on Cylinders Filled with an Elastic Core.
GM - 6- - 7520. 6-11, April 1960
Space Technology Laboratories, Inc.
14. Zak, A. R.: Stress Singularities in Bodies of Revolution
GALCIT SM 62-29, California Institute of Technology, July 1962.
(Submitted for Publication in Journal of Applied Mechanics).
15. Parr, C. H.: Stresses in a Solid Propellant Rocket under Axial Acceleration.
Rohm and Haas Company, Huntsville, Alabama
(Private Communication).
16. Weingarten, V. I.: The Buckling of Cylindrical Shells under Longitudinally Varying Loads.
Journal of Applied Mechanics, Vol. 29, March 1962.
17. Leaderman, H.: Proposed Nomenclature for Linear Viscoelastic Behavior.
Transactions of the Society of Rheology, Vol. 1, 1957, p. 213
18. Timoshenko, S.: Theory of Plates and Shells.
McGraw-Hill Book Co., Inc., New York, 1st Edition 1940, p. 391.
19. Schapery, R. A.: Two Simple Approximate Methods of Laplace Transform Inversion for Viscoelastic Analysis.
GALCIT SM 61-23, California Institute of Technology
November 1961.
20. Kruse, R. B.: The Role of Broad-Spectrum Mechanical Response Studies in Propellant Evaluation.
JANAF Physical Properties Panel (SPIA/APL - Johns Hopkins University) 20th Meeting Bulletin, Vol. 1, October 1961, p. 395

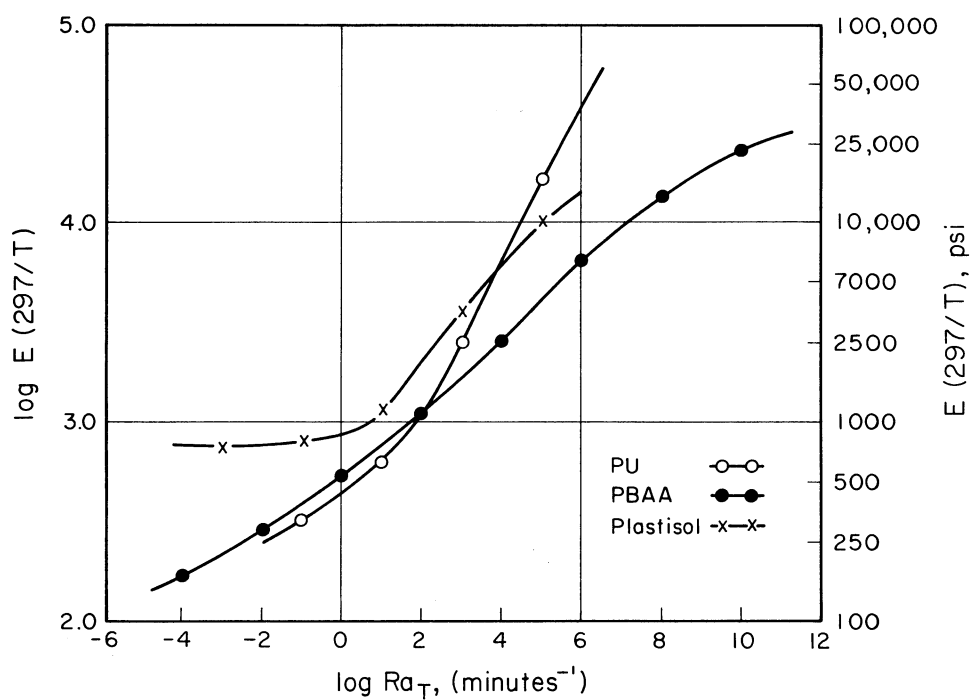


FIGURE 1.a NORMALIZED MODULUS VARIATION WITH REDUCED STRAIN RATE.

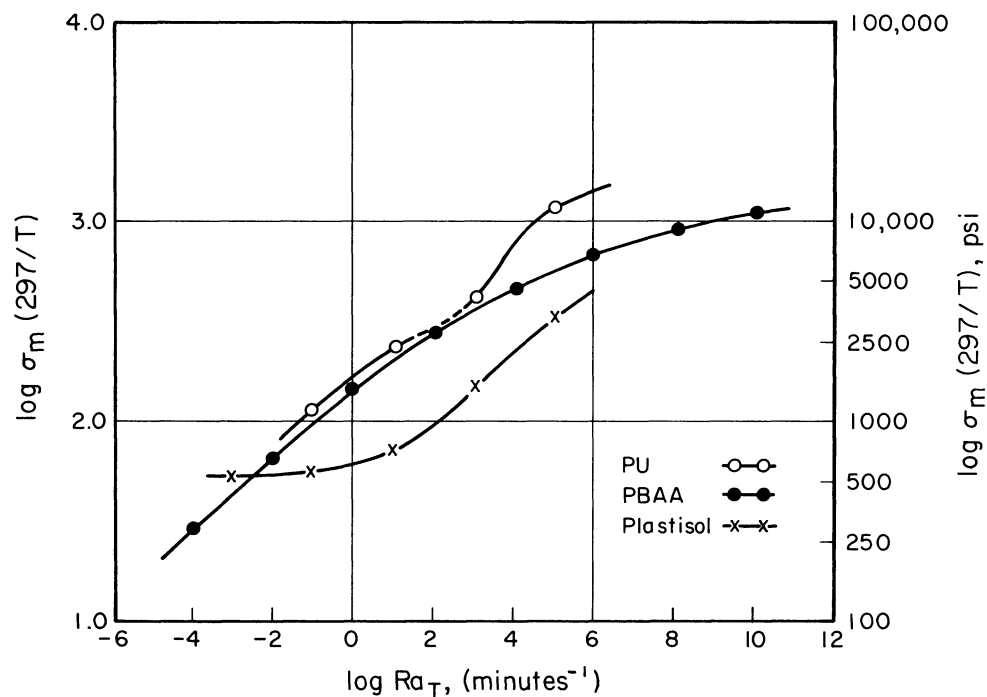


FIGURE 1.b NORMALIZED MAXIMUM TENSILE STRENGTH VARIATION WITH REDUCED STRAIN RATE.

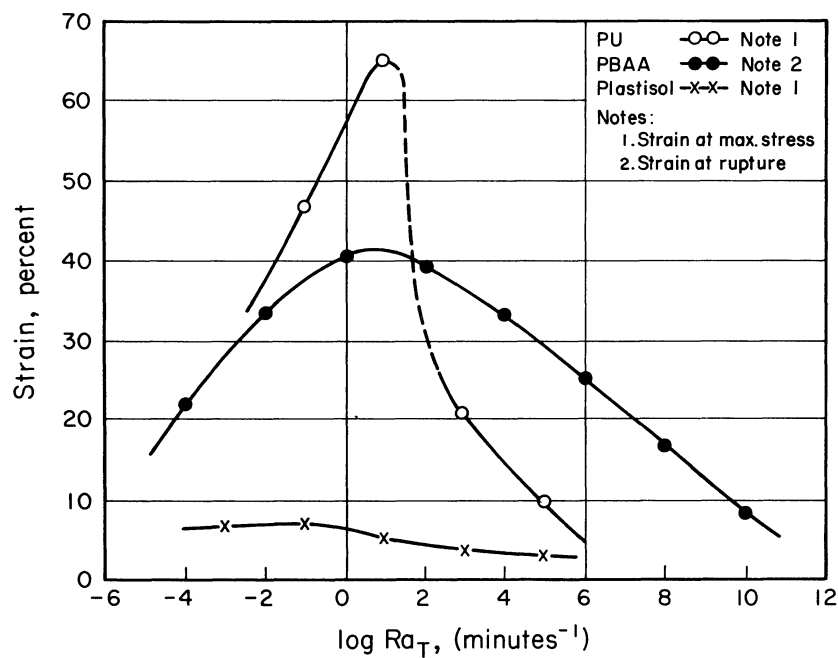


FIGURE 1.c CRITICAL STRAIN VARIATION WITH REDUCED STRAIN RATE.

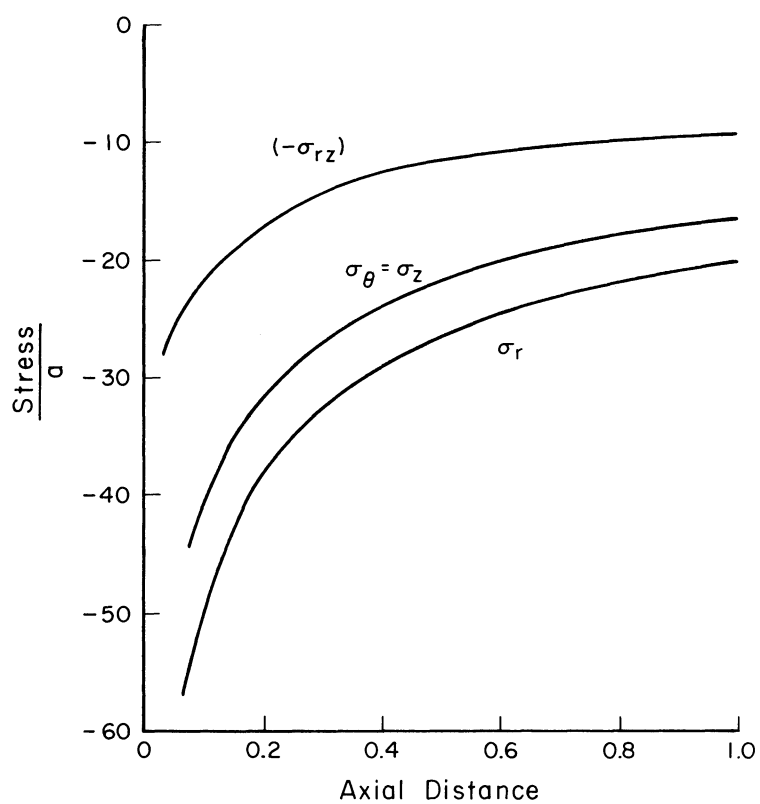


FIGURE 2. STRESSES BETWEEN THE PROPELLANT AND THE CASE.

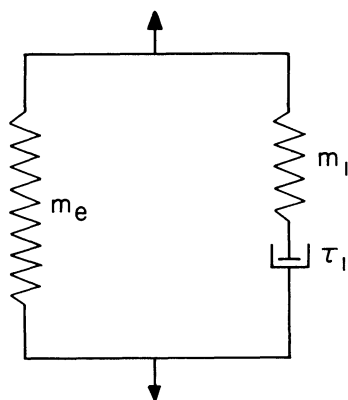


FIGURE 3. VISCOELASTIC MODEL FOR THE CORE.

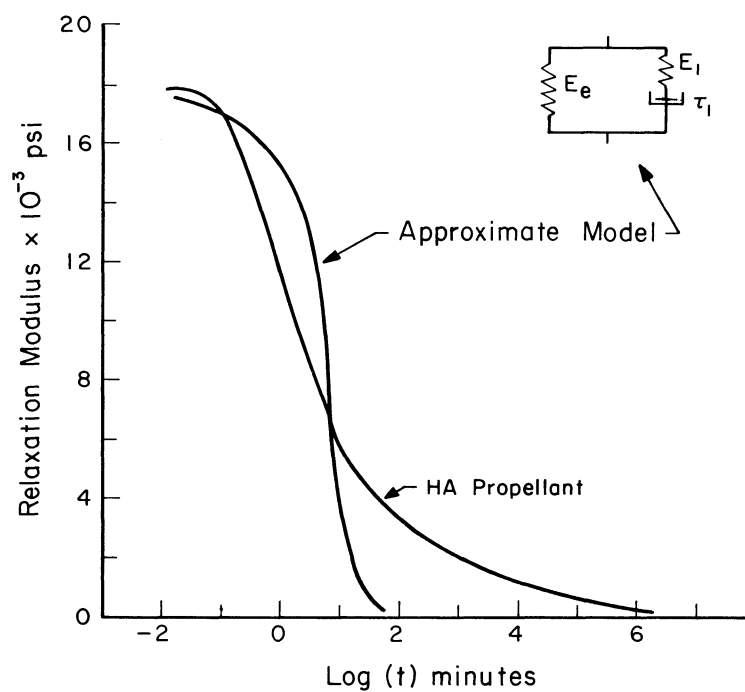


FIGURE 4. REAL AND APPROXIMATE RELAXATION MODULUS.

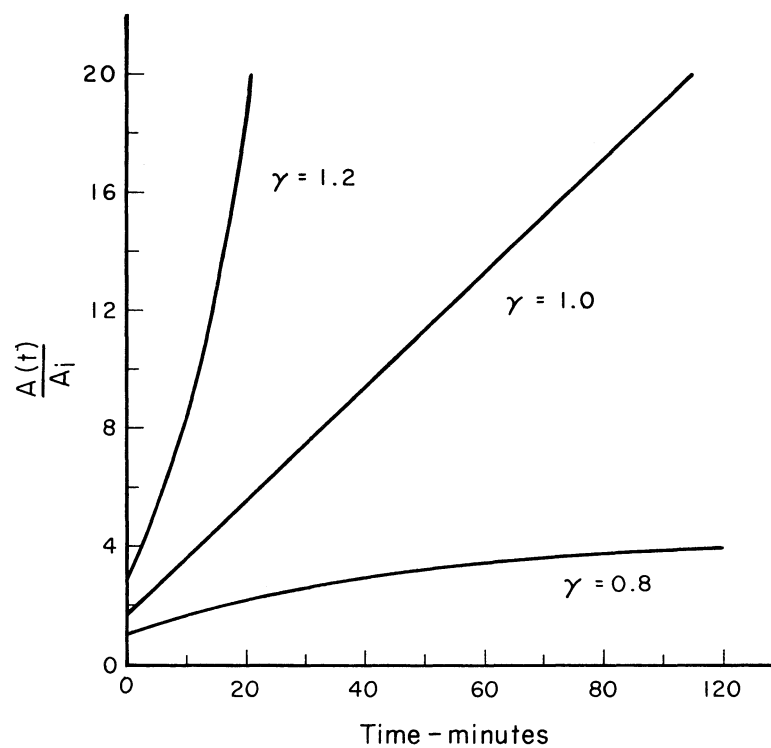


FIGURE 5. VARIATION OF DISPLACEMENT WITH TIME.

SIMILITUDE REQUIREMENTS FOR SCALE MODEL DETERMINATION OF SHELL BUCKLING UNDER IMPULSIVE PRESSURES

By Arthur A. Ezra

Martin Company, Denver, Colorado

SUMMARY

An analysis is made of the similitude requirements for scale model determination of the buckling of a thin shell structure of arbitrary shape and thickness under impulsive pressure loading, where the duration of the impulsive pressure is not short enough for it to be idealized as a pure impulse, nor long enough to be treated like a static pressure.

It is shown that if the same material is used for both model and prototype, then the magnitude of the applied pressure pulse must be the same for both and the duration must be scaled down in proportion to model size. If the magnitude and duration of the pressure pulse on the model cannot be controlled to these values, it is still possible to provide complete similitude for the pressure pulse by a suitable choice of a different materials for the model. In this case it becomes difficult to satisfy in addition the similitude requirements for Poisson's ratio and yield stress. However, if the problem is clearly one of elastic buckling, the result may not be strongly dependent on Poisson's ratio and yield stress so that a valid scale model test may still be achieved.

INTRODUCTION

It is well known that a pressure considerably larger than that which produces static buckling can be applied safely on a shell structure, provided that the duration is sufficiently short. On the other hand if a pressure is applied sufficiently rapidly and the duration is long enough, the structure may be expected to carry even less than it would statically. How to take advantage of the former situation and yet avoid the pitfall of the latter situation is the problem confronting the engineer when trying to design a minimum weight shell structure subjected to applied impulsive pressures.

Some difficulty exists in even defining the buckling impulse of a shell structure, let alone predicting it mathematically. A clarification of definitions for the purpose of this discussion is therefore in order. In this text, the impulse I will actually refer to a pressure impulse and is defined mathematically as $I = \int_0^T p dt$ where p is the magnitude of the impulsive pressure and T is the duration. A pure impulse is a mathematical idealization of an impulsive pressure and is defined as $\lim_{T \rightarrow 0} \int_0^T p dt$. The shape of the pressure-time diagram is important too, since for the same total impulse a more rapid build up to peak pressure will produce a greater structural response than a slower application of pressure. For a precise definition of impulsive pressures therefore, the entire pressure-time history must needs be specified.

Since for a given magnitude of impulse I there is no unique pressure-time relationship, it is not reasonable to ask for the maximum impulse, a particular shell structure will withstand without buckling. A more realistic statement of the buckling problem would be to ask the question: given an impulsive pressure with a particular pressure time history, will it buckle the shell structure? Here again a further clarification of shell buckling under impulsive pressures is necessary. A buckle may appear and then disappear after the pressure dies down. Should this be the definition of buckling? If the material is ductile, the engineer's answer would be no, implying that the load carrying capability is unimpaired. If a permanent buckle remains, then this is unquestionably a buckled condition. If the existence of a permanent buckle is accepted as the definition of buckling, this again emphasizes the difficulty of trying to define a buckling impulse for a structure. A lesser impulse may cause a buckle of smaller size and a larger impulse would cause a buckle of larger size. In order to make the definition unambiguous, the magnitude of a buckling impulse would have to be tied to the size of buckle or be defined as that impulse which would cause a permanent buckle of the smallest possible size. This illustrates the advisability of restating the problem to determine whether a particular shell structure will buckle or not under a given impulsive load.

The purpose of this paper is therefore directed towards the problem of answering, by means of scale model testing, whether a particular full scale thin shell structure will buckle or not under a prescribed impulsive pressure loading. The similitude requirements necessary to ensure valid results from a scale model test will therefore be derived.

DERIVATION OF SIMILITUDE REQUIREMENTS

It is possible to derive all the similitude requirements from a knowledge of the variables in the problem and their basic dimensions in terms of mass (M), length (L) and time (T). They are listed below along with their basic dimensions, and also shown for purposes of illustration in Fig. 1.

Variables	Dimensions
p = Impulsive pressure loading at any point on shell surface	$ML^{-1}T^{-2}$
T = Duration of impulsive pressure at any point on shell surface	T
h = Thickness of shell at any point of shell surface	L
R_1, R_2 = Radii of curvature at any point of shell surface	L
H = Height of shell structure	L
D = Diameter of shell opening	L
β = Semi-angle of shell opening	-
γ = Density of shell material	ML^{-3}
σ = Yield stress of shell material	$ML^{-1}T^{-2}$
E = Modulus of elasticity of shell material	$ML^{-1}T^{-2}$
ν = Poisson's ratio	-
P = Static internal pressure contained by the shell structure	$ML^{-1}T^{-2}$

The 13 variables may be combined into 10 dimensionless parameters since there are three basic dimensions (mass, length, time) in the problem. They are the following:

$$\begin{aligned}
 \pi_1 &= p/E \\
 \pi_2 &= T\sqrt{E/\delta D^2} \\
 \pi_3 &= R_1/D \\
 \pi_4 &= R_2/D \\
 \pi_5 &= D/h \\
 \pi_6 &= H/D \\
 \pi_7 &= \nu \\
 \pi_8 &= \beta \\
 \pi_9 &= \sigma/E \\
 \pi_{10} &= P/E
 \end{aligned}$$

The physical law expressing the buckling condition may be expressed as a function of the impulse and all the other variables pertaining to the structure in the following dimensionless form

$$F(p/E, T\sqrt{E/\delta D^2}, R_1/D, R_2/D, D/h, H/D, \nu, \beta, \sigma/E, P/E) = 0 \quad (1)$$

where F is some unknown function.

If all the dimensionless quantities in the parenthesis are made to have the same value in the model as they do in the prototype, then the buckling condition will be identical for both since the physical law, represented by the function F , is the same for both.* Thus the similitude requirements (or scale factors for the variables) are determined by making each of the dimensionless quantities in equation (1) the same for both model and prototype.

Since there are three basic dimensions in the problem (i.e. mass, length, and time), three scale factors may be chosen arbitrarily. All other scale factors will then be expressed in terms of them. Let the

*Providing the boundary conditions are the same for both.

three arbitrary scale factors be the following (the subscripts m and p refer to model and prototype, respectively):

$$(1) \quad n_1 = D_p/D_m$$

$$(2) \quad n_2 = \gamma_p/\gamma_m$$

$$(3) \quad n_3 = E_p/E_m$$

The scale factors expressing similitude requirements for the variables are therefore the following:

$$(4) \quad p_m = p_p/n_3$$

$$(5) \quad T_m = T_p \sqrt{n_3}/n_1 \sqrt{n_2}$$

$$(6) \quad R_{1m} = R_{1p}/n_1$$

$$(7) \quad R_{2m} = R_{2p}/n_1$$

$$(8) \quad H_m = H_p/n_1$$

$$(9) \quad h_m = h_p/n_1$$

$$(10) \quad \beta_m = \beta_p$$

$$(11) \quad \nu_m = \nu_p$$

$$(12) \quad \sigma_m = \sigma_p/n_3$$

$$(13) \quad P_m = P_p/n_3$$

SATISFACTION OF SIMILITUDE REQUIREMENTS

The scale factors (4) through (13) which express the similitude requirements for the variables in the problem are the most restrictive set, derived on the basis of no knowledge whatever of the nature of the function F in equation (1).

Scale factor (4) prescribes the magnitude of the impulsive pressure to be applied to the model. If the same material is used for both model and full scale, then $n_3 = 1$ and the same magnitude of pressure must be used for both. If a reduced pressure has to be used for a model test then the arbitrary scale factor n_3 must be chosen to have a value larger than 1. This can be done by using different materials for the model and prototype. For example if only half the prototype pressure can be provided for the model test, then the material for the model must have a modulus of elasticity half that of the prototype. However, it may then become difficult or impossible to satisfy simultaneously scale factor (11) for Poisson's ratio and scale factor (12), which is the similitude requirement for yield stress.

Scale factor (5) dictates the similitude requirements for the duration of the impulsive pressure. It can be seen that if the same material is used for both model and prototype i.e. $n_2 = n_3 = 1$ then the model pressure duration must be reduced in proportion to model size. If the durations of model impulsive pressure cannot be controlled, then dissimilar materials must be used for model and prototype and the length scale factor adjusted so as to satisfy scale factor (5). Again, difficulties may arise in simultaneously satisfying scale factors (11) and (12). The possibilities of scale model testing using dissimilar materials is discussed in more detail later.

Scale factors (6), (7), (8), (9) and (10) are concerned with providing geometrical similitude between model and prototype. The only difficulties to be anticipated here are the usual fabrication ones, and will not be discussed in detail.

Scale factor (13) provides the similitude requirements for the internal pressurization of the shell structure. This is easy to satisfy experimentally. When the shell buckles, the contained volume decreases and the internal pressure may rise appreciably. However, Koval (1) has shown in his work on the cylinder that this has no appreciable effect on the buckling load.

The degree of boundary restraint of the shell structure may have an appreciable effect on its resistance to buckling. Unless the boundaries of the full scale structure are either unrestrained or completely restrained, it is not an easy matter to define precisely the actual degree of restraint, let alone attempt to provide similitude requirements for them. However, it is a relatively simple matter to provide for the limiting cases of no restraint and full restraint in a scale model. The desired result falls between these two limiting cases and the most feasible experimental approach is to either conduct scale model tests at these extremes or choose that boundary condition for the model which will give conservative results.

USE OF DIFFERENT MATERIALS IN MODEL AND PROTOTYPE

The need for using different materials in model and prototype arises only if the same magnitude of impulsive pressure cannot be used for both, or if the duration of the impulsive pressure cannot be scaled down in proportion to model size, or if both difficulties are present simultaneously. The use of different materials in model and prototype is illustrated in the following typical example.

Example: It is desired to construct a scale model test of a 2014-T6 aluminum alloy dome subjected to an impulsive pressure of a prescribed peak magnitude and duration. A maximum model test pressure of only 10% of full scale can be provided with a duration 75% of full scale. The properties of the prototype dome are the following:

$$E_p = 10 \times 10^6 \text{ psi}$$

$$\gamma_p = 0.10 \text{ lbs/in}^3$$

$$\sigma_p = 66,000 \text{ psi}$$

$$\nu_p = 0.33$$

Solution: Consider mylar as a possible choice of model material.

The properties of the model material are the following.

$$E_m = 0.7 \times 10^6 \text{ psi}$$

$$\gamma_m = 0.05 \text{ lbs/in}^3$$

$$\sigma_m = 11,000 \text{ psi}$$

$$\nu_m = 0.30$$

Hence

$$n_2 = 0.10/0.05 = 2$$

$$n_3 = 10 \times 10^6 / 0.7 \times 10^6 = 14.3$$

The magnitude of the maximum required pressure for the model is $1/14.3$ or 7% of the maximum full scale pressure. This is within the test capability for the model. From scale factor (5),

$$n_1 = T_p \sqrt{n_3} / T_m \sqrt{n_2} = 0.75 \times \sqrt{14.3/2} = 0.75 \times 2.68 = 2$$

A half scale model using mylar will therefore be necessary to satisfy similitude requirements for magnitude and duration of impulsive pressure.

The value of Poisson's ratio for mylar is 0.30 compared to the value of 0.33 for aluminum. This is close enough for good similitude, since existing theoretical solutions for simple cases show that buckling impulse is not strongly dependent on Poisson's ratio. (2)

The required yield stress for the model material, according to scale factor (12) is $66,000/14.3 = 4,600$ psi, whereas the yield stress for mylar is 11,000 psi. However, if the problem is clearly one of elastic buckling, the yield stress of the material may not be a significant variable, and the corresponding lack of similitude may not be serious. This can be verified by conducting additional scale model tests with different materials suitably chosen to demonstrate this point.

CONCLUDING REMARKS

Excluding fabrication difficulties, it is possible to conduct valid scale model testing for buckling of shell structures under impulsive loading, subject to the following restrictions dictated by practical requirements.

(1) Scale model boundary restraints should be either completely free or completely fixed. This will provide either an upper or a lower bound on the true condition.

(2) The best similitude is provided by using the same material for both model and prototype. However in this case, the magnitude of the impulsive pressure for the scale model must be equal to the magnitude for the prototype, and the duration of the impulsive pressure must be scaled down in proportion to size.

(3) If there are practical limitations on the pressure magnitudes and durations that can be provided for the model, then different materials must be chosen for model and prototype in order to satisfy similitude requirements for pressure magnitude and duration.

(4) The use of different materials for model and prototype increases the difficulty of satisfying simultaneously the similitude requirements for the mechanical properties of the materials, unless the buckling is clearly elastic in nature, in which case it may be possible to violate the similitude requirement for yield stress.

REFERENCES

1. Koval, L. R. et al.: "Final Report on Buckling of Shells Under Dynamic Loads", Space Technology Laboratories, EM 11-22.
2. Humphreys, J. S. and Bodner, S. R.: "Dynamic Buckling of Shallow Shells Under Impulsive Loading", Journal of the Engineering Mechanics Division, Proceedings of the American Society of Civil Engineers, Vol. 88, No. EM 2, April 1962.
3. Abrahamson, G. R. and Goodier, J. N.: "Dynamic Plastic Flow Buckling of a Cylindrical Shell from Uniform Radial Impulse". Fourth U.S. National Congress of Applied Mechanics, Berkeley, June 18-21, 1962.

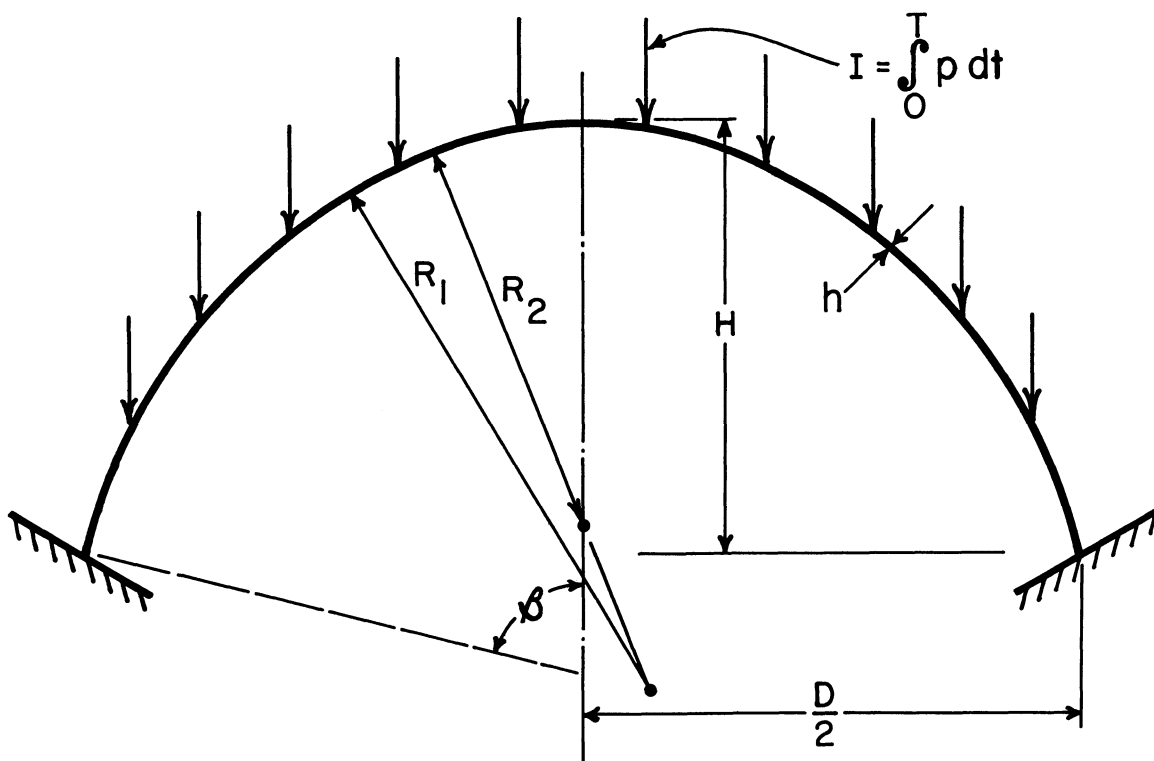


Figure 1.- Impulsive pressure loading on a shell structure.

STABILITY OF THIN TORISPHERICAL SHELLS UNDER UNIFORM INTERNAL PRESSURE

By John Mescall

Watertown Arsenal Laboratories
Watertown, Massachusetts

SUMMARY

The stability of the toroidal portion of a torispherical shell under internal pressure is considered from the point of view of the linear buckling theory. A detailed stress analysis of the prebuckled shell is made employing asymptotic integration. The change in potential energy of the shell is then minimized using a Rayleigh-Ritz procedure for actual computation of the critical pressure. Numerical results reveal that elastic buckling may occur for very thin shells whose material has a relatively high value of the ratio of yield stress to elastic modulus.

INTRODUCTION

Torispherical shells are frequently employed as end closures for cylindrical shells both in missile design and in a wide variety of industrial-type pressure vessels. Such shells generally consist of a shallow spherical cap joined to a toroidal segment, joined in turn to a cylindrical shell. This combined shell is then subjected to internal pressure. It was known (ref. 1) that large, compressive hoop stresses were developed in the torus, and that for very thin shells, elastic buckling was a distinct possibility. For shells whose thickness is heavy enough to avoid buckling, but which may still be rather thin compared to the toroidal radius, plastic deformation may occur. This has been examined in detail by Drucker and Shield (refs. 2 and 3). However, the elastic stability of torispherical shells was not considered a matter for concern until, recently, such a shell was actually observed to buckle under internal pressure. (See fig. 1.) The problem is an interesting one, since the prebuckling state of stress in such a shell is not a simple one. The membrane state, often employed to estimate prebuckling stresses, would actually predict a state of tension in the torus. Consequently a thorough stress analysis of the shell prior to the onset of instability must be made. This stress analysis is also useful (and necessary) in ascertaining the dividing line between those configurations which are likely to buckle and those which are likely to undergo plastic deformation.

In this report, prebuckling stresses in a shell of the type shown in figure 2, subjected to internal pressure, were determined by asymptotic integration techniques, with special attention being devoted to the particular solution. The vertical support on the cylinder was assumed to be sufficiently far removed from the junction of the torus that its specific form had little influence on the toroidal stresses. These results were then incorporated into the stability equations for the toroidal segment, and numerical results were obtained by applying a Rayleigh-Ritz approach to an appropriate potential energy expression. Since no prior theoretical results appear to be available, an experimental investigation of the same problem was undertaken simultaneously. The results of the two investigations compare favorably. Finally, a somewhat simplified stability criterion is proposed which provides results of essentially the same degree of accuracy, at a considerable saving in effort.

SYMBOLS

α, β	coordinates of middle surface of shell
z	coordinate normal to middle surface of shell
A, B	Lame' coefficients associated with α, β
R_1, R_2	principal radii of curvature
u, v, w	displacements in the α, β, z directions
u_1, v_1, w_1	additional displacements in the meridional, circumferential, and normal directions after buckling
$\epsilon_\alpha, \epsilon_\beta, \epsilon_{\alpha\beta}$	strains at any point in the shell
$\sigma_\alpha, \sigma_\beta, \sigma_{\alpha\beta}$	stresses at any point in the shell
U	strain energy of thin shell
$\hat{\epsilon}, \hat{\kappa}$	middle surface strains and curvature changes in a thin shell
$\omega_\alpha, \omega_\beta$	angle of rotation of normal to middle surface about tangent to lines $\beta = \text{constant}$, $\alpha = \text{constant}$
φ, θ	coordinates in meridional, circumferential direction on toroidal middle surface
b	radius of cross section of torus
a	distance from center line to center of toroidal cross section

r	$r = a + b \sin \varphi$, horizontal distance from center line to point on toroidal middle surface
λ	$\lambda = b/a$
$\bar{\lambda}$	$\bar{\lambda} = \frac{2\pi}{\pi - 2\varphi_0}$
h	shell thickness
E	Young's modulus of elasticity
ν	Poisson's ratio
D	flexural stiffness of torus: $\left[D = \frac{Eh^3}{12(1 - \nu^2)} \right]$
p	applied pressure
p_{cr}	critical pressure
n	wave number defining number of circumferential buckles in torus
$N_{\varphi_0}, N_{\theta_0}$	middle surface stress resultants prior to buckling
$M_{\varphi_0}, M_{\theta_0}$	middle surface stress couples prior to buckling

ANALYSIS OF THE ELASTIC STABILITY OF THIN TORISPHERICAL SHELLS UNDER UNIFORM INTERNAL PRESSURE

Theoretical Background

Equations governing both the equilibrium and the stability of a thin elastic shell may be obtained in the following manner (refs. 4 and 5). Beginning with an appropriate set of strain-displacement relations and a stress-strain law, one forms the strain energy integral associated with the thin shell under consideration. For a homogeneous isotropic thin shell this may be expressed as

$$U = \frac{1}{2} \iiint [\sigma_{\alpha} \epsilon_{\alpha} + \sigma_{\beta} \epsilon_{\beta} + \sigma_{\alpha\beta} \epsilon_{\alpha\beta}] AB \, d\alpha \, d\beta \, dz \quad (1)$$

Next, the principle of virtual work and the principle of stationary potential energy are applied. In this connection, consider a shell in a state of equilibrium characterized by displacements u_0, v_0, w_0 . This

state is said to be one of "neutral" equilibrium if there exists an adjacent equilibrium state differing from the first by an infinitesimal variation in the quantities characterizing that state. We therefore consider an alternate equilibrium state characterized by displacements

$$u = u_0 + \eta u_1 \quad v = v_0 + \eta v_1 \quad w = w_0 + \eta w_1 \quad (2)$$

where η is an infinitesimal, independent of α, β .

The strain energy associated with this second state becomes

$$U = U_0 + \eta U_1 + \eta^2 U_2. \quad (3)$$

The principle of stationary potential energy implies that for the second state to be one of equilibrium,

$$\delta U + \delta V = 0, \quad (4)$$

where δV is the work done by external loads due to a variation in displacements. Considering only variations in u_1, v_1, w_1 , we have:

$$\delta U_1 + \delta V_1 + \eta(\delta U_2 + \delta V_2) = 0. \quad (5)$$

But, since the first state was assumed to be an equilibrium state, the principle of virtual displacements implies that

$$\delta U_1 + \delta V_1 = 0. \quad (6)$$

Hence the condition that the first equilibrium state be unstable is that

$$\delta U_2 + \delta V_2 = 0. \quad (7)$$

To summarize, equation 6 yields equations governing the equilibrium of a state described by displacements u_0, v_0, w_0 , while equation 7 yields equations governing the stability of this state. This general

statement of the problem is valid for both large and small deflections. Thus, depending upon the generality of the strain-displacement relations and the stress-strain laws assumed, a variety of theories is possible. Kempner (ref. 5) delineates several of these in considerable detail and with attendant clarity.

Toroidal Geometry and Strain-Displacement Relations

We consider the coordinate system shown in figure 2 with φ, θ the middle surface coordinates in the meridional and circumferential directions and z normal to both, positive when directed inward. The principal radii of curvature R_1, R_2 are given by $R_1 = b$ and $R_2 \sin \varphi = a + b \sin \varphi = r$. The so-called Lamé coefficients for this system are $A_1 = b$ and $A_2 = R_2 \sin \varphi = r$. With this information it is a simple matter to obtain from reference 4 or 5 (with obvious changes in notation) the following strain-displacement relations, valid for small strains but large rotations:

$$\begin{aligned}\epsilon_{\varphi} &= \ell_{\varphi} + \frac{1}{2} (\omega_{\theta}^2) \\ \epsilon_{\theta} &= \ell_{\theta} + \frac{1}{2} (\omega_{\varphi}^2) \\ \epsilon_{\varphi\theta} &= \ell_{\varphi\theta} - \omega_{\varphi}\omega_{\theta}\end{aligned}\tag{8a}$$

where

$$\begin{aligned}\ell_{\varphi} &= \hat{\ell}_{\varphi} - z\kappa_{\varphi} & \ell_{\theta} &= \hat{\ell}_{\theta} - z\kappa_{\theta} \\ \ell_{\varphi\theta} &= \hat{\ell}_{\varphi\theta} - z\kappa_{\varphi\theta}\end{aligned}\tag{8b}$$

and

$$\begin{aligned}\hat{\ell}_{\varphi} &= \frac{1}{b}(u,_{\varphi} - w) & \hat{\ell}_{\theta} &= \frac{1}{r}(v,_{\theta} + u \cos \varphi - w \sin \varphi) \\ \hat{\ell}_{\varphi\theta} &= \frac{1}{b}(v,_{\varphi}) + \frac{1}{r}(u,_{\theta} - v \cos \varphi)\end{aligned}\tag{8c}$$

$$\begin{aligned}\kappa_{\varphi} &= -\frac{1}{b}(\omega_{\theta}),_{\varphi} & \kappa_{\theta} &= \frac{1}{r}(\omega_{\varphi}),_{\theta} - \frac{\cos\varphi}{r}(\omega_{\theta}) \\ \kappa_{\varphi\theta} &= \frac{r}{b}\left(\frac{\omega_{\varphi}}{r}\right),_{\varphi} - \frac{1}{r}(\omega_{\theta}),_{\theta}\end{aligned}\quad (8d)$$

$$\omega_{\varphi} = \frac{1}{r}(w,_{\theta} + v \sin \varphi) \quad \omega_{\theta} = -\frac{1}{b}(w,_{\varphi} + u) \quad (8e)$$

In obtaining these relations, in addition to the underlying assumptions of thinness of the shell and validity of Kirchhoff's hypothesis, we have made the further assumptions that components of strain and rotation are small compared to unity, and in addition, strains are small compared to rotations, i.e., $\epsilon = O(\ell) = O(\omega^2) \ll 1$. Further, we have assumed that ω_z , the component of rotation in the plane of the middle surface of the shell is much smaller than the other two components, ω_{φ} and ω_{θ} . Finally, it is possible to effect a considerable saving in algebra with a minimal expense of accuracy by neglecting in ω_{φ} and ω_{θ} the contribution of the u, v terms. This may be justified on an order of magnitude estimate of the terms involved, or by examination of the effect of this approximation on numerical results. The latter reinforces the former. This approximation results in what is sometimes referred to as a Donnell-type theory. In what follows, then, we take,

$$\omega_{\varphi} = \frac{1}{r}(w,_{\theta}) \quad \omega_{\theta} = -\frac{1}{b}(w,_{\varphi}) \quad (8f)$$

With a stress-strain law assumed in the form

$$\begin{aligned}\sigma_{\varphi} &= \frac{E}{1-\nu^2}(\epsilon_{\varphi} + \nu\epsilon_{\theta}) & \sigma_{\theta} &= \frac{E}{1-\nu^2}(\epsilon_{\theta} + \nu\epsilon_{\varphi}) \\ \sigma_{\varphi\theta} &= \frac{E}{2(1+\nu)}\epsilon_{\varphi\theta}\end{aligned}\quad (9)$$

the strain energy of the shell may be written out in detail, as well as the quantities U_1 and U_2 , sometimes referred to as the first and second variation of the strain energy. Specifically,

$$U_1 = \iiint (\sigma_{\varphi_0}\epsilon_{\varphi_1} + \sigma_{\theta_0}\epsilon_{\theta_1} + \sigma_{\varphi\theta_0}\epsilon_{\varphi\theta_1}) b r d\varphi d\theta dz \quad (10)$$

$$\begin{aligned}
U_2 = \frac{1}{2} \iiint (\sigma_{\varphi_1} \epsilon_{\varphi_1} + \sigma_{\theta_1} \epsilon_{\theta_1} + \sigma_{\varphi\theta_1} \epsilon_{\varphi\theta_1} \\
+ 2[\sigma_{\varphi_0} \epsilon_{\varphi_{11}} + \sigma_{\theta_0} \epsilon_{\theta_{11}} + \sigma_{\varphi\theta_0} \epsilon_{\varphi\theta_{11}}]) \text{brd}\varphi d\theta dz \quad (11)
\end{aligned}$$

where

$$\begin{aligned}
\epsilon_{\varphi_0} &= l_{\varphi_0} + \frac{1}{2}(w_{\varphi_0})^2 & \epsilon_{\theta_0} &= l_{\theta_0} + \frac{1}{2}(w_{\theta_0})^2 & \epsilon_{\varphi\theta_0} &= l_{\varphi\theta_0} - w_{\varphi_0} w_{\theta_0} \\
\epsilon_{\varphi_1} &= l_{\varphi_1} + w_{\theta_0} w_{\theta_1} & \epsilon_{\theta_1} &= l_{\theta_1} + w_{\varphi_0} w_{\theta_1} & \epsilon_{\varphi\theta_1} &= l_{\varphi\theta_1} - w_{\varphi_0} w_{\theta_1} \\
& & & & & - w_{\varphi_1} w_{\theta_0} \\
\epsilon_{\varphi_{11}} &= \frac{1}{2}(w_{\theta_1})^2 & \epsilon_{\theta_{11}} &= \frac{1}{2}(w_{\varphi_1})^2 & \epsilon_{\varphi\theta_{11}} &= -w_{\varphi_1} w_{\theta_1} \quad (12)
\end{aligned}$$

and where it is to be understood that the subscripted strain or rotation is to be evaluated in terms of the displacement of the same subscript. Finally, σ_{φ} , σ_{θ} and $\sigma_{\varphi\theta}$ are related to the appropriately subscripted strains according to equation 9.

Stability Criterion

Employing linearized strain-displacement relations we may obtain from equation 6 the equilibrium equations governing the (rotationally symmetric) prebuckling state of stress in the shell. We prefer to solve these in a somewhat different formulation however, and omit their presentation here. Proceeding directly to the stability relations we observe first that the prebuckled state is one of small deflections, governed by the classical (linear) theory. As Novozhilov (ref. 4) points out, then, we are justified in simplifying the expression for U_2 by omitting the w_0 terms in ϵ_{φ_1} , ϵ_{θ_1} and $\epsilon_{\varphi\theta_1}$. Upon integrating through the thickness, h , we may write

$$\begin{aligned}
U_2 = \frac{Eh}{2(1-\nu^2)} \iint \left\{ \hat{l}_{\varphi_1}^2 + \hat{l}_{\theta_1}^2 + 2\nu \hat{l}_{\varphi_1} \hat{l}_{\theta_1} + \frac{1-\nu}{2} \hat{l}_{\varphi\theta_1}^2 \right\} \text{brd}\varphi d\theta \\
+ \frac{Eh^3}{24(1-\nu^2)} \iint \left\{ \kappa_{\varphi_1}^2 + \kappa_{\theta_1}^2 + 2\nu \kappa_{\varphi_1} \kappa_{\theta_1} + 2(1-\nu) \kappa_{\varphi\theta_1}^2 \right\} \text{brd}\varphi d\theta \\
+ \frac{1}{2} \iint \left\{ N_{\varphi_0} (w_{\theta_1})^2 + N_{\theta_0} (w_{\varphi_1})^2 - 2N_{\varphi\theta_0} (w_{\varphi_1} w_{\theta_1}) \right\} \text{brd}\varphi d\theta \quad (13)
\end{aligned}$$

where N_{φ_0} , N_{θ_0} are the stress resultants of the prebuckled shell, and due to rotational symmetry prior to buckling, $N_{\varphi\theta_0} = 0$.

The potential energy of the external force system, V_2 , is equal to the product of the external load and the increase in volume enclosed by the shell. An approximate expression for V_2 for the toroidal shell segment under uniform internal pressure p is (ref. 6)

$$V_2 = \frac{p}{2} \iint \left\{ \frac{w}{b}(u, \varphi - w) + \frac{w}{r}(v, \theta + u \cos \varphi - w \sin \varphi) - \frac{v^2 \sin \varphi}{r} - \frac{u^2}{b} - uw, \varphi - \frac{vw, \theta}{r} \right\} br d\varphi d\theta. \quad (14)$$

Stability is governed by the relation

$$\delta(U_2 + V_2) = 0. \quad (15)$$

It is clear that solution of the differential equations governing the stability of the toroidal shell segment would be a formidable task even if the prebuckled state were a simple one. For this reason we employ a Rayleigh-Ritz approach and obtain an upper bound for the critical pressure. In this connection, guided somewhat by experimental observation of the buckled pattern in the toroidal segment, we choose the following set of displacements

$$\begin{aligned} u_1 &= \bar{A} r^2 \cos \bar{\lambda} (\varphi - \varphi_0) \cos (n\theta) \\ v_1 &= \bar{B} r^2 \sin \bar{\lambda} (\varphi - \varphi_0) \sin (n\theta) \\ w_1 &= \bar{C} r^2 \sin \bar{\lambda} (\varphi - \varphi_0) \cos (n\theta) \end{aligned} \quad (16)$$

where n is the number of lobes in the circumferential direction and \bar{A} , \bar{B} , \bar{C} are undetermined coefficients. The variations in u_1 , v_1 , w_1 are reduced to variations in \bar{A} , \bar{B} , \bar{C} . Inserting equation 16 into equation 15 and requiring that the resulting equation be satisfied for arbitrary values of $\delta\bar{A}$, $\delta\bar{B}$, $\delta\bar{C}$, we obtain a system of three linear homogeneous algebraic equations in \bar{A} , \bar{B} , \bar{C} , whose determinant set equal to zero yields an estimate of the critical pressure. Omitting details of intermediate algebra we may write

$$\frac{p_{cr}}{E} = \frac{h}{2(1-\nu^2)b} \left(\frac{N}{D} \right) \quad (17a)$$

where

$$\begin{aligned} N &= 4a_{11}a_{22}a_{33} - a_{11}(a_{23})^2 - a_{12}^2a_{33} + a_{12}a_{13}a_{23} - a_{22}a_{13}^2 \\ D &= 2a_{11}a_{23}b_{23} + a_{23}^2b_{11} + a_{12}^2b_{33} + 2a_{13}a_{22}b_{13} + a_{13}^2b_{22} \\ &\quad - a_{12}(a_{23}b_{13} + a_{13}b_{23}) - 4a_{33}(a_{22}b_{11} + a_{11}b_{22}) \\ &\quad - 4a_{11}a_{22}b_{33} \end{aligned} \quad (17b)$$

where:

$$\begin{aligned} a_{11} &= (5 + 4\nu) \left(\frac{12*}{b^3} \right) - 2(2 + \nu) \bar{\lambda} \left(\frac{25*}{b^4} \right) + \bar{\lambda}^2 \left(\frac{26*}{b^5} \right) + \frac{(1-\nu)n^2}{2} \left(\frac{11*}{b^3} \right) \\ a_{12} &= n(1 + 5\nu) \left(\frac{17*}{b^3} \right) - 2\nu n \bar{\lambda} \left(\frac{20*}{b^3} \right) - n \bar{\lambda} (1-\nu) \left(\frac{21*}{b^4} \right) \\ a_{13} &= -2(2 + \nu) \left(\frac{25*}{b^4} \right) + 2\bar{\lambda} \left(\frac{26*}{b^5} \right) - 2(1 + 2\nu) \left(\frac{18*}{b^3} \right) + 2\nu \bar{\lambda} \left(\frac{22*}{b^4} \right) \\ a_{22} &= n^2 \left(\frac{10*}{b^3} \right) + (1-\nu) \left(2 \left(\frac{15*}{b^3} \right) + \bar{\lambda} \left(\frac{25*}{b^4} \right) + \frac{\bar{\lambda}^2}{2} \left(\frac{27*}{b^5} \right) - \frac{3}{2} \left(\frac{13*}{b^3} \right) \right) \\ a_{23} &= -2n \left(\frac{19*}{b^3} \right) - 2\nu n \left(\frac{20*}{b^4} \right) \\ a_{33} &= \left(\frac{26*}{b^5} \right) + \left(\frac{14*}{b^3} \right) + 2\nu \left(\frac{22*}{b^4} \right) + \frac{h^2}{12b^2} \left\{ 8(1+\nu) \left(\frac{5*}{b} \right) + 4 \left(\frac{14*}{b^3} \right) \right. \\ &\quad + \bar{\lambda}^2 (17+8\nu) \left(\frac{12*}{b^3} \right) + \bar{\lambda}^4 \left(\frac{26*}{b^5} \right) - 8(1+\nu) \left(\frac{7*}{b^2} \right) + 20 \bar{\lambda} (1+\nu) \left(\frac{9*}{b^2} \right) \\ &\quad - 4 \bar{\lambda}^2 (1+\nu) \left(\frac{13*}{b^3} \right) - 4\bar{\lambda} (4+\nu) \left(\frac{18*}{b^3} \right) + 4\bar{\lambda}^2 \left(\frac{22*}{b^4} \right) + n^4 \left(\frac{1*}{b} \right) \\ &\quad + 4\nu n^2 \left(\frac{6*}{b^2} \right) - 2\bar{\lambda}^3 (4+\nu) \left(\frac{25*}{b^4} \right) + 2\nu \bar{\lambda}^2 n^2 \left(\frac{10*}{b^3} \right) - 2n^2 (1+3\nu) \left(\frac{3*}{b} \right) \\ &\quad \left. + 2n^2 \bar{\lambda} (1-6\nu) \left(\frac{8*}{b^2} \right) + 2n^2 (1-\nu) \bar{\lambda}^2 \left(\frac{11*}{b^3} \right) \right\} \end{aligned}$$

$$\begin{aligned}
b_{11} &= -\frac{1}{2} \left(\frac{27*}{b^5} \right) \\
b_{13} &= -\frac{1}{2} \left[\bar{\lambda} \left(\frac{27*}{b^5} \right) + \left(\frac{26*}{b^5} \right) - \left(\frac{25*}{b^4} \right) \right] \\
b_{22} &= -\frac{1}{2} \left(\frac{22*}{b^4} \right) \\
b_{23} &= n \left(\frac{20*}{b^4} \right) \\
b_{33} &= -\frac{1}{2} \left(\frac{26*}{b^5} \right) - \frac{1}{2} \left(\frac{22*}{b^4} \right) + K_2 \frac{n^2 b}{2} + \frac{K_1}{2b}
\end{aligned} \tag{17c}$$

where the quantities (1*), etc., are definite integrals of the form

$$(1*) = \int_{\varphi_0}^{\pi/2} r \sin^2 \bar{\lambda}(\varphi - \varphi_0) d\varphi,$$

and are listed in the Appendix. All these integrals may readily be evaluated explicitly in terms of trigonometric functions. Finally,

$$\begin{aligned}
K_2 &\equiv \int_{\varphi_0}^{\pi/2} N_{\theta_0} r^3 \sin^2 \bar{\lambda}(\varphi - \varphi_0) d\varphi \\
K_1 &= \int_{\varphi_0}^{\pi/2} N_{\varphi_0} r \left(2r r_{,\varphi} \sin \bar{\lambda}(\varphi - \varphi_0) + \bar{\lambda} r^2 \cos \bar{\lambda}(\varphi - \varphi_0) \right)^2 d\varphi.
\end{aligned} \tag{18}$$

Prebuckled State of Stress

In U_2 we encounter the integrals

$$\frac{1}{2} \iint N_{\varphi_0} \left(\frac{w, \varphi}{b} \right)^2 br d\varphi d\theta, \quad \frac{1}{2} \iint N_{\theta_0} \left(\frac{w, \theta}{r} \right)^2 br d\varphi d\theta \tag{19}$$

which assess the contribution of the prebuckled state of stress to the strain energy of the buckled state. Since the shells under consideration are very thin, the asymptotic method of solution of Reissner's equations for symmetric deformation of shells of revolution is most appropriate.

Clark (refs. 7 and 8) has presented asymptotic representations for both the homogeneous and particular solutions for the toroidal shell. These were employed in the present investigation.

In this connection, it may be well to digress for a moment to discuss the particular integral for toroidal shells. Galletley (ref. 1) has given ample warning that the frequently employed practice of using the membrane solution as a particular solution to the nonhomogeneous thin shell equations is not valid in the case of the torus. His results of a numerical integration of the complete differential equations for just such a tori-spherical-cylindrical shell show a markedly different stress pattern when compared to a solution using the membrane state as a particular solution. However, when the first two terms of an asymptotic particular solution developed by Clark (ref. 8) are used in conjunction with the homogeneous asymptotic solution, the results agree remarkably well with Galletley's. (See figure 3). This agreement is obtained at a value of the asymptotic parameter ($\mu \approx 15$) which is considerably smaller than the values assumed by the shells whose stability we wish to consider, and thus assures validity of application of the asymptotic method.

Very briefly, the prebuckling stresses may be written in terms of the two basic functions β and Ψ according to the relations:

$$\begin{aligned} N_{\varphi_0} &= \frac{Eh^2}{rm} (\Psi \cos \varphi + \Omega \sin \varphi) \\ N_{\theta_0} &= \frac{Eh^2}{mb} (\Psi_{,\varphi} + \frac{m}{Eh^2} r b p_H) \end{aligned} \quad (20)$$

where

$$\begin{aligned} \beta &= (1 + \nu \sin \varphi)^{-1/2} Q \{ A_0 h_{1r} - B_0 h_{1i} + C_0 h_{2r} - D_0 h_{2i} + \mu^{-2/3} (\lambda/D)^{1/2} \cdot \\ &\quad \cdot [F_0 T_r - G_0 T_i] + (\mu Q \Phi)^{-1} (\lambda/D)^{1/2} [G_0 Q^{-3} - G(\varphi)] \} \\ \Psi &= (1 + \lambda \sin \varphi)^{-1/2} Q \{ B_0 h_{1r} + A_0 h_{1i} + D_0 h_{2r} + C_0 h_{2i} + (\mu^{-2/3} (\lambda/D)^{1/2} \cdot \\ &\quad \cdot [F_0 T_i + G_0 T_r]) - (\mu Q \Phi)^{-1} (\lambda/D)^{1/2} [F_0 Q^{-3} - F(\varphi)] \} \end{aligned} \quad (21)$$

and

$$\begin{aligned}
\lambda &= b/a, \quad \mu = \frac{mb^2}{ah}, \quad m = \sqrt{12(1-v^2)}, \quad y = \mu^{1/3} \left(\frac{3}{2}\omega\right)^{2/3}, \\
\omega &= \int_0^\varphi \left(\frac{\sin\varphi}{1+\lambda\sin\varphi}\right)^{1/2} d\varphi, \quad Q = \left(\frac{3}{2}\omega\right)^{1/6} (\omega, \varphi)^{-1/2}, \\
\Omega &= \frac{m}{Eh^2} rV = -\frac{m}{Eh^2} \int r b p_V d\varphi, \quad F(\varphi) = \left(\frac{\mu mb}{Eh^2(1+\lambda\sin\varphi)}\right)^{1/2} (rV) \cos \varphi, \\
G(\varphi) &= \left(\frac{1+\lambda\sin\varphi}{\lambda Eh}\right)^{1/2} \left\{ \frac{b \cos \varphi}{r} \left(v + \frac{b \sin \varphi}{r}\right) (rV) - 2b^2 p \sin \varphi \cos \varphi \right. \\
&\quad \left. - b p r \cos \varphi \right\}, \quad F_0 \equiv F(\varphi_0) \quad G_0 \equiv G(\varphi_0), \quad (21a)
\end{aligned}$$

p_H and p_V are the horizontal and vertical components of applied pressure. In the above, h_{1r} , h_{1i} , h_{2r} , h_{2i} are the real and imaginary components of the modified Hankel functions of order one-third, of the first and second kind respectively. Their argument is understood to be (iy) . T_r , T_i are the real and imaginary parts of a special function introduced by Clark, and satisfying

$$T'' - iy T(y) = 1. \quad (22)$$

A_0 , B_0 , C_0 , D_0 are constants to be determined from the boundary conditions of the specific problem considered. In the present analysis, a shallow spherical segment was assumed joined to the torus at $\varphi = \varphi_0$, and a cylinder at $\varphi = \frac{\pi}{2}$. The vertical support on the cylinder was assumed to be sufficiently far removed from the junction of the torus that its specific form had little influence on the form of the toroidal stresses. N_{φ_0} , N_{θ_0} , M_{φ_0} and M_{θ_0} were evaluated along the length of the torus and then the integration indicated in equation 18 was carried out numerically. When this is done for a specific choice of geometric parameters, $\frac{p_{cr}}{E}$ remains a function of n . The minimum value of critical pressure was found by calculating p_{cr}/E over a range of n , subject to the condition that n be an integer.

Simplified Formula for Critical Pressure

The procedure outlined above was carried out initially using equation 17. It soon became apparent that certain terms could be

omitted without significantly affecting the numerical results, and at the same time affording considerable simplification of the relation for critical pressure. The validity of the approximation rests on the fact that the value of n found to minimize p_{cr}/E was always rather a large number compared to unity. This result is consistent with experimental observations of the buckling pattern. (See figure 1.)

The simplified relation for critical pressure may be written:

$$\frac{p_{cr}}{E} = \frac{h}{2(1-\nu^2)b} \frac{\bar{N}}{D} \quad (n \gg 1) \quad (23a)$$

where

$$\begin{aligned} \bar{N} &= 4 \bar{a}_{11} \bar{a}_{22} \bar{a}_{33} - \bar{a}_{11} \bar{a}_{23}^2 \\ D &= \bar{b}_{33}(\bar{a}_{12}^2 - 4 \bar{a}_{11} \bar{a}_{22}) \end{aligned} \quad (23b)$$

$$\begin{aligned} \bar{a}_{11} &= \left(\frac{1-\nu}{2} \right) n^2 \left(\frac{11*}{b^3} \right) \\ \bar{a}_{12} &= -n \bar{\lambda} \left(2\nu \left(\frac{20*}{b^3} \right) + (1-\nu) \left(\frac{21*}{b^4} \right) \right) \\ \bar{a}_{22} &= n^2 \left(\frac{10*}{b^3} \right) \\ \bar{a}_{23} &= -2n \left(\left(\frac{19*}{b^3} \right) + \nu \left(\frac{20*}{b^3} \right) \right) \\ \bar{a}_{33} &= \left(\frac{11*}{b^3} \right) + \left(\frac{26*}{b^5} \right) + 2\nu \left(\frac{22*}{b^4} \right) + \frac{h^2 n^4}{12b^2} \left(\frac{1*}{b} \right) \\ \bar{b}_{33} &= b_{33} = -\frac{1}{2} \left(\left(\frac{26*}{b^5} \right) + \left(\frac{22*}{b^4} \right) \right) + K_2 \frac{n^2 b}{2} + \frac{K_1}{2b} \end{aligned}$$

$$K_2 = \int_{\varphi_0}^{\pi/2} N_{\theta_0} r^3 \sin^2 \bar{\lambda}(\varphi - \varphi_0) d\varphi$$

$$K_1 = \int_{\varphi_0}^{\pi/2} N_{\varphi_0} r (2rr_{,\varphi} \sin \bar{\lambda}(\varphi - \varphi_0) + \bar{\lambda} r^2 (\cos \bar{\lambda}(\varphi - \varphi_0)))^2 d\varphi. \quad (23c)$$

Equation 23 is to be preferred over equation 17 for computational purposes when n is large. In all cases considered in this investigation, the value of n minimizing P_{cr} was greater than 40 and in most cases was greater than 60.

Numerical Results - Comparison With Experiment - Discussion

Computations of the critical pressure have been carried out thus far for a limited number of parameters. A typical set of numerical results is shown in figure 5. The parameters in these curves correspond to those involved in an experimental program concerned with the same problem. In each numerical evaluation of the critical pressure, a stress analysis of the unbuckled shell was made, the parameters K_1 and K_2 determined, and then the stability criterion evaluated.

In the experimental program*, scale models representative of those used in missile applications were tested. These models were made of poly-vinyl chloride, a material chosen among other reasons for its relatively high ratio of yield strength to elastic modulus. Some of the results of these tests are also shown in figure 5. In the case of the thickest shells tested, ($h/b > .007$) the disagreement between theory and experiment increased significantly. The prebuckling stress analysis for these shells revealed that at pressure levels below the predicted buckling pressure, the difference in principal stresses in the shell near the junction of torus and spherical cap had exceeded the yield stress of the material. Since our analysis has assumed elastic behavior throughout, it would not be expected to apply to the experimental material in this range of the parameters.

The following experimental result may also be of some interest. An aluminum torispherical bulkhead was tested under internal pressure. The parameters involved were

$$\phi_0 = 35^\circ \quad a = 34.43" \quad b = 18.07" \quad h_{average} = .081" \quad E = 10^7 \quad \nu = .3.$$

Dimples began to appear in the toroidal section at about $p = 25$ psi. The pressure level was increased to 40 psi, and when the load was released the dimples remained. The theoretical buckling pressure for a shell of this material (see fig. 5) is 64 psi. However, the prebuckling state of stress reveals that in the vicinity of $\phi = 45^\circ$, the value of $\frac{\sigma_\phi - \sigma_\theta}{p}$ on the inside and outside surfaces reaches a value of 1300 and

*This program was conducted by J. Adachi, formerly of Watertown Arsenal Laboratories, now associated with Materials Technology, Inc.

1015, respectively. Thus, for aluminum with a yield stress of 35,000 psi (as was the case in the test described) a value of $p = 25$ psi would produce stresses very close to yield.

The plastic models of this configuration, however, appeared to buckle elastically at 3.2 psi. (Theory predicts 2.9 psi.) This corresponds to an elastic buckling pressure of 70 psi for aluminum with $E = 10^7$. The stress level induced near 45° in the torus in the plastic models for $p = 2.9$ psi is in the vicinity of 3700 psi, which is below the yield stress of the plastic material used.

It is clear, then, that the phenomenon of elastic buckling of torispherical shells under internal pressure occurs only for very thin shells whose material has a relatively high value of the ratio of yield stress to elastic modulus. With the increasing role being played by such materials in space structures, it is believed that the analysis described in this report will assist the designer toward his objective of increased efficiency. Finally, it should be pointed out that the analysis may be applied to toriconical shells simply by replacing the spherical cap by a cone in determining the prebuckled state of stress.

REFERENCES

1. Galletley, G. D.: Torispherical Shells - a Caution to Designers. *Journal of Engineering for Industry* (Trans. ASME), vol. 81, Series B, 1959, pp. 51-62.
2. Drucker, D. C., and Shield, R. T.: Limit Analysis of Symmetrically Loaded Thin Shells of Revolution. *Journal of Applied Mechanics*, vol. 26, Trans ASME, vol. 81, Series E, 1959, pp. 61-68.
3. Shield, R. T., and Drucker, D. C.: Design of Thin Walled Torispherical and Toriconical Pressure Vessel Heads. *Journal of Applied Mechanics*, vol. 28, Trans ASME, vol. 83, Series E, 1961, pp. 292-297.
4. Novozhilov, V. V.: *Foundations of the Nonlinear Theory of Elasticity*. Graylock Press, Rochester, N. Y., 1953.
5. Kempner, J.: Unified Thin Shell Theory; Part I of A Symposium on the Mechanics of Plates and Shells for Industry Research Associates. Polytechnic Institute of Brooklyn, March 9-11, 1960.
6. Alfutov, N. A. (Moscow): On the Analysis of Shell Stability by the Energy Method. (Translated by M. I. Yarymovych, Columbia University.) Avco R & D. Translation, May 21, 1958.

7. Clark, R. A.: On the Theory of Thin Elastic Toroidal Shells. Journal of Mathematics and Physics, vol. 29, 1950, pp. 146-178.
8. Clark, R. A.: Asymptotic Solutions of Toroidal Shell Problems. Quarterly of Applied Mathematics, vol. 16, 1958, pp. 47-60.

APPENDIX

The following definite integrals occur in the expression for critical pressure (equation 17 or 23). In each instance the limits of integration are from φ_0 to $\pi/2$. The variable r is given by $r = a + b \sin \varphi$. All integrals may be evaluated explicitly in terms of trigonometric functions.

$$1* = \int r \sin^2 \bar{\lambda}(\varphi - \varphi_0) d\varphi$$

$$2* = \int r \sin \varphi \cos^2 \varphi \sin^2 \bar{\lambda}(\varphi - \varphi_0) d\varphi$$

$$3* = \int r \cos^2 \varphi \sin^2 \bar{\lambda}(\varphi - \varphi_0) d\varphi$$

$$4* = \int r \cos^3 \varphi \sin^2 \bar{\lambda}(\varphi - \varphi_0) d\varphi$$

$$5* = \int r \cos^4 \varphi \sin^2 \bar{\lambda}(\varphi - \varphi_0) d\varphi$$

$$6* = \int r^2 \sin \varphi \sin^2 \bar{\lambda}(\varphi - \varphi_0) d\varphi$$

$$7* = \int r^2 \sin \varphi \cos^2 \varphi \sin^2 \bar{\lambda}(\varphi - \varphi_0) d\varphi$$

$$8* = \int r^2 \cos \varphi \sin \bar{\lambda}(\varphi - \varphi_0) \cos \bar{\lambda}(\varphi - \varphi_0) d\varphi$$

$$9* = \int r^2 \cos^3 \varphi \sin \bar{\lambda}(\varphi - \varphi_0) \cos \bar{\lambda}(\varphi - \varphi_0) d\varphi$$

$$10* = \int r^3 \sin^2 \bar{\lambda}(\varphi - \varphi_0) d\varphi$$

$$11* = \int r^3 \cos^2 \bar{\lambda}(\varphi - \varphi_0) d\varphi$$

$$12* = \int r^3 \cos^2 \varphi \cos^2 \bar{\lambda}(\varphi - \varphi_0) d\varphi$$

$$13* = \int r^3 \cos^2 \varphi \sin^2 \bar{\lambda}(\varphi - \varphi_0) d\varphi$$

$$14* = \int r^3 \sin^2 \varphi \sin^2 \bar{\lambda}(\varphi - \varphi_0) d\varphi$$

$$15* = \int r^3 \cos^2 \varphi \sin^2 \bar{\lambda}(\varphi - \varphi_0) d\varphi$$

$$16* = \int r^3 \cos \varphi \sin^2 \bar{\lambda}(\varphi - \varphi_0) d\varphi$$

$$17* = \int r^3 \cos \varphi \sin \lambda(\varphi - \varphi_0) \cos \bar{\lambda}(\varphi - \varphi_0) d\varphi$$

$$18* = \int r^3 \sin \varphi \cos \varphi \sin \bar{\lambda}(\varphi - \varphi_0) \cos \bar{\lambda}(\varphi - \varphi_0) d\varphi$$

$$19* = \int r^3 \sin \varphi \sin^2 \bar{\lambda}(\varphi - \varphi_0) d\varphi$$

$$20* = \int r^4 \sin^2 \bar{\lambda}(\varphi - \varphi_0) d\varphi$$

$$21* = \int r^4 \cos^2 \bar{\lambda}(\varphi - \varphi_0) d\varphi$$

$$22* = \int r^4 \sin \varphi \sin^2 \bar{\lambda}(\varphi - \varphi_0) d\varphi$$

$$23* = \int r^4 \sin \varphi \cos^2 \bar{\lambda}(\varphi - \varphi_0) d\varphi$$

$$24* = \int r^4 \cos^2 \varphi \cos^2 \bar{\lambda}(\varphi - \varphi_0) d\varphi$$

$$25* = \int r^4 \cos \varphi \sin \bar{\lambda}(\varphi - \varphi_0) \cos \bar{\lambda}(\varphi - \varphi_0) d\varphi$$

$$26* = \int r^5 \sin^2 \bar{\lambda}(\varphi - \varphi_0) d\varphi$$

$$27* = \int r^5 \cos^2 \bar{\lambda}(\varphi - \varphi_0) d\varphi$$

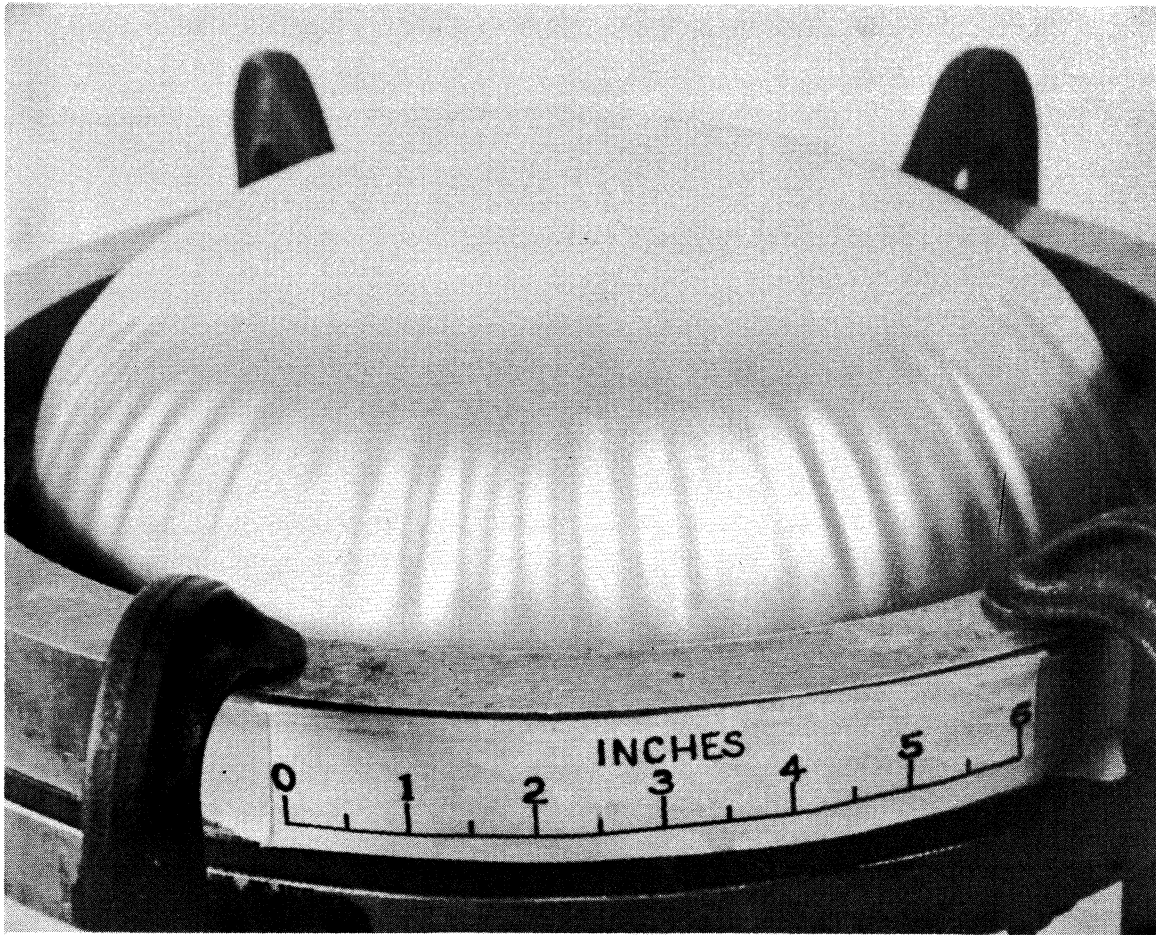


Figure 1.- Experimental setup.

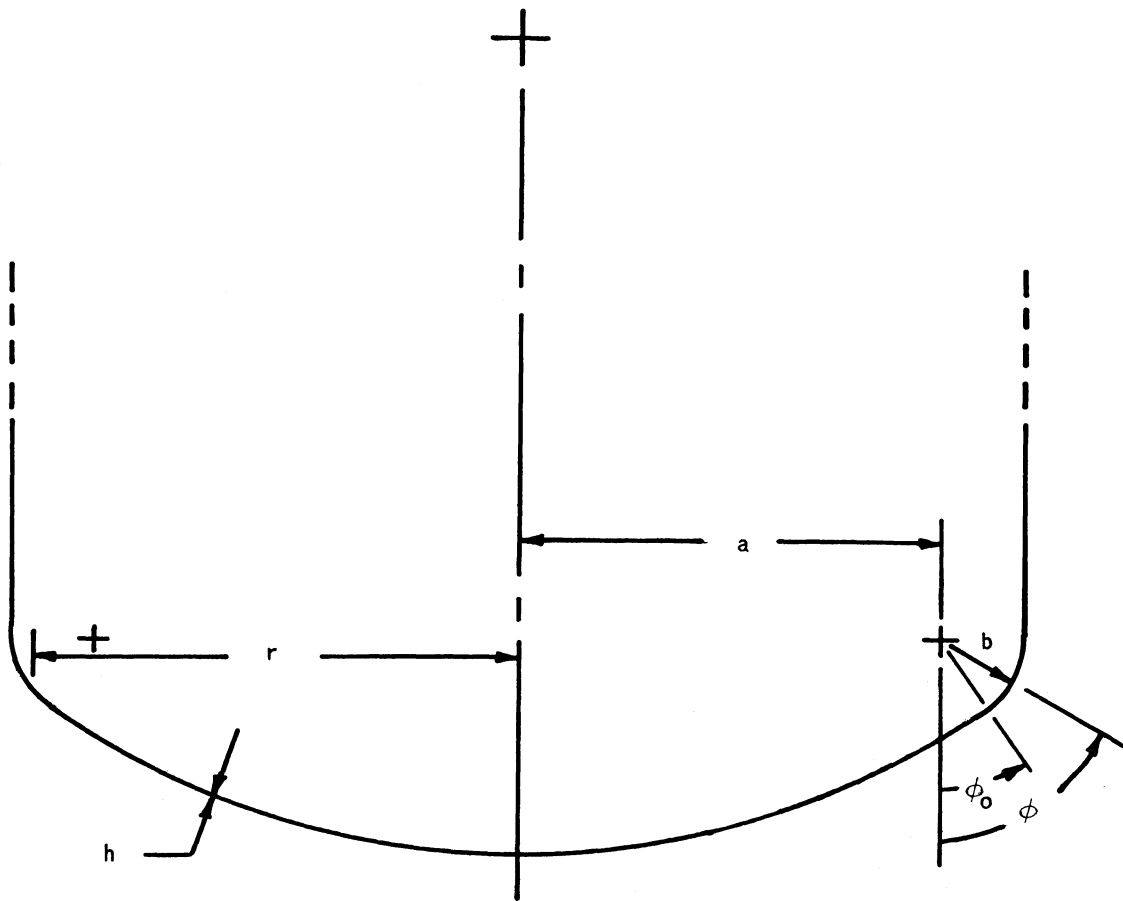


Figure 2.- Geometry of torispherical shell.

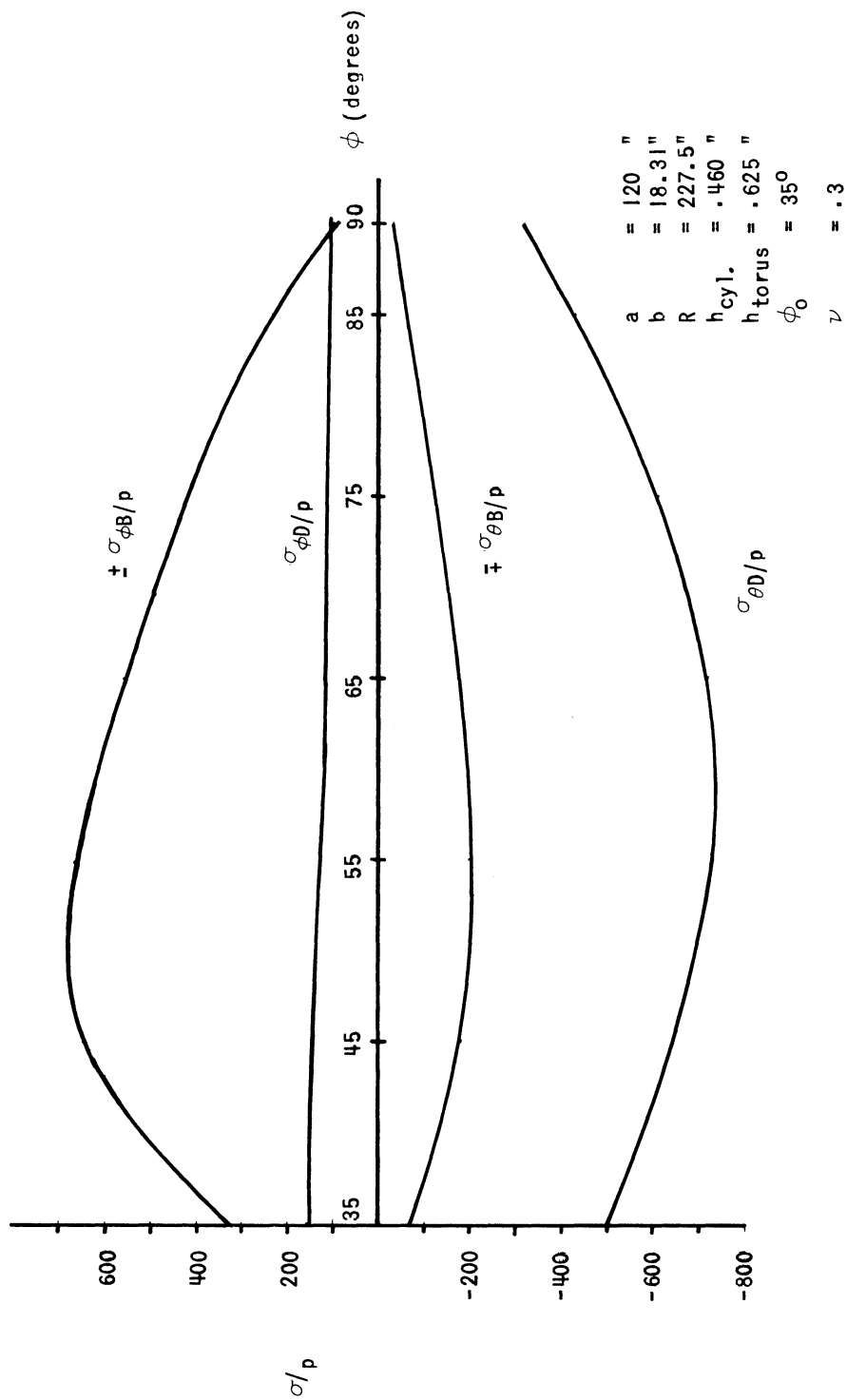


Figure 3.- Asymptotic solution corresponding to Galletley's (ref. 1) numerical solution.

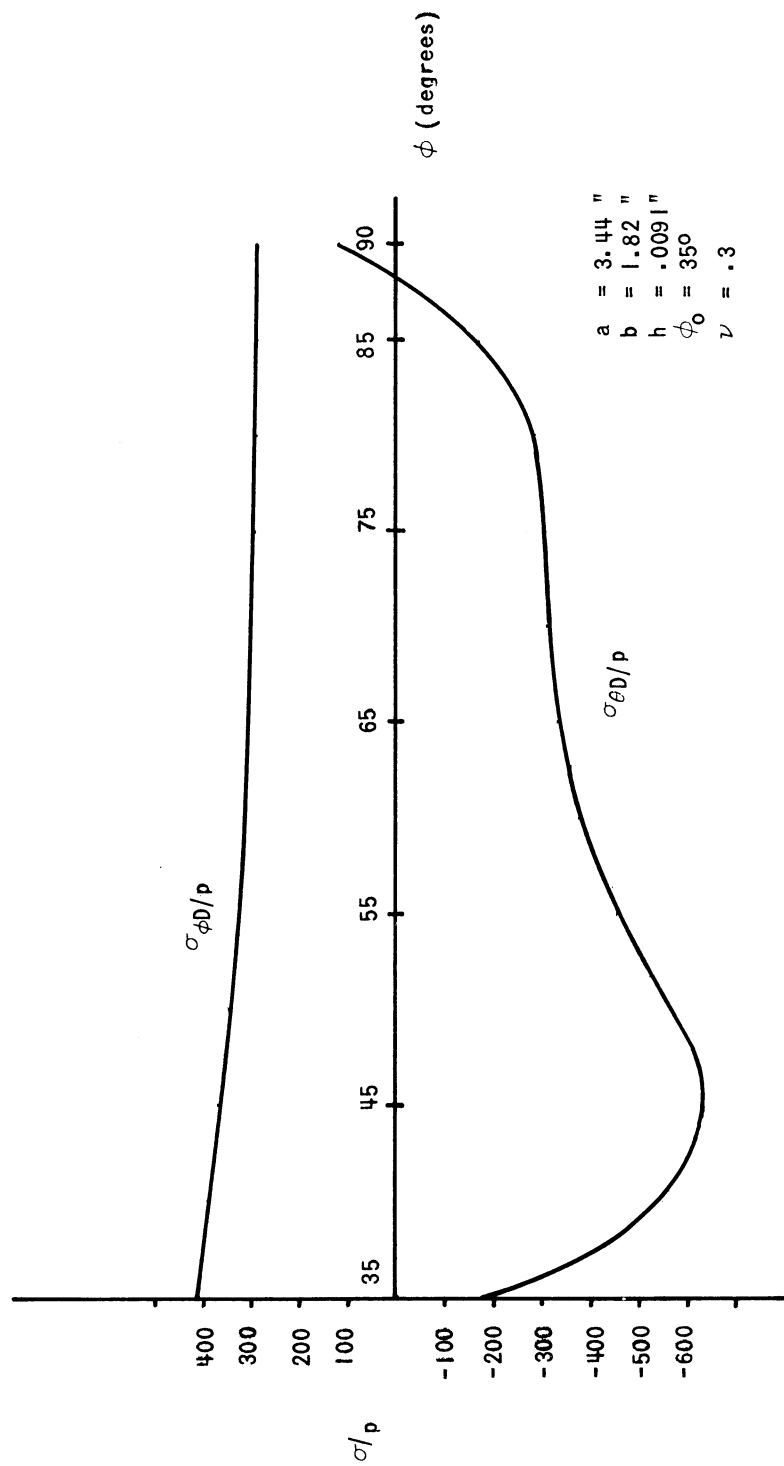


Figure 4.- Typical results of prebuckling stress analysis.

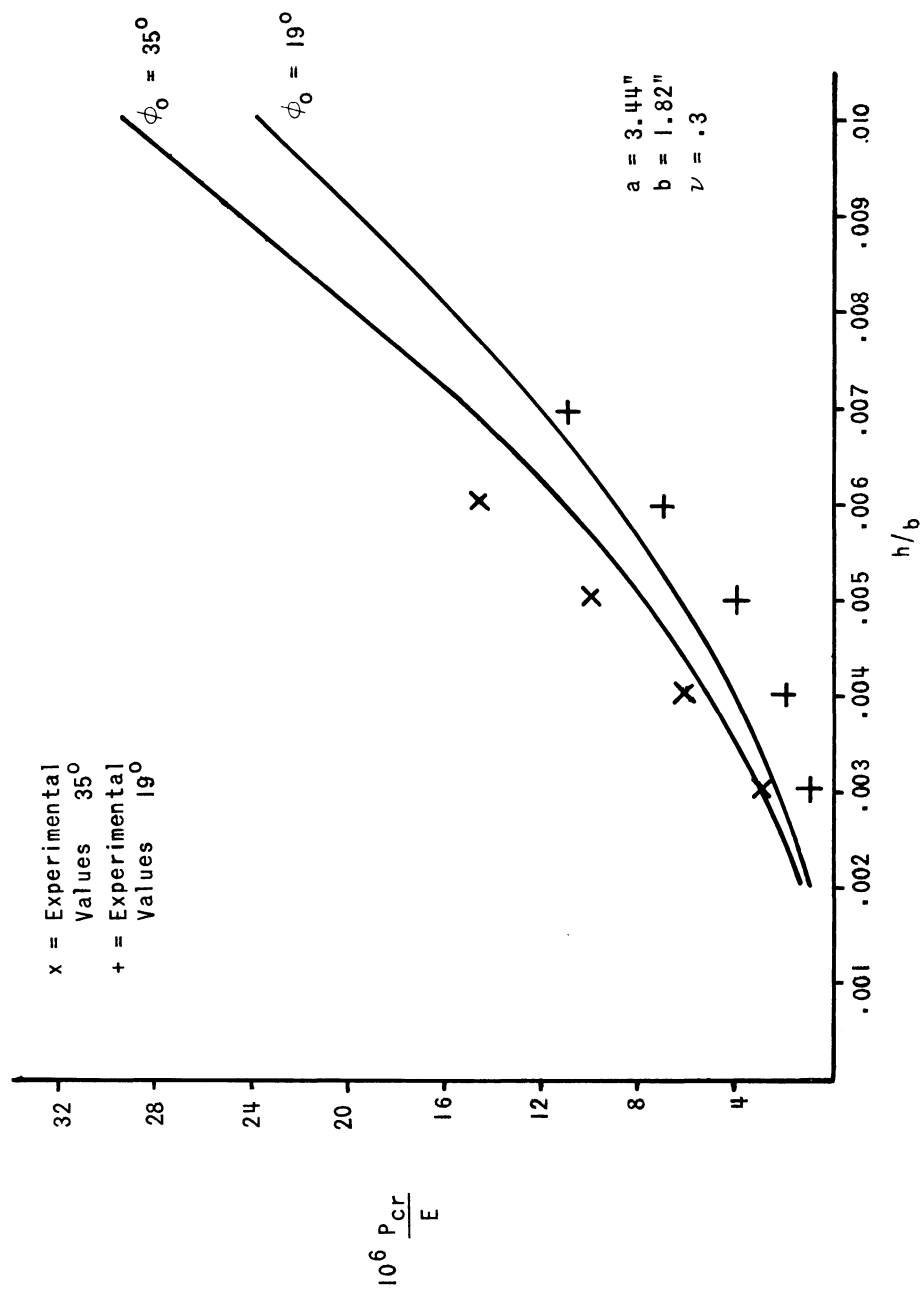


Figure 5.- Critical pressure levels.

ON SEVERAL RESEARCH PROBLEMS OF THE INSTABILITY
OF SHELL STRUCTURES

By Masatsugu Kuranishi

Nihon University, Japan

SUMMARY

First, the author describes the research results obtained by himself and his colleagues in his university on the instability of shell structures, that is, the buckling strength of full, and part of, circular and plane-walled cylinders under axial compression in elastic and plastic regions and sandwich circular cylinders under axial compression and twisting moment are treated. Then, he presents graphical methods for minimum weight design of sandwich cylinders. Lastly, the author introduces some results by Japanese researchers in this field of study.

INSTABILITY OF CIRCULAR CYLINDERS UNDER AXIAL COMPRESSION

Elastic Instability

From the theoretical point of view the necessity of investigating the origin and process of buckling of these structures exists to explain the considerable discrepancy of the classical buckling load from the experimental result. The discrepancy is too large to be attributed to some of the ordinary imperfection in the initial geometrical form, material property and loading condition. Most prevailing explanation at present, the author believes, is due to Th. v. Karman and H. S. Tsien, in which they introduced the idea of jump-over. The minimum possible buckling load corresponds in energy expression to the case where the jump over an energy barrier with equal energy level before and after the jump is possible. However, they gave no attention to the height of the energy barrier and origin of the energy variation sufficient to jump over the barrier (Ref. 1).

In Japan Y. Yoshimura and M. Uemura worked in the same line, gave some improvement in energy estimation, and extended to some cases for spherical shells (Ref. 2).

The present author suggested (Ref. 3) a new approach by

assuming a new type of buckling deformation pattern and a new process of computation of strains by comparing the initial and current shapes of elements in place of the ordinary process from the displacements of elements. The buckling deformation pattern assumed is only a preliminary attempt but in some points approximates the real pattern better than the classical ones. The tentative pattern represent the so-called diamond type of depression from the beginning of buckling and does not introduce no negative circumferential curvature even in the most depressed part of the cylindrical wall, which the experimental observation shows clearly.

The computation in this way was not sufficient to explain the discrepancy. However, the author expects success when more adequate buckling deformation pattern can be found with good approximation of the real pattern.

Plastic Buckling

The plastic buckling load becomes more important when the specific loading, that is, load per square or product of appropriately chosen overall dimensions of cylinders, increases beyond some magnitude, as will be seen in the section of minimum weight design in the following. The buckling deformation in this region is axial-symmetrical or has very small number of lobes.

The present author, having studied the difference of strains and stresses between the bulging-out part and the inward depressed part of the cylindrical wall in the axial-symmetrical deformation, gave the following effective modulus in the respective part. (Ref. 4). The tangent modulus in both the axial and circumferential directions for the bulging-out part and the Young's modulus in both directions for the inward depressed part were assigned as reasonable approximation. The computation showed the buckling load varied as $\frac{E_t}{E}$ instead of $\sqrt{\frac{E_t}{E}}$ which was given by J. W. Geckeler (Ref. 5) and only the bulging-out deformation predominates from the beginning of buckling and further on. The author believes that the result explains well the experimental data, for example, that of P. A. Robertson (Ref. 6).

BUCKLING STRENGTH OF CURVED RECTANGULAR PLATES COMPRESSED LONGITUDINALLY

The present author rearranged (Ref. 7) the experimental result obtained by J. R. Newell and W. H. Gale (Ref. 8), taking as a strength unit the following buckling strength σ_{kp} of rectangular flat plates supported freely at four edges:

$$\sigma_{kp} = \frac{\pi}{\sqrt{3(1-\nu^2)}} \cdot \sqrt{E\sigma_p} \cdot \frac{t}{b}$$

It should be noted that σ_p stands in place of σ_y which was first introduced by Th. v. Karman (Ref. 9), but the present author believes σ_p is much more suitable.

The buckling strength of curved rectangular plates in this strength unit was plotted against $\frac{b}{r}$ where b is the developed width and r the mean radius of the plates, and the author constructed the probable strength curves from these plots in dependence on the aspect ratio $\frac{a}{b}$ where a is the length of the plates, as shown in Fig. 1. He suggested also the buckling strength σ_k for very large aspect ratio in the following form:

$$\sigma_k = \sigma_{kp} + 0.18 E \frac{t}{r}$$

It was noted that there are flatter parts of curves in some range of $\frac{b}{r} < 0.1$. The author believes that only in this region the critical buckling stress and ultimate buckling strength are different, which is the prominent characteristic of flat plates in buckling.

INSTABILITY AND STRENGTH OF PLATE-WALLED CYLINDRICAL SHELLS UNDER AXIAL COMPRESSION (Ref. 10)

Closed Profiles

The plane-walled cylinders are here looked upon as a closed sequence of flat plates connected along the longitudinal edges successively. The basic assumptions for the calculation are:

1. The longitudinal wave length of the buckling deformation of any panel is the same and there is no phase difference.
2. In the critical buckling state no displacements are allowed at the edges.
3. Along an edge, the angle between the two adjacent panels is retained in the critical state and the bending moments on both sides are in equilibrium.
4. Each panel is long enough so that the end conditions at the loading edges have only negligible effect on the buckling load.

The author obtained the following condition to determine the critical buckling stress when the cylinder has m panels of equal thickness t and flexural rigidity D :

$$\begin{vmatrix} W_{a1} & W_{b1} & W_{a2} & -W_{b2} & 0 & 0 & 0 & 0 & - & - & - & 0 \\ 1 & 1 & -1 & 1 & 0 & 0 & 0 & 0 & - & - & - & 0 \\ 0 & 0 & W_{a2} & W_{b2} & W_{a3} & -W_{b3} & 0 & 0 & - & - & - & 0 \\ 0 & 0 & 1 & 1 & -1 & 1 & 0 & 0 & - & - & - & 0 \\ & & - & - & - & - & - & - & - & - & - & - \\ & & - & - & - & - & - & - & - & - & - & - \\ W_{a1} & -W_{b1} & 0 & 0 & & & & & 0 & & W_{am} & W_{bm} \\ -1 & 1 & 0 & 0 & & & & & 0 & & 1 & 1 \end{vmatrix} = 0$$

where

$$\begin{aligned} W_{an} &= m_1 \tanh \beta_n m_1 + m_2 \tanh \beta_n m_2 \\ W_{bn} &= m_1 \coth \beta_n m_1 - m_2 \cot \beta_n m_2 \end{aligned}$$

and β_n is the ratio of the width of n -th panel to a reference panel width a_v , ($n=1,2,\dots,m$). m_1 and m_2 are parameters originated from the fundamental differential equation. They determine the critical buckling stress σ_{cr} and the half wave length ℓ as follows:

$$\sigma_{cr} = \frac{2(m_1^2 + m_2^2)^2}{m_1^2 - m_2^2} \frac{D}{a_v^2 t}, \quad \pi \frac{a_v}{\ell} = \sqrt{2(m_1^2 - m_2^2)}$$

From the combinations of m_1 and m_2 satisfying the determinant we have to choose the combination which gives the least value of σ_{cr} . This is the actual critical buckling stress, and may be expressed as:

$$\sigma_{cr} = K_m \frac{D}{a_v^2 t}$$

K_m is, then, a coefficient depending on the profile form and proportion. From the second equation we obtain the corresponding half wave length.

In Fig. 2, 3, and 4 the computation results are illustrated. It should be noted here that only the sequence of the panels are concerned with the critical buckling stress, but the angles of intersection between panels do not have any effect on the buckling stress in this calculation. This is due to the edges remaining straight in the critical buckling state, which is supported by the observation in the tests. If the angle of intersection is very acute or obtuse, therefore, this theory does not apply.

Open Profiles

For open profiles the following additional basic assumptions are necessary:

1. The inner edge of the outermost panel with free edge has no deflection normal to the surface.

2. The outer edge of the second outermost panel may be deflected normal to that surface. The deflection is assumed to be restrained by the bending rigidity of the outermost panel in the normal direction to the second outermost panel.

The condition for determining the critical buckling stress may be given as follows, the number of any panel being counted from an outermost panel:

$$\begin{vmatrix} W_{g2} & W_{a3} & -W_{b3} & 0 & 0 & 0 & - & - & - & - & - & 0 \\ 1 & -1 & 1 & 0 & 0 & 0 & - & - & - & - & - & 0 \\ 0 & W_{a3} & W_{b3} & W_{a4} & -W_{b4} & 0 & - & - & - & - & - & 0 \\ 0 & 1 & 1 & -1 & 1 & 0 & - & - & - & - & - & 0 \\ & & & - & - & - & - & - & - & - & - & - \\ & & & - & - & - & - & - & - & - & - & - \\ 0 & 0 & - & - & - & - & 0 & W_{a,m-2} & W_{b,m-2} & W_{g,m-1} \\ 0 & 0 & - & - & - & - & 0 & 1 & 1 & -1 \end{vmatrix} = 0$$

where $W_{g,n}$ ($n=2$ or $m-1$) is given as:

$$W_{g,n} = \frac{P_o + P_r.r + P_s.s + P_{rs.rs}}{Q_o + Q_r.r + Q_s.s + Q_{rs.rs}}$$

$$P_o = -2m_1 + \left(\frac{m_1^2}{m_2 \cdot e} - m_2 \cdot e \right) \cdot \text{shm} \cdot \text{sim} + \left(e + \frac{1}{e} \right) \cdot \text{chm} \cdot \text{com}$$

$$P_r = (1+e) \cdot (-m_1 \cdot \text{chm} \cdot \text{sim} + m_2 \cdot \text{shm} \cdot \text{com})$$

$$P_s = -\left(\frac{1}{e}+1\right) \frac{m_1}{m_2} (m_1 \cdot \text{shm} \cdot \text{com} - m_2 \cdot \text{chm} \cdot \text{sim})$$

$$P_{rs} = -2m_1 + 2m_1 \cdot \text{chm} \cdot \text{com} - \left(\frac{m_1^2}{m_2} - m_2 \right) \cdot \text{shm} \cdot \text{sim}$$

$$Q_o = \frac{m_1}{e} \cdot \text{chm} \cdot \text{sim} - m_2 \cdot e \cdot \text{shm} \cdot \text{com}$$

$$Q_r = -(1+e) \cdot m_2 \cdot \text{shm} \cdot \text{sim}$$

$$Q_s = -\left(\frac{1}{e}+1\right) \cdot m_1 \cdot \text{chm} \cdot \text{com}$$

$$Q_{rs} = -m_1 \cdot \text{chm} \cdot \text{sim} + m_2 \cdot \text{shm} \cdot \text{com}$$

$$\text{chm} = \cosh 2\beta_n m_1, \text{shm} = \sinh 2\beta_n m_1, \text{com} = \cos 2\beta_n m_2,$$

$$\text{sim} = \sin 2\beta_n m_2$$

$$e = \frac{\left(1 - \frac{\nu}{2}\right) m_2^2 + \frac{\nu}{2} m_1^2}{\left(1 - \frac{\nu}{2}\right) m_1^2 + \frac{\nu}{2} m_2^2}$$

$$r = N_{r,1} \text{ or } m \cdot \frac{(m_1^2 - m_2^2)^2}{2m_2^2 \left(\left(1 - \frac{\nu}{2}\right) m_1^2 + \frac{\nu}{2} m_2^2 \right)} \cdot \beta_n m_2$$

$$s = -\frac{2}{W_{f,1} \text{ or } m \cdot a_\nu} \left(1 + \frac{1}{e} \right)$$

Here $W_{f,1}$ or m is the value of $\frac{P_o}{Q_o}$ for the outermost panel, therefore, β_1 or β_m should be used in place of β_n in the above cited equation, and $N_{r,1}$ or m is the bending rigidity of the outermost panel against the flexure of the adjacent panel edge, expressed in non-dimensional form. For example, $N_{r,m}$ is calculated from

$$N_{r,m} = \frac{E}{a_{m-1}D} \left(\frac{t a_m^2}{12} + \frac{a_m \cdot a_{e,m-1}}{a_m + a_{e,m-1}} t \frac{a_m^2}{4} - \frac{a_m + a_{e,m-1}}{a_{m-1}} \cdot \frac{(m_1^2 + m_2^2)^2}{(m_1^2 - m_2^2)^2} \right)$$

$N_{r,1}$ is expressed in the similar form. Here the first term presents the bending rigidity ratio taking account of the effective width $a_{e,m-1}$ or 2 in the second outermost panel, and the second term expresses the reduction due to the compressive stress in the area concerned. The effective width $a_{e,m-1}$ or 2 should be determined as a function of $\frac{t}{a_{m-1}}$ or 2 as well known in the literature

(Ref. 11). The calculated results for angles with stiffened edges, channels, hat and C profiles are given in Fig. 5, 6, 7 and 8.

The low values of K_m for small values of β are due to the poor values of N_r , and those for larger values of β are caused by the effect of the free edges. The most remarkable point, however, is that the summit values for suitable magnitude of β are comparable with those of the corresponding closed profiles.

Experimental Results and Comment

The present author made experiments for the wall buckling strength of rectangular closed cylinders, and C, hat and channel profiles made of aluminum alloy corresponding to 17S. The test results are converted to standard values which correspond to the critical buckling stress of rectangular flat plates supported freely along four edges. Considering some strength values exceed the proportional limit, the author converted the thickness ratio, $\frac{t}{a_v}$, that is, the ratio of the thickness to the width of reference to the standard thickness ratio $(\frac{t}{a})_{st}$ by the formula:

$$(\frac{t}{a})_{st} = (\frac{t}{a_v}) \frac{\sqrt{K_m}}{2\pi}$$

Here K_m is the coefficient for the test specimen. And it was received some correction in compliance with the actual sectional form of the specimen, for example, the round corners were assumed to have the strength as circular cylindrical wall.

The buckling strengths σ_k were plotted against $(\frac{t}{a})_{st}$ as shown in Fig. 9. The experimental points stand in comparatively narrow band, which may be deemed as substantiating the present theory. Then, the experimental curve was drawn. In the elastic region it was assumed to be a straight line just as it is the case for rectangular flat plates.

The buckling strength of channel profiles which were not included in Fig. 9 went very little above the critical buckling stress, and it may be assumed the critical and ultimate buckling stresses coincide with each other. The author believes the reason is in that the stress rearrangement beyond the critical buckling load which is allowed in other profiles can not be realized in channels because of the lack of equilibrium.

Although similar investigations have been published as well known, it may be remarked that the present author treated this problem in the most generalized form, and especially, in calculating N_r for open profiles he took full account of the effective width in the adjacent panel and the reduction of flexural rigidity due to the compressive stress in the area.

SANDWICH CYLINDRICAL SHELLS

Simple Theory (Ref. 12)

In the simple theory the conventional assumption was adopted that the face plates are very thin, the flexural rigidity of themselves may be neglected, and the normal and shear forces in the surface of cylinders are taken by the faces, and the shear force normal to the surface is taken by the core in which the deformation normal to the surface is excluded.

The result of computation shows that the buckling stress σ_k of sandwich circular cylinders under axial compression may be expressed as:

$$(a) \quad \sigma_k = \frac{E_f}{\sqrt{1-\nu_f^2}} \frac{h}{a} \left(2 - \frac{1}{\sqrt{1-\nu_f^2}} \cdot \frac{E_f \cdot t_f \cdot h}{G_c \cdot t_c \cdot a} \right)$$

provided

$$K_p = \frac{1}{\sqrt{1-\nu_f^2}} \cdot \frac{E_f \cdot t_f \cdot h}{G_c \cdot t_c \cdot a} \leq 1$$

If K_p is larger than 1,

$$\sigma_k = \frac{t_c}{t_f} G_c$$

Here t_f , $2t_c$ are the thickness of the face and core, respectively, $2h = 2t_c + t_f$, the center distance of two faces, and a is the mean radius of the cylinder. The other conventional notations for the face and core are distinguished by the subscripts f and c .

The buckling shear stress τ_k when long cylinders are twisted is given as:

$$\tau_k = 1.05 \cdot (1 - K_t) \frac{E_f}{(1 - \nu_f^2)^{3/4}} \cdot \left(\frac{h}{a}\right)^2$$

where

$$K_t = \frac{2}{2} \cdot \frac{1}{1 - \nu_f^2} \cdot \frac{E_f}{G_c} \cdot \frac{t_f}{t_c} \cdot \left(\frac{h}{a}\right)^2$$

provided $1 > K_t > 0$. Normally K_t is very small against 1 and we may put usually $K_t = 0$.

Similar results have been obtained by other authors (Ref. 13), only the coefficients being somewhat different.

More Accurate Theory

Since K_p in the preceding section can sometimes exceed unit, and in that region the flexural rigidity of face plates themselves and others are no more negligible, the authors developed, retaining only one basic assumption that the rigidness of core normal to the surface of cylinders continues to exist, we could show the buckling stress σ_k increases uniformly along with

$\frac{t_f}{a}$ or $\frac{h}{a}$ instead of remaining constant at the value, $\frac{t_c}{t_f} G_c$ as in the simple theory.

As an approximate expression satisfying the numerical examples we could suggest the following equation for σ_k :

$$(b) \sigma_k = \frac{E_f}{\sqrt{1-\nu_f^2}} \frac{h}{a} \cdot (1-K_p) + 56.5 \frac{E_f}{1-\nu_f^2} \cdot \frac{t_f}{a} \cdot \frac{h}{a} \cdot \left(1 + 16 \frac{1-\nu_f^2}{1-\nu_c^2} \frac{E_c}{E_f} \frac{t_c^2}{t_f^2}\right)$$

for $K_p \leq 1$, and if $K_p > 1$, put $K_p = 1$ in the equation.

GRAPHICAL APPROACHES OF MINIMUM WEIGHT DESIGN

Sandwich Cylinders under Axial Compression

The problem is the procedure to make the weight per axial length W minimum for a given total axial load P and mean radius a , or a given specific loading $\frac{P}{a}$ of sandwich cylinders such as treated in the preceding sections, the densities of face and core materials being ρ_f and ρ_c , respectively. They have the following relations:

$$\frac{P}{a} = \sigma_k \cdot 4\pi \frac{t_f}{a}$$

$$\frac{W}{a} = 4\pi \left(\rho_c \frac{h}{a} + \left(\rho_f - \frac{\rho_c}{2} \right) \frac{t_f}{a} \right)$$

$$\frac{P}{W} = \frac{\sigma_k}{\frac{h}{a} \cdot \rho_c \cdot \frac{a}{t_f} + \left(\rho_f - \frac{\rho_c}{2} \right)}$$

First, we assume we have the buckling strength curves of σ_k against $\frac{h}{a}$ for several prescribed values of $\frac{t_f}{a}$. These curves may be constructed from Eq. (a) or (b) in the preceding sections, taking account of an appropriate law of plasticity for σ_k above the proportional limit of the materials, or they may be experimental results. These curves are shown as an example on the right half of Fig. 10. The values in this figure are selected only for explanation and should not be regarded as actual example.

Taking a curve with a constant value of $\frac{t_f}{a}$ and multiplying the $\frac{h}{a}$ values with $\rho_c \cdot \frac{a}{t_f}$, construct a new curve of σ_k against

$\frac{h}{a} \cdot \rho_c \cdot \frac{a}{t_f}$ as shown in Fig. 11. Then, it is clear from the last of the above-mentioned equations the value of strength-weight ratio $\frac{P}{W}$ will, then, be determined by drawing straight lines from a point $-(\rho_f - \frac{\rho_c}{2})$ on the abscissa axis as drawn in the figure. The slope of the straight line is equal to $\frac{P}{W}$ which may be read on a ordinate line with appropriate scale. In Fig. 11 the ordinate axis was chosen, but for clearness the scale was transferred to a position on the left side.

From the values of σ_k and $\frac{h}{a}$ of the points of intersection we can compute the specific loading $\frac{P}{a}$ and the strength-weight ratio $\frac{P}{W}$. Varying values of $\frac{t_f}{a}$ we obtain the curves as shown in full lines in Fig. 12. If we choose stepwise the values of $\frac{t_f}{a}$, as in this example, then the uppermost parts of the curves correspond to the optimum selection of combination. When we change $\frac{t_f}{a}$ continuously, the envelope of the curves replaces them and each contact point will determine the optimum combination. In Fig. 12 the curves of $\frac{h}{a}$ for the optimum combination are shown in dotted lines. Consequently, we can determine easily the optimum set of $\frac{t_f}{a}$ and $\frac{h}{a}$ for a given value of $\frac{P}{a}$ and the resulting value of $\frac{P}{W}$ from the curves in the figure. Similarly we may construct curves of $\frac{W}{a}$ against $\frac{P}{a}$.

It should be noted here that the maximum point of $\frac{P}{W}$ for a prescribed value of $\frac{t_f}{a}$ is not necessarily the optimum point when the value of $\frac{t_f}{a}$ is varied.

If it is desired to compare the merit of density variation

of face and core, retaining the buckling strength, we have to change ρ_f and ρ_c in wide range. Then, it is suitable to keep the curves of σ_k against $\frac{h}{a}$ with $\frac{t_f}{a}$ as parameter and to change the starting points of the straight lines for $\frac{P}{W}$ to $-(\frac{\rho_f}{\rho_c} - \frac{1}{2})\frac{t_f}{a}$ as shown in Fig. 10, since we have the following rearranged equation:

$$\frac{P \cdot t_f}{W a \rho_c} = \frac{\sigma_k}{\frac{h}{a} + (\frac{\rho_f}{\rho_c} - \frac{1}{2}) \frac{t_f}{a}}$$

Consequently, in this method the slope should be multiplied by $\frac{a \rho_c}{t_f}$ to obtain the corresponding $\frac{P}{W}$ values.

Sandwich Cylinders under Column Effect

If sandwich cylinders under axial compression are so long that the column effect cannot be neglected, we have to extend the procedure of the minimum weight design to this range. For simplicity we assume that the wall buckling strength is as determined in the preceding sections and the bending buckling strength as a whole is determined only by the face plates, cylinder radius and length. In addition, the two types of buckling are assumed to have no interaction, although for both we have to give full consideration of the effect of plasticity for the stress above the proportional limit.

In this sort of problem we have to decide the optimum radius of the cylinder, $\frac{h}{a}$ and $\frac{t_f}{a}$ for a given set of the axial force P and the cylinder length L . To begin with, it is assumed that we have the buckling strength curve of σ_k against the slenderness number $(\frac{1}{L})^2$, that is, the reciprocal of the squared slenderness ratio, with $\frac{h}{a}$ as parameter for a prescribed value of $\frac{t_f}{a}$ as shown in Fig. 13. The equations expressing the relationship between the variables in the preceding section hold also in this case.

Therefore, dividing the ordinates in Fig. 13 by $\frac{h \cdot a}{a \cdot t_f} (\rho_c + (\rho_f - \frac{\rho_c}{2}))$, we get Fig. 14 for various values of $\frac{h}{a}$, m , a , b , c , e corresponding to the wall buckling strength with the same index in Fig. 13.

Connecting the corners, that is, the points of intersection of the curve from the bending buckling strength and the horizontal line from the wall buckling strength in Fig. 14, we obtain the optimum curve for the prescribed value of $\frac{t}{a}$. These optimum curves for several values of $\frac{t}{a}$ are shown in Fig. 15.

For a given set of P and L we select $\frac{P}{L}$ as the specific loading in this case. Accordingly, we transform the abscissa in Fig. 15 into the specific loading $\frac{P}{L}$ with the relation:

$$\frac{P}{L} = \sigma_k \cdot 16\pi \frac{t_f}{a} \cdot \frac{i^2}{L^2}$$

Thus, we get the curves of the strength-weight ratio $\frac{P}{W}$ against the specific loading $\frac{P}{L}$ as shown in Fig. 16. If the values of $\frac{t_f}{a}$ are chosen stepwise, the uppermost parts of the curves correspond to the optimum selection of $\frac{t_f}{a}$. If $\frac{t_f}{a}$ is varied continuously, the envelope of the curves will represent the optimum values of strength-weight ratio. Then, the contact point of the envelope with a curve determine the optimum value of $\frac{t_f}{a}$. The corresponding values of $\frac{h}{a}$ are read in Fig. 14. The values of $\frac{a}{L}$ will be given by the following relation from the slenderness number:

$$\frac{a^2}{L^2} = 4 \frac{i^2}{L^2}$$

These values of $\frac{h}{a}$ and $\frac{a}{L}$ were determined and given also in Fig. 16 against $\frac{P}{L}$ with $\frac{t_f}{a}$ as parameter.

It is noted that the most optimum part of $\frac{P}{W}$ when the values of $\frac{t_f}{a}$ are varied falls apart from the maximum point of $\frac{P}{W}$ for a prescribed value of $\frac{t_f}{a}$ somewhat more than in the case where the column effect is ignored.

Comment and Future Research

As can be seen from the results in preceding sections, in the minimum weight analysis the strength in the plastic region is much more important than that in the elastic region, because the weight-strength ratio is always favorable in the former region when the specific loading is high enough. On the contrary, if the specific loading is at low level, it is much advisable to resort to other types of structure, such as locally concentrated structures to ameliorate the weight-strength ratio by increasing the allowable stress. The present author believes, therefore, the analysis of stiffened structures is very important in the minimum weight design for low specific loading. Since the stiffeners, however, have chances of failure in many sorts of buckling, the analysis is quite complicated. Ordinarily, the bending buckling alone is considered. But there are evidences that the stiffeners fail through the torsional buckling or the wall buckling in many cases. Therefore, the theory of the minimum weight design taking account of every sort of failure is very much desired in the future.

We often express the results of analysis of minimum weight design by equations which contain some plasticity coefficients or reduced moduli and the specific loading. However, the plasticity coefficients and others are a certain function of the stress, consequently, that of the specific loading. Therefore, those expressions are not suitable for practical selection of optimum proportions of the structure.

OTHER RESEARCH RESULTS IN JAPAN

Buckling Strength of Circular Cylinders under
Bending and External or Internal Pressure

K. Ikeda after having studied theoretically and experimentally gave the following formula for the allowable bending moment M_k and pressure p_k (Ref. 14) (Fig. 17).

For external pressure:-

$$\frac{M_k^2}{M_{ko}^2} + \frac{p_k}{p_{ko}} = 1$$

where

$$M_{ko} = \frac{2\sqrt{2} \cdot E \pi r t^2}{9 \sqrt{1-\nu^2}} \quad (\text{Ref. 15})$$

$$p_{ko} = \frac{E}{4(1-\nu^2)} \cdot \frac{t^3}{r^3} \quad (\text{Ref. 16})$$

For internal pressure:-

$$\frac{M_k}{M_{ko}} = 0.65 + 0.835 \frac{(1 - \frac{p_k}{p_{ko}})^{\frac{1}{2}} \cdot (4.8 - \frac{2p_k}{p_{ko}})}{(3.25 - \frac{p_k}{p_{ko}})^{\frac{1}{2}} (6.5 - \frac{2p_k}{p_{ko}})}$$

And if p is comparatively high, i.e. $-p_k > p_{ko}$

$$\frac{M_k}{M_{ko}} = 1.49 + 0.56 \sqrt{1-\nu^2} \cdot \frac{r^2 - p_k}{t^2 E}$$

Buckling Strength of Circular Cylinders under
Torsion and External or Internal Pressure

Y. Yoshimura and H. Mōri investigated theoretically and gave the following experimental formula for the allowable torsional moment M_{tk} and pressure p_k (Ref. 17) (Fig. 18).

$$\left(\frac{M_{tk}}{(M_{tk})_{p=0}}\right)^{\frac{4}{3}} + \frac{p_k}{p_{ko}} = 1$$

Buckling Strength of Orthotropic Cylinders under Torsion

T. Hayashi showed that the well known Donnell's expression (Ref. 18) for the torsional buckling can be extended to this case only by putting: (Ref. 19).

$$B = \frac{\tau_k \cdot t}{\alpha_1(1-\nu_1\nu_2)} \sqrt{\frac{\alpha_1(1-\nu_1\nu_2)L^2}{12 D_2}}$$

$$J = \sqrt{\frac{12D_2}{\alpha_1(1-\nu_1\nu_2)}} \cdot \frac{1}{d^6}$$

where the orthotropic symmetry axes coincide with the longitudinal and circumferential directions and are denoted by 1 and 2, respectively, consequently, the extensional rigidity are designated as α_1, α_2 and the flexural rigidity by D_1, D_2 , respectively.

REFERENCES

1. Karman, Th., and Tsien, H. S.: The Buckling of Thin Cylindrical Shells under Axial Compression. J. A. S., vol. 8, no. 8, 1941, pp. 303-312.
Tsien, H. S.: A Theory for the Buckling of Thin Shells. J. A. S., vol. 9, no. 10, 1942, pp. 373-384.
2. Yoshimura, Y.: On the Mechanism of a Circular Cylindrical Shell (in Japanese). Rep. of Inst. of Sci. and Tech., vol. 5, 1951, pp. 179-198; NACA Techn. Mem. no. 1390, 1955.
Yoshimura, Y. and Uemura, M.: The Buckling of Spherical Shells due to External Pressure (in Japanese). Rep. of Inst. of Sci. and Tech., vol. 3, no. 12-13, 1951, pp. 316-322; vol. 6, no. 6, 1952, pp. 367-371.
3. Kuranishi, M. and Niisawa, J.: An Approach to the Real Buckling Stress of Thin Cylindrical Shells under Axial Compression. Proc. of Symp. on the Theory of Thin Elastic Shells, Delft, 1959, North-Holland Publ. Co., Amsterdam, 1960, pp. 189-201.

4. Kuranishi, M.: The Buckling Stress of Thin Cylindrical Shell under Axial Compressive Load, Forming Axial-Symmetrical Deformation. J. of Japan Soc. for Appl. Mech., vol. 3, no. 18, pp. 139-144.
5. Geckeler, J. W.: Plastische Knicken der Wandung von Hohlzylindern und einige andere Faltungserscheinungen von Schalen und Blechen. Z. Angew. Math. u. Mech., Bd. 8, 1928, p. 341.
6. Robertson, P. A.: The Strength of Tubular Struts. Aeron. Res. Comm., R. & M. no. 1185, 1927.
7. Kuranishi, M.: The Theory of Elasticity (Book in Japanese). Japan Soc. Mech. Engrs., 1948, p. 523.
8. Newell, J. S. and Gale, W. H.: Note on the Design of Metal Plates for Use in Airplane Structures. M. I. T. Report on Aircraft Material Research, 1931-1932.
9. Karman, Th., Sechler, E. E. and Donnell, L. H.: The Strength of Thin Plates in Compression. Trans. A. S. M. E., vol. 54, 1932, pp. 53-56.
10. Kuranishi, M.: The Wall Buckling Strength of Thin Plane--Walled Struts under Axial Compressive Load (in Japanese). J. of Soc. of Aeron. Sci. of Japan, vol. 2, no. 3-5, pp. 55-86, 259-284, 485-508.
11. Karman, Th.: Ueber die mitttragende Breite. A. Foeppl--Festschrift, 1924.
12. Kuranishi, M. and Nagao, H.: Bending and Buckling of Sandwich Beams, Plates and Shells, 1st Report (in Japanese). J. of Research Inst. of Technology, Nihon Univer., no. 15, pp. 196-213.
13. Teichman, F. K., Wang, C. T. and Gerard, G.: Buckling of Sandwich Cylinders under Axial Compression. J. A. S., vol. 18, no. 6, June, 1951, pp. 398-406.
Gerard, G.: Torsional Instability of a Long Sandwich Cylinder. Proc. 1st U. S. Nat. Congr. for Appl. Mech., 1951, pp. 391-394.
14. Ikeda, K.: Bending of Thin Circular Cylinders under Internal or External Pressure (in Japanese). J. of Soc. Aeron. Sci. of Japan, vol. 7, no. 68, 1940, pp. 1100-1120.

15. Brazier, L. G.: On the Flexure of Thin Cylindrical Shells and Other Thin Sections. Proc. Roy. Soc. London, Ser. A, vol. 116, 1927, pp. 104-114; or R. & M., no. 1081, 1927.
16. Bryan, H.: On the Stability of Elastic Systems. Proc. Cambridge Phil. Soc., vol. 6, 1888; or that cited in "Theory of Elastic Stability" by S. Timoshenko p. 220.
17. Yoshimura, Y. and Môri, H.: On the Torsional Buckling of Thin Circular Cylinders under Internal or External Pressure (in Japanese). Report of Aeron. Research Inst., Tokyo Univ., vol. 19, no. 264, 1943, pp. 347-359.
18. Donnell, L. H.: Stability of Thin-Walled Tubes under Torsion. NACA Tech. Rep. No. 479, 1933.
19. Hayashi, T.: On the Buckling of Orthotropic Circular Cylinders (in Japanese). J. of Naval Architects of Japan, vol. 9, no. 81, 1949, pp. 85-98.

BUCKLING STRENGTH OF CURVED PLATES

BUCKLING STRENGTH
RATIO

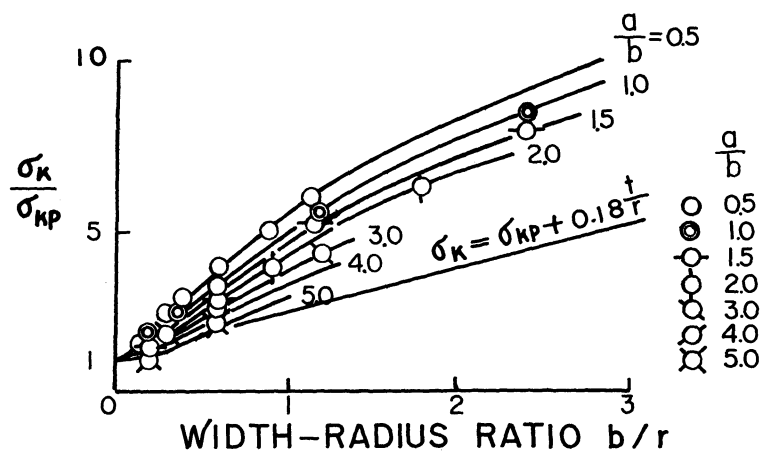


Figure 1

BUCKLING COEFFICIENTS OF RECTANGULAR CYLINDERS

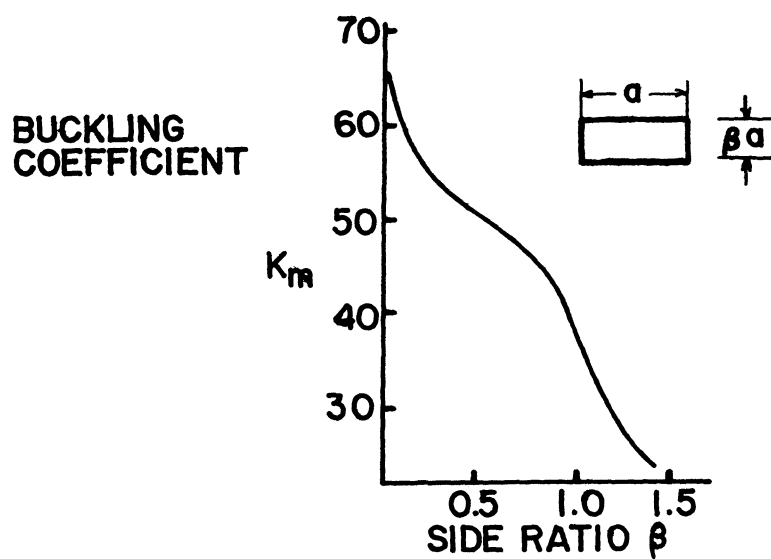


Figure 2

BUCKLING COEFFICIENTS OF TRAPEZOIDAL CYLINDERS

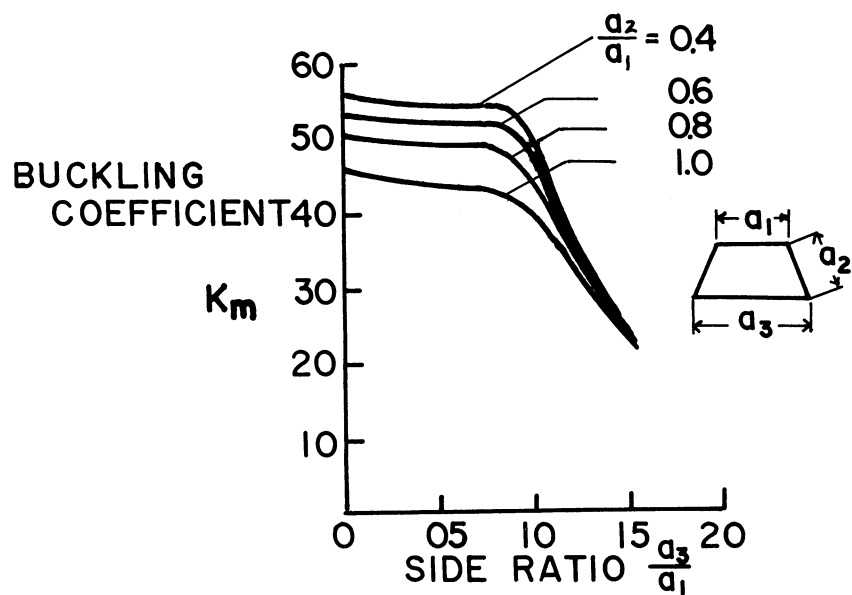


Figure 3

BUCKLING COEFFICIENTS OF ISOSCELES-TRIANGULAR CYLINDERS

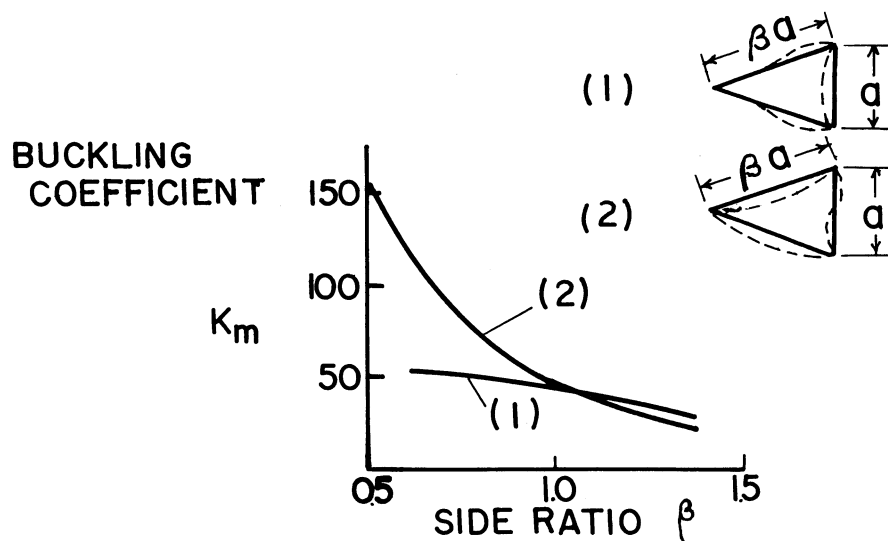


Figure 4

BUCKLING COEFFICIENTS OF ANGLES WITH STIFFENED EDGES

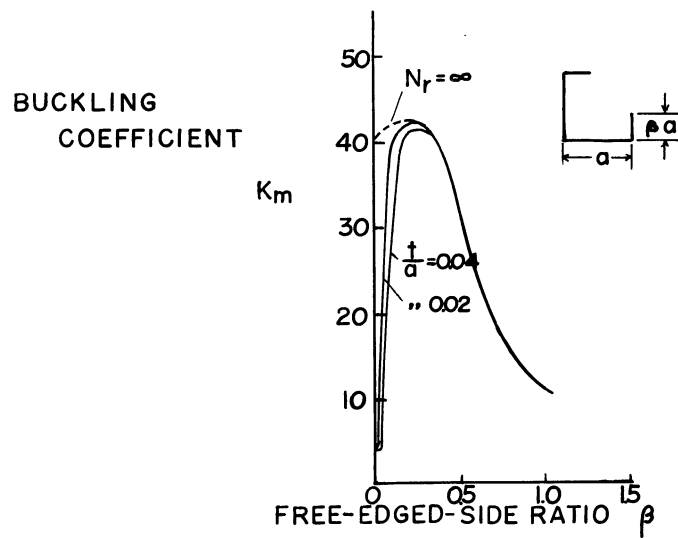


Figure 5

BUCKLING COEFFICIENTS OF CHANNELS

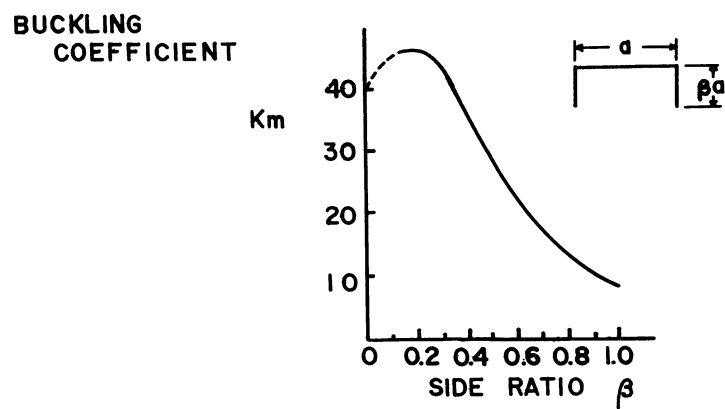


Figure 6

BUCKLING COEFFICIENTS OF C AND HAT PROFILES, SIDE RATIO=1,0

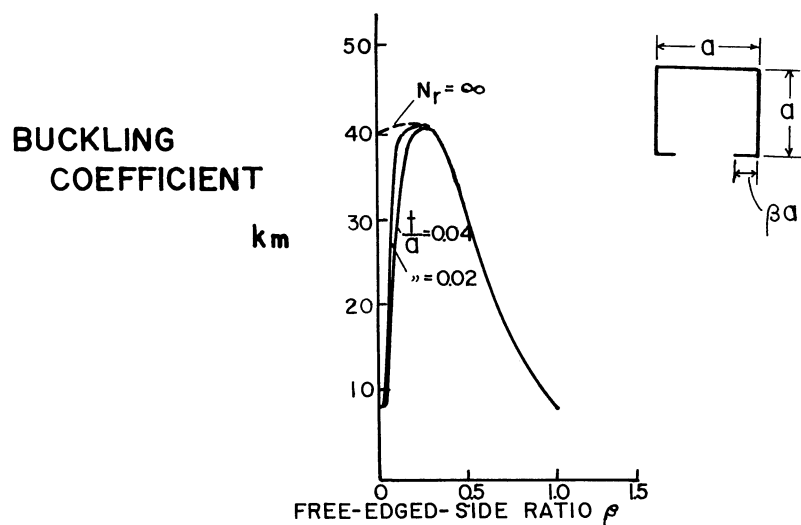


Figure 7

BUCKLING COEFFICIENT OF C AND HAT PROFILES, SIDE RATIO = 0.6

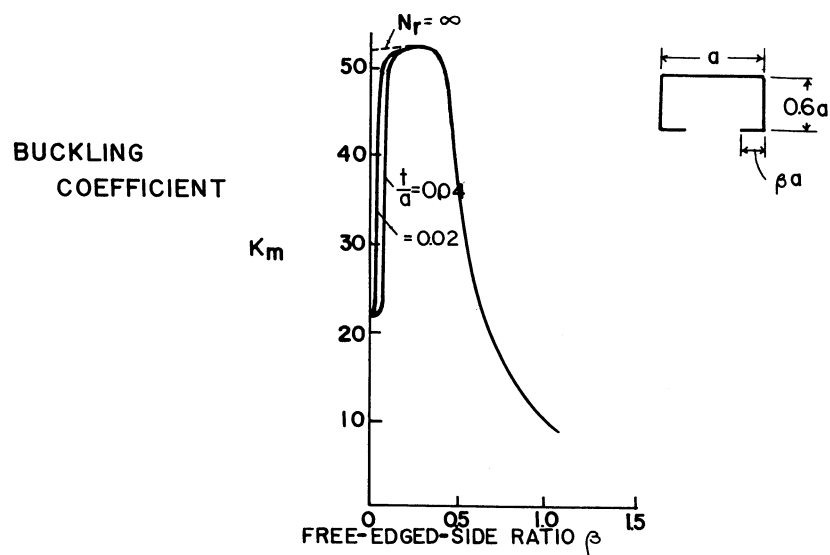


Figure 8

BUCKLING STRENGTH OF PLANE-WALLED CYLINDERS EXPERIMENTAL RESULTS

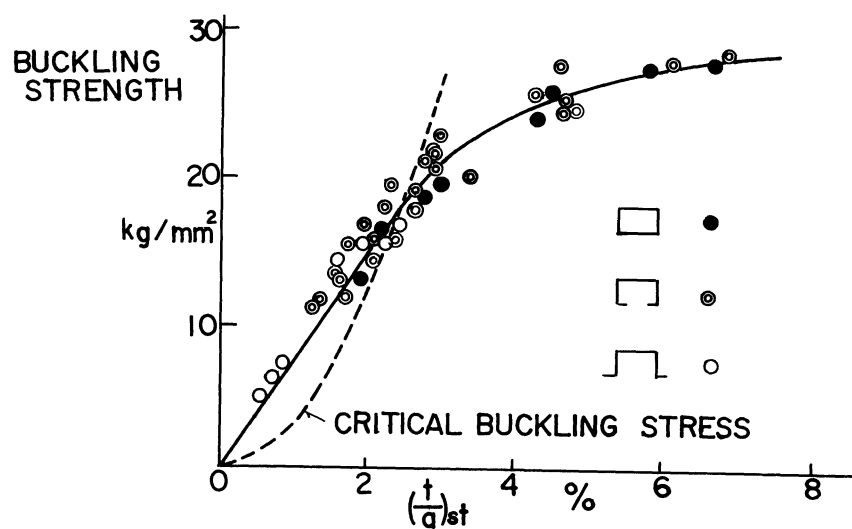


Figure 9

BUCKLING STRENGTH vs. h/a AND STRENGTH-WEIGHT RATIO

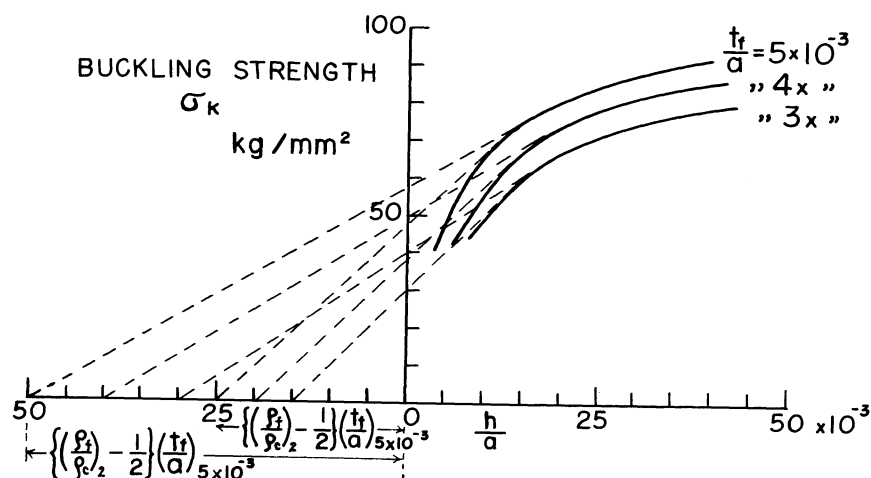


Figure 10

BUCKLING STRENGTH AND STRENGTH-WEIGHT RATIO

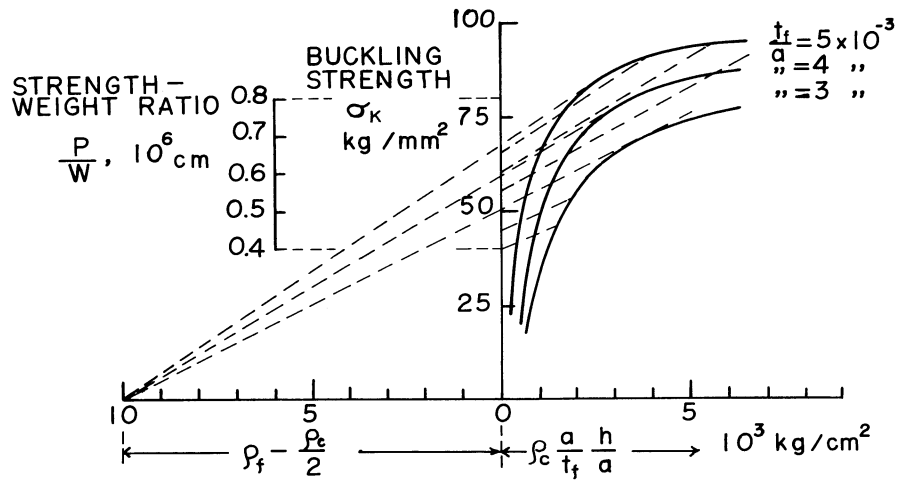


Figure 11

STRENGTH-WEIGHT RATIO vs. SPECIFIC LOADING, P/a^2

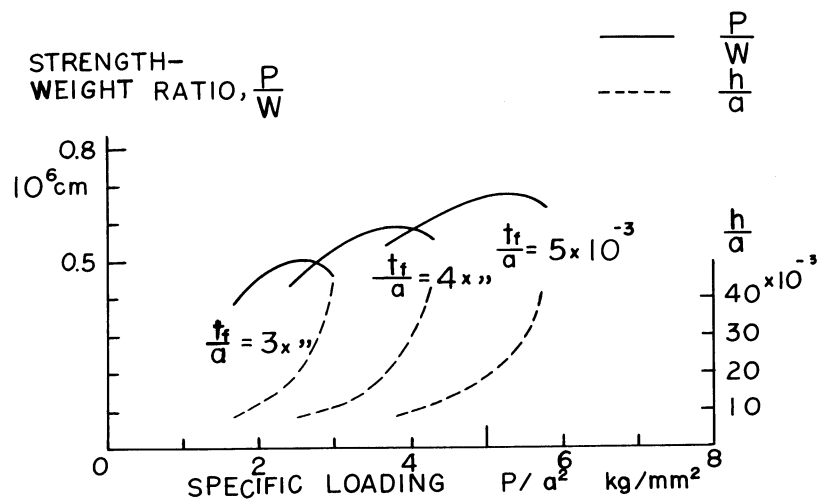


Figure 12

BUCKLING STRENGTH vs.
SLENDERNESS NUMBER, i^2/L^2

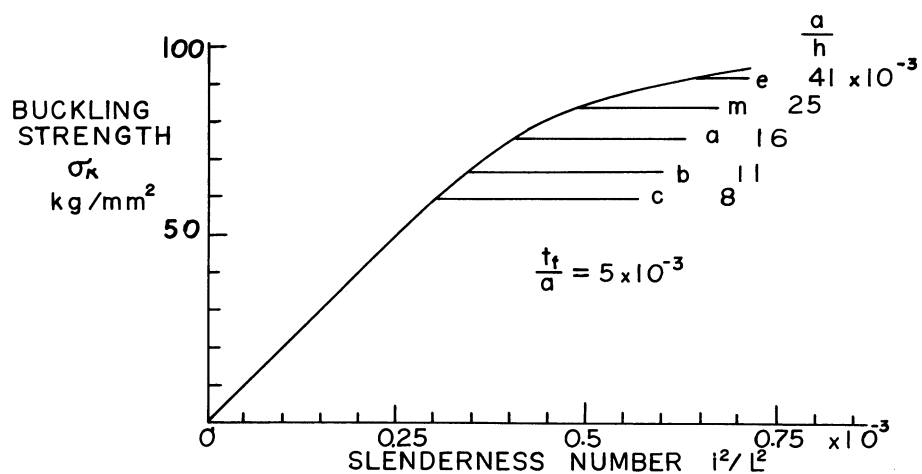


Figure 13

STRENGTH-WEIGHT RATIO $\frac{P}{W}$ vs.
SLENDERNESS NUMBER i^2/L^2
FOR A VALUE OF t_f/a

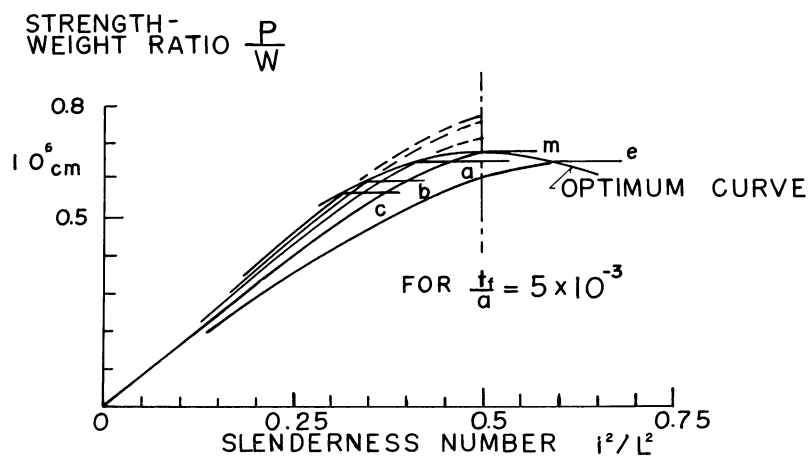


Figure 14

STRENGTH-WEIGHT RATIO vs.
SLENDERNESS NUMBER, i^2/L^2
OPTIMUM CURVES

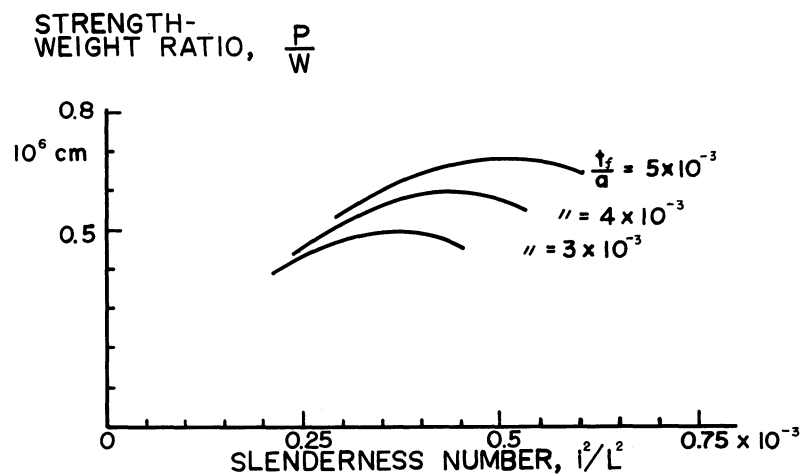


Figure 15

STRENGTH-WEIGHT RATIO vs.
SPECIFIC LOADING, P/L^2

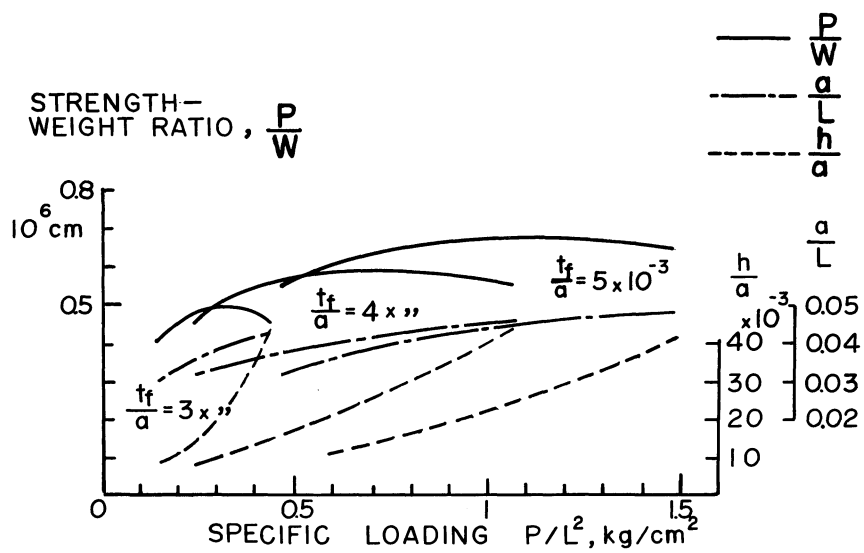


Figure 16

BUCKLING STRENGTH OF CIRCULAR CYLINDERS UNDER BENDING AND EXTERNAL OR INTERNAL PRESSURE

BENDING MOMENT

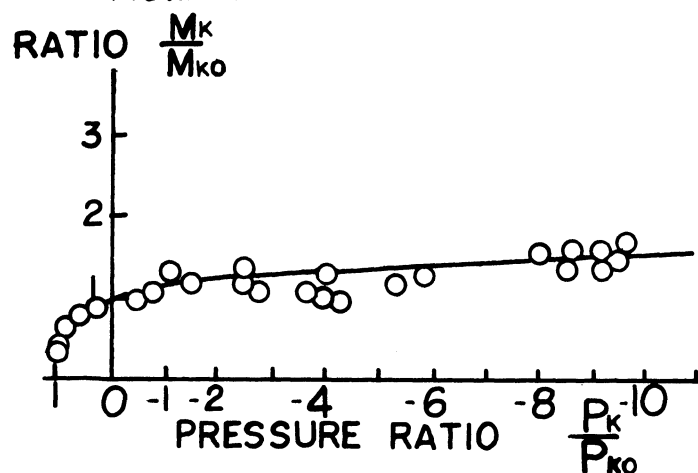


Figure 17

BUCKLING STRENGTH OF CIRCULAR CYLINDERS UNDER TORSION AND EXTERNAL OR INTERNAL PRESSURE

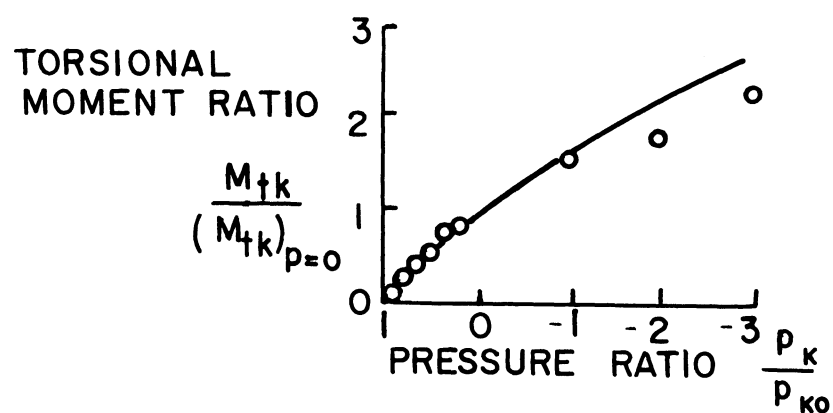


Figure 18

RECENT SOVIET CONTRIBUTIONS TO INSTABILITY OF
SHELL STRUCTURES

By George Herrmann

Northwestern University

SUMMARY

A review of major recent Soviet contributions to instability of shell structures is presented. Some current trends are discussed and established programs for future research are indicated. A representative bibliography is included.

INTRODUCTION

As in many other areas of applied mechanics, the Russian activities in the field of shell theory during the past decades have been extensive and varied. Research on shell instability, in particular, has been carried out at a considerable rate of increase over the past few years. As a consequence of imposed space limitations for papers of this symposium, however, it is the purpose of this review to discuss briefly only the major Soviet contributions of the last 3-4 years. The bibliography, even though limited, should still be broad enough to permit the reader to obtain more detailed information on a given specific problem.

The source material consisted primarily of publications in the Soviet periodical literature and listed in review journals such as Applied Mechanics Reviews and the Mechanics Section of the Soviet Reviews Journal. Fortunately, the language barrier which prevented many Western scientists and engineers from becoming acquainted with Russian work is less rigid now than in the past, thanks to numerous translation projects. In the field of shells attention should be called especially to translations published by NASA, by the American Rocket Society in the Russian Supplement to their journal, and by the ASME, in the translated Journal of Applied Mathematics and Mechanics, (PMM).

Before proceeding to a discussion of specific topics in shell stability, it appears appropriate to indicate certain general features and trends in the work of Russian scientists engaged in shell theory,

as these trends emerge from a study of recent publications. It can be noted that work on shell stability in Russia is spread over numerous institutions and that a large number of engineers and scientists are engaged in this field, representing the interests of aerospace, chemical, civil and mechanical engineering. In tackling stability problems a variety of assumptions is used, resulting in both linear and nonlinear governing differential equations. Statistical treatment of stability problems is commanding increased attention and the trend toward adaptation of approximate methods for use in conjunction with high speed computers is quite strong.

It was considered beyond the scope of this review to compare concrete results obtained in Russia with those available to Western scientists and thus the review is descriptive rather than critical.

A number of special conferences on plates and shells was held in the recent past, the last one in L'vov in September 1961, as reported in reference 1. Some sixty papers were presented, including such topics as: nonlinear problems and their effective solution, asymptotic methods in shell theory, postbuckling behavior based on the hypothesis of isometric properties of the middle surface, statistical methods of analysis of nonlinear problems in shell stability and application of multidimensional Markov processes to the stability analysis of shells subjected to random impact. In summarizing the discussions of this conference, the participants outlined areas of shell theory which should be emphasized in the future which included: general theory of elastic shells, behavior beyond the elastic limit, shells subjected to a variable thermal field, creep of shells, dynamic problems, and nonlinear problems. It was stressed that more experimental work is needed in shell theory and that a larger number of young scientists should be induced to work in shell theory. The next conference of this series is scheduled to take place in Erevan in October 1962.

INSTABILITY OF SHELLS

General

A number of recent papers is concerned with general questions associated with shell instability. Statistical methods in the nonlinear theory of elastic shells are presented in ref. 2 and applied in ref. 3 to evaluate more than 200 American test results reported in ref. 4.

A different method, based on probability considerations, is reported in ref. 5, where the difference in the influence of inaccuracies of shell properties and of loading are pointed out.

Effects of linearization of shell equations on stability are discussed in ref. 6 and conditions of applicability of variational methods are established in ref. 7. Plastic buckling of shells of revolution was examined in ref. 8.

Cylindrical Shells

A large number of papers reports studies on buckling of circular cylindrical shells subjected to various loadings. The linearized buckling equations are solved by energy or Galerkin methods in refs. 10 to 18. Stiffened cylindrical shells with various arrangement of stiffening members are considered in refs. 19 to 23, the last paper formulating the conclusion that it is more advantageous to place fewer stringers but of larger stiffness rather than vice versa. The influence of boundary conditions of buckling loads is established in refs. 24 and 25. The buckling problem in nonlinear formulation was considered in refs. 26 to 32. In particular, the critical stress of a cylindrical shell subjected to pure bending was found in ref. 33 to be equal to $0.26 E h / R$ and in ref. 34 equal to $0.295 E h / (R \sqrt{1 - \nu^2})$ where E is Young's modulus, h the thickness, R the radius and ν Poisson's ratio. The problem of the variation of the buckling region was considered in ref. 35. Ref. 36 deals with loss of stability in the plastic region of a shell subjected to axial compression.

Conical Shells

Stability of a conical shell of circular cross-section subjected to uniform external pressure was considered in ref. 37 and the critical combination of bending moments and pressure acting on such shells was found in ref. 38. The combination of axial compression and normal pressure was considered in ref. 39. Various approximate methods in studying a conical shell under lateral hydrostatic pressure were compared with experimental results in ref. 40.

Spherical Shells

The stability of a shallow spherical segment under the action of uniform external pressure was considered in ref. 41 on the basis of the Marguerre equations. Asymmetric buckling of a spherical shell undergoing large deflections under uniform pressure was analyzed in ref. 42. The influence of initial imperfections on axisymmetric form of buckling of such shells was studied in ref. 43. It was found that the lower critical pressure decreases about tenfold as a result of such imperfections.

Dynamic Loading

The stability of cylindrical shells subjected to dynamic loads was investigated in refs. 44 and 45. Whereas in this last reference, circumferential inertia was neglected, it is included in ref. 46. Rapidly varying and pulsating pressures acting on a cylindrical shell were considered in ref. 47 and 48. In this last reference the problem was reduced to a Mathieu equation and the amplitude was determined using the Mandel'shtam method. The stability of a complete spherical shell subjected to a periodically varying pressure superimposed on a constant pressure was investigated in ref. 49. Again, the problem was reduced to a Mathieu equation and the stability regions were established. Dynamic stability of shells filled with a liquid was considered in ref. 50.

Experimental Investigations

Celluloid and paper models were used in ref. 51 to determine experimentally the elastic stability of cylindrical and spherical shells subjected to external pressure. Results of axially compressed shells using again paper as the model material are reported in ref. 52. An experimental study of dynamic buckling of a shell is described in ref. 53. Critical pressures for conical shells were determined experimentally in ref. 54. Stability of bimetallic cylindrical shells under axial compression beyond the elastic limit was studied experimentally in ref. 55.

Miscellaneous

Stability of three-layered shells was investigated in refs. 56 and 57 and a general theory of shallow sandwich shells, the two facings having different properties, was evolved in ref. 58. Instability of helicoidal shells is discussed in ref. 59, of curved thin-walled tubes in ref. 60 and of shells of double curvature reinforced by stiffeners in ref. 61.

REFERENCES

1. Bolotin, V. V.: Paths in the Development of the Theory of Plates and Shells. Vestnik AN SSSR, Jan. 1962, pp. 136-138.
2. Bolotin, V. V.: Statistical Methods of the Nonlinear Theory of Elastic Shells. Izv. AN SSSR, Otd. tekhn. nauk, no. 3, 1958, pp. 33-41.

3. Makarov, B. P.: Application of Statistical Methods to Analysis of Experimental Values of Shell Stability. *Izv. AN SSSR, Otd. tekhn. nauk, Mekh. i Mashinostr.*, no. 1, 1962, pp. 157-158.
4. Suer, H. S., Harris, L. A., Skene, W. T., and Benjamin, R. J.: The Bending Stability of Thin-Walled Unstiffened Circular Cylinders Including the Effects of Internal Pressure. *Jour. Aeronautical Sci.*, vol. 25, 1958, pp. 281-287.
5. Goncharenko, V. M.: On the Probability Determination of Loss of Stability of a Shell. *Izv. AN SSSR, Otd. tekhn. nauk, Mekh. i Mashinostr.*, no. 1, 1962, pp. 159-160.
6. Vorovich, I. I.: Some Questions on Stability of Shells in the Large. *Dokl. AN SSSR*, vol. 122, no. 1, 1958, pp. 37-40.
7. Vorovich, I. I.: Error of Direct Methods in Nonlinear Shell Theory. *Dokl. AN SSSR*, vol. 122, no. 2, 1958, pp. 196-199.
8. Grigoliuk, E. I.: Plastic Buckling of Shells of Revolution. *Izv. AN SSSR, Otd. tekhn. nauk*, no. 2, 1958, pp. 130-132.
9. Darevskii, V. M. (editor): Strength of Cylindrical Shells. *Collect. of articles. Oborongiz, (Moscow)*, 1959, 159 pages.
10. Darevskii, V. M.: Stability of a Cantilevered Cylindrical Shell Subjected to Bending by a Transverse Force with Twist and Internal Pressure. In *collect. ed. by Darevskii (ref. 9, above)*, pp. 72-94. Translation available in *ARS Journal*, Jan. 1961, pp. 125-133.
11. Darevskii, V. M., Kukudzhanov, S. N.: Stability of a Cylindrical Orthotropic Shell under Twist and Normal Pressure. In *collect. ed. by Darevskii (ref. 9, above)*, pp. 95-108.
12. Darevskii, V. M., Kukudzhanov, S. N.: Torsional Stability of an Orthotropic Shell under Internal Pressure. *Soviet Physics - Dokl.*, vol. 3, no. 6, June 1959, pp. 1271-1274.
13. Darevskii, V. M., Kshniakin, R. I.: Stability of a Cantilevered Cylindrical Shell with a Clamped End under the Action of External Pressure. *Dokl. AN SSSR*, vol. 31, no. 6, 1960, pp. 1294-1297.
14. Prokhorov, S. V.: Determination of Critical Normal Pressure of a Cylindrical Shell of Variable Thickness. *Trudy Kazansk. khim.-tekhn. in-ta*, no. 22, 1957(59), pp. 295-300.

15. Kukudzhanov, S. N.: Stability of a Cylindrical Orthotropic Shell under External Lateral Pressure with Axial Extension and under Torsion with Axial Extension. In collect. ed. by Darevskii (ref. 9, above), pp. 109-117.
16. Mar'in, V. A.: Stability of a Cylindrical Shell under Torsion and Internal Pressure. In collect. Analysis of Spatial Structures, Gosstroizdat, (Moscow), no. 5, 1959, pp. 475-484.
17. Mar'in, V. A.: Stability of a Cylindrical Panel under Shear. In collect. Analysis of Spatial Structures, Gosstroizdat, (Moscow), no. 5, pp. 485-501.
18. Kukudzhanov, S. N.: Stability of Cylindrical Shells under the Action of Twisting Moments, Linearly Varying along the Length. Izv. AN SSSR, Otd. tekhn. nauk, Mekh. i Mashinostr., no. 1, 1961, pp. 180-182.
19. Arkhangorodskii, A. G., Popov, V. G.: Stability of Cylindrical Shells with Oblique Transverse Stiffeners. Izv. vyssh. uchebn. zaved. Mashinostroenie, no. 6, 1959, pp. 61-68.
20. Terebushko, O. I.: Analysis of Carrying Capacity of Circular Cylindrical Panel Reinforced by Ribs. In collect. Analysis of Spatial Structures, Gosstroizdat, (Moscow), no. 4, 1958, pp. 531-554.
21. Darevskii, V. M., Kshniakin, R. I.: Stability under External Pressure of a Cylindrical Shell Reinforced by Rings. Dokl. AN SSSR, vol. 134, no. 3, 1960, pp. 548-551.
22. Turkin, K. D.: General Stability of a Reinforced Cylindrical Shell under Transverse Bending. In collect. Analysis of Spatial Structures, Gosstroizdat, (Moscow), no. 5, 1959, pp. 450-474.
23. Arkhangorodskii, A. G., Popov, V. G.: Stability of Cylindrical Shells, Reinforced by Transverse and Longitudinal Stiffeners. Izv. vyssh. uchebn. zaved. Mashinostroenie, no. 3, 1960, pp. 3-13.
24. Palii, O. M.: Stability of a Circular Cylindrical Shell Clamped along Curvilinear Edges. Izv. AN SSSR, Otd. tekhn. nauk, no. 1, 1958, pp. 126-128.
25. Iumatov, V. P.: Some Generalization of Formulas, Determining upper Value of Critical Pressure on the Lateral Surface of a Cylindrical Shell. Izv. vyssh. uchebn. zaved. Mashinostroenie, no. 12, 1959, pp. 10-16.

26. Len'ko, O. N.: Stability of Orthotropic Cylindrical Shells. In collect. Analysis of Spatial Structures, Gosstroizdat, (Moscow), no. 4, 1958, pp. 499-524.
27. Immerman, A. G.: On Verification of Stability of Circular Cylindrical Shells under Axial and Lateral Compression. In collect. Analysis of Spatial Structures, Gosstroizdat, (Moscow), no. 4, 1958, pp. 525-530.
28. Alfutov, N. A., Sokolov, V. F.: Determination of Lower Critical Pressure of Elastic Cylindrical Shell and Behavior of Shell after Loss of Stability. In collect. Strength Analysis in Machine Construction, (Moskov. vyssh. tekhn. uchil. im. N. E. Baumana, vol. 89), (Moscow), 1958, pp. 95-110.
29. Golitsinskaia, E. D.: Some Problems of Stability of Thin Cylindrical Shells. Inzh. sbornik, vol. 25, 1959, pp. 145-153.
30. Golitsinskaia, E. D.: Stability of Thin Closed Cylindrical Shells. Trudy Belorussk. sel.-khov. akad., vol. 31, 1959, pp. 75-82.
31. Terebushko, O. I.: Stability of a Cylindrical Shell under Torsion, External Pressure and Compression. In collect. Analysis of Spatial Structures, Gosstroizdat, (Moscow), no. 5, 1959, pp. 502-522. (See also ARS Jour., 1961, p. 378.).
32. Len'ko, O. N.: On Stability of an Orthotropic Cylindrical Shell under Axial Force and External Pressure. In collect. Analysis of Spatial Structures, Gosstroizdat, (Moscow), no. 5, 1959, pp. 523-536. (See also ARS Jour., 1961, p. 1315).
33. Shevliakov, Iu. A., Manevich, L. I.: Stability of a Cylindrical Shell under Bending. Dopovidi AN URSR, no. 5, 1960, pp. 605-608.
34. Aksel'rad, E. L.: Bending and Loss of Stability of Thin-Walled Tubes under Hydrostatic Pressure. Izv. AN SSSR, Otd. tekhn. nauk, Mekh. i Mashinostr., no. 1, 1962, pp. 98-114.
35. Kornishin, M. S.: On the Problem of Variation of the Buckling Region. Izv. Kazan. Fil. AN SSSR, Ser. Fiz.-mat. i tekhn. nauk, no. 12, 1958, pp. 85-89.
36. Zubchaninov, V. G.: Axisymmetric Loss of Stability of a Circular Cylindrical Shell Beyond the Elastic Limit. Izv. AN SSSR, Otd. tekhn. nauk, Mekh. i Mashinostr., no. 5, 1961, pp. 131-132.
37. Sachenkov, A. V.: On Stability of Conical Shells of Circular

- Cross-Section Subjected to Uniform External Pressure. *Izv. Kazan. Fil. AN SSSR, Ser. Fiz.-mat. i tekhn. nauk*, no. 12, 1958, pp. 107-125.
38. Zagubizhenko, P. A., Manevich, L. I.: On the Stability of a Conical Shell in Bending. *Nauchn. zapiski Dnepropetrovsk. un-ta*, vol. 73, 1958 (1959), pp. 25-32.
39. Ivakhnin, I. I.: Stability of a Conical Shell of a Circular Cross-Section under Combined Action of Axial Compression and External Normal Pressure. *Dopovidy AN URSR*, no. 4, 1958, pp. 376-380.
40. Trapezin, I. I.: Stability of a Thin Conical Shell, Closed at the Top, Subjected to Lateral Hydrostatic Pressure. In collect. *Strength Analysis, Mashgiz, (Moscow)*, no. 5, 1960, pp. 249-258.
41. Krivosheev, N. I.: On Stability of a Shallow Spherical Segment under the Action of Uniform External Pressure. *Izv. vyssh. uchebn. zaved. Str.-vo i Arkhitekt.*, no. 5, 1959, pp. 48-54.
42. Grigoliuk, E. I.: Stability of a Spherical Shell with Large Deflections and Asymmetric Deformations. *Izv. AN SSSR, Otd. tekhn. nauk, Mekh. i Mashinostr.*, no. 6, 1960, pp. 68-73.
43. Gabril'iants, A. G., Feodos'ev, V. I.: On Axisymmetric Forms of Equilibrium of an Elastic Spherical Shell Subjected to Uniform Pressure. *PMM* vol. 25, no. 6, 1961, pp. 1091-1101.
44. Vol'mir, A. S.: On Stability of Dynamically Loaded Cylindrical Shells. *Soviet Physics - Doklady*, vol. 3, no. 6, June 1959, pp. 1287-1289.
45. Agamirov, V. L., Vol'mir, A. S.: Behavior of Cylindrical Shells under Dynamic Loading in the Form of All Around Pressure and Axial Compression. *Izv. AN SSSR, Otd. tekhn. nauk, Mekh. i Mashinostr.*, no. 3, 1959, pp. 78-83. English Translation in *ARS Jour. (Russian Supplement)*, vol. 31, no. 1, Jan. 1961, pp. 98-102.
46. Kadashevich, Iu. I., Pertsev, A. K.: On the Loss of Stability of a Cylindrical Shell under Dynamic Loading. *Izv. AN SSSR, Otd. tekhn. nauk, Mekh. i Mashinostr.*, no. 3, 1960, pp. 30-33. English Translation in *ARS Jour. (Russian Supplement)*, vol. 32, no. 1, Jan. 1962, pp. 140-143.
47. Terebushko, O. I.: Stability of Closed Cylindrical Shells Subjected to a Rapidly Varying Loading. Paper given at Conference

- at Riga in June 1960. See Izv. AN SSSR, Otd. tekhn. nauk, Mekh. i Mashinostr., no. 6, 1960, p. 183.
48. Gnuni, V. Ts.: On the Theory of Nonlinear Dynamic Stability of Shells. Izv. AN SSSR, Otd. tekhn. nauk, Mekh. i Mashinostr., no. 4, 1961, pp. 181-182.
 49. Bolotin, V. V.: Stability of a Thin-Walled Spherical Shell under the Action of a Periodic Pressure. Collect. Strength Analysis, Mashgiz, (Moscow), no. 2, 1958, pp. 284-289.
 50. Bublik, B. N., Merkulov, V. I.: On Dynamic Stability of Thin Elastic Shells Filled with a Liquid. PMM, vol. 24, no. 5, 1960, pp. 941-946.
 51. Kondrikov, D. V., Mel'nikov, A. M.: Some Problems Regarding Experimental Investigations of Elastic Stability of Cylindrical and Spherical Shells. Trudy Leningr. Korablestroit. in-ta., no. 29, 1959, pp. 211-219.
 52. Chebanov, V. M.: Some Problems of Shell Stability. Vestn. Leningr. Universiteta, no. 1, 1959, pp. 79-93.
 53. Vol'mir, A. S., Mineev, V. E.: An Experimental Investigation of the Buckling of a Shell under Dynamic Load. Soviet - Physics, Doklady, vol. 4, no. 2, Oct. 1959, pp. 464-465.
 54. Trapezin, I. I.: Experimental Determination of Critical Pressures of Conical Shells. In collect. Strength Analysis, Mashgiz, (Moscow), no. 6, 1960, pp. 217-230.
 55. Korolev, V. I., Smirnov, I. G., Stomma, R. P.: Study of Stability of Bimetallic Cylindrical Shells under Axial Compression beyond the Elastic Limit. Inzhenernyi Zhurnal, vol. 2, no. 1, 1962, pp. 98-110.
 56. Grigoliuk, E. I.: On Stability of Three-layered Shells and Plates beyond the Elastic Limit. Izv. AN SSSR, Otd. tekhn. nauk, no. 6, 1958, pp. 68-72.
 57. Kurshin, L. M.: On Stability of a Three-layered Shallow Cylindrical Shell under Compression. Izv. AN SSSR, Otd. tekhn. nauk, no. 8, 1958, pp. 97-100.
 58. Mushtari, Kh. M.: General Theory of Shallow Sandwich Shells. Izv. AN SSSR, Otd. tekhn. nauk, Mekh. i Mashinostr., no. 2, 1961, pp. 24-29.

59. Alumiaev, N. A.: Stability of Equilibrium of a Helicoidal Shell. PMM, vol. 21, no. 6, 1957, pp. 823-826.
60. Kostovetskii, D. L.: On Stability of Equilibrium of a Curved Thin-Walled Tube of Circular Cross-Section under External Pressure. Izv. AN SSSR, Otd. tekhn. nauk, Mekh. i Mashinostr., no. 1, 1961, pp. 177-179.
61. Kordashenko, A. B.: On Stability of Shells Reinforced by Ribs. Izv. AN SSSR, Otd. tekhn. nauk, Mekh. i Mashinostr., no. 1, 1962, pp. 115-120.

A REVIEW OF SOME AVAILABLE TECHNIQUES FOR PREDICTING
GENERAL INSTABILITY OF SHELL STRUCTURES

By Walter J. Crichlow

Lockheed-California Company

SUMMARY

The reliability of past methods of prediction for the general instability of complex light-weight shell structure has been shown to be less than adequate. A brief review of available data and methods of prediction is given, including empirical and high-speed computing techniques. These latter procedures show some promise for improvement in reliability (with empirical test-based correction factors) and success in handling more complex structure (by lumped element models in finite difference numerical techniques). Two analytical methods (Van der Neut, Becker) and two semi-empirical formulae (Michielsen, Ensrud) are correlated with the GALCIT test series under pure bending. In addition, shear loading test data are described and compared with numerical predictions on four highly orthotropic panels with flexible rib caps supported on rigid posts (truss type ribs).

SYMBOLS

E	Young's modulus of elasticity	
ν	Poisson's ratio	
b	spacing	
A_x	area	} of longitudinals
I_x	moment of inertia	
ρ_x	radius of gyration	
a	spacing	
A_y	area	} of rings
I_y	moment of inertia	
ρ_y	radius of gyration	
R	radius of circular cylinder	
t	thickness of skin	

ANALYTICAL METHODS

Van der Neut's Method

The method presented in Reference 1 by Van der Neut appears to be the most complete analysis of the general instability of stiffened cylindrical shells under axial compression. Its generality can be judged from the fact that the method not only covers symmetrical and non-symmetrical buckling modes, but also includes such limit cases as column instability of the whole cylinder and column failure of the longitudinal stiffeners. By comparing the theoretical solutions of the orthotropic shells with distributed section properties with the solution for the shell with a discrete frame, Van der Neut concludes that the two solutions differ only within a few percent if there are at least two frames per half wave length of the longitudinal buckling mode. The solution for the orthotropic shell with distributed section properties has been correlated with the GALCIT tests under pure bending (Reference 2) and the margins m

$$m [\%] = 100 \left(1 - \frac{\text{"computed"}}{\text{"test"}} \right) \quad (1)$$

are plotted in Figure 1. Van der Neut's critical stress has been modified by the inclusion of the tangent-modulus plasticity factor η_t .

The experimental critical stresses were obtained from the reported maximum strains in Reference 2, using the stress strain curve for 17ST material.

Twelve (12) GALCIT specimens were of such discrete stringer spacings that they could not qualify for distributed properties. The Van der Neut predictions for the remaining specimens are very good.

Becker's Method

Becker has derived a procedure (Reference 4) for the prediction of the general instability of orthotropic shells under axial compression, torsion, and external pressure, covering the entire range of lengths. The GALCIT tests (Reference 2) have been correlated with this method, for axial loading.

A comparison of any orthotropic theory with experimental data shows a discouraging discrepancy due to several uncertainties in the determination of the effective stiffness parameters. One approach is to assume several limit cases and to compare the theoretical results. The results

shown in Figure 1 (pertaining to Becker's formulae) have been obtained under the following assumptions:

- a. negligible effective width of skin in both directions
- b. negligible torsional rigidity of the sheet-stiffener-frame system
- c. the effective shear thickness of the cylinder wall $\bar{t} = \frac{2}{3}t$
- d. inclusion of a tangent-modulus plasticity reduction factor

It can be seen that the predicted values are generally conservative (positive margins).

SEMI-EMPIRICAL FORMULAE

During the past decade extensive studies have also been undertaken at Lockheed to establish semi-empirical formulae for the general instability of stiffened cylinders under compression and shear.

Michielsen's Approach

The formulae given below to predict general instability of a stiffened circular cylinder under compression is the result of studies by Michielsen commencing in 1954 (Reference 5). The theoretical development is made for an orthotropic cylinder as a linear problem. The relations between rigidity parameters and geometrical properties of the actual cylinder were derived, the theoretical buckling load per inch circumference is established, and a set of adjustments obtained from an extensive evaluation of available tests is introduced. These include considerably reduced shear rigidity of the (buckled) skin, empirical functions to account for the ratio between the critical bending stress and critical compression stress, and for plasticity. The best fit to test results was obtained by neglecting the skin completely in determining stiffness parameters connected with normal stresses.

GENERAL INSTABILITY OF FUSELAGES (LOCKHEED, 1954)

$$\begin{aligned}
 \Psi &= \rho_x / \rho_y; \quad K = A_x A_y / (a b t^2); \quad C = 10^4 \rho_x \rho_y / R^2 \\
 S &= 25 + .025 (b^2 / Rt)^2; \quad D = 1 + (\Psi - 1/\Psi)^2 / KS \\
 B &= (\Psi + 1/\Psi) + \sqrt{(\Psi - 1/\Psi)^2 + KS} \\
 M_e &= (0.1) E t R^2 \sqrt{CK/B} (1 + 0.25 \sqrt[4]{BCD})
 \end{aligned}
 \tag{2}$$

$$\begin{aligned}
 M_s &= 1.9 E R t^2 [1 + (S - 25)^{-0.5}] \\
 f_e &= \frac{M_e - M_s}{\pi (A_x/b) R^2} ; \quad M_{cr} = \frac{M_e - M_s}{\sqrt{1 + 0.5(f_e/f_y)^2}} + M_s \\
 f_y &= \text{yield stress of longitudinals} \\
 M_{id} &= \left| M_{ult} \right| + R \left| V_z \right| \\
 V_z &= \text{shear force}
 \end{aligned} \tag{2}$$

Ensrud's Approach

The semi-empirical method, based on distributed orthotropic properties, used in determining general instability of ring-stringer-stiffened cylindrical shells was developed by Ensrud (Reference 6).

Compression. - The allowable stress F_{ccr} is given by Equation 3.

$$F_{ccr} = \alpha_c \zeta_c \Gamma^{.375} (t'/R)^{.25} E \eta_1 \tag{3}$$

where α_c = buckling coefficient derived from one test of particular structure (=4.1 for GALCIT specimens)

$$\zeta_c = \left\{ 1 + \frac{b}{R} \sqrt[4]{\frac{I_x b}{K_x R}} \right\}^{-1}$$

$$t' = t + (A_x/b)$$

$$\Gamma = I_y / (a h R^2)$$

h = depth of ring

K_x = Saint-Venant torsion constant of longitudinals

$$\eta_1 = \sqrt{\eta_t}$$

and η_t is the tangent modulus plasticity reduction factor.

Shear. - The allowable stress F_{scr} is given by Equation 4

$$F_{scr} = \alpha_s \zeta_s \Gamma^{.375} (t'_s/t) E \eta_2 \quad (4)$$

where α_s = buckling coefficient derived from one test of particular structure.

$$\zeta_s = \left\{ 1 + \frac{\sqrt{ab}}{2R} \sqrt[4]{\frac{12 (1-\nu^2) I_y}{a t^3}} \right\}^{-1}$$

$$t'_s = (2t/3) + (A_x/b) \text{ for buckled skin}$$

$$\eta_2 = .83 \eta_s + .17 \eta_t$$

$$\eta_s = \text{secant modulus plasticity reduction factor}$$

The buckling coefficients α_c and α_s depend on the detail design of the ring-stringer intersection and have been determined from numerous tests.

The above semi-empirical formulae for compression (Equation 3) has been correlated with the GALCIT series (Reference 2) and the result is graphically presented in Figure 1. Correlations with a series of large curved fuselage type shear panel tests at Lockheed show similar comparisons for this loading case (Figure 2).

NUMERICAL STABILITY ANALYSIS OF COMPLEX STRUCTURES

From an approach proposed in Reference 5 a digital stability analysis procedure was developed which is equivalent to a small deflection buckling theory. It is programmed on a high speed digital computer in conjunction with a general program for the analysis of redundant structures. It is applicable to any structure represented in a lumped element (or finite difference) form.

The stability criterion is based on the equilibrium, in each node point of the lumped element structure, of internal and external forces in the critical deflection mode. This equilibrium is expressed by stipulating that the unbalances (residuals) of the internal loads in the critical displacement mode must be such that they cause that same displacement pattern. The critical mode can be expressed in terms of the deflection influence coefficients in each freedom of the lumped element structure, and the residuals in terms of unit residuals due to the

deflection coefficients. The stability criterion in form of the equilibrium in each freedom leads then to a set of homogeneous equations, of which the largest eigenvalue is the reciprocal of the smallest critical load level and the eigenvector determines the buckling mode.

Secondary bending (beam column) type problems can be handled in a similar way, including the effect of the displacements caused by the applied load condition at a given load level and the corresponding residuals. In this case, the system of equations is inhomogeneous, its solution vector determines the increment of deflections and internal loads due to secondary bending.

The method and the digital program have been checked out by simulation of continuous structures for which theoretical analytical results are available.

A column and a plate in compression, an arch and an isotropic cylinder in hoop compression were analysed, simulating the structure by lumped elements. The numerical result matched the theoretical analytical values very closely, the accuracy depending on the number of nodes defining the wave length of the buckling mode. On a straight column in compression, stability and column bending (with side load) were computed with an error of .4% for sixteen nodes per half-wave. On the arch and the isotropic cylinder in hoop compression, the error varied from .3% for twenty parts per half-wave to 5.5% for five parts per half-wave.

INSTABILITY OF INTEGRALLY STIFFENED WING SURFACE

General Instability

The general instability of flat orthotropic plates, representative of integrally stiffened wing surfaces, Figure 3, have been investigated in Reference 7. The integrally stiffened panel is simply supported along the front and rear beams and elastically supported by equally spaced flexible rib caps. Furthermore, each rib cap rests on equally spaced rigid posts (i.e. truss points). Even under the simplifying assumption of uniformly applied constant spanwise compression and shear load and elastic behavior, this structural problem illustrates a typical case for which numerical solutions have become possible only through the advent of high-speed digital computers.

The mathematical approach for finding the buckling loads under combined loading follows conventionally the Rayleigh-Ritz method. A standard iteration procedure (Reference 8) is applied to find the dominant

eigenvalue. To limit the computing time in case of excessively slow convergence, no more than 200 iterations were permitted. In the majority of the actual computed cases, no less than approximately fifty (50) parameters of the deflection function have been considered (including Lagrangian multipliers to consider the condition of zero deflection at the posts), and in some cases this number went as high as approximately one hundred (100).

Figure 4 shows a typical interaction curve (buckling coefficients K_S , K_C): It consists generally of three branches. The buckling pattern for Branch ① which applies for low values of K_C has a spanwise wave length $2\lambda = 4A$ with narrow chordwise waves and is similar to that for pure shear. As the value of K_C increases, Branch ② becomes critical. For this branch, $2\lambda = 3A$ while the chordwise waves are somewhat wider than for Branch ①. Branch ③ is practically unaffected by variations in the orthotropic plate stiffness ratio (D_x/D_y) but is strongly dependent on the aspect ratio (B/A) and the rib cap stiffness. This branch is characterized by a wave-length $2\lambda = 2A$ and the buckling pattern is similar to that of pure compression.

Local Buckling

In Reference 9, local buckling coefficients have been computed for the special case of an infinitely long, elastic, integrally stiffened plate under pure longitudinal compression, pure shear, and for various ratios of combined shear and longitudinal compression loads. The buckling problem for the individual plates (skin, stiffeners) has been treated by use of the differential equation for the deflection surface. The results have also been checked by using a modified version of the digital computer program for general instability (energy-method) and the agreement has been found excellent.

The results of shear tests are summarized in Table 1. These panels were subdivided into four bays by diagonal-truss ribs closely reproducing actual aircraft structure. The panels were tested in a picture-frame jig 72 inches x 57 inches between hinges (diagonal length 92 inches).

CONCLUSIONS AND RECOMMENDATION

The comparison in Figure 1 of the predictability of the general instability failure of stiffened cylinders under compression indicates the improvement to be achieved by the use of test based correction factors. The scope of the geometrical parameters covered by the GALCIT tests is limited compared with the requirements of modern shells. A large scale

test facility is urgently needed along with support for a comprehensive test program on specimens of a size and structural configuration to encompass current designs. It is strongly recommended that the NASA provide support for this necessary activity.

REFERENCES

1. Van der Neut, A.: The General Instability of Stiffened Cylindrical Shells Under Axial Compression. NLL Rep. S. 314, 1947.
2. GALCIT: Some Investigations of the General Instability of Stiffened Metal Cylinders. V. - Stiffened Metal Cylinders Subjected to Pure Bending. NACA TN 909, 1943.
3. Becker, Herbert: General Instability of Stiffened Cylinders. NACA TN 4273, July 1958.
4. Becker, Herbert and Gerard, George: Elastic Stability of Orthotropic Shells. Journ. Aeron. Sci., Vol. 29,5, May 1962.
5. Michielsen, H.F.: General Instability of Shell Structures - A Proposal for Further Development. Lockheed Report LR 12569, Sept. 1957, and AGARD Paper 1958.
6. Ensrud, A. F.: Procedures for Computing Fuselage Shell Allowables for Model P3V-1 (General Instability of Shell) Lockheed Report LR 14266, May 1960.
7. Mueller, F.M., Contini, Roberto, and Davis, C.S.: General Instability of Long Orthotropic Elastic Plates Supported by Flexible Rib Caps with Rigid Posts under Combined Longitudinal Compression and Shear. Lockheed Report LR 14724, September 1960.
8. Frazer, R.A., Duncan, W.J., and Collar, A.R.: Elementary Matrices. Cambridge Univ. Press, 1938.
9. Almroth, B.O.: Local Buckling of Integrally Stiffened Panels Under Combined Loads. Lockheed Report LR 13042, June 1958.

TABLE 1 - SHEAR PANEL TEST RESULTS

Panel	p in.	h in.	t _s in.	t _w in.	Rib Spacing in.	Failure Shear Stresses, ksi				Test/Computed	
						Predicted		Test			
						Local Buckling	General Instab.	Local Buckling	Ultimate Failure	Local Buckling	Ultimate Failure
1	2.00	1.250	.080	.112	18.0	42.9	42.1	45.9	47.7 ^(a)	1.07	1.13
2	2.00	1.170	.050	.112	18.0	38.5	41.2	40.4	49.6 ^(b)	1.05	1.20
3	2.10	.985	.073	.130	12.0	33.0	41.2	34.2	48.0 ^(c)	1.04	1.17
4	4.20	1.150	.070	.115	23.0	18.3	19.0	20.2	37.3 ^(d)	1.10	1.96

NOTES: (a) Clip Failure
 (b) Skin Tear-out
 (c) Buckled stiffeners, clip failures, and broken rib cap tab in corner of jig.
 (d) Catastrophic failure - post buckled state in pronounced tension field.

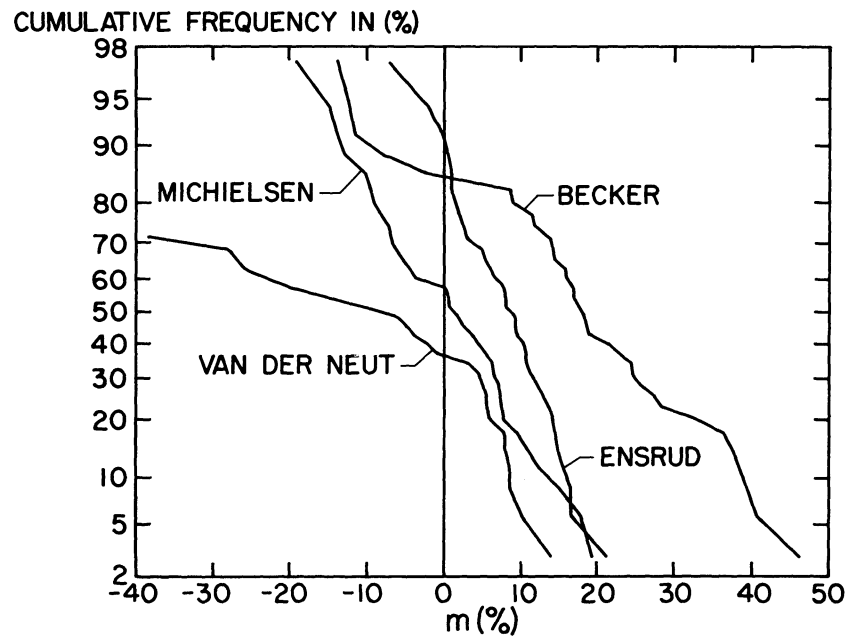


Figure 1.- Correlation of several methods of prediction with a GALCIT test series.

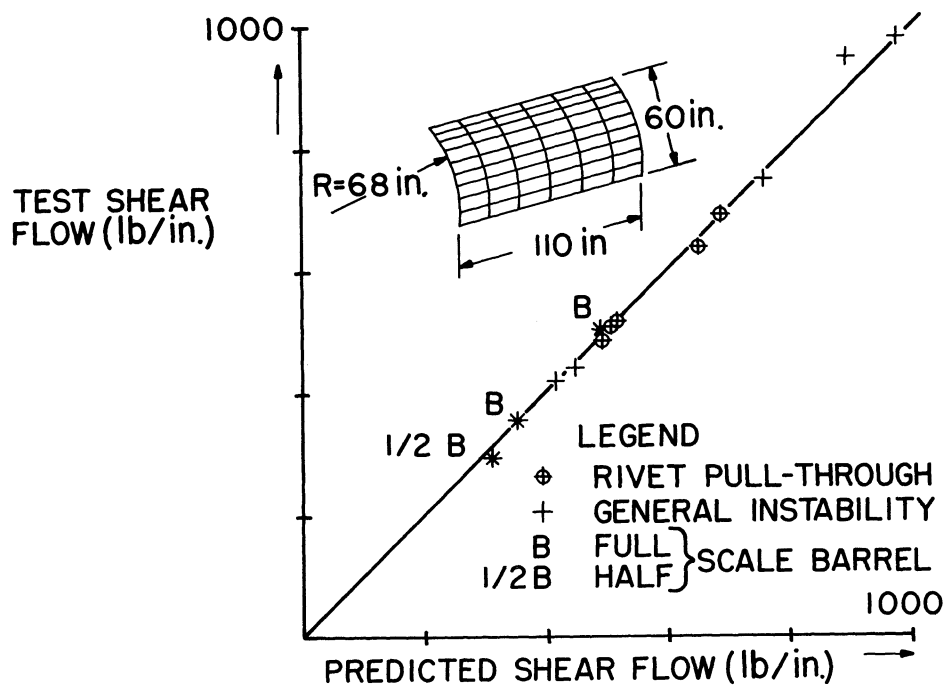


Figure 2.- Correlation of shear test results of stiffened curved panels and cylinders.

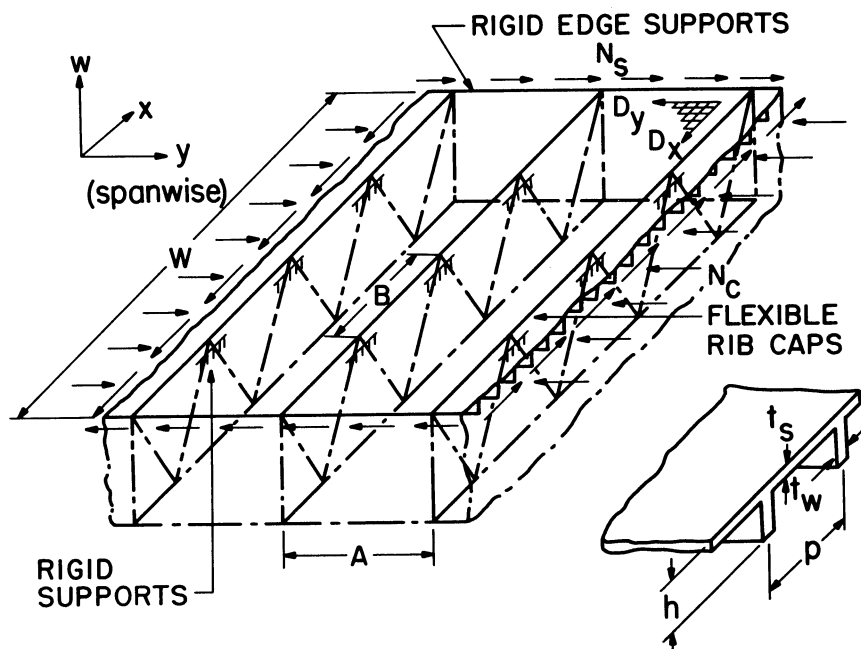


Figure 3.- Flexibly supported surface of integrally stiffened wing box beam.

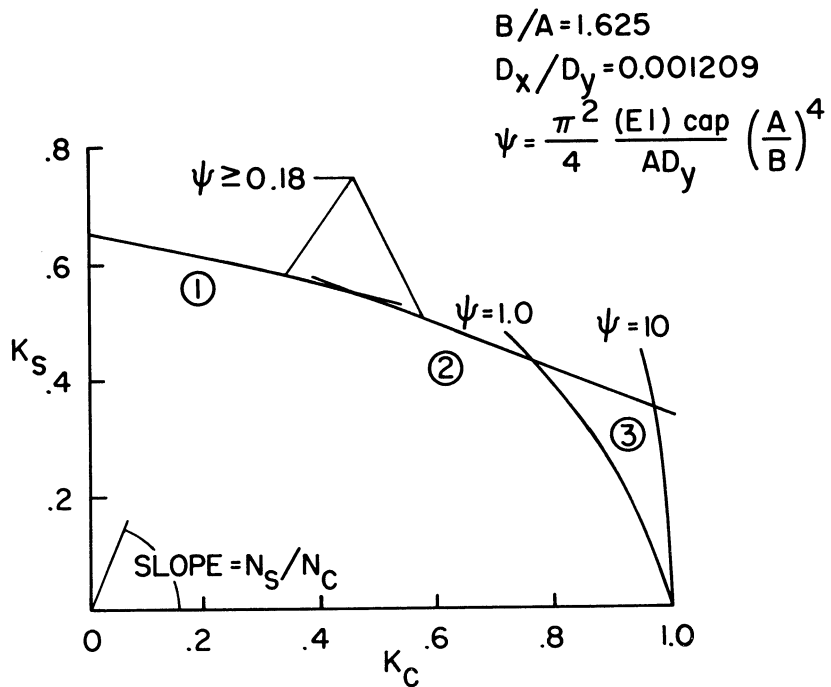


Figure 4.- Typical interaction curve for general instability of flexibly supported integrally stiffened panel.

A DIGITAL METHOD FOR THE ANALYSIS OF LARGE DEFLECTIONS
AND STABILITY OF COMPLEX STRUCTURES

By Dale S. Warren

Douglas Aircraft Company, Inc.

SUMMARY

The status of an extended program to develop a general digital method for geometrically nonlinear structures is reported. The program is based on the notion of superposing corrections upon the general solutions given by linear matrix methods. Thereby, full advantage is taken of the existing capability for linear analysis. The approach offers many desirable benefits, such as, (1) complete generality with respect to structural geometry, boundary conditions and thermo-mechanical loading, (2) an explicit description of the effects of initial eccentricities and (3) provisions to account for both short-time and time dependent plasticity, and local buckling. In addition, the linearized stability criterion for thermo-mechanical loading is available. These benefits have been realized for planar structures; generalizations for application to shell structures are under consideration.

INTRODUCTION

The trends in the designs of advanced aerospace vehicles and the high costs of testing in extreme environments have increased the demands on the reliability of methods for the analysis of complex structures. The need for improved methods for the analysis of geometrically nonlinear structures is especially significant, and therefore, an extended development program has been devoted to this need. The digital approach has been adopted to provide the generality required for practical application to complex structures.

The feasibility of the program was established by the development of the general matrix equations for geometrically nonlinear, discrete structures. The essentials of the development are as follows. It is observed that large deflections define two specific effects that are ignored in linear theories. These effects are identified as corrections to linear theory and incorporated in the general matrix equations that describe the internal forces and deflections of linear structures. The solution of the modified equations defines the internal forces and deflections of geometrically nonlinear structures. The resulting

equation of deflections is nonlinear and includes the linearized stability criteria for thermal, mechanical and combined thermo-mechanical loading. The development provides for discrete structural assemblies consisting of bars that carry direct, shearing, bending and torsional loads, and panels that carry shearing loads only. Assemblies of this type have been used successfully in linear analyses of many classes of complex structures, ranging from riveted and bonded joints to complete vehicles. It is believed that the reliability and versatility associated with this type of discrete idealization are directly applicable to the analysis of nonlinear structures.

Although simple in concept, the theoretical development is rather involved. Therefore, only an outline of the theory is presented. Because of the generality of the approach, an extensive series of applications is required to fully evaluate and appreciate the method. Representative applications are described in this paper.

OUTLINE OF THE THEORY

The Effects of Large Deflections in the Considerations of Equilibrium and Member Deformation

The conditions of equilibrium, compatibility and member deformation define the response of statically indeterminate structures. Properly, these conditions apply to the deformed state of the structure. The factors important in the equilibrium of an axially-loaded bar and the adjacent joints of a deformed structure are shown in Figure 1. The positions AB and A'B' represent the positions of the bar in the original and deformed states, respectively. The joints are in equilibrium under the action of the member force F , the linear force F' and the vector increment ϕ_n . The linear force F' is the member force that would be predicted if the deformation of the structure were neglected in the equations of equilibrium. Therefore, the vector increment ϕ_n can be considered as a correction to the linear force F' , to account for the effect of deflections in the equations of equilibrium. The correction is appropriately called a "fictitious force." From Figure 1,

$$\phi_n = \frac{F}{L} (\Delta_2 - \Delta_1) . \quad (1)$$

Since ϕ_n is linearly related to F , the fictitious forces for a system of axially-loaded bars can be written matrixally in the form

$$\phi_n = BF , \quad (2)$$

where ϕ_n is a matrix of fictitious forces, B is a linear transform and F is a matrix of member forces. The fictitious force associated with the warping of a shear panel is also linearly dependent upon the member force, and therefore Equation (2) is applicable to a composite structure consisting of axially-loaded bars and shear panels.

The consideration of member deformations must also be revised to account for large deflections. In Figure 2, the original and deformed positions of a bar are indicated by AB and A'B', respectively. Linear theory is developed in terms of the deformation of the bar, δL and the geometry of the undeformed structure. In this reference system, the difference between the length of the projection of A'B' and the original length is

$$(L + \delta L)\cos \theta - L = \delta L \cos \theta - L(1 - \cos \theta) . \quad (3)$$

Expanding $\cos \theta$ in a power series and neglecting higher order terms,

$$(L + \delta L) \cos \theta - L = \delta L - \frac{L}{2} \theta^2 . \quad (4)$$

From Equation (4), it is concluded that the effect of rotations of a bar can be approximately described by adding the "fictitious member deformation"

$$e_n = - \frac{L}{2} \theta^2 \quad (5)$$

to the linear equations of member deformation. The fictitious member deformation of a shear panel can be described in a similar form, and the complete set of fictitious member deformations of a composite structure can be described by a matrix e_n .

The General Equations for Internal Forces and Deflections, Accounting for Large Deflections

For a linear structure, the internal forces and deflections due to applied thermo-mechanical loading can be described in terms of influence coefficients by the matrix equations

$$F_L = F_\phi \phi + F_e e_T , \quad (6)$$

and

$$\Delta_L = \Delta_\phi \phi + \Delta_e e_T , \quad (7)$$

where F_L and Δ_L are the matrices of linear internal forces and deflections, respectively, due to the applied thermo-mechanical loading

described by the matrix of mechanical loads ϕ , and the matrix of unrestrained thermal deformations e_T . The matrices F_ϕ and F_e describe the internal forces due to conditions of unit applied mechanical loads and conditions of unit member deformations, respectively, and the matrices Δ_ϕ and Δ_e describe the deflections due to conditions of unit applied mechanical loads and unit member deformations, respectively. The influence coefficient matrices F_ϕ , F_e , Δ_ϕ and Δ_e can be derived in a routine manner by the use of linear matrix methods.

As defined, the fictitious forces are of the same physical form as ϕ , and the fictitious member deformations are of the same physical form as e_T . Further, ϕ_n and e_n are corrections to be added to the linear solution to account for large deflections. Therefore, for geometrically nonlinear structures, the forces and deflections due to applied thermo-mechanical loading are

$$F = F_\phi (\phi + \phi_n) + F_e (e_T + e_n), \quad (8)$$

and

$$\Delta = \Delta_\phi (\phi + \phi_n) + \Delta_e (e_T + e_n), \quad (9)$$

where F and Δ are the internal forces and deflections, respectively, accounting for large deflections.

Equations (8) and (9) can be solved approximately for the deflections. The result is (ref. 1)

$$\begin{aligned} [I - \Delta_\phi (\phi_n \phi_\Delta + \phi_n T_\Delta)] \Delta = \Delta_\phi \phi + \Delta_e e_T \\ + (\Delta_e + \Delta_\phi \phi_{n_e}) e_n, \end{aligned} \quad (10)$$

where I is the identity matrix, $\phi_n \phi_\Delta$ and $\phi_n T_\Delta$ are matrices of influence coefficients for the fictitious forces due to the combined effect of the unit deflections and the linear internal forces due to applied load and temperature, respectively, and ϕ_{n_e} is a matrix of fictitious forces due to the combined effect of the unknown deflections and the internal forces induced by unit member deformations.

The homogeneous form of Equation (10),

$$[I - \Delta_\phi (\phi_n \phi_\Delta + \phi_n T_\Delta)] \Delta = 0. \quad (11)$$

is the linearized stability criterion for buckling due to thermal, mechanical and combined thermo-mechanical loading. Equation (11) was developed by P. H. Denke in 1960 and has been the basis for the investigation of the elastic stability of various complex structures. It can be used in conjunction with a reduced modulus for cases of plastic buckling. However, since plastic buckling is dependent upon initial eccentricities, the general approach provided by Equations (8) and (10) is preferable. The following elaborations of these two equations were developed for practical application of the general approach to the analysis of buckling in creep environments (ref. 2):

$$\begin{aligned} \Delta = & \left[I - \Delta_{\phi} (C_{\phi} \phi_{n\phi_{\Delta}} + C_T \phi_{nT_{\Delta}}) \right]^{-1} \left\{ C_{\phi} \Delta_{\phi} \phi + C_T \Delta_e e_T \right. \\ & + \Delta_{\phi} (C_{\phi} \phi_{n\phi_{\Delta}} + C_T \phi_{nT_{\Delta}}) \Delta_o \\ & \left. + \left[\Delta_e + \Delta_{\phi} \phi_{ne\Delta} (\Delta + \Delta_o) \right] (e_p + e_n) \right\}, \end{aligned} \quad (12)$$

and

$$\begin{aligned} F = & C_{\phi} F_{\phi} \phi + C_T F_e e_T \\ & + F_{\phi} (C_{\phi} \phi_{n\phi_{\Delta}} + C_T \phi_{nT_{\Delta}}) (\Delta + \Delta_o) \\ & + \left[F_e + F_{\phi} \phi_{ne\Delta} (\Delta + \Delta_o) \right] (e_p + e_n). \end{aligned} \quad (13)$$

In Equations (12) and (13), Δ_o is the matrix of initial eccentricities, Δ is the matrix of deflections due to load and temperature, C_{ϕ} and C_T are scalars describing the intensity of the distributions of load and temperature, respectively, $\phi_{ne\Delta}$ is a three-dimensional array of fictitious forces due to the combined effect of unit deflections and internal

forces due to unit member deformation, and e_p is a matrix of nonlinear components of member deformations. The matrix e_p can be used to represent both plastic deformation and local buckling. Equations (12) and (13) are nonlinear and dependent, and therefore, special techniques are required for solution.

APPLICATIONS OF THE METHOD

Linearized Stability Solutions

In general, a linearized stability solution by the digital method includes the following steps: (1) computation of internal forces and deflection influence coefficients, (2) computation of the fictitious forces for conditions of unit deflection and (3) solution of the eigenvalue problem described by Equation (11). The results are the critical loads and corresponding buckling modes of the structure. A continuous computing process for the complete problem has been devised using existing digital methods and programs. Internal forces and deflection influence coefficients are computed using the Redundant Force Method, a fully automatic version of the Matrix Force Method. These data are transformed using a general purpose matrix abstraction program, and the eigenvalue problem is solved using a computer program originally developed for computation of vibration modes and frequencies. An indication of the generality of the method is provided by the complexity of the computations required for comparison of digital solutions with available data. From the viewpoint of the digital approach, most of these cases are degenerate, i.e., the typical stress distributions are uniform, and therefore the matrices of fictitious forces can be written by inspection.

The method has been applied to numerous cases of columns and panels. Columns were analyzed to evaluate the effect of the precision of discrete idealization. The results indicate that convergence is monotonic and that a high degree of precision is not required. As an example, a fixed-free column can be represented by two bars with an error of 5%, or by three bars with an error of 2%.

The digital method has been used to investigate several cases of panel buckling. A case of buckling of a simply supported, rectangular panel in shear was analyzed for the specific purpose of method verification. The critical shear stress computed by the digital method is 110% of the comparable value reported in reference 3, and buckling modes are in excellent agreement. The magnitude and sign of the error are consistent with the relatively crude idealization used in the analysis, and the error characteristics observed in the investigation of columns. On this basis, the agreement is considered to be excellent.

Large Deflection Solutions

A practical and convenient computing process has been developed for the analysis of large deflections of discrete structures (ref. 2). Linear influence coefficients are computed by the Redundant Force Method,

and Equations (12) and (13) are solved using a general purpose matrix abstraction program. For cases of elastic response without local buckling ($e_p = 0$), the equation of deflections is solved by an automatic iterative procedure. The solution of the equation of internal forces is then a routine process. The results are the internal forces and deflections for the specific thermo-mechanical condition described by C_ϕ and C_T . For cases of short-time or time dependent plasticity, or local buckling ($e_p \neq 0$), an incremental procedure is used. The results are a series of solutions describing the history of internal forces and deflections with respect to load and/or time.

A comparison of test data for a stiffened panel in compression at elevated temperature, and the results of the comparable incremental analysis are shown in figure 3. The peculiar shape of the deflection profile is of particular interest. The panel was stiffened unidirectionally and loaded in the direction of the stiffeners. In addition, a secondary loading was induced transversely to the stiffeners by an elastic restraint to Poisson deformation. The effect on the response of the panel was pronounced, even though the ratio of transverse to primary loads was only 5%. Without the secondary loading, the deflection profile would have been the characteristic shape indicated by the curve determined by linear analysis. The agreement of these data is an important contribution to the verification of the method.

Verification of the notion of fictitious member deformations is important to the use of the digital method for analysis of structures that exhibit failure due to large deflection instability. The results of an investigation for this purpose are shown in figure 4. It is concluded from this comparison that the idea of fictitious member deformations properly represents the effects peculiar to large deflection instability.

CONCLUSIONS

A general digital method for the analysis of nonlinear planar structures has been developed, programmed for efficient computations, and verified by application to a wide variety of structures. It is considered to be a practical and extremely valuable approach to the analysis of nonlinear structures and worthy of the effort required for generalization to include shells. When fully developed and understood, it is expected that the digital method will provide a sound basis for the analysis of the complicated nonlinear response of advanced aerospace

vehicles with sufficient reliability to allow a reduction in the scope of testing at elevated temperatures.

ACKNOWLEDGEMENTS

The development program reported in this paper is being conducted under the direction of M. Stone, Chief of the Aerostructural Mechanics Section, Aircraft Division, Douglas Aircraft Company, Inc. Technical direction of the program is the responsibility of P. H. Denke, Supervisor of Research and Development in the Aerostructural Mechanics Section. A major portion of the work reported herein was accomplished under the sponsorship of the Aeronautical Systems Division, AFSC, USAF, by authority of Contract No. AF 33(616)-8359, titled "Buckling of Structural Panels Subjected to Creep Environments."

REFERENCES

1. Denke, P. H.: Digital Analysis of Nonlinear Structures by the Force Method. Paper presented to the Structures and Materials Panel of AGARD, NATO, in Paris, France, July 1962.
2. Warren, D. S.: A Matrix Method for the Analysis of the Buckling of Structural Panels Subjected to Creep Environments. ASD Technical Report per Contract No. AF 33(616)-8359. (To be published.)
3. Stein, M. and Neff, J.: Buckling Stresses of Simply Supported Rectangular Flat Plates in Shear. NACA TN 1222, March 1947.

FICTITIOUS FORCES INDUCED BY ROTATION OF AN AXIALLY-LOADED BAR

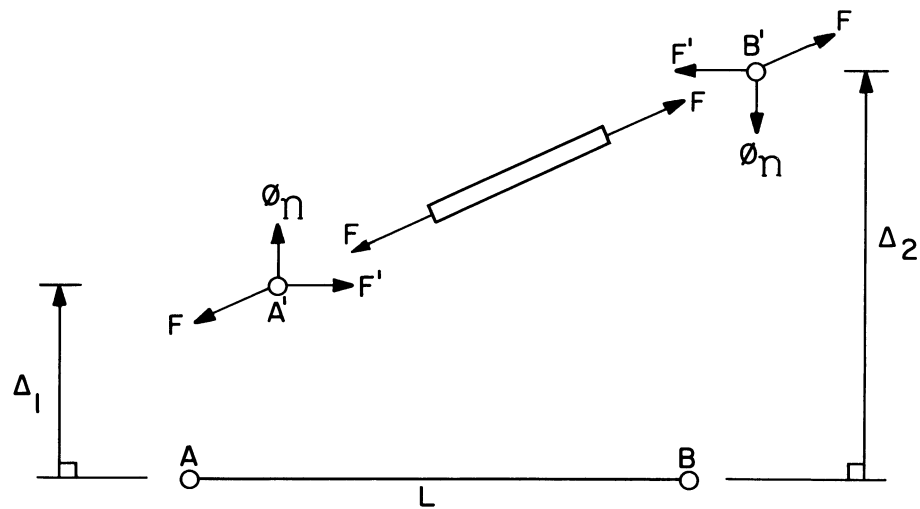


Figure 1

FICTITIOUS MEMBER DEFORMATION INDUCED BY ROTATION OF A BAR

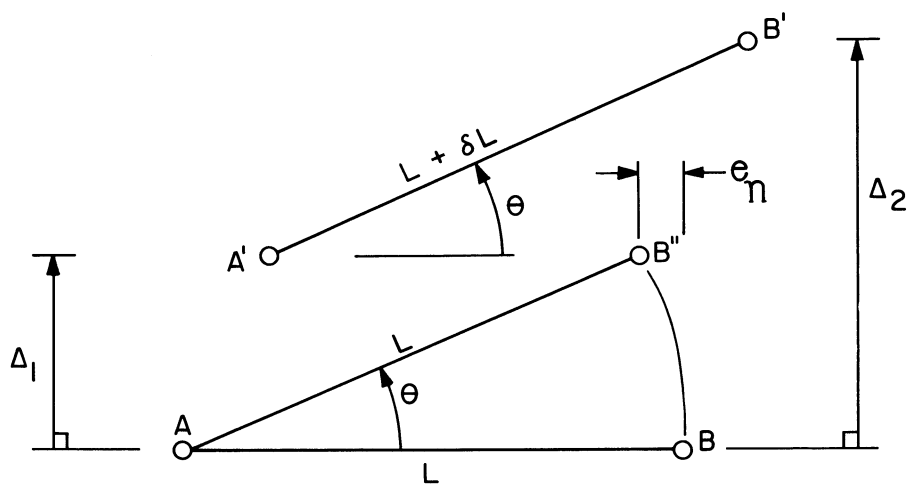


Figure 2

CREEP DEFLECTION OF A COMPRESSION PANEL

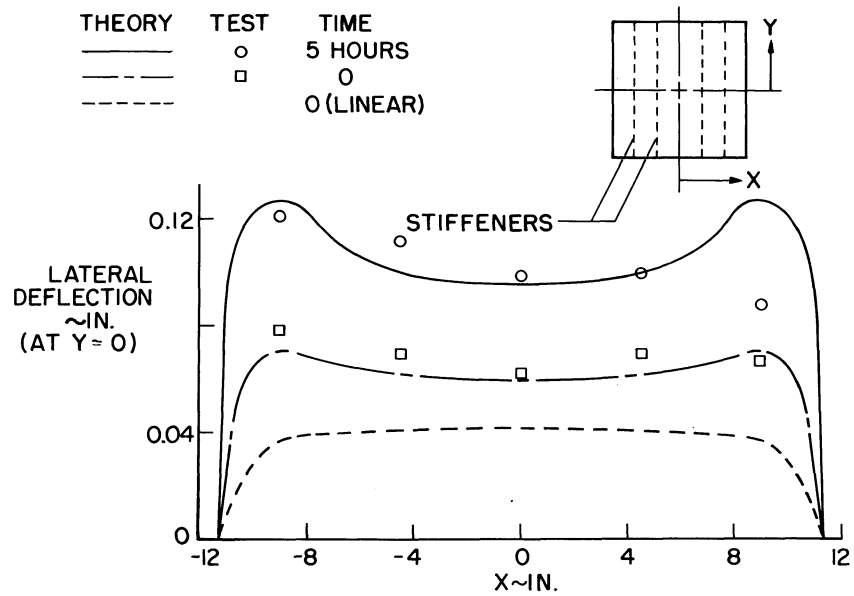


Figure 3

LARGE DEFLECTIONS AND STABILITY OF A TRUSS

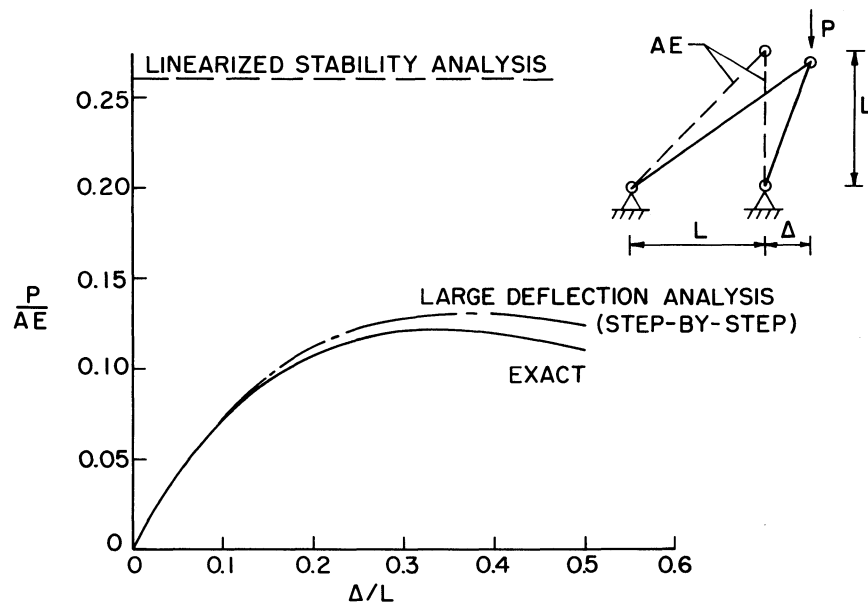


Figure 4

NON-LINEAR SHALLOW SHELL ANALYSIS BY

THE MATRIX FORCE METHOD

By Warner Lansing, Irving W. Jones
and Paul Ratner

Grumman Aircraft Engineering Corporation

SUMMARY

The matrix force method of redundant structure analysis is currently being extended by various users to cover a number of non-linear problems. One of these is the non-linear analysis of heated cambered wings, such as might be used in advanced flight vehicles. In this case the approach used by the present authors is equally applicable to shallow shells, the formulation of the strain-displacement and equilibrium relations being a finite element equivalent to that used by Marguerre. The solution is obtained by a combined iteration and step by step procedure utilizing a tangent flexibility matrix. Divergence in the calculations indicates that the range of stable configurations has been exceeded. Cambered plates subjected to several loadings are given as examples; for one, an exact solution is available for comparison.

It is believed that the basic concepts involved in this shallow shell analysis can be extended to apply to other, more general shell instability problems, and that useful solutions to the latter are probably within the capability of present day digital computers.

INTRODUCTION

Shell structures are one of the vital considerations in the design of aerospace vehicles. New methods are needed for analyzing the entire range of shells, from the very thin walled, pressurized membrane type, usually of relatively simple geometrical shape, to the reinforced shell type, with provision for such features as redistribution of large concentrated loads, discontinuities because of cutouts, irregular basic geometry, etc.

In cases where they are applicable, new solutions based upon extensions of the classical shell theory approaches would be preferred. However, when the shell structure and/or loading is sufficiently irregular, one of the finite element approaches is probably the only way out.

This paper presents a review of one such analysis for the non-linear behavior of shallow shells. This is of course a restricted problem, but it is believed that information gained from its solution will be of assistance in attacking the more important general shell case.

REVIEW OF THE METHOD

There are currently several finite element structural analysis methods in general use throughout the aerospace industry. Originally these methods were developed primarily with the linear analysis of airframes in mind; more recently they have been extended by a number of investigators to include various non-linear structural effects. See for example references 1 - 4.

Reference 5 treats the specific problem of a heated, cambered wing. The non-linear feature in this case is the effect of large deflections, rather than any material property consideration. While the procedure was developed with low aspect ratio wings in mind, it is equally applicable to shallow shells, the formulation of the strain and equilibrium relations being a finite element equivalent to that used by Marguerre (ref. 6).

Basically, the method consists of first carrying out two separate analyses, one for the bending behavior, the other for the membrane behavior. In so doing, the shell is idealized as consisting of a number of bars and shear panels. The output of the bending analysis is a conventional stiffness matrix which is independent of the lateral displacements. The membrane analysis, on the other hand, yields a stiffness matrix that is a function of the displacements. Its determination requires that one first assume a set of lateral displacements. From the two component stiffness matrices one can assemble a matrix equation giving the total loading carried by the shell structure in the assumed deflected configuration. This loading will not, in general, agree with the required loading. At this point, the assumed deflected configuration must be altered to correspond more nearly to the applied loading. Determining the correcting loads and displacements involves the calculation of a "tangent flexibility matrix".

Its calculation is the other key step in the analysis. It is obtained by the differentiation with respect to the displacements of the matrix equation for the total applied loads which was just discussed. The resulting tangent stiffness matrix for the composite structure is immediately inverted to give the corresponding tangent flexibility matrix. The elements of this matrix give the deflection at one point of the composite structure due to a unit load at another, assuming that the structure displaces linearly from its deflected shape.

With the tangent flexibility matrix available, it is possible to extrapolate linearly from the assumed deflected configuration to an improved one. The cycle may be repeated as many times as needed. The procedure merely determines at the end of each cycle how nearly the loads sustained by the structure agree with the actual applied loads, and terminates when the agreement is satisfactory.

For structures such as shallow shells, which have a characteristic non-linear applied load vs. deflection curve with continually decreasing slope, the determination of the buckling load can be carried out as follows: One first selects an applied load level and an assumed set of deflections, usually zero for the latter as a matter of convenience, and the iteration procedure is begun. When it has produced a stable set of deflections corresponding to the applied loading, these deflections and an increased applied load level are selected for a new iterative solution. This step-by-step procedure is continued until the slope of the load-deflection parameter curve has become practically horizontal, at which point the iteration procedure will no longer converge. The highest stable applied load level reached in this manner is a lower bound for the buckling load.

A more direct approach to the stability problem is also being explored in which the buckling load level is calculated directly. Indications are that this approach may be successful in cases where the equilibrium loading decreases distinctly after the structure becomes unstable.

NUMERICAL EXAMPLE

Description of Idealized Structure

Reference 7 contains an exact solution to a non-linear shallow shell problem, namely a cambered plate subjected to pure bending. A simplified idealization of this same type of structure but with a built up construction in mind has previously been programmed for a digital computer. It is therefore convenient to simulate the present cambered plate by appropriate bar and shear panel elements and to compare the resulting predictions of the computer program with the exact solution.

Figure 1 shows schematically the idealized structure representing the cambered plate. Because of double symmetry, only one quarter of the plate need be considered. The node points are shown numbered from one to fourteen. Interconnecting the node points at the upper and lower surfaces of the plate are the bars and shear panels. In the case of the bending structure analysis, standard methods for selecting effective

areas and gages are employed and yield satisfactory accuracy - see for example reference 5. For the membrane structure, one would customarily use the entire thickness of the plate as effective. However, with the total cross-section approximated by only five lumped areas, the moment of inertia of the finite element representation is 1.58 times the moment of inertia of the actual distributed cambered plate material. This could have been remedied by introducing more node points into the idealization. Instead, for simplicity, the effective thickness for the membrane structure was taken as $1/1.58$ times the actual value. This solution of the problem is not entirely satisfactory because when subjected to lateral loads, the cambered plate is now too flexible in shear. The results should nevertheless still be qualitatively correct in this situation, and should be much better when the loading is primarily bending.

The dimensions of the example structure are shown in figure 2. As can be seen there, the thickness t is 0.25 inches and the width a is 20 inches, while the rise of the parabolic cross section is 1.25 inches. Young's modulus E is taken as 10^7 psi, and Poisson's ratio is .316.

Loading By End Couples

The first loading considered is pure bending in the spanwise direction, for which an exact solution is available (ref. 7). This state is characterized by the conditions that (1) the stress distribution and the shape of the distorted cross-section are both constant for all cross-sections, (2) the curvature in the spanwise direction is also constant, i.e. spanwise elements of the plate bend circularly, and (3) the applied edge loads remain tangent to the plate surface as it deflects. For the state of pure bending to exist, the resultant moment M must be applied along the two cambered edges as a combination of membrane stresses and plate bending stresses. It is found that for the cambered plate proportions of figure 2 and for a very small value of M , 96% of M is carried in membrane action while only 4% is carried by plate bending. As M increases in value and the cambered plate tends to flatten out, a smaller amount of the total bending is carried in membrane action, until the structure becomes unstable. This is shown for the exact solution by the solid curve of figure 3, where the non-dimensional bending parameter $(12Ma)/(Et^4)$ is plotted against the longitudinal curvature parameter a^2/Rt . The quantity R is the radius of curvature of any spanwise line element in the mid-plane of the plate.

In the case of the finite element solution, the entire applied load M is arbitrarily introduced by an in-plane loading only, acting on the two cambered edges as indicated in figure 2. The five horizontal forces shown are distributed according to engineering beam theory. The small vertical forces, distributed in the same proportions, are introduced

in order to have the resultant forces remain approximately tangent to the median surface at the edge as the edge deflects. The magnitudes of the vertical forces are given a final adjustment by trial such that the reduction in camber is approximately uniform at all interior cross-sections. The results of several of these calculations are shown by the circled points in figure 3. The quantity R in the curvature parameter is now taken as the average of the radii of curvature along the five spanwise lumped bars, at the centerline. The agreement with the theoretical solution of reference 7 is surprisingly good for so crude an idealization. No real attempt has been made to obtain the idealized structure's maximum load because of the laborious way in which the end couples had to be introduced. For most applications this would not be a problem, since the directions of applied loads can usually be considered to remain constant during deflection.

Loading by Lateral Pressure

The other loading considered is a downward acting uniform pressure, resisted by a uniform line load at the transverse centerline. These effects are simulated on the finite element structure in the usual way, by equivalent concentrated forces acting at the node points.

The load-deflection behavior is again plotted on figure 3, the bending moment M now being the maximum value in the spanwise direction, occurring at the centerline. The curvature parameter is once more the average value at the centerline. Each of the triangular points shown represents an equilibrium configuration obtained by the iteration procedure. As the pressure is increased to a new value, the displacements for the preceding point are used as the starting point for the new sequence of iterations. The process is terminated when a very small increase in the pressure results in passage from a stable to an unstable configuration.

From a comparison of the curves for the two loadings it is obvious that the cambered plate is much more flexible for the lateral pressure loading than for pure bending. This should be expected in the actual cambered plate because of the rather large contribution of the shear deflections of the membrane structure in the lateral pressure case. This is exaggerated in the finite element idealization because of the reduced effective membrane thickness, as discussed previously.

CONCLUDING REMARKS

Although the shallow shell structure considered in the previous numerical example is of a rather special nature, and the idealization employed rather crude, the authors believe that the basic method should be adequate for the general shallow shell case. In particular, for axi-symmetric shells, trapezoidal panels can be readily substituted for the rectangular ones presented here. In keeping with other applications of these finite element methods, it should be possible to account for almost any type of irregularity in structure and/or loading. The application need only be sufficiently important to justify the cost of implementing the computer program.

In the progression toward the completely general shell instability problem, the case of cylinders and cones is next. Its solution by finite element analysis methods appears to be realizable. Considerable progress has already been made in developing these methods for semimonocoque shells. These have been employed in a relatively routine manner for stress distribution purposes by a number of airframe manufacturers. It should be fairly straight forward to extend this work to include a complete monocoque shell representation if desired, by the addition of certain element flexibilities.

The introduction of linear instability effects into these calculations should also be reasonably straight forward. Finally, it would appear that the non-linear effects of large deflections could be introduced by the initial imperfection concept. The method of solution would again use an iteration and step by step procedure based upon the tangent flexibility matrix notion.

The big question that remains is how large a computer and how much of a programming effort will be required to accomplish all this? The answer should not be too far away.

REFERENCES

1. Denke, Paul H.: Digital Analysis of Non-linear Structures by the Force Method. Presented to the Structures & Materials Panel, Advisory Group for Aeronaut. Research & Development, North Atlantic Treaty Organization, Paris, France, 6 July, 1962.
2. Turner, J.M., Dill, E.M., Martin, H.C. and Melosh, R.J.: Large Deflections of Structures Subjected to Heating and External Loads. Journal of the Aero/Space Sciences, February, 1960.
3. Gallagher, R.H.: Matrix Structural Analysis of Heated Airframes. Proceedings of Symposium on Aerothermoelasticity, Aeronaut. Sys. Div., TR 61-645, p. 879 (Oct. 1961).
4. Klein, B.: A Simple Method of Matrix Structural Analysis: Part IV Non-linear Problems. Journal of the Aero/Space Sciences, June, 1959.
5. Lansing, Warner, Jones, Irving W., and Ratner, Paul: Non-Linear Analysis of Heated, Cambered Wings by the Matrix Force Method. IAS Paper No. 62-107, presented at the IAS National Summer Meeting, Los Angeles, Calif., June 19-22, 1962.
6. Marguerre, K.: Zur Theorie der gekrummten Platte grosser Formanderung. Proc. Fifth Int. Cong. Appl. Mech. (Sept. 1938, Cambridge, Mass.), John Wiley & Sons, Inc., 1939, pp. 93-101.
7. Ashwell, D.G.: A Characteristic Type of Instability in the Large Deflections of Elastic Plates. Proc. Roy. Soc., Vol. 214A, 1952, pp. 98-118.

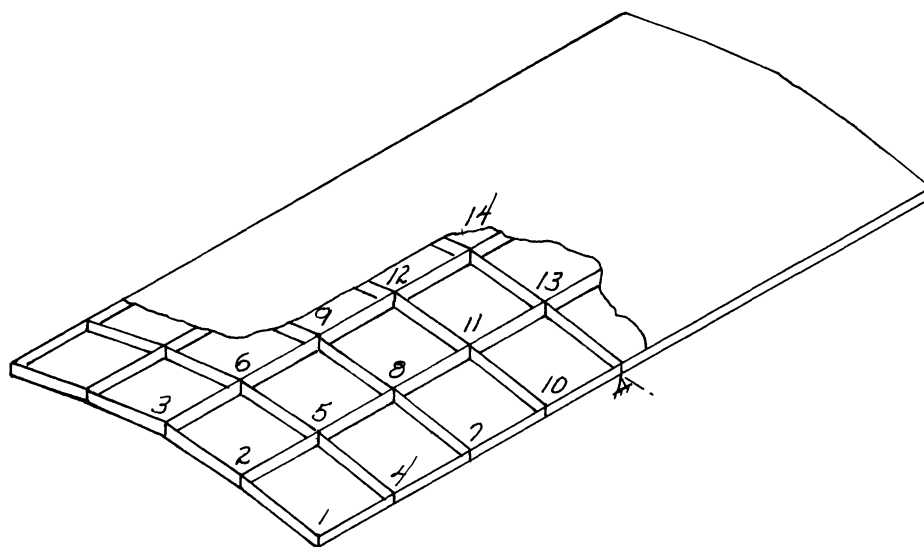


Figure 1.- Finite element idealization of cambered plate.

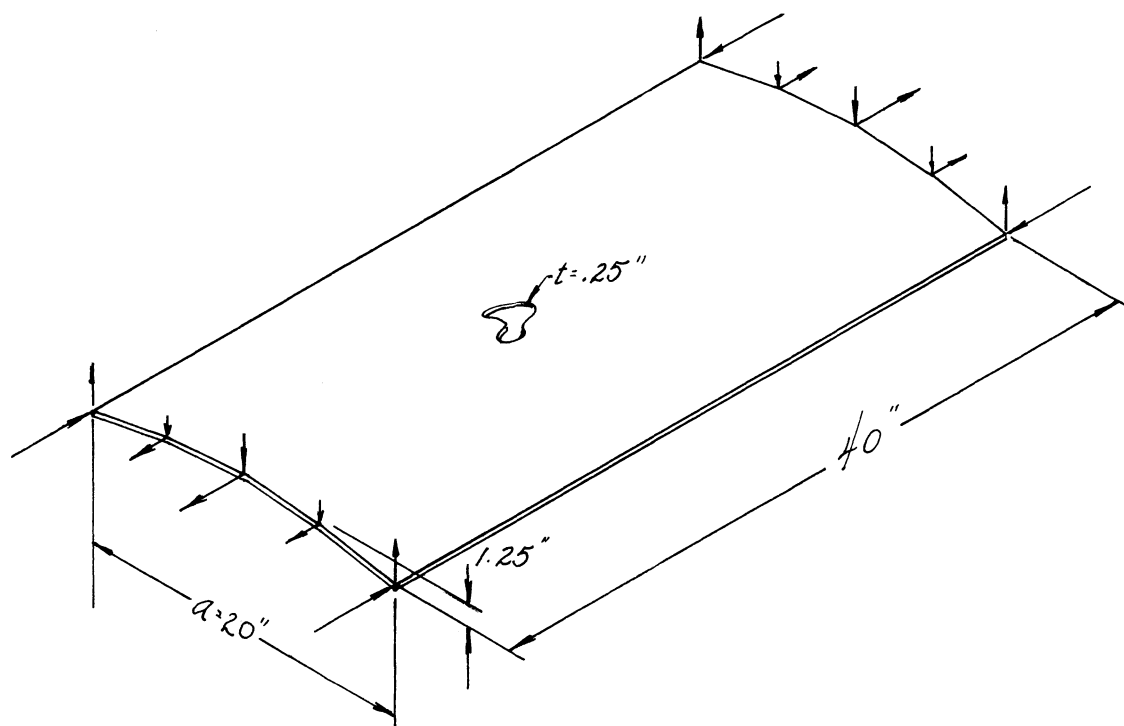


Figure 2.- Cambered plate subjected to pure bending.

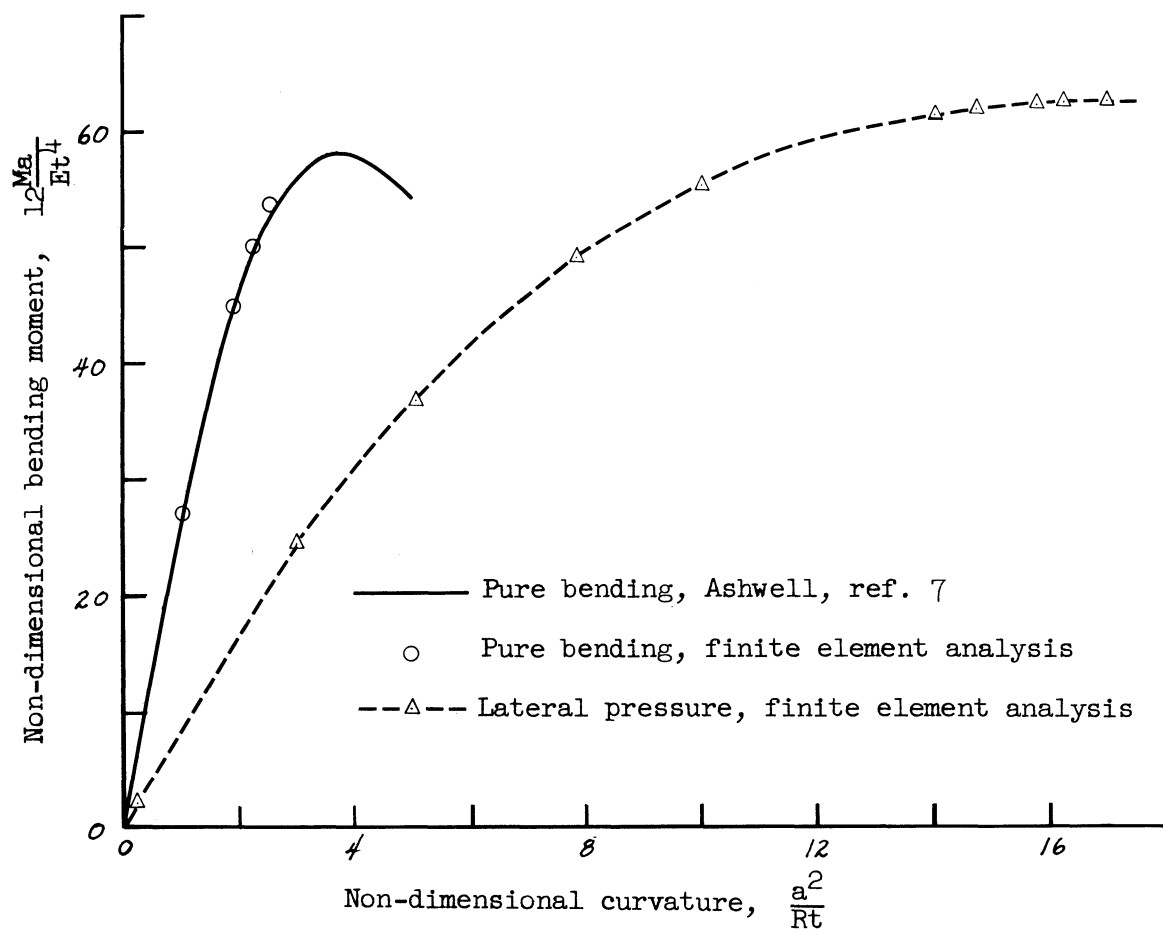


Figure 3.- Bending moment - curvature relationship for cambered plate.